

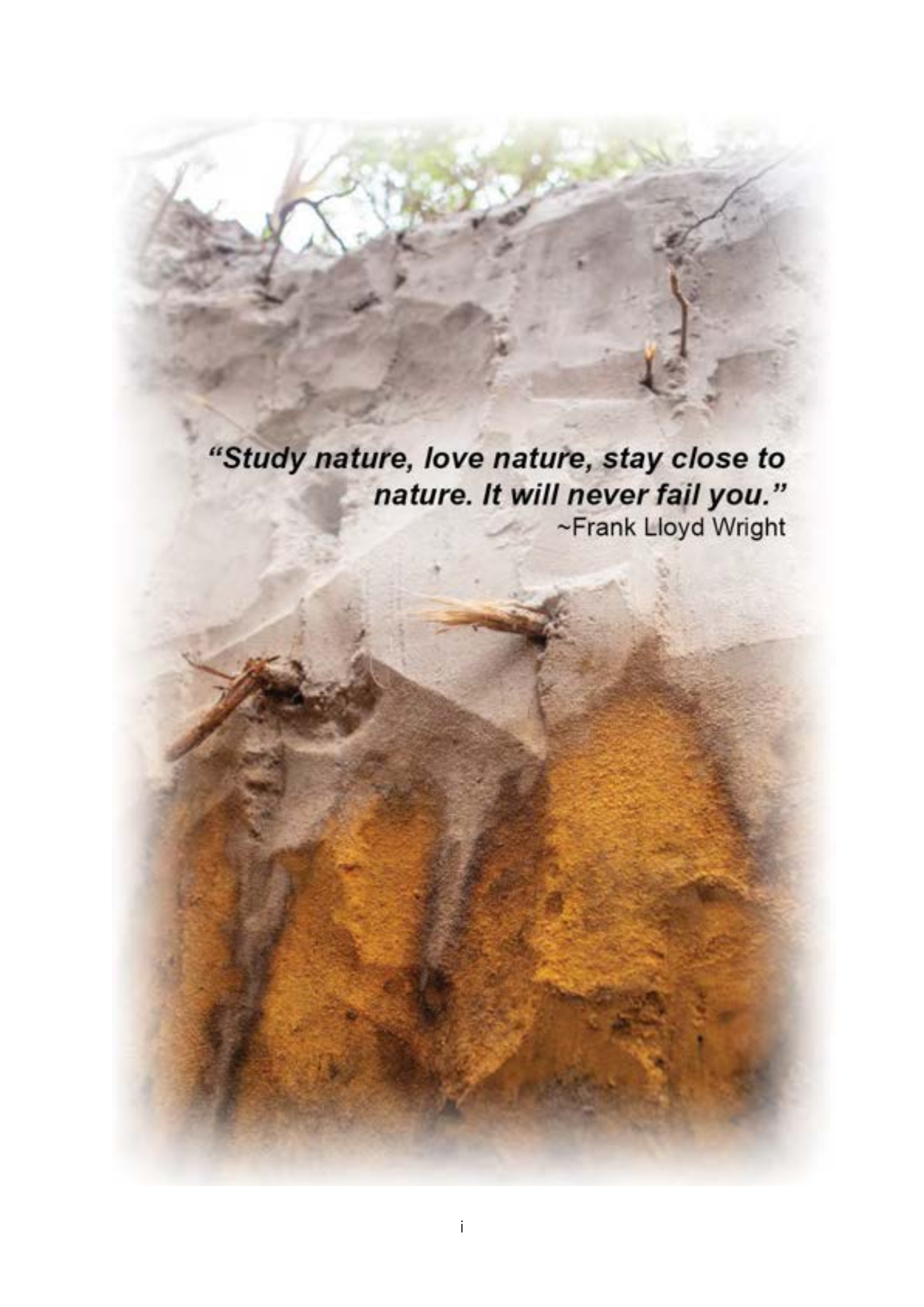


# Landscape evolution of the southeast Queensland dune fields, Australia

A thesis submitted in partial fulfilment of the requirements for the degree of Doctor of Philosophy in the  
School of Earth and Environment | *Te Kura Aronukurangi*  
University of Canterbury | *Te Whare Wānanga o Waitaha*

Nicholas R. Patton

Submitted June 2022 – Revised for print January 2024

A photograph of a sand dune with a quote overlaid. The dune is made of light-colored sand and has some small, dry, brown sticks and twigs protruding from it. The background shows some green foliage at the top of the dune. The quote is in a bold, black, sans-serif font and is centered on the dune. The text reads: "Study nature, love nature, stay close to nature. It will never fail you." followed by "~Frank Lloyd Wright" in a smaller font.

***"Study nature, love nature, stay close to nature. It will never fail you."***  
~Frank Lloyd Wright

# Abstract

The sub-tropical coastal dune fields of southeast Queensland, Australia are recognised for their outstanding beauty, cultural importance, and ecological diversity. Their soil and vegetation development have been intensively investigated and more recently, the geochronology of the dune fields has been expanded. However, there has been little focus on the evolution of the dune fields after the dunes stabilise. The aim of this thesis is to enhance our fundamental understanding of dune field evolution by evaluating the complete topographic development of the dunes from their emplacement (stabilisation) to maturity (denuded topography). Principles and concepts derived from hillslope geomorphology were used to determine styles and rates of landscape change. The Holocene section of the Cooloola Sand Mass (CSM) is the primary focus of this study, while Holocene dunes on K'gari (Fraser Island) were also investigated. The dune fields were selected because most of the major environmental factors contributing to landscape development in the Holocene can be constrained, and they contain one of the most complete coastal dunes sequences in the world.

Quantitative topographic analyses from high-resolution digital elevation models with landscape evolution theories (linear and nonlinear sediment transport) were used to better describe and understand dune fields and dune landforms. Principally, the foundational idea that gravitationally driven transport processes smooth dune landforms to their base-levels thereby reducing mean local relief, was used. The concept that landscapes smooths with time provides the framework to establish morphostratigraphical mapping, 2-D numerical modelling, and roughness-age modelling.

From the geomorphological mapping it is observed that the SE Queensland dune fields are constructed of five Holocene (including active dunes) and four Pleistocene dune morphosequence units. Dunes and their units systematically smooth with time and this evolution is well explained using surface roughness ( $\sigma_c$ ). It is demonstrated that Holocene dune  $\sigma_c$ -age relationships evolve in two distinct phases. The first phased is described well using nonlinear sediment transport with a soil transport coefficient (K) value of  $0.06 \text{ m}^2 \text{ yr}^{-1}$  and a critical gradient of  $0.65 \text{ m m}^{-1}$ , which is the angle of repose. The dune evolution switches to a K value of  $0.002 \text{ m}^2 \text{ yr}^{-1}$  after ca. 1 ka that can be modelled either using nonlinear or linear sediment transport.

The evolution of the whole landscape can be empirically described using an exponential function ( $(\partial\sigma_c)/\partial t \propto \sigma_c$ ). The predictable changes in dune topography permits a  $\sigma_c$ -age relationship to be calibrated on the CSM and tested against an independent OSL chronology from K'gari. The model generates age estimates for every dune thereby producing the first complete Holocene chronology in the dune field. This procedure can be easily expanded to dune fields globally to fill in chronological gaps using only high-resolution elevation data and a small number of absolutely dated dunes. The age estimates support the morphostratigraphical mapping and demonstrate dune emplacement peaking at ca. <0.5, 1.5, 4, and 8.5 ka. These ages are similar, but not identical, to the dune emplacement timings in the published literature but they tie closely to sea-level variability, which is the inferred primary cause of dune field activation.

The  $\sigma_c$ -age relationship was evaluated further by placing the modelled outputs into the context of sedimentary records from dune foot-slope positions. The first sediment transport phase corresponds with the period of rapid lowering of relief and elevated erosion/sedimentation rates ( $0.57 \pm 0.13 \text{ cm yr}^{-1}$ ) associated with the dominance of episodic sediment transport (i.e., dry-ravel and sheetwash). These transport styles are the consequence of fires on steep hillslope gradients. These events deposit charcoal as layers in foot-slope positions. This phase occurs for the first ca. 1-1.5 ka after dune emplacement until hillslopes are lowered below their angle of repose ( $0.65 \text{ m m}^{-1}$  or  $33^\circ$ ). In the second phase, erosion/sedimentation rates decrease by an order of magnitude ( $0.10 \pm 0.07 \text{ cm yr}^{-1}$ ) due to the dominance of slow and continuous sediment transport processes (i.e., biogenic soil creep and granular relaxation). Although fires are present, the absence of episodic sediment transport results in disseminated charcoal rather than charcoal layers in foot-slope positions. Nevertheless, fire frequency and intensity can be inferred from these records and the thesis highlights and develops the idea of utilising dune depositional records for fire histories. These deposits produce a ca. 7 cal ka BP fire record that identifies increased fire activity at ca. <0.3, 1.1-0.4, 2.2-1.6, 3.4-2.6, and 6.7-5.3 cal ka BP. These periods are consistent with local and regional fire histories from traditional charcoal records.

In summary, this thesis contributes new insights into landscape evolution using a dune field as a natural sandbox laboratory. It offers a novel perspective on aeolian systems and provides new lines of research into a variety of environmental processes from dunes.



# Financial support

Through my candidature, I was the recipient of the University of Queensland's 'Research Training Scholarship' and the University of Canterbury's 'College of Science Doctoral Scholarship'. This research was primarily funded by the Australian Research Council Discovery Grant project '*Climate and environmental history of SE Queensland dune fields*' (DP150101513). Additional funds for access to equipment, training, and analyses included ANSTO Portal Grants (AP12211, AP12591, AP12614, and AP12781), the Mason Trust Grant, and the British Geological Survey (BGS) University Funding Initiative (BUFI). Lastly, I received financial support by the Australian and New Zealand Geomorphology Group (ANZGG) to attend the 18th Biennial ANZGG conference.

# Declaration by author

The content of this thesis comprises of my original work that I have conducted since the commencement of my research candidature, which I started at The University of Queensland, Australia then transferred to the University of Canterbury, New Zealand. This work has not been submitted elsewhere for any other degree or tertiary institution. All material previously published is referenced and co-author contributions are included.

*Copyright © 2024 by Nicholas R. Patton.*

The copyright of this thesis rests with the author. No direct quotations or images from it should be used or published without the author's prior written consent.

# Acknowledgements

First and foremost, I would like to state my gratitude to Jamie Shulmeister. Who would have thought that meeting in Idaho seven years ago would have turned into a chance for me to obtain a PhD on the opposite side of the world. Thank you for the opportunity of a lifetime and being not just a great advisor but also a mentor and friend. Not all advisors would have allowed or even encouraged me to take on so many side projects. Thank you for being generous with your time, supportive of a work-life-balance, and taking me on as your student. How can I mention Jamie without mentioning my unofficial but official 'boss' of the PhD, Val. Thank you for always being someone I could look to for advice and to put things into perspective. You and Jamie have been my southern hemisphere family and I owe you both so much gratitude and appreciation. Without you both, I would have been living under a bridge, penniless, and starving during COVID lockdown and most of the PhD.

During my PhD, I transferred from the University of Queensland to the University of Canterbury to continue to work directly with Jamie. I had the privilege to work alongside amazing researchers from two fantastic departments. This move contributed to the success of my thesis and my development as a scientist. Thank you everyone that took the time to make my experience enjoyable (staff, faculty, techs, office mates, visiting academics and students). I would like to especially thank the following: Kevin Welsh, thanks for letting me tag along in the field and letting me continue our projects together. Melanie Leng and Mathew Jones, thank you for making me feel welcome at the University of Nottingham and the British Geological Survey. Tammy Rittenour, thank you for giving me the opportunity to take your short-course and stick around at Utah State University. David Fink, Toshi Fujioka, Kristin Simons and Quan Hua thank you for being supportive and a valuable resource throughout the PhD. I want to thank Peter Almond and Tim Stahl for being my NZ co-advisors. Lastly, I would like to thank the National Parks, Wildlife Service, and traditional owners of the Cooloola Sand Mass and K'gari (Fraser Island), the Kabi' Kabi' and Butchulla peoples and their elders past, present and emerging.

My success as a PhD student was not just developed over the last four years but throughout my entire academic career. I would like to thank my MSc advisor Kathleen Lohse for helping me build a strong foundation as a scientist, as this has undoubtedly made my transition from MSc to PhD a smooth one. Next, I would also like to thank Idaho State

University's Geology and Biology departments. Lastly, I would like to acknowledge California University of Pennsylvania's Geology and Chemistry departments.

To the hiking/coffee crew – Rasool, Inbar, and Arman. Thank you for the great times traveling through the New Zealand bush and for all the conversations about everything and nothing. Also, thank you for guilting me into learning geography. In addition to everyone already previously stated, I would like to extend my gratitude to those who made my time in Australia and New Zealand memorable – Chris, Dan, Jo, Patrick, Yuzhu, Dongliang, Jack, Al, Anna, Alex, Amanda, Valeria, Gretel, Kattie, Mia, Emily, Kegham, Ben, Clive, Pedro, Julia, Sulaiman, Eva, Rod, Jaime, Lauren, Holly, and Romy. I would also like to thank my friends that have kept in touch over the years and was always up for a chat – Carl, Sarah, Nick, Clar, Mitch, Courtney, Owen, and Bobby.

There are many people that have made an everlasting mark on my life and I am eternally grateful for their support. I would like to thank the Liehbold-Bardwell family for opening my eyes to a life beyond my hometown. Whether you realise it or not, the conversations around your dinner table inspired me to travel and continue to learn. You made a meaningful impact on my life and the choices I have made along the way. To Ashleigh. Thank you for bringing balance to my life and being the support system that I never knew I needed. I am grateful for all the times you dragged me out of the office/lab to enjoy nature. Every day you remind me that "I'm lucky", and that there is more to life than just work. I am excited to spend the rest of my life with you, and to see where our next adventure takes us. Last but certainly not least, I would like to thank and dedicate this thesis to my parents and my brothers who have helped me through the better part of a decade of struggle through school. Out of all the boys, I am just as surprised as you are that I made it. This is as much your PhD as it is mine.

Deputy Vice-Chancellor's Office  
Postgraduate Office

## Co-Authorship Form – Patton et al. (2019a)

This form is to accompany the submission of any thesis that contains research reported in co-authored work that has been published, accepted for publication, or submitted for publication. A copy of this form should be included for each co-authored work that is included in the thesis. Completed forms should be included at the front (after the thesis abstract) of each copy of the thesis submitted for examination and library deposit.

**Please indicate the chapter/section/pages of this thesis that are extracted from co-authored work and provide details of the publication or submission from the extract comes:**

*Chapter 2- High-resolution remapping of the coastal dune fields of south east Queensland, Australia: a morphometric approach*

*Published in Journal of Maps*

**Please detail the nature and extent (%) of contribution by the candidate:**

*80% of the research is the candidate's original work. All authors formulated the idea of the manuscript. N.R.P. did the mapping. N.R.P and D.E. drafted the manuscript with inputs from J.S. All authors assisted with writing and editing the manuscript.*

### **Certification by Co-authors:**

If there is more than one co-author then a single co-author can sign on behalf of all

The undersigned certifies that:

- The above statement correctly reflects the nature and extent of the PhD candidate's contribution to this co-authored work
- In cases where the candidate was the lead author of the co-authored work, he or she wrote the text

**Name:** James Shulmeister **Signature:** **Date:** 27<sup>th</sup> June 2022



Deputy Vice-Chancellor's Office  
Postgraduate Office

## Co-Authorship Form— Patton et al. (2022a)

This form is to accompany the submission of any thesis that contains research reported in co-authored work that has been published, accepted for publication, or submitted for publication. A copy of this form should be included for each co-authored work that is included in the thesis. Completed forms should be included at the front (after the thesis abstract) of each copy of the thesis submitted for examination and library deposit.

**Please indicate the chapter/section/pages of this thesis that are extracted from co-authored work and provide details of the publication or submission from the extract comes:**

*Chapter 3- Measuring landscape evolution from inception to maturity: insights from a coastal dune system*

*Published in Earth & Planetary Science Letters*

**Please detail the nature and extent (%) of contribution by the candidate:**

*80% of the research is the candidate's original work. N.R.P. formulated the idea of the manuscript. J.S. received funding for this project. N.R.P., D.E. and J.S. carried out fieldwork and the analyses. N.R.P. and J.S. drafted the manuscript with inputs from G.S., and D.E. G.S. and N.R.P. modelled landscape evolution. All authors assisted with writing and editing the manuscript.*

### **Certification by Co-authors:**

If there is more than one co-author then a single co-author can sign on behalf of all

The undersigned certifies that:

- The above statement correctly reflects the nature and extent of the PhD candidate's contribution to this co-authored work
- In cases where the candidate was the lead author of the co-authored work, he or she wrote the text

**Name:** James Shulmeister **Signature:** **Date:** 27<sup>th</sup> June 2022





Deputy Vice-Chancellor's Office  
Postgraduate Office

## Co-Authorship Form— Patton et al. (2022b)

This form is to accompany the submission of any thesis that contains research reported in co-authored work that has been published, accepted for publication, or submitted for publication. A copy of this form should be included for each co-authored work that is included in the thesis. Completed forms should be included at the front (after the thesis abstract) of each copy of the thesis submitted for examination and library deposit.

**Please indicate the chapter/section/pages of this thesis that are extracted from co-authored work and provide details of the publication or submission from the extract comes:**

*Chapter 4- Using calibrated surface roughness dating to estimate coastal dune ages at K'gari (Fraser Island) and the Cooloola Sand Mass, Australia*

*Published in Earth Surface Processes and Landforms*

**Please detail the nature and extent (%) of contribution by the candidate:**

*80% of the research is the candidate's original work. N.R.P. conceptualised the idea of the manuscript. J.S. received funding for this project. N.R.P., D.E., J.S., T.M.R., and T.S. completed all fieldwork. T.M.R. and N.R.P. carried out dating analyses. N.R.P created applied modelling. N.R.P. and J.S. drafted the manuscript. J.S., T.M.R. and P.C.A. are the primary supervisors of N.R.P. All authors assisted with writing and editing the manuscript.*

### **Certification by Co-authors:**

If there is more than one co-author then a single co-author can sign on behalf of all

The undersigned certifies that:

- The above statement correctly reflects the nature and extent of the PhD candidate's contribution to this co-authored work
- In cases where the candidate was the lead author of the co-authored work, he or she wrote the text

**Name:** James Shulmeister **Signature:** **Date:** 27<sup>th</sup> June 2022



Deputy Vice-Chancellor's Office  
Postgraduate Office

## Co-Authorship Form– Patton et al. (2023)

This form is to accompany the submission of any thesis that contains research reported in co-authored work that has been published, accepted for publication, or submitted for publication. A copy of this form should be included for each co-authored work that is included in the thesis. Completed forms should be included at the front (after the thesis abstract) of each copy of the thesis submitted for examination and library deposit.

**Please indicate the chapter/section/pages of this thesis that are extracted from co-authored work and provide details of the publication or submission from the extract comes:**

*Chapter 5- Reconstructing Holocene fire records using dune footslope deposits at the Cooloola Sand Mass, Australia*

*Published in Quaternary Research*

**Please detail the nature and extent (%) of contribution by the candidate:**

*80% of the research is the candidate's original work. N.R.P. conceptualised the idea of the manuscript. J.S. received funding for this project. N.R.P., D.E., J.S., J.G., A.G., and J.M.H. completed all field work. Q.H., J.M.H., T.R. and N.R.P. carried out dating analyses and age-depth modelling. N.R.P., J.S., and J.M.H. drafted the manuscript. J.S., T.R., and P.C.A. are the primary supervisors of N.R.P. All authors assisted with writing and editing the manuscript.*

### **Certification by Co-authors:**

If there is more than one co-author then a single co-author can sign on behalf of all

The undersigned certifies that:

- The above statement correctly reflects the nature and extent of the PhD candidate's contribution to this co-authored work
- In cases where the candidate was the lead author of the co-authored work, he or she wrote the text

# Table of Contents

ABSTRACT .....	II
FINANCIAL SUPPORT .....	IV
DECLARATION BY AUTHOR.....	V
ACKNOWLEDGEMENTS .....	VI
CO-AUTHORSHIP FORM – PATTON ET AL. (2019A) .....	VIII
CO-AUTHORSHIP FORM– PATTON ET AL. (2022A) .....	IX
CO-AUTHORSHIP FORM– PATTON ET AL. (2022B) .....	X
CO-AUTHORSHIP FORM– PATTON ET AL. (2023) .....	XI
TABLE OF CONTENTS.....	XII
LIST OF FIGURES .....	XV
LIST OF TABLES .....	XXVI
LIST OF SYMBOLS AND ABBREVIATIONS .....	XXVIII
LIST OF EQUATIONS.....	XXX
CHAPTER 1.....	1
1.1 Context .....	2
1.2 Thesis aims and objectives .....	3
1.3 Thesis structure .....	5
1.4 Scientific contributions .....	6
1.4.1 Peer-reviewed journal articles.....	7
1.4.2 Conferences presentations.....	8
CHAPTER 2.....	11
Abstract .....	12
2.1 Introduction.....	12
2.2 Study site .....	14
2.3 Materials and methods .....	16
2.3.1 Mapping assumptions and workflow .....	16
2.3.2 Dune delineation.....	16
2.3.3 Dune morphosequence delineation and supporting evidence.....	18
2.3.4 Mapping validation and supporting evidence .....	21
2.3.5 Mapping extrapolation .....	23
2.4 Results .....	23
2.4.1 CSM morphosequence unit delineation and validation.....	23
2.4.2 Mapping extrapolation .....	26
2.5 Discussion .....	27
2.5.1 Geomorphic evolution - foundation of this approach .....	27
2.6 Conclusion .....	28
CHAPTER 3.....	29
Abstract .....	30
3.1 Introduction.....	31
3.1.1 Study area: world premier chronosequence.....	33
3.1.2 Capturing landscape evolution with surface roughness .....	36
3.2 Methods .....	39
3.2.1 Dune selection and OSL dating overview .....	39
3.2.2 Dune delineation.....	39
3.2.3 Foot-slope excavation and depositional characterisation .....	39
3.2.4 Selection of topographic indices .....	40
3.2.5 Calculation of curvature and surface roughness.....	41
3.2.6 Two-dimensional dune evolution models .....	42

3.3 Result.....	42
3.4 Discussion .....	45
3.4.1 Parent material controls on dune evolution .....	45
3.4.2 Field observations and stratigraphic records .....	46
3.5 Conclusions.....	47
CHAPTER 4.....	49
Abstract .....	50
4.1 Introduction.....	50
4.2 Background.....	52
4.2.1 Surface roughness ( $\sigma_c$ ) as a proxy for landform.....	52
4.2.2 Surface roughness ( $\sigma_c$ ) in dune systems .....	53
4.2.3 Site description: Cooloola Sand Mass and K'gari.....	56
4.3 Methods .....	57
4.3.1 Dune mapping and remote sensing.....	57
4.3.2 Calculating surface roughness ( $\sigma_c$ ) .....	57
4.3.3 Optically stimulated luminescence (OSL) dating .....	58
4.3.4 Criteria for utilising previously OSL dated dunes .....	60
4.3.5 Surface roughness ( $\sigma_c$ )-age analysis and age extrapolation .....	60
4.3.6 Determination of dune emplacement through time .....	61
4.3.7 Sensitivity analysis.....	61
4.4 Results .....	62
4.4.1 OSL results and previous reported OSL ages.....	62
4.4.2 Surface roughness-age relationship .....	65
4.4.3 Predicted dune ages and their spatial relationships.....	66
4.4.4 Temporal frequency of dune emplacement.....	67
4.4.5 Sensitivity analysis.....	69
4.5 Discussion .....	69
4.5.1 Dune surface roughness and evolutionary processes.....	69
4.5.2 Timing of dune emplacement and regional story .....	70
4.5.3 Dune emplacement ages and sea-level variability .....	71
4.5.4 Surface roughness ( $\sigma_c$ )-age model application .....	75
4.6 Conclusions.....	76
CHAPTER 5.....	78
Abstract .....	79
5.1 Introduction.....	79
5.1.1 Fire in the Australian landscape .....	80
5.1.2 SE Queensland dune fields vegetation .....	83
5.1.3 SE Queensland dune fields fire history.....	84
5.2 Methods .....	87
5.2.1 Site selection and sampling design.....	87
5.2.2 Sediment sample preparation .....	89
5.2.3 Bulk density .....	89
5.2.4 Charcoal counting .....	89
5.2.5 Charcoal selection and preparation for radiocarbon ( $^{14}\text{C}$ ) dating.....	90
5.2.6 Age-depth model and combining charcoal records .....	91
5.3 Results .....	92
5.3.1 Field observations and soil characterizations.....	92
5.3.2 Charcoal concentrations.....	93
5.3.3 Radiocarbon ( $^{14}\text{C}$ ) analysis and age-depth modelling .....	93
5.3.4 CHAR records .....	98
5.4 Discussion .....	100
5.4.1 Charcoal preservation within dune foot-slope deposits .....	100
5.4.2 Sedimentation inferences from the age-depth models .....	102

5.4.3 Implications of charcoal layers in dune deposits .....	104
5.4.4 Comparison of paleofire records to the wider region.....	107
5.4.5 Causes of the high CHAR periods .....	109
5.4.6 Geomorphic and ecologic controls on dune paleofire records.....	111
5.4.7 Recommendations and future applications .....	112
<b>5.5 Conclusions.....</b>	<b>114</b>
<b>CHAPTER 6.....</b>	<b>116</b>
6.1 Key findings and contributions .....	117
6.2 Future directions .....	127
6.2.1 Automating dune delineation.....	128
6.2.2 Improving the application of $\sigma_c$ -age modelling.....	128
6.2.3 Quantifying and describing $\sigma_c$ -age transport mechanisms.....	129
6.2.4 Application in developing terrestrial fire histories .....	130
6.3 Summary .....	131
<b>REFERENCES.....</b>	<b>133</b>
<b>APPENDICES .....</b>	<b>160</b>
A.2 Supplementary Material to Chapter 2 .....	160
A.3 Supplementary Material to Chapter 3 .....	161
A.4 Supplementary Material to Chapter 4 .....	171
A.5 Supplementary Material to Chapter 5 .....	183
A.6 Chapters 2-4's original publications .....	194
A.6.1 Chapters 2 – Journal of Maps.....	194
A.6.2 Chapters 3 – Earth and Planetary Science Letters .....	206
A.6.3 Chapters 4 – Earth Surface Processes and Landforms.....	217
A.6.4 Chapters 5 – Quaternary Research .....	233

# List of Figures

- Figure 2.1:** (a) Study site location map of the SE Queensland dune fields with the eastern Australian longshore drift system and major rivers along the coast. Satellite images of (b) K’gari, (c) CSM, (d) Mulgumpin, (e) and Minjerribah .....14
- Figure 2.2:** Schematic flow chart of the mapping and validation procedures for dune morphosequence delineation.....18
- Figure 2.3:** Visual sequence of dune delineation example on Minjerribah (North Stradbroke Island) using (a) elevation and (b) slope DEMs, (c) satellite imagery, and (d) historical air photos. Note areas that are human disturbed (mining and road construction).....20
- Figure 2.4:** Workflow to produce mapping rasters. This figure demonstrates the methodology used to generate the topographic expressions as seen in the slope-elevation and slope-curvature layers. In each case a slope raster was superimposed at a 70% transparency on the elevation and curvature layers to generate the topographic expression. These topographic expressions were then applied to discriminate between morphosequence units.....21
- Figure 2.5:** The CSM morphosequence units and their validation. (a) Derived slope-curvature raster. (b) Final morphosequence map of the CSM. (c) Digitised version of Ward’s (2006) map. Note the strong similarity between panels b and c. In my final map I have added an extra Holocene unit (Freshwater) but eliminated a Pleistocene unit of Ward (2006) (Garawongera). (d) Examples of slope-curvature, slope-elevation and satellite images for each of the morphosequences. The heavy black line separating Triangle Cliff from Bowarrady marks the boundary between the Holocene and Pleistocene morphosequences. Note that the dune units become more diffuse and less well defined with increasing age. The units from the CSM were then applied to the sand islands.....22
- Figure 2.6:** Mapped morphosequence units and geomorphic characteristics. Final morphosequence maps for (a) K’gari, (b) the CSM, (c) Mulgumpin, and (d) Minjerribah dune fields. Note, dune fields are not to same scale. Panel (e) contains six graphs showing (i) percent land area for each unit; (ii) mean distance from coast, (iii) mean elevation, (iv) mean slope; (v) standard deviation of slope; (vi) standard deviation of curvature. The black line represents the mean values for all dune fields. Note that in all dune fields the parameters follow the same trends. Also note that for geomorphic characteristics there is a general progression from youngest to oldest morphosequences.....26
- Figure 3.1:** Regional and site location. (a) Satellite imagery of the SE Queensland dune fields in Australia, emphasising the location of the CSM. (b) Delineated Holocene dunes and their associated elevation at a 5 m resolution (black lines) and location of the 15 dated dunes and 4 soil pits used in this study (white circles and black dots, respectively) (obtained from Walker et al., (2018) and Ellerton et al., (2020), see Supplementary



Tables A.3.1, A.3.2, and A.3.3). Note, one soil pit was collected on a 2.14 ka dune that was not utilised in my topographic analyses (white triangle with black dot). A topographic transect aligned parallel to the dominant wind direction, (southeast to northwest), from juvenile to mature dunes is highlighted, see Figure 3.2. **(c)** Aerial view of an incipient parabolic dune forming along the margins of the Carlo Sand Blow near the township of Rainbow Beach (drone photography: “Wandering.the.Sky”). Note, this active dune (inception) is blown off the coast and extends inland through vegetation and over previously emplaced dunes creating over-steepened lee slopes, see Supplementary Figure A.3.1.....32

**Figure 3.2:** Changes in topographic variability at the CSM at a 5 m resolution. A transect aligned parallel to the dominant wind direction (northwest to southeast), seen in Figure 3.1b, indicates the transition from juvenile dunes (i) to more mature dunes (ii to vi) moving from the coast inland (right to left). When dunes are stabilised, they have highly variable surface topography. As time continues, their slope relaxes such that morphology is time independent and this evolution can best be described by the dune’s curvature, specifically a dune’s standard deviation of curvature ( $\sigma_c$ ) as a measure of surface roughness ( $(\partial\sigma_c)/\partial t \rightarrow 0$ ).....34

**Figure 3.3:** Idealised topography, chronosequence, and hillslope processes of the CSM, Australia. **(a)** The CSM dunes move inland from the coast across antecedent topography (dashed lines) until wind speeds decrease and dunes emplace (stabilise). With every subsequent dune emplacement, antecedent topography gradients increase therefore decreasing the distance dunes travel inland. **(b)** Conceptual diagram of hillslope positions and the contribution of erosion, deposition and flux (size of arrow). Once dunes’ hillslopes are lowered below their angle of repose (gradient of  $0.65 \text{ m m}^{-1}$  or angle of  $33^\circ$ ), I posit that nonlinear sediment transport effects become negligible. Here only diffusive hillslope processes are active and all sediment removed from crest and ridges can be accounted for in the hollows and valleys (a closed system). As time progresses ridges lower and hollows fill, reducing hillslope gradients and the maximum and minimum curvature values. Combined, I hypothesise a systematic decrease in erosion, deposition and flux rates with time.....36

**Figure 3.4:** Conceptual diagram (summarises hypotheses and main findings) inspired by Montgomery (2001). The relationship between change in elevation from base level, dominant transport styles, and curvature (C) distributions ( $\sigma_c$ ) for a dune landscape with time is shown. The dunes found at CSM are initially smooth (low  $\sigma_c$  and narrow C distributions) when they are actively migrating across the landscape (dune inception). As the dunes begin to stabilise, the competition between wind advection and vegetation stabilisation, results in an increase in topographic variability, broadening the C distribution (greater  $\sigma_c$ ) and thus increasing erosion rates. This positive change in  $\sigma_c$  represents a phase of landscape rejuvenation. Surface roughness reaches their highest values once dunes are fully stabilised (dune emplacement) and sediment transport is limited to hillslope processes, thus marking the relaxation phase (juvenile through old age stages). The lowering of crest and filling of hollows narrows C distribution (lower  $\sigma_c$ ) thus decreasing the dune’s erosion rates. Given ample time in a relaxation phase, the landscape will evolve towards senescence ( $(\partial\sigma_c)/\partial t \rightarrow 0$ )

where no local relief remains. I hypothesise that dune  $\sigma_c$  can only smooth (decrease) in the relaxation phase. Aerial images of the delineated dunes and the stage of their evolutionary development highlight these changes. Further description of dune stages can be found in Supplementary Tables A.3.1 and A.3.2.....38

**Figure 3.5:** Excavated depositional foot-slope soil profiles used to characterise erosion and sediment transport styles. Oldest profiles display disseminated charcoal through the full profile whereas the two youngest deposits have charcoal layers. Note the 2.14 ka dune record (not used in my  $\sigma_c$ -age analysis) with disseminated charcoal near the surface that switches to stratified charcoal layers near the base. This transition at  $\sim 1.1$  m corresponds with a depositional age of ca. 1 ka (determined by a radiocarbon age of  $1017 \pm 26$  yr BP (Wk50298) at 1.2-1.3 m, Supplementary Table A.3.4). I infer the presence of these layers are associated with fire induced episodic sediment transport (dry-ravel and sheetwash) when dunes are young and have steep slopes. As time progresses, hillslope gradients lower and charcoal layers become more diffuse and eventually become disseminated throughout the profile. These records highlight the transition between episodic to continuous sediment transport on dune evolution.....43

**Figure 3.6:** Measuring landscapes evolution through time at the CSM. **(a)** Observed curvature (C) distributions for four Holocene and one Pleistocene dune at the CSM. Note the normal distribution of C centred on planar topography ( $0 \text{ m}^{-1}$ ) and the gradual narrowing of distributions with time (dark to light frequency). **(b)** Measured dune age (with error bars,  $\pm 1\sigma$ ) with surface roughness ( $\sigma_c$ ) (white circles) and observed dominant transport styles. All dunes with excavated soil profiles are indicated with black dots. Additionally, the 2.14 ka dune with the excavated soil profile (not utilised in my topographic analyses) is represented by the white triangle. Initially, dunes are emplaced with over-steepened hillslopes at or above the critical gradient ( $S_c$ ). During this phase, there is a dominance of episodic sediment transport (dry-ravel and sheetwash ( $n=4$ )), purple dashed line. After dune's  $\sigma_c$  are lowered below a 'transitional zone' (at ca. 1 ka), only slow and continuous soil transport occurs (soil creep ( $n=11$ )), pink line. This behaviour continues and remains true for the Pleistocene dunes (grey diamonds, not included in this analysis).....44

**Figure 3.7:** Field images of typical soil transport styles. Commonly observed episodic (panels (a) and (b)) and continuous (Panels (c), (d), (e), and (f)) sediment transport mechanisms at the CSM. **(a)** Fire induced sand ravel and sheetwash movement on the steep lee facing hillslope of a 0.44 ka dune shortly after fire event and its associated **(b)** deposition. **(c)** Common mid-slope soil profile on a Holocene age dune highlighting the abundance of biogenic disturbed soil near the surface in the A horizon, where it becomes increasingly stable moving down profile as shown by the intact E and B horizons. Typical perturbation includes root growth and decay, **(d)** tree throw, **(e)** burrowing invertebrates, and **(f)** bird nest construction (photo credit: (c) Patrick Adams and (f) Kegham Hovsepian).....47

**Figure 4.1:** Conceptual diagram and result summary from *Chapter 3* between surface roughness ( $\sigma_c$ ) and dune age within the CSM dune field, Australia. **(a)** An idealised elevation profile of the CSM dune field. The dunes move inland from the coast through

sclerophyll forest and over antecedent topography (dashed lines) via the dominant south-easterly wind. Dunes are emplaced when wind speeds decrease and vegetation stabilises the dune surface. With every successive dune emplacement, antecedent topography gradients generally increase, thereby decreasing the distance dunes travel inland whilst preserving older dunes. Consequently, most dunes increase in age while decreasing in  $\sigma_c$  moving away from the coast. **(b)** Conceptual diagram of hillslope positions as defined by curvature (C) and the contribution of erosion, deposition and flux (size of arrow). All sediment removed from crest can be accounted for in the foot-slopes (a closed system). As time progresses ridges lower and hollows fill, reducing hillslope gradients and the maximum and minimum curvature values thus decreasing dune  $\sigma_c$ . **(c)** The general relationship between dune age, surface roughness ( $\sigma_c$ ), and sediment transport phases. Dunes with high  $\sigma_c$  (Phase 1) are best explained through non-linear sediment transport where episodic processes such as dry-ravelling and sheetwashing (comparable to grain flows and/or avalanching) occur. Once dune gradients are lowered below their angle of repose (gradient of  $0.65 \text{ m m}^{-1}$  or angle of  $33^\circ$ ) associated with the defined 'transitional zone', sediment transport is limited to slow and continuous processes (Phase 2) where their evolution can be explained with linear sediment transport.....54

**Figure 4.2:** **(a)** Satellite imagery of K'gari (Fraser Island), and the CSM, which make up the northern section of the SE Queensland (SEQ) dune field in Australia. The dune sediments are derived from the longshore drift system (dashed line and arrow) that is delivered to the coast by the dominant south-easterly winds (small arrows). **(b)** Close-up imagery of the coastline and dunes on K'gari (photo credit: Jürgen Wallstabe).....57

**Figure 4.3:** Locations of OSL dated dunes used in this chapter. Dunes utilised in the  $\sigma_c$ -age relationship are represented by grey dots, whereas, dunes used in the validation subset are white. For dunes with multiple dates, I preferentially selected ages from crest and/or stratigraphically lower positions. Samples that met my selection criteria but were not used in the model are marked with an 'X' .....65

**Figure 4.4:** Calculated surface roughness ( $\sigma_c$ )-age relationship from measured OSL dated dunes. **(a)** Dune  $\sigma_c$  depicts a strong exponential relationship with age ( $\pm 1\sigma$ ) (black line) bounded by 95% confidence intervals (shaded area) within the CSM and K'gari dune fields. The calibration ages (grey dots) come from the CSM ( $n=18$ ) whereas the remaining dates used as a validation subset (white dots) come from Inskip and K'gari ( $n=6$ ). **(b)** Model validation using predicted versus measured dune ages and their associated best-fit line (black line) using reduce major axis regression to account for uncertainty in both variables compared to a 1:1 line (solid black dashed line).....66

**Figure 4.5:** Predicted Holocene dune ages using  $\sigma_c$ -age model. **(a)** Aerial imagery of K'gari to the north and the CSM to the south with locations of Panels **(b)** northern K'gari, **(c)** southern K'gari, and **(d)** the CSM.....67

**Figure 4.6:** Normalised probability density functions (PDFs) of the combined K'gari and CSM dune fields derived from **(a)** OSL-dated dunes and **(b)** predicted ages. **(c)** Predicted ages normalised by total dune area. Vertical teal areas highlight phases of dune

emplacement. By far the largest number of dunes are small coastal blowouts, but cumulatively these dunes represent very little land area and are of only local significance. Area occupied by the dunes is critical as during major activation phases blowouts coalesce into much larger parabolic and transverse dune fields.....68

**Figure 4.7:** The combined K’gari and CSM dune fields PDF from predicted (dark grey) dune ages compared to local sea-level curves from Lewis et al. (2008) and Larcombe et al. (1995). Note there is a break in the relative sea-level axis so that both curves could be displayed on the same graph. I observe four emplacement phases (vertical teal areas) that are closely associated with the termination of the rising limb of sea-level events. The addition of my estimated ages permits me to better constrain the timing of dune emplacement (Ellerton et al., 2020) which has been associated with mapped dune units (Ward, 2006; *Chapter 2*): Cape ca. <0.5 ka; Station Hill ca.  $1.5 \pm 0.5$  ka; Freshwater ca.  $4 \pm 0.5$  ka; and Triangle Cliff ca.  $8.5 \pm 1.0$  ka.....73

**Figure 4.8:** Paleoclimate records through the Holocene from Laguna Pallcacocha in southern Ecuador (Moy et al., 2002), Swallow Lagoon in eastern Australia (Barr et al., 2019), and El Junco Lake in the Galápagos Islands (Conroy et al., 2008) compared to timing of major dune emplacement phases at K’gari and the CSM. Climate appears to have little direct link to dune emplacement.....74

**Figure 5.1: (a)** Total area burned in Australia during the 2019-2020 ‘Black Summers’ (red area) (DAWE, 2020) and the locations of sediment cores (white dots) used to generate Late-Quaternary fire records in Mooney et al. (2011). **(b)** Satellite imagery of the SE Queensland dune fields and location of fires during the 2019-2020 with yellow outline representing the ‘Fraser Fire’ and ‘Freshwater Road Fire’ on K’gari and the Cooloolo Sand Mass (CSM), respectively. The orange star marks the field site for this study, whereas the white stars indicate fire record locations compared in this research. Images of the **(c)** the Kings Bore Wildfire, **(d)** the Thannae Fire, and **(e)** the Freshwater Road Fire are provided as examples of wildfires that occurred within the SE Queensland dune fields during the ‘Black Summers’ (photo credit: Michael Ford Panel c and Erin Atkinson Panels d and e).....81

**Figure 5.2:** Site location. **(a)** Satellite imagery of the Cooloolo Sand Mass (CSM) with areas of interest, and the Rainbow Beach patterned fen complex (white star). **(b)** Close-up of the four dunes used in this study (dashed lines) and locations of the depositional foot-slope sites (stars) found on each dune’s North-facing slipface. The dunes selected in the research represent each of the four major Holocene dune activation/stabilisation phases (*Chapter 2*; *Chapter 4*; Ellerton et al., 2020) (see Supplementary Figure A.5.2) **(c)** Conceptual diagram of sediment transport (sand and charcoal) and deposition on a dune’s slipface. Charcoal particles are produced on the dune’s surface during fires (small black dots), transported down gradient, and deposited in the foot-slope position as disseminated charcoal or charcoal layers. I hypothesise that charcoal analysed in this study remains in stratigraphic order and is produced locally because sediment is retained within the CSM’s basins (*Chapter 3*) and charcoal particles are large (between  $180 \mu\text{m}$  and  $2 \text{ mm}$ ). The red box indicates the location that soil pits were excavated to obtain a fire record for this study. A sand auger was used at the

base of each pit to determine the depth of the underlining dune surface (i.e., maximum deposit thickness) which is inferred to represent the initiation of sediment deposition (i.e., dune age). **(d)** Soil profile looking up to crest on the 10 ka dune.....86

**Figure 5.3:** Charcoal concentrations for the **(a)** 0.5 ka, **(b)** 2 ka, **(c)** 5 ka, and **(d)** 10 ka dune depositional sites. For each depth interval (width of bar) charcoal was counted for all size classes 180-250  $\mu\text{m}$  (dark grey), 250-355  $\mu\text{m}$  (grey), and 355  $\mu\text{m}$ -2 mm (light grey). Charcoal layers identified in the profile face are indicated with a band of black dots and labelled (CL#). Samples collected for radiocarbon analysis are indicated with an orange star or an orange circle whether they were collected at a discrete depth or from a sample depth interval, respectively. Charcoal layers only occur on the two youngest dunes and were incorporated in multiple sample intervals due to predetermined sampled depths. Note, the Freshwater Road Fire severely burnt and deposited fresh charcoal at the surface of all sites (dashed lines labelled 'Freshwater Road Fire') after pit excavation and sample collection, but only produced a 0.1 m charcoal rich dry-ravel deposit at the 0.5 ka site. As a result, no charcoal concentrations were recorded for this interval. For more information on each soil profile see Supplementary Figures A.5.4 – A.5.8.....94

**Figure 5.4:** Bayesian age-depth models generated for the **(a)** 0.5 ka, **(b)** 2 ka, **(c)** 5 ka, and **(d)** 10 ka dune depositional sites. For each site, I set the age of the surface (0 m) to the date of pit excavation (vertical orange marker), and the basal age to the OSL-dated dune age collected from dune crest. All cal. ages are obtained through radiocarbon ( $^{14}\text{C}$ ) dating of charcoal fragments using the Southern Hemisphere calibration curve (SHCal20; Hogg et al., 2020) extended to the recent time using the Post-bomb Atmospheric calibration curve for Southern Hemisphere zone 1-2 (Bomb22SH1-2; Hua et al., 2022). Graphs were produced using 'rbacon' (Blaauw and Christen, 2011) in R (R Core Team 2022). The calibrated year probability distributions estimates are shown as blue and aqua markers for  $^{14}\text{C}$  and OSL ages, respectively. The red dashed line bounded by the grey dotted lines represents the age-depth model best fit and the 95% confidence intervals, respectively. Note, the y-axis only extends to 2.75 m, which covers all sample intervals, and does not include the complete age-depth model that extends to the base of each deposit (original dune deposits or onlapped topography). Additionally, samples collected from discrete depths are labelled with an orange star. ....95

**Figure 5.5:** Charcoal accumulation rates (CHAR) and the inferred timing of increased fire activity (peaks - vertical orange areas) for the **(a)** 0.5 ka, **(b)** 2 ka, **(c)** 5 ka, and **(d)** 10 ka dune depositional sites. Locations for all samples are marked with dots, such that white dots indicate episodic sediment transport (sheetwash or dry ravel) associated with the first 1.5 ka of sediment deposition, while black dots indicate slow and continuous sediment transport (soil creep). Charcoal layers (CL) found in profile faces (Figure 5.3) are indicated by a band of black dots and labelled (CL#). For more information on CHAR for each size class and the locations for all CL, see Supplementary Figure A.5.4. **(e)** A composite master charcoal record was derived from all four sites by dividing each record by its maximum CHAR value and then plotting the normalised CHAR with time. The white line represents a record composed of all CHAR values

(n=77) whereas the black area represents samples that only experienced continuous sediment transport (n=48).....99

**Figure 5.6: (a)** A log-log plot of the median sedimentation rate for all sampled intervals (dots) from each foot-slope deposit as a function of time since dune stabilisation. Sedimentation rates are initially high (dashed line) then abruptly decrease after ca 1.5 ka (solid line). **(b)** Box and whisker plots for sedimentation rates before and after this transition. Boxes are the interquartile range with the whiskers representing maximum and minimum values. The black dot is the mean and the horizontal black line represents the median. I hypothesise that the shift in sedimentation rates reflect the transition from episodic (dry-ravel and sheetwash) to continuous sediment transport styles (soil creep) and are associated with the presence or absence of charcoal in layers, respectively. Note that the separation between these two sedimentation rates occur ca 1.5 ka after dune emplacement which is comparable to the findings in *Chapter 3* where I estimated ca 1 ka for this transition to occur..... 103

**Figure 5.7:** Conceptual diagram of progressive vegetation succession, fire activity, charcoal production and stratigraphic deposit for an **(a)** active dune with steep gradients, **(b)** recently emplaced (stabilised) dune with steep gradients, and **(c)** emplaced dune with shallow gradients. When dunes are active, vegetation is sparse and fires are assumed to be infrequent and unproductive – panel a. As woody vegetation such as *Eucalyptus spp.* or *Corymbia spp.* becomes established, charcoal production increases (black dots). Charcoal can either be deposited in the foot-slope positions as layers (black lines – panel b) or disseminated throughout the profile (grey area – panels b and c). The presence or absence of charcoal layers is the result of episodic sediment transport processes (e.g., dry-ravel and sheetwash) and elevated charcoal production on dune gradients that are above the sand's angle of repose – panel b. The absence of layers but the presence of disseminated charcoal implies slow and continuous sediment transport (i.e., granular relaxation and biogenic soil creep) – panel c.....106

**Figure 5.8: (a)** Master charcoal record derived from only slow and continuous sediment transport for all sites in this study with increases in biomass burning (vertical orange bars) over three proposed periods of fire activity (black and white bar). My data is compared to other **(b)** local (Hanson et al., 2023), **(c-d)** regional sites (Donders et al., 2006; Mariani et al., 2019) as well as **(e)** a compilation of records from the subtropical high-pressure belt in eastern Australia (125 sites) (Mooney et al., 2011). Locations of local and regional records are indicated in Figure 5.1 as white stars. The fire records from the CSM sites are compatible with those from traditional fire records within SE Queensland (i.e., peats, bogs and lakes). Note (\*) indicates the lack of data.....108

**Figure 5.9: (a)** Master charcoal record derived from only slow and continuous sediment transport for all sites in this study (black area). I compare my results to the **(b)** Swallow Lagoon precipitation record (Barr et al., 2019), the **(c)** El Junco Lake in the Galápagos Islands and the **(d)** Lake Laguna Pallcacocha in southern Ecuador records of past El Niño event frequency (Moy et al., 2002; Conroy et al., 2008). Lastly, I compare the **(e)** probability density function for the timing of dune emplacement at the CSM (*Chapter 4*).....110



**Figure 5.10: (a)** World dryland distribution (orange areas) (Sorensen, 2007) and published paleofire records (white dots) from the Global Paleofire Database (Harrison et al., 2022). **(b)** Close-up view of Australia and the general locations of coastal (yellow) and continental (orange) dunes (Lees et al., 2006; Hesse, 2016). Note the abundant land area in Australia and the world that is both covered in drylands and lack fire histories. Dune depositional deposits present an opportunity to expand fire records from wetland areas into dryland regions which to this point have been underrepresented in paleofire studies.....113

**Supplementary Figure A.2.1:** High-resolution remapping of the SE Queensland dune fields.....160

**Supplementary Figure A.3.1:** Photos of the Carlo Sand Blow near the township of Rainbow Beach, photos location indicated in Figure 3.1c. **(a)** Photo taken near the western dune crest towards the Tasman Sea down the dune's stoss face. **(b)** Photo taken in the same location as panel a but down the dune crest towards the over-steepened lee face and forest canopy. Note the dune is extending inland through the tops of the open and closed Eucalyptus forest (canopy cover of 50-80% and >80%, respectively), which are approximately 20-30 m tall, and over previously emplaced dunes (photo credit: Patrick Adams).....161

**Supplementary Figure A.3.2:** A visualisation of the grid network depicting the 3 by 3 elevation submatrix utilised in this study to calculate curvature at the centre node ( $z_5$ ) (Zevenberger and Thorne, 1987; Moore et al., 1991). Here  $z$  is elevation and  $L$  is the length between nodes used in EQ.3.5 and EQ.3.6.....162

**Supplementary Figure A.3.3:** 2-D forward numerical modelling of dated CSM dunes. **(a)** Measured dune age and surface roughness ( $\sigma_c$ ) (large symbols) highlighting change in its topography every 1 ka for 10 ka for individual dunes (smaller symbols). The entire CSM evolution is described by nonlinear sediment transport with a  $K$  value of  $0.002 \text{ m}^2 \text{ yr}^{-1}$  and a  $S_c$  of  $0.65 \text{ m m}^{-1}$ , utilising a landscape evolution model from Booth et al. (2017). In reality the simulated topography appears to be more closely related to a  $K$  value of  $0.06 \text{ m}^2 \text{ yr}^{-1}$  for the first thousand years of the dune's development when  $\sigma_c$  is high (above the 'transitional zone',  $\sigma_c$  values between  $0.035$ - $0.045 \text{ m}^{-1}$ ). Only once dune  $\sigma_c$  is lowered below this point does their evolution switch to the  $K$  value  $0.002 \text{ m}^2 \text{ yr}^{-1}$  (not shown here). **(b)** Using the general evolution derived from the fix  $K$  value of  $0.002 \text{ m}^2 \text{ yr}^{-1}$  and a  $S_c$  of  $0.65 \text{ m m}^{-1}$ , I evaluate dune's  $\sigma_c$  relationship with modelled variability of erosion rate ( $\sigma_e$ ). I observe a shift in this relationship coinciding with the same observed transition zone in Figure 3.6, which I interpret as a phase when nonlinear sediment transport behaves similar to linear sediment transport, such that  $\sigma_c$  and  $\sigma_e$  become more uniform with time and their relationship can be described through EQ.3.3,  $\sigma_e \propto \sigma_c$ . Note  $\sigma_e$  and  $\sigma_c$  are autocorrelated; however, field observations support these modelled outcomes.....163

**Supplementary Figure A.3.4:** Slope map of modelled simulation for CSM dunes through nonlinear sediment transport. Utilising a 5 m DEM and the nonlinear sediment transport model from Booth et al. (2017) (fixed  $K$  and  $S_c$  values of  $0.002 \text{ m}^2 \text{ yr}^{-1}$  and  $0.65 \text{ m m}^{-1}$ , respectively) I provide dune topography, relative age, and geomorphic stage (Supplementary Tables A.3.1 and A.3.2) highlighting the evolution of a 0.44 ka dune (Dune 4). **(a)** Current dune topography in its juvenile phase with abundant steep slopes (dark browns). **(b)** Dune after being rapidly decayed for 1 ka until the ‘transitional zone’ has been reached ( $\sigma_c$  from  $0.035$ - $0.045 \text{ m}^{-1}$ ) depicting dune adolescence with shallower slopes (lighter browns). Once lowered below the ‘transitional zone’, dune evolution mimics linear slope dependent evolution where slow and continuous sediment transport processes dominate such that dune **(c)** maturity by 6 ka, and **(d)** old age is achieved by 12 ka. This is visually depicted with uniform and consistent slopes (yellows).....164

**Supplementary Figure A.4.1:** Equivalent Dose ( $D_E$ ) radial plots for the eight ( $n=8$ ) OSL samples used in this study.....171

**Supplementary Figure A.4.2:** **(a)** Dune frequency for active ( $n=103$ ) and emplaced Holocene aged ( $n=726$ ) dunes with 0.5 ka bin intervals. **(b)** Box and whisker plots depicting maximum distance travel from the modern eastern coast (not including dunes that originate on the western coast ( $n=15$ )). Horizontal bar is the median value whereas the black dot represents the average. In general, younger dunes are more common but on average do not travel far inland. In contrast, the oldest dunes which are less frequent are reported to travel up  $>10 \text{ km}$ . Note, bin interval varies to help account for sample size.....172

**Supplementary Figure A.4.3:** Comparison between probability density functions (PDFs) produced from OSL (dashed line with white area) and predicted (solid black line with grey fill) dated dunes within **(a)** both dune fields, **(b)** K’gari, and **(c)** the CSM.....173

**Supplementary Figure A.4.4:** Sensitivity analysis on PDF outcomes by varying original DEM resolution and bin interval. **(a)** PDFs generated from all modelled dune ages ( $n=726$ ) (assuming normally distributed age estimates) using 0.05 ka bin intervals for 12 ka (240 total bins). Each line represents a PDF from a surface roughness ( $\sigma_c$ )-age regression, derived at different DEM resolutions (1-50 m) (Supplementary Table A.4.3). Solid black lines are all PDFs that have  $\sigma_c$ -age relationships with a RMSE value  $<1.1 \text{ ka}$  and a  $r^2$  value  $>0.90$  ( $3\text{-}20 \text{ m}^2$  resolution). The full range of these PDFs are shaded in grey. The bold black line represents the PDF used in this study (5 m). All other PDFs are represented by grey dashed lines. An important note, besides the PDFs derived from the finest (1 and 2 m) and the coarsest resolutions (45 and 50 m), all PDFs show remarkable consistency in peaks when compared to the known dune emplacement events (vertical teal areas). **(b)** I evaluate the influence bin intervals have on modelled PDF outcomes on identical predicted ages (derive from 5 m DEM). As bin intervals increase (dark to light lines) the youngest peak ( $<0.5 \text{ ka}$ ) becomes increasingly subtle and by a bin interval of 1 ka, is completely removed.....174

**Supplementary Figure A.4.5:** Conceptual diagram summarising changes in dune age, geomorphic processes, and surface roughness ( $\sigma_c$ ), modified from *Chapter 3*. **(a)** The Coolooloa Sand Mass (CSM) contains thousands of dunes that have remarkably uniform evolution. When dunes are active, they have steep lee faces above or near the angle of repose ( $0.65 \text{ m m}^{-1}$  or  $33^\circ$ ) and shallow stoss faces that are controlled by wind advection processes, which prohibit the colonisation of vegetation when winds are high. Consequently, dunes are initially constructed with smooth topography (low  $\sigma_c$ ). As winds dissipate (either from the increase distance from the coast or a change in wind regime), dunes begin to become stabilised by vegetation. The competition between wind advection and vegetation stabilisation increases  $\sigma_c$ . The roughening of the topography continues until dunes are completely stabilised (dune emplacement) and  $\sigma_c$  is at a maximum. Emplacement marks the onset of dune relaxation where sediment transport is only active through hillslope processes (no wind advection) which causes  $\sigma_c$  to decline exponentially with time. Here, processes such as biogenic soil creep, rain-splash, and granular relaxation cause the lowering of crest and filling of adjacent foot-slopes decreasing local relief and  $\sigma_c$ . Examples of this process are observed on active and emplaced dunes and highlighted in **(b)** satellite imagery and **(c)** gradient maps. Note the exact relationship between  $\sigma_c$  and time for dunes stabilisation is not examined in this study but will be addressed in future research.....175

**Supplementary Figure A.5.1:** Evidence of increased sediment accumulation at the base of dune slipface after fire. **(a)** Episodic sediment transport initiated by the Freshwater Road Fire on the 0.5 ka dune looking up to dune crest. **(b)** Close-up image of the 0.1 m deposit with camera lens for reference. **(c)** Charcoal particle obtained at the deposit. ....183

**Supplementary Figure A.5.2:** Site location. **(a)** Satellite imagery of the Coolooloa Sand Mass (CSM) with areas of interest. **(b)** Close-up of the Holocene dune mapped dune units from *Chapter 2* and the four dunes used in this study (white stars). Note, a slope DEM was placed above the dune units at 70% transparency to help highlight dune the topography. ....184

**Supplementary Figure A.5.3:** Images of the locations used as a cross-site comparisons in this study, see Figure 5.1b for exact locations. **(a)** The CSM dry sclerophyll forest near my dune foot-slope deposits, **(b)** Rainbow Beach patterned fen complexes on Coolooloa, **(c)** Swallow Lagoon on Minjerribah (North Stradbroke Island) and **(d)** Lake Allom on K'gari (Fraser Island). Photo credits: **(b)** Kevin Welsh, **(c)** John Tibby, and **(d)** Queensland National Parks Service.....185

**Supplementary Figure A.5.4:** Charcoal accumulation rates (CHAR) for size classes  $355 \text{ }\mu\text{m}$ -2 mm (solid line),  $250\text{-}355 \text{ }\mu\text{m}$  (dashed line), and  $180\text{-}250 \text{ }\mu\text{m}$  (dotted line) for the **(a)** 0.5 ka, **(b)** 2 ka, **(c)** 5 ka, and **(d)** 10 ka dune depositional sites. The x-axis for the panels differs so that variability in CHAR trends with age can be observed. Charcoal layers identified in the profile face are indicated with a band of black dots and labelled (CL) and shaded areas are the inferred timing of increased fire activity identified in Figure 5.5. An important note is that trends are consistent between size classes and sites..186

<b>Supplementary Figure A.5.5:</b> Summary figure of data collected in the 0.5 ka Dune.....	187
<b>Supplementary Figure A.5.6:</b> Summary figure of data collected in the 2 ka Dune.....	188
<b>Supplementary Figure A.5.7:</b> Summary figure of data collected in the 5 ka Dune.....	189
<b>Supplementary Figure A.5.8:</b> Summary figure of data collected in the 10 ka Dune.....	190
<b>Supplementary Figure A.5.9:</b> Macro-Charcoal records (black areas) and micro-charcoal records (grey areas) from <b>(a)</b> the dune foot-slope deposits on the CSM, <b>(b)</b> Lake Allom on K'gari (Donders et al., 2006), and <b>(c)</b> Swallow Lagoon on Minjerribah (Mariani et al., 2019) versus major phases of dune emplacement (orange areas) ( <i>Chapter 2; Chapter 4</i> ). The same four Holocene dune emplacement phases have been mapped along the coastline of the SE Queensland dune fields ( <i>Chapter 2</i> ) and their ages have been determined through OSL dating and empirical relationships ( <i>Chapter 4</i> ; Ellerton et al., 2020). I observe that the timing of dune emplacement is inversely related to CHAR peaks, which may reflect the inability of fire to penetrate through active dune fields.....	191

# List of Tables

<b>Table 2.1:</b> Summary of CSM morphosequence units including mean age, surface characteristics, percent land cover, mean distance from the coast, mean elevation, mean slope, standard deviation of slope and standard deviation of curvature. All data was extracted using ArcGIS 10.6 (ESRI, Redlands, CA) zonal statistics tools. For more information on mean age and soil characteristic refer to Ellerton et al. (2018), Thompson (1981) and Walker et al. (2018).....	24
<b>Table 4.1:</b> Optically Stimulated Luminescence (OSL) age results and map location.....	63
<b>Table 4.2:</b> All dunes with their locations (Figure 4.3) and ages utilised in this study. Note, all italicised rows indicate the OSL ages that are not used in the surface roughness ( $\sigma_c$ )-age model and validation sets and are indicated with an 'X' in Figure 4.3.....	64
<b>Table 5.1:</b> All ages used to produce age-depth models in this study from woody macro-charcoal ( $^{14}\text{C}$ ) and primary dune sands (OSL) are reported in years relative to 1950 (Figure 5.4). Lab numbers beginning with 'Wk', 'OZ', and 'USU' were analysed at the Waikato Radiocarbon Dating Laboratory, ANSTO, and Utah State University Luminescence Laboratory, respectively. Age calibration was performed using the Southern Hemisphere calibration curve (SHCal20; Hogg et al., 2020) extended to the recent time using the Post-bomb Atmospheric calibration curve for Southern Hemisphere zone 1-2 (Bomb22SH1-2; Hua et al., 2022), and modelled ages were produced using 'rbacon' (Blaauw and Christen, 2011) in R (R Core Team 2022).....	96
<b>Supplementary Table A.3.1:</b> Additional dune data. Age data and supporting information used in Figure 3.1 and 3.6, and Supplementary Figures A.3.3, and A.3.4. (*) Indicates the area of the dune at the surface. (†) Indicates the distance dune travelled, parallel to trailing arm, from the current coastline position to its furthest inland extent.....	165
<b>Supplementary Table A.3.2:</b> Defining landscapes evolutionary stages. The development of the Cooloola Sand Mass dunes are set by their physical characteristics, soil development, and their primary and secondary transport processes (Reeve et al., 2008; <i>Chapter 2</i> ).....	166
<b>Supplementary Table A.3.3:</b> Soil characteristics from the excavated soil profile utilised in this study using standard survey methods from Schoenberger et al. (2002) .....	167
<b>Supplementary Table A.3.4</b> Accelerated mass spectrometry (AMS) radiocarbon dating results. One sample collected from the 2.14 ka depositional soil profile was obtained from a charcoal-rich layer. The sample was prepared using the acid–base–acid (ABA) protocol and dated at the University of Waikato Radiocarbon Dating Laboratory. Ages were calibrated at two sigma error using OxCal v4.3.2. (Ramsey, 2017) and the SHcal13 calibration curve (Hogg et al., 2013).....	170

<b>Supplementary Table A.4.1:</b> Soil descriptions of all sites containing newly acquired OSL samples used in this chapter.....	176
<b>Supplementary Table A.4.2:</b> Radioelement chemistry, water content, and grain size information.....	181
<b>Supplementary Table A.4.3:</b> Relationship between surface roughness ( $\sigma_c$ ) and all dated dunes (n=22) at varying resolutions to assess optimal and available DEM resolution to utilised the $\sigma_c$ -age model. (†) on dune resolution size indicates best-fit based on RMSE and $r^2$ values.....	182
<b>Supplementary Table A.5.1:</b> All modelled ages used in this study generated from age–depth models, see Table 5.1 and Figure 5.4. In this study, I utilise the median age for the mid-point of each sampling interval when placing charcoal concentrations and CHAR with time.....	192



# List of Symbols and Abbreviations

$^{14}\text{C}$	Radiocarbon	
2-D	Two-dimensional	
ABA	Acid-base-acid	
AMS	Accelerator mass spectrometry	
ARC	Australian Research Council	
$\text{BD}_{\text{CF}}$	Coarse fraction bulk density	$(\text{g cm}^{-3})$
$\text{BD}_{\text{FF}}$	Fine fraction bulk density	$(\text{g cm}^{-3})$
$\text{BD}_{\text{T}}$	Total bulk density	$(\text{g cm}^{-3})$
Bomb21SH12	Post-bomb Atmospheric calibration curve zone 1-2	
C	Curvature	$(\text{m}^{-1})$
CAM	Central Age Model	
CF	Coarse fraction	
Cfa	Köppen climate classification - humid sub-tropics	
CHAR	Charcoal accumulation rates	$(\text{cm}^{-2} \text{yr}^{-1})$
CL	Charcoal Layer	
CSM	Cooloola Sand Mass	
$D_{\text{E}}$	Equivalent dose	
DEM	Digital Elevation Model	
E	Erosion rate	$(\text{m yr}^{-1})$
ENSO	El Niño–Southern Oscillation	
FF	Fine fraction	
HCl	Hydrochloric acid	
GIS	Geographic information system	
ICP-AES	Inductively coupled plasma atomic emission spectroscopy	
ICP-MS	Inductively coupled plasma mass spectroscopy	
IPO	Interdecadal Pacific Oscillation	
K	Soil transport coefficient	$(\text{m}^2 \text{yr}^{-1})$
L	Length	
LED	Light emitting diodes	
LGM	Last glacial maximum	

LiDAR	Light Detection and Ranging	
MAP	Mean annual precipitation	
$M_{CF}$	Coarse fraction mass	(g)
$M_{FF}$	Fine fraction mass	(g)
$M_i$	Initial mass	(g)
$M_T$	Total mass	(g)
OSL	Optically stimulated luminescence	
PDF	Probability density function	
pMC	Percent modern carbon	
QGlobe	Queensland Globe	
QImagery	Queensland Imagery	
$q_s$	Sediment flux	( $m^2 \text{ yr}^{-1}$ )
RSE	Relative standard error	
SAR	Single-aliquot regenerative dose	
$S_c$	Critical gradient (hillslope threshold)	( $m \text{ m}^{-1}$ )
SE	Southeast	
SHCal20	Southern Hemisphere calibration curve	
SST	sea-surface temperatures	
STH	Sub-tropical high-pressure belt	
t	Time	(yr)
UAV	Unmanned aerial vehicles	
UNESCO	United Nations Educational, Scientific and Cultural Organization	
V	Volume	( $cm^{-3}$ )
$V_{CF}$	Coarse fraction volume	( $cm^{-3}$ )
$V_{FF}$	Fine fraction volume	( $cm^{-3}$ )
$V_T$	Total volume	( $cm^{-3}$ )
z	Elevation	(m)
$\sigma_C$	Surface roughness	( $m^{-1}$ )
$\sigma_E$	Variability of erosion rates	( $m \text{ yr}^{-1}$ )
$\nabla z$	Gradient	( $m \text{ m}^{-1}$ )
$\nabla^2 z$	Curvature	( $m^{-1}$ )
#	Number	

# List of Equations

<b>EQ.3.1</b>	$\mathbf{q_s} = -K\nabla\mathbf{z}$
<b>EQ.3.2</b>	$E = \nabla \cdot \mathbf{q_s} = -K\nabla^2\mathbf{z} = -KC$
<b>EQ.3.3</b>	$\sigma_E = -K \sigma(\nabla^2\mathbf{z}) = -K\sigma_C$
<b>EQ.3.4</b>	$\mathbf{q_s} = -K\nabla\mathbf{z} \left[1 - \left(\frac{ \nabla\mathbf{z} }{s_c}\right)^2\right]^{-1}$
<b>EQ.3.5</b>	$z = Ax^2y^2 + Bx^2y + Cxy^2 + Dx^2 + Ey^2 + Fxy + Gx + Hy + I$
<b>EQ.3.5a</b>	$A = [(z_1 + z_3 + z_7 + z_9) \div 4 - (z_2 + z_4 + z_6 + z_8) \div 2 + z_5] \div L^4$
<b>EQ.3.5b</b>	$B = [(z_1 + z_3 - z_7 - z_9) \div 4 - (z_2 - z_8) \div 2] \div L^3$
<b>EQ.3.5c</b>	$C = [(-z_1 + z_3 - z_7 + z_9) \div 4 + (z_4 - z_6) \div 2] \div L^3$
<b>EQ.3.5d</b>	$D = [(z_4 + z_6) \div 2 - z_5] \div L^2$
<b>EQ.3.5e</b>	$E = [(z_2 + z_8) \div 2 - z_5] \div L^2$
<b>EQ.3.5f</b>	$F = (-z_1 + z_3 + z_7 - z_9) \div 4L^2$
<b>EQ.3.5g</b>	$G = (-z_4 + z_6) \div 2L$
<b>EQ.3.5h</b>	$H = (z_2 - z_8) \div 2L$
<b>EQ.3.5i</b>	$I = z_5$
<b>EQ.3.6</b>	$\nabla^2\mathbf{z} = C = 2(D + E)$
<b>EQ.5.1a</b>	$M_{CF}/0.5 = V_{CF}$
<b>EQ.5.1b</b>	$V_T - V_{CF} = V_{FF}$
<b>EQ.5.1c</b>	$M_{FF}/V_{FF} = BD_{FF}$
<b>EQ.5.2</b>	$\text{Charcoal concentration} = \left(\frac{\#}{[M_i/BD_{FF}]}\right) = \left(\frac{\#}{[V]}\right)$

# Chapter 1.

## Introduction

**Preface:** This thesis includes a collection of four manuscripts (*Chapters 2-5*), three published and one ready for submission for publication. For consistency and completeness, all chapters start with a full citation including DOI and co-authors, and a brief introduction on how each chapter ties into each other. Each chapter is a unique body of work that focuses on different aspects of the southeast (SE) Queensland dune fields' evolution and contains a thorough review of the appropriate literature. Consequently, to avoid redundancy, this introduction chapter is kept brief and used only as a means to outline and summarise the main objectives of this thesis.

## 1.1 Context

This thesis presents a novel approach to understanding dune fields and dune landscapes. It examines dunes from the perspective of landscape evolution and focuses primarily on what happens after dunes stabilise. I focus my research on the Cooloola Sand Mass (CSM) and K'gari (Fraser Island) within the southeast (SE) Queensland dune fields along the eastern coast of Australia near the city of Brisbane. This coastal dune system is composed of dune fields and sand islands that occur from  $\sim 27.4^{\circ}\text{S}$  to  $\sim 25.5^{\circ}\text{S}$ . From its southern limit moving northwards lie Minjerribah (North Stradbroke Island), Mulgumpin (Moreton Island), Bribie Island, the CSM, and K'gari. The total area of the entire region covers roughly 2350 km<sup>2</sup> with dune crest reaching 285 meters above sea-level. The area is renowned for its outstanding beauty and for containing the three largest sand islands. In particular, K'gari holds half of the perched freshwater lakes, the largest unconfined aquifer on a sand island, thickest soils, and with the CSM the only extensive rainforest on dunes in the world (UNESCO, 2021).

At present, the dune fields are composed of predominantly stabilised (relic) parabolic and transgressive dune sheets in the interior and active blowouts/sheets along the coastline (e.g., Carlo Sandblow, Cooloola Sand Patch, and Sandy Cape) (Thompson, 1981). The successive dune onlapping has occurred through the mid- and late-Pleistocene with major dune building phases inferred to be associated with sea-level variability (Ellerton et al., 2020; *In Press*) resulting in compound and complex dune structures of varying ages (McKee, 1979). The dunes contain a vegetation succession from bare sand colonisers to a so-called 'Climax' vegetation of rainforest and/or tall wet sclerophyll forest and they act as a refugium for many relict and disjunct flora and fauna such as giant earthworms (*Digaster keastii*), Wallum rocketfrogs (*Litoria freycineti*), Fraser Island satinay (*Syncarpia hillii*). They also contain Ramsar-listed sub-tropical patterned fens (Walker et al., 1981; Moss et al., 2016; UNESCO, 2021).

Despite the global recognition of the SE Queensland dune fields very little was known regarding the processes that lead to their creation and evolution (Lees, 2006), except in terms of soil and vegetation development (i.e., Thompson, 1981; 1992; Walker et al., 1987; Wardell-Johnson, 2015). To address these questions, the Australian Research Council (ARC) Discovery Grant funded the project '*Climate and environmental history of SE Queensland dune fields*' in 2015 (DP150101513). The general goals were to provide novel paleoclimate and sea-level information from the sub-tropics and add universal significance to the World Heritage Listing.

I joined this project late in the research, when most of the dating and sea-level work was well under way. The strong chronology developed during the ARC project (e.g., Ellerton et al., 2020; *In Press*; Shulmeister et al. unpublished data) provided a chronological framework for my research. I have a strong background in landscape evolution and hillslope processes; therefore, I focused my research on dune evolution once aeolian processes had stopped and hillslope (diffusive) processes taken over.

In this thesis, I attempt to utilise foundational concepts in hillslope geomorphology that predicts how stabilised dunes will evolve from a newly constructed landform with high relief to a denuded landscape. The underpinning idea is that diffusional sediment transport is governed by gravitational forces acting on the landform thereby controlling erosion and deposition (e.g., Davis, 1892; Gilbert, 1909). The onlapping nature of the dune field provides an elegant space-for-time substitution study and its evolutionary outcomes are deterministic. Their composition of unconsolidated, uniform spherical particles are equivalent to those used in mathematical and laboratory-based models (a classic sandbox experiment) (e.g., Roering et al., 2001). Consequently, I can view the dunes as a ‘giant sandbox’ that are evolving under a limited set of known processes with defined boundary conditions. Any shifts in these processes or conditions (i.e., climate or base-level) will cause modifications to the topography and be recorded in depositional positions of the landscape (basins or foot-slopes). As a result, these locations may contain a previously unrecognised paleoenvironmental archive, which can be systematically targeted in aeolian research.

To my knowledge, no study has evaluated landscape evolution in a system that is truly transport limited (sediment availability is greater than sediment transport). Results here may show that dune fields are an ideal location to qualitatively and quantitatively test the assumptions of the landscape evolution literature that has persisted for over a century (Davis, 1892; Gilbert, 1909). If successful, application of these approaches will prove fruitful as dune fields are found globally (e.g., Martinez et al., 2004; Yan and Baas, 2015; Lancaster, 2016) and may provide the necessary information to connect local (grain) to regional (dune field) scale mechanisms to explain processes that lead to currently observed dune forms.

## 1.2 Thesis aims and objectives

The overarching theme of this research is to understand the landscape evolution of the SE Queensland dune fields in Australia. My goals are to enhance our fundamental

understanding of coastal dune fields by determining the complete evolution of dunes from their inception (activation) to maturity (denuded topography). Specifically, I focus my work on the Holocene age dunes from the CSM and K'gari. I aim to assess and test principals and concepts derived from hillslope geomorphology and apply them to a system that has primarily been evaluated with an aeolian geomorphology perspective. If successful, I will demonstrate that dunes' form and their depositional positions are previously unrecognised paleoenvironmental archives in aeolian research. Below is a list of objectives that will permit me to reach these aims:

- **Objective 1:** Produce an updated morphological map of the SE Queensland dune fields utilising modern remote sensing techniques to classify the dunes based on hillslope process parameters.
- **Objective 2:** Establish whether the SE Queensland dune fields are a suitable natural laboratory to evaluate landscape evolution.
- **Objective 3:** Assess and apply sediment transport theory to a dune system to understand its evolution once stabilised.
- **Objective 4:** Determine the dominant geomorphic processes controlling sediment erosion, transport, and deposition and their relative rates.
- **Objective 5:** Investigate whether landscape evolution metrics can be calibrated to determine dune chronology.
- **Objective 6:** Re-examine the environmental controls on dune activation and emplacement (i.e., climate change, sea-level, etc.).
- **Objective 7:** Identify and examine depositional records that might prove valuable in understanding dune field evolution.

### 1.3 Thesis structure

This thesis is composed of four research chapters (*Chapters 2-5*) that were written as standalone manuscripts. Therefore, I have provided a brief introduction to each chapter, their connection to each other, and how the objectives (*Section 1.2*) of this thesis are addressed:

*Chapter 2* presents the outcome of a mapping project with the aim to review and update the geomorphological dune units of the SE Queensland dune fields. The dune fields were first mapped by Ward (2006). I use topographic expression coupled with geomorphic, pedologic and biologic relationships to place dunes into morphostratigraphical units. The new maps allowed me to identify areas of interest and develop working hypotheses to address my aims and objectives. Some of the questions included: Are all the dune fields part of the same system and did they experience the same external perturbations? Are the same dune units preserved throughout the dune fields? What are the defining characteristics of the dune units? Finally, do units change systematically with inferred time? *Chapter 2* acts as the underpinning work for *Chapters 3-5* and directly addresses *Objective 1*.

*Chapter 3* explores and develops the application of sediment transport equations on stabilised dune hillslopes. I ask the following questions: Do the SE Queensland dune fields, specifically the CSM, have consistent boundary conditions and external forces that control dune evolution? Is there a topographic metric or measurement that can define and/or measure landscape change? What are the dominant styles and rates of sediment transport and deposition after dune emplacement? Lastly, can phases of dune evolution be defined based on sediment transport regimes and rates? This chapter provides the conceptual framework for *Chapter 4*, proposes locations to direct research in *Chapter 5*, offers critical progress to complete *Objectives 5 and 7*, and directly addresses *Objectives 2, 3 and 4*.

*Chapter 4* tests the application of sediment transport theory derived from *Chapter 3* to determine dune emplacement ages at the CSM and K'gari. In essence, this chapter acts as a methodological case study of roughness-age modelling on dunes, which has been previously applied in hillslope studies. In this chapter, I ask the following



questions: Can surface roughness be used to determine relative dune ages? What are the spatial and temporal patterns of dune ages for the dune fields? How do these trends differ from those interpreted from ‘traditional’ studies? Lastly, I re-examine whether climate or sea-level is the primary cause of dune activation and emplacement. The results from this chapter directly address *Objectives 5 and 6*, and provides additional support for *Objectives 1, 2, 3, and 4*.

Chapter 5 evaluates the role of fire in the dune field and whether foot-slope deposits identified in *Chapter 3* contain intact and reliable paleoenvironmental records. In this chapter, I address the following questions: What are the primary controls on episodic sediment transport on dunes? Does fire persist in the dune fields through the Holocene? How are fire events represented in stratigraphic records (charcoal layers or increased charcoal concentrations)? Do all fires cause a geomorphic response in the dune field (i.e., increased sedimentation rates)? Are these charcoal records compatible with those found locally and across the region from swamps and/or lakes? Finally, I consider what drives fire activity within the SE Queensland dune fields (i.e., changes in climate, vegetation, or human activity)? The outcomes of this chapter elucidates the potential of dune deposits as a means to develop paleoenvironmental records for areas unsuitable for the preservation of swamps, peats or other organic deposits. The results from this work directly addresses *Objective 7*, validates *Objective 4*, and offers supplementary support for *Objectives 2, and 3*.

Chapter 6 revisits the research aims and objectives, and summarises the main findings of the thesis. In this chapter, I also highlight the implications of the work and suggest future research directions.

## 1.4 Scientific contributions

*Chapters 2-5* were written initially as manuscripts. At the time of submission (06/09/2022), *Chapter 2* has been published in Journal of Maps, *Chapter 3* has been published in Earth and Planetary Science Letters, and *Chapter 4* has been published in Earth Surface Processes and Landforms, whereas, *Chapter 5* was later published in Quaternary Research (11/05/2023). *Chapters 2-5*’s original publications can be found in supplementary information

*Appendices A.6.* The fieldwork and analysis carried out during the thesis contributed to four other peer-reviewed publications where I was not the lead author. The content of this body of work is not included in the thesis but was vital in my understanding of the evolution of the dune fields as a whole. Additionally, findings for all chapters were presented at conferences as posters and/or oral presentations. Below I provide a complete list of published journal articles and conference presentations:

#### 1.4.1 Peer-reviewed journal articles

**Patton, N. R.,** Shulmeister, Hua, Q., Almond, P., Rittenour, T., Hanson, J. M., Grealy, A., Gilroy, J., & Ellerton, D. (2023) Reconstructing Holocene fire records using dune foot-slope deposits at the Cooloola Sand Mass, Australia. *Quaternary Research*, 1–23. <https://doi.org/10.1017/qua.2023.14>

**Patton, N. R.,** Shulmeister, J., Rittenour, T., Ellerton, D., Almond, P., & Santini, T. (2022b). Using calibrated surface roughness dating to estimate coastal dune ages at K'gari (Fraser Island) and the Cooloola Sand Mass, Australia. *Earth Surface Processes and Landforms*, 47(10), 2455-2470. <https://doi.org/10.1002/esp.5387>

**Patton, N. R.,** Shulmeister, J., Ellerton, D., & Seropian, G. (2022a). Measuring landscape evolution from inception to maturity: insights from a coastal dune system. *Earth and Planetary Science Letters*, 584, 17448. <https://doi.org/10.1016/j.epsl.2022.117448>

**Patton, N. R.,** Ellerton, D., & Shulmeister, J. (2019a). High-resolution remapping of the coastal dune fields of southeast Queensland, Australia: a morphometric approach. *Journal of Maps*, 15(2), 578-589. <https://doi.org/10.1080/17445647.2019.1642246>

**Not included as part of this thesis:**

Ellerton, D., Rittenour, T., Shulmeister, J., Roberts, A. P., Miot da Silva, G., Gontz, A., Hesp, P., Moss, P., **Patton, N. R.**, Santini, T., Welsh, K., & Zhao, X. (2022). Fraser Island (K'gari) and initiation of the Great Barrier Reef linked by Middle Pleistocene sea-level change. *Nature Geoscience*, 15, 1752-0894.

<https://doi.org/10.1038/s41561-022-01062-6>

Köhler, M., Shulmeister, J., **Patton, N. R.**, Rittenour, T. M., McSweeney, S., Ellerton, Daniel T., Stout, Justin C., & Hüneke, H. (2021). Holocene evolution of a barrier-spit complex and the interaction of tidal and wave processes, Inskip Peninsula, SE Queensland, Australia. *The Holocene*, 31(9), 1476-1488.

<http://dx.doi.org/10.1177/09596836211019092>

Gontz, A., McCallum, A., Ellerton, D., **Patton, N. R.**, & Shulmeister, J. (2020). The Teewah Transect: GPR-Derived Insights into the Younger Dune Morphosequences on the Great Sandy Coast, Queensland, Australia. *Journal of Coastal Research*, 95(SI), 500-504. <https://doi.org/10.2112/SI95-097.1>

Ellerton, D., Rittenour, T., Shulmeister, J., Gontz, A., Welsh, K. J., & **Patton, N. R.** (2020). An 800 kyr record of dune emplacement in relationship to high sea level forcing, Cooloolo Sand Mass, Queensland, Australia. *Geomorphology*, 354, 106999. <https://doi.org/10.1016/j.geomorph.2019.106999>

#### 1.4.2 Conferences presentations

**Patton, N. R.** Reconstructing Holocene fire records using dune foot-slope deposits at the Cooloolo Sand Mass, Australia. (2023). International Union for Quaternary Research (INQUA) Congress in Rome (Oral Presentation).

**Patton, N. R.** Using surface roughness to determine Holocene coastal dune ages at K'gari and Cooloolo, Australia. (2023). International Union for Quaternary Research (INQUA) Congress in Rome (Poster).

**Patton, N. R.** Reconstructing fire histories using dune depositional wedges. (2023). Friends of the Pleistocene (Oral Presentation).

**Patton, N. R.,** Shulmeister, J., Hua, Q., Almond, P., Rittenour, T. M., Hanson, J. M., Ellerton, D. T., and Seropian, G. The geomorphic influence of wildfire on stabilized dune fields, an example from the Cooloola Sand Mass, Australia. (2022). Geological Society of America (GSA) Denver, Colorado, USA (Oral Presentation).

**Patton, N. R.,** Shulmeister, J., Rittenour, T. M., Almond, P., Ellerton, D., & Santini, T. Using surface-roughness dating to estimate coastal dune ages at Fraser Island and the Cooloola Sand Mass, Australia. (2022). New World Luminescence Dating Workshop. Grand Junction, Colorado, USA. (Oral Presentation).

**Patton, N. R.** Utilising meteoric  $^{10}\text{Be}$  to define the mobile-stable regolith boundary within unconsolidated sediment. (2021). 15<sup>th</sup> International Conference on Accelerator Mass Spectrometry (AMS-15). (Oral Presentation).

**Patton, N. R.** Using surface roughness to determine ages of coastal dunes at K'gari (Fraser Island) and the Cooloola Sand Mass, Australia. (2021). Australasian Quaternary Association (AQUA) Pop-Up E Conference. (Oral Presentation). [Awarded 'Best Conference Presentation']

**Patton, N. R.** Measuring landscape evolution from inception to senescence; an example from the Cooloola Sand Mass, Australia. (2020). Geoscience Society of New Zealand (GSNZ) Annual Conference. Christchurch, NZ (Oral Presentation).

**Patton, N. R.** Systematic relaxation of geomorphic features: Application on the southeast Queensland dune fields, Australia. (2019). American Geophysical Union. San Francisco, CA, USA (Poster Presentation).

**Patton, N. R.** Landscape evolution of the southeast Queensland dune field, Australia. (2019). Australia's Nuclear Science and Technology Organization (ANSTO). Sydney, New South Wales, AUS (Oral Presentation).

**Patton, N. R.** Evaluating steady-state topography in the Cooloola Sand Mass, Australia. (2019). University of Utah Luminescence Laboratory. Logan, UT, USA. (Oral Presentation).

**Patton, N. R.** Creeping towards a steady-state topography: landscape evolution of the Cooloola Sand Mass, QLD. (2019). The Australian and New Zealand Geomorphology Group (ANZGG). Inverloch, VIC, AUS. (Poster Presentation).

**Patton, N. R.** Creeping towards a steady-state topography: landscape evolution of the Cooloola Sand Mass, QLD. The Australian and New Zealand Geomorphology Group (ANZGG). (2019). Inverloch, VIC, AUS. (Oral Presentation).

**Patton, N. R.** Remapping the coastal dune fields of South-east Queensland: a morphometric approach. (2018) University of Queensland. St. Lucia, QLD, AUS. (Oral Presentation in school seminar series).

**Patton, N. R.** Predicting soil thickness and its potential applications in Quaternary science. (2018). University of Nottingham. Beeston, UK. (Oral Presentation in departmental seminar series).

## Chapter 2.

### High-resolution remapping of the coastal dune fields of southeast Queensland, Australia: a morphometric approach

*This chapter has been modified from the original manuscript published in Journal of Maps*

Patton, N. R., Ellerton, D., & Shulmeister, J. (2019). High-resolution remapping of the coastal dune fields of southeast Queensland, Australia: a morphometric approach. *Journal of Maps*, 15(2), 578-589.

<https://doi.org/10.1080/17445647.2019.1642246>

**Preface:** This chapter is a mapping project aimed to update the morphological mapping of the SE Queensland dune fields, Australia. In this chapter, I developed a semi-objective mapping technique on the CSM that uses topographic expression and geomorphic relationships from high-resolution elevation data to group dunes in ‘morphosequence units’. The technique was then applied to K’gari (Fraser Island), Minjerribah (North Stradbroke Island), and Mulgumpin (Moreton Island). I provide a qualitative validation of the mapping results using soil development and vegetation type maps, along with a direct comparison with the previous mapping efforts by Ward (2006). Lastly, I compare the geomorphic and topographic characteristics for every morphosequence unit on each dune field. The results of *Chapter 2* provides the general observations that morphosequence units systematically decreases in topographic variability with time (based on the principle of superposition) and is the inspiration/foundation for both *Chapter 3* and *Chapter 4*.

N. R. Patton<sup>1</sup>, D. Ellerton<sup>1</sup> and J. Shulmeister<sup>1</sup>

<sup>1</sup>School of Earth and Environmental Sciences, University of Queensland, St Lucia, Australia

## Abstract

The sand islands and shore-attached dune fields of southeast (SE) Queensland form the world's oldest and largest coastal sand dune system. Here I present updated morphological maps for the dune fields based on topographic expression and geomorphic relationships. Dunes were delineated using high-resolution elevation data and were grouped into morphosequences based on the elevation, drainage patterns and slope characteristics. The slope characteristics focussed on high resolution derived slope-curvature and slope-elevation parameters. Morphosequences were recognised from cross-cutting relationships and relative position in the dune field. The method was developed for the Cooloola Sand Mass (CSM) and then applied to K'gari (Fraser Island), Mulgumpin (Moreton Island), and Minjerribah (North Stradbroke Island), the other major sand islands in SE Queensland. In total, five Holocene and four Pleistocene units have been identified. The new mapping underpins current work on the geomorphic evolution of the dune fields.

## 2.1 Introduction

The dune fields of SE Queensland comprise of one of the largest coastal sand dune systems in the world, incorporating Minjerribah (North Stradbroke Island), Mulgumpin (Moreton Island), Bribie and K'gari (Fraser Island) and the shore-attached Cooloola Sand Mass (CSM) (Miot da Silva and Shulmeister, 2016; Ward, 2006). They include the world's largest sand island (K'gari – 1820 km<sup>2</sup>) and are associated with the longest downdrift sand accumulation system in the world (Figure 2.1). The net northward longshore sand transport is approximately 500,000 m<sup>3</sup> yr<sup>-1</sup>, with the sand sourced from the rivers of central New South Wales more than 1000 km south of K'gari (Boyd et al., 2008; Roy and Thom, 1981). The dune fields, especially the CSM, have been the target of much research, primarily on the soils and biota. The giant podsols of the CSM are regarded as some of the thickest and most developed soils in the world (Thompson, 1981; 1983). The dune fields have been previously mapped by Ward (2006) who produced a map of all the major dune sequences. His maps were based on aerial photographs and extensive field-mapping. More recently, the dune fields have become

the focus of renewed geochronological (e.g., Brooke et al., 2015; Walker et al., 2018) and paleoenvironmental investigations (e.g., Petherick et al., 2008; Levin, 2011; Barr et al., 2013; Moss et al., 2013; Chang et al., 2015; Levin et al., 2017; Cadd et al., 2018). Previous investigations of the SE Queensland dune fields have defined dune building phases by the soil landscapes (Thompson, 1981; Chen et al., 2015), the periods of active deposition (Tejan-Kella et al., 1990) and morphostratigraphic relationships (Ward, 2006). Here, I use geomorphic properties along with these previously used characteristics to describe, identify and map the dune morphosequences of coastal SE Queensland. This chapter has taken advantage of the improved remotely sensed imagery that is now available for the entire dune fields, most notably complete LiDAR coverage which has permitted a significant refinement of the previous mapping.

Remote sensing has long been an invaluable tool for studying dune fields and has provided researchers with the means to map the global distribution of dune fields (McKee, 1979), study the interaction between sediment supply and wind direction (Wasson and Hyde, 1983; Roskin et al., 2013) and quantify dune morphodynamics (e.g., Ewing and Kocurek, 2010; Hugenholtz and Barchyn, 2010). More recently, LiDAR enables data resolutions down to sub-metre scales and permits the recognition of smaller scale geomorphic features. In the case of sand dunes, it facilitates the recognition of ripples and other small-scale structures on dune surfaces and can be used to track their gradual disappearance with increasing age. I took advantage of such features to examine surface roughness patterns to aid in the individual dune mapping at a much finer scale than was previously possible. This enabled me to distinguish areas of similar geomorphic characteristics within the dune field at a finer scale, thereby enabling me to distinguish late-Holocene units that appear identical on gross morphology. The technique presented in this chapter provides the foundation for future work to map and quantify phases of dune activity within stable dune fields as well as investigate how dune landscapes evolve through time.



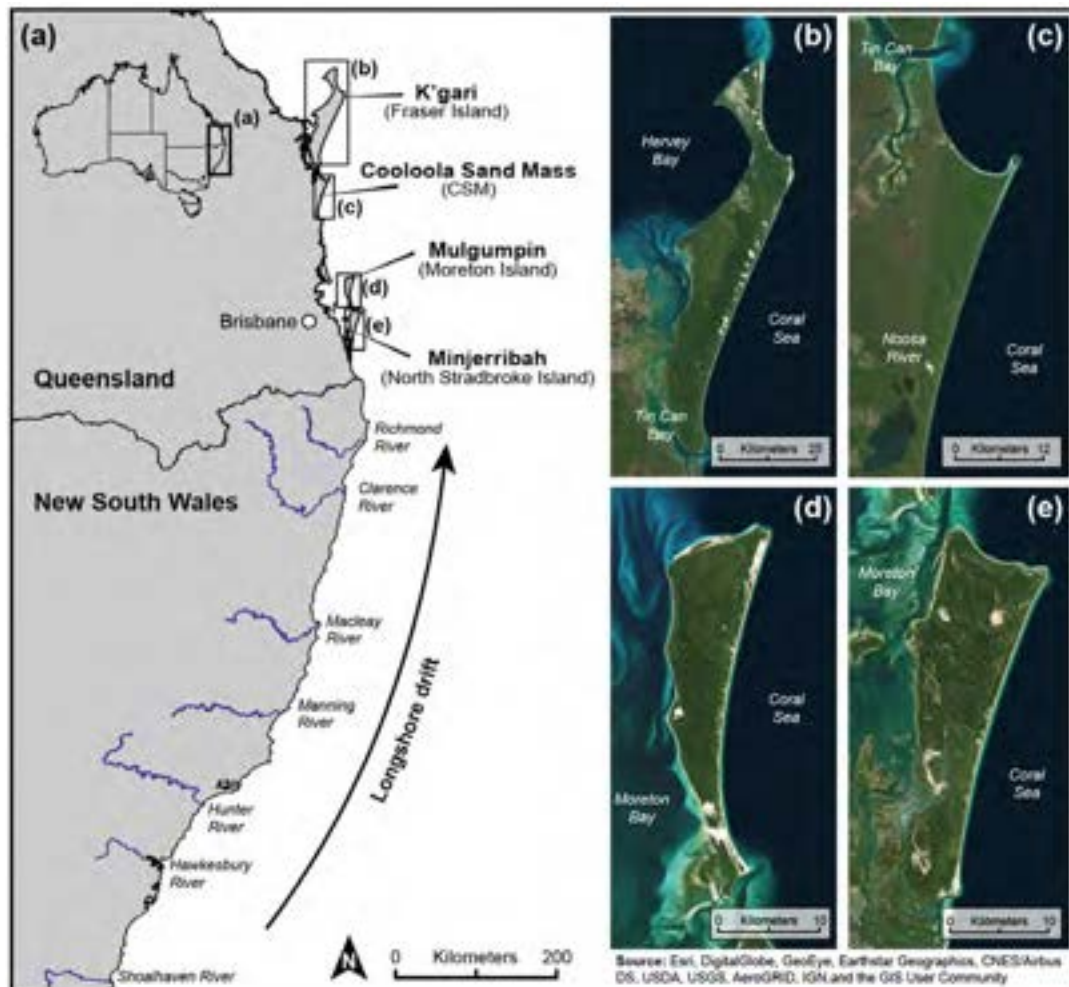


**Figure 2.1:** (a) Study site location map of the SE Queensland dune fields with the eastern Australian longshore drift system and major rivers along the coast. Satellite images of (b) K'gari, (c) CSM, (d) Mulgumpin, (e) and Minjerribah.

## 2.2 Study site

The sand islands of SE Queensland form an extensive series of coastal sand dune fields that include Mulgumpin and Minjerribah to the south and the Great Sandy Region to the north which comprises of the CSM (presently attached to the mainland) and K'gari (Figure 2.1). Minjerribah, situated offshore of Brisbane at  $\sim 27.4^{\circ}\text{S}$  forms the southern extent of these dune systems while K'gari forms the northern extent at  $\sim 25.5^{\circ}\text{S}$ . The dune fields are large, with the CSM, Mulgumpin and Minjerribah reaching lengths of approximately 40 km and widths of approximately 12 km. K'gari is significantly larger with a length of approximately 120 km and an average width of 24 km. The total land area of the dune fields is  $\sim 2350 \text{ km}^2$  and elevation ranges up to 285 meters above sea-level.

The entire region has a humid subtropical climate (Köppen classification Cfa) with warm, wet summers and mild and dry winters (Peel et al., 2007). Mean annual precipitation varies from ~1200 to ~1700 mm. February and March are the wettest months. South easterly winds persist year round with a more southerly component during the winter months and north-easterly winds occur during the spring (BOM, 2017).

The dune fields are notable for containing the world's largest area of rainforest on tall sand dunes (K'gari) (Gontz et al., 2015; Wardell-Johnson et al., 2015). Vegetation along the coastal eastern margin of the dune fields comprises of coastal shrubland and grasses that can tolerate strong winds and salty conditions. Moving inland, low open woodland gives way to tall open and closed forest with notophyllous vine forest in the swale areas. Along the western flanks of the dune fields, vegetation is dominated by open shrubland and heath communities (Longmore, 1997; Longmore and Heijnis, 1999; Donders et al., 2006; Gontz et al., 2015).

The dune fields are composed predominantly of stable parabolic dunes with localised blowouts and several small active transgressive dune sheets. The sediments of the dune fields are homogenous, well sorted and rounded siliceous sands derived from granites and Mesozoic metasediments from the tablelands of eastern New South Wales (Roy and Thom, 1981; Thompson, 1981; Pye, 1983). Bedrock exposures are limited to small rocky outcrops that mostly make up headlands at the northern ends of the dune fields. All of the dune field deposits have formed over successive phases of dune emplacement that have occurred since at least the mid-Pleistocene (Thompson, 1981; Pye, 1983; Ward, 2006). The dune emplacements have formed a series of onlapping dune units that increase in age moving away from the present coastline. Ward (2006) recognised nine periods of dune building based on soil development and morphological characteristics. More recently, Walker et al. (2018) identified 10 units at the CSM and used single grain optically stimulated luminescence (OSL) dating to identify periods of activity. They found that the oldest units at CSM date to ca. 725 ka, confirming earlier work by Tejan-Kella et al. (1990) and they also observed that dune emplacement has continued episodically.

Soil development across the dune fields ranges from weakly developed podsols to well-developed giant humus podsols that are primarily composed of siliceous sands with <2% heavy minerals, including zircon, rutile and ilmenite (Thompson, 1983). This composition reflects the sand delivered to the coast by the longshore drift system along the east Australian Coast. Marine derived sands extend to tens of meters below modern sea level (Ball, 1924).

Mean grain size ranges between 180 and 210  $\mu\text{m}$  and have high porosity at  $>600 \text{ mm h}^{-1}$  (Thompson and Moore, 1984; Reeve et al., 1985). Marked increases in soil development occur across the dune sequences with thick E (A2) and B horizons developed in older dunes located further inland (Thompson, 1981). Thompson (1981) suggested that there is little indication of large climatic, biotic, or lithological shifts within the dune field as indicated by the consistent shape of the dunes and the lack of deviation from podsol soil-forming trends.

## 2.3 Materials and methods

### 2.3.1 Mapping assumptions and workflow

Here I assume that all the SE Queensland coastal dune fields are part of the same depositional system and experience a similar formation and evolutionary history (Thompson, 1983; Ward, 2006). All changes in the character of the morphosequences are time dependent such that younger dunes will experience similar perturbations as older dunes, with the length of time since emplacement controlling the overall degree of erosion. This results in a unique erosional and depositional history for each dune morphosequence unit. In addition, I propose that each dune is systematically smoothing towards a morphological static state after its emplacement; that is, topography becomes increasingly uniform or ‘smoother’ with time (Montgomery, 2001; Bonetti and Porporato, 2017). Based on these assumptions I use changes in dune morphological characteristics supported by dune ancillary characteristics to map the dune fields (Figure 2.2). The CSM was the optimal location to establish this method because it contains the most complete dune sequence (Lees, 2006), the most ancillary (e.g., soil, chronology) information and has experienced little human disturbance.

### 2.3.2 Dune delineation

I utilise high-resolution elevation data, satellite imagery, and historical aerial photographs to identify individual dunes. Principally, I used a 5 m digital elevation model (DEM) derived from Light Detection and Ranging (LiDAR) and 1:5000 digital orthophoto imagery data. Elevation datasets for all areas of interest were obtained from the Digital Elevation Model (DEM) 5 m Grid of Australia created by merging 236 datasets collected between 2001 and 2015. Accuracy of elevation data met the Australian ICSM LiDAR

Acquisition Specifications with the vertical and horizontal data having an accuracy of no worse than  $\pm 0.30$  m and  $\pm 0.80$  m (95% confidence), respectively.

Orthophoto imagery was acquired through Queensland Globe (QGlobe), with a pixel resolution of 0.25 m and an accuracy of  $\pm 1.0$  m. In addition, historical aerial photographs were obtained through Queensland Imagery (QImagery) to determine any recent anthropogenic disturbances that may have altered the original topography, such as mining or logging, and provide locations and characteristics of previously visible dunes.

Where little to no anthropogenic disturbances occurred in the landscape, I identified individual dunes through large dune morphological features ( $>10$  m<sup>2</sup>) such as crests, trailing arms, and the slip face of the depositional lobes. An example of this process is provided in Figure 2.3. In ArcGIS 10.6 (ESRI, Redlands, CA) I delineated each dune at the base of their ridges and crests utilising elevation and slope rasters. For all points, slope was calculated using change in elevation in downhill direction which is presented here as degree slope. Curvature was obtained by the rate of change in slope, at a fixed position in all directions and multiplied by  $-100$  to remove the negative curvature convention (i.e., Patton et al., 2018).

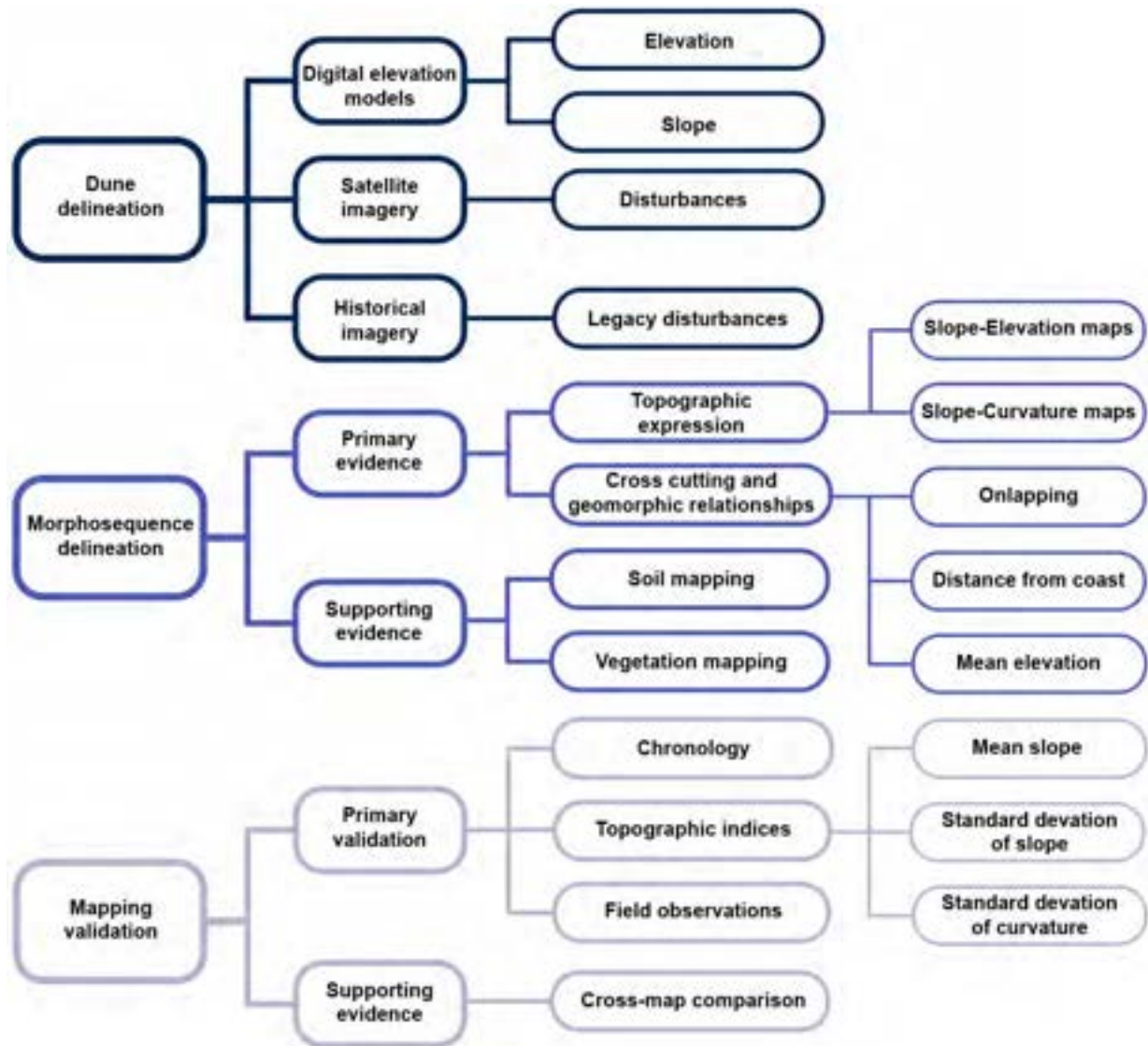


**Figure 2.2:** Schematic flow chart of the mapping and validation procedures for dune morphosequence delineation.

### 2.3.3 Dune morphosequence delineation and supporting evidence

Following dune delineation, I categorised dunes into separate morphosequences utilising crosscutting and geomorphic relationships. The CSM forms a classic onlapping dune sequence where dune units become increasingly older from the coast (east) moving inland (west) (Lees, 2006; Walker et al., 2018). In coastal dune fields, onlapping relationships allow me to determine the relative age sequence of the dune emplacements as younger dunes are superimposed on older units. To exemplify this, I measured the shortest mean distance from the furthest inland dune crest to the coast and the mean elevations for each morphosequence.

Where cross-cutting geomorphic relationships are not easily determined due to landscape complexity, I utilise small (<10 m) internal dune features to help delineate each morphosequence by using the topographic expression to 'fingerprint' each dune emplacement phase. The surface characteristics of the landscape can be defined by the relative surface texture, drainage patterns and landform elements present. The topographic fingerprint is best observed by combining and manipulating elevation, slope and curvature rasters. This was achieved by overlaying a 70% transparent slope raster with a white to black (low to high) gradient on an elevation raster with a continuous brightness colour ramp (Figure 2.4). Similar to elevation, I combined a transparent slope raster on a curvature raster with a diverging colour ramp. Due to the normal distribution of curvature around planar surfaces ( $0\text{ m}^{-1}$ ) a diverging colour ramp utilising quantile bins, is best suited to emphasise changes from convergent (hollows and valleys) to divergent (ridges and noses) topography (Figure 2.4). In combination, both rasters act as visual aids to identify the unique fingerprint of each depositional phase.



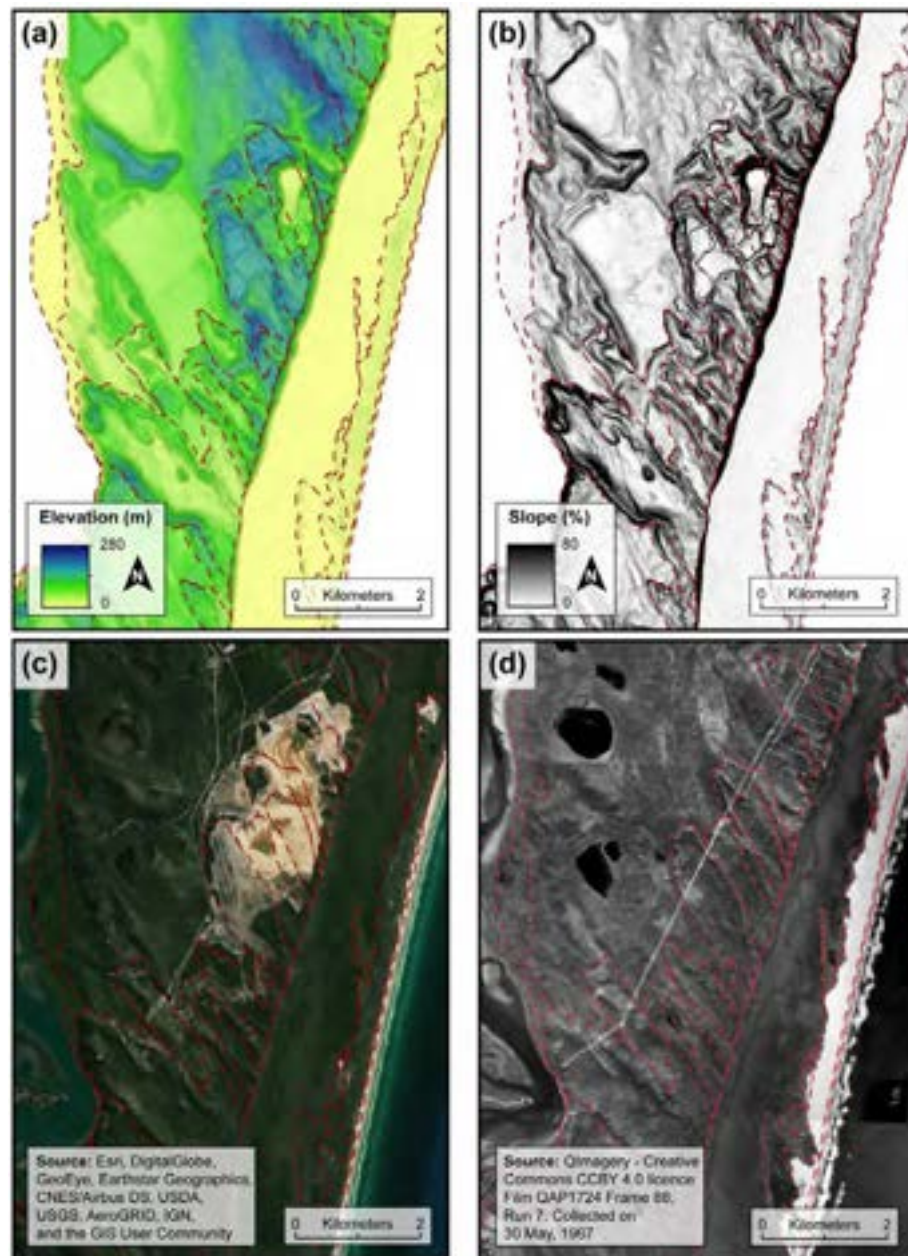


**Figure 2.3:** Visual sequence of dune delineation example on Minjerribah (North Stradbroke Island) using **(a)** elevation and **(b)** slope DEMs, **(c)** satellite imagery, and **(d)** historical air photos. Note areas that are human disturbed (mining and road construction).

This approach allows a simple visual comparison between each individual dune, permitting them to be delineated into separate morphosequence units; however, some discrepancies may still occur. Where internal dune features are limited or difficult to interpret due to depositional complexity, changes in base level or proximity to higher energy environments (such as Tin Can Bay, Noosa River or the Coral Sea) (see Figure 2.1) I used the available soil (Thompson, 1983), vegetation (Queensland Herbarium) and drainage direction data to complement and support my interpretations. Soil information helps provide a relative

age sequence of the dunes based on the increasing degree of pedogenesis with time (Chen et al., 2015). Field data was also used to confirm the onlapping relationships of each dune morphosequence.

I have opted to use the naming convention of Ward (2006) for the dune morphosequences. I use this convention rather than the numerical convention employed by Thompson (1981) and Walker et al. (2018), as using a number-based system can lead to issues if a new unit is identified or an existing unit is eliminated, as happened in the new mapping.

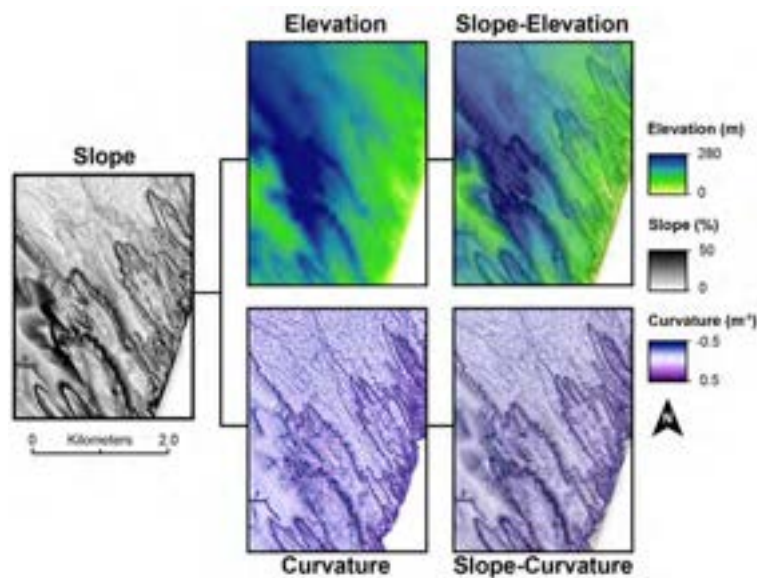


**Figure 2.4:** Workflow to produce mapping rasters. This figure demonstrates the methodology used to generate the topographic expressions as seen in the slope-elevation and slope-curvature layers. In each case a slope raster was superimposed at a 70% transparency on the elevation and curvature layers to generate the topographic expression. These topographic expressions were then applied to discriminate between morphosequence units.

### 2.3.4 Mapping validation and supporting evidence

To validate my approach for delineating dune morphosequence units, I focus on the CSM. Validation was achieved by cross-referencing each dune morphosequence with available unpublished chronological data and Walker et al. (2018). This was done to confirm the age relationships of each morphosequence using the weighted mean of the OSL ages. Each unit was plotted as the explanatory variable against mean distance from coast, mean elevation and extracted topographic indices. The topographic indices for each dune morphosequence were determined from ArcGIS zonal statistics as the mean and standard deviation of slope and the standard deviation of curvature. To eliminate any discrepancies



that may have altered the original topographic expression, portions of the landscape such as anthropogenic disturbances (e.g. roads), rock outcrops, and free-standing water were identified and removed from the analyses, along with an additional 10 m buffer.

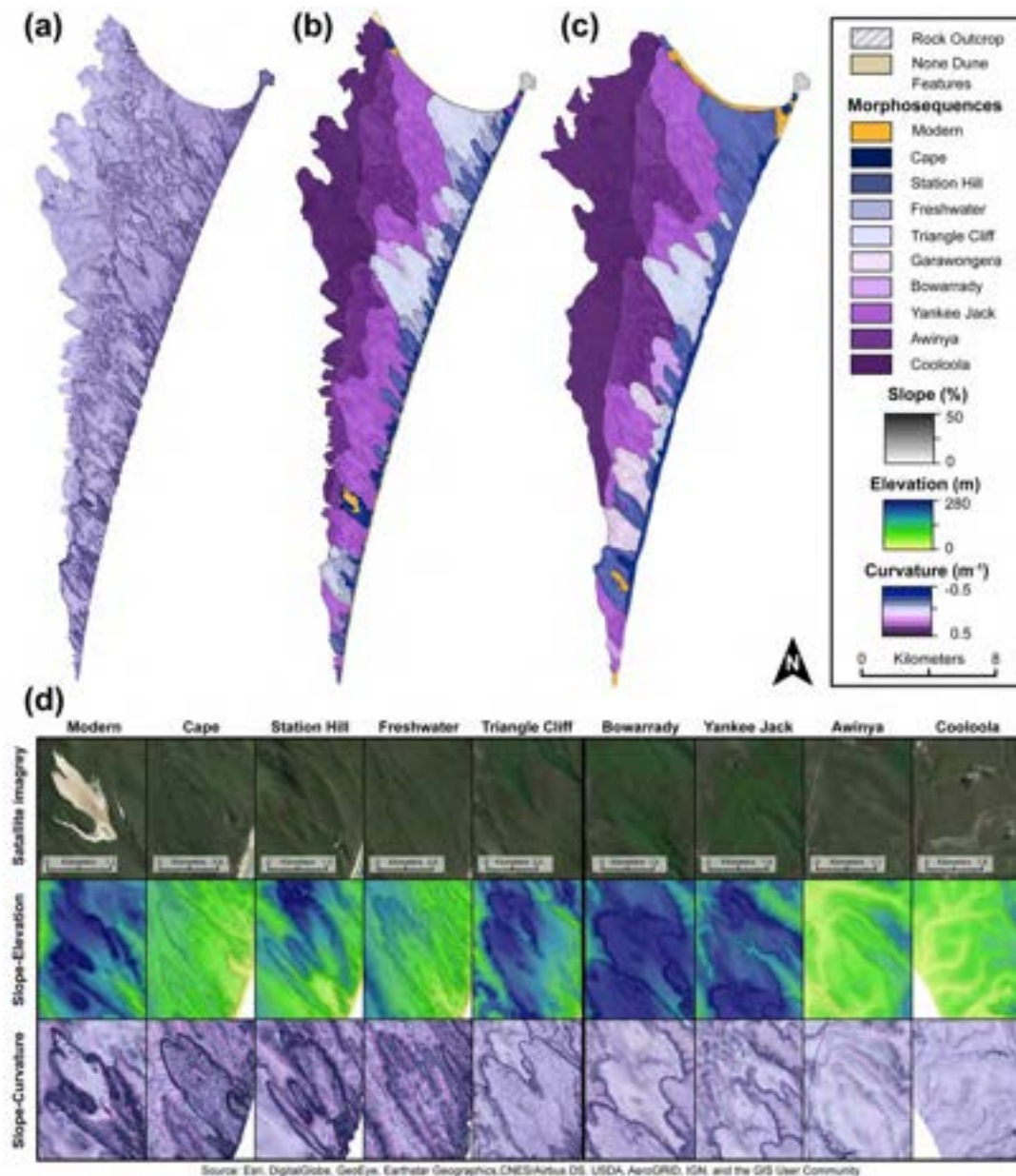


**Figure 2.5:** The CSM morphosequence units and their validation. **(a)** Derived slope-curvature raster. **(b)** Final morphosequence map of the CSM. **(c)** Digitised version of Ward's (2006) map. Note the strong similarity between panels b and c. In my final map I have added an extra Holocene unit (Freshwater) but eliminated a Pleistocene unit of Ward (2006) (Garawongera). **(d)** Examples of slope-curvature, slope elevation and satellite images for each of the morphosequences. The heavy black line separating Triangle Cliff from Bowarrady marks the boundary between the Holocene and Pleistocene morphosequence units. Note that the dune units become more diffuse and less well defined with increasing age. The units from the CSM were then applied to the sand islands.

A complementary assessment of my mapping efforts involved a comparison to the traditional, independently derived geomorphological map by Ward (2006). His study primarily used aerial imagery, soil data and field observations to map the CSM and extrapolated his findings across the remaining SE Queensland dune fields. I evaluated and compared each matching morphosequence unit between the studies. I acknowledge that this is by no means a true validation; however, comparisons of each map provide novel insight into the two techniques. To achieve this, Ward's map was digitised in the ArcGIS georeferencing tool, and I report the percent similarity of matching dune morphosequences.

### 2.3.5 Mapping extrapolation

I extrapolated my approach to the adjacent dune fields. In all dune fields, I delineated dunes and then grouped into the appropriate morphosequences based on the same topographic expression and geomorphic relationships seen at the CSM.

## 2.4 Results

### 2.4.1 CSM morphosequence unit delineation and validation

I recognise nine dune morphosequence units at the CSM composed of five Holocene (Modern, Cape, Station Hill, Freshwater and Triangle Cliff) and four Pleistocene units (Bowarrady, Yankee Jack, Awinya and Cooloola) see main map (Figures 2.5, Figure 2.6, and Supplementary Figure A.2.1). This chapter recognises an additional Holocene unit that was not mapped by Ward (2006), which I have named Freshwater. I have also removed one of Ward's Pleistocene units, Garawongera, which was not found in this study. Holocene morphosequences are characterised by decreases in crest sharpness and surface roughness, increases in podsolisation, elevation, and distance to coast with increasing age. They display little to no stream incision. Pleistocene units exhibit similar trends but all show evidence of increasing fluvial incision and decreasing crest elevation with age (Table 2.1).

**Table 2.1:** Summary of CSM morphosequence units including mean age, surface characteristics, percent land cover, mean distance from the coast, mean elevation, mean slope, standard deviation of slope and standard deviation of curvature. All data was extracted using ArcGIS 10.6 (ESRI, Redlands, CA) zonal statistics tools. For more information on mean age and soil characteristic refer to Ellerton et al. (2018), Thompson (1981) and Walker et al. (2018).

Dune Unit	Mean age (ka)	Surface characteristics	Soil characteristics	Land area (%)	Mean distance from coast (km)	Mean elevation (m)	Topographic Indices		
							Mean slope (%)	St. Dev slope (%)	St. Dev curvature (m <sup>-1</sup> )
Modern	< 0.4	Bare, presently active sand	No podsolisation	0.46	2.30	107	16.4	12.3	0.0232
Cape	0.4 ± 0.04	Sharp crested, parabolics that have been recently stabilised	No podsolisation	4.30	0.78	73.6	28.3	14.0	0.0490
Station Hill	0.8 ± 0.1	Elongate, sharp crested parabolics	Incipient podsol	5.77	0.78	80.9	22.6	12.4	0.0262
Freshwater	4.1 ± 0.24	Elongate, sharp crested parabolics.	Podsol	5.22	1.12	93.1	20.9	11.7	0.0191
Triangle	7.8 ± 0.26	Elongate, U-shaped parabolics. Large sand ripples within dune interior	Podsol	12.73	2.48	119	14.1	10.5	0.0128
Bowarrady	7.8 ± 132	Prominent dune relief with incised channels. Dune apex and ridges have been truncated. Found blocking major Yankee Jack channels.	Giant Podsol	1.66	3.10	158	13.3	7.89	0.0074
Yankee Jack	132 ± 3.9	Prominent dune relief with large incised channels. Dune apex and ridges have been truncated	Giant Podsol	30.42	3.23	132	17.2	9.51	0.0098
Awinya	648 ± 30.2	Subdued dune relief with significant incision and complex drainage patterns. Very little original dune morphology	Giant Podsol	17.64	5.81	89.2	16.7	8.32	0.0094
Cooloola	>648	Very subdued dune relief with no original dune morphology	Giant Podsol	21.79	8.33	6.61	6.61	4.62	0.0091

My results are consistent with the independent chronology of the CSM dune field based on OSL ages from both Walker et al., (2018) and my unpublished dataset. The weighted mean and standard error age for Cape, Station Hill, Freshwater, Triangle Cliff, Yankee Jack and Awinya units are ca.  $0.4 \pm 0.04$  ka,  $0.8 \pm 0.1$  ka,  $4.1 \pm 0.24$  ka,  $7.8 \pm 0.26$  ka,  $132 \pm 3.9$  ka,  $648 \pm 32$  ka, respectively. It should be noted here that OSL dates the last time sand grains were exposed to sunlight and these ages likely reflect the final phase of dune development rather than the time the dune was first initiated. It is likely that the time of initiation predates these ages. The Modern dunes are dunes that are currently active or were visibly active in historical imagery as shown by bare earth (lacking vegetation). The lack of original dune morphology suggests that the Cooloola unit has been extensively reworked, but is older than the Awinya unit (ca. >650 ka). The Bowarrady unit is recognised in my mapping but no age control is available for this dune morphosequence. Based on its morphostratigraphic position, emplacement occurred between the Yankee Jack and Triangle Cliff units and based on its morphology, the unit is clearly Pleistocene, as suggested by Ward (2006).

I observe that 90.3% and 97.8% similarity of my Holocene and Pleistocene mapped units, respectively, when compared to the Holocene and Pleistocene boundaries of the original mapping by Ward (2006). Direct comparisons of each morphosequence are complicated by the change in the number of units but I observe 5.3% Modern, 57.6% Cape, 21.4% Station Hill, 66.0% Triangle Cliff, 0% Bowarrady, 71.2% Yankee Jack, 70.7% Awinya, and 98.2% Cooloola congruence between my study and Ward's (2006). The new mapping of the CSM dune field agrees well with the chronology of the dune systems and is largely consistent with past mapping efforts, but provides increased resolution, especially in the Holocene dune units.

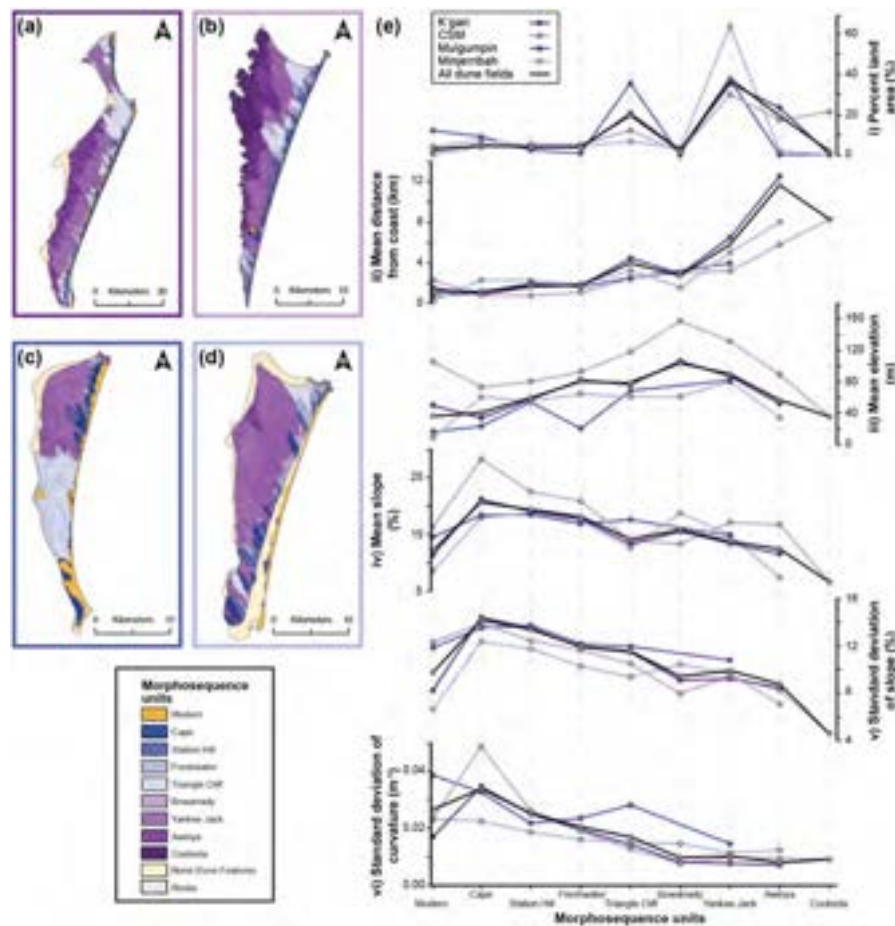


**Figure 2.6:** Mapped morphosequence units and geomorphic characteristics. Final morphosequence maps for (a) K'gari, (b) the CSM, (c) Mulgumpin, and (d) Minjerribah dune fields. Note, dune fields are not to same scale. Panel e contains six graphs showing (i) percent land area for each unit; (ii) mean distance from coast, (iii) mean elevation, (iv) mean slope; (v) standard deviation of slope; (vi) standard deviation of curvature. The black line represents the mean values for all dune fields. Note that in all dune fields the parameters follow the same trends. Also note that for geomorphic characteristics there is a general progression from youngest to oldest morphosequences.

## 2.4.2 Mapping extrapolation

Like Ward (2006), I extrapolated my morphosequence units across the SE Queensland dune fields. When plotting the topographic indices and geomorphic characteristics against each morphosequence unit, I observe similar landscape relationships between all study sites (Figure 2.6). The CSM contains all of the morphosequences recognised at other dune fields while none of the other dune fields contain the whole sequence. This confirms that the CSM is the most complete dune field sequence in SE Queensland and reinforces the need for conservation of this dune field.

## 2.5 Discussion

### 2.5.1 Geomorphic evolution - foundation of this approach

My mapping is based on the fundamental concept that all landforms are evolving towards their local base-level. This assumption can be problematic in dune fields as dunes can be easily reworked following a perturbation (Hugenholtz and Wolfe, 2005; Tsoar, 2005), especially in coastal environments (Hesp, 2002). The coastal dunes of SE Queensland show evidence of long-term stability despite the deep podsolisation, extensive incision and great antiquity of the Pleistocene units (Tejan-Kella et al., 1990; Lees, 2006; Walker et al., 2018). Following the earliest dune building events, subsequent phases of activation have not fully overrun and reworked previous deposits due to the high elevation and steep slopes of the antecedent topography. It is very likely that there have been periods of reworking (Walker et al., 2018); however, I argue that this has been more local and has not lead to the complete destruction of previous units. The patterns that I observed from the morphometric analyses at the CSM, indicates that these assumptions are reasonable and that, especially in the Holocene dune sequences, the approach allows me a better discrimination of dune units than was previously possible (Figure 2.5). Consistent with the CSM, I observe the same topographic patterns across the SE Queensland dune fields, indicating that my assumptions are reasonable and that all the dune fields are part of the same depositional system (Figure 2.6).

The previous mapping effort by Ward (2006) successfully delineated dune units based on cross-cutting relationships and large-scale features. This can be seen in the similarity of the Holocene and Pleistocene boundaries in both studies (Figure 2.5b-c). Where dune units are separated by a significant gap in time (e.g., Awinya and Yankee Jack) he was also able to accurately distinguish between the units. However, limitations with his map occurred in areas with complex terrain, dense vegetation cover, and/or where dune units were very similar in age. Where these conditions occurred, his maps became less reliable. My approach helps to improve and update the geomorphic mapping. For example, along the north eastern boundary of the CSM where significant dune onlapping and dense vegetation occurs, Ward (2006) mapped the entire area as Cape and Station Hill, whereas I was able to individually delineate all Holocene morphosequences in this area.

With respect to limitations of this work, the main constraints are around the manual nature of dune delineation which makes the procedure quite time-consuming. There are

specific challenges in areas of complex topography because the mapping requires the operator to identify individual dunes. In areas of heavy drainage dissection or complex dune interactions, this may not always be accurate and depends on the familiarity of the operator with the dune forms. Only a few small areas of the dune field are affected by this phenomenon.

In order to apply this method to other systems, high-resolution elevation data are needed along with an understanding of the processes dominating the landscape. How changes to base level, climate and antecedent topography have influenced the depositional and erosional history is important to understand the patterns observed. An example of this is the role of pre-existing topography on dune unit extent. In areas where high dunes are preserved younger dune units are compressed, as they need energy to migrate up and over the older systems. In contrast, in north-central K'gari, early-Holocene dunes propagated onto a lower topography and succeeded in migrating many kilometres to the west.

## 2.6 Conclusion

Here I have presented a novel method to interpret and delineate dune morphosequence units across the coastal dune fields of SE Queensland, Australia based on work from the Cooloola Sand Mass (CSM). This study combined traditional approaches with the assumption that landscapes are systematically smoothing through time. I used two primary parameters to undertake this work, topographic expression and geomorphic relationships to define the morphosequences. The mapped units were validated using chronology, topographic indices and field observations. Using these parameters, I have been able to successfully sub-divide the dunes into five Holocene and four Pleistocene units.

The mapping approach presented in this chapter has advantages over visual mapping of the dune morphosequences in that it is semi-objective and could be automated. Based on my analyses, it is likely to be more robust than traditional mapping. Future coastal dune field studies can use the techniques I provide here as a first-order approach to delineate landforms based on relative age. In addition, I was able to extrapolate with confidence across the entire SE Queensland dune fields into areas with little to no previous chronological information. The mapping will help underpin ongoing paleoclimate and geomorphological research in the SE Queensland dune fields.

## Chapter 3.

### **Measuring landscape evolution from inception to maturity: insights from a coastal dune system**

*This chapter has been modified from the original manuscript published in Earth & Planetary Science Letters*

Patton, N. R., Shulmeister, J., Ellerton, D., & Seropian G. (2022a). Measuring landscape evolution from inception to maturity: insights from a coastal dune system. *Earth & Planetary Science Letters*, 584, 17448 <https://doi.org/10.1016/j.epsl.2022.117448>

**Preface:** This chapter explores the observations of *Chapter 2* that the average morphosequence unit's topography become increasingly smooth with time but on the individual dune scale. In this chapter, I first provide evidence that the Holocene sections of the SE Queensland dune field is an ideal natural laboratory to evaluate landscape evolution. I demonstrate that dune topographic evolution within the CSM can be numerically explained through hillslope sediment transport theory and these findings are validated through field observations and forward numerical models. This chapter explores the conditions and mechanisms that control both style and rate of landscape change. Critically, the results of *Chapter 3* provides the theoretical framework for the surface roughness-age relationship used in *Chapter 4* and the rationale for evaluating fire frequency in *Chapter 5*.



N. R. Patton<sup>1,2</sup>, J. Shulmeister<sup>1,2</sup>, D. Ellerton<sup>3,2</sup> and G. Seropian<sup>1</sup>

<sup>1</sup>School of Earth and Environment, University of Canterbury, Christchurch, New Zealand

<sup>2</sup>School of Earth and Environmental Sciences, University of Queensland, St Lucia, Australia

<sup>3</sup>Department of Geological Sciences, Stockholm University, Sweden.

## Abstract

The concept of the geomorphic cycle is a foundational principle in geology and geomorphology, but the topographic evolution of a single landscape from inception to maturity has been difficult to demonstrate in nature. The onlapping dunes of the Cooloola Sand Mass (CSM) in eastern Australia provide an ideal chronosequence to evaluate landscape evolution. Here commonly assumed properties on which landscape models are based (i.e., conservation of mass and major factors contributing to landscape change) can be physically measured and accounted for. My field-based measurements and forward numerical models demonstrate that dunes, like other landscapes, relax in an exponential manner. The emplaced dunes evolve through an initial phase of rapid topographic adjustment associated with the dominance of episodic sediment transport. This phase continues for ca. 1 ka until hillslope gradients are lowered below their angle of repose ( $0.65 \text{ m m}^{-1}$  or  $33^\circ$ ). Once sufficiently lowered, the dunes evolve through slow, continuous sediment transport. These findings of dual transport regimes are validated by stratigraphic records at all excavated dune foot-slopes, and I propose that this evolution can be measured by the distribution of curvature ( $C$ ) of a landform, specifically its standard deviation ( $\sigma_C$ ), as a measure of surface roughness. Surface roughness smooths with time through diffusional sediment transport that lowers local relief. The value and its rate of smoothing can define the stage in evolutionary development and help infer processes, which makes it an important morphometric tool for understanding landscapes. These observations highlight that under stable evolutionary conditions, the development of the landscape is governed by the physical properties of the dune's parent material. In addition, my findings support landscape evolution inferences from numerical and physical models and the coupling of granular material physics with landscape change.

### 3.1 Introduction

The idea of the geomorphic cycle is embedded in our understanding of landscape evolution (Davis, 1892; Gilbert, 1909). The underpinning concept is that gravitationally driven transport processes and consequential erosion and deposition, relax landscapes towards their base-levels while reducing mean local relief (Carson and Kirkby, 1972; Montgomery, 2001). However, it is difficult to measure and describe the complete process in a natural setting. This is due to the fact that landscape evolution typically occurs over geological time scales (Fernandes and Dietrich, 1997) and few systems have adequate dating control over the full duration of erosion to investigate the entire process; nor are many intermediate stages usually preserved. Nevertheless, studies utilise space-for-time substitutions for their experimental design (e.g., Rosenbloom and Anderson, 1994; Stolar et al., 2007; Hilley and Arrowsmith, 2008; Fryirs et al., 2012; Micallef et al., 2014). However, tectonic, lithologic, biologic and climatic forcings that contribute to landscape change are rarely uniform in time and space and cannot be accurately constrained nor can critical assumptions be verified (McKean et al., 1993; Whipple, 2001).

As highlighted by reviews across the geosciences (e.g., Tucker and Hancock, 2010; Minasny et al., 2015; Pawlik and Šamonil, 2018; Jerolmack and Daniels, 2019; Richter et al., 2020), identifying landscapes that can facilitate the use of interdisciplinary methods is vital for understanding earth systems' processes. In this chapter, I first highlight that the Cooloola Sand Mass (CSM) dune field in Australia provides a true time-for-space substitution to evaluate landscape evolution, see Figure 3.1. Here I note that this dune field offers the closest real-world approximation to sandbox models and the application of purely diffusional transport theory is appropriate (a commonly used laboratory-based analogue to illustrate erosion and deposition). I then demonstrate this evolution is well characterised by surface roughness ( $\sigma_c$ ), as defined by the standard deviation of curvature ( $C$ ), due to curvature's mechanistic and empirical relationship with landscape drivers. Lastly, I validate my inferences with sedimentological records and by simulating dune evolution using a two-dimensional numerical evolutionary model.

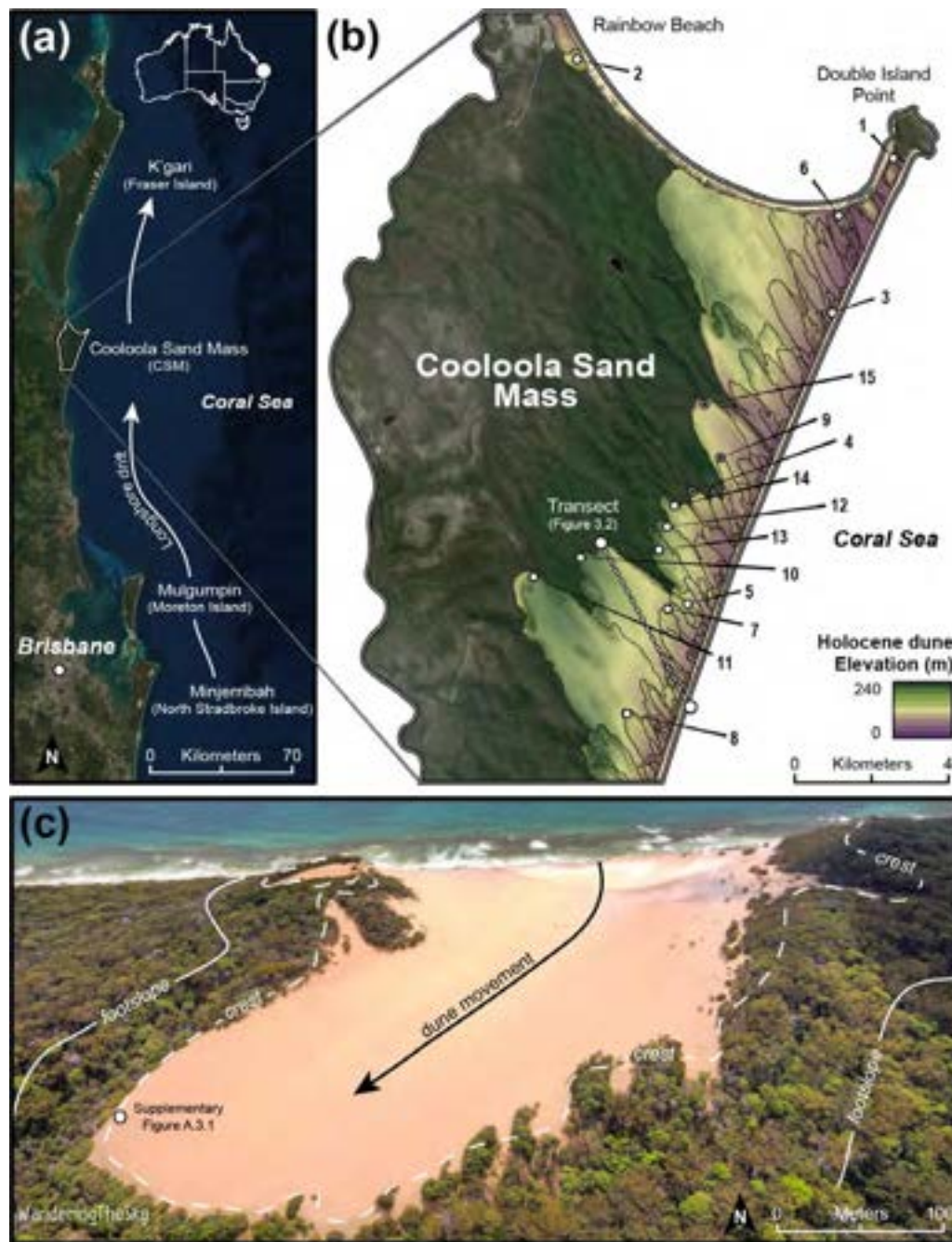


**Figure 3.1:** Regional and site location. **(a)** Satellite imagery of the SE Queensland dune fields in Australia, emphasising the location of the CSM. **(b)** Delineated Holocene dunes and their associated elevation at a 5 m resolution (black lines) and location of the 15 dated dunes and 4 soil pits used in this chapter (white circles and black dots, respectively) (obtained from Walker et al., (2018) and Ellerton et al., (2020), see Supplementary Tables A.3.1, A.3.2, and A.3.3). Note, one soil pit was collected on a 2.14 ka dune that was not utilised in my topographic analyses (white triangle with black dot). A topographic transect aligned parallel to the dominant wind direction, (southeast to northwest), from juvenile to mature dunes is highlighted, see Figure 3.2. **(c)** Aerial view of an incipient parabolic dune forming along the margins of the Carlo Sand Blow near the township of Rainbow Beach (drone photography: “Wandering.the.Sky”). Note, this active dune (inception) is blown off the coast and extends inland through vegetation and over previously emplaced dunes creating over-steepened lee slopes, see Supplementary Figure A.3.1.

### 3.1.1 Study area: world premier chronosequence

The Cooloola Sand Mass (CSM) in southeast Queensland, Australia contains coastal dunes that extend back nearly 800 ka (Ellerton et al., 2020) (Figure 3.1). The Holocene dunes comprise ~30% of the total area containing >190 parabolic dunes (*Chapter 2*), which were created and evolved under similar conditions. The dunes are composed of sands derived from one of the world's longest longshore drift systems (~1500 km) which has generated a nearly limitless supply of homogenous parent material that is >98% medium-fine quartz sand (Boyd et al., 2008). The CSM has been tectonically inactive during this period and experienced only minor eustatic/hydro-isostatic changes in local elevation (sea-level) since the Holocene sea-level highstand (Lewis et al., 2008). In addition, the regional climate has been stable and pollen/ palynological proxy records indicate no major changes in vegetation types (e.g., Barr et al., 2017; Schreuder et al., 2019).

Consistent dune activation and emplacement mechanisms promote remarkably uniform morphology. Initiating near the Coral Sea coastline, dunes advance inland by the prevailing wind (dune inception) (Thompson, 1981). The dunes migrate through stands of tall (20-30 m in height) open and closed Eucalyptus Forest (canopy cover of 50-80% and >80%, respectively). Their path inland gradually steepens, limiting their progress and permitting rapid colonisation of vegetation on the bare hillslopes, thereby emplacing dunes and preserving older dunes. The buttressing of hillslopes and rapid growth of vegetation enable dunes to have over-steepened lee slopes built near or above the sand's unmodified angle of repose (gradient of 0.65 m m<sup>-1</sup> or an angle of 33°) (see Supplementary Figure A.3.1). As a result, the onlapping dune sequences create a landscape that increases in age while decreasing in topographic variability moving inland from the coast (Figure 3.2).

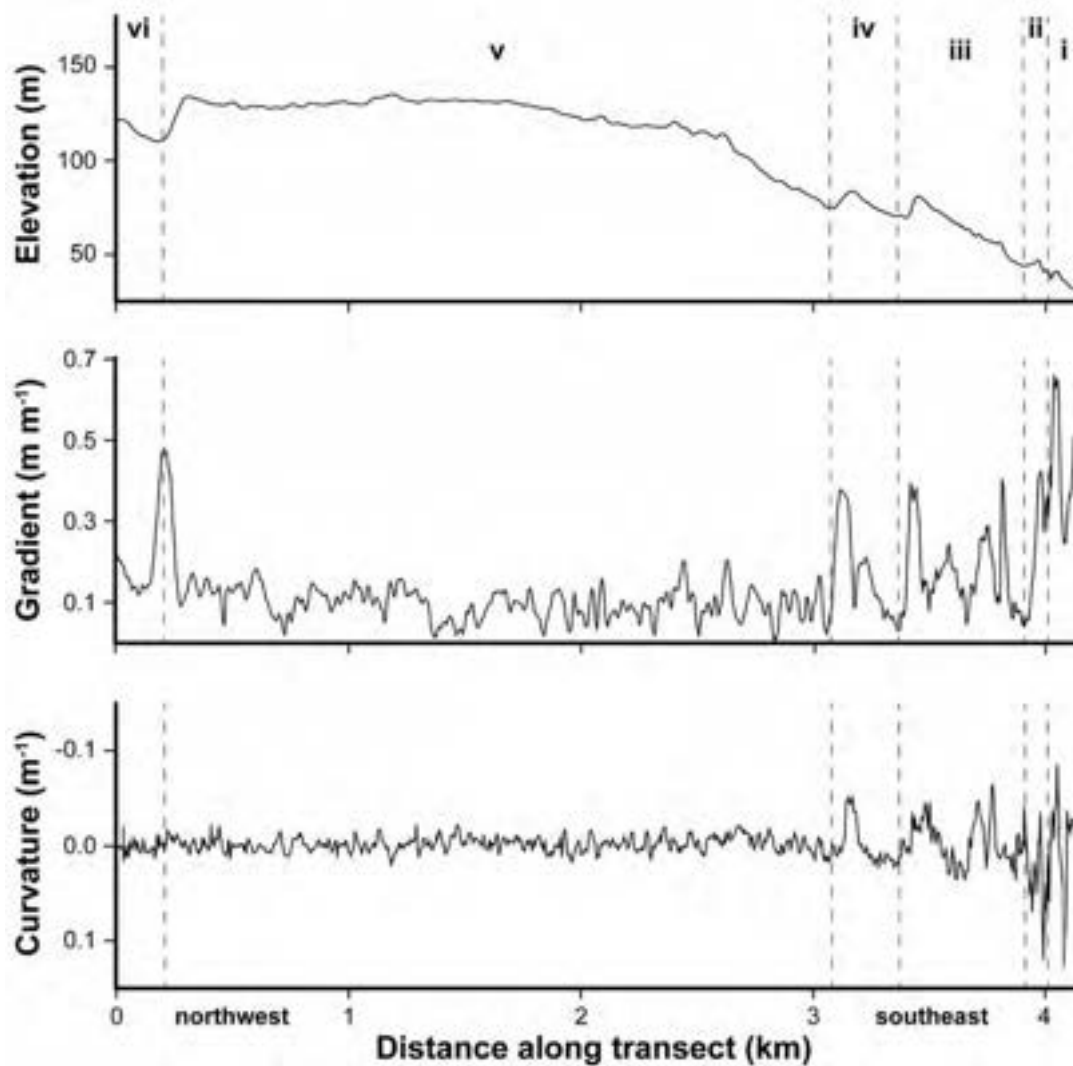


**Figure 3.2:** Changes in topographic variability at the CSM at a 5 m resolution. A transect aligned parallel to the dominant wind direction (northwest to southeast), seen in Figure 3.1b, indicates the transition from juvenile dunes (i) to more mature dunes (ii to vi) moving from the coast inland (right to left). When dunes are stabilised, they have highly variable surface topography. As time continues, their slope relaxes such that morphology is time independent and this evolution can best be described by the dune's curvature, specifically a dune's standard deviation of curvature ( $\sigma_c$ ) as a measure of surface roughness, ( $(\partial\sigma_c)/\partial t \rightarrow 0$ ).

Dune emplacement marks the onset of topographic relaxation (juvenile through old-age stages). The CSM dunes evolve by the reduction of local relief with time under a limited set of sediment (soil) transport processes. The smooth, undissected topography reflects the absence of fluvial transport, which is suppressed by high soil infiltration rates ( $>600 \text{ mm hr}^{-1}$ ) (Reeve et al., 1985). There is consequently a dominance of diffuse grain-by-grain processes. Since the dune sands and the soils they generate are virtually identical with regard to transportability (i.e., similar bulk density, grain size, and structure), the landscape is not

defined and/or limited by development of soil horizons (pedogenesis) – a truly transport limited system. The lack of hillslope-scale water-driven transport and the presence of dune onlapping, limits sediment removal from internal basins, effectively making the Holocene dunes a closed system. As a result, mass is conserved within the boundaries of the CSM, such that all sediment eroded (loss of elevation) is transported only through gravitational hillslope processes and can be accounted for in depositional locations adjacent to the dune ridges as gain of elevation (Figure 3.3). Thus, the CSM presents a true space-for-time substitution and illuminates the evolution of an initial topographic form by purely hillslope processes. The dunes retain the depositional legacy of those processes in inland basins, allowing process style and tempo to be inferred. Because of these conditions, I can apply conservation of mass equations to this landscape.

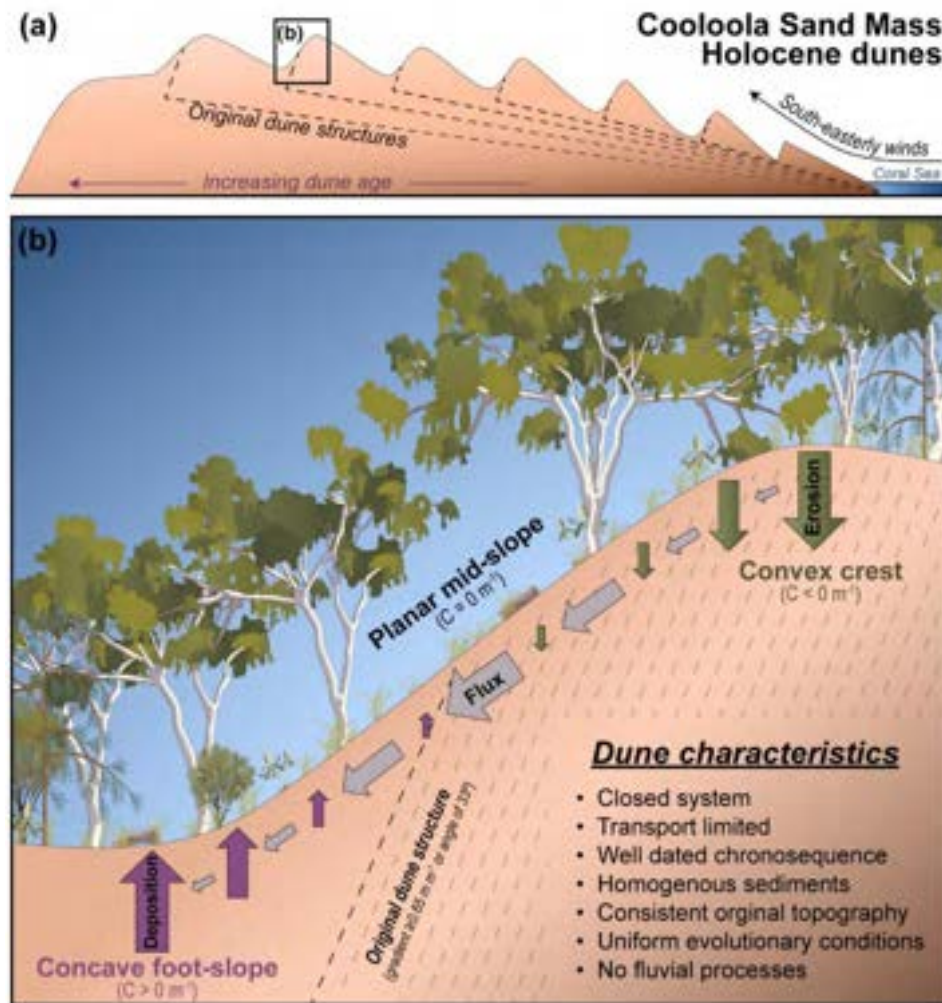


**Figure 3.3:** Idealised topography, chronosequence, and hillslope processes of CSM, Australia. **(a)** The CSM dunes move inland from the coast across antecedent topography (dashed lines) until wind speeds decrease and dunes emplace (stabilise). With every subsequent dune emplacement, antecedent topography gradients increase therefore decreasing the distance dunes travel inland. **(b)** Conceptual diagram of hillslope positions and the contribution of erosion, deposition and flux (size of arrow). Once dunes' hillslopes are lowered below their angle of repose (gradient of  $0.65 \text{ m m}^{-1}$  or angle of  $33^\circ$ ), I posit that nonlinear sediment transport effects become negligible. Here only diffusive hillslope processes are active and all sediment removed from crest and ridges can be accounted for in the hollows and valleys (a closed system). As time progresses ridges lower and hollows fill, reducing hillslope gradients and the maximum and minimum curvature values. Combined I hypothesise a systematic decrease in erosion, deposition and flux rates with time.

### 3.1.2 Capturing landscape evolution with surface roughness

On shallow hillslopes, soil transport is commonly described by a linear slope-dependent transport law where soil flux is solely gradient dependent. In this circumstance, sediment flux ( $q_s$ ) per unit width is proportional to hillslope gradient (i.e.,  $\nabla z$ ) (Davis, 1892; Gilbert, 1909):

$$\mathbf{q}_s = -K\nabla z, \quad (\text{EQ.3.1})$$

where  $K$  is the soil transport coefficient. Here erosion rates ( $E$ ), can be determined by the divergence of  $\mathbf{q}_s$ :

$$E = \nabla \cdot \mathbf{q}_s = -K\nabla^2 z = -KC, \quad (\text{EQ.3.2})$$

such that curvature ( $C$ ) ( $\nabla^2 z$ , where  $z$  is elevation) is proportional to erosion rate ( $E$ ) (Hurst et al., 2013). As a result, where only diffusive hillslope processes act, the smoothing of the landscape will depend on surface roughness, expressed in terms of standard deviation of  $C$  ( $\sigma_C$ ):

$$\sigma_E = -K \sigma(\nabla^2 z) = -K\sigma_C, \quad (\text{EQ.3.3})$$

where  $\sigma_C$  captures the spatial variability of erosion rates ( $\sigma_E$ ) such that  $\sigma_E \propto \sigma_C$ . However, when gradients are steep,  $\mathbf{q}_s$  responds nonlinearly to gradient (nonlinear slope-dependent transport) (Roering et al., 1999):

$$\mathbf{q}_s = -K\nabla z \left[ 1 - \left( \frac{|\nabla z|}{S_c} \right)^2 \right]^{-1}, \quad (\text{EQ.3.4})$$

such that  $\mathbf{q}_s$  becomes infinite as a hillslope's gradient approaches a critical gradient or threshold slope ( $S_c$ ), which is associated with the angle of repose (Roering et al., 1999). In this circumstance,  $E$  is no longer linearly related to  $C$ , showing instead greater sensitivity at higher gradients.

Despite this apparent theoretical limitation on steeper slopes, recent studies have highlighted surface roughness as a promising metric to empirically measure and characterise landscape form. It shows consistent relationships to erosion rates and processes in landscapes where diffusional processes act. While evaluating catchment-wide soil thicknesses, Patton et al., (2018) found that across diverse sites, catchments with broad  $C$  distributions (high surface roughness), relate to a general increase in catchment  $E$ , soil thickness variability and sediment transport styles (i.e., soil creep to landslides), even when landscapes are steep and suggest nonlinear transport (EQ.3.1 or EQ.3.4). Moreover, it has been observed on landslide deposits, that changes in surface roughness can be used to define landform ages and this evolution is best described through nonlinear sediment transport (Booth et al., 2017; LaHusen et al., 2020). Combined, the results of these studies and others (e.g., Korzeniowska et al., 2018; Berti et al., 2013), suggest that surface roughness is an essential morphometric tool to measure and define a landscape's stage of geomorphic evolution. I hypothesise surface roughness ( $\sigma_C$ ) to have enhanced utility in the CSM where transport is purely diffusional (juvenile through



old-age stages) because of the linear relationship between E and C, except where slopes approach the angle of repose, which only comprises <2% of the CSM's total land area, see Figure 3.4.

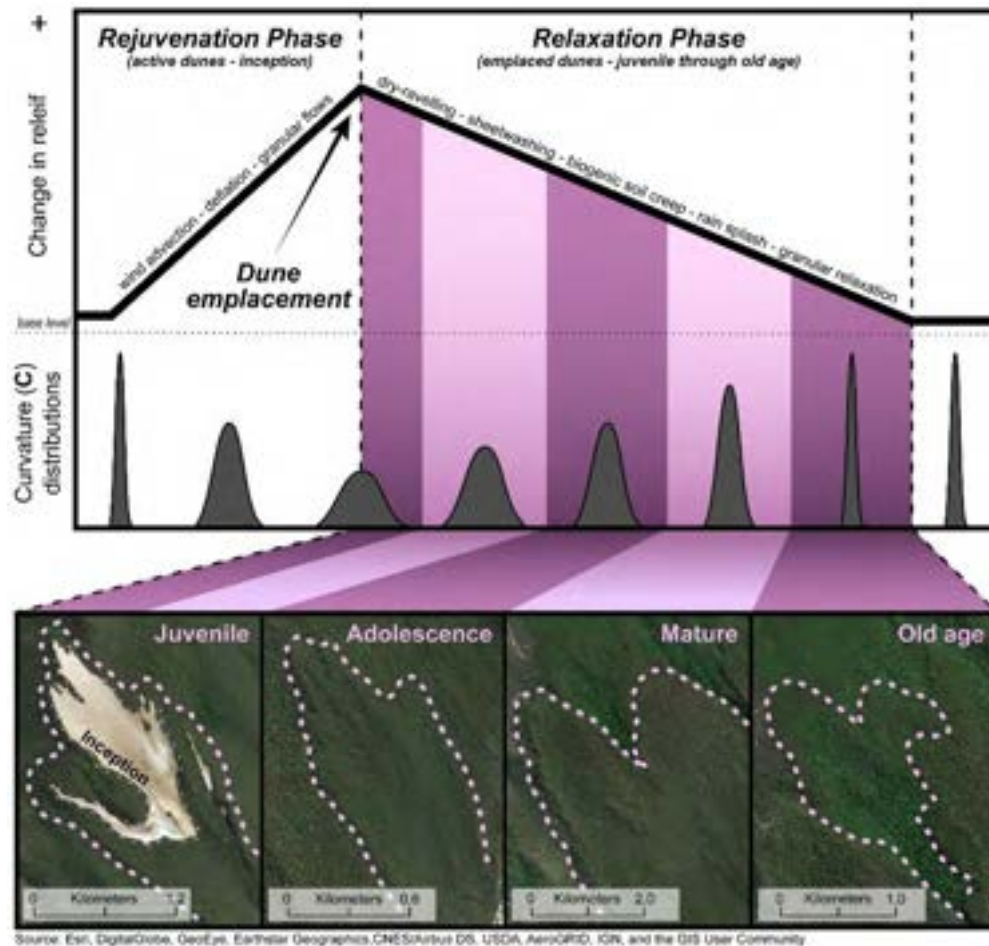


**Figure 3.4:** Conceptual diagram (summarises hypotheses and main findings) inspired by Montgomery (2001). The relationship between change in elevation from base level, dominant transport styles, and curvature ( $C$ ) distributions ( $\sigma_C$ ) for a dune landscape with time is shown. The dunes found at the CSM are initially smooth (low  $\sigma_C$  and narrow  $C$  distributions) when they are actively migrating across the landscape (dune inception). As the dunes begin to stabilise, the competition between wind advection and vegetation stabilisation, results in an increase in topographic variability, broadening the  $C$  distribution (greater  $\sigma_C$ ) and thus increasing erosion rates. This positive change in  $\sigma_C$  represents a phase of landscape rejuvenation. Surface roughness reaches their highest values once dunes are fully stabilised (dune emplacement) and sediment transport is limited to hillslope processes, thus marking the relaxation phase (juvenile through old age stages). The lowering of crest and filling of hollows narrows  $C$  distribution (lower  $\sigma_C$ ) thus decreasing the dune's erosion rates. Given ample time in a relaxation phase, the landscape will evolve towards senescence ( $(\partial\sigma_C)/\partial t \rightarrow 0$ ) where no local relief remains. I hypothesise that dune  $\sigma_C$  can only smooth (decrease) in the relaxation phase. Aerial images of the delineated dunes and the stage of their evolutionary development highlight these changes. Further description of dune stages can be found in Supplementary Tables A.3.1 and A.3.2.

## 3.2 Methods

### 3.2.1 Dune selection and OSL dating overview

I focus on the Holocene sections of the CSM, as mapped by Ward (2006) and *Chapter 2*. I acquired all previously published small aliquot (Ellerton et al., 2020) and single grain (Walker et al., 2018) Optically Stimulated Luminescence (OSL) ages from emplaced Holocene dunes within the CSM (juvenile through mature dunes). Dates represent the time of dune emplacement and consequently the initiation of dune relaxation. I choose to select ages either from dune apices or along the crest of the trailing ridges to ensure primary aeolian deposition. If dunes have multiple ages, I preferentially select dates obtained at dune crests and from stratigraphically lower positions. In total, 15 dunes met my criteria and were utilised to produce the age-roughness relationship, see Supplementary Tables A.3.1.

### 3.2.2 Dune delineation

I use high-resolution elevation data, satellite imagery and a series of field campaigns to identify and validate my mapping efforts. Principally, I used publicly available 1 m resolution digital elevation model (DEM) derived from Light Detection and Ranging (LiDAR) (2011 Queensland LiDAR data) and Orthophoto imagery (1:5000) acquired through Queensland Globe. Dated dunes are individually defined as polygons in ArcMAP and delineated at the base of crests and trailing arms. Each dune was allocated into a geomorphic stage according to definitions given in Supplementary Table A.3.2. A more detailed explanation of the mapping procedures can be found in *Chapter 2*.

### 3.2.3 Foot-slope excavation and depositional characterisation

I utilise depositional foot-slope positions from parabolic dunes ranging in age and surface roughness ( $\sigma_c$ ) to evaluate and characterise records of sediment transport and erosion. Sites are selected with similar aspects and hillslope lengths (parallel to contemporary sediment transport direction). At each site, I identify and record depositional and erosional features (scarps, lobes, burrows, pits and mounds) to help infer active sediment transport styles (landsliding, sheetwashing, biogenic soil creep, etc.). Soil profiles (1 m by 2 m) are excavated to a depth >1.75 m and described using standard field protocols (i.e., grain size, sorting, roundness, bedding structures, Munsell colour and texture).

### 3.2.4 Selection of topographic indices

In this chapter, I have evaluated the application of common morphometric variables such as elevation, slope, and curvature for all delineated dunes. Ultimately curvature ( $C$ ), and more specifically the standard deviation of curvature ( $\sigma_C$ ), as a measurement of surface roughness was chosen for the study for four main reasons:

1) Curvature governs the convergence and divergence of sediment transport hence influences water flow paths (Bogaart and Troch, 2006), nutrient redistribution (Ritchie et al., 2007; Patton et al., 2019b), and soil characteristics (Minasny and McBratney, 2016). These consequently affect landscape evolution. In particular,  $C$  has been used as a surrogate for mobile soil (regolith) thickness (Dietrich et al., 1995; Catani et al., 2010; Patton et al., 2018) and in the derivation of soil production functions and erosion rates (Heimsath et al., 1997; Hurst et al., 2012; Gabet et al., 2021; Struble and Roering, 2021). This makes  $C$  a logical candidate to describe landscape evolution.

2)  $C$  and  $\sigma_C$  normalise for antecedent topography on which dunes were emplaced and allow me to compare dunes of varying ages across the whole dune field. Curvature is the spatial rate of change of gradient from a fixed position in all directions and hence is insensitive to gradient biases introduced by broad-scale topography. Despite initial similarity in most respects, antecedent topography plays a role in controlling initial slope conditions. Dunes that have advanced over a flat plain have internal basins with different (lower) slopes than those that have advanced through previously emplaced dune sequences (Figures 3.2 and 3.3). A desirable feature of  $C$  is that all landforms' curvature distributions are centered at zero (Patton et al., 2018), which makes it possible to make straightforward comparisons between dunes'  $\sigma_C$  values.

3)  $\sigma_C$  follows Hani et al.'s (2011) recommendations for ideal morphometric variables. In short,  $\sigma_C$  provides unique values that are independent of rotations or translations, discriminates between varying surfaces (i.e., amplitudes, frequencies, and correlations), describes innate properties of the landscape surfaces, represents local (not global) measurements, are physically meaningful, and easy to derive.

4) More complex methods have been used to describe topographic variability (e.g., root mean squared-based models, two dimensional variograms, and wavelet lifting schemes);

however, the difference between each method's outcome is likely insignificant and largely site specific, see Berti et al., (2013) for a discussion on this.

### 3.2.5 Calculation of curvature and surface roughness

Curvature (C) was calculated using the equation derived from Zevenberger and Thorne (1987) and Moore et al., (1991) in ArcGIS (version 10.8.1) spatial analysis tools. This calculation utilises a 3 by 3 matrix around a central node ( $z_5$ ) (Supplementary Figure A.3.2) and fits a surface ( $z$ ) to the surrounding nine nodes using a moving window:

$$z = Ax^2y^2 + Bx^2y + Cxy^2 + Dx^2 + Ey^2 + Fxy + Gx + Hy + I, \quad (\text{EQ.3.5})$$

where the nine coefficients (A through I) are:

$$A = [(z_1 + z_3 + z_7 + z_9) \div 4 - (z_2 + z_4 + z_6 + z_8) \div 2 + z_5] \div L^4 \quad (\text{EQ.3.5a})$$

$$B = [(z_1 + z_3 - z_7 - z_9) \div 4 - (z_2 - z_8) \div 2] \div L^3 \quad (\text{EQ.3.5b})$$

$$C = [(-z_1 + z_3 - z_7 + z_9) \div 4 + (z_4 - z_6) \div 2] \div L^3 \quad (\text{EQ.3.5c})$$

$$D = [(z_4 + z_6) \div 2 - z_5] \div L^2 \quad (\text{EQ.3.5d})$$

$$E = [(z_2 + z_8) \div 2 - z_5] \div L^2 \quad (\text{EQ.3.5e})$$

$$F = (-z_1 + z_3 + z_7 - z_9) \div 4L^2 \quad (\text{EQ.3.5f})$$

$$G = (-z_4 + z_6) \div 2L \quad (\text{EQ.3.5g})$$

$$H = (z_2 - z_8) \div 2L \quad (\text{EQ.3.5h})$$

$$I = z_5 \quad (\text{EQ.3.5i})$$

Curvature is calculated from the above equations:

$$\nabla^2 z = C = 2(D + E). \quad (\text{EQ.3.6})$$

The original equation by Zevenberger and Thorne (1987) and Moore et al., (1991) differentiates the slope in percent rather than the actual gradient, and reverses the sign, so to compute curvature values in units  $1 \text{ m}^{-1}$ ; I removed -100 from their equation. This makes positive values represent concavity (hollows) and negative values represent convexity (ridges/crest).

I elected to resample the original DEM using bilinear interpolation to a 5 m resolution to dampen topographic noise, removing DEM artefacts, decrease roughness associated with dense vegetation (Berti et al., 2013; *Chapter 2*), and to help place the curvature values in the context of previous work (Patton et al., 2018). Surface roughness ( $\sigma_c$ ) was determined by calculating the standard deviation of C for the defined polygon of each dune. All areas

presently undergoing active local reactivation, recently disturbed (e.g., streets, mines, and buildings), and/or currently water affected (e.g., lakes and swamps) were removed and not included within my statistical analysis. Note,  $C$  and  $\sigma_C$  are extremely sensitive to the quality of the original elevation model or changes to boundary conditions (i.e., extent of the DEM and/or shape and size which statistics are calculated), methodology, and/or processes. Minor variability in absolute values may occur; however, overall trends remain consistent.

### 3.2.6 Two-dimensional dune evolution models

I utilised two-dimensional (2-D) sediment transport models to provide a general explanation of landscape evolution for the dune field and to examine the ability of surface roughness ( $\sigma_C$ ) to change with time. I applied the 5 m DEM from the CSM and ran linear and nonlinear landscape evolution with  $K$  values (spanning from  $0.001 \text{ m}^2 \text{ yr}^{-1}$  to  $0.100 \text{ m}^2 \text{ yr}^{-1}$  covering a range of previously reported values (Hurst et al., 2013)) for a model time of 10 ka.

The linear simulated land surface evolved by solving EQ.3.2, using a forward finite difference scheme with yearly time steps. At each time step,  $C$  and  $E$  were calculated and  $E$  was then multiplied by the time step to compute land surface lowering (erosion) or rise (deposition). For nonlinear evolution, I utilised a 2-D model from Booth et al., (2017) which uses EQ.3.4. Similar to the linear model, I make multiple simulations with different parameterisations of the physical properties of the dune sands. I used a selected  $S_C$  value of  $0.65 \text{ m m}^{-1}$  to represent the angle of repose of the original dune material. I performed simulations and calculated  $\sigma_C$  and the standard deviation of  $E$  ( $\sigma_E$ ) for each dune every 1 ka. I selected  $K$  values and chose one (based on observed goodness of fit with all of the measured dune  $\sigma_C$ ). Note, simulated dune evolution is utilised to produce general age-roughness relationships, such that  $(\partial\sigma_C)/\partial t \propto \sigma_C$  and modelled  $\sigma_E \propto \sigma_C$  can be evaluated.

## 3.3 Result

Four ( $n=4$ ) depositional soil profiles at the base of  $<70 \text{ m}$  hillslopes were excavated from dunes ranging in  $\sigma_C$  (from  $0.046$  to  $0.016 \text{ m}^{-1}$ ) and ages (from  $0.44$  to  $9.82 \text{ ka}$ ) to  $>1.75 \text{ m}$  in depth, Figure 3.5 and Supplementary Table A.3.1. All sites contain evidence of slow, continuous sediment transport (burrows, pit and mounds, and root growth and decay); whereas, only the youngest dune displayed evidence of episodic sediment transport with a

0.1 m sheetwash deposit from a recent fire event. All soil profiles have abundant charcoal records with the highest concentrations near the surface. The oldest two sites (4.89 ka and 9.82 ka) have charcoal evenly disseminated through the full excavated profile. In contrast, the 2.14 ka site has disseminated charcoal within the top 1.1 m; however, below this depth (marking the first thousand years of sediment deposition, Supplementary Tables A.3.3 and A.3.4) charcoal is present in distinct layers. The youngest site (0.44 ka) only contains one charcoal layer near the surface.

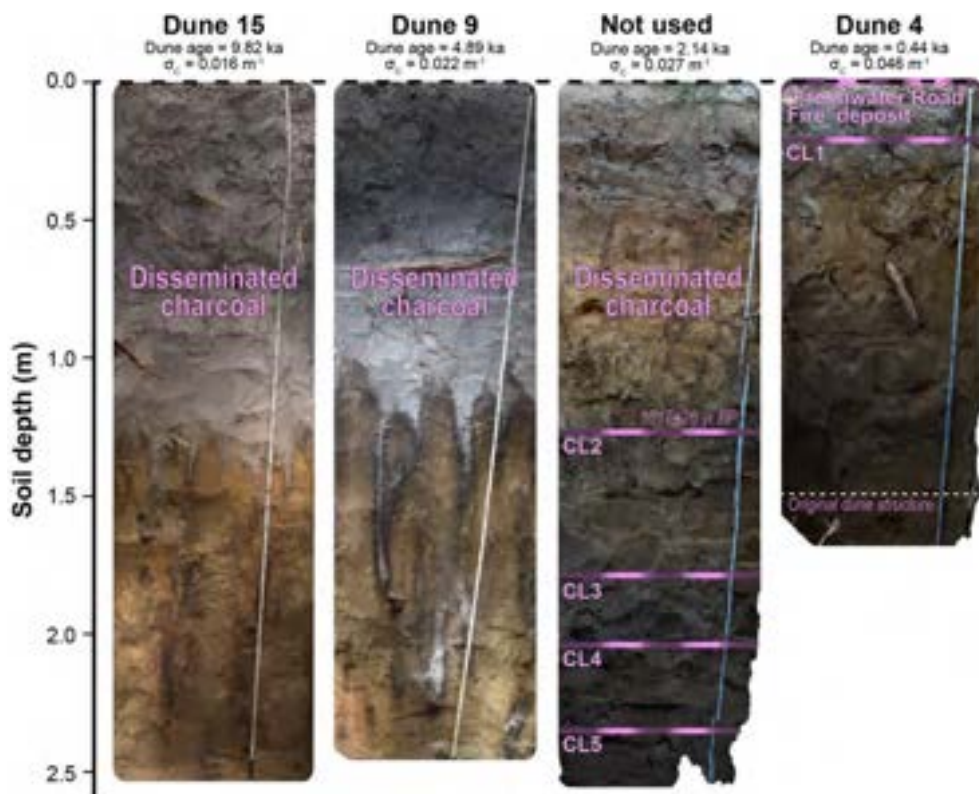


**Figure 3.5:** Excavated depositional foot-slope soil profiles used to characterise erosion and sediment transport styles. Oldest profiles display disseminated charcoal through the full profile whereas the two youngest deposits have charcoal layers. Note the 2.14 ka dune record (not used in my  $\sigma_c$ -age analysis) with disseminated charcoal near the surface that switches to stratified charcoal layers (CL#) near the base. This transition at  $\sim 1.1$  m corresponds with a depositional age of ca. 1 ka (determined by a radiocarbon age of  $1017 \pm 26$  yr BP (Wk50298) at 1.2-1.3 m, Supplementary Table A.3.4). I infer the presence of these layers are associated with fire induced episodic sediment transport (dry-ravel and sheetwash) when dunes are young and have steep slopes. As time progresses, hillslope gradients lower and charcoal layers become more diffuse and eventually become disseminated throughout the profile. These records highlight the transition between episodic to continuous sediment transport on dune evolution.

In total, 15 OSL dated dunes were used in this chapter, Supplementary Table A.3.1. All CSM dunes exhibit normal distributions of  $C$  of mean  $\sim 0 \text{ m}^{-1}$  and their surface roughness ( $\sigma_c$ ) declines by a factor of about 5 (from 0.083 to  $0.015 \text{ m}^{-1}$ ) as dunes increase in age and decrease in local relief and hillslope gradients (Figure 3.6a). The time series of  $\sigma_c$  depicts a ‘horizontal hockey stick’ with two distinct phases: 1) an initial rapid decay within the first thousand years after dune emplacement; 2) transitioning to a phase of gradual decline between a  $\sigma_c$  of  $0.035$ – $0.045 \text{ m}^{-1}$  (Figure 3.6b). I define this measured  $\sigma_c$  interval as the ‘transitional zone’ where the presence of episodic sediment transport is no longer observed as dunes increase in age (values between Dunes 4 and 5).

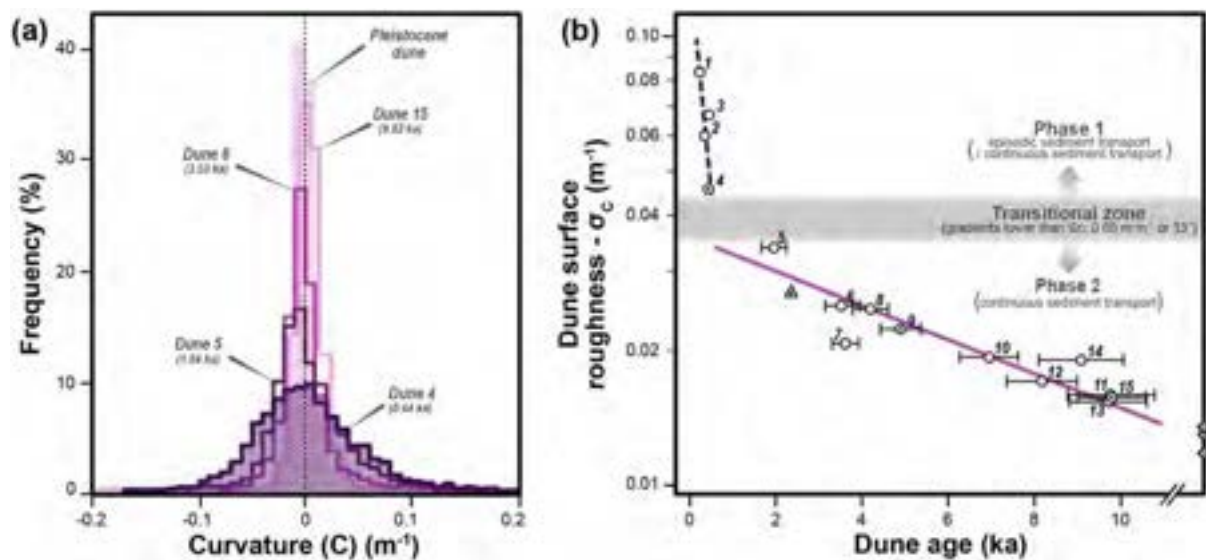


**Figure 3.6:** Measuring landscapes evolution through time at the CSM. **(a)** Observed curvature ( $C$ ) distributions for four Holocene and one Pleistocene dune at the CSM. Note the normal distribution of  $C$  centred on planar topography ( $0 \text{ m}^{-1}$ ) and the gradual narrowing of distributions with time (dark to light frequency). **(b)** Measured dune age (with error bars,  $\pm 1\sigma$ ) with surface roughness ( $\sigma_c$ ) (white circles) and observed dominant transport styles. All dunes with excavated soil profiles are indicated with black dots. Additionally, the 2.14 ka dune with the excavated soil profile (not utilised in my topographic analyses) is represented by the white triangle. Initially, dunes are emplaced with over-steepened hillslopes at or above the critical gradient ( $S_c$ ). During this phase, there is a dominance of episodic sediment transport (dry-ravel and sheetwash ( $n=4$ )), purple dashed line. After dune's  $\sigma_c$  are lowered below a ‘transitional zone’ (at ca. 1 ka), only slow and continuous soil transport occurs (soil creep ( $n=11$ )), pink line. This behaviour continues and remains true for the Pleistocene dunes (grey diamonds, not included in this analysis).

The evolution of surface roughness ( $\sigma_c$ ) for the entire CSM is explained well by nonlinear sediment transport with a fixed  $K$  value of  $0.002 \text{ m}^2 \text{ yr}^{-1}$  and a  $S_c$  of  $0.65 \text{ m m}^{-1}$ . In

reality, simulated topography appears to be more closely represented by an initial  $K$  value of  $0.06 \text{ m}^2 \text{ yr}^{-1}$  then switching to  $0.002 \text{ m}^2 \text{ yr}^{-1}$  at the ‘transitional zone’ near ca. 1 ka (Supplementary Figures A.3.3 and A.3.4). My selected  $K$  values are comparable to other values derived from transport-limited systems and sand pile experiments (e.g., Hurst et al., 2013 and Roering et al., 2001). All simulated dune topography continues to have normally distributed  $C$  with means centred on  $\sim 0 \text{ m}^{-1}$ , and distributions that gradually narrow with time. Regardless of the transport mode (linear or nonlinear), dune  $\sigma_C$  has a positive monotonic relationship with its modelled variability of erosion rate ( $\sigma_E$ ), and this relationship continues as dunes relax (Supplementary Figure A.3.3b).

## 3.4 Discussion

### 3.4.1 Parent material controls on dune evolution

My results indicate that the measured break in topographic decay at the ‘transitional zone’ reflects a shift in dominant transport styles associated with soil transport efficiency ( $K$ ). Booth et al., (2017) observed a similar rapid decay in surface roughness within the first thousand years on landslide deposits. They suggested this phase change was likely due to higher  $K$  values during the initial emplacement linked to shifts in climate and vegetation. In the CSM, climate and vegetation are stable throughout this period, so I propose this break reflects an internal transition to a reduction of slope below the critical gradient ( $S_C$ ). In fact, this topographic adjustment has been demonstrated in sandbox experiments and modelled as the transition between episodic to continuous sediment transport processes (Roering et al., 2001). The ‘transitional zone’ value is set by the physical properties of the dune sands (i.e., surface roughness values associated with the presence or absence of gradients greater than its angle of repose) and as a result, the measured ‘transition zone’ is specific to the CSM.

The early phase of evolution of the youngest dunes, which retain steep slopes, corresponds with the period when episodic sediment transport on steeper slopes is significant (purple dashed line Figure 3.6b). When hillslope gradients are below the  $S_C$ , slow continuous soil creep prevails and a simple first order relationship of the form  $(\partial \sigma_C)/\partial t \propto \sigma_C$  is apparent (pink line Figure 3.6b). In this phase, all dune erosion rates become increasingly uniform and their evolution behaves in a linear slope dependent way (Supplementary Figure A.3.3b). These results follow my field observations that younger dunes experience a wider variety of



sediment transport styles that are both discontinuous in frequency and magnitude compared to older dunes. I infer that disturbances, such as burning or storms, switches the dunes from essentially slow, continuous sediment transport to episodic sediment transport, but these episodic styles are only manifested on the younger, steeper dunes with higher surface roughness (increased  $\sigma_c$ ) values.

### 3.4.2 Field observations and stratigraphic records

Field observations support the presence of two phases of dune evolution (Figures 3.5 and 3.7). On active dunes built above their  $S_c$ , episodic sediment transport (i.e., dry-ravelling and sheetwashing) is observed. After emplacement, episodic sediment transport continues to operate as a result of disturbance-driven events, mostly fires. Fires temporarily generate hydrophobic surface soils and increase local soil transport efficiency ( $K$ ) (Bridge and Ross, 1983), thereby promoting rapid lowering of relief. Although fires occur on dunes of all ages (Moss et al., 2013), higher erosion and flux rates caused by episodic sediment transport is limited to the first thousand years of dune development (Figure 3.6b). After the dunes' gradients are reduced below the  $S_c$ , gradual transport regimes controlled by continuous sediment transport (i.e., granular relaxation, bioturbation, and rain splash) and podsolisation is well expressed. As a result, these degraded dunes are resistant to episodic sediment transport.

A major fire event in 2019 only shows evidence of mass movement on younger dunes, initiating on over-steepened, lee slopes near dune crests. Though short-lived, the landscape was efficiently smoothed by lowering local highs and filling local lows (Jyostna and Haff, 1997) (Figure 3.7b) and within just three months, the disturbed portions of the landscape were stabilised by new vegetation growth.

These types of disturbance-driven events are recorded in depositional foot-slopes (Figure 3.5) (Roering and Gerber, 2005). Within the early stages of dune evolution, sedimentary infills are characterised by stratified layers of charcoal, associated with episodic sediment transport. As time progresses, these layers become more diffuse and eventually charcoal is disseminated through the profile due to the influence of slow, continuous sediment transport and mixing. These records of dual transport regimes are found at all

excavated foot-slope positions and demonstrate the consistency of the landscape to transition from episodic to continuous processes.

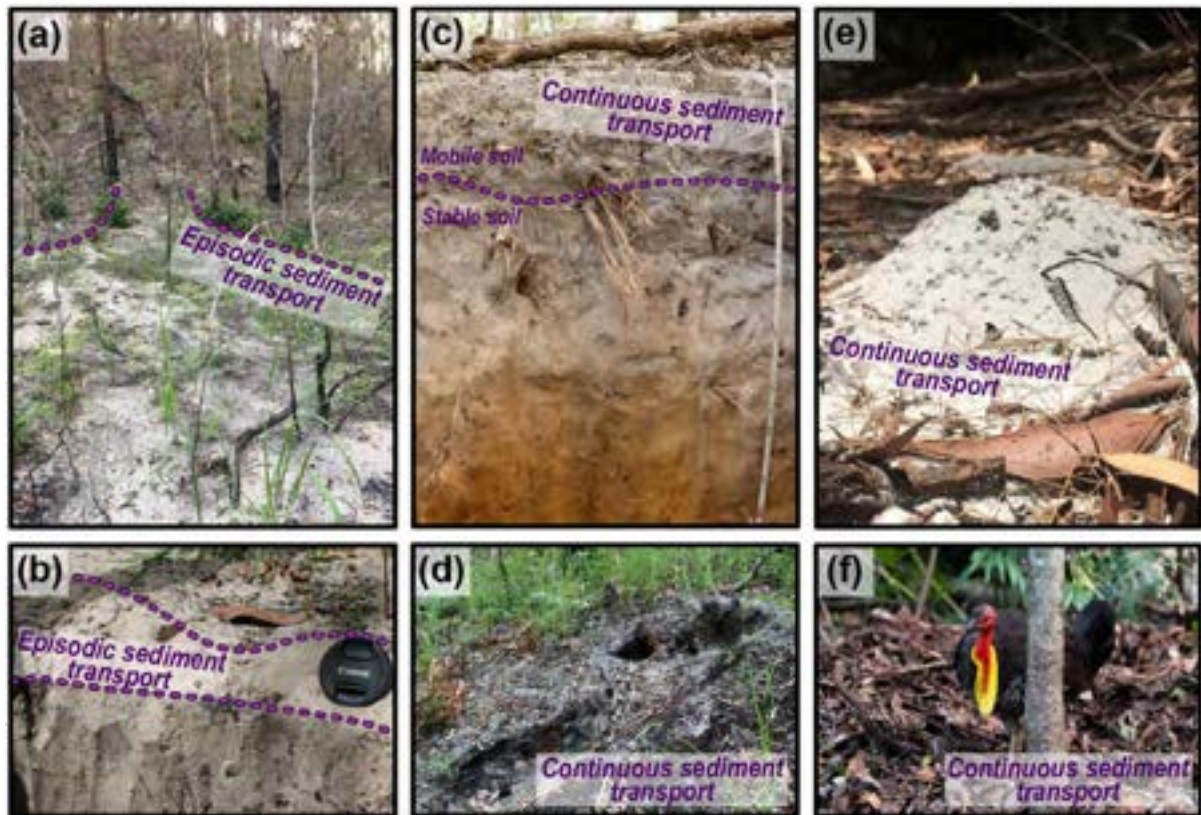


**Figure 3.7:** Field images of typical soil transport styles. Commonly observed episodic (panels (a) and (b)) and continuous (Panels (c), (d), (e), and (f)) sediment transport mechanisms at the CSM. **(a)** Fire induced sand ravel and sheetwash movement on the steep lee facing hillslope of a 0.44 ka dune shortly after fire event and its associated **(b)** deposition. **(c)** Common mid-slope soil profile on a Holocene age dune highlighting the abundance of biogenic disturbed soil near the surface in the A horizon, where it becomes increasingly stable moving down profile as shown by the intact E and B horizons. Typical perturbation includes root growth and decay, **(d)** tree throw, **(e)** burrowing invertebrates, and **(f)** bird nest construction (photo credit: (c) Patrick Adams and (f) Kegham Hovsepian).

### 3.5 Conclusions

The Holocene dunes in the Cooloola Sand Mass (CSM) provide a highly resolved space-for-time substitution where most major factors contributing to landscape evolution are known. The fidelity of the landscape to preserve dunes from inception to topographic maturity makes it possible to demonstrate how transport processes, erosion, and deposition act on topography to relax landscapes. The dominance of diffusional processes and the assumption of sediment mass balance from erosional into depositional positions is valid,

whereas this is not demonstrable in most landscapes. As a result, the dunes' topographic and stratigraphic records validate the presence of dual soil transport regimes. The early phase of dune development evolves through episodic sediment transport, which is facilitated by wildfires on over steepened gradients. Once lowered below their  $S_c$ , the later phase of continuous sediment transport processes persist. This transition is preserved as infill at all foot-slope positions and confirms that variations in sediment delivery to depositional areas are due to changes in hillslope steepness and not a shift in climate.

Adopting  $C$  as a surrogate for landscape change, I evaluate dunes'  $C$  distribution ( $\sigma_c$ ) as a measure of surface roughness and capture the CSM's full morphological evolution. When  $C$  distributions are broad (larger  $\sigma_c$  values) erosion and deposition rates reach more extreme values with a wider variety of transport styles compared to narrow distributions (smaller  $\sigma_c$  values). Once gradients are lowered below their  $S_c$  and soil creep dominates, the landscape can be numerically explained through process-based conservation of mass equations (EQ.3.1-EQ.3.3). The marked shift of  $\sigma_c$  coinciding with the transition between episodic to continuous sediment transport processes provides evidence that evaluating  $\sigma_c$  with time can highlight changes in geomorphic processes and/or their rates (Patton et al., 2018). My findings reveal the complete evolution of a dune sequence and identifies these systems as an ideal natural laboratory to understand landscape change. I demonstrate that forward numerical models generate outcomes that closely parallel the evolution of the CSM. The physical properties of the original dune material are the primary control on how the dune evolves and the  $\sigma_c$  value associated with the 'transitional zone'. Consequently, my observations validate landscape evolution inferences from sandbox modelling (e.g., Roering et al., 2001) and supports the coupling between granular material physics and landscape change (e.g., Deshpande et al., 2021).

## Chapter 4.

### Using calibrated surface roughness dating to estimate coastal dune ages at K'gari (Fraser Island) and the Cooloola Sand Mass, Australia

*This chapter has been modified from the original manuscript published in Earth Surface Processes and Landforms*

Patton, N. R., Shulmeister, J., Rittenour, T., Ellerton, D., Almond, P., & Santini, T. (2022b). Using calibrated surface roughness dating to estimate coastal dune ages at K'gari (Fraser Island) and the Cooloola Sand Mass, Australia. *Earth Surface Processes and Landforms*, 47(10), 2455-2470. <https://doi.org/10.1002/esp.5387>

**Preface:** This chapter is largely a methodological case study of roughness-age modelling on the SE Queensland dune fields, Australia. In this chapter, I utilise the theoretical findings in *Chapter 3* and develop a surface roughness ( $\sigma_c$ )-age model from Holocene dated dunes on the CSM and validated its utility on K'gari (Fraser Island). Using surface roughness from each dune, I am able to estimate dune age and uncertainty for every dune in the dune field. The model output highlights interesting spatial and temporal patterns of dune emplacement. This chapter answers the long-lasting debate on the dominant processes controlling dune activity and emplacement between sea-level and climate variability. Additionally, the results provides more supporting evidence for the use of the mapping technique in *Chapter 2* and field evidence of the mechanisms controlling dune field evolution stated in *Chapter 3*.

N. R. Patton<sup>1,2</sup>, J. Shulmeister<sup>1,2</sup>, T. M. Rittenour<sup>3</sup>, P. Almond<sup>4</sup>, D. Ellerton<sup>5</sup> and T. Santini<sup>6</sup>

<sup>1</sup>School of Earth and Environment, University of Canterbury, Christchurch, New Zealand

<sup>2</sup>School of Earth and Environmental Sciences, University of Queensland, St Lucia, Queensland, Australia

<sup>3</sup>Department of Geology, Utah State University, Logan, Utah, United States of America

<sup>4</sup>Department of Soil and Physical Sciences, Lincoln University, Christchurch, New Zealand

<sup>5</sup>Department of Geological Sciences, Stockholm University, Stockholm, Sweden.

<sup>6</sup>School of Agriculture and Environment, The University of Western Australia, Perth, Australia

## Abstract

Here I present a novel application of landscape smoothing with time to generate a detailed chronology of a large and complex dune field. K'gari (Fraser Island) and the Cooloola Sand Mass (CSM) dune fields host thousands of emplaced (relict) and active onlapping parabolic dunes that span 800,000 years in age. While the dune fields have a dating framework, their sheer size (~1930 km<sup>2</sup>) makes high resolution dating of the entire system infeasible. Leveraging newly acquired (n=8) and previously published (n=20) optically stimulated luminescence (OSL) ages from K'gari and the CSM, I estimate the age of Holocene dunes by building a surface roughness ( $\sigma_c$ )-age relationship model. In this chapter, I define  $\sigma_c$  as the standard deviation of topographic curvature for a dune area and I demonstrate an exponential relationship ( $r^2 = 0.942$ , RMSE = 0.892 ka) between  $\sigma_c$  and timing of dune emplacement on the CSM. This relationship is validated using ages from K'gari. I calculate  $\sigma_c$  utilising a 5 m digital elevation model (DEM) and apply my model to predict the ages of 726 individually delineated Holocene dunes. The timing of dune emplacement events are assessed by plotting cumulative probability density functions (PDFs) derived from both measured and predicted dune ages. I demonstrate that both dune fields had four major phases of dune emplacement peaking at ca. <0.5, 1.5, 4, and 8.5 ka. I observe that my predicted dune ages did not create or remove major events when compared to the OSL-dated sequence, but instead reinforced these patterns. My study highlights that  $\sigma_c$ -age modelling can be an easily applied relative or absolute dating tool to dune fields globally. This systematic approach can fill in chronological gaps using only high-resolution elevation data (3-20 m resolution) and a limited set of dune ages.

## 4.1 Introduction

Coastal dunes are important environmental systems that are found globally around both seas and lakes (Martinez and Psuty, 2004; Yan and Baas, 2015; Lancaster et al., 2016)

and provide a rich record of climatic, geologic and geomorphic information (e.g., Pye, 1983; Swezey, 2001; Wells and Goff, 2007; Lindhorst and Betzler, 2016; Ellerton et al., *In Press; Chapter 3*). However, uncovering and deciphering the information from these systems is challenging because they lie at the interface of terrestrial, aquatic, and atmospheric processes which vary on decadal to millennial timescales (Pye, 1983).

The timing and mechanisms of dune field activation and consequent stabilisation (dune emplacement hereafter) are ascribed to changes in climate and sediment supply, which affect vegetation, storminess, fire frequency, sea-surface temperatures and sea-level (e.g., Yan and Baas, 2017; Shumack and Hesse, 2018; Han et al., 2021; Vimpere et al., 2021). These interpretations have largely been demonstrated on active and/or recently emplaced sections of dune fields where physical measurements or repeat aerial/satellite imagery are available (e.g., Tsoar, 2005; Marín et al., 2005; Levin et al., 2017). These mechanisms have been extended to emplaced dune systems; however, the direct landscape-process relationship is unknown, and it is difficult to infer these processes unless a strong chronological framework is established.

Coastal dune fields' temporal relationships appear chaotic, and it is difficult to determine whether emplaced dunes were once active simultaneously or asynchronously across the dune field. Stochastic (random) dune activity can be indicative of local perturbations but not related to regional changes in environmental conditions because dunes can simultaneously be active and emplace under the same conditions (Yizhaq et al., 2007). In contrast mass activation or emplacement of entire dune fields may provide clues about regional environmental forcings (e.g., Lees, 2006). While the direct dating of dunes can be achieved using optically stimulated luminescence (OSL) and/or radiocarbon dating, these techniques are costly and finding suitable dating targets for radiocarbon is often challenging. To offset these limitations, it is common to either establish geobotanical chronosequences (morphological, biological, or pedological units) (e.g., Thompson, 1981; Shulmeister and Lees, 1992), or to date organic rich sediments in adjacent deposits as a means to help place the dunes into a chronosequence (e.g., Wilson, 2002). In both scenarios, these estimates often have large spatial and temporal uncertainty, even in locations where there are clear sequences of overlapping dunes (e.g., Lees, 2006; Swezey, 2001). Consequently, dune sequences that are composed of tens or even thousands of individual dunes are typically

secured by only a handful of ages with wide age constraints that can lead to misinterpretations (e.g., Ward, 2006).

To validate age inferences, and hence improve our understanding of former dune activation and stabilisation, a means of extending dune ages to all (or most) dunes within a dune field would be a useful tool. In this chapter, I explore the implications of *Chapter 3's* observed relationship between dune surface roughness ( $\sigma_c$ ) and dune age to explain landscape smoothing with time. I test whether this provides a basis for dating dunes where high-resolution elevation data and a rough geochronological framework are in place.

## 4.2 Background

### 4.2.1 Surface roughness ( $\sigma_c$ ) as a proxy for landform

In most aeolian research, surface roughness characterises the near-surface meteorological boundary layer over dunes as a means to understand airflow and sediment transport (e.g., Gillette and Stockton, 1989; Raupach et al., 1993; Wiggs et al., 1996; Lancaster and Baas, 1998; Levin et al., 2008; Jerolmack et al., 2012; Pelletier, 2013). For this study, surface roughness ( $\sigma_c$ ) is used to measure and define a dune's topographic development (colluvial not aeolian processes). Surface roughness ( $\sigma_c$ ) has been defined as a metric of topographic variability (local relief) within a defined spatial area or window (e.g., Korzeniowska et al., 2018). Its application has been utilised across earth science disciplines as a metric to identify and map spatial patterns and as a surrogate to build empirical relationships (Smith, 2014). An important application of  $\sigma_c$  is its utility as a proxy for relative age. This relationship has been predominantly applied to constrain the timing of landslide deposition (e.g., McKean and Roering, 2004; Glenn et al., 2006; Booth et al., 2009; 2017; Bell et al., 2012; Goetz et al., 2014; LaHusen et al., 2020), but has also been used on alluvial fans (Frankel and Dolan, 2007), earth flows (Schanz and Colee, 2021), and planetary surfaces (Pommerol et al., 2012).

Surface roughness ( $\sigma_c$ ) gradually smooths due to diffusive processes of sediment transport (Booth et al., 2017; *Chapter 3*). The basic principle is that local relief reduces with time due to weathering and erosion such that features smooth (ridges erode and valleys fill) on surfaces that are not affected by advective processes (e.g., sediment transport by water-driven processes). LaHusen et al. (2020) utilised this principle to build a  $\sigma_c$ -age relationship

from a minimal set of dated landslide deposits and predicted ~10,000 ages in the Pacific Northwest, USA. The utility of this model was not only that ages could be predicted, but more particularly that previously undated landforms could be placed into the context of regional records of climate and landscape change. Consequently, they determined that rainfall, not earthquake activity, was the major driver of landslide activation inland of the Cascadia Subduction Zone.

#### 4.2.2 Surface roughness ( $\sigma_c$ ) in dune systems

Surface roughness ( $\sigma_c$ ) has been used to map dune landforms (e.g., Korzeniowska et al., 2018); however, the application of  $\sigma_c$  as an indicator of landform age ( $\sigma_c$ -age relationship) has not yet been applied and tested in a dune system. *Chapter 3* highlighted the utility of  $\sigma_c$  within the Cooloola Sand Mass (CSM) dune field as an important metric and to characterise and define the stage of geomorphologic development of dune forms. I demonstrated that dune  $\sigma_c$ , as measured by standard deviation of curvature for a given dune area, could be related to sediment transport theory. I found that dunes are initially emplaced with remarkably uniform surface roughness ( $\sigma_c$ ) that smooths with time and this evolution can be simulated using nonlinear and linear sediment transport models (Figure 4.1).



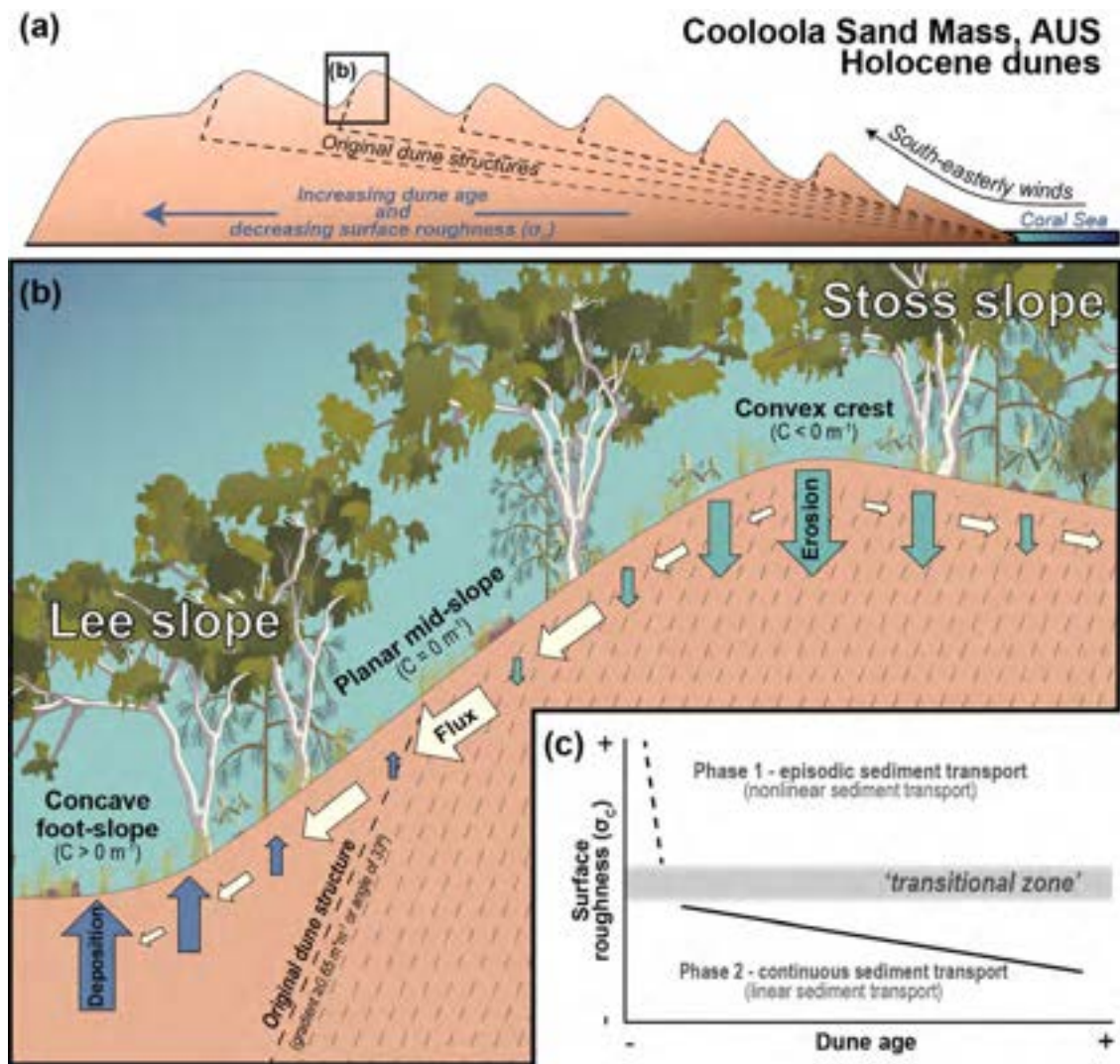


**Figure 4.1:** Conceptual diagram and result summary from *Chapter 3* between surface roughness ( $\sigma_c$ ) and dune age within the CSM dune field, Australia. **(a)** An idealised elevation profile of the CSM dune field. The dunes move inland from the coast through sclerophyll forest and over antecedent topography (dashed lines) via the dominant south-easterly wind. Dunes are emplaced when wind speeds decrease, and vegetation stabilises the dune surface. With every successive dune emplacement, antecedent topography gradients generally increase, thereby decreasing the distance dunes travel inland whilst preserving older dunes. Consequently, most dunes increase in age while decreasing in  $\sigma_c$  moving away from the coast. **(b)** Conceptual diagram of hillslope positions as defined by curvature ( $C$ ) and the contribution of erosion, deposition and flux (size of arrow). All sediment removed from crest can be accounted for in the foot-slopes (a closed system). As time progresses ridges lower and hollows fill, reducing hillslope gradients and the maximum and minimum curvature values thus decreasing dune  $\sigma_c$ . **(c)** The general relationship between dune age, surface roughness ( $\sigma_c$ ), and sediment transport phases. Dunes with high  $\sigma_c$  (Phase 1) are best explained through non-linear sediment transport where episodic processes such as dry-ravelling and sheetwashing (comparable to grain flows and/or avalanching) occur. Once dune gradients are lowered below their angle of repose (gradient of  $0.65 \text{ m m}^{-1}$  or angle of  $33^\circ$ ) associated with the defined 'transitional zone', sediment transport is limited to slow and continuous processes (Phase 2) where their evolution can be explained with linear sediment transport.

In *Chapter 3*, I determined that dunes evolve in two distinct phases (Figure 4.1c). The first phase occurs within ca. 1 ka after dune emplacement and is explained through nonlinear sediment transport. This is a period when dune gradients and  $\sigma_c$  is large, erosion and deposition rates are more rapid, and there is a wider variety of transport styles. During this initial period, dune-surface gradients are lowered as a result of disturbance-driven perturbations such as fires and storms. These disturbances may remove vegetation, increase hydrophobicity and consequently increase the soil's efficiency to move downslope, promoting dry-ravel and sheetwash processes (similar to avalanching and grain flows observed on active dune slip-faces). This phase continues until dune relief is lowered and  $\sigma_c$  values reach the 'transitional zone', as seen in Figure 4.1c. This zone was defined by an observed shift in dominant transport style and the absence of gradient greater than the sands' angle of repose ( $33^\circ$  or gradients of  $0.65 \text{ m m}^{-1}$ ). Once gradients are lowered beyond this zone, the second phase of dune evolution begins; wherein sediment transport is proportional to hillslope gradient (linear sediment transport). During this period, dune  $\sigma_c$  is small and sediment transport is limited to slow and continuous processes (e.g., biogenic soil creep, rain-splash, and granular relaxation) where erosion occurs at the dune crests and sediment is deposited within the adjacent foot-slopes (Figure 4.1b). This mechanism is inferred to continue until all relief is either removed or increased due to dune activation or sea-level fall.

In *Chapter 3*, I alluded to an apparent exponential relationship between dune  $\sigma_c$  and age; however, I chose not to prescribe a single function to explain the dune field's evolution. Instead, I retain the two distinct erosional phases to ensure sediment transport processes were not conflated. Despite this decision, I argued that because the dune fields have limited hillslopes that exceed the angle of repose and a dominance of linear sediment transport dune  $\sigma_c$  will smooth with time and ascribing a single exponential fit is appropriate.

The goal of this chapter is to test and, if appropriate, apply surface roughness ( $\sigma_c$ )-age modelling to a pair of adjacent coastal dune fields, the CSM and K'gari (Fraser Island) in SE Queensland. These large and once connected systems are dominated by active and emplaced parabolic dunes. At the CSM many of these dunes have been dated and the younger parabolic sequences span the mid- to late-Holocene. Once emplaced, the evolution of the dunes (erosion and deposition) is controlled by a limited set of known diffusional processes that are morphologically trackable through time. I first establish a  $\sigma_c$ -age relationship on the CSM and test its validity on K'gari. If the model proves to be successful for the dated dunes, I will utilise

it to estimate ages of the remaining Holocene-age dunes in both dune fields. Although my study focuses specifically on two locations, the research provides insights on the evolution of onlapping coastal dune systems and a means to produce a more complete chronological framework for multi-phase dune fields globally.

#### 4.2.3 Site description: Cooloola Sand Mass and K'gari

The SE Queensland dune fields in Australia (Figure 4.2) are composed of K'gari (aka Fraser Island), and the mainland-attached Cooloola Sand Mass (CSM) immediately to the south. The dune fields have been developing for over 800 kyr (Walker et al., 2018; Ellerton et al., 2020). These dune systems are currently separated by the entrance to the Great Sandy Strait and the Inskip Peninsula, but recent work (Köhler et al., 2021) has demonstrated that this separation dates back only to the early mid-Holocene. Stretching for more than 200 km of coastline (26.17°S to 24.41°S), these two systems cover a combined land area of ~1930 km<sup>2</sup>, with most of the dune fields on K'gari. They contain one of the longest and most complete coastal dune field sequences in the world (Thompson, 1981) and include over 700 Holocene dunes (Ward, 2006; *Chapter 2*) covering roughly 640 km<sup>2</sup>, which are the focus of this chapter.

Both dune fields have nearly limitless sediment supply with an estimated 500,000 m<sup>3</sup> of sediment transported yearly along the regional longshore drift system (Patterson and Patterson, 1983; Boyd et al., 2008). The parent material is a uniform 98% medium to fine quartz sand (180-250 µm) that is well-sorted and sub-rounded to rounded (Thompson, 1992). The majority of onlapping dunes are parabolic with local transgressive dune waves, which travel inland under the influence of the dominant south-easterly winds (Coaldrake, 1962; Ellerton et al., 2018). The region has been tectonically inactive (Roy and Thom, 1981) with only minor variability in local base-level, between +2 to -0.5 m since the Holocene sea-level highstand (Lewis et al., 2008). The vegetation communities have been relatively stable (e.g., Moss et al., 2013; Atahan et al., 2015) with tall open/close sclerophyll forest making up the majority of the inland vegetation and coastal scrubland dominating the eastern side of the dune fields (Harrold et al., 1987). Additionally, the climate has remained sub-tropical (Cfa) during this period (Donders et al., 2006).



**Figure 4.2:** (a) Satellite imagery of K'gari (Fraser Island), and the CSM, which make up the northern section of the SE Queensland dune field in Australia. The dune sediments are derived from the longshore drift system (dashed line and arrow) that is delivered to the coast by the dominant south-easterly winds (small arrows). (b) Close-up imagery of the coastline and dunes on K'gari (photo credit: Jürgen Wallstabe).

## 4.3 Methods

### 4.3.1 Dune mapping and remote sensing

In this chapter, I individually remap the Holocene and modern dunes for both the K'gari and the CSM first identified in *Chapter 2*. Dunes were identified using a 1 m resolution digital elevation model (DEM) derived from Light Detection and Ranging (LiDAR) (publically available from Geoscience Australia; Fraser Coastal Project), 1:5000 orthophoto imagery retrieved from Queensland Globe, and field observations. Each dune was delineated by hand in ArcGIS (version 10.6) at the base of slip-faces and trailing arms and defined as polygons.

### 4.3.2 Calculating surface roughness ( $\sigma_c$ )

Surface roughness ( $\sigma_c$ ) is calculated by determining the standard deviation of curvature ( $C$ ) for each mapped dune area, defined by a map polygon. This calculation of  $\sigma_c$  is utilised because  $C$  distributions are centred at zero (Patton et al., 2018) making it possible to compare dunes without biases introduced by broad-scale topography (e.g., variations in initial

morphology caused from the antecedent topography) (*Chapter 3*). Curvature was generated in ArcMap, which utilises equations from Zevenberger and Thorne (1987) and Moore et al. (1991), that calculate curvature from the slope in percent and reverses the sign (negative curvature convention). Therefore, I divide ArcMap's curvature output by -100 such that positive values represent concavity (hollows/foot-slopes), and negative values represent convexity (ridges/crest), see *Chapter 3* and Supplementary Figure A.3.2 for more detail. It is important to highlight that  $\sigma_c$  values are sensitive to methodology and boundary conditions and/or processes. Minor variabilities in  $\sigma_c$  values may occur but overall trends remain consistent.

Prior to the  $\sigma_c$  calculation, I chose to resample the original DEM using bilinear interpolation to a 5 m resolution. The reduction of resolution dampened noise and lowered elevation uncertainty by removing DEM processing artefacts and vegetation effects (Berti et al., 2013) while preserving dune morphology (*Chapter 3*). My assumption in calibrating a  $\sigma_c$ -age relationship was that dune  $\sigma_c$  values monotonically decline with dune age. Hence, I limited my areas of calibration and application to where diffusive processes and not advective processes (e.g., wind and fluvial transport which can increase relief and roughness) prevailed. Additionally, all water (water bodies, bogs, coastal cliffs, etc.) and/or anthropogenic modifications (roads, build-up areas, mining, etc.) were also excluded. Once removed, the 'zonal statistics' tool in ArcMap was used to determine  $\sigma_c$ .

### 4.3.3 Optically stimulated luminescence (OSL) dating

Optically stimulated luminescence (OSL) dating provides an age estimate of the time since quartz grains were last exposed to sunlight (burial) (Huntley et al., 1985); therefore, OSL dates represent timing of dune emplacement (Lancaster, 2008). For each dune, OSL samples were collected at dune crests utilising a sand auger with a 15 cm bucket. Dune stratigraphy was described using standard field protocols (i.e., grain size, sorting, roundness, bedding structures, Munsell colour and texture). An OSL sampling head was attached with an aluminium insert and once the sample was recovered, the tube was capped, sealed and stored for later analysis. Dose-rate and moisture content samples were collected from the auger samples above and below the OSL sample depth. Eight ( $n=8$ ) samples were collected, dating six dunes ( $n=6$ ). On two dunes, I collected multiple OSL samples to increase confidence in

measured ages and field interpretations. One dune had samples from the same auger hole and is believed to be equivalent in age. The other dune had samples collected on separate parallel ridges on a transgressive wave, and these ages may slightly vary. These ages are used to supplement those previously collected and reported in (Walker et al., 2018; Ellerton et al., 2020; Köhler et al., 2021).

All OSL samples were processed and analysed at the Utah State University Luminescence Laboratory. Ages were determined utilising single-aliquot regenerative dose (SAR) analysis of small aliquots of quartz sand (Murray and Wintle, 2000; Murray et al., 2021). Samples were analysed using small aliquot (~10 grain) analysis to reduce scatter caused by grain-to-grain variability in dose rate (micro-dosimetry) (e.g., Guérin et al., 2015; Ellerton et al., 2020). Sample preparation followed standard luminescence protocols (i.e., Wintle, 1997).

All dose rates were determined using representative sub-samples that were analysed using ICP-MS and ICP-AES techniques to determine the concentrations of the K, Rb, Th, and U in the sediment. Moisture content (*in-situ*) was calculated for all samples. If the measured value was below 5%, I assumed a value of  $5 \pm 2\%$  which represents the average moisture history (Ellerton et al., 2020). Dose rates are determined from sediment chemistry, cosmic ray contribution, and water content (Aitken and Xie, 1990; Aitken, 1998) using conversion factors from Guérin et al. (2011). The contribution of cosmic radiation to the dose rate was calculated using sample depth, elevation, and latitude/longitude following the calculations of Prescott and Hutton (1994).

Optical measurements were performed on small-aliquot (1 mm diameter, ~10 grains per disk) samples using Risø TL/OSL Model DA-20 readers with blue-green light emitting diodes (LED) ( $470 \pm 30$  nm) as the stimulation source. The luminescence signal was measured through 7.5 mm UV filters (U-340) over 40–60 s (250 channels) at 125 °C with LED diodes at 70–90% power (~45 mW/cm<sup>2</sup>) and calculated by subtracting the average of the last 5s (background signal) from the first 0.7s (4 channels) of the signal decay curve. The luminescence signals show rapid decay dominated by the fast component of the signal (Murray and Wintle, 2003). For those samples with <1 Gy equivalent dose ( $D_E$ ), dose response curves were fitted linearly between the zero dose and repeated regenerative doses. Results of a preheat-plateau dose-recovery (PP-DR) test (Wintle and Murray, 2006) suggest that a 200 °C preheat for 10 s produces the best results for samples in this study. Equivalent dose values were calculated using the Central Age Model (CAM) of Galbraith and Roberts (2012) using at

least 14 accepted aliquots of quartz sand. Aliquots were rejected if they had evidence of feldspar contamination, a recycling ratio beyond 20% of unity ( $<0.8$  or  $>1.2$ ), recuperation  $>1$  Gy, or natural  $D_E$  greater than the highest regenerative dose given. Errors on  $D_E$  and age estimates are reported at one sigma standard error and include errors related to instrument calibration, and dose rate and equivalent dose calculations and the errors were calculated in quadrature using the methods of Aitken and Alldred (1972) and Guérin et al. (2011).

#### 4.3.4 Criteria for utilising previously OSL dated dunes

I utilise the following sampling criteria for dune ages from previously published studies. 1) Dates must reflect the age of the dune surface morphology (i.e., the uppermost dune unit that forms the surface morphology was dated). 2) Dunes must be emplaced (i.e., stabilised, not active). Lastly, 3) ages must be collected from dune apices or the crest of the trailing ridges and in physically little altered (B/C, C, soil parent material) soil horizons. These criteria were set to ensure that ages represented primary aeolian deposition.

#### 4.3.5 Surface roughness ( $\sigma_c$ )-age analysis and age extrapolation

A single empirical relationship was generated using all OSL-dated dunes within the CSM. I hypothesise that both the CSM and K'gari dune fields are governed by identical mechanisms controlling dune activation and evolution because they were once part of a connected dune field (Köhler et al., 2021) and have been mapped as a part of the same dune system (Ward, 2006; *Chapter 2*). As a result, I assume the same surface roughness ( $\sigma_c$ )-age relationship can be applied at both sites.

For use in the  $\sigma_c$ -age model and validation subset, where dunes have multiple dates, I preferentially selected ages that were collected nearest to the dune crest and/or from sand with minimal pedogenic alterations (C horizon). Any ages that met my sampling criteria but were not used in the model are recorded. All OSL-dated dunes from the CSM were utilised to build the  $\sigma_c$ -age model (model set). The remaining OSL-dated dunes from the Inskip Peninsula and K'gari are used as the validation subset. I fit the  $\sigma_c$ -age data with an exponential curve given that relief lowers through diffusional processes with time (Booth et al., 2017; LaHusen et al., 2020; *Chapter 3*). I demonstrate the model output by predicting dune ages from the

validation subset and using reduced major axis regression I compare the slope of the predicted versus measured dune ages to 1.

A map of estimated dune ages is produced using my  $\sigma_c$ -age model to convert dune  $\sigma_c$  to time since dune emplacement. Mapped dune polygons are reclassified to their estimated ages. Given that the  $\sigma_c$ -age relationship is constructed from dunes that are emplaced, I do not predict ages for active sections of the dune field, but rather assigned them absolute ages of 0 ka. Active sections are identified by aerial imagery as landforms constructed with little to no vegetation and steep lee slopes with gradients greater than  $0.65 \text{ m m}^{-1}$  (slopes  $> 33^\circ$ , which is at or above the angle of repose). All areas previously removed during the calculation of  $\sigma_c$  (e.g., sections of dunes with water bodies or anthropogenic disturbances) are incorporated back into the total area to show the full extent of the dune fields and produce the final predictive age map but their surface roughness is not incorporated in the results.

#### 4.3.6 Determination of dune emplacement through time

To evaluate frequency of dune emplacement through time, I determine cumulative probability density functions (PDFs) for the CSM, K'gari, and the combined Holocene dune fields (not including active sections). I calculate separate PDFs for OSL dated and modelled dune ages with 0.05 ka bin intervals for 12 ka (240 total bins) and assume that the age estimates represent the median value with normally distributed errors. As a conservative estimate of error, I utilise a constant 10% relative standard error (RSE) for predictive age, which is frequently applied for OSL dating (Murray et al., 2021). I normalise each PDF by total number of dunes used to generate the curve. Additionally, PDFs produced from predictive ages are also normalised by dune area (dune area divided by total Holocene dune area – not including active dune area). This is to remove bias towards younger dunes caused by the preservation of numerous small, younger dunes. I visually compare PDFs and assess dune emplacement through time.

#### 4.3.7 Sensitivity analysis

I calculate  $\sigma_c$  for all map dune polygons at a range of DEM resolutions (1 - 50 m). For each resolution, a  $\sigma_c$ -age relationship is produced and its  $r^2$  and RMSE is recorded. I predict all dune ages and generate cumulative probability density functions (PDFs) utilising these



relationships and their respective DEM resolutions. I compare all PDFs to the OSL derived PDF. Although the latter does not provide a quantitative assessment of my analysis it does offer a sense of uncertainty and a foundation to examine how enhanced resolution and bin intervals may influence my interpretations.

## 4.4 Results

### 4.4.1 OSL results and previous reported OSL ages

The eight ( $n=8$ ) newly acquired OSL ages from six individual ( $n=6$ ) dunes are shown in Table 4.1 and Figure 4.3. For each sample, supporting information such as soil descriptions, geochemistry, water content, and over dispersion are found within the Supplementary Figure A.4.1 and Supplementary Tables A.4.1, and A.4.2. From previously published work, twenty ( $n=20$ ) OSL ages met my sample criteria, dating sixteen dunes ( $n=16$ ) (specifically Walker et al., 2018; Ellerton et al., 2020; Köhler et al., 2021) (Table 4.2 and Figure 4.3). All dunes with multiple ages were consistent with my expectations. Samples collected from the same auger hole indicate equivalent ages (e.g., Dune 11); whereas, samples from different locations from the same dune yielded ages that consistently increased moving towards the dune's inland limit (e.g., Dune 16 and 17). In total (newly acquired and previously published), twenty-eight ( $n=28$ ) OSL ages met my criteria dating twenty-two dunes ( $n=22$ ). All ages that met my sampling criteria but were not preferred are denoted by italicised text in Table 4.2.

**Table 4.1:** Optically Stimulated Luminescence (OSL) age results and map location.

Dune number	Map ID	Location	Depth (m)	Lab number	Number of aliquots <sup>†</sup>	Dose rate (Gy/ka) <sup>‡</sup>	Equivalent Dose ( $D_e$ ) <sup>2</sup> $\pm 2\sigma$ (Gy) <sup>§</sup>	OSL age $\pm 1\sigma$ (ka)
4	4	K'gari	1-1.13	USU-2742	20 (34)	$0.59 \pm 0.04$	$0.27 \pm 0.07$	$0.45 \pm 0.07$
5	5	K'gari	1-1.16	USU-2743	14 (35)	$0.34 \pm 0.03$	$0.16 \pm 0.06$	$0.47 \pm 0.10$
6	6	K'gari	1.97-2.24	USU-2730	16 (22)	$0.40 \pm 0.03$	$0.51 \pm 0.07$	$1.27 \pm 0.16$
11	11a	CSM	1.90-2.05	USU-3020	19 (31)	$0.56 \pm 0.04$	$1.41 \pm 0.23$	$2.51 \pm 0.32$
11	11a'	CSM	3.88-4.07	USU-3021	20 (32)	$0.62 \pm 0.04$	$1.33 \pm 0.23$	$2.14 \pm 0.27$
12	12	K'gari	4.40-4.50	USU-2397	17 (31)	$0.25 \pm 0.03$	$1.00 \pm 0.14$	$4.05 \pm 0.63$
17	17a	K'gari	3.15-3.20	USU-2390	18 (22)	$0.30 \pm 0.03$	$1.79 \pm 0.21$	$5.96 \pm 0.82$
17	17b	K'gari	3.05-3.15	USU-2389	20 (27)	$0.35 \pm 0.03$	$2.5 \pm 0.27$	$7.24 \pm 0.92$

<sup>†</sup> OSL age analysis using the single-aliquot regenerative-dose procedure of Murray and Wintle (2000) on 1-mm small-aliquots of quartz sand. Number of aliquots used in age calculation and number of aliquots analysed in parentheses.

<sup>‡</sup> See Supplementary information for radioisotope concentrations of surrounding sediment and cosmic contribution to dose rate.

<sup>§</sup> Equivalent dose ( $D_e$ ) calculated using the Central Age Model (CAM) Galbraith and Roberts (2012).

**Table 4.2:** All dunes with their locations (Figure 4.3) and ages utilised in this chapter. Note, all italicised rows are OSL ages that are not used in the surface roughness ( $\sigma_c$ )-age model and validation sets and are indicated with an 'X' in Figure 4.3.

Dune number	Map ID	Location	Latitude, longitude (°S, °E)	Surface roughness (m <sup>-1</sup> )	Model or validation set	Lab number	Mean depth (m)	OSL age $\pm 1 \sigma$ (ka)	Study
1	1	CSM	25.93, 153.18	0.0684	Model	USU-2011	7.40	0.23 $\pm$ 0.05	Ellerton et al., 2020
2	2	CSM	25.98, 153.16	0.0506	Model	USU-2010	1.50	0.43 $\pm$ 0.06	Ellerton et al., 2020
3	3	CSM	26.01, 153.13	0.0368	Model	USU-2283	2.19	0.44 $\pm$ 0.10	Ellerton et al., 2020
4	4	K'gari	25.16, 153.27	0.0465	Validation	USU-2742	1.07	0.45 $\pm$ 0.12	This study
5	5	K'gari	25.19, 153.26	0.0593	Validation	USU-2743	1.08	0.47 $\pm$ 0.18	This study
6	6	K'gari	25.60, 153.08	0.0406	Validation	USU-2730	2.20	1.27 $\pm$ 0.22	This study
7	7	CSM	26.04, 153.12	0.0275	Model	USU-2267	3.45	1.94 $\pm$ 0.28	Ellerton et al., 2020
8	8	CSM	26.04, 153.12	0.0154	Model	Map 2; Sample 2	0.80	3.6 $\pm$ 0.30	Walker et al., 2018
9	9	CSM	26.01, 153.14	0.0236	Model	USU-2265	2.15	2.37 $\pm$ 0.23	Ellerton et al., 2020
10	10	CSM	25.95, 153.16	0.0191	Model	USU-2012	3.25	3.53 $\pm$ 0.38	Ellerton et al., 2020
11	11a	CSM	26.01, 153.13	-	-	USU-3020	1.98	2.51 $\pm$ 0.32	<i>This study</i>
11	11a'	CSM	26.01, 153.13	0.0268	Model	USU-3021	4.00	2.14 $\pm$ 0.27	This study
12	12	K'gari	25.13, 153.25	0.0189	Validation	USU-2397	4.45	4.05 $\pm$ 0.80	This study
13	13	CSM	25.13, 153.25	0.0178	Model	USU-2284	3.62	4.89 $\pm$ 0.45	Ellerton et al., 2020
14	14	CSM	26.06, 153.11	0.0200	Model	Map 3; Sample 3	0.85	4.2 $\pm$ 0.40	Walker et al., 2018
15	15	Inskip	25.82, 153.05	0.0190	Validation	USU-2744	2.55	4.84 $\pm$ 0.46	Köhler et al., 2021
16	16a	CSM	26.02, 153.12	-	-	USU-2268	8.90	5.91 $\pm$ 0.61	<i>Ellerton et al., 2020</i>
16	16b	CSM	26.03, 153.12	0.0138	Model	USU-2269	1.48	6.96 $\pm$ 0.71	Ellerton et al., 2020
17	17a	K'gari	25.04, 153.24	-	-	USU-2390	3.15	5.96 $\pm$ 1.03	<i>This study</i>
17	17b	K'gari	25.04, 153.25	0.0120	Validation	USU-2389	3.10	7.24 $\pm$ 1.13	This study
18	18a	CSM	26.06, 153.09	-	-	Map 6; Sample 7	0.75	6.7 $\pm$ 0.60	<i>Walker et al., 2018</i>
18	18b	CSM	26.03, 153.08	-	-	Map 4; Sample 4	0.80	6.2 $\pm$ 0.80	<i>Walker et al., 2018</i>
18	18b'	CSM	26.03, 153.08	0.0113	Model	Map 4; Sample 5	1.05	9.8 $\pm$ 0.80	Walker et al., 2018
19	19	CSM	26.02, 153.12	0.0120	Model	USU-2282	6.85	8.17 $\pm$ 0.82	Ellerton et al., 2020
20	20	CSM	26.02, 153.12	0.0138	Model	USU-2270	1.48	9.1 $\pm$ 0.96	Ellerton et al., 2020
21	21	CSM	25.99, 153.13	0.0108	Model	USU-2285	2.62	9.82 $\pm$ 0.98	Ellerton et al. 2020
22	22a	CSM	26.03, 153.10	-	-	Map 5; Sample 6	0.80	8.3 $\pm$ 0.70	<i>Walker et al., 2018</i>
22	22b	CSM	26.04, 153.12	0.0109	Model	USU-2748	6.40	9.74 $\pm$ 0.90	Ellerton et al., 2020

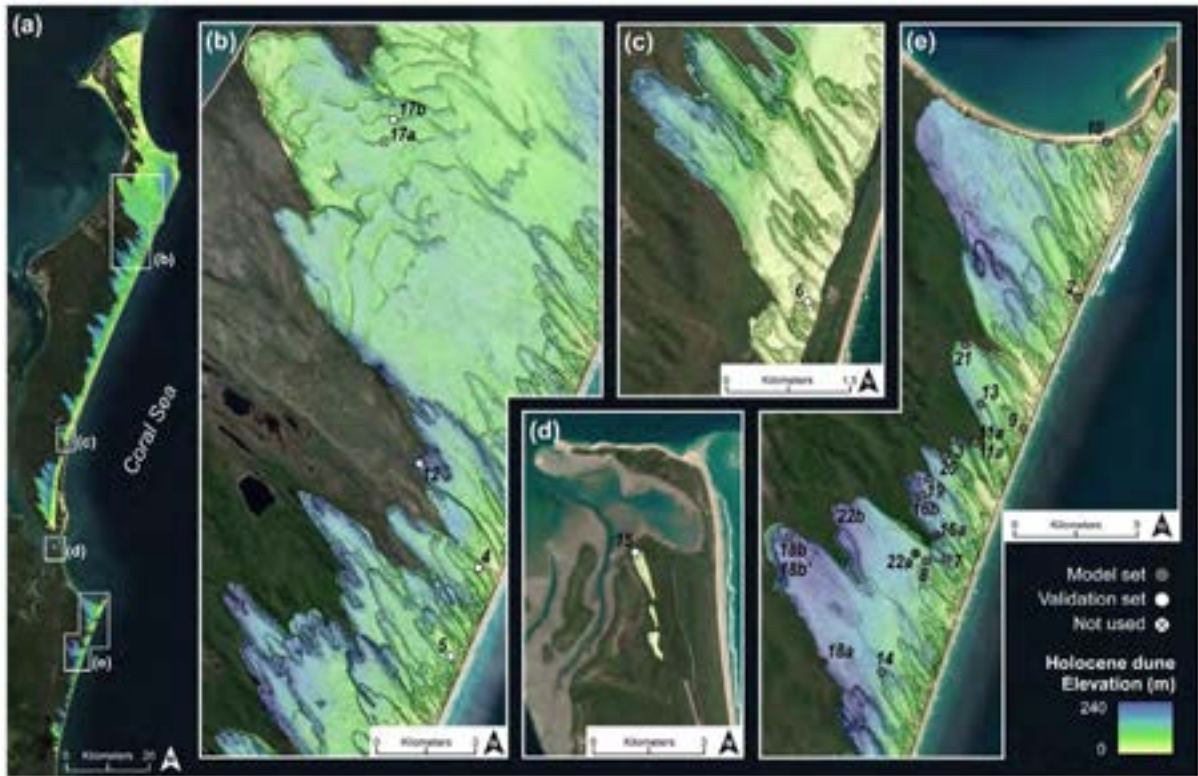


**Figure 4.3:** Locations of OSL dated dunes used in this chapter. Dunes utilised in the  $\sigma_c$ -age relationship are represented by grey dots; whereas, dunes used in the validation subset are white. For dunes with multiple dates, I preferentially selected ages from crest and/or stratigraphically lower positions. Samples that met my selection criteria but were not used in the model are marked with an 'X'.

#### 4.4.2 Surface roughness-age relationship

The dune calibration ages ( $n=16$ ) span from  $0.23 \pm 0.05$  ka to  $9.82 \pm 0.98$  ka with surface roughness ( $\sigma_c$ ) declining from  $0.068 \text{ m}^{-1}$  to  $0.016 \text{ m}^{-1}$  with age (see Table 4.2). An exponential regression fits the data well,  $Dune\ Age = 32.1 * \text{Exp}(-108.9 * \sigma_c)$ , with an  $r^2 = 0.942$ , RMSE = 0.892 ka, and  $p\text{-value} < 0.0001$  (Figure 4.4a). The validation subset from dunes on K'gari and Inskip Peninsula ( $n=6$ ) fall within the predictions of the model set and demonstrates the predictive power of this model with a slope of 0.805 (Figure 4.4b). Similar to past studies, high  $\sigma_c$  associated with younger dunes rapidly decreases within the first thousand years, and after this period  $\sigma_c$  values decrease more gradually, which is best described by a negative exponential function (Booth et al., 2017; LaHusen et al., 2020; Chapter 3).

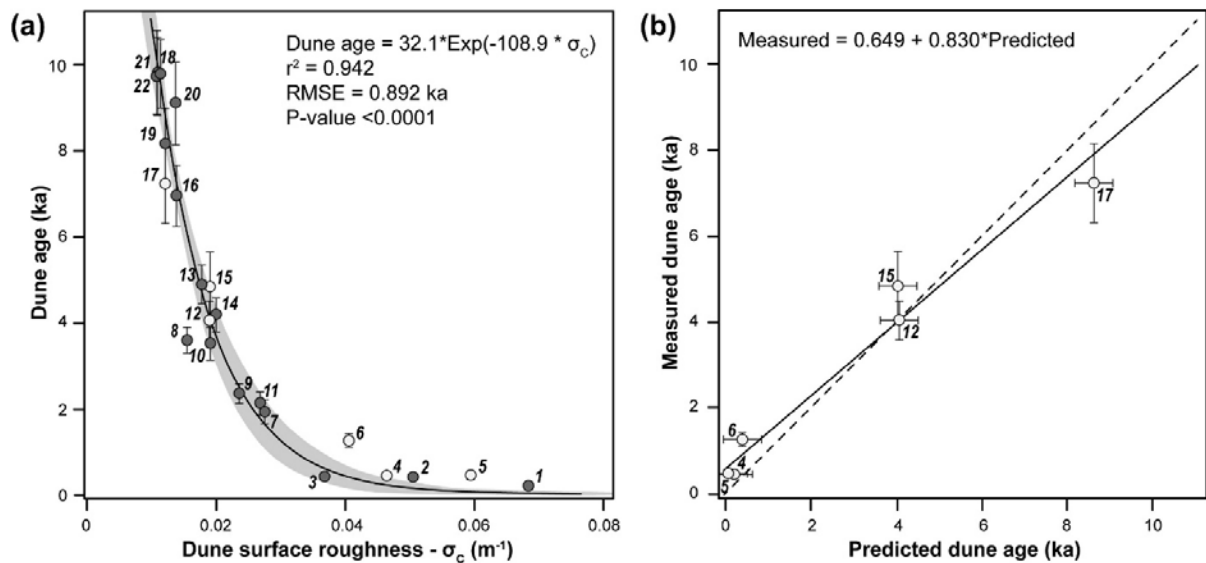


**Figure 4.4:** Calculated surface roughness ( $\sigma_c$ )-age relationship from measured OSL dated dunes. **(a)** Dune  $\sigma_c$  depicts a strong exponential relationship with age ( $\pm 1\sigma$ ) (black line) bounded by 95% confidence intervals (shaded area) within the CSM and K'gari dune fields. The calibration ages (grey dots) come from the CSM ( $n=18$ ) whereas the remaining dates used as a validation subset (white dots) come from Inskip Peninsula and K'gari ( $n=6$ ). **(b)** Model validation using predicted versus measured dune ages and their associated best-fit line (black line) using reduce major axis regression to account for uncertainty in both variables compared to a 1:1 line (solid black dashed line).

#### 4.4.3 Predicted dune ages and their spatial relationships and characteristics

In this chapter, I remotely mapped 92 and 11 active dunes (total 103), and 535 and 191 emplaced Holocene (total 726) dunes on K'gari and the CSM, respectively, covering a total area of  $640 \text{ km}^2$  -- 33% of both dune fields total land area. Utilising the  $\sigma_c$ -age function above, I estimate the emplacement ages for the Holocene dunes. Generally, the oldest dunes (lowest surface roughness) were located further inland despite having large sections overlapped by subsequent dune emplacement (Supplementary Figure A.4.2). Dunes become progressively younger moving towards the east coast (west to east) (Figure 4.5 and Supplementary Figure A.4.2). The oldest dunes tend to be larger and less numerous across the landscape, whereas younger dunes are smaller in size but greater in number (Supplementary Figure A.4.2). Overlapping relationships revealed by the roughness analysis obey the principle of superposition, consistently showing younger dunes superimposed on older dunes.

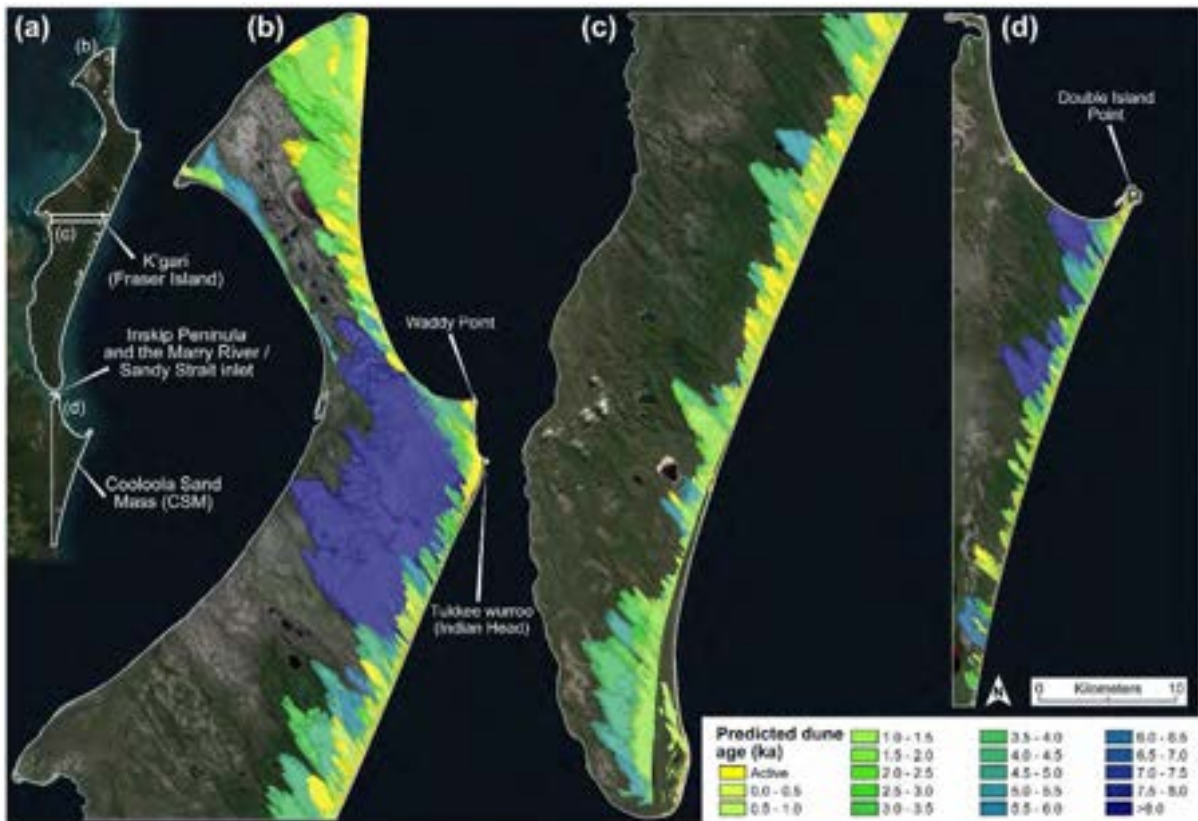


**Figure 4.5:** Predicted Holocene dune ages using  $\sigma_c$ -age model. **(a)** Aerial imagery of K'gari to the north and the CSM to the south with locations of Panels **(b)** northern K'gari, **(c)** southern K'gari, and **(d)** the CSM.

#### 4.4.4 Temporal frequency of dune emplacement

Overall, there is good visual correspondence between probability density function (PDF) peaks from the OSL age control and predicted dune ages (Figure 4.6 vertical teal areas). Utilising dated dunes and their measurement error ( $n=22$ ), PDFs depict four major peaks that occur at ca. 0.5, 2.2, 4, and 9.5 ka. When separating the OSL ages into two unique PDFs for both locations, I observe similar trends between K'gari ( $n=6$ ) and the CSM ( $n=16$ ) suggesting my sampling efforts captured consistent emplacement events despite having limited OSL dates (white PDFs in Supplementary Figure A.4.3b and c, respectively).

Using predicted ages derived from the  $\sigma_c$ -age model (not including active dunes) ( $n=726$ ) I produce PDFs for dune emplacement. PDFs derived from non-normalised estimated dune ages depict one major significant peak at ca. 1 ka that rapidly decreases with increasing dune age (Figure 4.6b). This is observed for both the combined and separated PDFs and is a reflection of the abundant number of mapped dunes (~60%) emplace during the last 1 ka (Supplementary Figure A.4.2a). When accounting for dune area, the combined normalised

PDF has four peaks centred at ca. <0.5, 1.5, 4, and 8.5 ka (Figure 4.6c). The same peaks are common to the PDFs generated for the two areas when treated separately (Supplementary Figure A.4.3b and c).

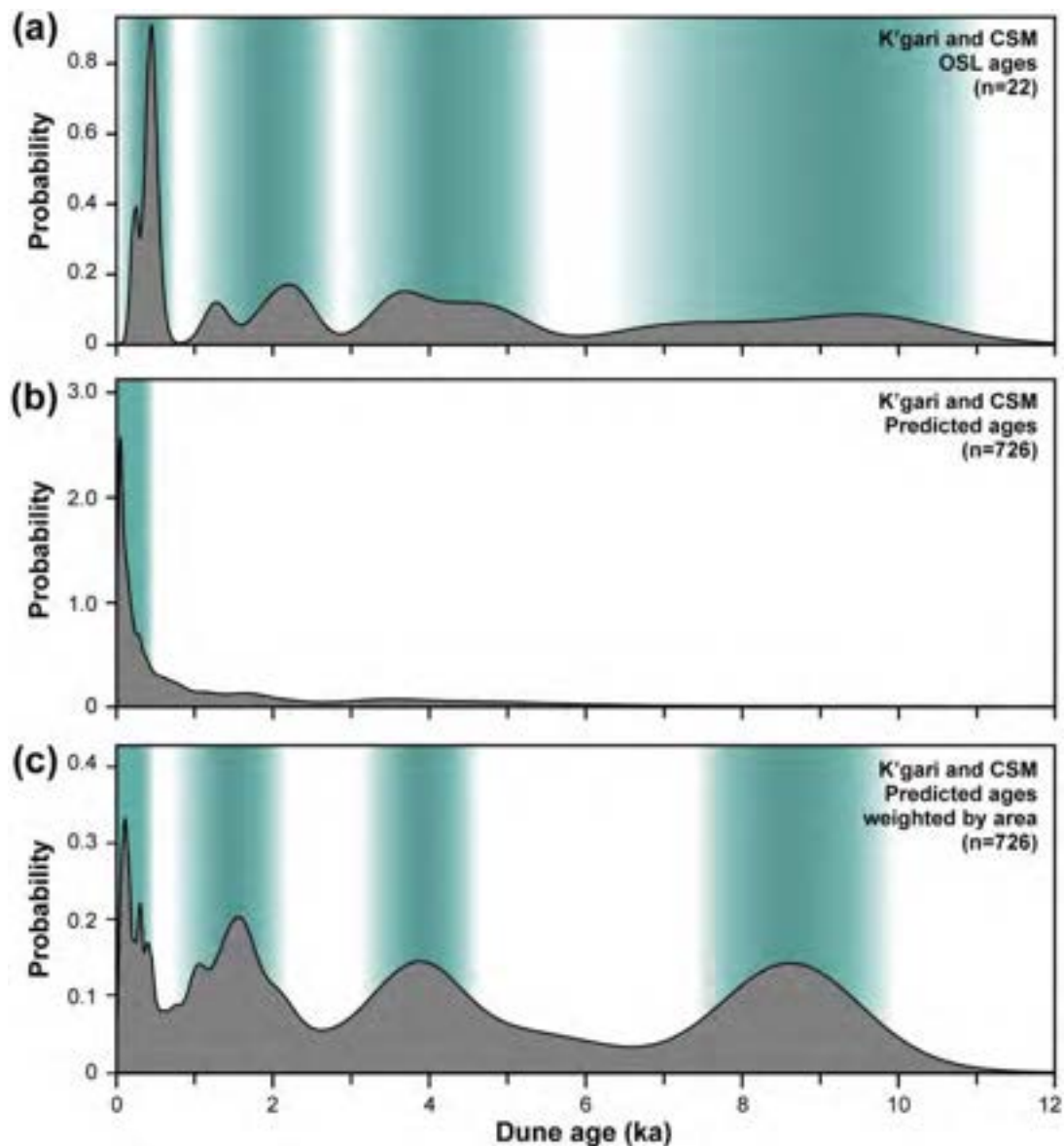


**Figure 4.6:** Normalised probability density functions (PDFs) of the combined K'gari and CSM dune fields derived from **(a)** OSL-dated dunes and **(b)** predicted ages. **(c)** Predicted ages normalised by total dune area. Vertical teal areas highlight phases of dune emplacement. By far the largest number of dunes are small coastal blowouts, but cumulatively these dunes represent very little land area and are of only local significance. Area occupied by the dunes is critical as during major activation phases blowouts coalesce into much larger parabolic and transverse dune fields.

#### 4.4.5 Sensitivity analysis

Surface roughness ( $\sigma_c$ )-age relationships for a range of DEM resolutions (1 - 50 m) and their associated  $r^2$  and RMSE are reported in Supplementary Table A.4.3. I find that a wide range of resolutions provide a good fit (3 - 20 m) with their  $r^2 > 0.90$  and  $RMSE < 1.1$  ka with the best resolutions being 5 and 6 m. I observe the poorest relationship (low  $r^2$  and high RMSE) for the highest and lowest resolutions (1 m and 50 m). Generally, I observe that PDFs determined from DEM resolution between 3 - 20 m show similar frequency, magnitude, and timing of dune emplacement compared to PDFs derived from measured OSL dated dunes (Supplementary Table A.4.3 and Supplementary Figure A.4.4).

### 4.5 Discussion

#### 4.5.1 Dune surface roughness and evolutionary processes

While dunes are active, they are dominated by wind advection and deflation that controls their movement near the lee slope slip-face (Pye, 1982; Hesp, 2002). The migrating dunes' surfaces are barren of vegetation with shallow stoss gradients and over-steepened lee slopes that are smooth (low  $\sigma_c$ ). The dune continues to move while vegetation begins to stabilise dune segments along the trailing arms and furthest from the active sections (Levin, 2011; Yan and Baas, 2017). Topographic variability begins to emerge as sand is entrained within and/or forced around vegetation patches. This increases local relief, roughening the dune surface resulting in an increase in  $\sigma_c$ . This progresses until the vegetation have fully covered and stabilised the dune's surface, marking the onset of dune emplacement and the highest recorded  $\sigma_c$  values (Supplementary Figure A.4.5). My observations match those seen in other dune systems (e.g., Hesp, 2002; Stallins and Parker, 2003; Pelletier et al., 2009), indicating that dune emplacement through to the stage of vegetation stabilisation is a mechanism that roughens topography.

Once dunes are emplaced, their topographic evolution can be described by diffusive sediment transport theory which includes two phases of smoothing (decreasing  $\sigma_c$  with time) (*Chapter 3*). The first phase of rapid smoothing is induced by frequent episodic sediment transport from dry-ravel and sheetwash processes. This persists until all slopes are lowered below their angle of repose. This is followed by the second phase which is dominated by slow and continuous transport processes such as bioturbation and granular relaxation. I



hypothesise that this continues as erosion rates lower, and the styles of transport become increasingly uniform until no relief remains,  $\sigma_c \rightarrow 0 \text{ m}^{-1}$  (Supplementary Figure A.4.5). This general evolution is supported by my field observations that steep slopes persist on young dunes (<1 ka), geomorphic processes are consistent on K'gari, and the validation subset fits well.

#### 4.5.2 Timing of dune emplacement and regional story

The  $\sigma_c$ -age relationship calibrated from the CSM accurately predicts the ages of the OSL dated dunes on K'gari. The findings support the idea that both dune fields are part of the same system undergoing similar evolutionary development with distinct emplacement phases in the Holocene (e.g., Ward, 2006; Ellerton et al., 2020; *Chapter 2*). Critically, I was able to predict the age of every emplaced Holocene dune in the dune field, which significantly amplifies my ability to extract chronological signals from dune fields that have, to this point, been limited.

My approach allows me to observe patterns within the dune fields that would otherwise be obscure. For example, the oldest of the Holocene emplacement phases at the CSM and K'gari is the so-called 'Triangle Cliff' unit (Ward, 2006; *Chapter 2*). It is comprised of large parabolic dunes, and more locally, large transverse dune waves. This unit was mapped uniformly across the dune fields (Ward, 2006; *Chapter 2*) suggesting that the entire coastline was simultaneously active during the early Holocene. This is consistent with the expectation that the dune fields would be generally active during the main post-glacial transgression (e.g., Thom, 1978; Thompson, 1981; Pye, 1983; Pye and Bowman, 1984; Cook, 1986; Shulmeister and Lees, 1992; Lees, 2006). However, the age estimates indicate a slightly different pattern, I observe the main preservation of these older Holocene dunes are immediately (within ~20 km) south of rocky headlands (i.e., Double Island Point on the CSM; Tukkee Wurroo (aka Indian Head) and Waddy Point on K'gari) (Figure 4.5). I hypothesise that these headlands act as pinning points for the beaches and long-term rotation of the coastline into swash alignment south of the headlands which has resulted in enhanced erosion and the consequential loss of older Holocene dunes in the southern parts of both dune fields (Stephens et al., 1981). In addition, eroded sediment tends to accumulate south of the headlands, as can be observed inland from Tukkee Wurroo. The one exception is near the southern limit of K'gari where the

northward migration of the Mary River/Sandy Strait inlet during the mid- to late-Holocene (Köhler et al., 2021) has increased local sediment supply, promoting coastal accretion (Figure 4.5). This has consequently preserved some mid-Holocene parabolic dunes behind beach ridge complexes.

Paleoenvironmental interpretations from dune fields are constrained by dune chronologies and are often based on a handful of ages (e.g., Shulmeister and Lees, 1992). In fact, many of the current interpretations for the coastal dune fields are from sparse data sets which are limited to inferred key events, for example, the onset/intensification of the El Niño Southern Oscillation (ENSO) or even the post glacial transgression. My method provides a systematic and inexpensive means to substantially expand these chronologies, and a way to increase the robustness of interpretations by providing realistic ages for all the dunes in the dune field. The enhanced chronology is important because patterns of dune activation and emplacement are complex and may encompass both significant, region dependent, time lags and local signals (Lancaster et al., 2016).

#### 4.5.3 Dune emplacement ages and sea-level variability

Overall, the predicted ages support previous inferences about the dune fields. Whether the SE Queensland dune fields, including the CSM and K'gari, have been activated by sea-level or climate change has been strongly debated (e.g., Ward, 1978; Thompson, 1981; Young et al., 1993; Walker et al., 2018; Ellerton et al., 2020) but the idea that the main dune forming events were associated with the glacial maximum has become embedded in the popular literature (e.g., the listing for the Fraser Island | K'gari World Heritage Area). The most comprehensive chronology comes from Ellerton et al. (2020) who constrained the ages of the mapped Pleistocene and Holocene dune units and related these emplacement phases to sea-level. In our study, they noted that sea-level rise is likely the main driver inducing dune activity owing to the erosion of sand from the coast and nearshore and consequent reworking of sediment into the dune fields (Cooper-Thom model) (Cooper, 1958; Thom, 1978).

I re-examine this hypothesis by comparing the PDF results from the  $\sigma_c$ -age model with local sea-level curves from Lewis et al. (2008) and Larcombe et al. (1995). Similar to Ellerton et al. (2020), my findings support the Cooper-Thom model. I observe four major peaks in the

Holocene at ca. 0.5, 1.5, 4, and 8.5 ka that are primarily tied to sea-level variability (Figure 4.7).

The clear advantage of my method compared with OSL generated PDFs is that the peaks are much better defined. This is particularly true for the two older events which are larger and more pronounced, which this is not the case for the OSL derived PDF (Figure 4.6). To maintain consistency with previous papers, I use names of dune units to represent phases of dune emplacement (Ward, 2006; Ellerton et al., 2020; *Chapter 2*). The oldest emplacement phase (Triangle Cliff) changes from a poorly defined period between ca. 11 and 6.5 ka (Ellerton et al., 2020), to a tighter defined event at ca.  $8.5 \pm 1.0$  ka. This coincides well with the termination of the rapid component of post-glacial transgression (e.g., Larcombe et al., 1995). For the two younger events there is a shift in their peaks, in both cases making the peak slightly younger than the OSL based peaks. For the Freshwater (ca.  $4 \pm 0.5$  ka) and Station Hill (ca.  $1.5 \pm 0.5$  ka) emplacement phases, the revised ages are clearly younger than the sea-level rise they are interpreted to be associated with. This is sensible as the dune ages reflect the timing of sand burial, hence dune emplacement. New dune activation ceases when sea-level rise stops but the dunes that are active, can remain active for decades to centuries after the initiation process has stopped (e.g., Levin, 2011; Houser et al., 2015; Levin et al., 2017).

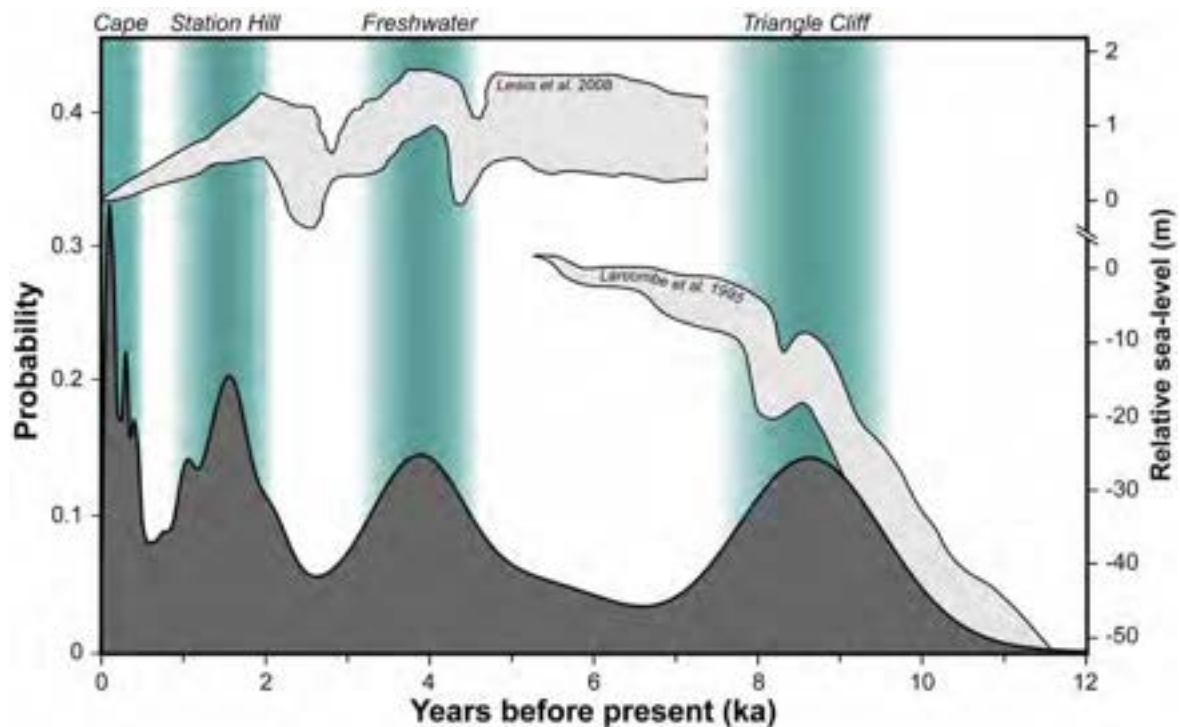


**Figure 4.7:** The combined K'gari and CSM dune fields PDF from predicted (dark grey) dune ages compared to local sea-level curves from Lewis et al. (2008) and Larcombe et al. (1995). Note, there is a break in the relative sea-level axis so that both curves could be displayed on the same graph. I observe four emplacement phases (vertical teal areas) that are closely associated with the termination of the rising limb of sea-level events. The addition of the estimated ages permits me to better constrain the timing of dune emplacement (Ellerton et al., 2020) which has been associated with mapped dune units (Ward, 2006; *Chapter 2*): Cape ca. <0.5 ka; Station Hill ca.  $1.5 \pm 0.5$  ka; Freshwater ca.  $4 \pm 0.5$  ka; and Triangle Cliff ca.  $8.5 \pm 1.0$  ka.

The most recent dune emplacement event (Cape) occurred within the last 0.5 ka which does not correspond with increased sea-level. This phase has been ascribed to increased human activity (Aboriginal fires and European clearance and fires) (Cook, 1986), but it has also been proposed that sea-surface temperatures (SST), specifically the intensification of ENSO and the Interdecadal Pacific Oscillation (IPO) may account for this activation (Levin, 2011). While very little is known about the long-term history of the IPO, its direct effect on beach processes in this area has recently been confirmed (Kelly et al., 2019) and it is associated with a change in incident wave direction and effective wave height (McSweeney and Shulmeister, 2018). More positive IPO conditions in the last few centuries may account for this increased coastal dune formation. There is one caveat. Coastal blowouts are formed continuously and are a function of local storms, fires and other disturbances as well as regional events (Levin, 2011; Hesp, 2002). The large number of very young dunes may well

simply be a reflection of stochastic process, where these dunes have little long-term preservation potential.

It is important to note that I observe little evidence to support the hypothesis that climate is the major control on widespread dune activity, as proposed by Young et al. (1993) (Figure 4.8). It has been inferred from paleoclimate records that there was an intensification of ENSO during the mid-Holocene which may have led to increased storminess and climate variability (Shulmeister and Lees, 1995; Moy et al., 2002; Donders et al., 2006; Conroy et al., 2008; Barr et al., 2019) resulting in widespread dune activity. However, this is unlikely in these dune fields. Pollen studies have shown that vegetation type in the dune field was not modified by climate change in the Holocene. In fact, dune vegetation was remarkably consistent. Instead, any impact of ENSO will be through interactions with the IPO on wave climate and on enhanced sea-surface temperatures, triggering more frequent or stronger storms.

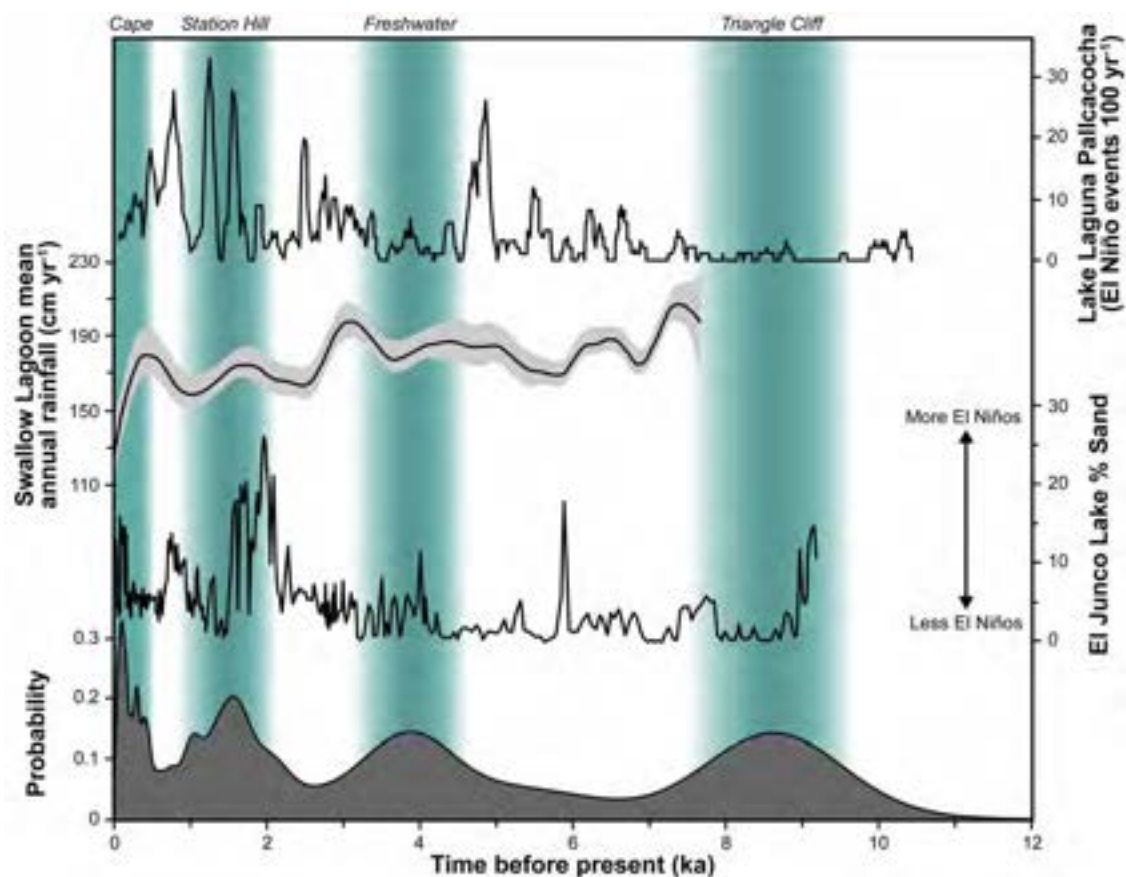


**Figure 4.8:** Paleoclimate records through the Holocene from Laguna Pallcacocha in southern Ecuador (Moy et al., 2002), Swallow Lagoon in eastern Australia (Barr et al., 2019), and El Junco Lake in the Galápagos Islands (Conroy et al., 2008) compared to timing of major dune emplacement phases at K’gari and the CSM. Climate appears to have little direct link to dune emplacement.

#### 4.5.4 Surface roughness ( $\sigma_c$ )-age model application

In this chapter, I have demonstrated that the surface roughness ( $\sigma_c$ )-age model is a potentially powerful tool for applying in dune settings. The advantage of this approach is that it produces systematic dune ages and only requires high-resolution elevation data and a limited number of constraining dune ages. It also has the ability to detect previously non-identified map units. Dunes can be placed in clusters of similar  $\sigma_c$  to help infer the number of emplacement events and their relative sequence even when dune units are not contiguous and/or age control is absent. Furthermore, reasonable age estimates can be obtained for these undated events. These analyses can be used to target and direct future sampling strategies to ensure all events are confirmed and sampled for dating, while avoiding areas of reactivation so that a robust chronology can be constructed.

In contrast to dune ages, high-resolution elevation data is becoming increasingly available as unmanned aerial vehicles (UAVs) and other remote sensing techniques are being extensively employed to capture topographic information. Indeed, the sensitivity analysis highlights that a wide range of DEM resolutions can produce robust age predictions, the PDFs of which correspond well with previously described emplacement events. I determine that  $\sigma_c$  calculated with DEM resolutions of between 3 and 20 m produce similar results. Beyond this range (i.e., finer or coarser resolution), the relationships deteriorate (Supplementary Table A.4.3 and Supplementary Figure A.4.4). Additionally, it is important to recognise that not all elevation models are equal, and researchers must use their own discretion to determine if their data adequately describes the dunes surface at the necessary resolution. For example, areas with dense vegetation and/or canopy cover, Light Detection and Ranging (LiDAR) should be considered because of its vegetation penetrating abilities (i.e., bare-earth DEM) rather than a photogrammetry derived DEM which may not capture the 'true topography'.

I expect that my  $\sigma_c$ -age model will be applicable in many other dune settings. The model has three major assumptions: initial landforms are formed with significant surface roughness, landscape evolution is time dependent, and only diffusive hillslope processes are active. These suggest that all dunes within the same system will have identical evolutionary trajectories ( $\sigma_c$ -age regression) and their topography will only smooth with time (decreasing  $\sigma_c$ ). Within K'gari and the CSM these assumptions are known to be valid and is clearly demonstrated by the strength of the model in both locations. Similar to K'gari and the CSM,

many coastal dune systems have relatively stable base-levels in the mid- to late-Holocene, well defined and stable wind fields, and have uniform, well-sorted, and unconsolidated material. These boundary conditions apply on the Oregon coast (Peterson et al., 2007) and Great Lakes of the USA (Hansen et al., 2020), Northern Ireland and Scotland (Wilson et al., 2004; Sommerville et al., 2007), the SE Brazil coast (Giannini et al., 2007), and Israel (Levin et al., 2008), amongst many others.

Despite superficial similarities, each of these dune systems vary dramatically in climate and biota which may lead to changes in the rate  $\sigma_c$  decays with time between sites. As discussed by Booth et al. (2017) and *Chapter 3*, the rate of decline for the regression is controlled by soil diffusivity (which is the combined effect of all environmental factors influencing the efficiency of sediment to move downslope). As a result, there is no one dune field  $\sigma_c$ -age regression that is applicable at all sites. A new model calibration and validation is critical in each case. Nevertheless, the decline in  $\sigma_c$  with time and its value can help infer transport processes, characterise dune evolution, and place tighter constraints on dune field development with respect to regional climate/sea-level models.

The key limitation of the method is when non-diffusive (advective) processes such as knickpoint erosion also affect dune evolution. For this reason, applications of the method should initially be limited to Holocene dunes and avoid sites with significant fluvial reworking and/or rapid base-level change. My intention is to adapt the model to Pleistocene sections of the CSM and K'gari dune fields in due course, a process that will involve developing a model that incorporates the effect of base-level changes into the evolving  $\sigma_c$ .

## 4.6 Conclusions

Determining age control for landforms is important within the earth sciences for several reasons, notably for providing the rates of processes driving landscape evolution. However, acquiring the volume of ages necessary to develop the complete record of dune emplacement events for a field area is challenging and, in most cases, not feasible. This is mainly due to sample availability, time, cost, and methodological constraints, but may also arise from environmental degradation caused by sampling and travel in sensitive areas. The K'gari and the Cooloola Sand Mass (CSM) dune fields are ideal locations to validate this approach as within the Holocene most major factors contributing to landscape evolution can

be measured and constrained. I apply an exponential fit to the dune surface roughness ( $\sigma_c$ )-age measurements and this relationship can be numerically explained through conservation of mass equations. K'gari and the CSM provides a field site where greater than 700 dunes spanning the last 10 ka are preserved and which can be readily compared with paleo-records of climate, sea-level, and vegetation. Despite numerous dating campaigns, only slightly over 20 luminescence dated Holocene dunes are reported (Tejan-Kella et al., 1990; Walker et al., 2018; Ellerton et al., 2020; Köhler et al., 2021). This only accounts for <3% of dunes preserved and <1% of the total land area (*Chapter 2*). To fully understand the spatial and temporal relationship of dune emplacement, many additional ages are required. Utilising a roughness-age empirical model, I provide the first high-resolution coastal dune chronology. Its application gives a more robust insight on coastal system evolution than can be derived from limited chronological constraints.

This model provides realistic estimates for every Holocene dune which is not only useful in understanding where dunes of certain ages are located, but it also adds significance to the timing of major dune emplacement events. For instance, when only OSL dated dunes are utilised, the timing of these events are broad and poorly defined. With the addition of the predicted ages, the time constraints on the events narrow and peaks are more pronounced (e.g., the Triangle Cliff dune unit being reclassified from ca. 11 to 6.5 ka by Ellerton et al. (2020) to ca.  $8.5 \pm 1.0$  ka event). At K'gari and the CSM, my results confirm that major phases of dune activity are governed by sea-level fluctuations. In addition, the age pattern allows me to demonstrate that their spatial distributions are controlled by changes in swash/drift alignment of the coast. The oldest Holocene dunes are concentrated near headlands that act as pinning points for coastal rotation and are less erosion prone. These observations highlight the power of the method to yield new insights on landform evolution in a coastal dune field.



## Chapter 5.

### Reconstructing Holocene fire records using dune foot-slope deposits at the Cooloola Sand Mass, Australia

*This chapter is in preparation to be submitted to Quaternary Research*

Patton, N. R., Shulmeister, Hua, Q., Almond, P., Rittenour, T., Hanson, J. M., Greal, A., Gilroy, J., & Ellerton, D. (2023) Reconstructing Holocene fire records using dune foot-slope deposits at the Cooloola Sand Mass, Australia. *Quaternary Research*, 1–23. <https://doi.org/10.1017/qua.2023.14>.

**Preface:** This chapter evaluates the utility of dune foot-slope deposits to record intact, stratigraphic fire records. In this chapter, I excavate soil profiles at the base of four different aged dunes in the CSM, Australia. Charcoal concentrations are determined for predetermined sample depth intervals for three size classes. I generate high-resolution age-depth models to place charcoal accumulation rates (CHAR) in the context of time and compare the results to other more traditional records (i.e., lakes and bogs) locally and regionally. The outcomes of this chapter highlight a previously unrecognised deposit that can be used in both coastal and continental dune systems as a means to evenly distribute geomorphic (erosion and sedimentation) and ecologic (fire) records globally. Additionally, the findings add supporting evidence for *Chapter 3* that fire is an important disturbance in the dune fields.

Nicholas R. Patton<sup>1,2</sup>, James Shulmeister<sup>1,2</sup>, Quan Hua<sup>3</sup>, Peter Almond<sup>4</sup>, Tammy M. Rittenour<sup>5</sup>, Johanna M. Hanson<sup>1</sup>, Aloysius Grealy<sup>2</sup>, Jack Gilroy<sup>2</sup>, and Daniel Ellerton<sup>2,6</sup>

<sup>1</sup>School of Earth and Environment, University of Canterbury, Christchurch 8041, NZ

<sup>2</sup>School of Earth and Environmental Sciences, The University of Queensland, Brisbane 4072, AUS

<sup>3</sup>Australian Nuclear Science and Technology Organisation, Kirrawee DC, NSW, 2232, AUS

<sup>4</sup>Department of Soil and Physical Sciences, Lincoln University, Christchurch 7647 New Zealand

<sup>5</sup>Department of Geology, Utah State Luminescence Laboratory, Utah State University Logan, UT 84322, USA

<sup>6</sup>Department of Geological Sciences, Stockholm University, SE 10961 Stockholm, SE

## Abstract

In this study, I assess charcoal records from aeolian deposits within the Cooloola Sand Mass, a subtropical coastal-dune system in eastern Australia, to determine whether they can be used as a proxy for Holocene fire history. I excavate four profiles in depositional wedges at the base of dune slipfaces (foot-slope deposits) and calculate charcoal concentrations for three size classes (180-250  $\mu\text{m}$ , 250-355  $\mu\text{m}$ , and 355  $\mu\text{m}$ -2 mm) at predetermined depth intervals. Age-depth models are constructed for each profile using radiocarbon measurements ( $n=46$ ) and basal OSL ages ( $n=4$ ). All records appear intact with little evidence of post-depositional mixing as demonstrated by minimal age-reversals and consistent trends in charcoal concentration and accumulation rates (CHAR) amongst size classes. Combining all four records, I generate a ca 7 cal. ka BP terrestrial fire history that depicts distinct peaks representing periods of increased local fire activity at <0.3, 1.1-0.4, 2.2-1.6, 3.4-2.6, and 6.7-5.3 cal. ka BP. My findings parallel regional records and highlight the utility of dune foot-slopes as ecological and sedimentary archives. As dune fields are much more common than wetlands and lakes in semi-arid and arid areas, these deposits have the potential to increase the spatial resolution of fire records globally.

## 5.1 Introduction

Wildfires are prevalent across much of the world; however, fire records are primarily limited to regions with abundant aquatic archives (e.g., Power et al., 2008; Harrison et al., 2022). As a result, identifying a potential sediment deposit that are commonly found within these areas, such as drylands, would provide a valuable target for paleoclimate studies and a means to evenly distribute fire records globally. The goal of this study is to assess the utility of dune foot-slope deposits to reconstruct fire histories. As a case study, I focus on stabilise Holocene dunes at the Cooloola Sand Mass (CSM) within the southeast (SE) Queensland dune

fields (Figure 5.1). The dunes are well dated (Walker et al., 2018; Ellerton et al., 2020; *Chapter 4*), their evolution is well-understood (Levin, 2011; *Chapter 3*), and there are several aquatic records which can be used for comparison and validation (Donders et al., 2006; Mariani et al., 2019; Hanson et al., 2023). Specifically, the main objectives were to (i) assess whether sites contain stratigraphically intact units with preserved depositional charcoal for developing a fire record; (ii) evaluate the sensitivity of the records to charcoal size classes; (iii) place the spatially aggregated charcoal records into the context of other records found in the SE Queensland dune fields; and (iv) consider improvements to the data gathering and/or interpretation techniques. The outcomes will aid in the development of charcoal records from areas where fire is a rare event (wetlands/lakes) into regions where fire may be the dominant geomorphic and ecological process.

### 5.1.1 Fire in the Australian landscape

Fire is one of the most dominant landscape disturbances on Earth (Hennessy et al., 2005; Bowman et al., 2009; McLauchlan et al., 2020). This was clearly demonstrated in the 2019-2020 'Black Summers' bushfires in Australia, which burned ~240,000 km<sup>2</sup>, destroyed over 3000 houses, killed an estimated one-billion animals, and displaced thousands of people (Figure 5.1) (DAWE, 2020; Filkov et al., 2020; Richards et al., 2020; Gallagher et al., 2021; Canadell et al., 2021). Fire activity (both frequency and severity) has been projected to increase due to changes in land use and climate (McKenzie et al., 2004; IPCC, 2021). It is therefore imperative to understand the role, frequency and intensity of fire in Australia as it is one of the world's most fire-prone landscapes (Bradstock et al., 2002; Russell-Smith et al., 2007; Bradstock, 2010; Van der Wef et al., 2017) and one that has a long legacy of both natural and anthropogenic fire occurrence.

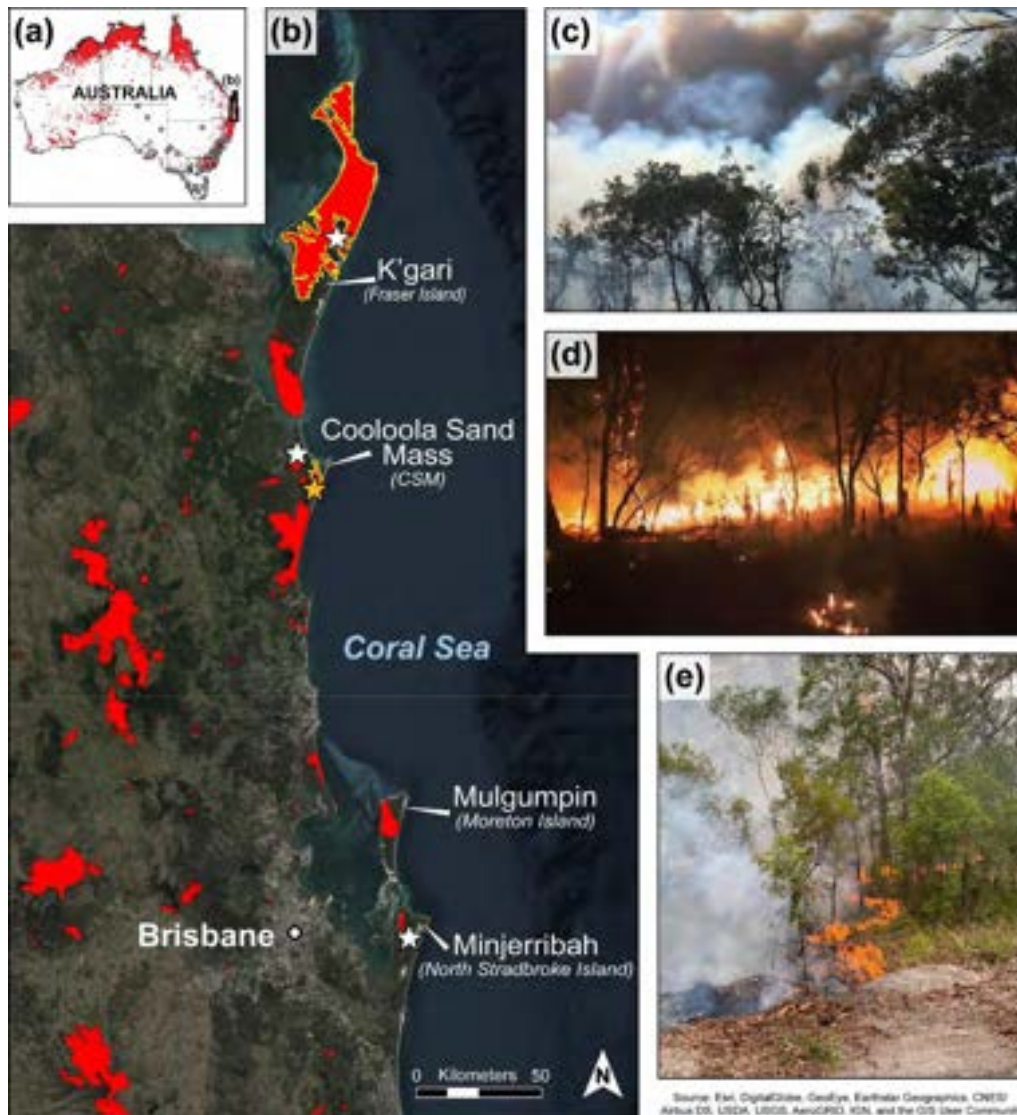


**Figure 5.1:** (a) Total area burned in Australia during the 2019-2020 'Black Summers' (red area) (DAWE, 2020) and the locations of sediment cores (white dots) used to generate Late-Quaternary fire records in Mooney et al. (2011). (b) Satellite imagery of the SE Queensland dune fields and location of fires during the 2019-2020 with yellow outline representing the 'Fraser Fire' and 'Freshwater Road Fire' on K'gari and the Cooloola Sand Mass (CSM), respectively. The orange star marks the field site for this study, whereas the white stars indicate fire record locations compared in this research. Images of the (c) the Kings Bore Wildfire, (d) the Thannae Fire, and (e) the Freshwater Road Fire are provided as examples of wildfires that occurred within the SE Queensland dune fields during the 'Black Summers' (photo credit: Michael Ford Panel c and Erin Atkinson Panels d and e).

Prior to the arrival of humans ca 70-65 ka, evidence of fire in sedimentological records is intermittent and sparse, and is presumed to be of minor importance in Australia (Singh et al., 1981; Moss and Kershaw, 2000; Clarkson et al., 2017). After this period, the subsequent substantial increase in fire activity is commonly ascribed to indigenous arrival (Kershaw, 1986; Turney et al., 2001) due to their frequent use of small, low-intensity fire across the landscape,

aka ‘fire-stick farming’ (Russell-Smith et al., 1997; Bowman, 1998). However, more recent studies have suggested little evidence of variations in fire regimes after human arrival, instead ascribing increased fire activity to changes in climate (e.g., Mooney et al., 2011).

The relationship between humans and fire is difficult to address in sedimentological records because the timing of initial human arrival is not precisely known and there are autocorrelations between climate, vegetation, and fire (Bowman, 1998; Archibald et al., 2013). Not until European arrival and a shift to fire suppression and cessation in the last 200 years, do I see a clear anthropogenic signal (Moss et al., 2011; 2015; Hanson et al., 2022). Indeed, the transition from traditional fire management to fire suppression is inferred to be responsible for not only increased fire severity, but also a shift in vegetation structure, boundaries, and community composition (Thompson and Moore, 1984; Pyne, 1998; Fletcher et al., 2021; Mariani et al., 2022; Stone et al., 2022).

Regardless of its origin, the role of fire in controlling Australian ecosystems and landscapes is widely accepted as significant (Bowman, 1998). There are large and growing paleofire datasets (e.g., Marlon et al., 2015; Gross et al., 2018; Hawthorne et al., 2018; Harrison et al., 2022) but the records in these databases are strongly biased towards wetland areas and consequently, for Australia, there is a strong emphasis on the SE region (Figure 5.1a). To broaden the coverage of fire histories there is a need to extend records beyond peat bogs, swamps, and lakes; however, much of the Australian landscape is not suitable to sustain long-term organic records (Bridgman and Timms, 2012; Chang et al., 2014; 2017) and therefore, finding suitable sites for the preservation of sedimentary charcoal is challenging (e.g., Leys et al., 2018). As a result, there are spatial discrepancies in data coverage across the continent, particularly in the interior and in the tropics and subtropics. A means to extend fire histories to the continental interior, where fires may be the dominant ecological process, is needed. In this study, I examine dune deposits as potential archives of fire history within the SE Queensland dune fields because these landforms are abundant within the interior and along the coastlines of Australia (Lees, 2006; Hesse, 2016), and many parts of the world (Lancaster et al., 2016).

### 5.1.2 SE Queensland dune fields vegetation

The SE Queensland dune fields (aka the Great Sandy Coast) in Australia (24.4°S – 27.5°S) include the three largest sand islands in the world: K’gari (Fraser Island), Minjerribah (North Stradbroke Island), and Mulgumpin (Moreton Island), and the Cooloola Sand Mass (CSM) on the mainland (Figure 5.1b). These dune fields have existed since ca 800 ka (Ellerton et al., 2020; 2022). They are composed of large parabolic dunes, which contain the world’s largest rainforest and unconfined aquifer on a sand island and are home to rare flora and fauna (UNESCO, 2021). Their vegetation structure follows a climax succession moving inland from the coast (Walker et al., 1981; 2010). Biozones change from coastal pioneer communities, through dry sclerophyll forest (e.g., *Eucalyptus*, *Casuarina*, and *Banksia*), to wet sclerophyll forest (e.g., *Satinay* (*Syncarpia hillii*), *Araucaria*, and ferns), and rainforest landward, with heathlands and coastal wetlands on the western (inland) side of the dune sequences (Queensland Herbarium, 2021).

While this shift in vegetation structure and composition is inferred to be reliant on nutrient and water availability (Walker et al., 1981; 1987; Thompson, 1992; Thomas, 2003), fire plays an important role in shaping this landscape (Thompson and Moore, 1984; Walker et al., 1987; Spencer and Baxter, 2006). For example, heathlands and dry sclerophyll forest often require frequent, low intensity fires at a minimum spacing of 8-years to reduce ground cover and canopy shading, and to incorporate nutrients into the soils (Keeley, 1995; Bowman et al., 2014; Queensland Herbarium, 2021).

Wet sclerophyll forest (composed of tall sclerophyll trees, with relatively dense understory vegetation such as ferns) is characterised by less frequent fires occurring in SE Queensland at a minimum of 20-year intervals (Queensland Herbarium, 2021). In these areas, fires are generally suppressed by the forest moisture content. Even wetter are the rainforests, or more accurately, notophyllous vine thickets, that typically avoid burning in all but the driest and most extreme conditions. Local patches of rainforest within the dune fields are associated with the low-lying dune swales that are perennially wet and when fires penetrate, they are usually low intensity; however, these systems are extremely sensitive to fire (Collins, 2019; Queensland Herbarium, 2021).

### 5.1.3 SE Queensland dune fields fire history

The oldest fire record from the dune island of Minjerribah, c. 160 km south of the CSM, has preserved fire activity for at least the last ca 210 ka. There are documented indigenous traditions of frequent, low intensity burning on these dune fields (Fensham, 1997; Mulholland, 2021). The oldest archaeological site on Minjerribah is at Wallen Wallen Creek and is dated to 21 ka (Neal and Stock, 1986). Dated archaeological sites on K'gari and the CSM are much younger with the oldest published age at ca 5.5 ka (McNiven, 1991), but it is likely that these areas have been inhabited at least as long as Minjerribah.

More recently, indigenous land management has been absent from the dune fields and replaced by a fire suppression regime that dates to the expansion of the timber industry ca 1870 AD (Hawkins, 1975; Spenser and Baxter, 2006). The consequent shift to less frequent fires is easily identified in palaeoecological studies (e.g., Moss et al., 2015) and has led to the transition of wet sclerophyll forests to rainforest through local fire exclusion (Krishnan et al., 2018). It is also linked to rare, higher intensity fire events. For example, in late 2020 AD, the 'Fraser Island Fire' burned over 50% (~870 km<sup>2</sup>) of K'gari (Figure 5.1b) and is believed to have had a devastating effect on the biota of the dune fields and may be responsible for an acceleration of dune migration (Mulholland, 2021).

Indeed, fire plays a critical role in transforming the landscape (Figure 5.1c-e). It is well documented that fire may lead to the formation, acceleration, and/or erosion of dunes (Levin et al., 2012; Shumack and Hesse, 2018; Ellerton et al., 2018; *Chapter 3*). Ellerton et al. (2018) discovered that the most recent activation of the Carlo Blowout in the CSM was initiated by fire and posited that this was unlikely to be a one-time occurrence. As I discussed in *Chapter 3*, fire is one of the primary factors creating the necessary conditions to destabilise steep dune hillslopes. I found that the burned sections of the 2019 'Freshwater Road Fire' (Figure 5.1e) induced dry-ravel and sheetwash (similar to sand avalanching) but was limited to the youngest dunes (Figure 5.1b and Supplementary Figure A.5.1). I hypothesised that this was due to changes in sediment transport styles associated with hillslope gradients after fire. This study aims to help elucidate the effects of fire on dune erosional and depositional processes over multi-millennial periods, and how these changes may influence our interpretations of charcoal records.

Landscapes such as the SE Queensland dune fields, with high fuel loads and proximity to consistent winds, are prone to wildfires (Filion, 1984; Thompson and Moore, 1984; Srivastava et al., 2012; Shumack et al., 2017; Ellerton et al., 2018); however, dune environments are rarely targeted for paleofire reconstruction. This is most likely because they are regarded as too ephemeral or too difficult to extract reliable multi-millennial environmental records. There are few bogs in the CSM so there are no fire records documented within the immediate dunes despite the inferred importance of fire in maintaining the local environment. This is in contrast to the other SE Queensland dune fields (i.e., K'gari and Minjerribah) which have multiple charcoal records (e.g., Donders et al., 2006; Moss et al., 2013; Barr et al., 2013; 2017; Atahan et al., 2015; Schreuder et al., 2019; Mariani et al., 2019; Kemp et al., 2021; Maxson et al., 2021) from bog, lake and fen settings. The closest records from the CSM dune field are from the Rainbow Beach patterned fen complexes approximately 10 km north-west of the dune field (Figure 5.2) (Moss, 2014; Hanson et al., 2023) which provide local records to compare with records from the CSM.



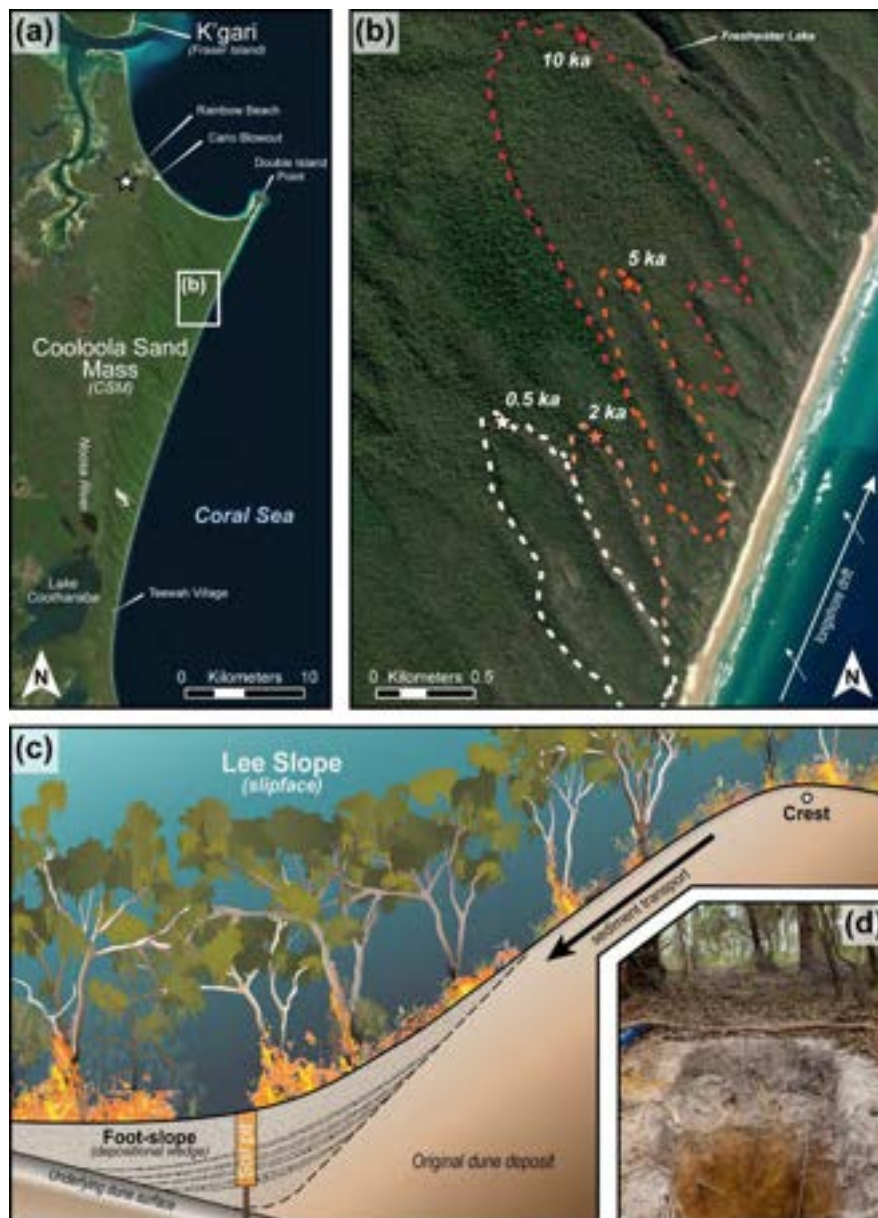


**Figure 5.2:** Site location. **(a)** Satellite imagery of the Coolooloola Sand Mass (CSM) with areas of interest, and the Rainbow Beach patterned fen complex (white star). **(b)** Close-up of the four dunes used in this study (dashed lines) and locations of the depositional foot-slope sites (stars) found on each dune's North-facing slipface. The dunes selected in the research represent each of the four major Holocene dune activation/stabilisation phases (*Chapter 2*; *Chapter 4*; Ellerton et al., 2020) (see Supplementary Figure A.5.2) **(c)** Conceptual diagram of sediment transport (sand and charcoal) and deposition on a dune's slipface. Charcoal particles are produced on the dune's surface during fires (small black dots), transported down gradient, and deposited in the foot-slope position as disseminated charcoal or charcoal layers. I hypothesise that charcoal analysed in this study remains in stratigraphic order and is produced locally because sediment is retained within the CSM's basins (*Chapter 3*) and charcoal particles are large (between 180  $\mu\text{m}$  and 2 mm). The red box indicates the location that soil pits were excavated to obtain a fire record for this study. A sand auger was used at the base of each pit to determine the depth of the underlining dune surface (i.e., maximum deposit thickness) which is inferred to represent the initiation of sediment deposition (i.e., dune age). **(d)** Soil profile looking up to crest on the 10 ka dune.

## 5.2 Methods

### 5.2.1 Site selection and sampling design

The CSM in SE Queensland, Australia is positioned approximately 150 km north of Brisbane and immediately south of the sand island K'gari. The dune field has an area of 240 km<sup>2</sup> and is composed of large parabolic dunes with crests up to 240 meters above sea-level. They are comprised of >98% well-sorted siliceous sands (180-250  $\mu$ m) (Thompson, 1983; 1992; Tejan-Kella et al., 1990). The freely drained soils and the humid subtropical climate with warm, wet summers and mild, dry winters (MAP 1500 mm) (Peel et al., 2007; BOM, 2019) promote podsolisation. Sediments are retained within inter-dune and foot-slope positions due to the lack of fluvial and aeolian erosion following stabilisation by vegetation (*Chapter 3*). The land-surface stability coupled with high porosity and permeability lead to the unabated development of giant podsols (Thompson, 1981). Changes in dune-form age correspond with systematic changes in soil and vegetation development. The dune field has been extensively dated (Tejan-Kella et al., 1990; Walker et al., 2018; Ellerton, et al., 2020; *Chapter 4*; Ellerton et al., 2023) and mapped (Ward, 2006; *Chapter 2*).

Most dunes initiate near the coastline from disturbances such as sea-level rise, storms, and/or fires (Levin, 2011; *Chapter 4*). Their path inland is maintained by the nearly limitless sediment supply from the longshore drift system (Boyd et al., 2008) and consistent SE winds (Coaldrake, 1962) until they are ultimately stabilised by vegetation (Levin, 2011). The timing of dune stabilisation is penecontemporaneous with the initiation of dune sediment erosion and deposition (i.e., the transition from aeolian to colluvial processes) (*Chapter 4*). These processes have been occurring for at least 800 kyr, resulting in one of the oldest and most complex coastal dune sequences in the world (Ellerton et al., 2020; 2022).

In this study, I sampled depositional wedges at the base of four closely adjacent Holocene parabolic dunes with emplacement (stabilisation) ages of  $0.44 \pm 0.10$  ka,  $2.14 \pm 0.27$  ka,  $4.89 \pm 0.45$  ka, and  $9.82 \pm 0.98$  ka, hereafter referred to as the 0.5 ka, 2 ka, 5 ka, and 10 ka dunes, respectively (Figure 5.2b). The age of each dune was determined by optically stimulated luminescence (OSL) dating from dune crest positions and represent each of the four major Holocene dune activation/stabilisation phases (*Chapter 2*; Ellerton et al., 2020; *Chapter 4*) (Supplementary Figure A.5.2). Sample sites were chosen from depositional settings at the base of the lee-side slipface of each dune (Figure 5.2b). All sampled soil pits have a

similar upslope source area (a planar hillslope length of <70 m to the dune crest) on a north-facing dune slipface (Figure 5.2c-d) and are located in 'dry' sclerophyll forest with similar vegetation types and canopy cover. The dominant taxa include Pink Bloodwood (*Corymbia intermedia*), Scribbly Gum (*Eucalyptus signata*), Forest-oak (*Casuarina torulosa*), Black She-oak (*Casuarina littoralis*), Banksia (*Banksia serrata*), and Blackbutt (*Eucalyptus pilularis*) with a canopy cover between ~60-80%.

Each site was hand excavated to a minimum depth of 1.75 m (Figure 5.2d). Additionally, I augered at the base of each pit to determine the depth of the underlying dune surface (i.e., deposit thickness) which was identified by the presence of buried horizons (Figure 5.2c). This depth is inferred to represent the initiation of sediment deposition and the timing of dune stabilisation (i.e., the transition from aeolian to colluvial sediment transport); therefore, I utilised the OSL ages collected from dune crest to reflect the maximum basal age of dune foot-slope deposits (white dot in Figure 5.2c). The profile face was cleaned and described using standard soil description protocols (i.e., Schoenberger et al., 2002). Descriptions included characterising soil horizons, grain size, boundaries of horizons, rooting depths, and soil structure. All charcoal layers and bioturbation features (e.g., ant burrows, nest construction, root growth and decay, and/or evidence of tree-throws) were recorded. Charcoal fragments visible on the exposure face were sampled, labelled, and saved for radiocarbon ( $^{14}\text{C}$ ) analysis.

For each soil profile, sediment samples and bulk density cores were extracted (~2000 cm<sup>3</sup> and ~260 cm<sup>3</sup>, respectively) at predetermined depths with highest sampling density near the surface. Samples were extracted contiguously across the profile face at 0.05 m intervals from 0-0.1 m and then at 0.1 m intervals to 1.5 m after which intervals of 0.25 m were used. In this study, I assign the mid-point for each sample depth interval when placing them in the context of depth and time (e.g., a depth range of 0.1-0.2 m would be reported as being at 0.15 m). Bulk density was measured using the short core extraction method (Blake and Hartge, 1986), which involves driving a core into the pit face and carefully removing it with a flat edged soil knife. All samples were collected from the bottom of the profile upward to avoid contamination. The sampling was not initially designed with a fire record in mind and limitations created by the sampling design are discussed later.

### 5.2.2 Sediment sample preparation

All samples were dried for 48 hrs at 50° C. Dried samples were passed through a 2 mm stainless steel sieve to remove the coarse fraction (CF). Very little CF was present (average  $0.34 \pm 0.73\%$  by mass) and only consisted of root and charcoal fragments. This is not surprising in an aeolian sand deposit. Coarse charcoal particles in the CF were handpicked and saved for radiocarbon dating. The remaining fine fraction (FF) (<2 mm) soil samples were saved and labelled to be later sub-sampled for charcoal counting.

### 5.2.3 Bulk density

Bulk density cores retrieved from the field were oven dried for 48 hrs at 105 °C to remove all moisture and then weighed. A 2 mm sieve was used to partition soils into CF and FF and weighed ( $M_{CF}$  and  $M_{FF}$ , respectively). The volume of the CF ( $V_{CF}$ ) was determined for each core by dividing the  $M_{CF}$  by the density of the CF, which is assumed to be a constant  $0.5 \text{ g cm}^{-3}$  (EQ.5.1a). This density value was selected because charcoal and fine roots range between  $0.4 \text{ g cm}^{-3}$  and  $0.6 \text{ g cm}^{-3}$  as determined through water displacement. The  $V_{CF}$  was subtracted from the bulk density core volume ( $V_T$ ),  $\sim 260 \text{ cm}^3$ , to obtain the FF volume ( $V_{FF}$ ) (EQ.5.1b). Finally, FF bulk density ( $BD_{FF}$ ) was calculated by dividing the mass by the volume (EQ.5.1c) of the fine fraction.

$$M_{CF}/0.5 = V_{CF} \quad (\text{EQ.5.1a})$$

$$V_T - V_{CF} = V_{FF} \quad (\text{EQ.5.1b})$$

$$M_{FF}/V_{FF} = BD_{FF} \quad (\text{EQ.5.1c})$$

### 5.2.4 Charcoal counting

Charcoal retained in sedimentological records has been used as a proxy for fire activity and regimes (e.g., Whitlock and Larsen, 2001; Marlon et al., 2016; Hennebelle et al., 2020). Most traditional aquatic archives, such as lakes and bogs, utilise micro-charcoal particles (e.g., <125  $\mu\text{m}$ ) that are associated with distal sources through either airborne fall-out (generally c. 1-2 km) and/or by inlet streams from the surrounding catchment area (Whitlock & Millspaugh, 1996; Whitlock and Larsen, 2001; Higuera et al., 2007). As a result, these records typically represent broad, regional fire signals that may include an amalgamation of vegetation type and biozones (Marlon et al., 2006; Vachula et al., 2018). In this study, I focus

my analyses on larger macro-charcoal which represents local (in-situ) fire production originating within c. 100 m of the dune soil profiles (e.g., Clark et al., 1998; Gavin et al., 2003; Higuera et al., 2005; Sanborn et al., 2006; Iglesias et al., 2015; Itter, et al., 2017; Leys et al., 2017; Morris et al., 2017). I analysed charcoal >180 µm because smaller fragments are more susceptible to eluviation processes (the vertical transport of particles through the soil profile), due to the homogenous (180-250 µm) and well drained (600 mm hr<sup>-1</sup>) dune sands (Reeve et al., 1985).

Fine fraction (FF) soil samples for all depth intervals were homogenised, sub-sampled using a riffle splitter (~5 g) and if necessary, treated with 15 mL of 10% HCl for 24 hrs to remove any sesquioxide coatings on sand grains (i.e., samples collected from well-developed B horizons). Each sample was sequentially wet sieved at 355 µm, 250 µm, and 180 µm. Care was taken not to damage the charcoal fragments. Under a dissecting microscope (2-20x magnification) all charcoal was counted (#) in the following size classes (180-250 µm, 250-355 µm, and 355 µm-2 mm). Charcoal counts are converted to charcoal concentration by dividing the charcoal count by the sub-sample volume (V). The volume is calculated by using the initial sub-sample mass (M<sub>i</sub>) divided by the BD<sub>FF</sub> from the appropriate depth interval (see EQ.2). This was completed for all samples for each profile and results are plotted against depth. Additionally, I compare charcoal concentrations between each size class.

$$\text{Charcoal concentration} = \left( \frac{\#}{[M_i/BD_{FF}]} \right) = \left( \frac{\#}{[V]} \right) \quad (\text{EQ.5.2})$$

### 5.2.5 Charcoal selection and preparation for radiocarbon (<sup>14</sup>C) dating

Even in regions with homogenous geomorphology and ecology, it is necessary to acquire a large number of dates to adequately resolve fire history. To build a chronological framework for each depositional profile, I selected charcoal samples to be radiocarbon (<sup>14</sup>C) dated by accelerator mass spectrometry (AMS). My primary targets were >2 mm diameter charcoal fragments picked directly from the profile face of known absolute depths (n=24). I supplemented these samples with charcoal within the coarse fraction (n=22) and although these charcoal samples have inherently higher uncertainty with regard to depth (i.e., they come from intervals of 0.05 m to 0.25 m), they provide a means to evenly distribute radiocarbon dating across all profiles.

Radiocarbon samples were dated at two laboratories, with 46 samples dated in total. Twelve samples were dated at the Waikato Radiocarbon Dating Laboratory in 2019 and 2021. A further 34 samples were dated at the Australian Nuclear Science and Technology Organisation (ANSTO) radiocarbon laboratory in 2021 and 2022 (Fink et al., 2004). At both laboratories, the charcoal samples were pre-treated using the standard acid-base-acid (ABA) protocol before being combusted and graphitised (Hua et al., 2001). Sample graphite was then loaded into aluminium cathodes and measurements were determined by AMS. The results were reported in conventional radiocarbon age or percent modern carbon (pMC) (see Table 5.1).

### 5.2.6 Age-depth model and combining charcoal records

For all profiles, age-depth models were created using the 'rbacon' package (Blaauw and Christen, 2011) in R (R Core Team, 2022) with the calibration data being the Southern Hemisphere calibration curve (SHCal20; Hogg et al., 2020) extended to the recent time using the post-bomb atmospheric calibration curve for Southern Hemisphere zone 1-2 (Bomb22SH12; Hua et al., 2022). All the modelled ages were reported in calibrated years before 1950 (cal. yr BP) at 95% confidence interval (CI). Additionally, I set the surface age to 2019 (i.e., -69 cal. yr BP; date of sample collection) and the basal ages to the OSL-dated dune ages collected from dune crest (Figure 5.2c). I attributed the age for each sample to the mid-point of each sample depth range. Charcoal records are evaluated by plotting sample depth to charcoal concentration (particles  $\text{cm}^{-3}$ ). I normalise for changes in sedimentation rates within and between sites by calculating charcoal accumulation rates (CHAR) expressed in units of particles  $\text{cm}^{-2} \text{yr}^{-1}$  (Long et al., 1998). Charcoal production can vary amongst sites due to local conditions (i.e., moisture content, fire intensity, and biomass); therefore, I rescaled each record to range from 0-1 by dividing by the maximum CHAR value (Power et al., 2008). Once normalised, records were combined and plotted against time to establish a composite master charcoal record for the Holocene dune field. For each dune and master charcoal records, CHAR peaks were identified visually.

Our results were compared to published charcoal records from a nearby patterned fen complex (Hanson et al., 2023), and two lake records with similar forest types and, presumably, similar fire histories (Donders et al., 2006; Mariani et al., 2019) (white stars in

Figure 5.1b, Supplementary Figure A.5.3). Additionally, I compared the results to Mooney et al. (2011) and Williams et al. (2015) subtropical high-pressure belt (25°S – 45°S) record of biomass burning. The purpose of this cross-site comparison is to assess whether my master charcoal record depicted reasonable local trends and/or evidence of broad regional fire-regime changes as compared to those derived from more traditional (aquatic) archives.

## 5.3 Results

### 5.3.1 Field observations and soil characterizations

Soil profiles were excavated to a maximum depth of 2.75 m and were classified from youngest to oldest as an inceptisol, rudimentary podsol, podsol, and podsol (Figure 5.3). As expected, all soils have uniform grain size distributions concentrated between 180-250  $\mu\text{m}$ . The younger profiles from the 0.5 ka and 2 ka dunes have minimal pedogenic development and charcoal is dispersed throughout the profile; however, distinct charcoal layers (CL) are observed. The 0.5 ka profile had one layer (CL1: 0.2-0.3 m) and no charcoal was observed >1.5 m. All sediment below 1.6 m was classified as primary dune sediments due to its lack of soil development and absence of organic material. The 2 ka profile had four charcoal layers near the base (CL2: 1.20-1.30 m, CL3: 1.70-1.80 m, CL4: 1.90-2.10 m, and CL5: 2.20-2.40 m). In contrast, the oldest profiles from the 5 ka and 10 ka dunes have distinct transitions between the pedogenic horizons, with the exception of the boundary between the A and E horizons, which is diffuse. Charcoal was disseminated throughout the profile with elevated concentrations at the base and near the surface. Additionally, several months after pit excavations the 'Freshwater Road Fire' (Figure 5.1b and e) burnt all site locations. The fire removed vegetation and deposited charcoal at the surface, but only induced a ~0.1 m sand ravel deposit on the 0.5 ka dune foot-slope (Figure 5.3a and Supplementary Figure A.5.1). This deposit was not included in my charcoal analyses and is only utilised as a point of discussion.

For all sites, root growth and decay are the most prevalent forms of post-depositional mixing. This activity is greatest at the surface and rapidly decreases with depth, such that most roots are confined within the A horizon (<0.5 m depth). Unexpectedly, I observed little evidence of other common forms of bioturbation (i.e., ant mounds, rodent burrows, tree throws, and/or nest construction). This is in stark contrast to the upslope, eroding positions

at the CSM where all these processes are commonly observed, and where I visually estimated up to three ant colonies per  $\text{m}^{-2}$  along the hillslope surface.

### 5.3.2 Charcoal concentrations

Charcoal at all sites was well-preserved (black, angular and opaque). Concentrations were consistent across all the sites and all size classes depicted similar trends with depth (Figure 5.3, Supplementary Figure A.5.4). The 180-250  $\mu\text{m}$  size class contributes approximately half of the cumulative charcoal concentrations for each depth interval, whereas the larger size classes (250-355  $\mu\text{m}$  and 355  $\mu\text{m}$ -2 mm) each contributed about a quarter of the cumulative charcoal concentrations. For this reason, I simplify my results by only reporting aggregate charcoal concentrations hereafter. Combined charcoal concentrations from all size classes (i.e., combined charcoal counts from 180  $\mu\text{m}$ -2 mm) are measured from 0 to 49.4 particles  $\text{cm}^{-3}$  with the highest values found near the surface. Out of the 78 sampled depth intervals, only three samples lacked charcoal (not including samples at depths >160 cm from the 0.5 ka dune which constitutes the original dune deposit). The average charcoal concentrations for each profile generally increased with dune age from  $3.9 \pm 5.7$ , through  $5.8 \pm 2.8$ , and  $14.5 \pm 16.6$ , to  $13.9 \pm 11.6$  particles  $\text{cm}^{-3}$ .

### 5.3.3 Radiocarbon ( $^{14}\text{C}$ ) analysis and age-depth modelling

Radiocarbon results from 46 charcoal particles produced ages ranging from 0.01 to 7.125 cal. ka BP (Table 5.1). Twelve, 14, and 17 radiocarbon samples from the 2 ka, 5 ka, and 10 ka dunes were analysed, respectively. The 0.5 ka dune had few radiocarbon targets and only yielded three ages. Due to my sampling strategy, 52% of the total dates are less than 2 cal. ka BP. I observe consistent trends with depth, with only four age reversals ( $> \pm 2\sigma$ ) (Figure 5.4). The ages of the sampled intervals represent a range of ages owing to the contiguous sampling design, see Supplementary Table A.5.1; however, I find samples from the same depth interval within sites yield similar ages (e.g., Samples 33 and 34; Samples 44 and 45 in the 10 ka dune). Sedimentation rates are the highest where charcoal layers are present (i.e., the entire 0.5 ka dune and below 1.20 m on the 2 ka dune). In general, rates decrease moving up the excavated profiles, towards the surface.



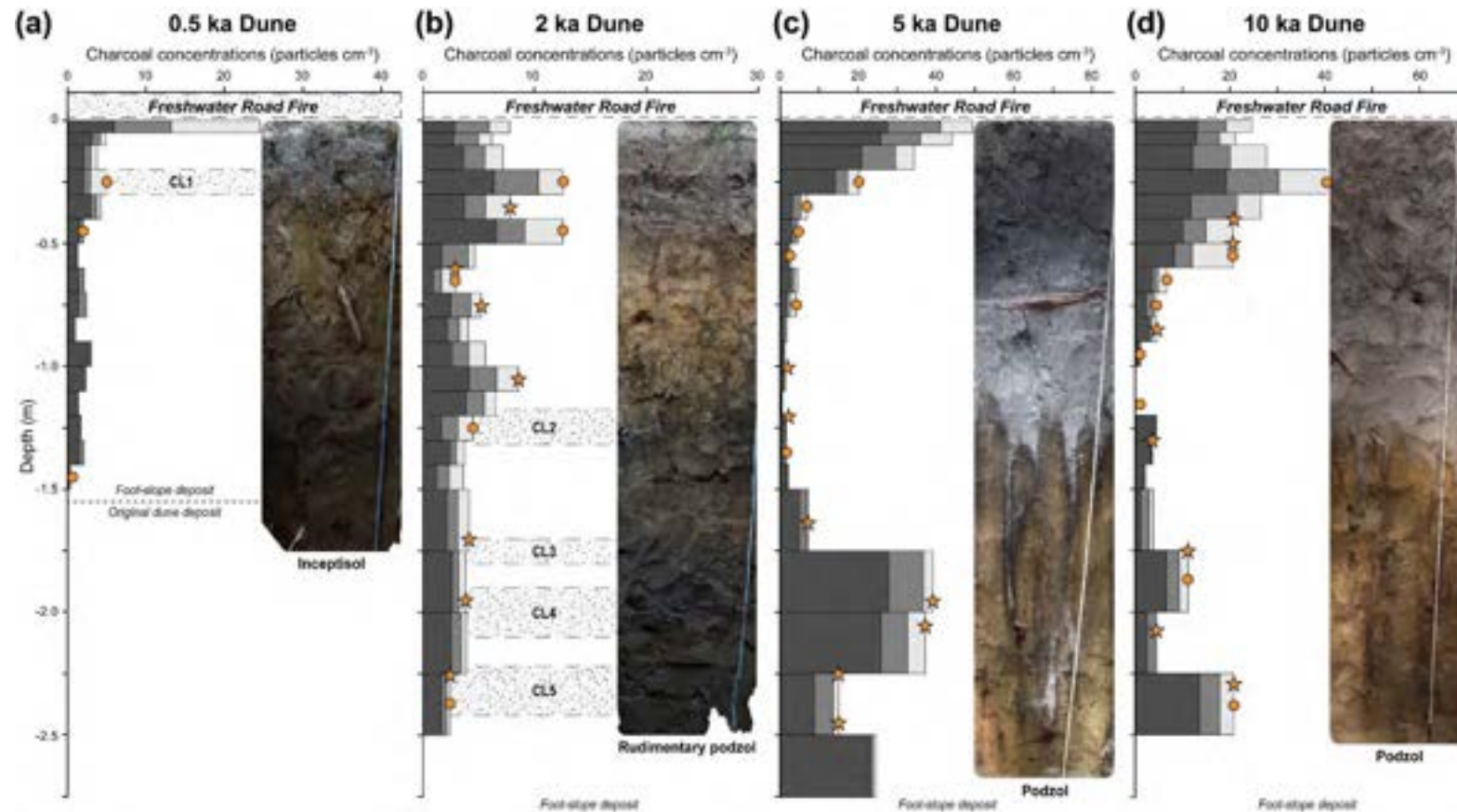


**Figure 5.3:** Charcoal concentrations for the (a) 0.5 ka, (b) 2 ka, (c) 5 ka, and (d) 10 ka dune depositional sites. For each depth interval (width of bar) charcoal was counted for all size classes 180-250  $\mu\text{m}$  (dark grey), 250-355  $\mu\text{m}$  (grey), and 355  $\mu\text{m}$ -2 mm (light grey). Charcoal layers identified in the profile face are indicated with a band of black dots and labelled (CL#). Samples collected for radiocarbon analysis are indicated with an orange star or an orange circle whether they were collected at a discrete depth or from a sample depth interval, respectively. Charcoal layers only occur on the two youngest dunes and were incorporated in multiple sample intervals due to predetermined sampled depths. Note, the Freshwater Road Fire severely burnt and deposited fresh charcoal at the surface of all sites (dashed lines labelled 'Freshwater Road Fire') after pit excavation and sample collection, but only produced a 0.1 m charcoal rich dry-ravel deposit at the 0.5 ka site. As a result, no charcoal concentrations were recorded for this interval. For more information on each soil profile see Supplementary Figures A.5.4 – A.5.8.

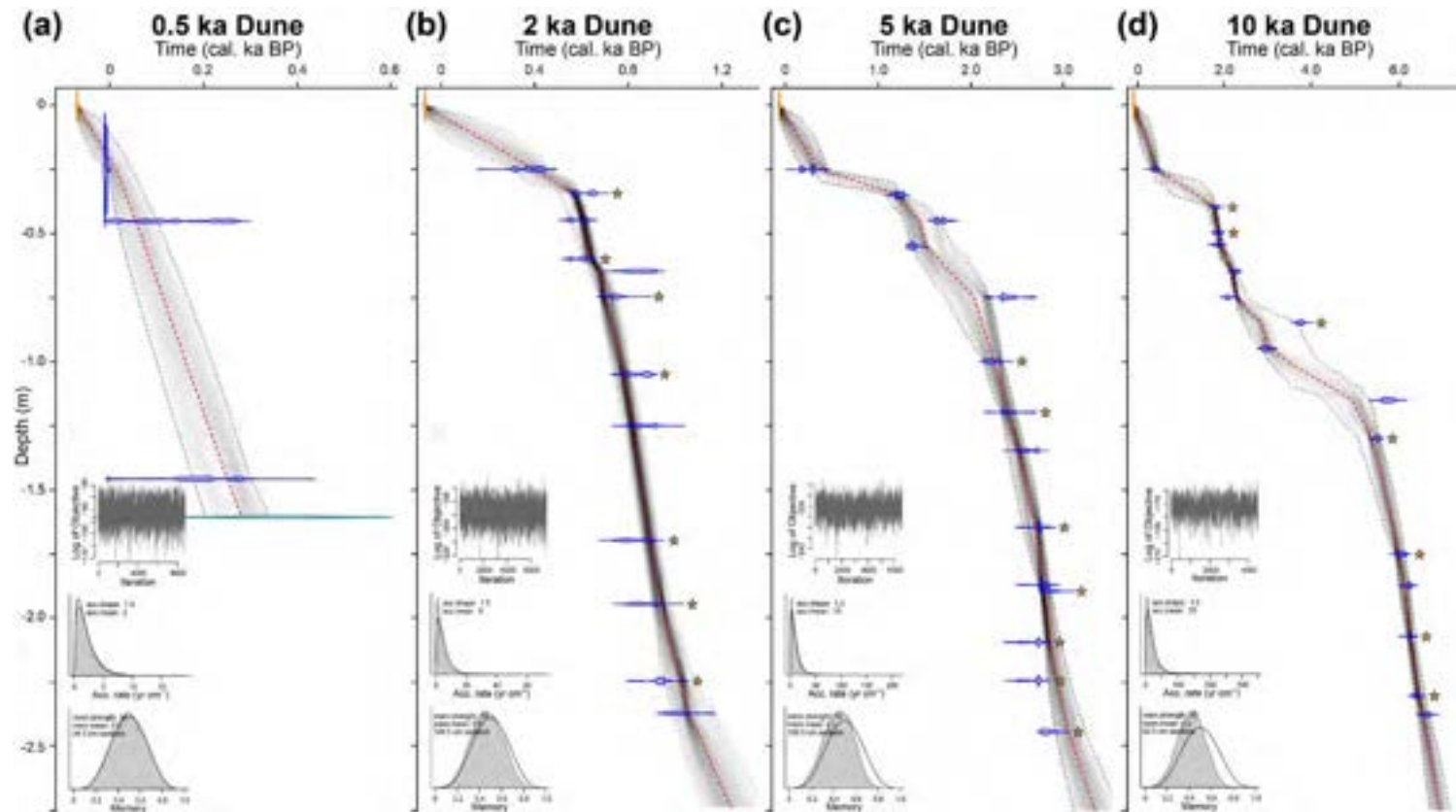


**Figure 5.4:** Bayesian age-depth models generated for the (a) 0.5 ka, (b) 2 ka, (c) 5 ka, and (d) 10 ka dune depositional sites. For each site, I set the age of the surface (0 m) to the date of pit excavation (vertical orange marker), and the basal age to the OSL-dated dune age collected from dune crest. All cal. ages are obtained through radiocarbon ( $^{14}\text{C}$ ) dating of charcoal fragments using the Southern Hemisphere calibration curve (SHCal20; Hogg et al., 2020) extended to the recent time using the Post-bomb Atmospheric calibration curve for Southern Hemisphere zone 1-2 (Bomb22SH1-2; Hua et al., 2022). Graphs were produced using 'rbacon' (Blaauw and Christen, 2011) in R (R Core Team 2022). The calibrated year probability distributions estimates are shown as blue and aqua markers for  $^{14}\text{C}$  and OSL ages, respectively. The red dashed line bounded by the grey dotted lines represents the age-depth model best fit and the 95% confidence intervals, respectively. Note, the y-axis only extends to 2.75 m, which covers all sample intervals, and does not include the complete age-depth model that extends to the base of each deposit (original dune deposits or overlapped topography). Additionally, samples collected from discrete depths are labelled with an orange star.

**Table 5.1:** All ages used to produce age-depth models in this study from woody macro-charcoal ( $^{14}\text{C}$ ) and primary dune sands (OSL) are reported in years relative to 1950 (Figure 5.4). Lab numbers beginning with ‘Wk’, ‘OZ’, and ‘USU’ were analysed at the Waikato Radiocarbon Dating Laboratory, ANSTO, and Utah State University Luminescence Laboratory, respectively. Age calibration was performed using the Southern Hemisphere calibration curve (SHCal20; Hogg et al., 2020) extended to the recent time using the Post-bomb Atmospheric calibration curve for Southern Hemisphere zone 1-2 (Bomb22SH1-2; Hua et al., 2022), and modelled ages were produced using ‘rbacon’ (Blaauw and Christen, 2011) in R (R Core Team 2022).

Sample #	Lab ID	Depth (m)	OSL ages (ka $\pm 1\sigma$ )	Conventional $^{14}\text{C}$ ages (yr BP $\pm 1\sigma$ )	Calibrated ages (95% CI) (cal. yr BP)	Modelled cal. ages (95% CI) (cal. yr BP)
<i>0.5 ka Dune</i>						
-	Surface	0	-	-	-69 <sup>§</sup>	-69 (-66 - -72)
1	OZAF02	0.20 – 0.30	-	102.61 $\pm$ 0.32*	-5 (0 - -9)	11 (49 - -4)
2	OZAF03	0.40 – 0.50	-	170 $\pm$ 25	116 (278 - -3)	59 (102 - 17)
3	OZAF04	1.40 – 1.50	-	220 $\pm$ 25	192 (298 - -4)	266 (300 - 178)
-	<sup>1</sup> USU-2283	<sup>†</sup> 1.60	0.44 $\pm$ 0.10	-	-	292 (344 - 205)
<i>2 ka Dune</i>						
-	Surface	0	-	-	-69 <sup>§</sup>	-69 (-66 - -72)
4	OZAE96	0.20 – 0.30	-	335 $\pm$ 25	389 (448 - 300)	398 (463 - 299)
5	Wk-52211	0.35	-	718 $\pm$ 18	628 (666 - 565)	575 (598 - 512)
6	OZAE97	0.40 – 0.50	-	625 $\pm$ 25	604 (635 - 535)	608 (633 - 555)
7	Wk-52212	0.60	-	640 $\pm$ 19	608 (636 - 545)	644 (673 - 613)
8	OZAE98	0.60 – 0.70	-	980 $\pm$ 30	852 (924 - 771)	680 (712 - 639)
9	Wk-52213	0.75	-	882 $\pm$ 21	745 (793 - 683)	703 (751 - 680)
10	Wk-52214	1.05	-	960 $\pm$ 19	852 (907 - 768)	780 (814 - 745)
11	<sup>2</sup> Wk-50298	1.20 – 1.30	-	1017 $\pm$ 26	857 (930 - 798)	820 (855 - 791)
12	OZAE99	1.70	-	955 $\pm$ 30	834 (917 - 740)	895 (928 - 864)
13	Wk-50299	1.95	-	1023 $\pm$ 24	859 (955 - 800)	945 (981 - 908)
14	OZAF01	2.25	-	1080 $\pm$ 25	944 (1047 - 908)	1031 (1082 - 957)
15	Wk-50300	2.35 – 2.41	-	1166 $\pm$ 24	1013 (1062 - 960)	1060 (1169 - 1002)
-	<sup>3</sup> USU-3021	<sup>†</sup> 5.10	2.14 $\pm$ 0.27	-	-	2373 (2679 - 2109)
<i>5 ka Dune</i>						
-	Surface	0	-	-	-69 <sup>§</sup>	-69 (-66 - -72)
16	OZAE83	0.2 – 0.3	-	270 $\pm$ 25	285 (322 - -4)	354 (456 - 184)
17	OZAE84	0.3 – 0.4	-	1350 $\pm$ 25	1225 (1285 - 1177)	1203 (1282 - 1085)
18	OZAE85	0.4 – 0.5	-	1815 $\pm$ 25	1662 (1747 - 1590)	1425 (1661 - 1282)
19	OZAE86	0.5 – 0.6	-	1535 $\pm$ 20	1367 (1411 - 1314)	1502 (1811 - 1361)
20	Wk-50296	0.7 – 0.8	-	2397 $\pm$ 26	2381 (2671 - 2179)	2056 (2211 - 1732)
21	OZAE87	1.0	-	2290 $\pm$ 25	2225 (2341 - 2143)	2253 (2343 - 2148)
22	OZAE88	1.20	-	2410 $\pm$ 25	2401 (2684 - 2332)	2406 (2489 - 2336)

23	OZAE89	1.30 – 1.40	-	2585 ± 25	2626 (2753 - 2493)	2523 (2605 - 2410)
24	OZAE90	1.65	-	2665 ± 25	2752 (2845 - 2718)	2717 (2767 - 2570)
25	OZAE92	1.75 – 2.00	-	2695 ± 25	2769 (2849 - 2737)	2783 (2854 - 2741)
26	OZAE91	1.90	-	2795 ± 25	2848 (2946 - 2772)	2796 (2868 - 2760)
27	OZAE93	2.10	-	2630 ± 30	2734 (2777 - 2516)	2858 (2979 - 2805)
28	Wk-50297	2.25	-	2624 ± 25	2733 (2767 - 2518)	2932 (3076 - 2840)
29	OZAE94	2.45	-	2760 ± 30	2818 (2920 - 2754)	3059 (3246 - 2922)
-	<sup>1</sup> USU-2284	<sup>†</sup> 5.30	4.89 ± 0.45	-	-	5716 (6328 - 5197)
<i>10 ka Dune</i>						
-	Surface	0	-	-	-69 <sup>§</sup>	-69 (-66 - -72)
30	OZZ591	0.20 – 0.30	-	560 ± 25	-	-
31	OZZ592	0.20 – 0.30	-	365 ± 35	392 (487 - 309)	421 (493 - 308)
32	OZAE76	0.40	-	1905 ± 25	1792 (1875 - 1725)	1752 (1824 - 1611)
33	OZAE77	0.50	-	1955 ± 25	1858 (1928 - 1749)	1856 (1924 - 1761)
34	OZZ594	0.50 – 0.60	-	1950 ± 35	1852 (1985 - 1746)	1905 (1998 - 1834)
35	OZAE78	0.60 – 0.70	-	2275 ± 25	2231 (2337 - 2140)	2174 (2271 - 2105)
36	OZZ596	0.70 – 0.80	-	2160 ± 35	2087 (2298 - 2003)	2284 (2524 - 2225)
37	Wk-50293	0.85	-	3534 ± 24	3768 (3871 - 3652)	2823 (3699 - 2445)
38	OZAE79	0.90 – 1.00	-	2860 ± 25	2926 (3060 - 2848)	3008 (3960 - 2849)
39	OZZ597	1.10 – 1.20	-	5040 ± 70	5743 (5900 - 5600)	4982 (5358 - 4285)
40	OZAE80	1.30	-	4815 ± 25	5522 (5590 - 5334)	5381 (5570 - 5074)
41	Wk-50294	1.75	-	5305 ± 26	6062 (6183 - 5934)	5997 (6152 - 5922)
42	OZAE81	1.75 – 2.00	-	5485 ± 30	6240 (6308 - 6125)	6123 (6235 - 6011)
43	OZAE82	2.07	-	5495 ± 30	6246 (6385 - 6128)	6277 (6385 - 6197)
44	Wk-50295	2.30	-	5648 ± 26	6375 (6483 - 6305)	6455 (6602 - 6359)
45	OZZ598	2.25 – 2.50	-	5880 ± 35	6659 (6778 - 6502)	6553 (6688 - 6442)
46	OZZ599	2.90	-	5995 ± 35	6788 (6895 - 6670)	7124 (7393 - 6834)
-	<sup>1</sup> USU-2285	<sup>†</sup> 4.50	9.82 ± 0.98	-	-	10,215 (11196 - 9414)

\* – Indicates a modern sample, whose measured <sup>14</sup>C content was reported in percent modern carbon (pMC) instead of conventional <sup>14</sup>C age.

<sup>†</sup> – Depth indicates the maximum depth of each profile and basal ages obtained from OSL ages.

<sup>§</sup> – Surface date in cal. yr BP. <sup>1</sup> – Date from Ellerton et al. (2020), <sup>2</sup> date from *Chapter 3*, <sup>3</sup> date from *Chapter 4*. OSL ages were collected from dune crest and were used to represent the basal age of each subjacent foot-slope deposit.

### 5.3.4 CHAR records

Charcoal concentrations are converted into charcoal accumulation rates (CHAR) using accumulation rates derived from the age-depth models. I find that all CHAR values ranged from 0 to 11.6 particles  $\text{cm}^{-2} \text{yr}^{-1}$  and each record shows distinct peaks in CHAR that are detected amongst sites and size classes (Figure 5.5 and Supplementary Figure A.5.4). The 0.5 ka dune has one peak at the surface whereas the 2 ka dune has a peak between ca 1.1 and 0.4 cal. ka BP. The 5 ka dune record has two peaks. The most recent occurred within the last 0.3 ka and the earlier peak at ca 3.4-2.6 cal. ka BP. The 10 ka dune has four peaks at ca 6.7-5.3 cal. ka BP, peaks between ca 3.0-2.6 and 2.2-1.6 cal. ka BP, and the most recent started ca 0.5 cal. ka BP. When combined into a composite master record I observe five peaks occurring between ca <0.3, 1.1-0.4, 2.2-1.6, 3.4-2.6, and 6.7-5.3 cal. ka BP (vertical orange bars in Figure 5.5e) regardless of including or excluding CHAR values associated with episodic sediment transport (white line or black area, respectively). In general, CHAR peaks increase in frequency after ca 3.4 cal. ka BP with the highest values in the last century.

Not all CHAR peaks register as visible charcoal layers in the soil profiles. Charcoal layers (CL1-CL5) are only observed within the two youngest sites (Figure 5.3a-b). These differences are due to the relatively coarse and contiguous sampling intervals and that not all charcoal used for radiocarbon dating were from discrete depths. This caused charcoal layers to be incorporated in multiple samples (Figure 5.3), including those with low charcoal concentrations, which result in a smoothed CHAR record.

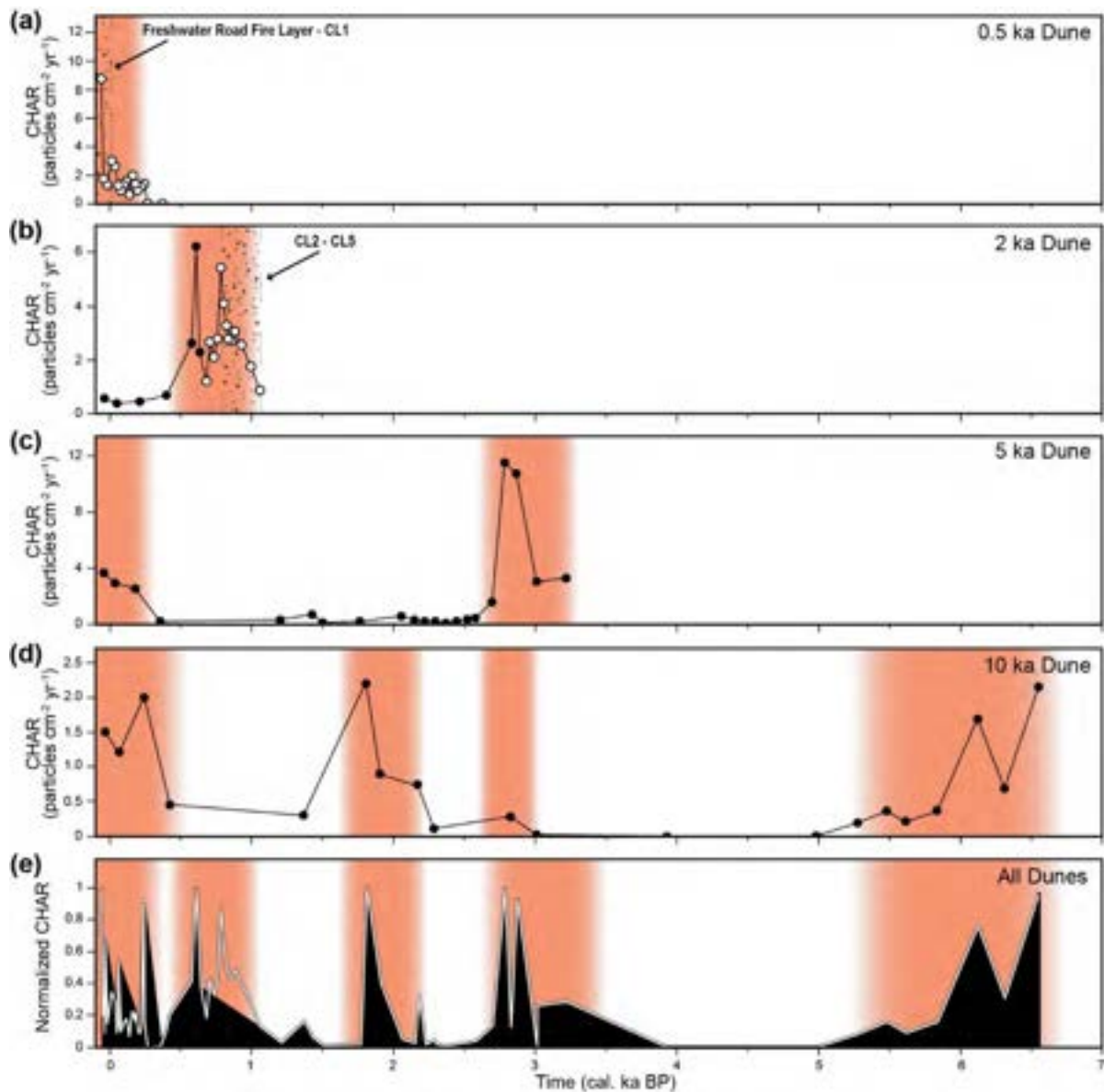


**Figure 5.5:** Charcoal accumulation rates (CHAR) and the inferred timing of increased fire activity (peaks - vertical orange areas) for the (a) 0.5 ka, (b) 2 ka, (c) 5 ka, and (d) 10 ka dune depositional sites. Locations for all samples are marked with dots, such that white dots indicate episodic sediment transport (sheetwash or dry ravel) associated with the first 1.5 ka of sediment deposition, while black dots indicate slow and continuous sediment transport (soil creep). Charcoal layers (CL) found in profile faces (Figure 5.3) are indicated by a band of black dots and labelled (CL#). For more information on CHAR for each size class and the locations for all CL, see Supplementary Figure A.5.4. (e) A composite master charcoal record was derived from all four sites by dividing each record by its maximum CHAR value and then plotting the normalised CHAR with time. The white line represents a record composed of all CHAR values (n=77) whereas the black area represents samples that only experienced continuous sediment transport (n=48).

## 5.4 Discussion

### 5.4.1 Charcoal preservation within dune foot-slope deposits

Previous studies have successfully used charcoal records from paleosols in blowouts, deflation basins, and swales to understand dune activity with respect to changes in climate and fire regimes (e.g., Fillion, 1984; Seppala, 1995; Käyhkö et al., 1999; Mann et al., 2002; Arbogast and Packman, 2004; Carcaillet et al., 2006; Matthews and Seppala, 2014). This study represents the first attempt to systematically target dune foot-slopes (depositional wedges in front of dune slipfaces) to reconstruct a fire record. I propose that dune foot-slopes are appropriate targets for paleofire reconstruction. Foot-slopes at the CSM are depositional systems that produce sequences of locally derived sediments. Most or all inorganic sediments produced on the adjacent hillslope (dune front avalanche face) are inferred to be deposited and preserved with little disruption or mixing. Short-term hiatuses are likely present, but field observations demonstrate only minor physical post-depositional mixing of particles  $>180\ \mu\text{m}$ . These are limited to the near surface through root growth and decay. The lack of physical mixing is supported by intact and distinct soil horizons, consistent charcoal concentrations amongst size classes, and consistent increases in age with depth. Only four age reversals are observed in my records, and they likely record minor reworking in upbuilding soil A horizons (Almond and Tonkin, 1999) (Figure 5.4).

Fires are common in the dune field (e.g., Mulholland et al., 2021) and charcoal is present throughout the profile of the colluvial foot-slope deposits. As the sites are located within a c. 2 km radius from each other, the similarity of the records is expected and indeed necessary, if these types of sites are to be used to produce reliable fire histories. As depicted in the 0.5 ka dune (Figure 5.3a), there is no evidence of macro-charcoal ( $>180\ \mu\text{m}$ ) found within the original dune deposit ( $>1.6\ \text{m}$  depth) which suggest charcoal in these depositional profiles must be incorporated after dune emplacement (stabilisation). In fact, my previous studies indicated no evidence of charcoal in the primary aeolian deposits from my sampled Holocene dunes (Ellerton et al., 2020; Köhler et al., 2021; *Chapter 4*). The absence of charcoal from primary dune sands within the CSM likely reflects the limited area for fire to initiate in the up-wind direction (i.e., the Coral Sea) and the challenge for fire to penetrate into active dunes due to their limited woody fuel loads (Figure 5.2b).

My local records indicate wildfires that occurred within the CSM's dry sclerophyll forest impacted most dune slopes. Perhaps the best evidence for the preservation of paleofire records are that CHAR peaks are traceable between the different profiles (Figure 5.5) and the trends are consistent regardless of charcoal size classes (Supplementary Figure A.5.4). For instance, the 0.5 ka, 5 ka, and 10 ka deposits identified the same ca <0.3 ka CHAR peak, the 5 ka and 10 ka foot-slope share the CHAR peak at ca 3 cal. ka BP, and all sites had fresh charcoal deposited on their surfaces from the Freshwater Road Fire (Figure 5.3).

An important observation is that I observe minor variability between my records. Fires can be extremely localised and confined to specific sections of the dune field due to the direction of fire propagation or naturally occurring firebreaks (i.e., low-lying swales with high humidity and/or barren sand patches). Indeed, this may explain the differences between my depositional records, especially when episodic sediment transport dominates (within the first ca 1.5 ka of sediment deposition). However, it could be the result of my sampling design, which lacks the necessary resolution to capture all changes in charcoal production and/or events (Figure 5.5). For instance, the 2 ka dune depicts one CHAR peak, which incorporates four charcoal layers (CL2-CL5) from ca 1.1-0.4 cal. ka BP, which did not register at the older sites despite being positioned windward of those sites. This is inferred to be the result of the coarse sample size which incorporated both periods of low and high biomass burning within the same sample, thereby obscuring potential CHAR peaks (see sample locations - dots in Figure 5.5c-d).

Alternatively, the discrepancies could reflect variations in charcoal production or preservation between sites. Cohen-Ofri et al. (2007) demonstrated that oxidising conditions may degrade charcoal structure thereby lowering charcoal preservation potential, like those found within the CSM (<5 pH). The charcoal found within my depositional foot-slopes are large, woody, and are structurally strong (slightly hard to hard consistency). Moreover, I find that average charcoal concentrations between the oldest and youngest sites are nearly four times greater despite having been exposed to acidic conditions longer. Although my coarse sampling design prohibited me from addressing this concern, I believe that chemical degradation of charcoal into fragments smaller than my analyses (180  $\mu$ m-2 mm) is minor and thus not affecting my interpretations. Nevertheless, future studies should consider the preservation potential of charcoal in acidic soil conditions when constructing a fire history.



### 5.4.2 Sedimentation inferences from the age-depth models

In my previous work, I characterised the first phase of dune hillslope development as occurring through episodic sediment transport (dry-ravel and sheetwash) induced by disturbances such as fire on the steep initial dune gradients (*Chapter 3*). These perturbations resulted in rapid topographic adjustments (increased foot-slope sedimentation rates). I discovered that once dune gradients are lowered below their angle of repose ( $0.65 \text{ m m}^{-1}$  or  $33^\circ$ ) which occurs ca 1 kyr after dune stabilisation, a second phase of gradual hillslope evolution with steady and continuous sediment transport (soil creep processes) begins. Indeed, my geochronological and sedimentological data in this study support these assertions.

The age-depth models from the four deposits yield similar trends of increasing age with depth (Figure 5.4) and indicate no substantial break in sedimentation or evidence of erosion (truncated horizons), which support the idea that these dune positions are consistently depositional (*Chapter 3*). Additionally, I find that sedimentation rates decrease with dune age which is to be expected due to the ‘Sadler Effect’ (Sadler, 1981) which may lead to biases in sedimentological records if not accounted for (Vachula et al., 2022). I attempt to account for this effect by averaging the median sediment rate in 100-year intervals for each foot-slope deposit and find that sedimentation rates decrease with age from  $0.34 \pm 0.17$ , through  $0.16 \pm 0.13$ , and  $0.05 \pm 0.05$ , to  $0.03 \pm 0.02 \text{ cm yr}^{-1}$ .

When plotting my sedimentation rates for each sample interval as a function of time since dune stabilisation, I find a distinct transition at ca 1.5 ka (Figure 5.6a). Interestingly, the abrupt shift in sedimentation rates coincides with the presence or absence of charcoal layers found within the excavated sections of the foot-slope deposits. For example, the ca. 1.5 ka transition occurs at 0.35 m depth on the 2 ka Dune which is above the boundary between charcoal preserved in distinct layers and where the charcoal is dispersed throughout (Figure 5.3b).

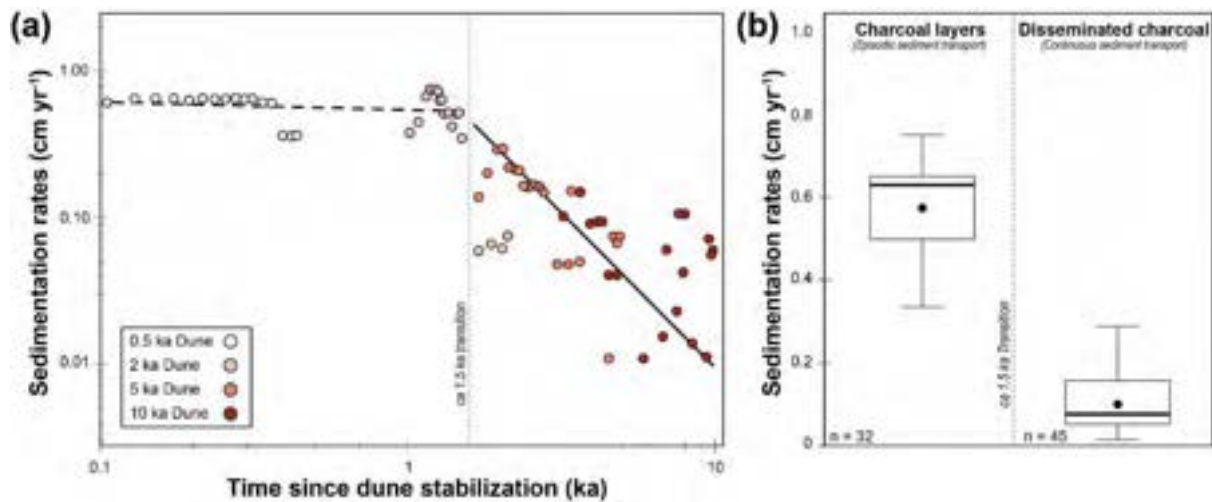


**Figure 5.6:** (a) A log-log plot of the median sedimentation rate for all sampled intervals (dots) from each foot-slope deposit as a function of time since dune stabilisation. Sedimentation rates are initially high (dashed line) then abruptly decrease after ca 1.5 ka (solid line). (b) Box and whisker plots for sedimentation rates before and after this transition. Boxes are the interquartile range with the whiskers representing maximum and minimum values. The black dot is the mean and the horizontal black line represents the median. I hypothesise that the shift in sedimentation rates reflect the transition from episodic (dry-ravel and sheetwash) to continuous sediment transport styles (soil creep) and are associated with the presence or absence of charcoal in layers, respectively. Note that the separation between these two sedimentation rates occur ca 1.5 ka after dune emplacement which is comparable to the findings in Chapter 3 where I estimated ca 1 ka for this transition to occur

I find a substantial difference in the average sedimentation rate between sampled intervals before and after the 1.5 ka transition (i.e., sections associated with either charcoal layers or disseminated charcoal) with mean values of  $0.57 \pm 0.13$  and  $0.10 \pm 0.07$  cm yr<sup>-1</sup>, respectively (Figure 5.6b). My results support the differences in sedimentation rates are associated with the transition from the dominance of episodic to continuous sediment transport on the dune hillslopes (*Chapter 3*) (Figure 5.6). Moreover, these findings highlight the idea that the change from presence to absence of charcoal layers reflects a geomorphic process (the transition from dominance of episodic to continuous sediment transport).

In fact, the observed 0.1 m deposit during the Freshwater Road Fire of 2019 (Figure 5.3a and Supplementary Figure A.5.1) onto the foot-slope of the 0.5 ka dune is consistent with the sedimentation rates during the first phase of sedimentation when charcoal layers are present. For sclerophyll forest, such as those found on the CSM, fires are estimated to occur at ca 20 yr intervals (Keith, 2004). Assuming the Freshwater Road Fire is representative of past fires and that the multi-millennial fire frequency-magnitude relationship is appropriate; I

would expect a fire to deposit ~10 cm of sediment on average within each 20 yr interval (equivalent to a fire-induced sedimentation rate of  $0.5 \text{ cm yr}^{-1}$ ). This estimate is consistent with the sedimentation rates observed in the 0.5 ka and 2 ka deposits, and reflects the contribution associated with episodic sediment transport. Sediment will also actively move downslope even without the perturbation of fire through continuous soil transport processes (e.g., granular relaxation, rain splash, and biogenic soil creep) which I estimated to be an order of magnitude lower (*Chapter 3*).

### 5.4.3 Implications of charcoal layers in dune deposits

Rates of sedimentation and the presence or absence of charcoal layers (CL) are intimately coupled with geomorphic and ecologic processes and must be considered when generating fire records. In the section, I discuss whether CHAR peaks and/or CL in pit faces represent fire-based events (Figure 5.5 and Figure 5.3, respectively) and provide plausible mechanisms for their presence within my dune deposits.

It is not straightforward to determine if CHAR peaks or CL represent individual wildfires. For CHAR peaks, sampling intervals could span more than one fire event and even where sampling intervals are narrow, these intervals may reflect several centuries of accumulation. This is particularly true for fire records that lack a strong chronological framework (limited age constraints) and have charcoal samples with large inbuilt ages which can make interpretations difficult. Although I am confident in my age-depth modelling due to my large quantity of radiocarbon and OSL dates ( $n=50$ ) and small inbuilt ages (ca 10 yrs, Sample 2 in Table 1) there are always uncertainties in these analyses (e.g., Whitlock and Larsen, 2001). Therefore, it is inappropriate to claim elevated CHAR values represent single fire events, such as those found in sections where sedimentation rates are low (e.g., peak at ca 2.2-1.6 cal. ka BP in Figure 5.5d). I propose that individual fire events cannot be identified from CHAR peaks alone, but rather should be used to indicate phases of increased biomass burning (Long et al., 1998; Remy et al., 2018).

Charcoal layers, however, are likely an event-based deposit (Mathews and Seppala, 2014) (i.e., CL1-CL5 in Figure 5.5a-b and Supplementary Figures A.5.5 and A.5.6). As discussed earlier, layers are only formed before ca 1.5 ka after dune stabilisation, when dune hillslope gradients are above their angle of repose and perturbations such as fires can induce episodic

sediment transport near the dune crest. The short (<70 m) and steep ( $0.65 \text{ m m}^{-1}$  or  $33^\circ$ ) hillslopes promote the rapid delivery of sediments to their subjacent foot-slopes (e.g., as I observed following the Freshwater Road Fire, Supplementary Figure A.5.1). These observations indicate that long-term storage of charcoal on hillslopes during this phase is unlikely; therefore, I propose that CL in pit faces are associated with individual fire events.

An important caveat is that not all fires on over steepened slopes induce episodic sediment transport and those that do, do not induce sediment transport evenly across the landscape. To initiate dry-ravel and sheetwash (similar to a sand avalanche), soil cohesion needs to be decreased (Reid and Dunne, 1996; Roering and Gerber, 2005). This can occur by either the removal of organic matter, reduction of water content and roots, or by the production of hydrophobic surface soils (Bridge and Ross, 1983; Doerr et al., 2000; Shakesby and Doerr, 2006). These disturbances to the hillslope are dependent on the severity of the fire and are unlikely to be consistent between events (DeBano, 1981). This was demonstrated during the Freshwater Road Fire where episodic sediment transport styles were not observed evenly across all slipfaces near or at the angle of repose. It is reasonable to assume that only the largest and hottest fires are likely to be represented as woody charcoal layers across multiple sampling locations, whereas layers that occur at only one sample site are likely to reflect local fire conditions.

From my dune foot-slope sites, I find that there is a clear geomorphic and ecologic record preserved within the stratigraphy. I observe three stratigraphic deposits within my sites: 1) sand lacking charcoal; 2) sand with charcoal in layers; and 3) sand with dispersed charcoal. I hypothesise that these records directly relate to the vegetation structure, composition and the dominant active sediment transport style (Figure 5.7). While dunes are active or stabilising, woody charcoal producing fire is rare. In this phase, sand is exposed with only minor patches of vegetation that are composed of grasses and small shrubs (Levin, 2011). The ability of fire to spread is limited and the lack of woody biomass hinders the production of charcoal, specifically in those larger size classes I utilised in this study. Consequently, the sediment delivered from dune crest to the foot-slopes through slipface avalanching and granular flows is barren of macro-charcoal (Figure 5.7a).

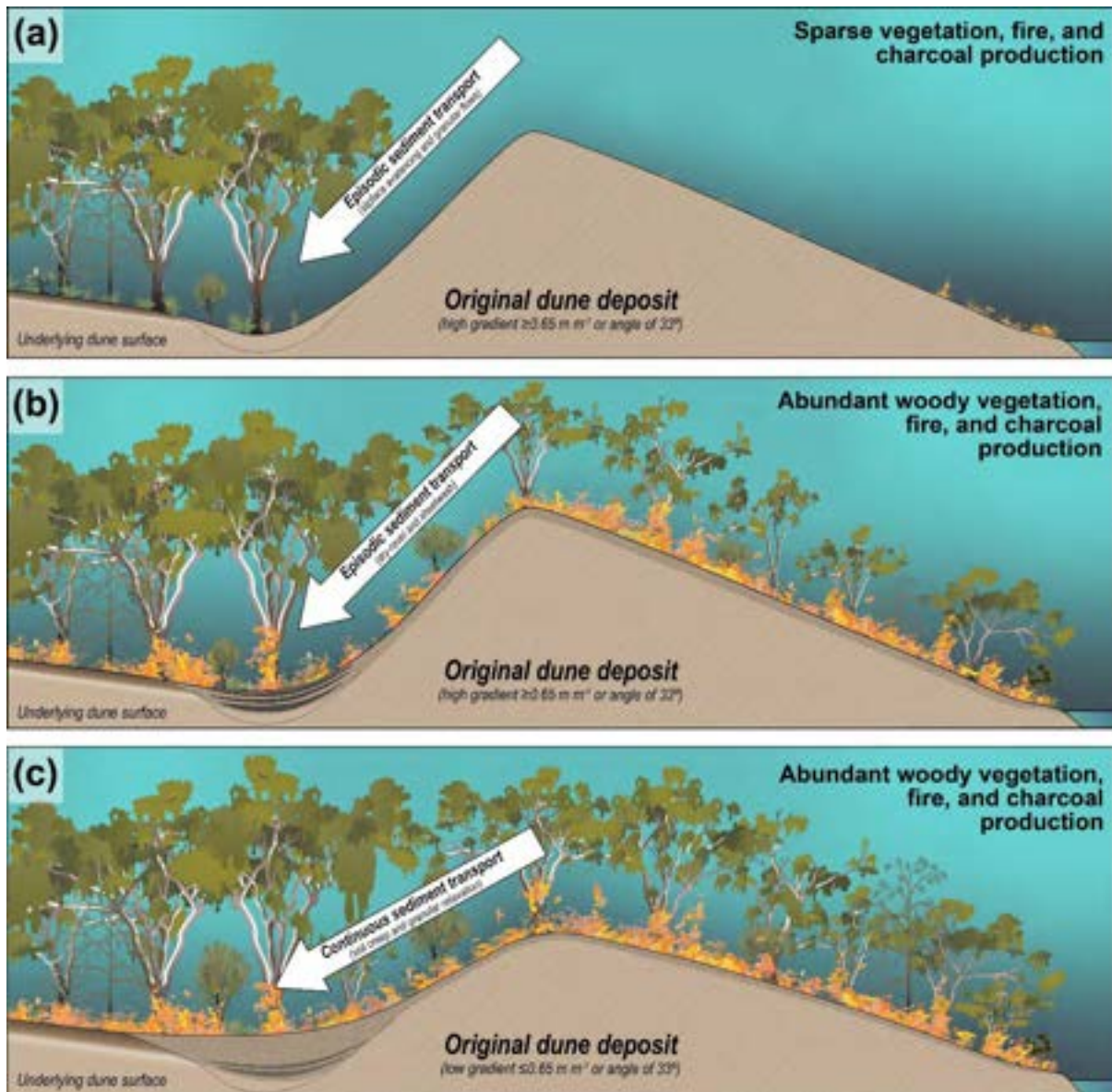


**Figure 5.7:** Conceptual diagram of progressive vegetation succession, fire activity, charcoal production and stratigraphic deposit for an (a) active dune with steep gradients, (b) recently emplaced (stabilised) dune with steep gradients, and (c) emplaced dune with shallow gradients. When dunes are active, vegetation is sparse and fires are assumed to be infrequent and unproductive – panel a. As woody vegetation such as *Eucalyptus spp.* or *Corymbia spp.* becomes established, charcoal production increases (black dots). Charcoal can either be deposited in the foot-slope positions as layers (black lines – panel b) or disseminated throughout the profile (grey area – panels b and c). The presence or absence of charcoal layers is the result of episodic sediment transport processes (e.g., dry-ravel and sheetwash) and elevated charcoal production on dune gradients that are above the sand's angle of repose – panel b. The absence of layers but the presence of disseminated charcoal implies slow and continuous sediment transport (i.e., granular relaxation and biogenic soil creep) – panel c.

Once the dunes are stabilised, dry sclerophyll forest begins to develop through vegetation succession (Walker et al., 1981), hence fire becomes more prevalent and woody

charcoal production increases. I estimate this succession in the CSM to occur ca. 0.3 ka after dune stabilisation due to the presence of ~1 m diameter Pink Bloodwood (*Corymbia intermedia*) found on the 0.5 ka Dune upslope positions that are estimated to be ca 175-350 years old (Ngugi et al., 2020) (Supplementary Figure A.5.1a). Charcoal produced on the slopes is rapidly transported down gradient through dry-ravel and sheetwash forming charcoal layers (Figure 5.7b). However, episodic sediment transport only occurs while the gradients are above the angle of repose of the dry unconsolidated dune sands. Once gradients are lowered below this threshold, only continuous sediment processes such as granular relaxation or soil creep prevails (Roering et al., 1999; BenDror & Goren, 2018; *Chapter 3*). This transition is estimated to occur ca 1.5 ka after dune stabilisation as indicated by the significant decrease in the sedimentation rates beginning at 0.35 m in the 2 ka Dune (Figure 5.4b and Figure 5.6). Despite the potential for fire and charcoal production to remain high during this phase, the absence of episodic sediment transport results in only the preservation of disseminated charcoal, with higher and lower CHAR rates representing increasing or decreasing biomass burning, respectively (Figure 5.7c).

#### 5.4.4 Comparison of paleofire records to the wider region

CHAR values from CL provide useful insights on sediment transport styles and local fire events; however, these layers should be used cautiously when developing fire records due to their spatial variability within a small area. Therefore, to compare my findings with other local and regional records I utilise the composite master charcoal record from CHAR values linked to consistent sedimentation styles and rates (disseminated charcoal) (black area in Figure 5.5e and Figure 5.8a) as these deposits should reflect general trends of biomass burning without conflating geomorphic and ecologic processes.

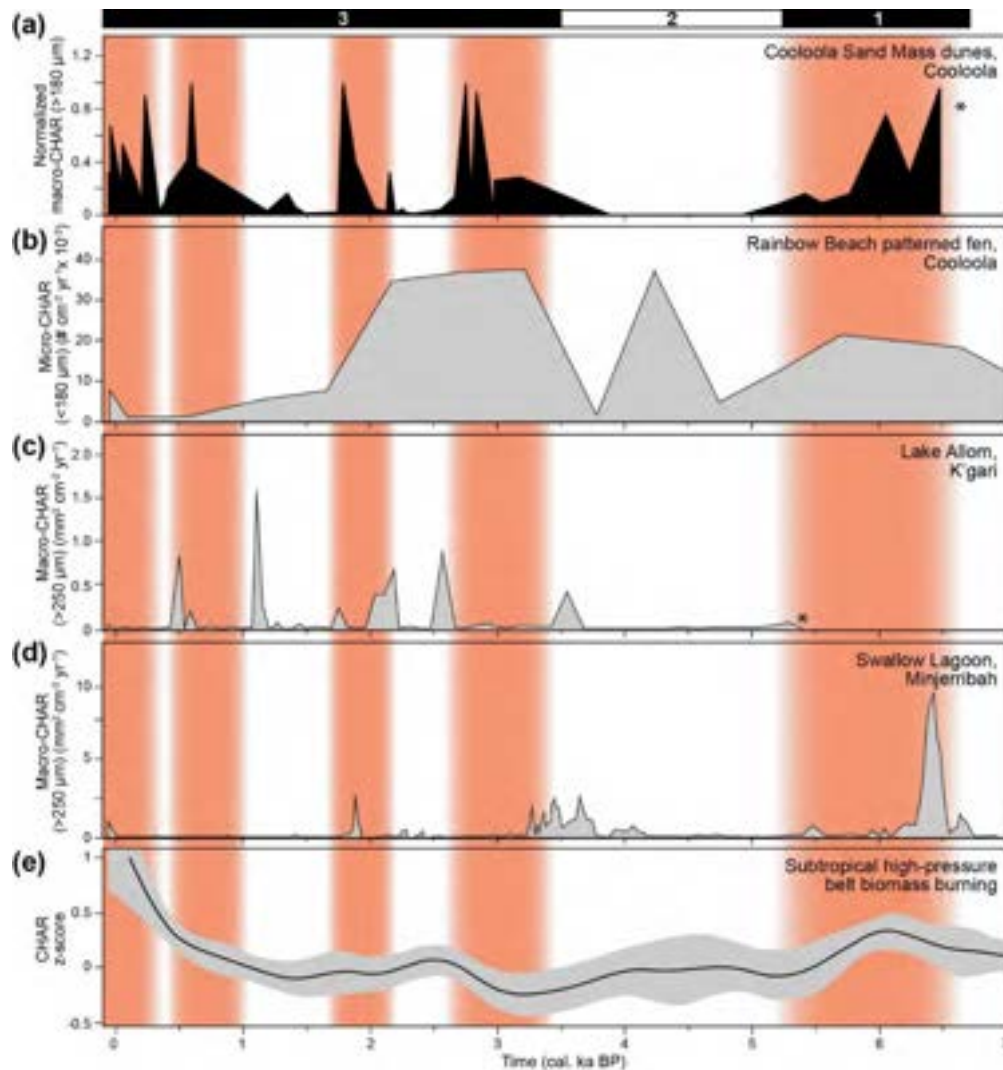


**Figure 5.8:** (a) Master charcoal record derived from only slow and continuous sediment transport for all sites in this study with increases in biomass burning (vertical orange bars) over three proposed periods of fire activity (black and white bar). My data is compared to other (b) local (Hanson et al., 2023), (c-d) regional sites (Donders et al., 2006; Mariani et al., 2019) as well as (e) a compilation of records from the subtropical high-pressure belt in eastern Australia (125 sites) (Mooney et al., 2011). Locations of local and regional records are indicated in Figure 5.1 as white stars. The fire records from the CSM sites are compatible with those from traditional fire records within SE Queensland (i.e., peats, bogs and lakes). Note (\*) indicates the lack of data.

My composite master charcoal record three major periods of fire activity in the past ca 7 cal. ka BP that reflect those records derived from lake and swamp deposits in the SE Queensland dune fields and in the wider subtropical high-pressure belt of eastern Australia (24°S – 45°S) (Figure 5.8). I observe that the earliest peak at ca 6.7-5.3 cal. ka BP corresponds with charcoal records from Minjerribah (Figure 5.8d) and a compilation of sites across the non-tropical east coast of Australia (Figure 5.8e). The Lake Allom record on K’gari (Figure 5.8c)



registers elevated CHAR values at ca 7 cal. ka BP prior to a hiatus from ca 6.5-5.4 cal. ka BP (Donders et al., 2006). In the wider region a downward trend in CHAR is observed during this period (Mooney et al., 2011). The only exception is the ca 4.5 ka charcoal event at the Rainbow Beach patterned fen complex (Moss, 2014; Hanson et al., 2023) where a local fire close to the patterned fen is the likely source of the elevated CHAR (Figure 5.8b). This period of reduced burning was followed by an upswing in fire activity with a large CHAR peak from ca 3.4-2.6 cal. ka BP with a smaller peak in CHAR at ca 2.2-1.6 cal. ka BP that is observed in all local and regional records. These late Holocene events are only observed in SE Queensland. At ca 1.1-0.4 cal. ka BP there is a gradual increase in burning and CHAR peaks at the CSM, at the Rainbow Beach patterned fen complex, and Lake Allom. Although this peak is absent from the macro-charcoal record from Swallow Lagoon on Minjerribah (Figure 5.8b), it is present within their micro-charcoal record (Mariani et al., 2019). All records show a marked increase in CHAR over the last few centuries between ca 5 and 0.2 cal. ka BP. In summary, the CSM's dune foot-slope fire records are compatible with those from traditional fire records found within SE Queensland.

#### 5.4.5 Causes of the high CHAR periods

As noted in Figure 5.8, the charcoal records in the SE Queensland dune fields can be divided into three major periods. Period 1, prior to ca 5.3 cal. ka BP shows elevated charcoal indicating increased local burning, while Period 2 has little evidence of fires between ca 5.3 ka and 3.4 cal. ka BP. This matches records obtained from K'gari and Minjerribah (Donders et al., 2006; Atahan et al., 2015; Schreuder et al., 2019; Mariani et al., 2019), and across the subtropical high-pressure belt (Mooney et al., 2011; Williams et al., 2015). The disruption in biomass burning coincides with increases in total rainfall with lower relative variability associated with less frequent El Niño events during Period 2 (Figure 5.9 b-d) (Barr et al., 2019). An alternative explanation for the transition may be the result of the termination of the post-glacial transgression (Lewis et al., 2008). Prior to ca 5.5 cal. ka BP the coastline would have extended significantly seaward from its modern position, which would result in more dune field (land) being seaward of all foot-slope deposits and increasing the likelihood of fire reaching the sample sites. These hypotheses are not mutually exclusive and indeed likely are the result of both scenarios.



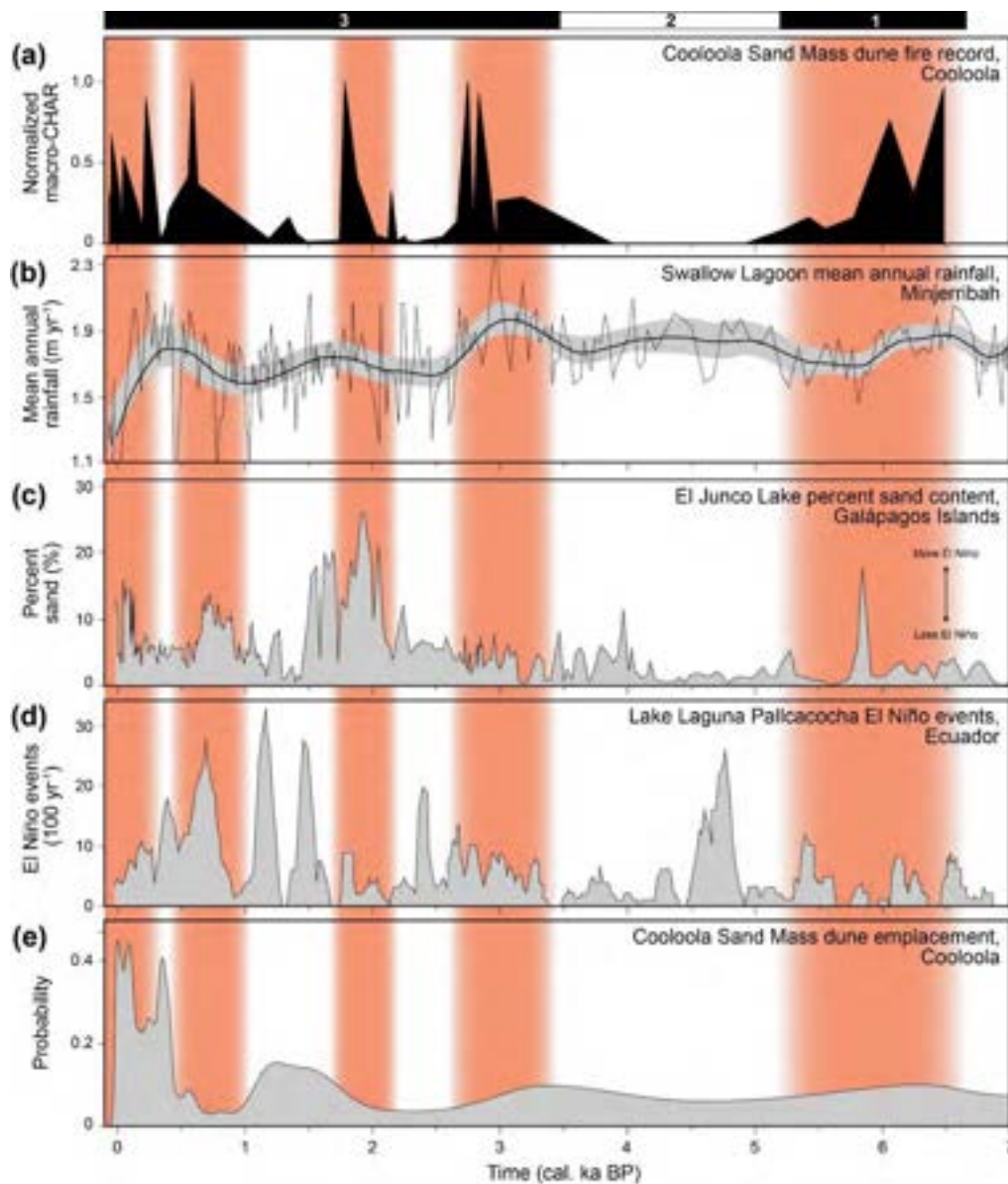


**Figure 5.9:** (a) Master charcoal record derived from only slow and continuous sediment transport for all sites in this study (black area). I compare my results to the (b) Swallow Lagoon precipitation record (Barr et al., 2019), the (c) El Junco Lake in the Galápagos Islands and the (d) Lake Laguna Pallcacocha in southern Ecuador records of past El Niño event frequency (Moy et al., 2002; Conroy et al., 2008). Lastly, I compare the (e) probability density function for the timing of dune emplacement at the CSM (*Chapter 4*).

Period 3 shows that fire frequency has gradually increased over the last ca 3.4 cal. ka BP (Figure 5.8). This increase in CHAR is observed within many SE Queensland records. K’gari records indicate that after ca 4 cal. ka BP fire activity progressively increased (e.g., Donders et al., 2006; Atahan et al., 2015; Schreuder et al., 2019). The elevated fire activity was ascribed to increased occupation and amplified indigenous burning practices (Schreuder et al., 2019);

however, this is difficult to evaluate due to the limited archaeological data available. Alternatively, the increased fire activity is hypothesised to relate to changes in the hydrological cycle primarily through the intensification of the El Niño–Southern Oscillation (ENSO) (Shulmeister and Lees, 1995; Moy et al., 2002; Donders et al., 2006; Conroy et al., 2008; Barr et al., 2019) with minor shifts in vegetation type (Donders et al., 2007; Mariani et al., 2019). Again, it is likely that both intensification of human usage and ENSO affected the fire records but may also reflect an artifact of increase sampling frequency in these sediment sections.

At the end of Period 3, there is an increase in biomass burning which is widely observed in records across Australia and the world (e.g., Kershaw et al., 2002; Power et al., 2008; Mooney et al., 2011; Williams et al., 2015). This elevated biomass burning in Australia is inferred to be a direct result of climate change (Power et al., 2008; Mooney et al., 2011) exacerbated by European fire suppression (Mariani et al., 2022; Hanson et al., 2022).

Climate variability drives vegetation communities and thereby available fuel load and fire frequency in the dry sclerophyll forest of subtropical Australia (Mariani et al., 2019). In years with higher water availability, fuel loads increase but fires are suppressed by the moisture content. Whereas dry years enable fires to occur, but the reduced fuel loads make them less intense and frequent. In both scenarios, stable wet or dry climates result in relatively reduced fire risk. In contrast, when interannual climate varies strongly, such as the SE Queensland dune fields have experienced in the late Holocene (Barr et al., 2019), fuel loads are able to build up in wet years and cure in the subsequent dry ones resulting in increased fire activity and intensity (Bradstock, 2010).

#### 5.4.6 Geomorphic and ecologic controls on dune paleofire records

Biomass burning can be primarily ascribed to climate mediated vegetation changes; however, it is important to consider how geomorphic processes may influence vegetation, fire activity, and charcoal deposition (Figure 5.7). Across the SE Queensland dune field, CHAR records closely reflect progressive vegetation succession associated with phases of dune activation and emplacement (stabilisation) (Figure 5.9 and Supplementary Figure A.5.9). I observe that CHAR peaks are inversely related to the timing of major phases of dune emplacement and likely reflects the inability of fire to penetrate through active dune fields.

The presence of charcoal in the dune foot-slope deposits are partially controlled by the local composition of vegetation in the windward direction (SE) on the dune hillslopes (Figure 5.7). The first evidence of charcoal occurs directly after the first phases of dune activation  $8.5 \pm 1.0$  ka during the post-glacial transgression (Ellerton et al, 2020; *Chapter 4*) (Figure 5.9 and Supplementary Figure A.5.9). As sea-level rose, dunes were active off the coast and migrated inland (vegetation free landscape) for years to centuries before stabilising (e.g., Houser et al., 2015; Levin, 2011; Levin et al., 2017). While the dunes are active, they act as a natural fire break which hinders the encroachment of fire spreading from the windward direction (Figure 5.7a). Not until the emergence of woody vegetation such as *Eucalyptus spp.* or *Corymbia spp.* do woody charcoal bearing fires occur (Figure 5.7b-c). These findings matched those found in the Nebraska Sand Hills in the USA where fire frequency and pollen abundance were inversely related to aeolian activity (Schmieder et al., 2013).

An important caution is that dune activation does not influence fire records equally. Although, dune activation will result in some form of disruption to the vegetation, only the largest dunes will make a significant impact to the charcoal records. For example, only large active dunes that extend several kilometers inland would pose a substantial barrier for fires. Once vegetated with grasses and shrubs, these dunes become highly flammable ignition sources. These same processes will occur on small dunes but to a lesser extent and under localised conditions.

#### 5.4.7 Recommendations and future applications

Wildfires are prevalent across the world, but fire histories are limited to where wetland sediment records are relatively abundant (Figure 5.10). My study identifies dune foot-slope deposits as a previously unrecognised record that can help explain past fire regimes and/or provide evidence for how ecosystems, such as those found in Australia, are adapted or not adapted to fire (Figure 5.10). Although, this study is based on large, coastal dunes in SE Queensland I believe these outcomes are not unique to this area. Other similar high-quality records should be present in smaller and older dunes across the world, and I encourage further exploration and methodological development in these archives. A clear path of future research would be to target under-represented regions such as drylands where fire records are sparse. I highlight Mediterranean regions, California and the southwestern

USA, northern and southern Africa, and central China as likely high value targets for this work (Figure 5.10a). Below I provide suggestions on selecting sites and sampling strategies in future studies.

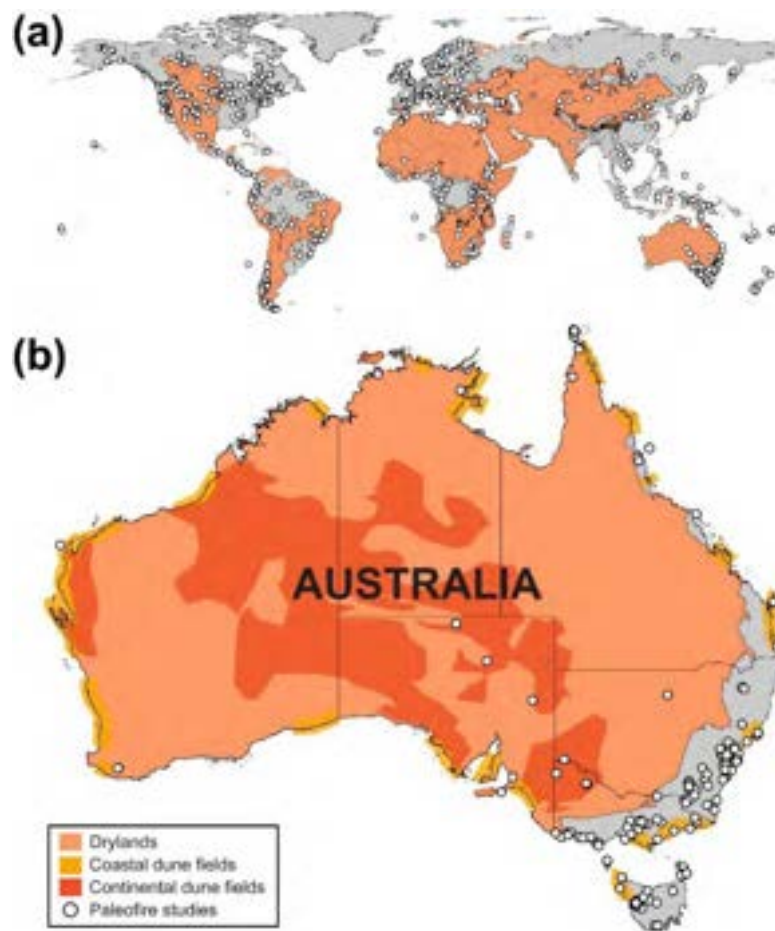


**Figure 5.10: (a)** World dryland distribution (orange areas) (Sorensen, 2007) and published paleofire records (white dots) from the Global Paleofire Database (Harrison et al., 2022). **(b)** Close-up view of Australia and the general locations of coastal (yellow) and continental (orange) dunes (Lees et al., 2006; Hesse, 2016). Note the abundant land area in Australia and the world that is both covered in drylands and lack fire histories. Dune depositional deposits present an opportunity to expand fire records from wetland areas into dryland regions which to this point have been underrepresented in paleofire studies

As developed in this study, a network of depositional sites to construct a fire record is encouraged but not necessary. A singular site of significant antiquity coupled with a higher resolution sampling design can provide useful and continuous local fire records. However, I suggest targeting multiple older, Pleistocene aged dunes that cover similar time periods. This will increase record length, improve comparison between sites, and reduce biases created by over sampling younger depth intervals. Moreover, it is critical to avoid dunes that have experienced recent reactivations, as their foot-slopes are prone to hiatuses and large shifts in

sediment rates. These datasets are necessary if we are attempting to understand broad scale shifts in fire regimes over glacial-interglacial cycles.

The largest improvement to this study is to undertake a higher resolution, consistent sampling regime, like those used on lake sediment cores (e.g., 1 cm samples collected every 2 or 5 cm). This would ensure that CHAR peaks are not obscured,  $^{14}\text{C}$  dates are collected at discrete depths, and age-depth models are representative of each site. Furthermore, it is important to select samples for fire reconstruction from intervals with consistent sedimentation rates and styles to decrease the risk of conflating geomorphic and ecologic processes. As my work highlights, the first ca 1.5 ka of sediment deposition is dynamic and fire records may reflect extremely localised and stochastic signals (i.e., CL2-5 in Figure 5.5b). After this point, sedimentation rates are reduced, and the dominant signal is inferred to represent more regional trends in biomass burning. Determining the timing of this transition is critical, as this shift from episodic to continuous sediment transport is unique to each site and relates to the physical properties of the dune sands (*Chapter 4*). However, the transition can be easily recognised from the change-over from charcoal layers to dispersed charcoal. While charcoal layers (CL) do not record regional trends in fire activity, they should not be discounted or ignored. Their presence in deposits elucidate processes, relative rates, and indicates local fire events. Moreover, this simple identification of CL in deposits can rapidly aid in site selection, without the immediate need for  $^{14}\text{C}$  dating and age-depth modelling.

## 5.5 Conclusions

The largest spatial gaps in fire records come from semi-arid and arid regions, which lack the aquatic records favourable for preserving charcoal (Leys et al., 2018; Harrison et al., 2022). However, in these regions' dunes are abundant (Thomas and Wiggs, 2008) and may provide a useful target for paleofire reconstruction. In this study, I demonstrate the potential of dune foot-slope deposits as an archive of multi-millennial fire records. I establish that the sclerophyll forest on the stabilised dunes in the Cooloola Sand Mass (CSM), Australia have burnt repeatedly and produced abundant charcoal over a ca 7 ka period.

The large charcoal size classes (180-250  $\mu\text{m}$ , 250-355  $\mu\text{m}$ , and 355  $\mu\text{m}$ -2 mm) selected to represent the presence of local fires, show consistent concentrations and accumulation rates (CHAR) with depth from all my sites. These findings support the hypothesis that foot-

slope deposits have experienced limited post-depositional mixing and those sites contain intact and reliable stratigraphic records of fire activity. I find that the dune depositional stratigraphy reflects one of three distinct phases with respect to charcoal production and preservation:

- 1) Absent to sparse charcoal: As dunes are active or becoming stabilised, there is insufficient vegetation to allow fires to fully develop and penetrate.
- 2) Charcoal layers: Once the dunes are stabilised by the colonisation of vegetation, charcoal production increases and episodic sediment transport dominates. This results in the creation of charcoal layers associated with individual major fire events.
- 3) Dispersed charcoal: After dune slopes lower below their angle of repose and transition to slow and continuous sediment transport (at ca 1.5 ka), charcoal continues to be deposited but is dispersed through the profile. During these times individual fires cannot be identified but relative biomass burning can be inferred.

I observe five CHAR peaks found within the three major periods that are traceable between dune foot-slope records. In general, fire becomes more abundant after ca 3.4 cal. ka BP, which is seen in other records from lakes and swamps in the SE Queensland dune fields (i.e., K'gari's Lake Allom, CSM's patterned fen complex, and Minjerribah's Swallow Lagoon). My findings correlate with earlier inferences that the shift in fire activity is partially due to changes in the hydrological cycle through the ENSO intensification and its impact on fuel loads. This increase may also reflect intensification of fire usage by the indigenous people. However, I also propose an alternative hypothesis that the mechanism causing fire variability is through vegetation changes in the dune field driven by dune activity itself.

The consistent trends of increasing age with depth and relatively minor uncertainty make these depositional foot-slope positions ideal targets for paleofire reconstruction. I propose that other dune deposits will yield comparable findings and that these records can expand fire histories from areas where fire is a rare event (wetlands/lakes) into the parts of the landscape where fire may be an important or the dominant ecological process. Furthermore, this method opens many new regions for paleofire studies and can give new insights on fire frequency and intensity in regions globally (Figure 5.10).

## Chapter 6. Conclusion

**Preface:** In this chapter, I summarise the key findings and scientific contributions with respect to my research objectives stated in *Chapter 1*. The outcomes of these objectives are placed in the context of our current knowledge of the SE Queensland dune fields and offer future research directions.

## 6.1 Key findings and contributions

This thesis aimed to enhance our fundamental understanding of dune fields by determining the complete evolution of a dune and dune morphosequence unit from its inception (activation) to maturity (denuded topography). Below I restate my research objectives and demonstrate how each objective was met by synthesising my main findings.

***Objective 1:*** *Produce an updated morphological map of the SE Queensland dune fields utilising modern remote sensing techniques to classify the dunes based on hillslope process parameters.*

I present the first geographic information system (GIS)-based morphostratigraphical maps for the SE Queensland dune fields that built upon prior work from Ward (2006) to address *Objective 1*. Chapter 2 provides a semi-objective, qualitative mapping approach based on the fundamental concept that all landforms are relaxing with time towards their base levels. This assumption is validated in *Chapters 3- 5*. Hundreds of dunes were delineated using LiDAR derived elevation data and grouped into morphosequence units based on the cross-cutting/onlapping relationships, topographic expression, and soil/vegetation development. My approach was first developed on the Cooloola Sand Mass (CSM) because it was thought to have the most complete and continuous dune record compared to the other major dune fields and sand islands in SE Queensland. This was confirmed in *Chapter 2, Chapter 4*, and in Ellerton et al. (2020). I then applied the mapping technique to K'gari (Fraser Island), Mulgumpin (Moreton Island), and Minjerribah (North Stradbroke Island) (Supplementary Figure A.2.1). My mapping work was validated with field observations, cross-referencing dunes of known ages, and by making a comparison with the earlier map created by Ward (2006) (Figure 2.5). The cross-map comparison highlighted the areas that traditional mapping techniques failed to capture, because of the complexity of the dune field (e.g., densely vegetated areas, compound and complex dune structures, and/or dunes of similar ages).

The mapping of the dune field has proven instrumental in driving research questions and for identifying ideal targets for OSL-dating (*Chapters 3-5*; Ellerton et al., 2020; Gontz et al., 2020; Köhler et al., 2021). The main findings from this work



demonstrate that there are five Holocene (including an active unit) and four Pleistocene morphosequence units in the SE Queensland dune fields, adding a previously unidentified Holocene unit. I demonstrated that these units are found on all the dune fields and despite not being continuous (connected between sites); their morphological structure and topographic indices (i.e., mean and standard deviation of slope and curvature) indicate they have experienced similar formation and environmental perturbations (e.g., changes in climate and base-level). This was supported by Köhler et al. (2021) and *Chapter 4*, where I demonstrated that the CSM was connected to K'gari at Inskip Peninsula and that both dune fields have identical Holocene emplacement ages. Although morphostratigraphical units are only a reflection of gross morphology and may not directly relate to chronostratigraphic units, a first-order age constraint for each dune unit was established using newly acquired dune ages (OSL-dated and estimated) (*Chapter 4*; Ellerton et al., 2020; Köhler et al., 2021).

***Objective 2:*** *Establish whether the SE Queensland dune fields are a suitable natural laboratory to evaluate landscape evolution.*

I address *Objective 2* by reviewing and utilising previously published literature to act as the foundation of my research. The large body of work from the late 1970's to the early 1990's provided the necessary information to help identify the internal and external processes that control dune evolution. My literature review and field observations support that the SE Queensland dune fields, specifically the Holocene dunes with limited anthropogenic disturbances (i.e., built-up areas and mining), provides an ideal natural laboratory and indeed a premier chronosequence to evaluate landscape evolution (Figure 3.3). The Holocene sections are composed of many hundreds of dunes covering an area of 670 km<sup>2</sup> (*Chapter 2*). These dunes were constructed almost continuously in space and time over the Holocene with punctuated periods of increased activity (*Chapter 4*). The dunes are composed of identical sands that are homogenous (>98%) sub-rounded and well sorted, medium-fine quartz sand from the longshore drift system. The dune fields have been

tectonically inactive during the Quaternary and only minor eustatic/hydro-isostatic changes have occurred after the Holocene highstand due to sea-level variability (-0.5 to 2 m). The region has experienced only minor fluctuations in climate, mostly related to changes in ENSO, the IPO and the position of the sub-tropical high-pressure belt (*Chapter 4* and *Chapter 5*). Additionally, previously published pollen and paleoenvironmental records indicate no major shifts in regional vegetation types. The only minor changes in vegetation are due to localised disturbances such as dune activity, fire, and/or storms (*Chapter 4* and *Chapter 5*). My observations confirm that the well-drained, unconsolidated dune parent material coupled with consistent activation and emplacement mechanisms promote uniform dune landforms (*Chapter 3* and *Chapter 4*). Dunes are initially stabilised with over-steepened lee slopes constructed  $>0.65 \text{ m m}^{-1}$  (sand's angle of repose) with shallow stoss slopes dictated by the antecedent topography onto which the dune overlapped. I highlight in *Chapter 3*, that the absence of fluvial incision and changes in soil cohesion with time, generates a transport-limited system that is as close to a closed-system as you can find in nature (Figure 3.3). In summary, the dune fields are an ideal natural laboratory because their chronology, and their initial and boundary conditions are well constrained such that their evolution is deterministic. This work is critical for this thesis as it facilitates the use of interdisciplinary methods and establishing the use of sediment transport theory in *Chapter 3* and *Chapter 4*.

**Objective 3:** *Assess and apply sediment transport theory to a dune system to understand its evolution once stabilised.*

To address *Objective 3*, I first needed to constrain the initial/boundary conditions and establish all active transport processes (advective or diffusive) present within the landscape. As mentioned in *Objective 2* and demonstrated in *Chapter 3*, the Holocene sections of the SE Queensland dune fields, specifically the CSM and K'gari, are an ideal natural laboratory to evaluate landscape evolution. Dunes emplace with consistent structures. The overlapping dunes produce a landscape that increases in age moving inland from the coast. Their homogenous parent material and high infiltration

rates restrict sediment transport to purely diffusional processes. All material eroded on dune crests are transported downslope and deposited in the depositional positions where it remains – an effectively closed-system. I confirm this inference in *Chapter 3* and *Chapter 5*, by only observing diffusive hillslope processes (i.e., dry-ravel, sheetwash, soil creep, and granular relaxation) with neglectable fluvial or aeolian processes acting on the Holocene dunes. Aeolian advection of dust does occur but at the scale of the dune is sedimentologically unimportant. All sediment is accounted for in their adjacent foot-slope positions, which preserves both sediment transport style and tempo.

In *Chapter 3*, I identified surface roughness ( $\sigma_c$ ) as an easy and effective topographic variable to measure and define the dune field's evolution. As mentioned in *Chapter 2*, dune units' landscapes and topographic indices appeared to be systematically smoothing and decreasing with time, respectively. The optimal index was the standard deviation of curvature (C) as a measure of  $\sigma_c$ . In *Chapter 3* and *Chapter 4*, I endorsed the utility of  $\sigma_c$  as an ideal variable due to C's intimate coupling with landscape change parameters, ability to be normalised based on antecedent topography, simplicity in its derivation, and it has been shown to be a promising metric to characterise landscapes. I demonstrate that the  $\sigma_c$  time series derived from OSL-dated dunes ( $n=15$ ) on the CSM depicts a 'horizontal hockey stick' that appears to follow  $(\partial\sigma_c)/\partial t \propto \sigma_c$ . This 'horizontal hockey stick' pattern can be split into two distinct phases the 'blade' and the 'shaft'. The first phase (blade) is a rapid decay within the first thousand years associated with episodic (nonlinear) sediment transport. The second phase (shaft) involves a gradual evolution where only slow, continuous (linear) sediment transport occurs. I find in *Chapter 3* that the break in these two phases, which I dubbed the 'transitional zone', occurs ca. 1 ka after emplacement due to the internal reduction of dune gradients below their angle of repose (critical gradient –  $S_c$ ). This is confirmed in *Chapter 3* and *Chapter 5* from depositional foot-slope records that depict a distinct change in stratigraphy (charcoal layers versus disseminated charcoal) associated with changes in transport styles (dry-ravel and sheetwash to soil creep processes) between sites. Moreover, and unsurprisingly, in *Chapter 5* I find that this transition results in a significant decrease in sedimentation rates.

I support these findings in *Chapter 3* by applying 2-D linear and nonlinear sediment transport evolutionary models to the CSM. I find that the CSM's evolution is explained well by nonlinear sediment transport with a fixed  $K$  value of  $0.002 \text{ m}^2 \text{ yr}^{-1}$  and a  $S_c$  of  $0.65 \text{ m m}^{-1}$ . Once gradients are lowered below their angle of repose, dune evolution behaves similarly to linear sediment transport and appears to follow the  $(\partial \sigma_c)/\partial t \propto \sigma_c$  relationship such that  $\sigma_E \propto \sigma_c$  is apparent. The application of the model was confirmed in *Chapter 3* and *Chapter 4* when the measured OSL-dated dunes followed similar age-roughness trends on the CSM and K'gari, respectively. However, I posited that fires disproportionately affect young dunes by temporarily increasing  $K$  values thus altering sedimentation/erosion rates. Although this is yet to be rigorously vetted, forward numerical modelling supports these claims. The simulated topography appears to be more closely represented by an initial  $K$  value of  $0.06 \text{ m}^2 \text{ yr}^{-1}$  that switches to  $0.002 \text{ m}^2 \text{ yr}^{-1}$  ca. 1.5 ka after dune emplacement (*Chapter 3* and *Chapter 5*). Nevertheless, it is clear that the application of sediment transport theory is appropriate and advantageous for understanding dune evolution.

**Objective 4:** *Determine the dominant geomorphic processes controlling sediment erosion, transport, and deposition and their relative rates.*

To address *Objective 4*, I first needed to use remote sensing to elucidate the geomorphic processes acting on the SE Queensland dune fields (*Chapter 2*). The smooth topography with convex ridges and concave hollows indicated the dominance of diffusive sediment transport, which was confirmed from field observations (*Chapter 3* and *Chapter 5*). I conducted a series of field campaigns in 2018-2019 throughout the CSM where I excavated soil profiles along <70 m transects on four Holocene aged dunes. On these transects biogenic soil creep processes were the most prevalent form of soil transport. This includes root growth and decay, burrowing, nest construction, and tree throw processes that are predominately confined to the top 0.5 m of soil (A horizon) (Figure 3.7). The steepest gradients on the youngest dunes yielded similar processes; however, dry-ravel and sheetwash processes were present after wildfires (Supplementary Figure A.5.1). This is in contrast to active and Pleistocene aged dunes

where advective processes are important contributors to landscape evolution, dominated by aeolian and fluvial processes respectively. Below, I present the mechanisms controlling dune evolution from their inception to maturity and provide sedimentation/erosion rates associated with geomorphic processes (conceptualised in Figure 3.4, Figure 5.7, and Figure A.4.5):

Active dunes - topographic rejuvenation: While dunes are active (dune inception), they are dominated by wind advection and deflation that creates sand ripples in their interior that are void of vegetation (e.g., Carlo Blowout) (Figure 3.1c and Supplementary Figure A.3.1). This controls their movement near the lee slope through episodic granular flows and slipface avalanching. The minimum Holocene dune migration rate is  $1.05 \pm 0.45 \text{ m yr}^{-1}$  where dunes are  $>3 \text{ km}$  from the coastline. As this rate decreases, vegetation begins to stabilise along the trailing arms and sections furthest from the crest. As sand is entrained within the newly vegetated patches, local topography emerges; therefore, increasing surface roughness. This process continues until wind advection is negligible, dunes stabilise, hillslope processes dominate and surface roughness values are at their highest (*Chapter 4*).

Holocene dunes – topographic relaxation: On all stabilised dunes, their topography relaxes (smooths) with time due to hillslope processes. For dunes emplaced during the Holocene, their topographic evolution can be explained through two phases of diffusive sediment transport. I demonstrate in *Chapter 3*, that the first phase starts immediately after dunes are emplace and is characterised by a rapid topographic adjustment. The dune hillslopes experience episodic sediment transport such as dry-ravel and sheetwash processes on over-steepened slipfaces built near or above the sand's angle of repose (gradient of  $0.65 \text{ m m}^{-1}$  or an angle of  $33^\circ$ ). I hypothesise that the primary cause for this response is through disturbances like wildfires that reduce soil cohesion (i.e., removal of organic matter, water content, and roots) and produce hydrophobic surface soils. I find that that episodic transport is best described through nonlinear sediment transport with a fixed  $K$  value of  $0.06 \text{ m}^2 \text{ yr}^{-1}$  and a  $S_c$  of  $0.65 \text{ m m}^{-1}$  with an average sedimentation/erosion rate of  $0.57 \pm 0.13 \text{ cm yr}^{-1}$  (*Chapter 3* and *Chapter 5*). This rate is validated by the  $0.5 \text{ cm yr}^{-1}$  estimated from the sheetwash deposit induced by the large and uncontrolled 'Freshwater Road Fire'

in 2019. Although episodic sediment transport results in the most apparent topographic changes during this phase, specifically on steep slipfaces, soil creep processes remain active. This is supported by the lack of observable episodic transport on shallow stoss slopes through remote sensing (*Chapter 2*) and presence of bioturbation and root growth and decay in slipface soil profiles (*Chapter 3* and *Chapter 5*). For these sections in space and time, nonlinear sediment transport with a fixed  $K$  value of  $0.002 \text{ m}^2 \text{ yr}^{-1}$  is the most appropriate (*Chapter 3*).

The second phase of dune evolution occurs within the first ca. 1.5 ka after dune stabilisation, associated with the 'transitional zone' (i.e., break in the age-roughness relationship depicted in Figure 3.6). This zone reflects an internal transition to a reduction of slope below the sand's angle of repose suggested in *Chapter 3* and confirmed in *Chapter 5*. I find that this phase is controlled by slow and continuous sediment transport processes such as granular relaxation, biogenic soil creep, and rain splash. Although fires are present on all dune gradients, higher erosion and sedimentation rates associated with episodic sediment transport are absent because degraded dunes are resistant to these type of transport styles (validated in *Chapter 5*). This was confirmed during the 'Freshwater Road Fire' where no accelerated erosion due to episodic transport was present on dunes older than ca. 2 ka. Forward numerical models indicates that the continuous dune evolution in this phase can be explained with either linear or nonlinear sediment transport with a fixed  $K$  value of  $0.002 \text{ m}^2 \text{ yr}^{-1}$  and a  $S_c$  of  $0.65 \text{ m m}^{-1}$ . In *Chapter 5*, I estimate the average sedimentation/erosion rate to  $0.10 \pm 0.07 \text{ cm yr}^{-1}$ , which is an order of magnitude lower than its episodic counterpart. While in the second phase, sediment transport styles and their rates become increasingly uniform until no relief remains (dune senescence) or a change in base-level occurs (i.e., Pleistocene dunes) (Supplementary Figure A.4.5).

Pleistocene dunes – topographic relaxation: The Pleistocene dunes are dominated by diffusive processes that smooth their topography with time. Similar to the Holocene dunes in the second phase of evolution, their evolution can be explained by linear or nonlinear sediment transport with a fixed  $K$  value of  $0.002 \text{ m}^2 \text{ yr}^{-1}$  and a  $S_c$  of  $0.65 \text{ m m}^{-1}$  due to their subdued dune relief (*Chapter 3*). However, in contrast with the Holocene dunes, the Pleistocene topography has been heavily dissected. This

provides strong evidence of significant fluvial processes such as stream incision and knickpoint erosion (*Chapter 2*). Active streams are sparse which suggests that fluvial processes are not the current dominant process. In fact, the degraded, smoothed channels indicate these processes have not been present for some time, at least during the Holocene.

***Objective 5:*** Investigate whether landscape evolution metrics can be calibrated to determine dune chronology.

To address *Objective 5*, I utilised the concept that surface roughness ( $\sigma_c$ ) gradually smooths with time as identified in *Chapter 2* and numerically explained in *Chapter 3*. Dunes are initially constructed with uniform, high  $\sigma_c$  values that decrease as a function of time and this evolution is deterministic. As long as no advective processes are active, dune topography experiences diffusive sediment transport processes that can be simulated using either nonlinear or linear evolutionary models (*Objectives 2-4*). A single exponential function was not applied to the  $\sigma_c$ -age relationship in *Chapter 3* due to the risk of conflating episodic and continuous sediment transport processes. However, the assumed dominance of linear sediment transport across 98% of the landscape in *Chapter 3* indicates that a singular function is acceptable when describing this general empirical relationship.

Utilising this assumption in *Chapter 4*, I built a  $\sigma_c$ -age relationship using previously published OSL-dated Holocene dune ages from the CSM. I find the  $\sigma_c$ -age relationship is explained well with an exponential function for DEM resolutions between 3 - 20 m. I validate this finding with newly acquired OSL-dated dunes on K'gari and Inskip Peninsula, which follow the same  $(\partial\sigma_c)/\partial t \propto \sigma_c$  relationship. This finding supports the idea that these dune fields are controlled by consistent evolutionary mechanisms and are a part of the same dune system.

Using Holocene dunes from the CSM and K'gari that were first identified in *Chapter 2* and individually remapped in *Chapter 4*, the emplacement ages were estimated from  $\sigma_c$  values and the  $\sigma_c$ -age empirical relationship. This resulted in a high-resolution Holocene chronology that includes 103 active and 726 Holocene dunes

(Figure 4.5). My  $\sigma_c$ -age model makes it possible to observe patterns in dune systems that have been to this point been only inferred. My chronology maps reconfirm the onlapping nature of the dune fields with the oldest dunes located further inland that become progressively younger moving towards the east coast. The oldest dunes tend to be larger and less numerous across the landscape, whereas younger dunes ( $< 1$  ka) are smaller in size but much greater in number ( $\sim 60\%$  total dune preserved). From my new observations, I find the main preservation of older occur immediately south of rocky headlands due to the long-term rotation of the coastline into swash alignment. Moreover, the new Holocene chronology validates the presence of four major emplacement phases at ca.  $<0.5$ , 1.5, 4, and 8.5 ka. In summary, my  $\sigma_c$ -age approach provides a systematic way to predict the age of every Holocene dune and a means to produce a rigorous dating framework for dune fields globally.

**Objective 6:** *Re-examine the environmental controls on dune activation and emplacement (i.e., climate change, sea-level, etc.).*

The factors controlling the SE Queensland dune fields activation and emplacement have been strongly debated by Ward (1978; 2006), Thompson (1981), Young et al. (1993), Lees (2006), Walker et al. (2018), and Ellerton et al. (2020). The prevalent hypotheses for dune activation are associated with either formation during cold, dry periods, specifically the glacial maxima, or under rising sea-levels. I address this long-lasting debate in *Chapter 4* by first producing a high-resolution Holocene chronology (obtained in *Objective 5*) from the CSM and K'gari. I generate probability density functions (PDFs) for each dune field. I discover that dune activation and emplacement appear to be continuous along most of the coastline possibly reflecting local storms, fires and other disturbances. There were, however, major phases of dune building at ca.  $<0.5$ , 1.5, 4, and 8.5 ka. I compare my PDF results with local and regional sea-level curves (Figure 4.7) and paleoclimate records (Figure 4.8). My results demonstrate a strong correlation between dune activation and emplacement with sea-level variability whereas there is little to no evidence for climate change at these times. This strongly supports the Cooper-Thom model for dune activity at the CSM and



K'gari, and consequently the SE Queensland dune fields (Cooper, 1958; Thom, 1978) as proposed by Lees (2006).

**Objective 7:** *Identify and examine depositional records that might prove valuable in understanding dune field evolution.*

In *Chapter 3*, I recognised the slopes of Holocene aged dunes are as close to a closed-system as you can find in nature. All sediment eroded from the dune crest are transported down gradient to their subjacent foot-slope positions. I theorised that once deposited, (virtually) all material must be retained in the basins due to the dominance of hillslope and the lack of fluvial and aeolian, processes; thus, creating an ideal archive for dune field geomorphic and ecologic evolution that has been previously undocumented. To address *Objective 7*, I set out in *Chapter 5*, to determine if this is indeed true by evaluating sedimentation/erosion rates and fire histories in the CSM. I chose foot-slope deposits on four closely adjacent parabolic dunes (i.e., the 0.5, 2, 5, and 10 ka dunes). Their depositional basal ages span the Holocene and have comparable north-facing slipfaces that are <70 m in length and covered in dry sclerophyll forest. As a result, these sites make a well-designed space-for-time study to evaluate this objective.

Dunes that are less than ca. 1.5 cal ka BP are dominated by episodic sediment transport induced by disturbances. This produces sedimentation rates that are an order of magnitude higher than older dunes that are governed by slow and continuous sediment transport ( $0.57 \pm 0.13 \text{ cm yr}^{-1}$  and  $0.10 \pm 0.07 \text{ cm yr}^{-1}$ , respectively) (Figure 5.6). I propose these shifts in transport styles coupled with charcoal production are reflected in three types of depositional stratigraphy: 1) the absence of or limited charcoal due to the lack of charcoal production on active dunes, 2) charcoal layers associated with fire induce by episodic sediment transport on steep slopes, and 3) disseminated charcoal when hillslope gradients are shallow and only continuous sediment transport occurs (Figure 5.7). To my knowledge, this has not been previously documented and provides useful environmental insights for dune fields.

Utilising these observations along with charcoal accumulation rates (CHAR), I was able to construct a ca. 7 cal ka BP aggregated master charcoal record for the CSM. Five CHAR peaks are observed at ca. <0.3, 1.1-0.4, 2.2-1.6, 3.4-2.6, and 6.7-5.3 cal. ka BP within three major periods of enhanced fire. These findings parallel fire records regionally and in the wider sub-tropical high-pressure belt in eastern Australia (24°S-45°S). In general, fire becomes more abundant after ca. 3.4 cal ka BP, which has been previously ascribed to changes in fire activity associated with ENSO and/or the intensification of fire usage by local indigenous people. However, I observe in *Chapter 5* that my fire record appears to be inversely related to dune emplacement (stabilisation) ages. As an alternative hypothesis, I suggest that the variations in CHAR records over the Holocene reflect shifts in vegetation due to successive phases of dune activation and emplacement in the up-wind direction (Figure 5.9). By answering *Objective 7*, I have proven the value of dune depositional positions for providing a contiguous, multi-millennial record to understand dune field's ecologic and geomorphic evolution.

This thesis has expanded our knowledge of dune fields and landforms evolution by achieving all proposed research aims and objectives. In summary, I confirm the application and benefits of using hillslope geomorphology evolution theories to better describe and understand dune systems. I demonstrate that dune form coupled with numerical theory, and their depositional positions provide a valuable paleoenvironmental archives for future aeolian research.

## 6.2 Future directions

This thesis highlighted an innovative approach to understanding dune fields and dune landscapes by using a hillslope geomorphology prospective. Although key research objectives were established to understand the complete topographic evolution of a dune field and its dunes, there are a number of new directions for potential research. Below, I present specific examples:

### 6.2.1 Automating dune delineation

A major contribution of the thesis is the use of morphological characteristics and topographic indices to map and determine relative ages for dune sequences. These two findings are powerful because they reduce the subjectivity of mapping and can be classified within ArcGIS (ESRI, Redlands, CA) or other GIS tool kits. The clear limitation with these techniques is the necessity for all dunes to be manually delineated prior to placing them into a morphosequence unit or determining their surface roughness ( $\sigma_c$ ) value. This step is both sometimes ambiguous and incredibly time-consuming. An obvious next step would be to transition to a fully automated mapping approach using either using artificial intelligence to self-delineate dunes or by calculating  $\sigma_c$  using a moving window analysis for each cell rather than a delineated polygon. In theory, this should only require training the model with previously identified dunes and determining the appropriate size window to calculate the  $\sigma_c$  values. This would vastly improve model efficiency, reduce time, and limit human error.

### 6.2.2 Improving the application of $\sigma_c$ -age modelling

The  $\sigma_c$ -age model developed in this thesis provides a means to generate high-resolution chronologies in relic dune fields. The obvious next step is to apply this technique to other systems; however, in order to apply this approach to other systems the  $\sigma_c$ -age relationship must be recalibrated. In future research, I plan to establish  $\sigma_c$ -age relationships across other dune fields. The SE Queensland dune fields are just one of many sets of dune complexes along the eastern Australia coast. I plan to firstly test and establish  $\sigma_c$ -age relationships on all dune fields to the south and north that are supplied by the same longshore drift system. This would include Myall Lakes, New Castle Bright, and Kurnell in the south and extended up to Shell Harbour, Shoalwater Bay, Hinchinbrook Island, Cape Flattery, Cape Bedford, Orford Ness and Shelburne Bay to the north. Next, I would look to apply these approaches into continental dune fields. If my hypothesis is correct and all  $\sigma_c$ -age relationships are site specific, I will be able to identify plausible causes in the rate of smoothing between sites (i.e., changes in K values due to climate, biology, fires, and/or lithology). Alternatively, if all  $\sigma_c$ -age relationships are identical, recalibration for each function would not be necessary and my model created in *Chapter 4* could be used universally.

As mentioned in *Chapter 3* and *Chapter 4*, the  $\sigma_c$ -age model is built for systems that are dominated by colluvial transport where landscape evolution is diffusive. Adapting this model to include advective processes which cause an increase in surface erosion would be highly useful as it would significantly increase the opportunities to apply the work. For instance, the Pleistocene sections of the SE Queensland dune fields have gone through multiple phases of sea-level rise and fall, which has caused knickpoint erosion to affect dune evolution. Future research could adapt my surface  $\sigma_c$ -age approach to incorporate the effect of base-level changes into the evolving  $\sigma_c$ . This will be advantageous for refining the chronology of the Pleistocene section of the dune fields, which make up roughly two-thirds of the total land area. It would also allow a variant of the model to be developed for other regions where advective processes are important.

Lastly, the concept of topography smoothing with time is widely observed and should be utilised in other systems outside of dune fields. Indeed, the original application of surface roughness-age modelling was generated for landslide deposits. In future work, I plan to target beach ridge complexes (e.g., the southern limit of K'gari, north of the Mary River/Sandy Strait inlet). Similar to dunes, these systems have consistent composition, uniform topography and their initial structures are set by the sand's unmodified angle of repose. I can build topographic relationships by using OSL ages and the average profile curvature (change in slope in the downslope direction) on the beach ridge crest. This empirical relationship can be calibrated and used to estimate every beach ridge age in a given area, thus providing a high-resolution beach ridge chronology and local sea-level curve.

### 6.2.3 Quantifying and describing $\sigma_c$ -age transport mechanisms

The observation that surface roughness ( $\sigma_c$ ) records two phases of topography decay with time has been recorded from 'sandbox' experiments but this is the first application in a dune field. As I demonstrate in *Chapter 4*, K'gari and the CSM's dunes develop in a similar manner but both systems share identical critical slope angles ( $S_c$ ) which relate to the same source material. Is this similar in other systems or are the SE Queensland dune fields unique? My expectation is that the basic model should be robust. What will be different are the rates of change in  $\sigma_c$  as a response to local climatic, edaphic and anthropogenic conditions. Therefore, I encourage the examination of my proposed two phases of landscape evolution

and its relationship to transport styles, soil transport coefficients (K values) and  $S_c$  in other dune fields.

These systems provide an ideal natural laboratory to observe and measure geomorphic processes and model landscape evolution. This permitted the estimation of general  $\sigma_c$ -age relationships and K values based on 2-D sediment transport models and observed goodness of fit. Although these findings fall within previously reported K values, they should be further assessed. In future work I plan to calculate K values from sedimentation/erosion rates collected in *Chapter 5* to assess how values change through space and time. This would permit me to test whether episodic sediment transport is caused by a reduction of K on hillslopes above their critical gradient (dunes with high  $\sigma_c$ ). Moreover, measured K values would refine both the linear and nonlinear sediment transport models and directly test the inferred  $(\partial\sigma_c)/\partial t \propto \sigma_c$  and  $\sigma_E \propto \sigma_c$  relationships. This could give researchers a better idea whether a landscape or landform has greater potential to change (erode or smooth) with time.

#### 6.2.4 Application in developing terrestrial fire histories

I identified dune foot-slope positions as a novel and previously unrecognised depositional record for ecologic and geomorphic processes, specifically its ability to record fire histories. Unlike other charcoal records, dune foot-slopes are controlled by a limited set of evolutionary processes, which reduces the complexities related to charcoal transport and source. Most charcoal is locally produced on the dunes but still provides records of apparent regional applicability. As I previously highlight, wildfires are prevalent across the Australian landscape; however, fire records are limited to the SE corner of Australia where wetland sediment records are relatively abundant. These foot-slope records would allow the expansion of fire records into dryland and fully arid regions for past fire regimes and may provide evidence for how ecosystems in Australia are adapted (or not adapted) to fire. In fact, fire records are sparse in dryland regions worldwide; therefore, a clear path of future research would be to target dune deposits to expand fire histories into under-represented regions across the globe. I highlight Mediterranean regions, California and the southwestern USA and southern Africa as likely high value targets for this work.

Although my work focuses on Holocene records, there is no reason older deposits cannot and should not be targeted. For instance, these records have the potential to unlock the role climate and/or indigenous peoples had on the landscape from regions where they are rare or absent. Deciphering these types of questions requires long-term multi-millennial records that extend beyond the timing of first occupation (>65 ka in Australia) which could be available with these deposits. It would be exciting to see this work extended into the Kimberley and the dune areas along the northern Australian coast where human occupation is likely to be the oldest.

## 6.3 Summary

In this thesis, I have presented a hillslope geomorphology perspective to understand dune fields and dune landscapes. I adopt the idea that landscapes smooth with time, which has allowed for the complete evolution of a dune from its inception to maturity to be evaluated and measured. My work identifies two previously unrecognised paleoenvironmental archives. The first are the dune landforms themselves. Although dunes morphologies have been utilised as a means to identify past wind fields or environmental conditions, evaluating the changes in their topography after deposition has not been rigorously assessed. I find that dune fields are an ideal natural laboratory to study landscape change. Their evolution is analogous to 'sandbox' experiments used to illustrate erosion and deposition because initial and boundary conditions can be identified, and the application of purely diffusional transport theory is appropriate. I found that a systematic change in dune topography with time permits the calibration of surface roughness-age models and the prediction of every Holocene dune age within my field area. As a result, spatial and temporal patterns of dune emplacement were assessed and the Cooper-Thom model of dune field activation with rising sea-levels was strongly supported for the Holocene SE Queensland dune fields. The second archive discovered is depositional foot-slopes. These topographic positions have been shown to record quasi-continuous sedimentological records that can be used to indicate both sediment transport styles and rates. I observed that in the CSM, fires play an important role in dune fields and their frequency can be evaluated from these locations. Both records can be used independently or together to understand not only dune landscapes but also qualitatively test the validity of the landscape evolution literature. This thesis highlights

significant advantages of looking at dunes from a landscape evolution perspective and provides new lines of research into dune field processes and evolution.

## References

- Aitken, M.J. (1998). Introduction to optical dating: the dating of Quaternary sediments by the use of photon-stimulated luminescence. Clarendon Press.
- Aitken, M.J., & Alldred, J.C. (1972). The assessment of error limits in thermoluminescent dating. *Archaeometry*, 14(2), 257-267. doi.org/10.1111/j.1475-4754.1972.tb00068.x
- Aitken, M.J., & Xie, J. (1990). Moisture correction for annual gamma dose. *Ancient TL*, 8(2), 6-9.
- Almond, P.C., & Tonkin, P.J. (1999). Pedogenesis by upbuilding in an extreme leaching and weathering environment, and slow loess accretion, south Westland, New Zealand. *Geoderma*, 92(1-2), 1-36. doi.org/10.1016/S0016-7061(99)00016-6
- Arbogast, A.F., & Packman, S.C. (2004). Middle-Holocene mobilization of aeolian sand in western upper Michigan and the potential relationship with climate and fire. *The Holocene*, 14, 464-471. doi.org/10.1191/0959683604hl723rr
- Archibald, S., Lehmann, C.E., Gómez-Dans, J.L., & Bradstock, R.A. (2013). Defining pyromes and global syndromes of fire regimes. *Proceedings of the National Academy of Sciences*, 110(16), 6442-6447. doi.org/10.1073/pnas.1211466110
- Atahan, P., Heijnis, H., Dodson, J., Grice, K., Le Metayer, P., Taffs, K., Hembrow, S., Woltering, M., & Zawadzki, A. (2015). Pollen, biomarker and stable isotope evidence of late Quaternary environmental change at Lake McKenzie, southeast Queensland. *Journal of Paleolimnology*, 53(1), 139-156. doi.org/10.1007/s10933-014-9813-3
- Ball, L.C. (1924). Report on oil prospecting, near Tewantin. *Queensland Government Mining Journal*, 25(293), 354-360.
- Barr, C., Tibby, J., Leng, M.J., Tyler, J.J., Henderson, A.C.G., Overpeck, J.T., Simpson, G.L., Cole, J.E., Phipps, S.J., Marshall, J.C., McGregor, G.B., Hua, Q., & McRobie, F.H. (2019). Holocene el Niño–southern Oscillation variability reflected in subtropical Australian precipitation. *Scientific Reports*, 9(1), 1-9. doi.org/10.1038/s41598-021-86998-2
- Barr, C., Tibby, J., Marshall, J.C., McGregor, G.B., Moss, P.T., Halverson, G.P., & Fluin, J. (2013). Combining monitoring, models and palaeolimnology to assess ecosystem response to environmental change at monthly to millennial timescales: the stability of Blue Lake, North Stradbroke Island, Australia. *Freshwater Biology*, 58(8), 1614-1630. doi.org/10.1111/fwb.12154
- Barr, C., Tibby, J., Moss, P.T., Halverson, G.P., Marshall, J.C., McGregor, G.B., & Stirling, E. (2017). A 25,000-year record of environmental change from Welsby Lagoon, North



## References

- Stradbroke Island, in the Australian subtropics: *Quaternary International*, 449, 106-118. doi.org/10.1016/j.quaint.2017.04.011
- Bell, R., Petschko, H., Röhrs, M., & Dix, A. (2012). Assessment of landslide age, landslide persistence and human impact using airborne laser scanning digital terrain models. *Geografiska Annaler: Series A, Physical Geography*, 94(1), 135-156. doi:10.1111/j.1468-0459.2012.00454.x
- BenDror, E., & Goren, L. (2018). Controls over sediment flux along soil-mantled hillslopes: insights from granular dynamics simulations. *Journal of Geophysical Research: Earth Surface*, 123, 924–944. doi.org/10.1002/2017JF004351
- Berti, M., Corsini, A., & Daehne, A. (2013). Comparative analysis of surface roughness algorithms for the identification of active landslides. *Geomorphology*, 182, 1-18. doi.org/10.1016/j.geomorph.2012.10.022
- Blaauw, M., & Christen, J.A. (2011). Flexible paleoclimate age-depth models using an autoregressive gamma process. *Bayesian analysis*, 6(3), 457-474. doi.org/10.1214/11-BA618
- Blake, G.R., & Hartge, K.H. (1986). Bulk density. *Methods of soil analysis: Part 1 Physical and mineralogical methods*, 5, 363-375.
- Bogaart, P.W., & Troch, P.A. (2006). Curvature distribution within hillslopes and catchments and its effect on the hydrological response. *Hydrology and Earth System Sciences Discussions*, European Geosciences Union 3 (3), 1071-1104. doi.org/10.5194/hess-10-925-2006
- Bonetti, S., & Porporato, A. (2017). On the dynamic smoothing of mountains. *Geophysical Research Letters*, 44(11), 5531-5539. doi.org/10.1002/2017GL073095
- Booth, A.M., LaHusen, S.R., Duvall, A.R., & Montgomery D.R. (2017). Holocene history of deep-seated landsliding in the North Fork Stillaguamish River valley from surface roughness analysis, radiocarbon dating, and numerical landscape evolution modeling: *Journal of Geophysical Research: Earth Surface* 122 (2), 456-472. doi.org/10.1002/2016JF003934
- Booth, A.M., Roering, J.J., & Perron, J.T. (2009). Automated landslide mapping using spectral analysis and high-resolution topographic data: Puget Sound lowlands, Washington, and Portland Hills, Oregon. *Geomorphology*, 109(3-4), 132-147. doi.org/10.1016/j.geomorph.2009.02.027
- Bowman, D.M. (1998). The impact of Aboriginal landscape burning on the Australian biota. *The New Phytologist*, 140(3), 385-410. doi.org/10.1046/j.1469-8137.1998.00289.x

- Bowman, D.M., Balch, J.K., Artaxo, P., Bond, W.J., Carlson, J.M., Cochrane, M.A., D'Antonio C.M., DeFries R.S., Doyle J.C., Harrison S.P., & Johnston F.H. (2009). Fire in the Earth system. *Science*, 324(5926), 481-484. DOI:10.1126/science.1163886
- Bowman, D.M., Murphy, B.P., Neyland, D.L., Williamson, G.J., & Prior, L.D. (2014). Abrupt fire regime change may cause landscape-wide loss of mature obligate seeder forests. *Global Change Biology*, 20(3), 1008-1015. doi.org/10.1111/gcb.12433
- Boyd, R., Ruming, K., Goodwin, I., Sandstrom, M., & Schröder-Adams, C. (2008). Highstand transport of coastal sand to the deep ocean: A case study from Fraser Island, southeast Australia: *Geology*, 36.1, 15-18. doi.org/10.1130/G24211A.1
- Bradstock, R.A. (2010). A biogeographic model of fire regimes in Australia: current and future implications. *Global Ecology and Biogeography*, 19, 145–158. doi.org/10.1111/j.1466-8238.2009.00512.x
- Bradstock, R.A., Williams, J.E., & Gill, A.M. (2002). Flammable Australia: the fire regimes and biodiversity of a continent. Cambridge University Press, Cambridge.
- Bridge, B.J., & Ross, P.J. (1983). Water erosion in vegetated sand dunes at Cooloola, south-east Queensland. *Zeitschrift für Geomorphologie, Supplementband* 45, 227–244.
- Bridgman, H., & Timms, B.V. (2012). Australia, climate and lakes. In *Encyclopedia of Lakes and Reservoirs*. (Eds L. Bengtsson, RW Herschy and RW Fairbridge.) 73–80.
- Bronk Ramsey, C. (2009). Bayesian analysis of radiocarbon dates. *Radiocarbon*, 511, 337–360. doi.org/10.1017/S0033822200033865.
- Brooke, B.P., Pietsch, T.J., Olley, J.M., Sloss, C.R., & Cox, M.E. (2015). A preliminary OSL chronology for coastal dunes on Moreton Island, Queensland, Australia—Marginal deposits of a large-scale quaternary shelf sediment system. *Continental Shelf Research*, 105, 79-94. doi.org/10.1016/j.csr.2015.06.002
- Bureau of Meteorology (BOM). (2017). Climate data online [online] (Vol. 2017), Australian Government, Bureau of Meteorology.
- Bureau of Meteorology (BOM). (2019). Climate Data Online [online]. Australian Government, Bureau of Meteorology
- Bureau of Meteorology (BOM) & Commonwealth Scientific and Industrial Research Organisation (CSIRO). (2020). State of the climate 2020.
- Cadd, H.R., Tibby, J., Barr, C., Tyler, J., Unger, L., Leng, M., J. Marshall, J. C., McGregor, G., Lewis, R., Arnold, L.J., & Lewis, T. (2018). Development of a southern hemisphere subtropical wetland (Welsby Lagoon, south-east Queensland, Australia) through the last glacial cycle. *Quaternary Science Reviews*, 202, 53-65. doi.org/10.1016/j.quascirev.2018.09.010

## References

- Canadell, J.G., Meyer, C.P., Cook, G.D., Dowdy, A., Briggs, P.R., Knauer, J., Pepler, A., & Haverd, V. (2021). Multi-decadal increase of forest burned area in Australia is linked to climate change. *Nature communications*, 12(1), 1-11. doi.org/10.1038/s41467-021-27225-4
- Carcaillet, C., Richard, P.J., Asnong, H., Capece, L., & Bergeron, Y. (2006). Fire and soil erosion history in East Canadian boreal and temperate forests. *Quaternary Science Reviews*, 25(13-14), 1489-1500. doi.org/10.1016/j.quascirev.2006.01.004
- Carson, M.A., & Kirkby, M.J. (1972). Hillslope Form and Process: Cambridge University Press, New York.
- Catani, F., Segoni, S., & Falorni, G. (2010). An empirical geomorphology-based approach to the spatial prediction of soil thickness at catchment scale. *Water Resources Research*, 46(5). doi.org/10.1029/2008WR007450
- Chang, J.C., Shulmeister, J., Woodward, C., Steinberger, L., Tibby, J., & Barr, C. (2015). A chironomid-inferred summer temperature reconstruction from subtropical Australia during the last glacial maximum (LGM) and the last deglaciation. *Quaternary Science Reviews*, 122, 282-292. doi.org/10.1016/j.quascirev.2015.06.006
- Chang, J.C., Woodward, C., & Shulmeister, J. (2014). A snapshot of the limnology of eastern Australian water bodies spanning the tropics to Tasmania: the land-use, climate, limnology nexus. *Marine and Freshwater Research*, 65, 872-883. doi-org.ezproxy.library.uq.edu.au/10.1071/MF13265.
- Chang, J.C., Woodward, C., & Shulmeister, J. (2017). Reconstructing terrestrial temperatures in the Australian sub-tropics and tropics: A chironomid-based transfer function approach. *Quaternary International*, 449, 136-148. doi.org/10.1016/j.quaint.2016.11.006.
- Chen, C.R., Hou, E.Q., Condon, L.M., Bacon, G., Esfandbod, M., Olley, J., & Turner, B.L. (2015). Soil phosphorus fractionation and nutrient dynamics along the Cooloola coastal dune chronosequence, southern Queensland, Australia. *Geoderma*, 257, 4-13. doi.org/10.1016/j.geoderma.2015.04.027
- Clark, J.S., Lynch, J., Stocks, B.J., & Goldammer, J.G. (1998). Relationships between charcoal particles in air and sediments in west-central Siberia. *The Holocene*, 8(1), 19-29. doi.org/10.1191/095968398672501165
- Clarkson, C., Jacobs, Z., Marwick, B., Fullagar, R., Wallis, L., Smith, M., Roberts, R.G., Hayes, E., Lowe, K., Carah, X., Florin, S.A., McNeil, J., Cox, D., Arnold, L.J., Hua, Q., Huntley, J., Brand, H.E.A., Manne, T., Fairbairn, A., Shulmeister, J., Lyle, L., Salina, M., Page, M., Connell, K., Park, G., Norman, K., Murphy, T., & Pardoe, C. (2017). Human occupation of northern Australia by 65,000 years ago. *Nature*, 547, 306-310. doi-org.ezproxy.library.uq.edu.au/10.1038/nature22968

- Coaldrake, J.E. (1962). The coastal sand dunes of southern Queensland. *Proceedings of the Royal Society of Queensland*, 72, 101-16.
- Cohen-Ofri, I., Weiner, L., Boaretto, E., Mintz, G., & Weiner, S. (2006). Modern and fossil charcoal: aspects of structure and diagenesis. *Journal of Archaeological Science*, 33, 428–439. doi.org/10.1016/j.jas.2005.08.008
- Collins, L. (2019). Eucalypt forests dominated by epicormic resprouters are resilient to repeated canopy fires. *Journal of Ecology*, 108, 310–324. doi-org.ezproxy.library.uq.edu.au/10.1111/1365-2745.13227.
- Conroy, J.L., Overpeck, J.T., Cole, J.E., Shanahan, T.M. & Steinitz Kannan, M. (2008). Holocene changes in eastern tropical Pacific climate inferred from a Galápagos lake sediment record. *Quaternary Science Reviews*, 27(11–12), 1166–1180. doi.org/10.1016/j.quascirev.2008.02.015
- Cook, P.G. (1986). A review of coastal dune building in Eastern Australia. *Australian Geographer*, 17(2), 133-143. doi.org/10.1080/00049188608702912
- Cooper, W.S. (1958). Coastal sand dunes of Oregon and Washington. doi.org/10.1130/MEM72-p1
- Davis, W.M. (1892). The convex profile of badland divides: *Sciences*, 20, 245. doi:10.1126/science.ns-20.508.245.a
- DeBano, L.F. (1981). Water repellent soils: a state-of-the-art (Vol. 46). US Department of Agriculture, Forest Service, Pacific Southwest Forest and Range Experiment Station.
- Department of Agriculture, Water and the Environment (DAWE). (2020). Preliminary analysis for environmental analysis – 2019/20 fires. Canberra (Australia): Department of Agriculture, Water and the Environment. www.environment.gov.au/fed/catalog/search/resource/details.page?uuid=%7B9ACDCB09-0364-4FE8-9459-2A56C792C743%7D (15, May 2022).
- Deshpande, N.S., Furbish, D.J., Arratia, P.E., & Jerolmack, D.J. (2021). The perpetual fragility of creeping hillslopes. *Nature Communications*, 12 (1), 1-7. doi.org/10.1038/s41467-021-23979-z
- Dietrich, W.E., Reiss, R., Hsu, M.L. & Montgomery, D.R. (1995). A process-based model for colluvial soil depth and shallow landsliding using digital elevation data. *Hydrological Processes*, 9, 383–400. doi.org/10.1002/hyp.3360090311
- Doerr, S.H., Shakesby, R.A., & Walsh, R. (2000). Soil water repellency: its causes, characteristics and hydro-geomorphological significance. *Earth-Science Reviews*, 51(1-4), 33-65. doi.org/10.1016/S0012-8252(00)00011-8

## References

- Donders, T.H., Haberle, S.G., Hope, G., Wagner, F., & Visscher, H. (2007). Pollen evidence for the transition of the Eastern Australian climate system from the post-glacial to the present-day ENSO mode. *Quaternary Science Reviews*, 26(11-12), 1621-1637. doi.org/10.1016/j.quascirev.2006.11.018
- Donders, T.H., Wagner, F., & Visscher, H. (2006). Late Pleistocene and Holocene subtropical vegetation dynamics recorded in perched lake deposits on Fraser Island, Queensland, Australia. *Palaeogeography, Palaeoclimatology, Palaeoecology*, 241(3-4), 417-439. doi.org/10.1016/j.palaeo.2006.04.008
- Ellerton, D., Rittenour, T., Miot da Silva, G., Gontz, A., Shulmeister, J., Hesp, P., Santini, T., & Welsh, K. J. (2018). Late-Holocene cliff-top blowout activation and evolution in the Cooloolo Sand Mass, south-east Queensland, Australia. *The Holocene*, 28(11), 1697-1711. doi.org/10.1177/0959683618788679
- Ellerton, D., Rittenour, T., Shulmeister, J., Gontz, A., Welsh, K.J., & Patton N.R. (2020). An 800 kyr record of dune emplacement in relationship to high sea level forcing, Cooloolo Sand Mass, Queensland, Australia: *Geomorphology*, 354, 106999. doi.org/10.1016/j.geomorph.2019.106999
- Ellerton, D., Rittenour, T., Shulmeister, J., Roberts, A.P., Miot da Silva, G., Gontz, A., Hesp, P., Moss, P., Patton N.R., Santini, T., Welsh, K., & Zhao, X. (2023). Fraser Island (K'gari) and initiation of the Great Barrier Reef linked by Middle Pleistocene sea-level change. *Nature Geoscience*, 15, 1017-1026. doi.org/10.1038/s41561-022-01062-6
- Ewing, R.C., & Kocurek, G.A. (2010). Aeolian dune interactions and dune-field pattern formation: White Sands Dune Field, New Mexico. *Sedimentology*, 57(5), 1199-1219. doi.org/10.1111/j.1365-3091.2009.01143.x
- Fairfax, R., Rowland, J., Ryan, T., & Drimer, J. (2011). A preliminary investigation into 'patterned fens' of the Great Sandy Region. Unpublished report to the Commonwealth Department of Sustainability, Environment, Water, Population and Communities. Queensland Herbarium, Queensland Department of Environment and Resource Management, Brisbane.
- Fensham, R.J. (1997). Aboriginal fire regimes in Queensland, Australia: analysis of the explorers' record. *Journal of Biogeography*, 24(1), 11-22. doi.org/10.1111/j.1365-2699.1997.tb00046.x
- Fernandes, N. F., & Dietrich, W. E. (1997). Hillslope evolution by diffusive processes: The timescale for equilibrium adjustments: *Water Resources Research*, 33, 1307-1318. doi.org/10.1029/97WR00534
- Filion, L. (1984). A relationship between dunes, fire and climate recorded in the Holocene deposits of Quebec. *Nature*, 309(5968), 543-546. doi.org/10.1038/309543a0

- Filkov, A.I., Ngo, T., Matthews, S., Telfer, S., & Penman, T.D. (2020). Impact of Australia's catastrophic 2019/20 bushfire season on communities and environment. Retrospective analysis and current trends. *Journal of Safety Science and Resilience*, 1, 44–56. doi.org/10.1016/j.jnlssr.2020.06.009.
- Fink, D., Hotchkis, M., Hua, Q., Jacobsen, G., Smith, A.M., Zoppi, U., Child, D., Mifsud, C., van der Gaast, H., Williams, A., & Williams, M. (2004). The ANTARES AMS Facility at ANSTO. *Nuclear Instruments and Methods in Physics Research B*, 223-224, 109-115. doi.org/10.1016/j.nimb.2004.04.025.
- Fletcher, M.S., Hall, T., & Alexandra, A.N. (2021). The loss of an indigenous constructed landscape following British invasion of Australia: An insight into the deep human imprint on the Australian landscape. *Ambio*, 50(1), 138-149. doi.org/10.1007/s13280-020-01339-3
- Frankel, K.L., & Dolan, J.F. (2007). Characterizing arid region alluvial fan surface roughness with airborne laser swath mapping digital topographic data. *Journal of Geophysical Research: Earth Surface*, 112(F2). doi.org/10.1029/2006JF000644
- Fryirs, K., Brierley, G.J., & Erskine, W.D. (2012) Use of ergodic reasoning to reconstruct the historical range of variability and evolutionary trajectory of rivers. *Earth Surface Processes and Landforms*, 37(7), 763-773. doi.org/10.1002/esp.3210
- Gabet, E.J., Mudd, S.M., Wood, R.W., Grieve, S.W.D., Binnie, S. A., & Dunai, T. J. (2021). Hilltop curvature increases with the square root of erosion rate. *Journal of Geophysical Research: Earth Surface*, 126(5). doi.org/10.1029/2020JF005858
- Galbraith, R.F., & Roberts, R.G. (2012). Statistical aspects of equivalent dose and error calculation and display in OSL dating: an overview and some recommendations. *Quaternary Geochronology*, 11, 1-27. doi.org/10.1016/j.quageo.2012.04.020
- Gallagher, R.V., Allen, S., Mackenzie, B.D., Yates, C.J., Gosper, C.R., Keith, D.A., Merow, C., White, M.D., Wenk, E., Maitner, B.S., & He, K., (2021). High fire frequency and the impact of the 2019–2020 megafires on Australian plant diversity. *Diversity and Distributions*, 27, 1166–1179. doi.org/10.1111/ddi.13265.
- Gavin, D.G., Brubaker, L.B., & Lertzman, K.P. (2003). An 1800-year record of the spatial and temporal distribution of fire from the west coast of Vancouver Island, Canada. *Canadian Journal of Forest Research*, 33(4), 573-586. doi.org/10.1139/x02-196
- Giannini, P.C., Sawakuchi, A.O., Martinho, C.T., & Tatum, S.H. (2007). Eolian depositional episodes controlled by Late Quaternary relative sea level changes on the Imbituba–Laguna coast (southern Brazil). *Marine Geology*, 237(3-4), 143-168. doi.org/10.1016/j.margeo.2006.10.027
- Gilbert, G.K. (1909). The convexity of hilltops: *The Journal of Geology*, 17 (4), 344–350. doi.org/10.1086/621620

## References

- Gillette, D.A., & Stockton, P.H. (1989). The effect of nonerodible particles on wind erosion of erodible surfaces. *Journal of Geophysical Research: Atmospheres*, 94(D10), 12885-12893. doi.org/10.1029/JD094iD10p12885
- Glenn, N.F., Streutker, D.R., Chadwick, D.J., Thackray, G.D., & Dorsch, S.J. (2006). Analysis of LiDAR-derived topographic information for characterizing and differentiating landslide morphology and activity. *Geomorphology*, 73(1-2), 131-148. doi.org/10.1016/j.geomorph.2005.07.006
- Goetz, J.N., Bell, R., & Brenning, A. (2014). Could surface roughness be a poor proxy for landslide age? Results from the Swabian Alb, Germany. *Earth Surface Processes and Landforms*, 39(12), 1697-1704. doi.org/10.1002/esp.3630
- Gontz, A., McCallum, A., Ellerton, D., Patton, N., & Shulmeister, J. (2020). The Teewah Transect: GPR-Derived Insights into the Younger Dune Morphosequences on the Great Sandy Coast, Queensland, Australia. *Journal of Coastal Research*, 95(SI), 500-504. doi.org/10.2112/SI95-097.1
- Gontz, A., Moss, P.T., Sloss, C.R., Petherick, L.M., McCallum, A., & Shapland, F. (2015). Understanding past climate variation and environmental change for the future of an iconic landscape—K'gari Fraser Island, Queensland, Australia. *Australasian Journal of Environmental Management*, 22(2), 105-123. doi.org/10.1080/14486563.2014.1002120
- Gontz, A., Zhang, Y., Ellerton, D., Kemp, J., & Shulmeister, J. (In Review) Evidence for dune field reactivation and implication for retrogressive plant communities, eastern Cooloola Sand Mass, Queensland, Australia: *Geomorphology*.
- Greenslade, P., & Thompson, C. (1984). Ant distribution, veg and soil relationships in the Cooloola-Noosa River area, Queensland. *Vegetation Classification in Australia*, 192.
- Gross, W., Morrill, C., & Wahl, E. (2018). New advances at NOAA's World data service for paleoclimatology—Promoting the FAIR principles. *Past Global Changes Magazine*, 26(2), 58–58. doi.org/10.22498/pages.26.2.58
- Guérin, G., Jain, M., Thomsen, K.J., Murray, A.S., & Mercier, N. (2015). Modelling dose rate to single grains of quartz in well-sorted sand samples: the dispersion arising from the presence of potassium feldspars and implications for single grain OSL dating. *Quaternary Geochronology*, 27, 52-65. doi.org/10.1016/j.quageo.2014.12.006
- Guérin, G., Mercier, N., & Adamiec, G. (2011). Dose-rate conversion factors: update. *Ancient TL*, 29(1), 5-8.
- Han, M., Kim, J.C., Yang, D.Y., Lim, J., & Yi, S. (2021). The main periods and environmental controls of coastal dune development along the west coast of the Korean Peninsula

- during the mid to late Holocene. *Palaeogeography, Palaeoclimatology, Palaeoecology*, 569, 110345. doi.org/10.1016/j.palaeo.2021.110345
- Hani, A.F., Sathyamoorthy, D., & Asirvadam, V.S. (2011). A method for computation of surface roughness of digital elevation model terrain via multiscale analysis. *Computures & Geosciences*, 37,177–192. doi.org/10.1016/j.cageo.2010.05.021.
- Hansen, E., DeVries-Zimmerman, S., Davidson-Arnott, R., Dijk, D.V., Bodenbender, B., Kilibarda, Z., Thompson, T. & Yurk, B. (2020). *Dunes of the Laurentian Great Lakes. In Inland Dunes of North America*, 65-120. Springer, Cham.
- Hanson, J.M., VanderGragt, M.L., Welsh, K.J., & Moss, P.T. (2022). Variations in wetland conditions within the Fitzroy Basin, north-eastern Australia: a palaeoecological approach. *Marine and Freshwater Research*, 73(1), 35-47. doi.org/10.1071/MF21082
- Hanson, J.M., Welsh, K.J., Moss, P.T., & Gadd, P. (2023). Implications of sea level variability on the formation and evolution of subtropical Rainbow Beach patterned fen complexes, Queensland, Australia: *The Holocene*. 33, 49-60. doi.org/10.1177/0959683622112612
- Harrison, S.P., Villegas-Diaz, R., Cruz-Silva, E., Gallagher, D., Kesner, D., Lincoln, P., Shen, Y., Sweeney, L., Colombaroli, D., Ali, A. & Barhoumi, C. (2022). The Reading Palaeofire database: an expanded global resource to document changes in fire regimes from sedimentary charcoal records. *Earth System Science Data*, 14(3), 1109-1124. doi.org/10.17864/1947.319
- Harrold, A.G., McDonald, W.J.F., Hopkins, M.S., Walker, J., Sandercoe, C.S., & Thompson, C.H. (1987). Studies in landscape dynamics in the Cooloola-Noosa River area, Queensland. Vascular plants. Divisional Report, Division of Soils, CSIRO, Australia, (89).
- Hawkins, P.J. (1975). Forest management of Cooloola State Forest. *In Proceedings of the Ecological Society of Australia*.
- Hawthorne, D., Mustaphi, C.J.C., Aleman, J.C., Blarquez, O., Colombaroli, D., Daniau, A.L., Marlon, J.R., Power, M., Vanniere, B., Han, Y. & Hantson, S. (2018). Global Modern Charcoal Dataset (GMCD): A tool for exploring proxy-fire linkages and spatial patterns of biomass burning. *Quaternary International*, 488, 3-17. doi.org/10.1016/j.quaint.2017.03.046
- Heimsath, A., Dietrich, W., Nishiizumi, K., & Finkel, R.C. (1997). The soil production function and landscape equilibrium. *Nature*, 388, 358–361. doi.org/10.1038/41056
- Hennebelle, A., Aleman, J.C., Ali, A.A., Bergeron, Y., Carcaillet, C., Grondin, P., Landry, & J., Blarquez, O. (2020). The reconstruction of burned area and fire severity using charcoal from boreal lake sediments. *The Holocene*, 30, 1400–1409. doi.org/10.1177/0959683620932979



## References

- Hennessey, K., Lucas, C., Nicholls, N., Bathols, J., Suppiah, R., & Ricketts, J. (2005). Climate change impacts on fire-weather in south-east Australia. Climate Impacts Group, CSIRO Atmospheric Research and the Australian Government Bureau of Meteorology, Aspendale.
- Hesp, P. (2002). Foredunes and blowouts: initiation, geomorphology and dynamics. *Geomorphology*, 48(1-3), 245-268. doi.org/10.1016/S0169-555X(02)00184-8
- Hesse, P.P. (2016). How do longitudinal dunes respond to climate forcing? Insights from 25 years of luminescence dating of the Australian desert dunefields. *Quaternary International*, 410, 11-29. doi.org/10.1016/j.quaint.2014.02.020
- Higuera, P.E., Sprugel, D.G., & Brubaker, L.B. (2005). Reconstructing fire regimes with charcoal from small-hollow sediments: a calibration with tree-ring records of fire. *The Holocene*, 15(2), 238-251. doi.org/10.1191/0959683605hl789rp
- Higuera, P.E., Peters, M.E., Brubaker, L.B., & Gavin, D.G. (2007). Understanding the origin and analysis of sediment-charcoal records with a simulation model. *Quaternary Science Reviews*, 26, 1790–1809. doi.org/10.1016/j.quascirev.2007.03.010
- Hilley, G.E. & Arrowsmith, J.R. (2008) Geomorphic response to uplift along the Dragon's Back pressure ridge, Carrizo Plain, California: *Geology*, 36 (5), 367-370. doi.org/10.1130/G24517A.1
- Hogg, A.G., Heaton, T.J., Hua, Q., Palmer, J.G., Turney, C.S., Southon, J., Bayliss, A., Blackwell, P.G., Boswijk, G., Bronk Ramsey, C., Pearson, C., Petchey, F., Reimer, P., Reimer, R., & Wacker, L. (2020). SHCal20 Southern Hemisphere calibration, 0–55,000 years cal BP. *Radiocarbon*, 62, 759–778. doi.org/10.1017/RDC.2020.59.
- Houser, C., Wernette, P., Rentschlar, E., Jones, H., Hammond, B., & Trimble, S. (2015). Post-storm beach and dune recovery: Implications for barrier island resilience. *Geomorphology*, 234, 54-63. doi.org/10.1016/j.geomorph.2014.12.044
- Hua, Q., Jacobsen, G.E., Zoppi, U., Lawson, E.M., Williams, A.A., Smith, A.M., & McGann, M.J. (2001). Progress in radiocarbon target preparation at the ANTARES AMS Centre. *Radiocarbon*, 43(2A), 275-282. doi:10.1017/S003382220003811X
- Hua, Q., Turnbull, J.C., Santos, G.M., Rakowski, A.Z., Ancapichún, S., De Pol-Holz, R., Hammer, S., Lehman, S.J., Levin, I., Miller, J.B. Palmer, J.G., & Turney, C.S.M. (2022). Atmospheric radiocarbon for the period 1950–2019. *Radiocarbon*, 64, 723-745. doi.org/10.1017/RDC.2021.95.
- Hugenholtz, C.H., & Barchyn, T.E. (2010). Spatial analysis of sand dunes with a new global topographic dataset: new approaches and opportunities. *Earth surface processes and landforms*, 35(8), 986-992. doi.org/10.1002/esp.2013

- Hugenholtz, C.H., & Wolfe, S.A. (2005). Biogeomorphic model of dunefield activation and stabilization on the northern Great Plains. *Geomorphology*, 70(1-2), 53-70. doi.org/10.1016/j.geomorph.2005.03.011
- Huntley, D.J., Godfrey-Smith, D.I. & Thewalt, M.L. (1985). Optical dating of sediments. *Nature*, 313(5998), 105-107. doi.org/10.1038/313105a0
- Hurst, M.D., Mudd, S.M., Walcott, R., Attal, M., & Yoo, K. (2012). Using hilltop curvature to derive the spatial distribution of erosion rates. *Journal of Geophysical Research: Earth Surface*, 117(F2). doi.org/10.1029/2011JF002057
- Hurst, M.D., Mudd, S.M., Yoo, K., Attal, M., & Walcott, R. (2013). Influence of lithology on hillslope morphology and response to tectonic forcing in the northern Sierra Nevada of California. *Journal of Geophysical Research: Earth Surface*, 118 (2), 832-851. doi.org/10.1002/jgrf.20049
- Iglesias, V., Yospin, G.I., & Whitlock, C. (2015). Reconstruction of fire regimes through integrated paleoecological proxy data and ecological modelling. *Frontiers in Plant Science*, 5, 785. doi.org/10.3389/fpls.2014.00785
- IPCC, 2021: Climate Change 2021: The Physical Science Basis. Contribution of Working Group I to the Sixth Assessment Report of the Intergovernmental Panel on Climate Change [Masson-Delmotte, V., P. Zhai, A. Pirani, S.L. Connors, C. Péan, S. Berger, N. Caud, Y. Chen, L. Goldfarb, M.I. Gomis, M. Huang, K. Leitzell, E. Lonnoy, J.B.R. Matthews, T.K. Maycock, T. Waterfield, O. Yelekçi, R. Yu, & B. Zhou (eds.)]. Cambridge University Press, Cambridge, United Kingdom and New York, NY, USA, 2391 pp. doi:10.1017/9781009157896.
- Itter, M.S., Finley, A.O., Hooten, M.B., Higuera, P.E., Marlon, J.R., Kelly, R., & McLachlan, J.S. (2017). A model-based approach to wildland fire reconstruction using sediment charcoal records. *Environmetrics*, 28(7), e2450. doi.org/10.1002/env.2450
- Jerolmack, D.J., & Daniels, K.E. (2019). Viewing Earth's surface as a soft-matter landscape. *Nature Reviews Physics*, 1-15. doi.org/10.1038/s42254-019-0111-x
- Jerolmack, D.J., Ewing, R.C., Falcini, F., Martin, R.L., Masteller, C., Phillips, C., Reitz, M.D., & Buynevich, I. (2012). Internal boundary layer model for the evolution of desert dune fields. *Nature Geoscience*, 5(3), 206-209. doi.org/10.1038/ngeo1381
- Jyotsna R., & Haff, P.K. (1997). Microtopography as an indicator of modern hillslope diffusivity in arid terrain. *Geology*, 25, 695–698. doi.org/10.1130/0091-7613(1997)025<0695:MAAIOM>2.3.CO;2
- Käyhkö, J.A., Worsley, P., Pye, K., & Clarke, M.L. (1999). A revised chronology for aeolian activity in subarctic Fennoscandia during the Holocene. *The Holocene*, 9(2), 195-205. doi.org/10.1191/095968399668228352

## References

- Keeley, J.E. (1995). Seed-germination patterns in fire-prone Mediterranean-climate regions. *Ecology and Biogeography of Mediterranean ecosystems in Chile, California, and Australia*. (pp. 239-273). Springer, New York, NY.
- Keith, D. (2004). Ocean shores to desert dunes: the native vegetation of New South Wales and the ACT. Department of Environment and Conservation, Hurstville.
- Kelly, J.T., McSweeney, S., Shulmeister, J., & Gontz, A.M. (2019). Bimodal climate control of shoreline change influenced by Interdecadal Pacific Oscillation variability along the Cooloola Sand Mass, Queensland, Australia. *Marine Geology*, 415, 105971. doi.org/10.1016/j.margeo.2019.105971
- Kemp, C., Tibby, J., Barr, C., & Arnold, L. (2021). Climate, fire and vegetation history from subtropical North Stradbroke Island (Minjerribah), eastern Australia, during the last three interglacials. *Journal of Quaternary Science*, 36(7), 1201-1213. doi.org/10.1002/jqs.3355
- Kershaw, A.P. (1986). Climatic change and Aboriginal burning in north-east Australia during the last two glacial/interglacial cycles. *Nature* 322, 47-49. doi.org/10.1038/322047a0.
- Kershaw, A.P., Clark, J.S., Gill, A.M., & D'Costa, D.M. (2002). A history of fire in Australia. *Flammable Australia: the fire regimes and biodiversity of a continent*, 1, 3-25.
- Köhler, M., Shulmeister, J., Patton, N.R., Rittenour, T.M., McSweeney, S., Ellerton, D.T., Stout, J.T., & Hüneke, H. (2021). Holocene evolution of a barrier-spit complex and the interaction of tidal and wave processes, Inskip Peninsula, SE Queensland, Australia. *The Holocene*, 31(9), 1476-1488. doi.org/10.1177/09596836211019092
- Korzeniowska, K., Pfeifer, N., & Landtwing, S. (2018). Mapping gullies, dunes, lava fields, and landslides via surface roughness. *Geomorphology*, 301, 53-67. doi.org/10.1016/j.geomorph.2017.10.011
- Krishnan, V., Robinson, N., Firn, J., Applegate, G., Herbohn, J., & Schmidt, S. (2018). Without management interventions, endemic wet-sclerophyll forest is transitioning to rainforest in World Heritage listed K'gari (Fraser Island), Australia. *Ecology and Evolution*, 9(3), 1378-1393. doi.org/10.1002/ece3.4853
- LaHusen, S.R., Duvall, A.R., Booth, A.M., Grant, A., Mishkin, B.A., Montgomery, D.R., Struble, W., Roering, J.J., & Wartman, J. (2020). Rainfall triggers more deep-seated landslides than Cascadia earthquakes in the Oregon Coast Range, USA. *Science Advances*, 6 (38), eaba6790. doi.org/10.1126/sciadv.aba6790
- Lancaster, N. (2008). Desert dune dynamics and development: insights from luminescence dating. *Boreas*, 37(4), 559-573. doi.org/10.1111/j.1502-3885.2008.00055.x
- Lancaster, N., & Baas, A. (1998). Influence of vegetation cover on sand transport by wind: field studies at Owens Lake, California. *Earth Surface Processes and Landforms, The Journal*

- of the British Geomorphological Group*, 23(1), 69-82. doi.org/10.1002/(SICI)1096-9837(199801)23:1<69::AID-ESP823>3.0.CO;2-G
- Lancaster, N., Wolfe, S., Thomas, D., Bristow, C., Bubenzer, O., Burrough, S., Duller, G., Halfen, A., Hesse, P., Roskin, J. & Singhvi, A. (2016). The INQUA dunes atlas chronologic database. *Quaternary International*, 410, 3-10. doi.org/10.1016/j.quaint.2015.10.044
- Larcombe, P., Carter, R.M., Dye, J., Gagan, M.K., & Johnson, D.P. (1995). New evidence for episodic post-glacial sea-level rise, central Great Barrier Reef, Australia. *Marine Geology*, 127(1-4), 1-44. doi.org/10.1016/0025-3227(95)00059-8
- Lees, B. (2006). Timing and formation of coastal dunes in northern and eastern Australia. *Journal of Coastal Research*, 22(1), 78-89. doi.org/10.2112/05A-0007.1
- Levin, N. (2011). Climate-driven changes in tropical cyclone intensity shape dune activity on Earth's largest sand island. *Geomorphology*, 125(1), 239-252. doi.org/10.1016/j.geomorph.2010.09.021
- Levin, N., Ben-Dor, E., Kidron, G.J., & Yaakov, Y. (2008). Estimation of surface roughness (z0) over a stabilizing coastal dune field based on vegetation and topography. *Earth Surface Processes and Landforms: The Journal of the British Geomorphological Research Group*, 33(10), 1520-1541. doi.org/10.1002/esp.1621
- Levin, N., Jablon, P.E., Phinn, S., & Collins, K. (2017). Coastal dune activity and foredune formation on Moreton Island, Australia, 1944–2015. *Aeolian research*, 25, 107-121. doi.org/10.1016/j.aeolia.2017.03.005
- Levin, N., Levental, S., & Morag, H. (2012). The effect of wildfires on vegetation cover and dune activity in Australia's desert dunes: A multisensor analysis. *International Journal of Wildland Fire*, 21(4), 459-475. doi.org/10.1071/WF10150
- Lewis, S.E., Wüst, R.A., Webster, J.M., & Shields, G.A. (2008). Mid-late Holocene sea-level variability in eastern Australia: *Terra Nova*, 20.1, 74-81. doi.org/10.1111/j.1365-3121.2007.00789.x
- Leys, B.A., Commerford, J.L., & McLauchlan, K.K. (2017). Reconstructing grassland fire history using sedimentary charcoal: Considering count, size and shape. *PLoS One*, 12(4), e0176445. doi.org/10.1371/journal.pone.0176445
- Leys, B.A., Marlon, J.R., Umbanhowar, C., & Vannière, B. (2018). Global fire history of grassland biomes. *Ecology and evolution*, 8(17), 8831-8852. doi.org/10.1002/ece3.4394
- Lindhorst, S., & Betzler, C. (2016). The climate-archive dune: Sedimentary record of annual wind intensity. *Geology*, 44(9), 711-714. doi.org/10.1130/G38093.1

## References

- Little, I.P. (1986). Numerical analysis of soil development in a chronosequence on Fraser Island, southeastern Queensland. *Soil Research*, 24(3), 321-330. doi.org/10.1071/SR9860321
- Long, C.J., Whitlock, C., Bartlein, P.J., & Millspaugh, S.H. (1998). A 9000-year fire history from the Oregon Coast Range, based on a high-resolution charcoal study. *Canadian Journal of Forest Research*, 28(5), 774-787. doi.org/10.1139/x98-051
- Longmore, M.E. (1997). Quaternary palynological records from perched lake sediments, Fraser Island, Queensland, Australia: rainforest, forest history and climatic control. *Australian Journal of Botany*, 45(3), 507-526. doi.org/10.1071/BT96109
- Longmore, M.E., & Heijnis, H. (1999). Aridity in Australia: Pleistocene records of palaeohydrological and palaeoecological change from the perched lake sediments of Fraser Island, Queensland, Australia. *Quaternary International*, 57, 35-47. doi.org/10.1016/S1040-6182(98)00048-2
- Mann, D.H., Heiser, P.A., & Finney, B.P. (2002). Holocene history of the Great Kobuk sand dunes, northwestern Alaska. *Quaternary Science Reviews*, 21(4-6), 709-731. doi.org/10.1016/S0277-3791(01)00120-2
- Mariani, M., Connor, S.E., Theuerkauf, M., Herbert, A., Kuneš, P., Bowman, D., Fletcher, M.S., Head, L., Kershaw, A.P., Haberle, S.G. & Stevenson, J. (2022). Disruption of cultural burning promotes shrub encroachment and unprecedented wildfires. *Frontiers in Ecology and the Environment*. 20, 292-300. doi.org/10.1002/fee.2395
- Mariani, M., Tibby, J., Barr, C., Moss, P., Marshall, J.C., & McGregor, G.B. (2019). Reduced rainfall drives biomass limitation of long-term fire activity in Australia's subtropical sclerophyll forests. *Journal of Biogeography*, 46(9), 1974-1987. doi.org/10.1111/jbi.13628
- Marín, L., Forman, S.L., Valdez, A., & Bunch, F. (2005). Twentieth century dune migration at the Great Sand Dunes National Park and Preserve, Colorado, relation to drought variability. *Geomorphology*, 70(1-2), 163-183. doi.org/10.1016/j.geomorph.2005.04.014
- Marlon, J., Bartlein, P.J., & Whitlock, C. (2006). Fire-fuel-climate linkages in the northwestern USA during the Holocene. *The Holocene*, 16(8), 1059-1071. doi.org/10.1177/095968360606939
- Marlon, J.R., Kelly, R., Daniau, A.L., Vannière, B., Power, M.J., Bartlein, P., Higuera, P., Blarquez, O., Brewer, S., Brucher, T. & Feurdean, A. (2015). Reconstructions of biomass burning from sediment-charcoal records to improve data-model comparisons. *Biogeosciences*, 13(11), 3225-3244. doi.org/10.5194/bg-13-3225-2016
- Martínez, M.L., & Psuty, N.P. (2004). *Coastal dunes*. Springer Verlag.

- Matthews, J.A., & Seppälä, M. (2014). Holocene environmental change in subarctic aeolian dune fields: The chronology of sand dune re-activation events in relation to forest fires, palaeosol development and climatic variations in Finnish Lapland. *The Holocene*, 24(2), 149-164. doi.org/10.1177/0959683613515733
- Maxson, C., Tibby, J., Marshall, J., Kent, M., Tyler, J., Barr, C., McGregor, G., Cadd, H., Schulz, C. & Lomax, B.H. (2021). Fourier transform infrared spectroscopy as a tracer of organic matter sources in lake sediments. *Palaeogeography, Palaeoclimatology, Palaeoecology*, 581, 110622. doi.org/10.1016/j.palaeo.2021.110622
- McFarland, D.C. (1988). Fire and the vegetation composition and structure of sub-tropical heathlands in southeastern Queensland. *Australian Journal of Botany*, 36(5) 533 – 546. doi.org/10.1071/BT9880533
- McKean, J.A., Dietrich, W.E., Finkel, R.C., Southon, J.R., & Caffee, M.W. (1993). Quantification of soil production and downslope creep rates from cosmogenic <sup>10</sup>Be accumulations on a hillslope profile. *Geology*, 21(4), 343-346. doi.org/10.1130/0091-7613(1993)021<0343:QOSPAD>2.3.CO;2
- McKean, J., & Roering, J. (2004). Objective landslide detection and surface morphology mapping using high-resolution airborne laser altimetry. *Geomorphology*, 57(3-4), 331-351. doi.org/10.1016/S0169-555X(03)00164-8
- McKee, E. D. (1979). Introduction to a study of global sand seas. In A study of global sand seas (Vol. 1052, pp. 1-19). US Government Printing Office.
- McKenzie, D., Gedalof, Z., Peterson, D., & Mote, P. (2004). Climatic Change, wildfire and conservation. *Conservation Biology*, 890-902. doi.org/10.1111/j.1523-1739.2004.00492.x
- McLauchlan, K.K., Higuera, P.E., Miesel, J., Rogers, B.M., Schweitzer, J., Shuman, J.K., Tepley, A.J., Varner, M., Veblen, T.T., Adalsteinsson, S.A., Balch, J.K., Baker, P., Batllori, E., Bigio, E., Brando, P., Cattau, M., Chipman, M.L., Coen, J., Crandall, R., Daniels, L., Enright, N., Gross, W. S., Harvey, B.J., Hatten, J.A., Hermann, S., Hewitt, R.E., Kobziar, L.N., Landesmann, J.B., Loranty, M.M., Maezumi, S.Y., Mearns, L., Moritz, M., Myers, J.A., Pausas, J.G., Pellegrini, A. F.A., Platt, W.J., Roozeboom, J., Safford, H., Santos, F., Scheller, R.M., Sherriff, R.L., Smith, K.G., Smith, M.D., & Watts, A.C. (2020). Fire as a fundamental ecological process: research advances and frontiers. *Journal of Ecology*, 108, 2047– 2069. doi.org/10.1111/1365-2745.13403
- McNiven, I.J. (1991). Teewah Beach: New evidence for Holocene coastal occupation in southeast Queensland, *Australian Archaeology*, 33, 14-27. doi.org/10.1080/03122417.1991.11681428
- McSweeney, S., & Shulmeister, J. (2018). Variations in wave climate as a driver of decadal scale shoreline change at the Inskip Peninsula, southeast Queensland, Australia. *Estuarine, Coastal and Shelf Science*, 209, 56-69. doi.org/10.1016/j.ecss.2018.04.034

## References

- Micallef, A., Ribó, M., Canals, M., Puig, P., Lastras, G., & Tubau, X. (2014). Space-for-time substitution and the evolution of a subterre canyon–channel system in a passive progradational margin. *Geomorphology*, 221, 34-50. doi.org/10.1016/j.geomorph.2014.06.008
- Minasny, B., Finke, P., Stockmann, U., Vanwalleghe, T., & McBratney, A.B. (2015). Resolving the integral connection between pedogenesis and landscape evolution. *Earth Science Reviews*, 150, 102-120. doi.org/10.1016/j.earscirev.2015.07.004
- Minasny, B., & McBratney, A.B. (2016). Digital soil mapping: A brief history and some lessons. *Geoderma*, 264, 301-311. doi.org/10.1016/j.geoderma.2015.07.017
- Miot da Silva, G., & Shulmeister, J. (2016). A review of coastal dunefield evolution in Southeastern Queensland. *Journal of Coastal Research*, (75 (10075)), 308-312. doi.org/10.2112/SI75-062.1
- Montgomery, D.R. (2007). Characterization of topographic steady state in Taiwan. *Earth and Planetary Science Letters*, 261 (3-4), 421-431. doi.org/10.1016/j.epsl.2007.07.045
- Montgomery, D.R. (2001). Slope distributions, threshold hillslopes, and steady-state topography: *American Journal of Science*, 301, 432–454. doi.org/10.2475/ajs.301.4-5.432
- Mooney, S.D., Harrison, S.P., Bartlein, P.J., Daniau, A.L., Stevenson, J., Brownlie, K.C., Buckman, S., Cupper, M., Luly, J., Black, M., Colhoun, E., D’Costa, D., Dodson, J., Haberle, S., Hope, G.S., Kershaw, P., Kenyon, C., McKenziel, M., & Williams, N. (2011). Late Quaternary fire regimes of Australasia. *Quaternary Science Reviews*, 30(1-2), 28-46. doi.org/10.1016/j.quascirev.2010.10.010
- Moore, I.D., Grayson, R.B., & Landson, A.R. (1991). Digital terrain modeling: a review of hydrological, geomorphological, and biological applications: *Hydrological Processes*, 5, 3–30. doi.org/10.1002/hyp.3360050103
- Morris, J.L., Higuera, P.E., Haberle, S., & Whitlock, C. (2017). Modern pollen from small hollows reflects *Athrotaxis cupressoides* density across a wildfire gradient in subalpine forests of the Central Plateau, Tasmania, Australia. *The Holocene*, 27(11), 1781-1788. doi.org/10.1177/0959683617702228
- Moss, P.T. (2014). Investigation of the vegetation and fire history of the EPBC, RAMSAR and WHA wetlands of the Great Sandy Strait, *Unpublished Report*, University of Queensland, Australia.
- Moss, P.T., & Kershaw, P.A. (2000). The last glacial cycle from the humid tropics of northeastern Australia: comparison of a terrestrial and a marine record. *Palaeogeography, Palaeoclimatology, Palaeoecology*, 155(1-2), 155-176. doi.org/10.1016/S0031-0182(99)00099-1

- Moss, P., Mackenzie, L., Ulm, S., Sloss, C., Rosendahl, D., Petherick, L., Steinberger, L., Wallis, L., Heijnis, H., Petchey, F., & Jacobsen, G. (2015). Environmental context for late Holocene human occupation of the South Wellesley Archipelago, Gulf of Carpentaria, northern Australia. *Quaternary International*, 385, 136-144. doi.org/10.1016/j.quaint.2015.02.051
- Moss, P.T., Petherick, L., & Neil, D. (2011). Environmental change at Myora Springs, North Stradbroke Island over the last millennium. *Proceedings of the Royal Society of Queensland*, 117, 133–140. doi/10.3316/informit.551525558476472
- Moss, P.T., Tibby, J., Petherick, L., McGowan, H., & Barr, C. (2013). Late Quaternary vegetation history of North Stradbroke Island, Queensland, eastern Australia. *Quaternary Science Reviews*, 74, 257–272. doi/10.1016/J.QUASCIREV.2013.02.019
- Moss, P., Tibby, J., Shapland, F., Rairfax, R., Stewart, P., Barr, C., Petherick, L., Gontz, A., & Sloss, C. (2016). Patterned fen formation and development from the Great Sandy Region, south-east Queensland, Australia, *Marine and Freshwater Research*, 67(6), 816-827. doi.org/10.1071/MF14359
- Moy, C.M., Seltzer, G.O., Rodbell, D.T., & Anderson, D.M. (2002). Variability of El Niño/Southern Oscillation activity at millennial timescales during the Holocene epoch. *Nature*, 420(6912), 162-165. doi.org/10.1038/nature01194
- Mulholland, C. (2021). Fighting to save an international icon-K'gari (Fraser Island). *The Australian Journal of Emergency Management*, 36(4), 40-43. doi/10.3316/informit.194168525918020
- Murray, A., Arnold, L.J., Buylaert, J.P., Guérin, G., Qin, J., Singhvi, A.K., Smedley, R., & Thomsen, K.J. (2021). Optically stimulated luminescence dating using quartz. *Nature Reviews Methods Primers*, 1(1), 1-31. doi.org/10.1038/s43586-021-00068-5
- Murray, A.S., & Wintle, A.G. (2000). Luminescence dating of quartz using an improved single-aliquot regenerative-dose protocol. *Radiation measurements*, 32(1), 57-73. doi.org/10.1016/S1350-4487(99)00253-X
- Murray, A.S., & Wintle, A. G. (2003). The single aliquot regenerative dose protocol: potential for improvements in reliability. *Radiation measurements*, 37(4-5), 377-381. doi.org/10.1016/S1350-4487(03)00053-2
- Neal, R., & Stock, E. (1986). Pleistocene occupation in the south-east Queensland coastal region. *Nature*, 323(6089), 618-621. doi.org/10.1038/323618a0
- Ngugi, M.R., Knight, J., Hua, Q., Dowling, R., Kington, D., & Burns, D. (2020). Ageing culturally significant relic trees in southeast Queensland to support bushfire management strategies. *Ecological Management & Restoration*, 21(2), 147-150. doi.org/10.1111/emr.12404



## References

- Patterson, C.C., & Patterson, D.C. (1983). Gold Coast longshore transport, in Proceedings of the Sixth Australian Coastal and Ocean Engineering Conference: Australia: Gold Coast, Queensland, Australia, The Institute of Engineers, p. 251–256.
- Patton, N.R., Ellerton, D., & Shulmeister, J. (2019a). High-resolution remapping of the coastal dune fields of south east Queensland, Australia: a morphometric approach: *Journal of Maps*, 15 (2), 578-589. doi.org/10.1080/17445647.2019.1642246
- Patton, N.R., Lohse, K.A., Godsey, S.E., Crosby, B.T., & Seyfried, M. (2018). Predicting soil thickness on soil mantled hillslopes: *Nature Communications*, 9 (1), 1-10. doi.org/10.1038/s41467-018-05743-y
- Patton, N.R., Lohse, K.A., Seyfried, M.S., Godsey, S.E., & Parsons, S.B. (2019b). Topographic controls of soil organic carbon on soil-mantled landscapes. *Scientific Reports*, 9(1), 1-15. doi.org/10.1038/s41598-019-42556-5
- Patton, N.R., Shulmeister, J., Ellerton, D., & Seropian, G. (2022a). Measuring landscape evolution from inception to maturity: Insights from a coastal dune system. *Earth and Planetary Science Letters*, 584, 117448. doi.org/10.1016/j.epsl.2022.117448
- Patton, N.R., Shulmeister, J., Rittenour, M.T., Almond, P., Ellerton, D.T., & Santini T. (2022b). Using calibrated surface roughness dating to estimate coastal dune ages at K'gari (Fraser Island) and the Cooloola Sand Mass, Australia. *Earth Surface Processes and Landforms*, 47(10), 2455-2470. doi.org/10.1002/esp.5387
- Pawlik, Ł., & Šamonil, P. (2018). Soil creep: the driving factors, evidence and significance for biogeomorphic and pedogenic domains and systems—a critical literature review: *Earth Science Reviews*, 178, 257-278. doi.org/10.1016/j.earscirev.2018.01.008
- Peel, M.C., Finlayson, B.L., & McMahon, T.A. (2007). Updated world map of the Köppen-Geiger climate classification. *Hydrology and Earth System Sciences*, 11(5), 1633-1644. doi.org/10.5194/hess-11-1633-2007
- Pelletier, J.D. (2013). Deviations from self-similarity in barchan form and flux: The case of the Salton Sea dunes, California. *Journal of Geophysical Research: Earth Surface*, 118(4), 2406-2420. doi.org/10.1002/2013JF002867
- Pelletier, J.D., Mitasova, H., Harmon, R.S., & Overton, M. (2009). The effects of interdune vegetation changes on eolian dune field evolution: a numerical-modeling case study at Jockey's Ridge, North Carolina, USA. *Earth Surface Processes and Landforms*, 34(9), 1245-1254. doi.org/10.1002/esp.1809
- Peterson, C.D., Stock, E., Price, D.M., Hart, R., Reckendorf, F., Erlandson, J.M., & Hostetler, S.W. (2007). Ages, distributions, and origins of upland coastal dune sheets in Oregon, USA. *Geomorphology*, 91(1-2), 80-102. doi.org/10.1016/j.geomorph.2007.02.005

- Petherick, L., McGowan, H., & Moss, P. (2008). Climate variability during the Last Glacial Maximum in eastern Australia: evidence of two stadials?. *Journal of Quaternary Science: Quaternary Research Association*, 23(8), 787-802. doi.org/10.1002/jqs.1186
- Pommerol, A., Chakraborty, S., & Thomas, N. (2012). Comparative study of the surface roughness of the Moon, Mars and Mercury. *Planetary and Space Science*, 73(1), 287-293. doi.org/10.1016/j.pss.2012.08.020
- Power, M.J., Marlon, J., Ortiz, N., Bartlein, P.J., Harrison, S.P., Mayle, F.E., Ballouche, A., Bradshaw, R.H.W., Carcaillet, C., Cordova, C., Mooney, S., Moreno, P.I., Prentice, I.C., Thonicke, K., Tinner, W., Whitlock, C., Zhang, Y., Zhao, Y., Ali, A.A., Anderson, R.S., Beer, R., Behling, H., Briles, C., Brown, K.J., Brunelle, A., Bush, M., Camill, P., Chu, G.Q., Clark, J., Colombaroli, D., Connor, S., Daniau, A.L., Daniels, M., Dodson, J., Doughty, E., Edwards, M.E., Finsinger, W., Foster, D., Frechette, J., Gaillard, M.J., Gavin, D.G., Gobet, E., Haberle, S., Hallett, D.J., Higuera, P., Hope, G., Horn, S., Inoue, J., Kaltenrieder, P., Kennedy, L., Kong, Z.C., Larsen, C., Long, C.J., Lynch, J., Lynch, E.A., McGlone, M., Meeks, S., Mensing, S., Meyer, G., Minckley, T., Mohr, J., Nelson, D.M., New, J., Newnham, R., Noti, R., Oswald, W., Pierce, J., Richard, P.J.H., Rowe, C., Sanchez Goñi, M.F., Shuman, B.N., Takahara, H., Toney, J., Turney, C., Urrego-Sanchez, D.H., Umbanhowar, C., Vandergoes, M., Vanniere, B., Vescovi, E., Walsh, M., Wang, X., Williams, N., Wilmshurst, J., & Zhang, J.H. (2008). Changes in fire regimes since the Last Glacial Maximum: an assessment based on a global synthesis and analysis of charcoal data. *Climate dynamics*, 30 (7), 887-907. doi.org/10.1007/s00382-007-0334
- Prescott, J.R., & Hutton, J.T. (1994). Cosmic ray contributions to dose rates for luminescence and ESR dating: *Radiation Measurements*, 23, 497-500. doi.org/10.1016/1350-4487(94)90086-8
- Pye, K. (1982). Morphological development of coastal dunes in a humid tropical environment, Cape Bedford and Cape Flattery, North Queensland. *Geografiska Annaler: Series A, Physical Geography*, 64 (3-4), 213-227. doi.org/10.1080/04353676.1982.11880067
- Pye, K. (1983). Coastal dunes. *Progress in Physical Geography*, 7(4), 531-557. doi.org/10.1177/030913338300700403
- Pye, K. & Bowman, G.M. (1984). Holocene marine transgression as a forcing function in episodic dune activity on the eastern Australian coast. In: Thom, B.G. Editor, editor/s. Coastal geomorphology in Australia. Sydney: Academic Press, 179-196.
- Pyne S.J. (1998). Burning Bush: A Fire History of Australia. Henry Holt, New York.
- Queensland Herbarium (2021). Regional Ecosystem Description Database (REDD). Version 12.1 Queensland Department of Environment and Science, Brisbane. [online] www.qld.gov.au/environment/plants-animals/plants/ecosystems (01 April 2022).
- R Core Team (2020). R: A language and environment for statistical computing, R Foundation for Statistical Computing, Vienna, Austria, <https://www.R-project.org/>.

## References

- Ramsey, C.B. (2017). Methods for summarizing radiocarbon datasets. *Radiocarbon*, 59 (6), 1809-1833. doi:10.1017/RDC.2017.108
- Raupach, M.R., Gillette, D.A., & Leys, J.F. (1993). The effect of roughness elements on wind erosion threshold. *Journal of Geophysical Research: Atmospheres*, 98(D2), 3023-3029. doi.org/10.1029/92JD01922
- Reeve, R., Fergus, I.F., & Thompson, C.H. (1985). Studies in landscape dynamics in the Cooloola-Noosa River area, Queensland. 4. *Hydrology and water chemistry*. In: *CSIRO Aust. Div. Soils Divisional Report*, 73, (42).
- Reid, L. M., & Dunne, T. (1996). Rapid evaluation of sediment budgets (Vol. 29). *Reiskirchen, Germany: Catena*.
- Remy, C.C., Fouquemberg, C., Asselin, H., Andrieux, B., Magnan, G., Brossier, B., Grondin, P., Bergeron, Y., Talon, B., Girardin, M.P., Blarquez, O., Bajolle, L., & Ali, A.A. (2018). Guidelines for the use and interpretation of palaeofire reconstructions based on various archives and proxies. *Quaternary Science Reviews*, 193, 312-322. doi.org/10.1016/j.quascirev.2018.06.010
- Richards, L., Brew, N., & Smith, L. (2020). 2019-2020 Australian bushfires—frequently asked questions: a quick guide. Parliament of Australia, Research Paper Series 2019–2020. Retrieved from: [www.aph.gov.au/About\\_Parliament/Parliamentary\\_Departments/Parliamentary\\_Library/pubs/rp/rp1920/Quick\\_Guides/AustralianBushfires](http://www.aph.gov.au/About_Parliament/Parliamentary_Departments/Parliamentary_Library/pubs/rp/rp1920/Quick_Guides/AustralianBushfires)
- Richter, D.D., Eppes, M.C., Austin, J.C., Bacon, A.R., Billings, S.A., Brecheisen, Z., Ferguson, T.A., Markewitz, D., Pachon, J., Schroeder, P.A., & Wade, A.M. (2020). Soil production and the soil geomorphology legacy of Grove Karl Gilbert. *Soil Science Society of America Journal*, 84(1), 1-20. doi.org/10.1002/saj2.20030
- Ritchie, J.C., McCarty, G.W., Venteris, E.R., & Kaspar, T.C. (2007). Soil and soil organic carbon redistribution on the landscape. *Geomorphology*, 89(1-2), 163-171. doi.org/10.1016/j.geomorph.2006.07.021
- Roering, J.J., & Gerber, M. (2005). Fire and the evolution of steep, soil-mantled landscapes: *Geology*, 33 (5), 349-352. doi.org/10.1130/G21260.1
- Roering, J.J., Kirchner, J.W., & Dietrich, W.E. (1999). Evidence for nonlinear, diffusive sediment transport on hillslopes and implications for landscape morphology: *Water Resources Research*, 35(3), 853-870. doi.org/10.1029/1998WR900090
- Roering, J.J., Kirchner, J.W., Sklar, L.S., & Dietrich, W.E. (2001). Hillslope evolution by nonlinear creep and landsliding: An experimental study: *Geology*, 29 (2), 143-146. doi.org/10.1130/0091-7613(2001)029<0143:HEBNCA>2.0.CO;2

- Rosenbloom, N.A., & Anderson, R.S. (1994). Hillslope and channel evolution in a marine terraced landscape, Santa Cruz, California. *Journal of Geophysical Research: Solid Earth*, 99(B7), 14013-14029. doi.org/10.1029/94JB00048
- Roskin, J., Katra, I., & Blumberg, D.G. (2013). Late Holocene dune mobilizations in the northwestern Negev dunefield, Israel: A response to combined anthropogenic activity and short-term intensified windiness. *Quaternary International*, 303, 10-23. doi.org/10.1016/j.quaint.2012.10.034
- Roy, P.S., & Thom, B.G. (1981). Late Quaternary marine deposition in New South Wales and southern Queensland—an evolutionary model. *Journal of the Geological Society of Australia*, 28(3-4), 471-489. doi.org/10.1080/00167618108729182
- Russell-Smith, J., Lucas, D., Gapindi, M., Gunbunuka, B., Kapiirigi, N., Namingum, G., Lucas, K., Giuliani, P., & Chaloupka, G. (1997). Aboriginal resource utilization and fire management practice in western Arnhem Land, monsoonal northern Australia: notes for prehistory, lessons for the future. *Human Ecology*, 25(2), 159-195. doi.org/10.1023/A:1021970021670
- Russell-Smith, J., Yates, C.P., Whitehead, P.J., Smith, R., Craig, R., Allan, G.E., Thackway, R., Frakes, I., Cridland, S., Meyer, M.C. & Gill, A.M. (2007). Bushfires 'down under': patterns and implications of contemporary Australian landscape burning. *International Journal of Wildland Fire*, 16, 361–377. doi.org/10.1071/WF07018.
- Sadler, P.M. (1981). Sediment accumulation rates and the completeness of stratigraphic sections. *The Journal of Geology*, 89(5), 569-584. doi.org/10.1086/628623
- Sanborn, P., Geertsema, M., Jull, A.T., & Hawkes, B. (2006). Soil and sedimentary charcoal evidence for Holocene forest fires in an inland temperate rainforest, east-central British Columbia, Canada. *The Holocene*, 16(3), 415-427. doi.org/10.1191/0959683606hl937rp
- Schanz, S.A., & Colee, A.P. (2021). Development of a surface roughness curve to estimate timing of earthflows and habitat development in the Teanaway River, central Washington State, USA. *Earth Surface Dynamics Discussions*, 1-24. doi.org/10.5194/esurf-2021-61
- Schmieder, J., Fritz, S.C., Grimm, E.C., Jacobs, K.C., Brown, K.J., Swinehart, J.B., & Porter, S.C. (2013). Holocene variability in hydrology, vegetation, fire, and eolian activity in the Nebraska Sand Hills, USA. *The Holocene*, 23(4), 515-527. doi.org/10.1177/0959683612463100
- Schoenberger, P.J., Wysocki, D.A., Benham, E.C., & Broderson, W.D. (2002). Field book for describing and sampling soils. Version 2.0. *Natural Resources Conservation Service*, National Soil Survey Center, Lincoln, Nebraska.

## References

- Schreuder, L.T., Donders, T.H., Mets, A., Hopmans, E.C., Damsté, J.S.S., & Schouten, S. (2019). Comparison of organic and palynological proxies for biomass burning and vegetation in a lacustrine sediment record (Lake Allom, Fraser Island, Australia). *Organic Geochemistry*, 133, 10-19. doi.org/10.1016/j.orggeochem.2019.03.002
- Seppälä, M. (1995). Deflation and redeposition of sand dunes in Finnish Lapland. *Quaternary Science Reviews*, 14(7-8), 799-809. doi.org/10.1016/0277-3791(95)00057-7
- Shakesby, R.A., & Doerr, S.H. (2006). Wildfire as a hydrological and geomorphological agent. *Earth-Science Reviews*, 74(3-4), 269-307. doi.org/10.1016/j.earscirev.2005.10.006
- Shulmeister, J. (1999). Australasian evidence for mid-Holocene climate change implies precessional control of Walker Circulation in the Pacific. *Quaternary International*, 57, 81-91. doi.org/10.1016/S1040-6182(98)00052-4
- Shulmeister, J., & Lees, B.G. (1992). Morphology and chronostratigraphy of a coastal dune field; Groote Eylandt, northern Australia. *Geomorphology*, 5(6), 521-534. doi.org/10.1016/0169-555X(92)90023-H
- Shulmeister, J. & Lees, B.G. (1995). Pollen evidence from tropical Australia for the onset of an ENSO-dominated climate at c. 4000 BP. *The Holocene*, 5(1), 10-18. doi.org/10.1177/095968369500500102
- Shumack, S., & Hesse, P. (2018). Assessing the geomorphic disturbance from fires on coastal dunes near Esperance, Western Australia: Implications for dune destabilisation. *Aeolian Research*, 31, 29-49. doi.org/10.1016/j.aeolia.2017.08.005
- Shumack, S., Hesse, P., & Turner, L. (2017). The impact of fire on sand dune stability: Surface coverage and biomass recovery after fires on Western Australian coastal dune systems from 1988 to 2016. *Geomorphology*, 299, 39-53. doi.org/10.1016/j.geomorph.2017.10.001
- Singh, G., Kershaw, A.P., & Clark, R. (1981). Quaternary vegetation and fire history in Australia. *Fire and the Australian biota*, 23-54.
- Smith, M.W. (2014). Roughness in the earth sciences. *Earth-Science Reviews*, 136, 202-225. doi.org/10.1016/j.earscirev.2014.05.016
- Sommerville, A.A., Hansom, J.D., Housley, R.A., & Sanderson, D.C.W. (2007). Optically stimulated luminescence (OSL) dating of coastal aeolian sand accumulation in Sanday, Orkney Islands, Scotland. *The Holocene*, 17(5), 627-637. doi.org/10.1177/0959683607078987
- Sorensen, L. (2007). A spatial analysis approach to global delineation of dryland area of relevance to CBD Programme of Work on Dry and Subhumid Lands. UNEP-WCMC, Cambridge. [Online: <http://datadownload.unep-wcmc.org/datasets>]

- Spenser, R.J., & Baxter, G.S. (2006). Effects of fire on the structure and composition of open eucalypt forests. *Austral Ecology*, 31(5), 638-646. doi.org/10.1111/j.1442-9993.2006.01616.x
- Srivastava, S.K., King, L., Mitchell, C., Wiegand, A., Carter, R.W., Shapcott, A., & Russell-Smith, J. (2012). Ecological implications of standard fire-mapping approaches for fire management of the World Heritage Area, Fraser Island, Australia. *International Journal of Wildland Fire*, 22(3), 381-393. doi.org/10.1071/WF11037
- Stallins, J.A., & Parker, A.J. (2003). The influence of complex systems interactions on barrier island dune vegetation pattern and process. *Annals of the Association of American Geographers*, 93(1), 13-29. doi.org/10.1111/1467-8306.93102
- Stephens, A., Roy, P., & Jones, M. (1981). Geological Model of Erosion on a Littoral Drift Coast. In: Fifth Australian Conference on Coastal and Ocean Engineering, 1981: Offshore Structures. Barton, A.C.T.: Institution of Engineers, Australia, 1981: 174-179. <https://search.informit.org/doi/10.3316/informit.925679732664746>
- Stewart, P.L.C., Moss, P.T., & Farrell, R. (2020). Land change analysis of moon point vegetation on Fraser Island, East Coast, Queensland, Australia. *International Journal of Ecology and Environmental Sciences*, 46(1), 25-39.
- Stolar, D.B., Willett, S.D., & Stewart, P.L.C., Moss, P.T., & Farrell, R. (2020). Land change analysis of moon point vegetation on Fraser Island, East Coast, Queensland, Australia. *International Journal of Ecology and Environmental Sciences*, 46(1), 25-39. doi.org/10.1016/j.epsl.2007.07.045
- Stone, Z.L., Maron, M., & Tasker, E. (2022). Reduced fire frequency over three decades hastens loss of the grassy forest habitat of an endangered songbird. *Biological Conservation*, 270, 109570. doi.org/10.1016/j.biocon.2022.109570
- Struble, W.T., & Roering, J.J. (2021). Hilltop curvature as a proxy for erosion rate: Wavelets enable rapid computation and reveal systematic underestimation. *Earth Surface Dynamics*, 9, 1279-1300. doi.org/10.5194/esurf-9-1279-2021, 2021
- Swezey, C. (2001). Eolian sediment responses to late Quaternary climate changes: temporal and spatial patterns in the Sahara. *Palaeogeography, Palaeoclimatology, Palaeoecology*, 167 (1-2), 119-155. doi.org/10.1016/S0031-0182(00)00235-2
- Tejan-Kella, M.S., Chittleborough, D.J., Fitzpatrick, R.W., Thompson, C.H., Prescott, J.R., & Hutton, J.T. (1990). Thermoluminescence dating of coastal sand dunes at Cooloola and North Stradbroke Island, Australia. *Soil Research*, 28(4), 465-481. doi.org/10.1071/SR9900465
- Thom, B.G. (1978). Coastal sand deposition in southeast Australia during the Holocene. *Landform evolution in Australasia*, (pp. 197-214). ANU Press Canberra.

## References

- Thomas, A. (2003). Fraser Island World Heritage Area fire management systems: fire strategy. *Queensland Government, Queensland Parks and Wildlife Service*. (Brisbane, Qld).
- Thomas, D.S., & Wiggs, G.F. (2008). Aeolian system responses to global change: challenges of scale, process and temporal integration. *Earth Surface Processes and Landforms: The Journal of the British Geomorphological Research Group*, 33(9), 1396-1418. doi.org/10.1002/esp.1719
- Thompson, C.H. (1981). Podzol chronosequences on coastal dunes of eastern Australia. *Nature*, 291(5810), 59-61. doi.org/10.1038/291059a0
- Thompson, C.H. (1983). Development and weathering of large parabolic dune systems along the subtropical coast of Eastern Australia. *Zeitschrift fuer Geomorphologie*, 205-225.
- Thompson, C.H. (1992). Genesis of podzols on coastal dunes in southern Queensland. Field relationships and profile morphology. *Soil Research*, 30(5), 593-613. doi.org/10.1071/SR9920593
- Thompson, C.H., & Moore, A.W. (1984). Studies in landscape dynamics in the Cooloola-Noosa River area, Queensland. *Divisional Report – CSIRO, Australia, Division of Soils Article*, v. 73.
- Tsoar, H. (2005). Sand dunes mobility and stability in relation to climate. *Physica A: Statistical Mechanics and its Applications*, 357(1), 50-56. doi.org/10.1016/j.physa.2005.05.067
- Tucker, G.E., & Hancock, G.R. (2010). Modelling landscape evolution. *Earth Surface Processes and Landforms*, 35(1), 28-50. doi.org/10.1002/esp.1952
- Turney, C.S., Kershaw, A.P., Moss, P., Bird, M.I., Fifield, L.K., Cresswell, R.G., Santos, G.M., Di Tada, M.L., Hausladen, P.A., & Zhou, Y. (2001). Redating the onset of burning at Lynch's Crater (North Queensland): implications for human settlement in Australia. *Journal of Quaternary Science: Published for the Quaternary Research Association*, 16(8), 767-771. doi.org/10.1002/jqs.643
- United Nations Educational, Scientific and Cultural Organization (UNESCO) World Heritage Convention (2021). *K'gari (Fraser Island) listing*. (01 January, 2022). <https://whc.unesco.org/en/list/630/>
- Vachula, R.S., Russell, J.M., Huang, Y., & Richter, N. (2018). Assessing the spatial fidelity of sedimentary charcoal size fractions as fire history proxies with a high-resolution sediment record and historical data. *Palaeogeography, Palaeoclimatology, Palaeoecology*, 508, 166-175. doi.org/10.1016/j.palaeo.2018.07.032
- Vachula, R.S., Sheppard, R.Y., & Cheung, A.H. (2022). Preservation biases are pervasive in Holocene paleofire records. *Palaeogeography, Palaeoclimatology, Palaeoecology*, 602, 111165. doi.org/10.1016/j.palaeo.2022.111165

- Van Der Werf, G.R., Randerson, J.T., Giglio, L., Van Leeuwen, T.T., Chen, Y., Rogers, B.M., Mu, M., van Marle, M.J.E., Morton, D.C., Collatz, G.J., Yokelson, R.J., & Kasibhatla, P.S. (2017). Global fire emissions estimates during 1997–2016. *Earth System Science Data*, 9(2), 697-720. doi.org/10.5194/essd-9-697-2017
- Vimpere, L., Watkins, S.E., & Castelltort, S. (2021). Continental interior parabolic dunes as a potential proxy for past climates. *Global and Planetary Change*, 206, 103622. doi.org/10.1016/j.gloplacha.2021.103622
- Wagstaff, S.J., & Clarkson, B.R. (2012). Systematics and ecology of the Australasian genus *Empodisma* (Restionaceae) and description of a new species from peatlands in northern New Zealand. *PhytoKeys*, (13), 39. doi:10.3897/phytokeys.13.3259
- Walker, J., Lees, B., Olley, J., & Thompson, C. (2018). Dating the Cooloola coastal dunes of south-eastern Queensland, Australia. *Marine Geology*, 398, 73-85. doi.org/10.1016/j.margeo.2017.12.010
- Walker, J., Thompson, C.H., Fergus, I.F., & Tunstall, B.R. (1981). Plant succession and soil development in coastal sand dunes of subtropical eastern Australia. In *Forest Succession* (pp. 107-131). Springer, New York. doi: 10.1007/978-1-4612-5950-3\_9
- Walker, J., Thompson, C.H., & Lacey, C.J. (1987). Morphological differences in lignotubers of *Eucalyptus intermedia* RT Bak. and *E. signata* F. Muell. associated with different stages of podzol development on coastal dunes, Cooloola, Queensland. *Australian Journal of Botany*, 35(3), 301-311. doi.org/10.1071/BT9870301
- Walker, L.R., Wardle, D.A., Bardgett, R.D., & Clarkson, B.D. (2010). The use of chronosequences in studies of ecological succession and soil development. *Journal of Ecology*, 98(4), 725-736. doi.org/10.1111/j.1365-2745.2010.01664.x
- Ward, R. (1978). Australian legend re-visited. *Australian Historical Studies*, 18(71), 171-190. doi.org/10.1080/10314617808595586
- Ward, W.T. (2006). Coastal dunes and strandplains in southeast Queensland: sequence and chronology. *Australian Journal of Earth Sciences*, 53(2), 363-373. doi.org/10.1080/08120090500507354
- Wardell-Johnson, G., Schoeman, D., Schlacher, T., Wardell-Johnson, A., Weston, M.A., Shimizu, Y., & Conroy, G. (2015). Re-framing values for a World Heritage future: what type of icon will K'gari-Fraser Island become?. *Australasian Journal of Environmental Management*, 22(2), 124-148. doi.org/10.1080/14486563.2014.985267
- Wasson, R.J., & Hyde, R. (1983). Factors determining desert dune type. *Nature*, 304(5924), 337-339. doi.org/10.1038/304337a0



## References

- Wells, A., & Goff, J. (2007). Coastal dunes in Westland, New Zealand, provide a record of paleoseismic activity on the Alpine fault. *Geology*, 35(8), 731-734. doi.org/10.1130/G23554A.1
- Whipple, K.X. (2001). Fluvial landscape response time: How plausible is steady-state denudation?. *American Journal of Science*, 301(4-5), 313-325. doi.org/10.2475/ajs.301.4-5.313
- Whitlock, C., & Larsen, C. (2001). Charcoal as a fire proxy. *Tracking environmental change using lake sediments* (pp. 75-97). Springer, Dordrecht. doi:10.1007/0-306-47668-1\_5
- Whitlock, C. & Millspaugh, S.H. (1996). Testing assumptions of fire history studies: an examination of modern charcoal accumulation in Yellowstone National Park. *The Holocene*, 6: 7–15. doi.org/10.1177/095968369600600102
- Wiggs, G.F., Livingstone, I., Thomas, D.S., & Bullard, J.E. (1996). Airflow and roughness characteristics over partially vegetated linear dunes in the southwest Kalahari Desert. *Earth Surface Processes and Landforms*, 21(1), 19-34. doi.org/10.1002/(SICI)1096-9837(199601)21:1<19::AID-ESP508>3.0.CO;2-P
- Williams, A.N., Mooney, S.D., Sisson, S.A., & Marlon, J. (2015). Exploring the relationship between Aboriginal population indices and fire in Australia over the last 20,000 years. *Palaeogeography, Palaeoclimatology, Palaeoecology*, 432, 49-57. doi.org/10.1016/j.palaeo.2015.04.030
- Wilson, P., (2002). Holocene coastal dune development on the South Erradale peninsula, Wester Ross, Scotland. *Scottish Journal of Geology*, 38(1), pp.5-13. doi.org/10.1144/sjg38010005
- Wilson, P., McGourty, J., & Bateman, M.D. (2004). Mid-to late-Holocene coastal dune event stratigraphy for the north coast of Northern Ireland. *The Holocene*, 14(3), 406-416. doi.org/10.1191/0959683604hl716rp
- Wintle, A.G. (1997). Luminescence dating: laboratory procedures and protocols. *Radiation measurements*, 27(5-6), 769-817. doi.org/10.1016/S1350-4487(97)00220-5
- Wintle, A.G., & Murray, A.S. (2006). A review of quartz optically stimulated luminescence characteristics and their relevance in single-aliquot regeneration dating protocols. *Radiation measurements*, 41(4), 369-391. doi.org/10.1016/j.radmeas.2005.11.001
- Yan, N., & Baas, A.C. (2015). Parabolic dunes and their transformations under environmental and climatic changes: Towards a conceptual framework for understanding and prediction. *Global and Planetary Change*, 124, 123-148. doi.org/10.1016/j.gloplacha.2014.11.010

- Yan, N., & Baas, A.C. (2017). Environmental controls, morphodynamic processes, and ecogeomorphic interactions of barchan to parabolic dune transformations. *Geomorphology*, 278, 209-237. doi.org/10.1016/j.geomorph.2016.10.033
- Yizhaq, H., Ashkenazy, Y., & Tsoar, H. (2007). Why do active and stabilized dunes coexist under the same climatic conditions?. *Physical Review Letters*, 98(18), 188001. doi.org/10.1103/PhysRevLett.98.188001
- Young, R. W., Bryant, E. A., Price, D. M., Wirth, L. M., & Pease, M. (1993). Theoretical constraints and chronological evidence of Holocene coastal development in central and southern New South Wales, Australia. *Geomorphology*, 7(4), 317-329. doi.org/10.1016/0169-555X(93)90061-6
- Zevenbergen, L.W., & Thorne, C.R. (1987). Quantitative analysis of land surface topography. *Earth Surface Process Landforms*, 12, 47–56. doi.org/10.1002/esp.3290120107

# Appendices

## A.2 Supplementary Material to Chapter 2

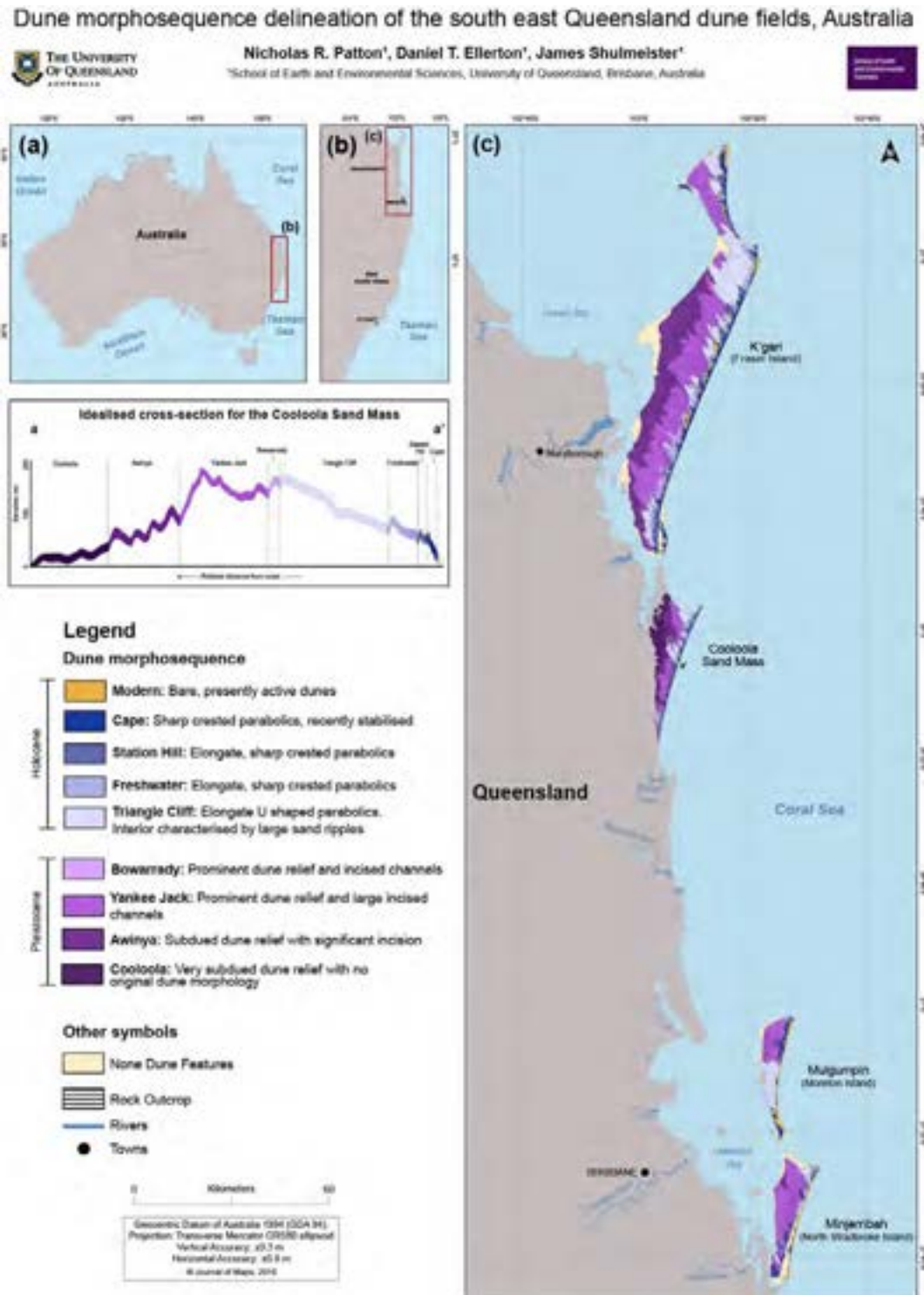


**Figure A.2.1:** High-resolution remapping of the SE Queensland dune fields.

## A.3 Supplementary Material to Chapter 3



**Figure A.3.1:** Photos of the Carlo Sand Blow near the township of Rainbow Beach, photos location indicated in Figure 3.1c. **(a)** Photo taken near the western dune crest towards the Tasman Sea down the dune's stoss face. **(b)** Photo taken in the same location as panel a but down the dune crest towards the over-steepened lee face and forest canopy. Note the dune is extending inland through the tops of the open and closed Eucalyptus forest (canopy cover of 50-80% and >80%, respectively), which are approximately 20-30 m tall, and over previously emplaced dunes (photo credit: Patrick Adams).

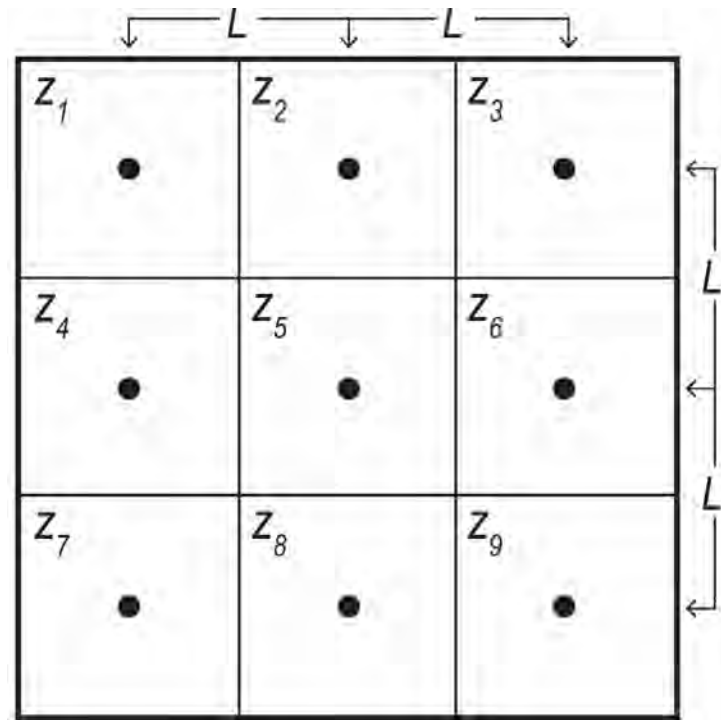


**Figure A.3.2:** A visualisation of the grid network depicting the 3 by 3 elevation submatrix utilised in this study to calculate curvature at the centre node ( $z_5$ ) (Zevenberger and Thorne, 1987; Moore et al., 1991). Here  $z$  is elevation and  $L$  is the length between nodes used in EQ.3.5 and EQ.3.6.

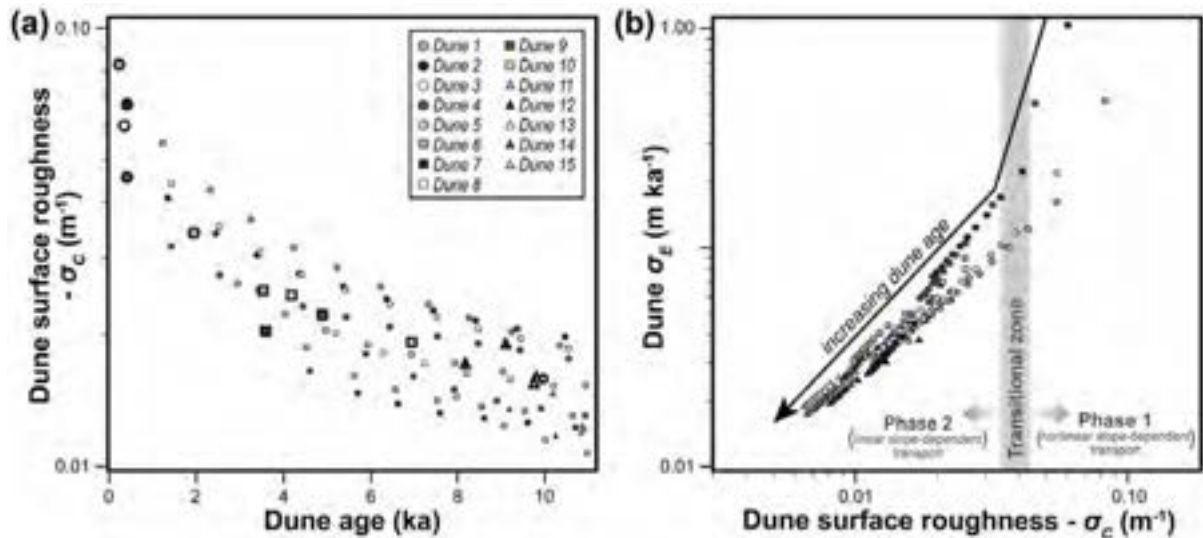


**Figure A.3.3:** 2-D forward numerical modelling of dated CSM dunes. **(a)** Measured dune age and surface roughness ( $\sigma_c$ ) (large symbols) highlighting change in its topography every 1 ka for 10 ka for individual dunes (smaller symbols). The entire CSM evolution is described by nonlinear sediment transport with a  $K$  value of  $0.002 \text{ m}^2 \text{ yr}^{-1}$  and a  $S_c$  of  $0.65 \text{ m m}^{-1}$ , utilising a landscape evolution model from Booth et al. (2017). In reality the simulated topography appears to be more closely related to a  $K$  value of  $0.06 \text{ m}^2 \text{ yr}^{-1}$  for the first thousand years of the dunes development when  $\sigma_c$  is high (above the 'transitional zone',  $\sigma_c$  values between  $0.035$ - $0.045 \text{ m}^{-1}$ ). Only once dune  $\sigma_c$  is lowered below this point does their evolution switch to the  $K$  value  $0.002 \text{ m}^2 \text{ yr}^{-1}$  (not shown here). **(b)** Using the general evolution derived from the fix  $K$  value of  $0.002 \text{ m}^2 \text{ yr}^{-1}$  and a  $S_c$  of  $0.65 \text{ m m}^{-1}$ , I evaluate dune's  $\sigma_c$  relationship with modelled variability of erosion rate ( $\sigma_E$ ). I observe a shift in this relationship coinciding with the same observed 'transition zone' in Figure 3.6, which I interpret as a phase when nonlinear sediment transport behaves similar to linear sediment transport, such that  $\sigma_c$  and  $\sigma_E$  become more uniform with time and their relationship can be described through EQ.3.3,  $\sigma_E \propto \sigma_c$ . Note  $\sigma_E$  and  $\sigma_c$  are autocorrelated; however, field observations support these modelled outcomes.



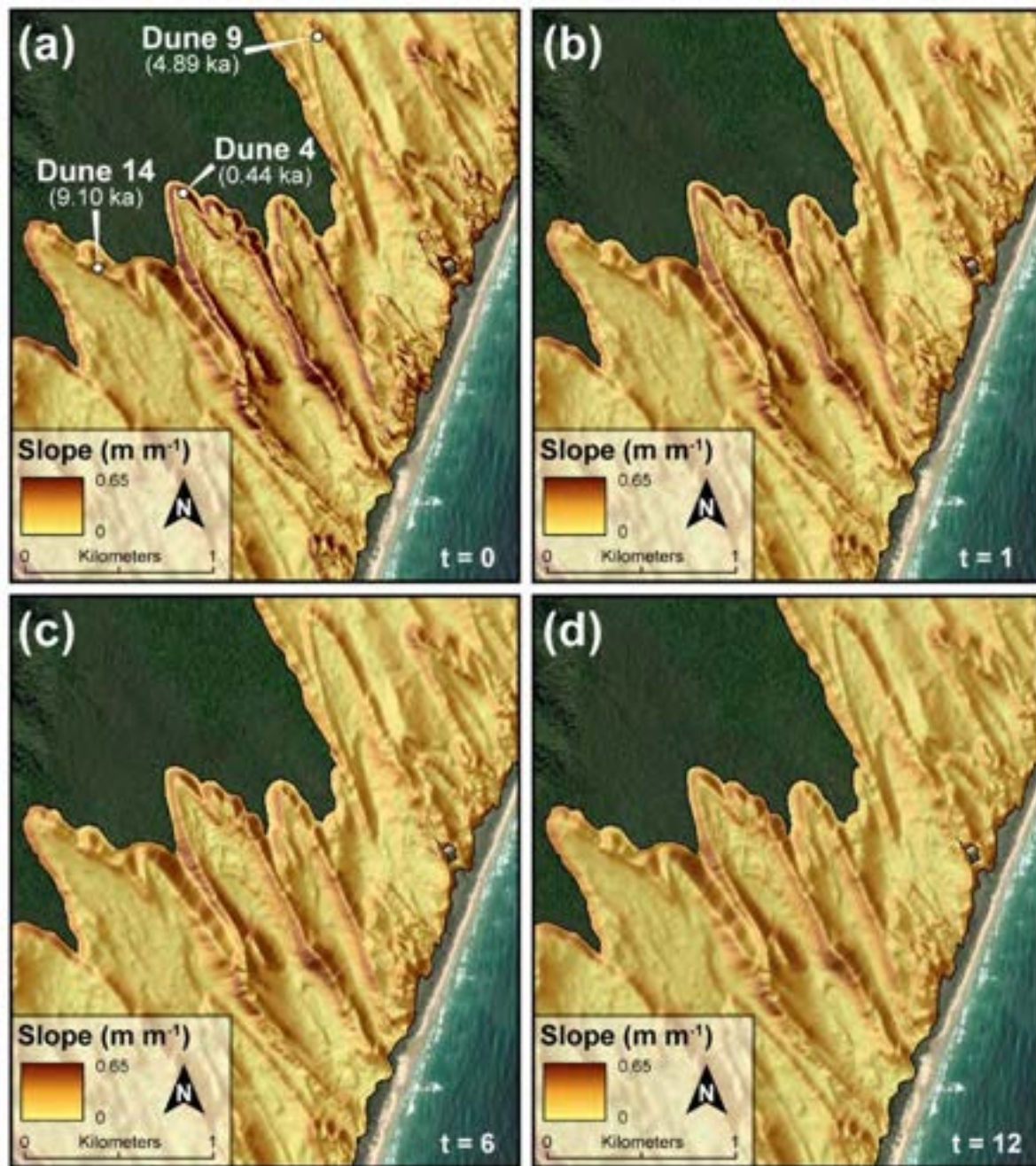


**Figure A.3.4:** Slope map of modelled simulation for CSM dunes through nonlinear sediment transport. Utilising a 5 m DEM and the nonlinear sediment transport model from Booth et al. (2017) (fixed  $K$  and  $S_c$  values of  $0.002 \text{ m}^2 \text{ yr}^{-1}$  and  $0.65 \text{ m m}^{-1}$ , respectively) I provide dune topography, relative age, and geomorphic stage (Supplementary Tables A.3.1 and A.3.2) highlighting the evolution of a 0.44 ka dune (Dune 4). **(a)** Current dune topography in its juvenile phase with abundant steep slopes (dark browns). **(b)** Dune after being rapidly decayed for 1 ka until the 'transitional zone' has been reached ( $\sigma_c$  from  $0.035$ - $0.045 \text{ m}^{-1}$ ) depicting dune adolescence with shallower slopes (lighter browns). Once lowered below the 'transitional zone', dune evolution mimics linear slope dependent evolution where slow and continuous sediment transport processes dominate such that dune **(c)** maturity by 6 ka, and **(d)** old age is achieved by 12 ka. This is visually depicted with uniform and consistent slopes (yellows).

**Table A.3.1:** Additional dune data. Age data and supporting information used in Figure 3.1 and 3.6, and Supplementary Figures A.3.3, and A.3.4. (\*) Indicates the area of the dune at the surface. (†) Indicates the distance dune travelled, parallel to trailing arm, from the current coastline position to its furthest inland extent.

Map code	Age (ka)	Age error (ka)	*Dune area (km <sup>2</sup> )	†Dune length from coast (km)	Mean slope (m m <sup>-1</sup> )	Standard deviation of slope (m m <sup>-1</sup> )	Hillslope $\sigma_c$ (m <sup>-1</sup> )	Evolutionary stage	Dating method	Lab ID	References
1	0.23	0.05	0.06	0.53	0.27	0.19	0.083	Juvenile	Single-aliquot	USU-2011	Ellerton et al., 2020
2	0.36	0.11	0.14	0.64	0.42	0.21	0.060	Juvenile	Single-aliquot	USU-2002	Ellerton et al., 2018
3	0.43	0.06	0.02	0.29	0.34	0.16	0.067	Juvenile	Single-aliquot	USU-2010	Ellerton et al., 2020
4	0.44	0.10	0.54	1.80	0.34	0.20	0.046	Juvenile	Single-aliquot	USU-2283	Ellerton et al., 2020
5	1.94	0.28	0.15	0.87	0.28	0.12	0.034	Adolescence	Single-aliquot	USU-2267	Ellerton et al., 2020
6	3.53	0.38	0.14	1.24	0.30	0.11	0.025	Mature	Single-aliquot	USU-2012	Ellerton et al., 2020
7	3.60	0.30	0.27	1.45	0.23	0.09	0.020	Mature	Single grain	Sample Number 2	Walker et al., 2018
8	4.20	0.40	0.53	1.47	0.23	0.13	0.025	Mature	Single grain	Sample Number 3	Walker et al., 2018
9	4.89	0.45	0.48	1.47	0.20	0.13	0.022	Mature	Single-aliquot	USU-2284	Ellerton et al., 2020
10	6.96	0.71	0.79	2.48	0.24	0.14	0.019	Mature	Single-aliquot	USU-2269	Ellerton et al., 2020
11	9.80	0.80	8.19	5.28	0.13	0.11	0.016	Mature	Single grain	Sample Number 5	Walker et al., 2018
12	8.17	0.82	0.80	2.28	0.17	0.11	0.017	Mature	Single-aliquot	USU-2282	Ellerton et al., 2020
13	9.74	0.90	4.34	3.92	0.14	0.12	0.015	Mature	Single-aliquot	USU-2748	Ellerton et al., 2020
14	9.10	0.96	0.73	2.40	0.22	0.13	0.019	Mature	Single-aliquot	USU-2270	Ellerton et al., 2020
15	9.82	0.98	1.86	2.57	0.16	0.12	0.016	Mature	Single-aliquot	USU-2285	Ellerton et al., 2020



**Table A.3.2:** Defining landscapes evolutionary stages. The development of the Cooloola Sand Mass dunes are set by their physical characteristics, soil development, and their primary and secondary transport processes (Reeve et al., 2008; *Chapter 2*).

Dune development	Description	Dominant transport processes	Secondary transport processes	Soil development
<i>Inception</i>	Dune creation. Active landform constructed with little to no vegetation.	Wind advection, granular flows, and deflation.	Dry-ravelling, granular relaxation, and rain-splash	No podsolisation
<i>Juvenile</i>	Newly emplaced dune with vegetation. Some sections may contain bare sand features. Gradients are steep, with lee facing slopes near or above $0.65 \text{ m m}^{-1}$ ( $33^\circ$ ). Sharp crest and trailing arms. Episodic sediment transport the dominant transport process.	Granular flows, sheetwashing, and dry-ravelling	Dry-ravelling, granular relaxation, bioturbation, and rain-splash	Incipient Podsol (weak B horizon)
<i>Adolescence</i>	Stabilised dune with vegetation. Gradients remain steep with sharp crest and trailing arms. However, all gradients are less than $0.65 \text{ m m}^{-1}$ ( $33^\circ$ degrees) and no episodic sediment transport is present.	Soil creep, rain-splash, bioturbation, and granular relaxation	NA	Podsol (well defined B and E horizons)
<i>Mature</i>	Stabilised dune with vegetation. Diffuse hillslopes with rounded crests. Continuous sediment transport controls the development of the dune's evolution.	Soil creep, rain-splash, bioturbation, and granular relaxation	NA	Podsol (well defined B and E horizons)
<i>Old age</i>	Lacks many of the dune original structures. Diffuse hillslope with no episodic sediment transport. Continuous sediment transport controls the development of the dunes evolution.	Soil creep, rain-splash, bioturbation, and granular relaxation	NA	Well-developed Podsol (E horizon > 5 m)

**Table A.3.3:** Soil characteristics from the excavated soil profile utilised in this study using standard survey methods from Schoenberger et al. (2002).

Dune Site	Dune Age (ka)	Sample Depth Interval (cm)	Soil Horizon	Grain Size ( $\mu\text{m}$ )	Sorting	Roundness	Structure	Mansell Colour (Dry)	Mansell Colour (Wet)	Charcoal
Dune 15	9.82	0-5	A <sub>1</sub>	180-250	Well Sorted	Sub-Rounded	1 F Sbk	10YR 6/2	10YR 4/1	Present
		5-10	A <sub>1</sub>	180-250	Well Sorted	Sub-Rounded	1 F Sbk	10YR 6/1	10YR 4/1	Present
		10-20	A <sub>1</sub>	180-250	Well Sorted	Sub-Rounded	1 F Sbk	10YR 6/1	10YR 4/1	Present
		20-30	A <sub>2</sub>	180-250	Well Sorted	Sub-Rounded	1 F-M Sbk	10YR 5/1	10YR 3/1	Present
		30-40	A <sub>2</sub>	180-250	Well Sorted	Sub-Rounded	1 F-M Sbk	10YR 6/1	10YR 4/1	Present
		40-50	A <sub>3</sub>	180-250	Well Sorted	Sub-Rounded	1 F-M Sbk	10YR 6/1	10YR 4/1	Present
		50-60	AE	180-250	Well Sorted	Sub-Rounded	1 F-M Sbk	10YR 6/1	10YR 4/1	Present
		60-70	AE	180-250	Well Sorted	Sub-Rounded	1 F-M Sbk	10YR 6/1	10YR 4/1	Present
		70-80	E	180-250	Well Sorted	Sub-Rounded	1 F-M Sbk	7.5YR 6/1	7.5YR 4/1	Present
		80-90	E	180-250	Well Sorted	Sub-Rounded	Massive	7.5YR 6/1	7.5YR 5/1	Present
		90-100	E	180-250	Well Sorted	Sub-Rounded	Massive	7.5YR 7/1	7.5YR 4/1	Present
		100-110	E	180-250	Well Sorted	Sub-Rounded	Massive	7.5YR 7/2	7.5YR 5/2	Present
		110-120	E	180-250	Well Sorted	Sub-Rounded	Massive	7.5YR 6/2	7.5YR 5/3	Present
		120-130	E	180-250	Well Sorted	Sub-Rounded	Massive	7.5YR 6/3	7.5YR 4/3	Present
		130-140	BE	180-250	Well Sorted	Sub-Rounded	2 M Sbk	7.5YR 5/3	7.5YR 4/4	Present
		140-150	BE	180-250	Well Sorted	Sub-Rounded	2 M Sbk	7.5YR 5/4	7.5YR 4/4	Present
		150-175	BE-B	180-250	Well Sorted	Sub-Rounded	3 M-VC Sbk	7.5YR 4/4	7.5YR 3/4	Present
		175-200	B-BC	180-250	Well Sorted	Sub-Rounded	3 M-VC Sbk	7.5YR 4/4	7.5YR 3/3	Present
		200-225	BC	180-250	Well Sorted	Sub-Rounded	3 M-VC Sbk	7.5YR 4/4	7.5YR 3/3	Present
		225-250	BC	180-250	Well Sorted	Sub-Rounded	3 M-VC Sbk	7.5YR 5/4	7.5YR 4/4	Present
Dune 9	4.89	0-5	A <sub>1</sub>	180-250	Well Sorted	Sub-Rounded	1 F Sbk	10YR 6/1	10YR 4/1	Present
		5-10	A <sub>1</sub>	180-250	Well Sorted	Sub-Rounded	1 F Sbk	10YR 6/1	10YR 4/1	Present
		10-20	A <sub>2</sub>	180-250	Well Sorted	Sub-Rounded	1 F-M Sbk	10YR 5/1	10YR 4/1	Present

## Appendices

		20-30	A <sub>2</sub>	180-250	Well Sorted	Sub-Rounded	1 F-M Sbk	10YR 5/1	10YR 4/1	Present
		30-40	A <sub>3</sub>	180-250	Well Sorted	Sub-Rounded	1 F-M Sbk	10YR 5/1	10YR 4/1	Present
		40-50	AE	180-250	Well Sorted	Sub-Rounded	1 F-M Sbk	10YR 5/1	10YR 4/1	Present
		50-60	AE	180-250	Well Sorted	Sub-Rounded	1 F-M Sbk	10YR 5/1	10YR 4/1	Present
		60-70	E	180-250	Well Sorted	Sub-Rounded	Massive	10YR 5/1	10YR 4/1	Present
		70-80	E	180-250	Well Sorted	Sub-Rounded	Massive	10YR 5/1	10YR 4/1	Present
		80-90	E	180-250	Well Sorted	Sub-Rounded	Massive	7.5YR 5/1	7.5YR 3/1	Present
		90-100	E	180-250	Well Sorted	Sub-Rounded	Massive	7.5YR 5/2	7.5YR 3/1	Present
		100-110	E	180-250	Well Sorted	Sub-Rounded	Massive	7.5YR 5/1	7.5YR 3/1	Present
		110-120	E	180-250	Well Sorted	Sub-Rounded	2 M Sbk	7.5YR 4/2	7.5YR 3/1	Present
		120-130	E-BC	180-250	Well Sorted	Sub-Rounded	2 M Sbk	7.5YR 4/2	7.5YR 3/2	Present
		130-140	BC	180-250	Well Sorted	Sub-Rounded	2 M Sbk	7.5YR 3/2	7.5YR 2.5/2	Present
		140-150	BC	180-250	Well Sorted	Sub-Rounded	2 M Sbk	7.5YR 4/3	7.5YR 3/3	Present
		150-175	BC-CB	180-250	Well Sorted	Sub-Rounded	3 M-VC Sbk	7.5YR 4/3	7.5YR 3/3	Present
		175-200	CB	180-250	Well Sorted	Sub-Rounded	3 M-VC Sbk	7.5YR 5/3	7.5YR 3/3	Present
		200-225	CB	180-250	Well Sorted	Sub-Rounded	3 M-VC Sbk	7.5YR 5/4	7.5YR 3/4	Present
		225-250	CB	180-250	Well Sorted	Sub-Rounded	3 M-VC Sbk	7.5YR 5/4	7.5YR 3/4	Present
		250-275	CB	180-250	Well Sorted	Sub-Rounded	3 M-VC Sbk	7.5YR 6/4	7.5YR 4/4	Present
Not used in age- $\sigma_c$ model	2.14	0-5	A <sub>1</sub>	180-250	Well Sorted	Sub-Rounded	1 Vf-F Sbk	10YR 6/2	10YR 4/2	Present
		5-10	A <sub>1</sub>	180-250	Well Sorted	Sub-Rounded	1 Vf-F Sbk	10YR 6/1	10YR 5/1	Present
		10-20	A <sub>1</sub>	180-250	Well Sorted	Sub-Rounded	1 Vf-F Sbk	10YR 6/1	10YR 5/1	Present
		20-30	A <sub>2</sub>	180-250	Well Sorted	Sub-Rounded	1 Vf-M Sbk	10YR 5/1	10YR 4/1	Present
		30-40	A <sub>2</sub>	180-250	Well Sorted	Sub-Rounded	1 Vf-M Sbk	7.5YR 5/2	7.5YR 3/4	Present
		40-50	AB <sub>w</sub>	180-250	Well Sorted	Sub-Rounded	1 F-M Sbk	7.5YR 5/2	7.5YR 3/4	Present
		50-60	B <sub>w</sub> C	180-250	Well Sorted	Sub-Rounded	2 F-M Sbk	7.5YR 5/3	7.5YR 4/3	Present
		60-70	B <sub>w</sub> C	180-250	Well Sorted	Sub-Rounded	2 F-M Sbk	7.5YR 6/3	7.5YR 4/3	Present
		70-80	B <sub>w</sub> C	180-250	Well Sorted	Sub-Rounded	2 F-M Sbk	10YR 5/4	10YR 4/4	Present
		80-90	B <sub>w</sub> C	180-250	Well Sorted	Sub-Rounded	2 F-M Sbk	10YR 5/3	10YR 4/3	Present

		90-100	B <sub>w</sub> C	180-250	Well Sorted	Sub-Rounded	2 F-M Sbk	10YR 5/4	10YR 4/4	Present
		100-110	B <sub>w</sub> C	180-250	Well Sorted	Sub-Rounded	2 F-M Sbk	10YR 5/3	10YR 4/3	Present
		110-120	B <sub>w</sub> C	180-250	Well Sorted	Sub-Rounded	2 F-M Sbk	10YR 5/3	10YR 4/3	Present- Layers
		120-130	C <sub>1</sub>	180-250	Well Sorted	Sub-Rounded	2 F-Co Sbk	10YR 5/4	10YR 4/4	Present- Layers (dated)
		130-140	C <sub>1</sub>	180-250	Well Sorted	Sub-Rounded	2 F-Co Sbk	10YR 5/3	10YR 4/3	Present
		140-150	C <sub>1</sub>	180-250	Well Sorted	Sub-Rounded	2 F-Co Sbk	10YR 5/3	10YR 4/3	Present
		150-175	C <sub>1</sub> -C <sub>2</sub>	180-250	Well Sorted	Sub-Rounded	2 F-Co Sbk	10YR 5/3	10YR 4/3	Present
		175-200	C <sub>2</sub>	180-250	Well Sorted	Sub-Rounded	2 F-Co Sbk	10YR 5/2	10YR 3/4	Present- Layers
		200-225	C <sub>2</sub>	180-250	Well Sorted	Sub-Rounded	2 F-Co Sbk	10YR 5/3	10YR 4/3	Present- Layers
		225-250	C <sub>2</sub>	180-250	Well Sorted	Sub-Rounded	2 F-Co Sbk	10YR 5/3	10YR 4/3	Present- Layers
Dune 4	0.44	0-5	A <sub>1</sub>	180-250	Well Sorted	Sub-Rounded	1 F Sbk	10YR 7/2	10YR 4/2	Present- Layers
		5-10	A <sub>1</sub>	180-250	Well Sorted	Sub-Rounded	1 F Sbk	10YR 6/2	10YR 4/2	Present- Layers
		10-20	A <sub>1</sub> -A <sub>2</sub>	180-250	Well Sorted	Sub-Rounded	1 F-M Sbk	10YR 6/2	10YR 4/2	Present- Layers
		20-30	A <sub>2</sub> -AB <sub>w</sub>	180-250	Well Sorted	Sub-Rounded	1 F-M Sbk	10YR 5/3	10YR 4/3	Present- Layers
		30-40	AB <sub>w</sub>	180-250	Well Sorted	Sub-Rounded	2 F-M Sbk	10YR 5/4	10YR 4/4	Present- Layers
		40-50	ABW	180-250	Well Sorted	Sub-Rounded	2 M Sbk	10YR 6/4	10YR 5/4	Absent
		50-60	CB <sub>w</sub>	180-250	Well Sorted	Sub-Rounded	2 M Sbk	10YR 6/4	10YR 5/4	Absent
		60-70	CB <sub>w</sub> -C	180-250	Well Sorted	Sub-Rounded	2 M Sbk	10YR 6/4	10YR 5/4	Absent
		70-80	C	180-250	Well Sorted	Sub-Rounded	3 M-VC Sbk	10YR 6/4	10YR 5/4	Absent
		80-90	C	180-250	Well Sorted	Sub-Rounded	3 M-VC Sbk	10YR 6/4	10YR 5/4	Absent
		90-100	C	180-250	Well Sorted	Sub-Rounded	3 M-VC Sbk	10YR 6/4	10YR 5/4	Absent
		100-110	C	180-250	Well Sorted	Sub-Rounded	3 M-VC Sbk	10YR 6/4	10YR 5/4	Absent
		110-120	C	180-250	Well Sorted	Sub-Rounded	3 M-VC Sbk	10YR 6/4	10YR 5/4	Absent
		120-130	C	180-250	Well Sorted	Sub-Rounded	3 M-VC Sbk	10YR 6/4	10YR 5/4	Absent
		130-140	C	180-250	Well Sorted	Sub-Rounded	3 M-VC Sbk	10YR 6/4	10YR 5/4	Absent
		140-150	C	180-250	Well Sorted	Sub-Rounded	Massive-original dune structure	10YR 6/4	10YR 5/4	Absent
		150-175	C	180-250	Well Sorted	Sub-Rounded	Massive-original dune structure	10YR 6/4	10YR 5/4	Absent

**Table A.3.4** Accelerated mass spectrometry (AMS) radiocarbon dating results. One sample collected from the 2.14 ka depositional soil profile was obtained from a charcoal-rich layer. The sample was prepared using the acid–base–acid (ABA) protocol and dated at the University of Waikato Radiocarbon Dating Laboratory. Ages were calibrated at two-sigma error using OxCal v4.3.2. (Ramsey, 2017) and the SHcal13 calibration curve (Hogg et al., 2020).

Lab ID	Depth Interval (m)	Material	AMS measurement results (yr BP $\pm$ 2 $\sigma$ )	2 $\sigma$ calibrated date range (cal yr BP)
Wk50298	1.2-1.3	Charcoal –wood/twig	1017 $\pm$ 26	800-940

## A.4 Supplementary Material to Chapter 4

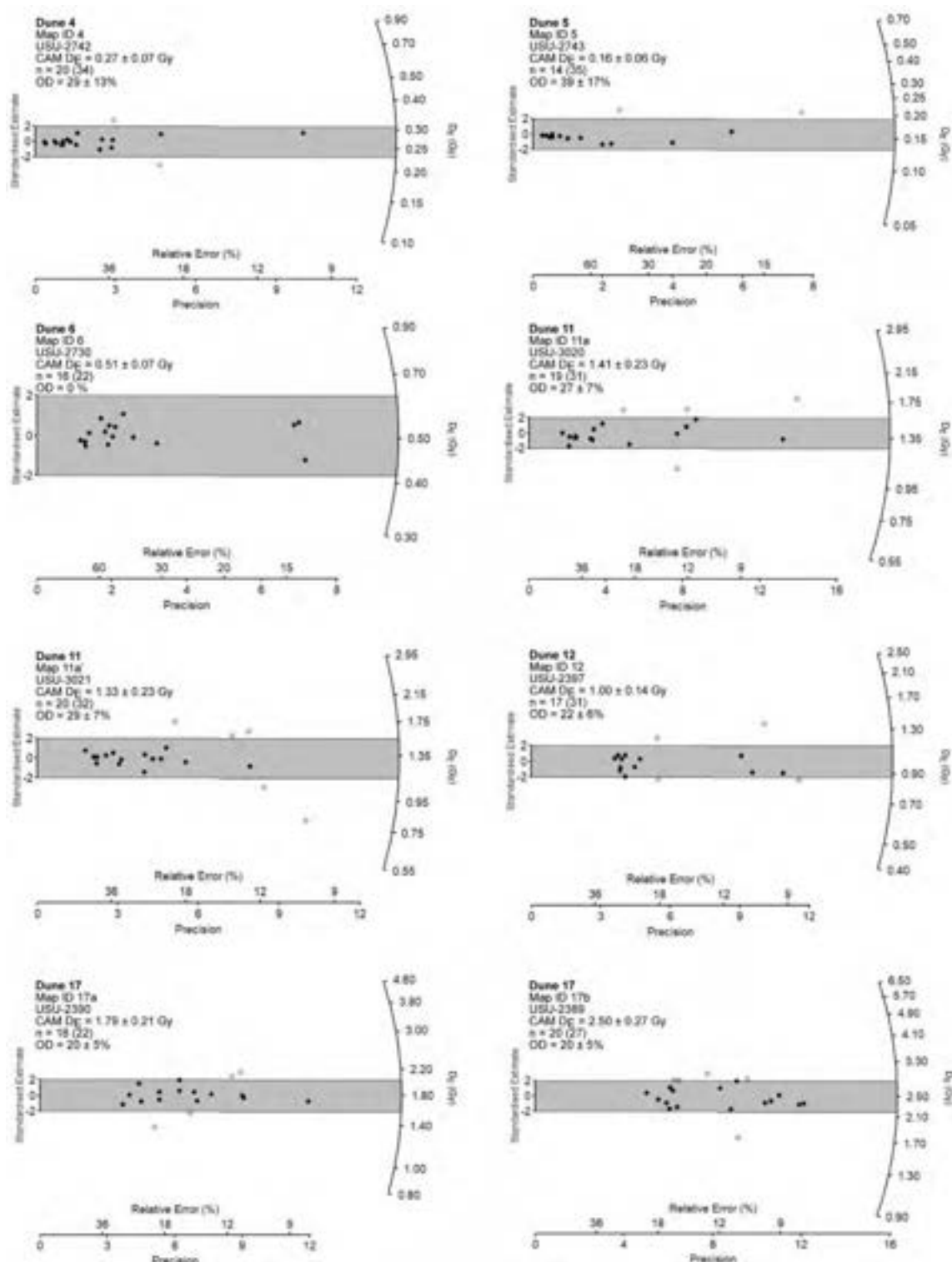


**Figure A.4.1:** Equivalent Dose ( $D_e$ ) radial plots for the eight ( $n=8$ ) OSL samples used in this study.

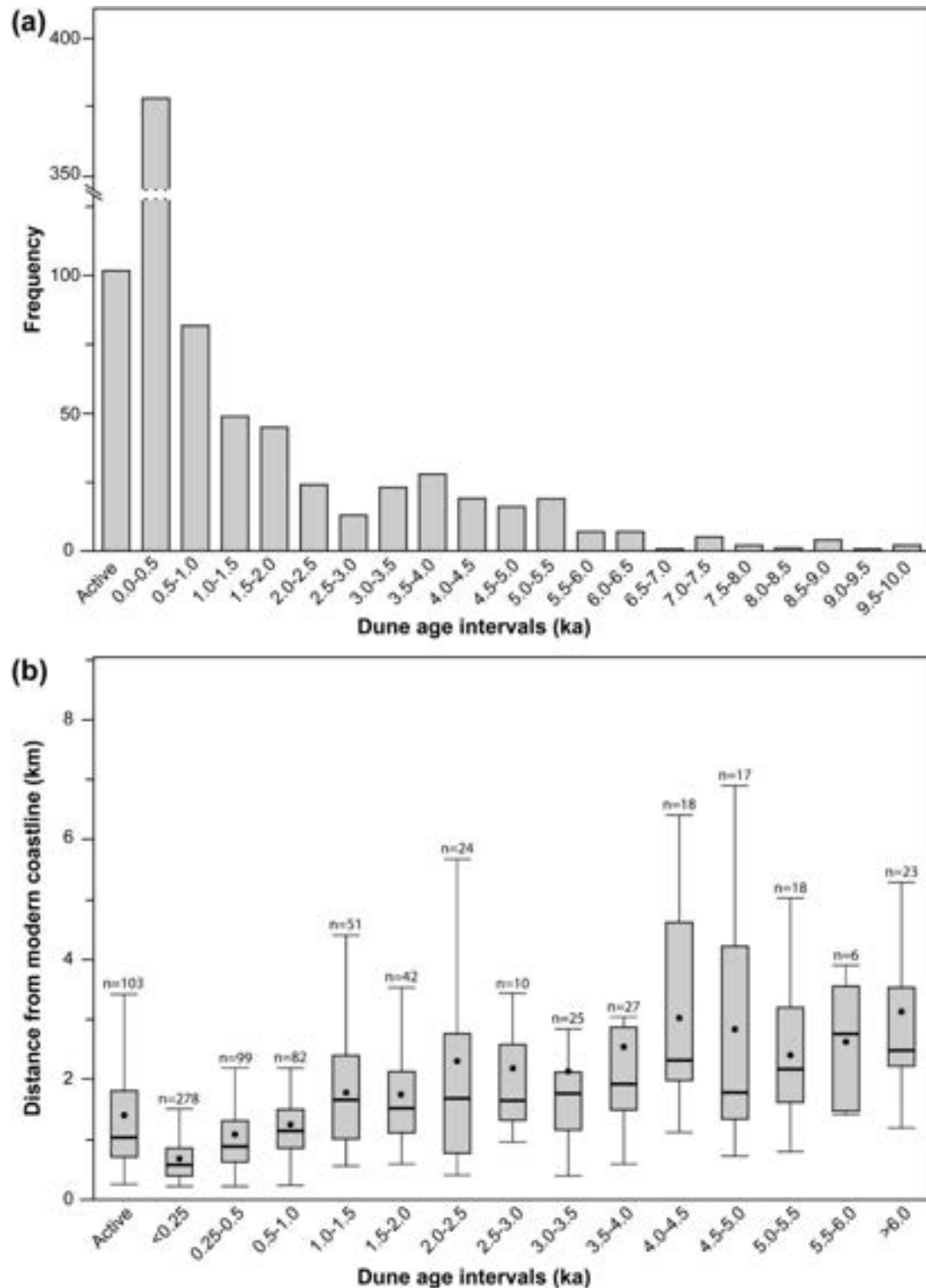


**Figure A.4.2: (a)** Dune frequency for active ( $n=103$ ) and emplaced Holocene aged ( $n=726$ ) dunes with 0.5 ka bin intervals. **(b)** Box and whisker plots depicting maximum distance travel from the modern eastern coast (not including dunes that originate on the western coast ( $n=15$ )). Horizontal bar is the median value whereas the black dot represents the average. In general, younger dunes are more common but on average do not travel far inland. In contrast, the oldest dunes which are less frequent are reported to travel up >10 km. Note, bin interval varies to help account for sample size.

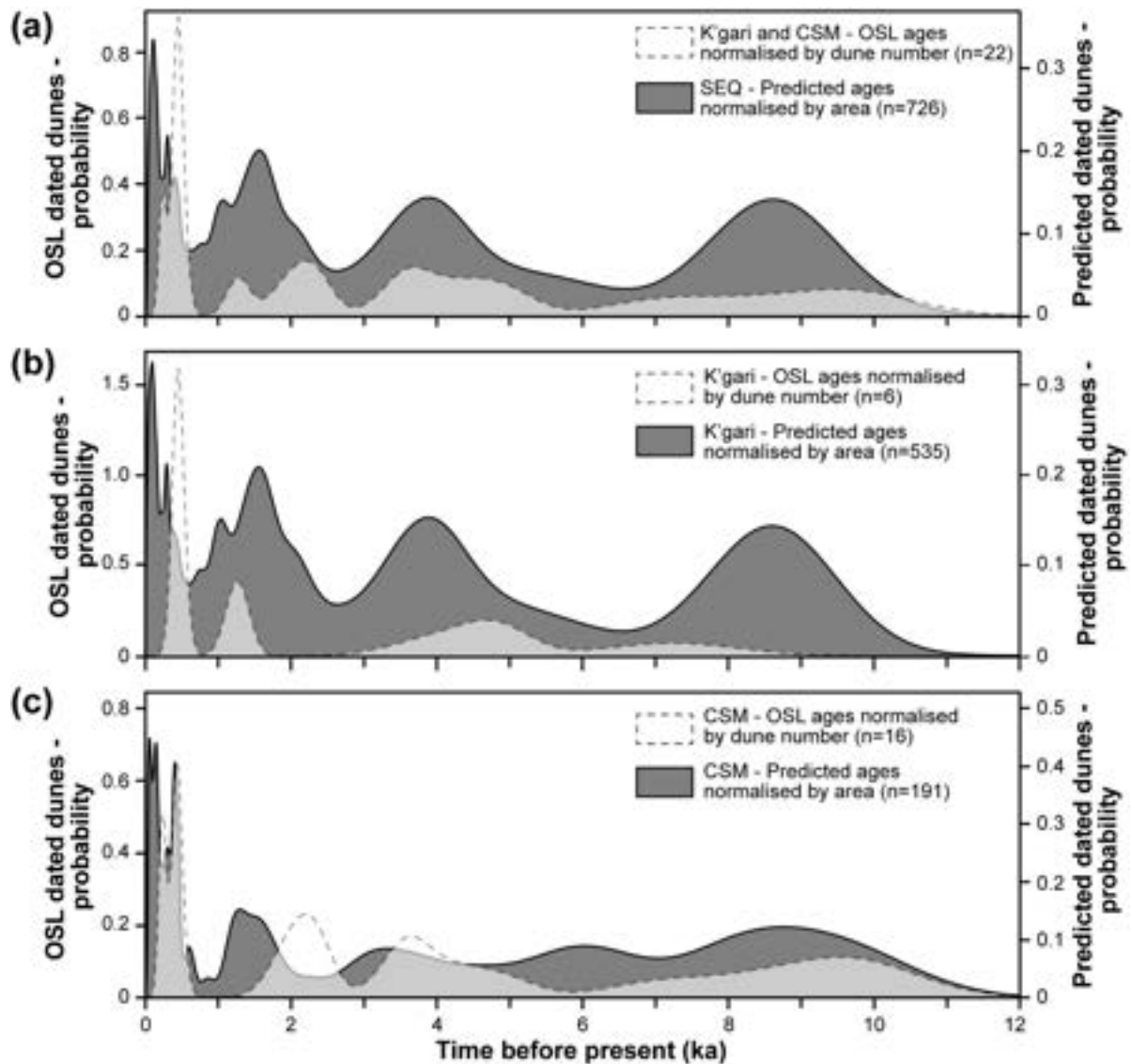


**Figure A.4.3:** Comparison between probability density functions (PDFs) produced from OSL (dashed line with white area) and predicted (solid black line with grey fill) dated dunes within (a) both dune fields, (b) K'gari, and (c) the CSM.



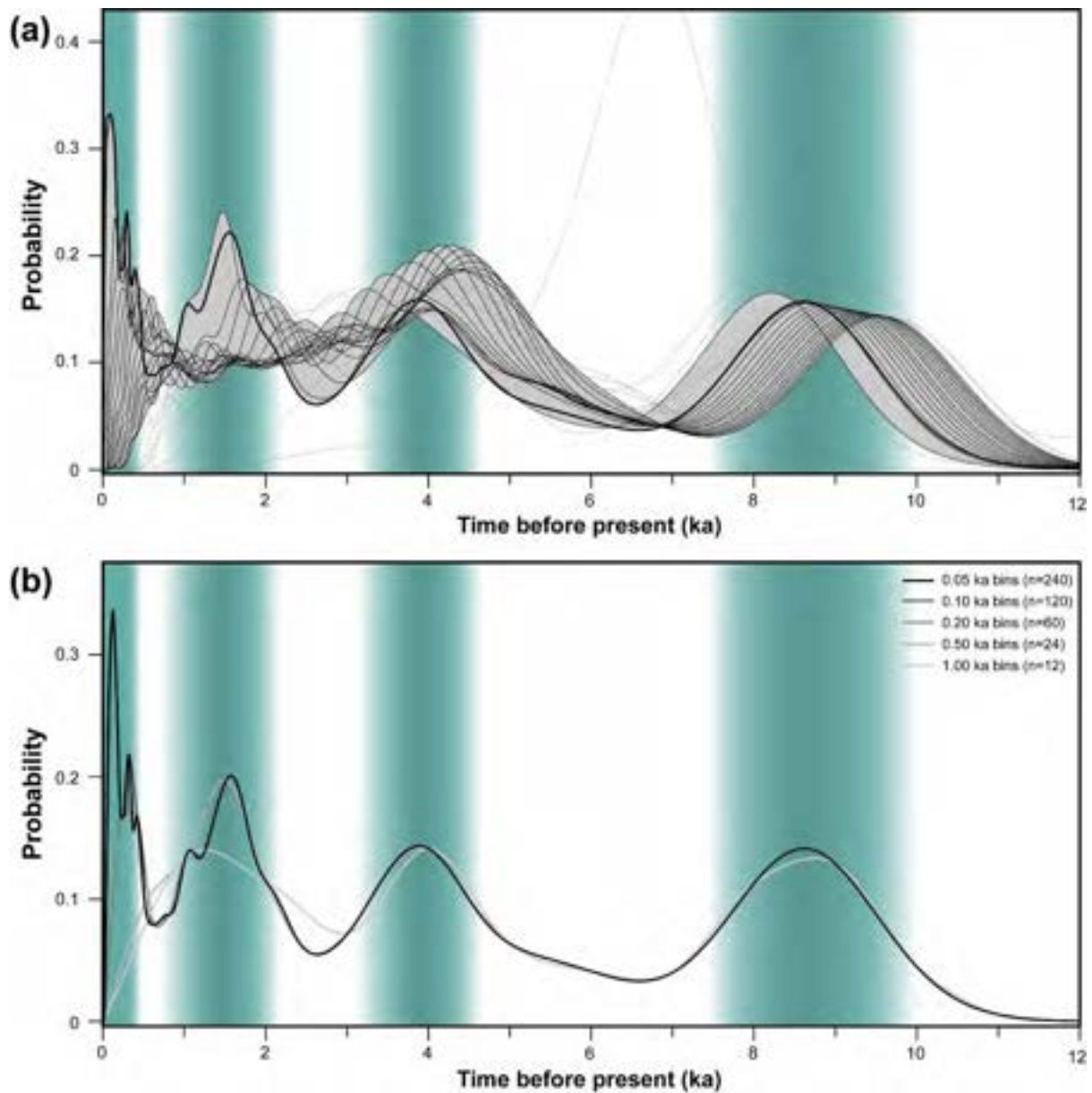


**Figure A.4.4:** Sensitivity analysis on PDF outcomes by varying original DEM resolution and bin interval. **(a)** PDFs generated from all modelled dune ages (n=726) (assuming normally distributed age estimates) using 0.05 ka bin intervals for 12 ka (240 total bins). Each line represents a PDF from a surface roughness ( $\sigma_c$ )-age regression, derived at different DEM resolutions (1-50 m) (Supplementary Table A.4.3). Solid black lines are all PDFs that have  $\sigma_c$ -age relationships with a RMSE value  $< 1.1$  ka and a  $r^2$  value  $> 0.90$  (3-20 m<sup>2</sup> resolution). The full range of these PDFs are shaded in grey. The bold black line represents the PDF used in this study (5 m). All other PDFs are represented by grey dashed lines. An important note, besides the PDFs derived from the finest (1 and 2 m) and the coarsest resolutions (45 and 50 m), all PDFs show remarkable consistency in peaks when compared to the known dune emplacement events (vertical teal areas). **(b)** I evaluate the influence bin intervals have on modelled PDF outcomes on identical predicted ages (derive from 5 m DEM). As bin intervals increase (dark to light lines) the youngest peak ( $< 0.5$  ka) becomes increasingly subtle and by a bin interval of 1 ka, is completely removed.

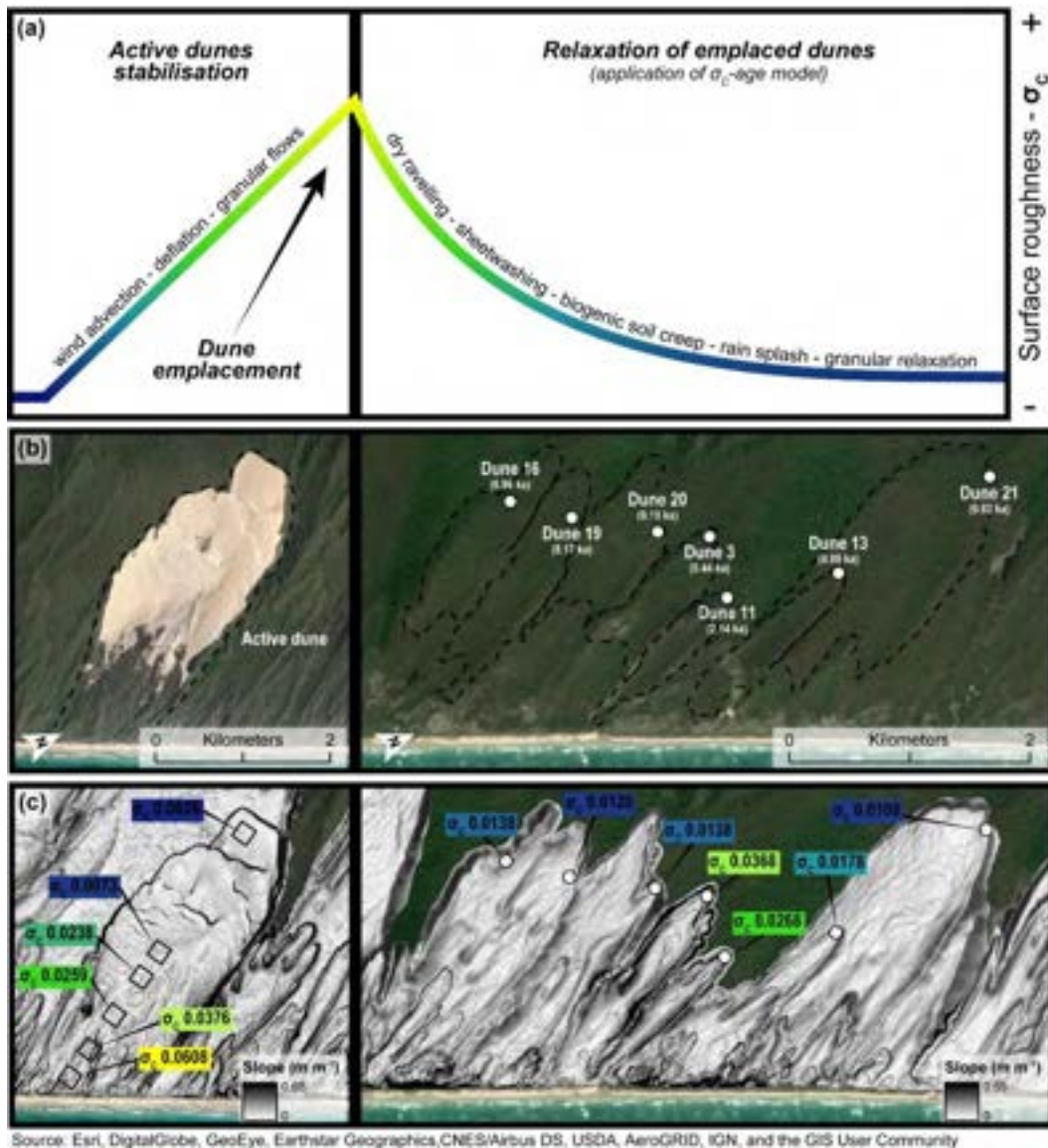


**Figure A.4.5:** Conceptual diagram summarising changes in dune age, geomorphic processes, and surface roughness ( $\sigma_c$ ), modified from *Chapter 3*. **(a)** The Cooloola Sand Mass (CSM) contains thousands of dunes that have remarkably uniform evolution. When dunes are active, they have steep lee faces above or near the angle of repose ( $0.65 \text{ m m}^{-1}$  or  $33^\circ$ ) and shallow stoss faces that are controlled by wind advection processes which prohibit the colonisation of vegetation when winds are high. Consequently, dunes are initially constructed with smooth topography (low  $\sigma_c$ ). As winds dissipate (either from the increase distance from the coast or a change in wind regime), dunes begin to become stabilised by vegetation. The competition between wind advection and vegetation stabilisation increases  $\sigma_c$ . The roughening of the topography continues until dunes are completely stabilised (dune emplacement) and  $\sigma_c$  is at a maximum. Emplacement marks the onset of dune relaxation where sediment transport is only active through hillslope processes (no wind advection) which causes  $\sigma_c$  to decline exponentially with time. Here, processes such as biogenic soil creep, rain-splash, and granular relaxation cause the lowering of crest and filling of adjacent foot-slopes decreasing local relief and  $\sigma_c$ . Examples of this process are observed on active and emplaced dunes and highlighted in **(b)** satellite imagery and **(c)** gradient maps. Note the exact relationship between  $\sigma_c$  and time for dunes stabilisation is not examined in this study but will be addressed in future research.

## Appendices

**Table A.4.1:** Soil descriptions of all sites containing newly acquired OSL samples used in this chapter.

<b>Map ID: 4</b> Date: 13/10/2017 Dune number: 4 OSL lab number: USU-2742 Sample name: FRAS131017-13 Site description: Crest of parabolic dune. GPS coordinates (Latitude, Longitude): -25.16°S, 153.27°E						
Horizon	Depth (cm)	Structure	Texture	Colour	Boundary	Notes/special features
O	-1-0	Slightly decomposed <i>Eucalyptus</i> leaf litter at surface				
O/A	0-16	Apedal, single grain sand	Medium sand	10YR 4/1	Clear smooth	Fine roots throughout
A/C	16-32	Apedal, single grain sand	Medium sand	10YR 5/4	Clear smooth	
C	32-38	Apedal, single grain sand	Medium sand	10YR 5/6	Clear smooth	
C	38-50	Apedal, single grain sand	Medium sand	10YR 5/6	Clear smooth	
C	50-62	Apedal, single grain sand	Medium sand	10YR 6/6	Clear smooth	
C	62-74	Apedal, single grain sand	Medium sand	10YR 6/6	Clear smooth	
C	74-76	Apedal, single grain sand	Medium sand	10YR 7/6	Clear smooth	
C	76-88	Apedal, single grain sand	Medium sand	10YR 6/6	Clear smooth	
C	88-99	Apedal, single grain sand	Medium sand	10YR 6/6	Clear smooth	Dose rate.
C	99-113	Apedal, single grain sand	Medium sand	10YR 6/6	Clear smooth	OSL sample.
C	113-123	Apedal, single grain sand	Medium sand	10YR 6/6	Clear smooth	Dose rate.
<b>Map ID: 5</b> Date: 13/10/2017 Dune number: 5 OSL lab number: USU-2743 Sample name: FRAS131017-14 Site description: Crest of parabolic dune. GPS coordinates (Latitude, Longitude): -25.19°S, 153.26°E						
Horizon	Depth (cm)	Structure	Texture	Colour	Boundary	Notes/special features
O	-2-0	Slightly decomposed <i>Eucalyptus</i> leaf litter at surface				
O/A	0-17	Apedal, single grain sand	Medium sand	10YR 5/3	Clear smooth	Fine roots throughout
A/C	17-33	Apedal, single grain sand	Medium sand	10YR 5/3	Clear smooth	
C	33-42	Apedal, single grain sand	Medium sand	10YR 6/6	Clear smooth	
C	42-57	Apedal, single grain sand	Medium sand	10YR 6/6	Clear smooth	
C	57-72	Apedal, single grain sand	Medium sand	10YR 6/6	Clear smooth	
C	72-85	Apedal, single grain sand	Medium sand	10YR 6/6	Clear smooth	
C	85-99	Apedal, single grain sand	Medium sand	10YR 6/6	Clear smooth	Dose rate.
C	99-116	Apedal, single grain sand	Medium sand	10YR 6/6	Clear smooth	OSL sample.
C	116-124	Apedal, single grain sand	Medium sand	10YR 6/6	Clear smooth	Dose rate.

**Map ID: 6**

Date: 10-10-17

Dune number: 6

OSL lab number: USU-2730

Sample name: FRAS-101017-1

Site description: Crest of parabolic dune.

GPS coordinates (Latitude, Longitude): -25.60°S, 153.08°E

Horizon	Depth (cm)	Structure	Texture	Colour	Boundary	Notes/special features
O	-2-0	Slightly decomposed <i>Eucalyptus</i> leaf litter at surface				
O/A	0-17	Apedal, single grain sand	Fine sand	10YR 4/2	Clear smooth	Fine roots throughout
A	17-34	Apedal, single grain sand	Fine sand	10YR 4/2	Clear smooth	
B	34-45	Apedal, single grain sand	Fine sand	10YR 5/2	Clear smooth	
B	45-57	Apedal, single grain sand	Fine sand	10YR 6/3	Clear smooth	
B	57-69	Apedal, single grain sand	Fine sand	10YR 5/4	Clear smooth	
B	69-83	Apedal, single grain sand	Fine sand	10YR 5/4	Clear smooth	
B	83-93	Apedal, single grain sand	Fine sand	10YR 5/6	Clear smooth	
B/C	93-108	Apedal, single grain sand	Medium sand	10YR 5/6; 10YR 7/4	Abrupt smooth	
C	108-120	Apedal, single grain sand	Medium sand	10YR 7/4	Clear smooth	
C	120-134	Apedal, single grain sand	Medium sand	10YR 7/3	Clear smooth	
C	134-146	Apedal, single grain sand	Medium sand	10YR 7/4	Clear smooth	
C	146-160	Apedal, single grain sand	Medium sand	10YR 7/4	Clear smooth	
C	160-172	Apedal, single grain sand	Medium sand	10YR 7/4	Clear smooth	
C	172-184	Apedal, single grain sand	Medium sand	10YR 7/4	Clear smooth	
C	184-197	Apedal, single grain sand	Medium sand	10YR 7/4	Clear smooth	Dose rate.
C	197-224	Apedal, single grain sand	Medium sand	10YR 7/4	Clear smooth	OSL sample.
C	224-232	Apedal, single grain sand	Medium sand	10YR 7/4	Clear smooth	Dose rate.

**Map ID: 11**

Date: 09/04/2019

Dune number: 11a and 11a'

OSL lab number: USU-3020 and USU-3021

Sample name: EFBR17\_190-205 and EFBR17\_388-407

Site description: Crest of parabolic dune.

GPS coordinates (Latitude, Longitude): -26.01°S, 153.13°E

Horizon	Depth (cm)	Structure	Texture	Colour	Boundary	Notes/special features
O	-1-0	Slightly decomposed <i>Eucalyptus</i> leaf litter at surface				
A1	0-25	Apedal, single grain sand	Fine sand	10YR 5/1	Clear smooth	Fine roots throughout
A1	25-50	Apedal, single grain sand	Fine sand	10YR 5/1	Clear smooth	
A2	50-55	Apedal, single grain sand	Fine sand	10YR 5/1	Clear smooth	
AB	55-62	Apedal, single grain sand	Fine sand	10YR 5/1	Abrupt smooth	
B	62-89	Apedal, single grain sand	Fine sand	10YR 5/4	Clear smooth	

## Appendices

B	89-102	Apedal, single grain sand	Medium sand	10YR 4/4	Clear smooth	
B	102-113	Apedal, single grain sand	Medium sand	10YR 4/6	Clear smooth	
BC	113-132	Apedal, single grain sand	Medium sand	10YR 5/6	Clear smooth	
BC	132-146	Apedal, single grain sand	Medium sand	10YR 6/6	Clear smooth	
CB	146-166	Apedal, single grain sand	Medium sand	10YR 6/6	Abrupt smooth	
C	166-176	Apedal, single grain sand	Medium sand	10YR 7/6	Clear smooth	
C	176-190	Apedal, single grain sand	Medium sand	10YR 7/6	Clear smooth	Dose rate.
C	190-205	Apedal, single grain sand	Medium sand	10YR 7/6	Clear smooth	OSL sample.
C	205-215	Apedal, single grain sand	Medium sand	10YR 7/6	Clear smooth	Dose rate.
C	215-232	Apedal, single grain sand	Medium sand	10YR 6/6	Clear smooth	
C	232-247	Apedal, single grain sand	Medium sand	10YR 6/6	Clear smooth	
C	247-271	Apedal, single grain sand	Medium sand	10YR 6/6	Clear smooth	
C	271-276	Apedal, single grain sand	Medium sand	10YR 6/6	Clear smooth	
C	276-292	Apedal, single grain sand	Medium sand	10YR 6/6	Clear smooth	
C	292-306	Apedal, single grain sand	Medium sand	10YR 6/6	Clear smooth	
C	306-320	Apedal, single grain sand	Medium sand	10YR 6/6	Clear smooth	
C	320-338	Apedal, single grain sand	Medium sand	10YR 6/6	Clear smooth	
C	338-349	Apedal, single grain sand	Medium sand	10YR 6/6	Clear smooth	
C	349-363	Apedal, single grain sand	Medium sand	10YR 6/6	Clear smooth	
C	363-378	Apedal, single grain sand	Medium sand	10YR 6/6	Clear smooth	
C	378-388	Apedal, single grain sand	Medium sand	10YR 6/6	Clear smooth	Dose rate.
C	388-407	Apedal, single grain sand	Medium sand	10YR 6/6	Clear smooth	OSL sample.
C	407-412	Apedal, single grain sand	Medium sand	10YR 6/6	Clear smooth	Dose rate.

---

**Map ID: 12**  
Date: 24/24/2016  
Dune number: 12  
OSL lab number: USU-2397  
Sample name: Fras-062416-14  
Site description: Crest of parabolic dune along the road, migrating from the coast.  
GPS coordinates (Latitude, Longitude): -25.13°S, 153.25°E

Horizon	Depth (cm)	Structure	Texture	Colour	Boundary	Notes/special features
E/A1	0-20	Apedal, single grain sand	Fine sand	10YR 6/1	Clear smooth	Fine roots throughout
E/A2	20-40	Apedal, single grain sand	Fine sand	10YR 6/1	Clear smooth	
E/A3	40-50	Apedal, single grain sand	Fine sand	10YR 7/2	Clear smooth	
E/A4	50-65	Apedal, single grain sand	Fine sand	10YR 7/2	Clear smooth	
E1	65-85	Apedal, single grain sand	Fine sand	10Y 7/1	Clear smooth	
E2	85-100	Apedal, single grain sand	Fine sand	10Y 7/1	Clear smooth	non-coherent mottles
E3	100-115	Apedal, single grain sand	Fine sand	7.5YR 8/1	Clear smooth	
E4	115-130	Apedal, single grain sand	Fine sand	10YR 8/1	Clear smooth	
E5	130-150	Apedal, single grain sand	Fine sand	7.5YR 8/1	Clear smooth	

B1	150-170	Apedal, single grain sand	Medium sand	7.5YR 8/1; 10YR 7/4	Abrupt smooth	non-coherent mottles
B1	170-185	Apedal, single grain sand	Medium sand	10YR 6/4; 10YR 7/6	Clear smooth	non-coherent mottles
B2	185-200	Apedal, single grain sand	Medium sand	10YR 8/1; 10YR 5/3; 10YR 7/6	Clear smooth	non-coherent mottles
B2	200-210	Apedal, single grain sand	Medium sand	10YR 8/1; 10YR 5/3; 10YR 3/2; 10YR 7/6	Clear smooth	non-coherent mottles
B2	210-220	Apedal, single grain sand	Medium sand	10YR 8/2; 10YR 5/3; 10YR 6/3	Clear smooth	non-coherent mottles
B2	220-235	Apedal, single grain sand	Medium sand	10YR 8/1; 10YR 5/3	Clear smooth	non-coherent mottles
B3	235-250	Apedal, single grain sand	Medium sand	10YR 4/3; 10YR 5/4	Clear smooth	non-coherent distinct mottles
B3	250-265	Apedal, single grain sand	Medium sand	10YR 8/1; 10YR 5/2; 10YR 3/1; 10YR 7/6	Clear smooth	non-coherent distinct mottles
B3	265-280	Apedal, single grain sand	Medium sand	10YR 4/3	Clear smooth	non-coherent distinct mottles
B3	280-295	Apedal, single grain sand	Medium sand	10YR 4/3	Clear smooth	non-coherent distinct mottles
B4	295-305	Apedal, single grain sand	Medium sand	10YR 5/3	Clear smooth	non-coherent mottles
B4	305-320	Apedal, single grain sand	Medium sand	10YR 5/3	Clear smooth	non-coherent mottles
B4	320-335	Apedal, single grain sand	Medium sand	10YR 5/4	Clear smooth	non-coherent mottles
B5	335-350	Apedal, single grain sand	Medium sand	10YR 5/4	Clear smooth	
B5	350-365	Apedal, single grain sand	Medium sand	10YR 5/4; 10YR 6/4	Clear smooth	
B5	365-380	Apedal, single grain sand	Medium sand	10YR 4/4	Clear smooth	
B5	380-390	Apedal, single grain sand	Medium sand	10YR 4/3	Clear smooth	
B5	390-405	Apedal, single grain sand	Medium sand	10YR 5/4	Clear smooth	
B5	405-415	Apedal, single grain sand	Medium sand	7.5YR 4/3	Clear smooth	
B5	415-425	Apedal, single grain sand	Medium sand	7.5YR 4/3	Clear smooth	
B/C	425-440	Apedal, single grain sand	Medium sand	10YR 5/4	Clear smooth	Dose rate.
B/C	440-450	Apedal, single grain sand	Medium sand	10YR 5/4	Clear smooth	OSL sample.
B/C	450-470	Apedal, single grain sand	Medium sand	10YR 5/4	Clear smooth	Dose rate.

**Map ID: 17a**

Date: 22/06/2016

Dune number: 17

OSL lab number: USU-2390

Sample name: Fras-062216-7

Site description: Crest of transverse sand wave.

GPS coordinates (Latitude, Longitude): -25.04°S, 153.24°E

Horizon	Depth (cm)	Structure	Texture	Colour	Boundary	Notes/special features
Oi	-2-0	Slightly decomposed <i>Eucalyptus</i> leaf litter at surface				
Ah1	0-20	Apedal, single grain sand	Fine sand	10YR 4/1	Clear smooth	Fine roots throughout
Ah2	20-40	Apedal, single grain sand	Fine sand	10YR 5/2	Clear smooth	
Ah3	40-60	Apedal, single grain sand	Fine sand	10YR 8/2	Clear smooth	Substantially lighter than Ah1 and Ah2
E	60-80	Apedal, single grain sand	Fine sand	10YR 8/1	Abrupt smooth	Substantially lighter than Ah1 and Ah2
Bs1	80-95	Apedal, single grain sand	Fine sand	2.5Y 7/6	Clear smooth	
Bs2	95-110	Apedal, single grain sand	Fine sand	2.5Y 6/6	Clear smooth	
Bs3	110-125	Apedal, single grain sand	Medium sand	10YR 6/6	Clear smooth	50% darker non-coherent mottles, 10YR 4/4 dark yellowish brown

## Appendices

Bs4	125-135	Apedal, single grain sand	Medium sand	10YR 5/6	Clear smooth	
Bs5	135-150	Apedal, single grain sand	Fine sand	10YR 7/6	Clear smooth	
Bs6	150-165	Apedal, single grain sand	Fine sand	10YR 5/6	Clear smooth	
Bs7	165-230	Apedal, single grain sand	Fine sand	10YR 7/6	Clear smooth	
Bs8	230-245	Apedal, single grain sand	Medium sand	10YR 7/6	Clear smooth	
Bs9	245-275	Apedal, single grain sand	Medium sand	10YR 6/6	Clear smooth	5-10% non-coherent lighter and darker mottles
Bs10	275-290	Apedal, single grain sand	Medium sand	10YR 5/6	Clear smooth	50% non-coherent lighter and darker mottles
Bs11	290-315	Apedal, single grain sand	Medium sand	10YR 5/6	Clear smooth	Dose rate.
Bs12	315-330	Apedal, single grain sand	Medium sand	10YR 6/6	Clear smooth	OSL sample.
Bs13	330-345	Apedal, single grain sand	Medium sand	10YR 7/6	Clear smooth	Dose rate.

<b>Sample site: 17b</b>						
Date: 22/06/2016						
Sample number: 17						
OSL lab number: USU-2389						
Sample name: Frs-062216-6						
Site description: Crest of transverse sand wave						
GPS coordinates (Latitude, Longitude): -25.04°S, 153.25°E						
Horizon	Depth (cm)	Structure	Texture	Colour	Boundary	Notes/special features
Oi	-2-0	Slightly decomposed <i>Banksia</i> and <i>Eucalyptus</i> leaf litter at surface, some <i>Xanthorrhoea</i> stems and needles				
Ah1	0-20	<10 % soft very friable fine subangular blocky peds	Fine sand	10YR 4/1	Abrupt smooth	Fine roots throughout
Ah2	20-40	Apedal, single grain sand	Fine sand	10YR 4/2	Abrupt smooth	Some fine roots
Ah3	40-60	Apedal, single grain sand	Medium sand	10YR 6/2	Gradual smooth	Still enough organics for Ah3 rather than E horizon
Bsw	60-80	Apedal, single grain sand	Medium sand	10YR 6/4	Clear smooth	
Bs1	80-95	Apedal, single grain sand	Medium sand	10YR 6/6	Clear smooth	
Bs2	95-110	Apedal, single grain sand	Medium sand	10YR 7/6	Clear smooth	
Bs3	110-125	Apedal, single grain sand	Medium sand	10YR 6/6	Clear smooth	
Bs4	125-140	Apedal, single grain sand	Medium sand	10YR 7/6	Clear smooth	
Bs5	140-170	Apedal, single grain sand	Medium sand	10YR 7/6	Clear smooth	10% friable distinct mottles, darker in colour
Bs6	170-190	Apedal, single grain sand	Medium sand	10YR 7/6	Clear smooth	50% non-coherent distinct mottles, darker in colour
Bs7	190-250	Apedal, single grain sand	Medium sand	10YR 7/6	Clear smooth	
Bs8	250-265	Apedal, single grain sand	Medium sand	10YR 8/6	Clear smooth	
Bs9	265-305	Apedal, single grain sand	Medium sand	10YR 7/6	Clear smooth	Dose rate.
Bs10	305-315	Apedal, single grain sand	Medium sand	10YR 7/6	Clear smooth	OSL sample.
Bs11	315-335	Apedal, single grain sand	Medium sand	10YR 7/6	Clear smooth	Dose rate.

**Table A.4.2:** Radioelement chemistry, water content, and grain size information.

Map ID	Sample ID number	Lab number	In-situ H <sub>2</sub> O (%) <sup>†</sup>	Grain size (μm)	K (%) <sup>‡</sup>	Rb (ppm) <sup>‡</sup>	Th (ppm) <sup>‡</sup>	U (ppm) <sup>‡</sup>	Cosmic (Gy/kyr) <sup>§</sup>
4	FRAS131017-13	USU-2742	3.1	180-250	0.06±0.01	2.9±0.1	3.9±0.4	0.5±0.1	0.17±0.02
5	FRAS131017-14	USU-2743	3.6	180-250	0.06±0.01	2.9±0.1	0.9±0.2	0.2±0.1	0.19±0.02
6	FRAS-101017-1	USU-2730	1.7	180-250	0.07±0.01	3.3±0.1	1.9±0.2	0.3±0.1	0.15±0.01
11a	EFBR17_190-205	USU-3020	3.8 <sup>¶</sup>	180-250	0.13±0.01	5.3±0.2	3.1±0.3	0.4±0.1	0.15±0.02
11a'	EFBR17_388-407	USU-3021	4.8 <sup>¶</sup>	180-250	0.14±0.01	5.6±0.2	4.0±0.4	0.5±0.1	0.12±0.01
12	Fras-062416-14	USU-2397	4.7	180-250	0.03±0.01	1.3±0.1	1.0±0.2	0.2±0.1	0.12±0.01
17a	Fras-062216-7	USU-2390	3.9	180-250	0.06±0.01	2.7±0.1	1.1±0.2	0.2±0.1	0.13±0.01
17b	Fras-062216-6	USU-2389	4.3	180-250	0.06±0.01	3.1±0.1	1.4±0.2	0.3±0.1	0.13±0.01

<sup>†</sup> Assumed  $7.0 \pm 2.1\%$  for all samples as moisture content over burial history, unless otherwise noted.

<sup>‡</sup> Radioelemental concentrations determined using ICP-MS and ICP-AES techniques. Dose rate is derived from concentrations by alpha, beta, and gamma conversion factors from Guérin et al. (2011).

<sup>§</sup> Contribution of cosmic radiation to the dose rate was calculated by using sample depth, elevation, and longitude/latitude following Prescott and Hutton (1994).

<sup>¶</sup> Assumed  $5.0 \pm 2.0\%$  for all samples as moisture content over burial history.



**Table A.4.3:** Relationship between surface roughness ( $\sigma_c$ ) and all dated dunes (n=22) at varying resolutions to assess optimal and available DEM resolution to utilised the  $\sigma_c$ -age model. (†) on dune resolution size indicates best-fit based on RMSE and  $r^2$  values.

Resolution (m)	$\sigma_c$ -age relationship	Root Mean Square Error (ka)	$r^2$
1	Dune Age = 10.41 * EXP (-3.960 * $\sigma_c$ )	3.16	0.18
2	Dune Age = 69.45 * EXP (-52.50 * $\sigma_c$ )	1.36	0.84
3	Dune Age = 54.82 * EXP (-89.84 * $\sigma_c$ )	0.97	0.92
4	Dune Age = 34.97 * EXP (-97.62 * $\sigma_c$ )	0.88	0.93
5 <sup>†</sup>	Dune Age = 32.12 * Exp (-108.9 * $\sigma_c$ )	0.84	0.94
6 <sup>†</sup>	Dune Age = 27.02 * EXP (-106.9 * $\sigma_c$ )	0.84	0.94
7	Dune Age =26.57 * EXP (-112.7 * $\sigma_c$ )	0.85	0.94
8	Dune Age =26.57 * EXP (-118.2 * $\sigma_c$ )	0.85	0.94
9	Dune Age =26.82 * EXP (-124.1 * $\sigma_c$ )	0.85	0.94
10	Dune Age =27.04 * EXP (-129.6 * $\sigma_c$ )	0.86	0.93
11	Dune Age =27.45 * EXP (-135.9 * $\sigma_c$ )	0.88	0.93
12	Dune Age =27.92 * EXP (-142.3 * $\sigma_c$ )	0.89	0.93
13	Dune Age =28.06 * EXP (-147.6 * $\sigma_c$ )	0.89	0.93
14	Dune Age =28.58 * EXP (-154.5 * $\sigma_c$ )	0.92	0.93
15	Dune Age =28.83 * EXP (-160.5 * $\sigma_c$ )	0.94	0.92
16	Dune Age =29.18 * EXP (-167.1 * $\sigma_c$ )	0.96	0.92
17	Dune Age =29.58 * EXP (-174.1 * $\sigma_c$ )	0.99	0.91
18	Dune Age =29.65 * EXP (-179.6 * $\sigma_c$ )	1.03	0.91
19	Dune Age =30.01 * EXP (-186.8 * $\sigma_c$ )	1.05	0.90
20	Dune Age =30.55 * EXP (-195.2 * $\sigma_c$ )	1.09	0.90
25	Dune Age =32.19 * EXP (-234.5 * $\sigma_c$ )	1.33	0.85
30	Dune Age =33.36 * EXP (-276.8 * $\sigma_c$ )	1.60	0.79
35	Dune Age =33.53 * EXP (-318.9 * $\sigma_c$ )	1.86	0.71
40	Dune Age =32.27 * EXP (-358.1 * $\sigma_c$ )	2.13	0.62
45	Dune Age =30.93 * EXP (-402.6 * $\sigma_c$ )	2.45	0.50
50	Dune Age =25.43 * EXP (-396.9 * $\sigma_c$ )	2.61	0.44

## A.5 Supplementary Material to Chapter 5

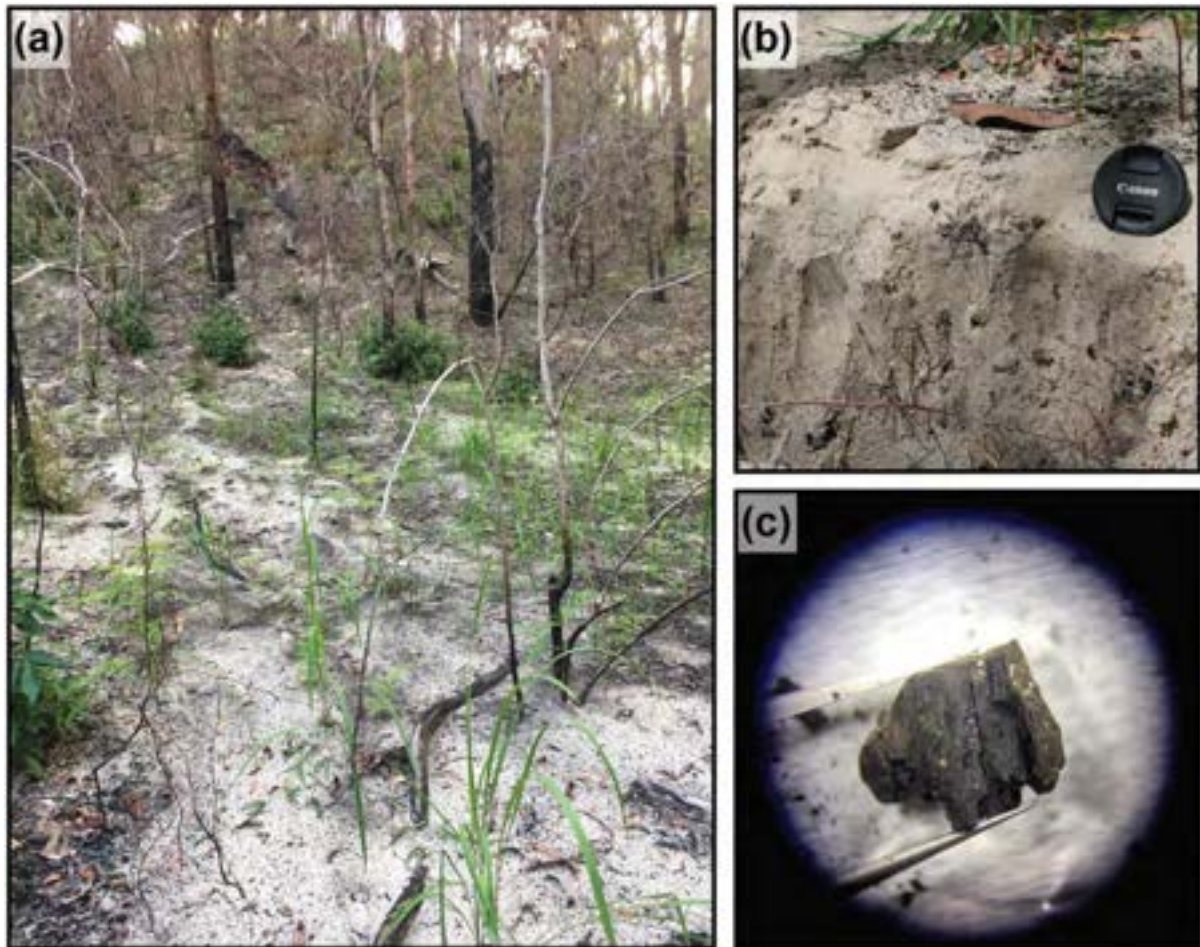


**Figure A.5.1:** Evidence of increased sediment accumulation at the base of dune slipface after fire. **(a)** Episodic sediment transport initiated by the 'Freshwater Road Fire' on the 0.5 ka dune looking up to dune crest. **(b)** Close-up image of the 0.1 m deposit with camera lens for reference. **(c)** Charcoal particle obtained at the deposit.

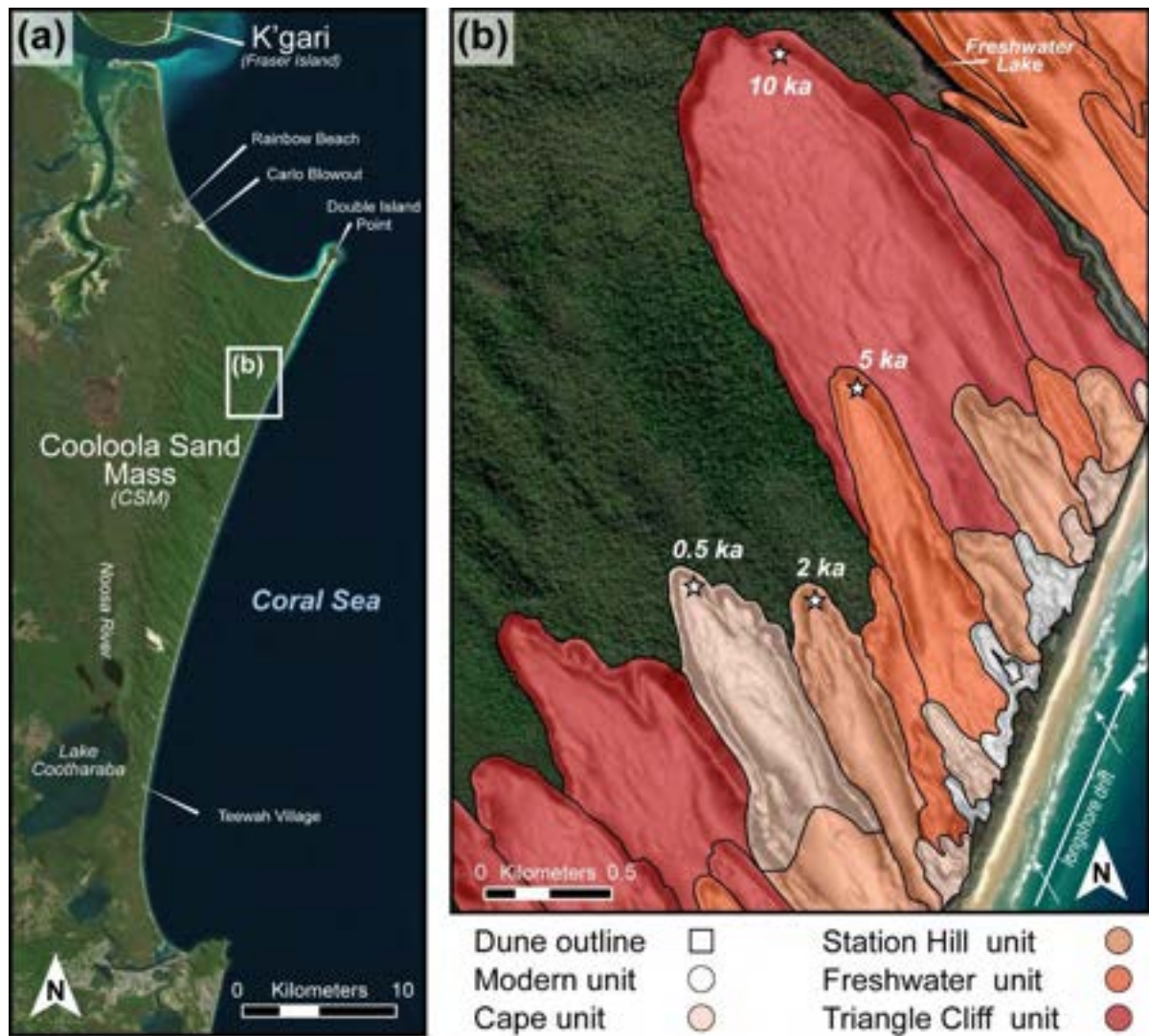


**Figure A.5.2:** Site location. **(a)** Satellite imagery of the Cooloola Sand Mass (CSM) with areas of interest. **(b)** Close-up of the Holocene dune mapped dune units from *Chapter 2* and the four dunes used in this study (white stars). Note, a slope DEM was placed above the dune units at 70% transparency to help highlight the dune topography.



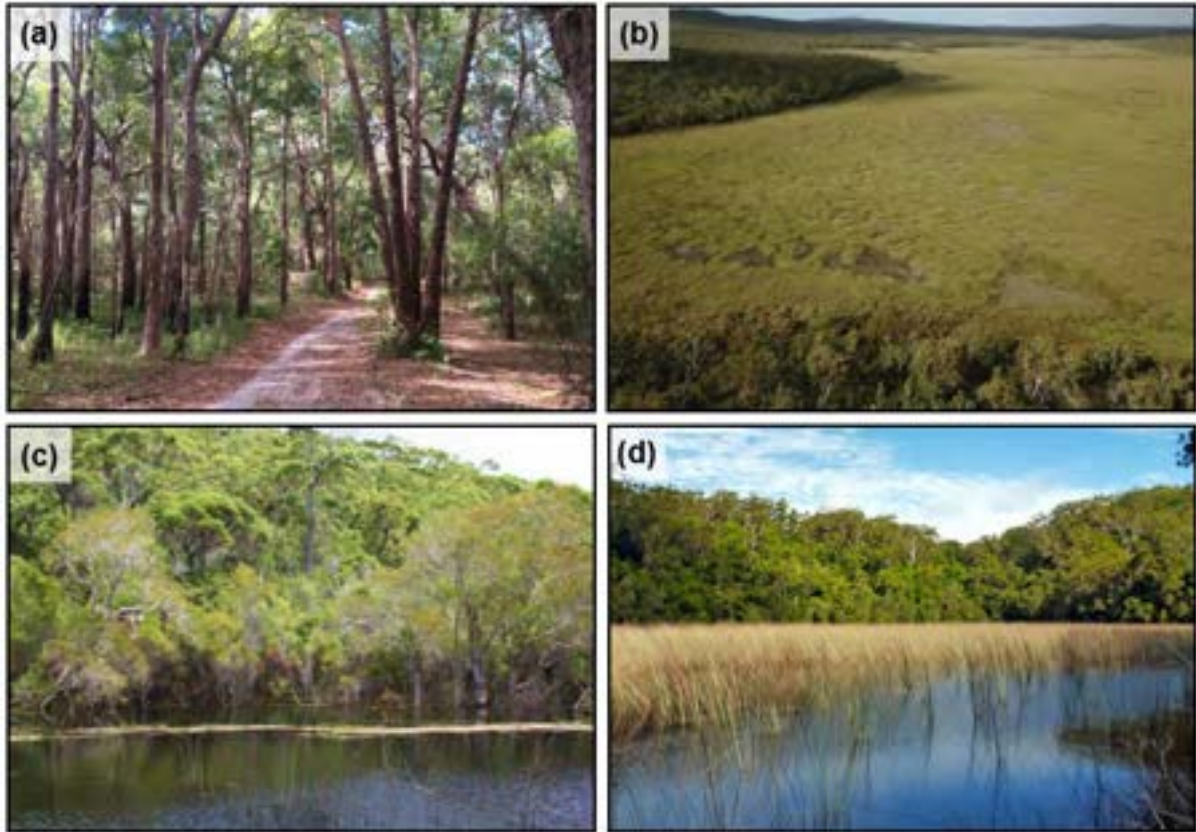


**Figure A.5.3:** Images of the locations used as a cross-site comparisons in this study, see Figure 5.1b for exact locations. **(a)** The CSM dry sclerophyll forest near my dune foot-slope deposits, **(b)** Rainbow Beach patterned fen complexes on Cooloola, **(c)** Swallow Lagoon on Minjerribah (North Stradbroke Island) and **(d)** Lake Allom on K'gari (Fraser Island). Photo credits: (b) Kevin Welsh, (c) John Tibby, and (d) Queensland National Parks Service.

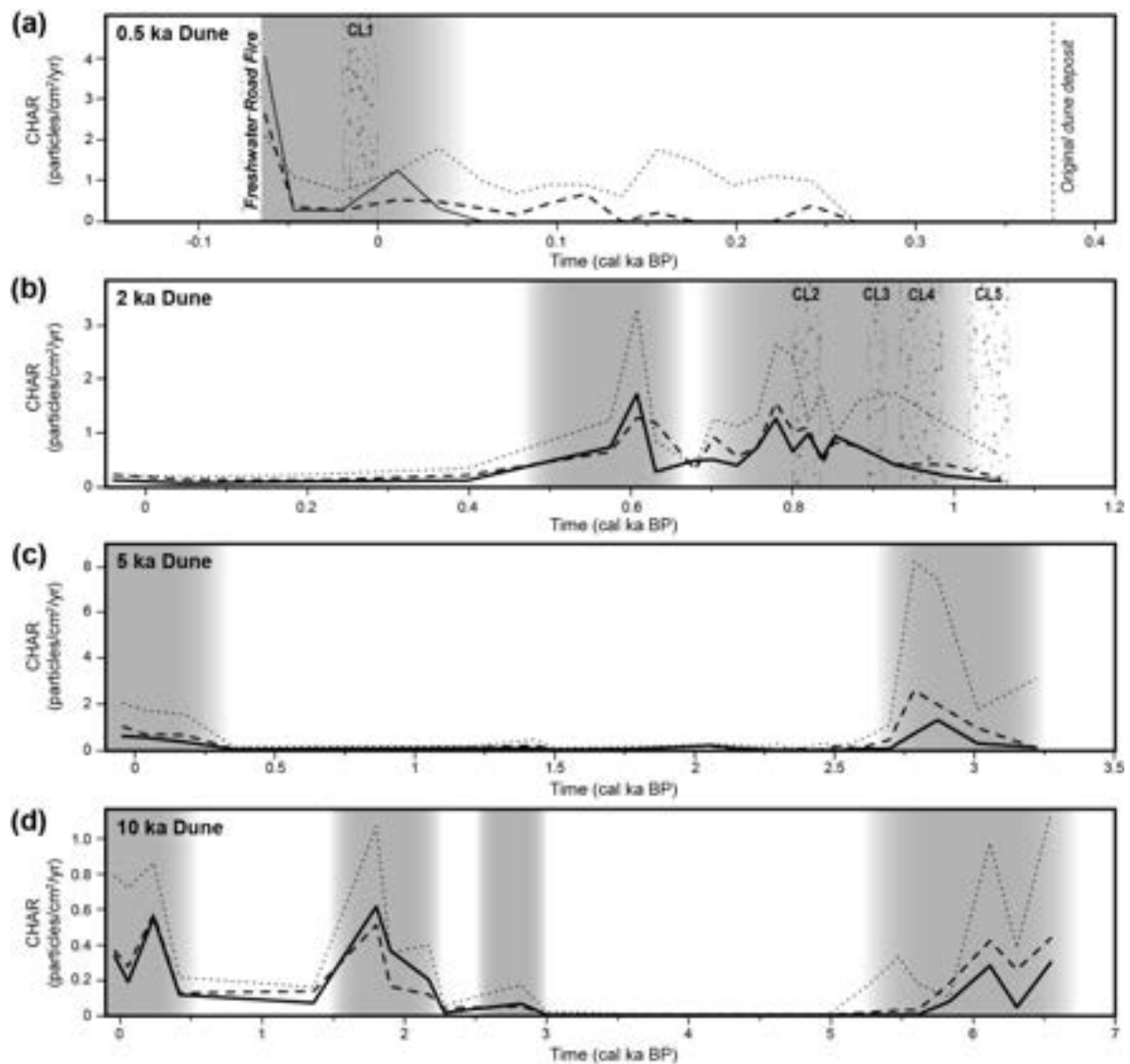


**Figure A.5.4:** Charcoal accumulation rates (CHAR) for size classes 355 µm-2 mm (solid line), 250-355 µm (dashed line), and 180-250 µm (dotted line) for the (a) 0.5 ka, (b) 2 ka, (c) 5 ka, and (d) 10 ka dune depositional sites. The x-axis for the panels differs so that variability in CHAR trends with age can be observed. Charcoal layers identified in the profile face are indicated with a band of black dots and labelled (CL) and shaded areas are the inferred timing of increased fire activity identified in Figure 5.5. An important note is that trends are consistent between size classes and sites.

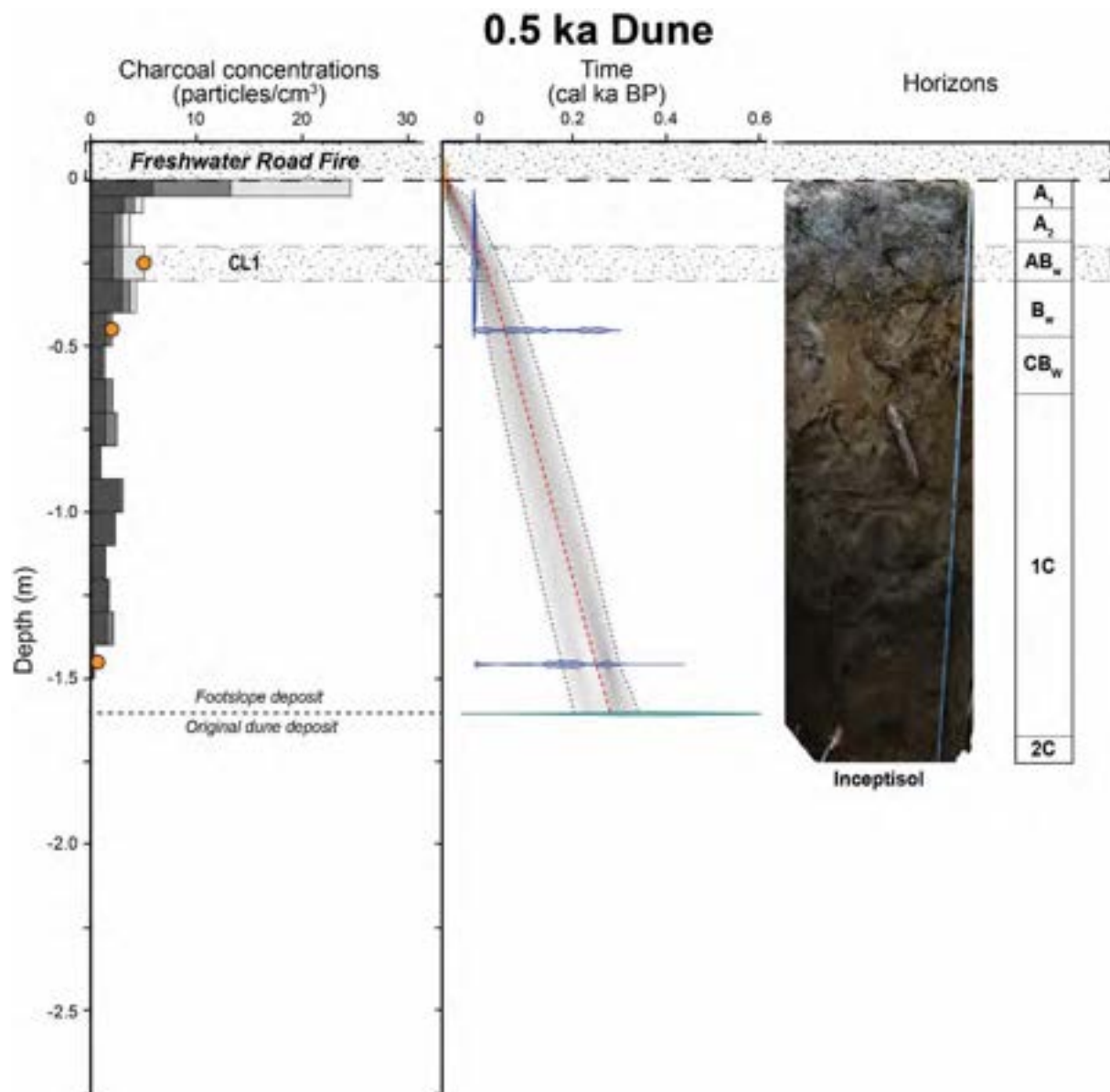


**Figure A.5.5:** Summary figure of data collected in the 0.5 ka Dune.

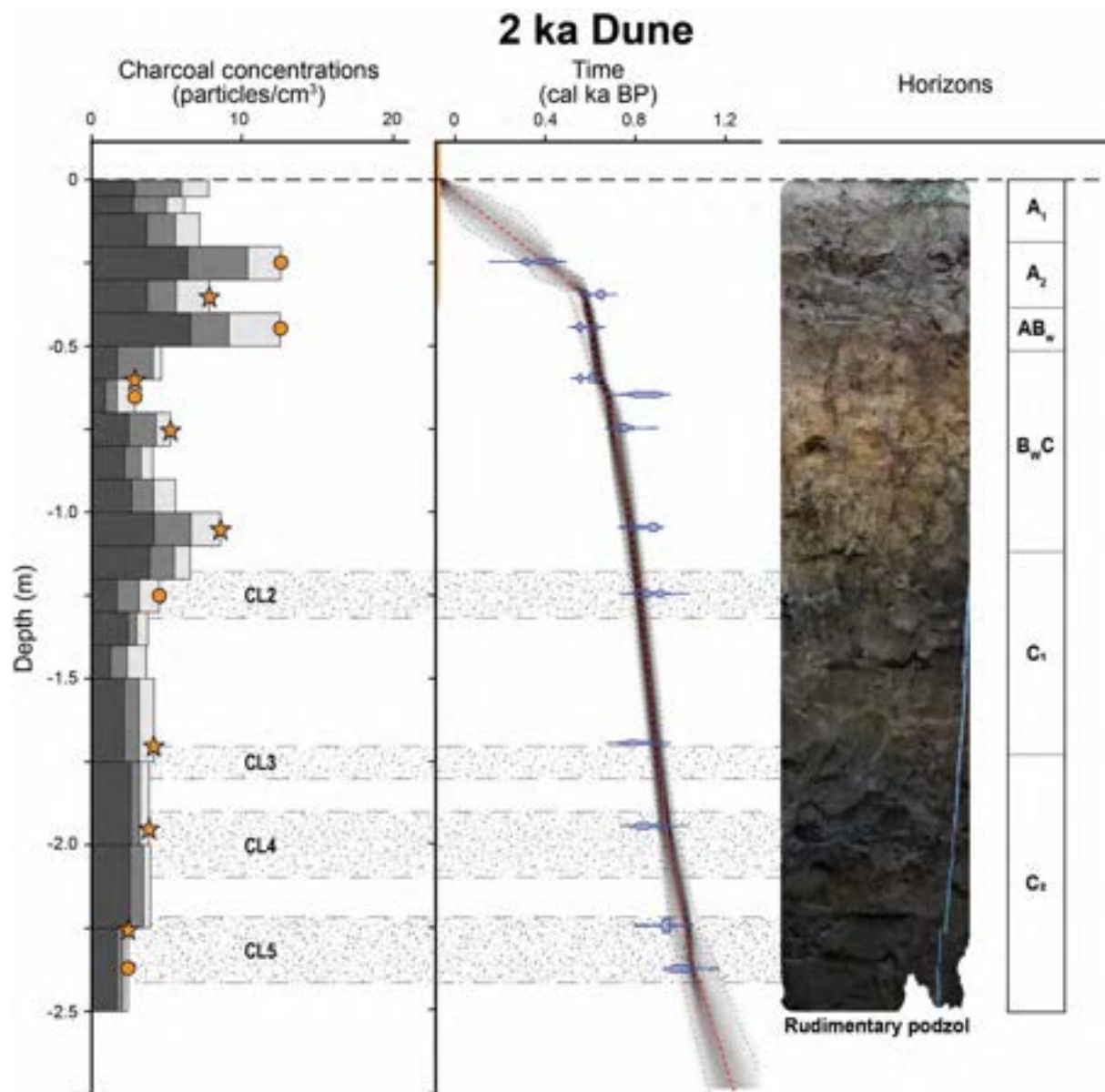


**Figure A.5.6:** Summary figure of data collected in the 2 ka Dune.

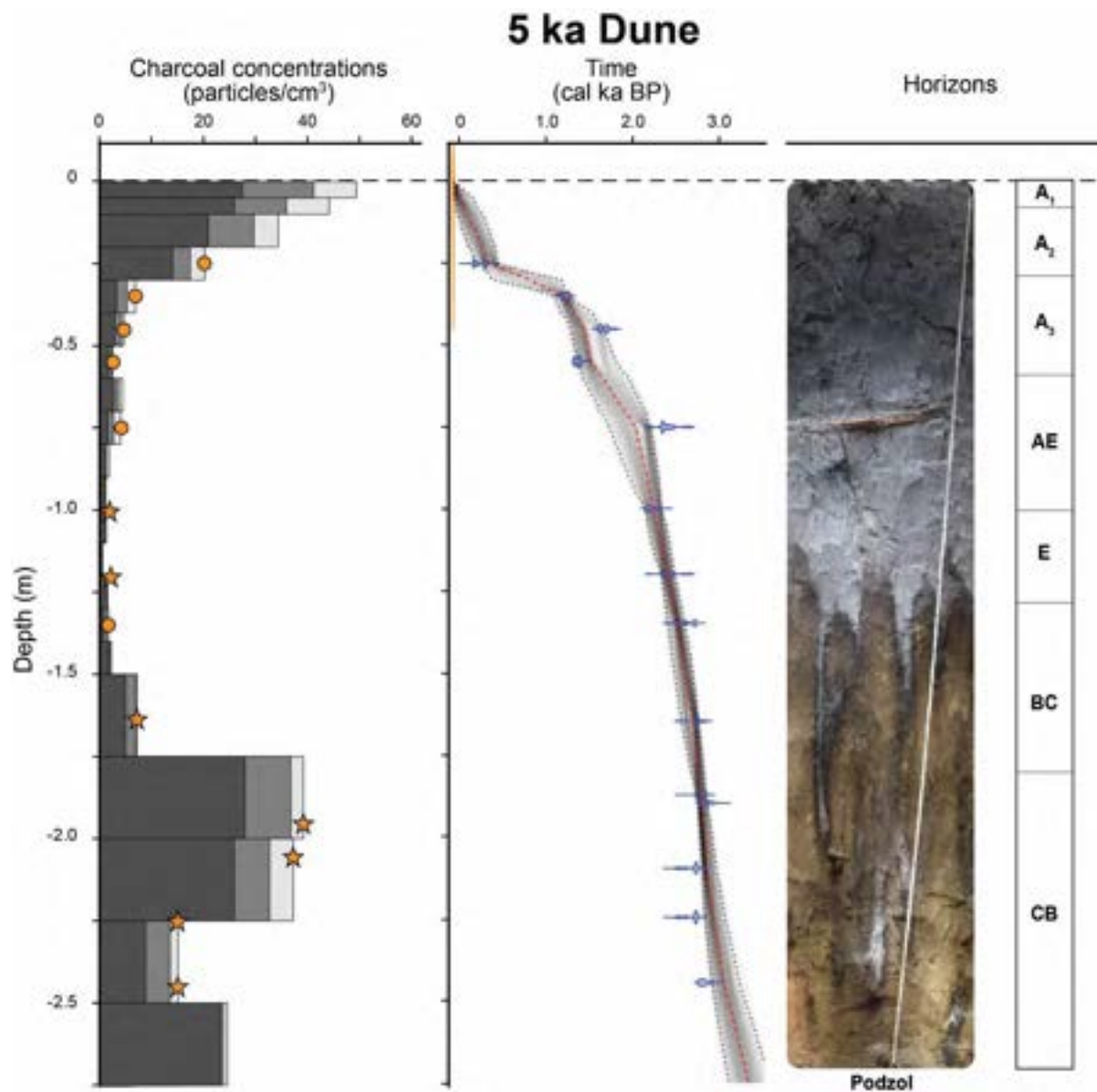


**Figure A.5.7:** Summary figure of data collected in the 5 ka Dune.



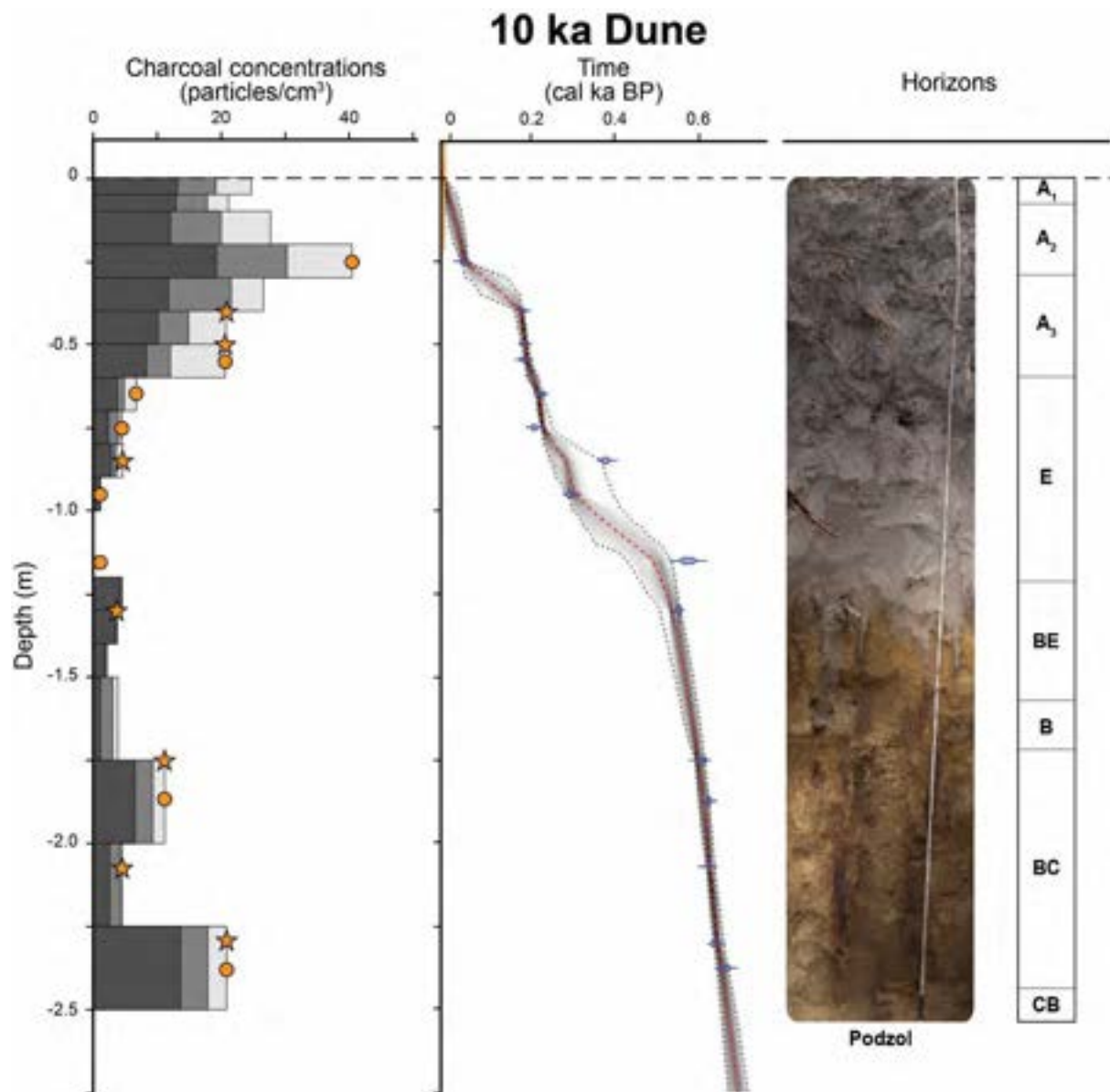


**Figure A.5.8:** Summary figure of data collected in the 10 ka Dune.

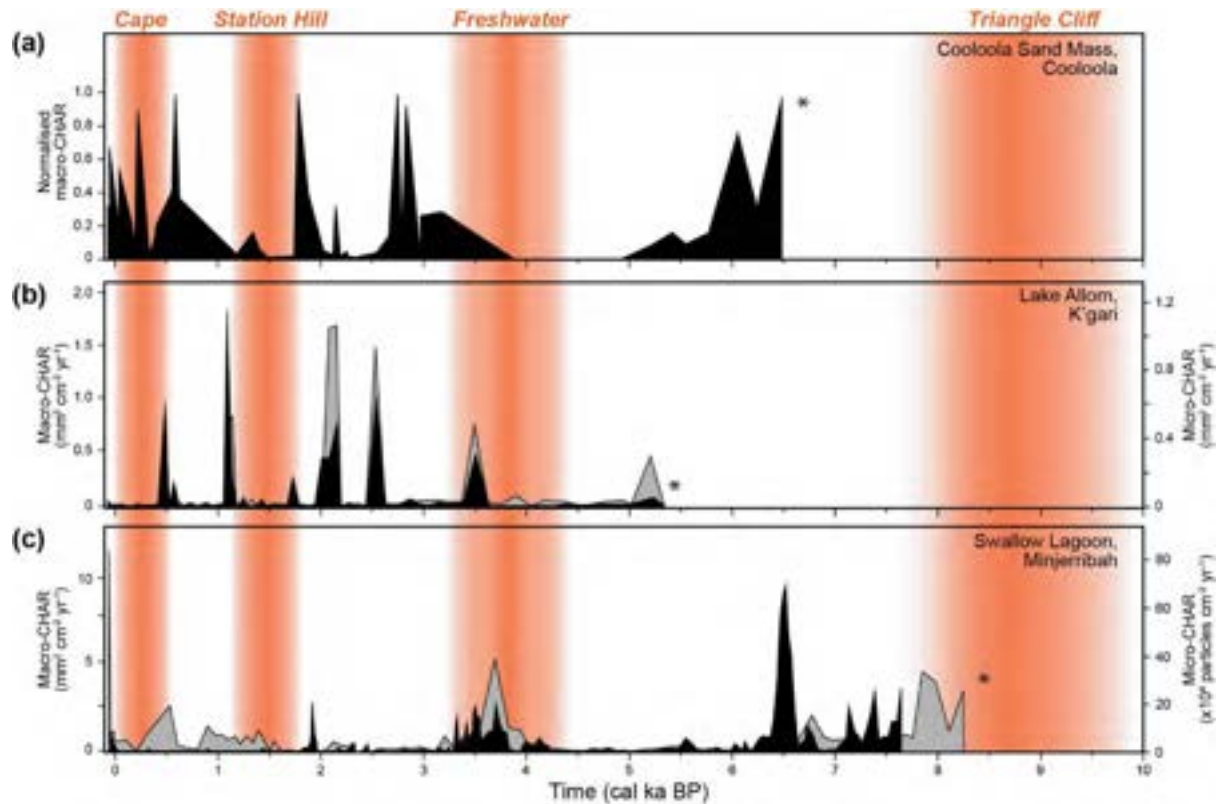


**Figure A.5.9:** Macro-Charcoal records (black areas) and micro-charcoal records (grey areas) from **(a)** the dune foot-slope deposits on the CSM, **(b)** Lake Allom on K'gari (Donders et al., 2006), and **(c)** Swallow Lagoon on Minjerribah (Mariani et al., 2019) versus major phases of dune emplacement (orange areas) (*Chapter 2*; *Chapter 4*). The same four Holocene dune emplacement phases have been mapped along the coastline of the SE Queensland dune fields (*Chapter 2*) and their ages have been determined through OSL dating and empirical relationships (*Chapter 4*; Ellerton et al., 2020). I observe that the timing of dune emplacement is inversely related to CHAR peaks, which may reflect the inability of fire to penetrate through active dune fields.

**Table A.5.1:** All modelled ages used in this study generated from age–depth models, see Table 5.1 and Figure 5.4. In this study, I utilise the median age for the mid-point of each sampling interval when placing charcoal concentrations and CHAR with time.<sup>a</sup>

Sampled depth interval (cm)	Modelled cal. age ranges for each sample interval (cal. yr BP) <sup>b</sup>	Mid-point depth (cm)	Modelled cal. ages (95% confidence interval) (cal. yr BP)
<b>0.5 ka Dune</b>			
0-5	-69 to -55	-2.5	-63 (-69 to -50)
5-10	-55 to -37	-7.5	-47 (-64 to -17)
10-20	-37 to -3	-15	-20 (-49 - 18)
20-30	-3-23	-25	11 (-4 - 49)
30-40	23-46	-35	34 (6 - 75)
40-50	46-68	-45	59 (17 - 102)
50-60	68-87	-55	77 (30 - 125)
60-70	87-106	-65	96 (45 - 147)
70-80	106-126	-75	116 (60 - 169)
80-90	126-146	-85	136 (76 - 189)
90-100	146-166	-95	156 (93 - 210)
100-110	166-188	-105	177 (109 - 229)
110-120	188-209	-115	198 (126 - 248)
120-130	209-231	-125	220 (143 - 266)
130-140	231-254	-135	242 (161 - 283)
140-150	254-274	-145	266 (178 - 300)
<b>2 ka Dune</b>			
0-5	-69-3	-2.5	-40 (-67 - 13)
5-10	3-107	-7.5	47 (-38 - 173)
10-20	107-309	-15	211 (45 - 356)
20-30	309-494	-25	398 (299 - 463)
30-40	494-592	-35	575 (512 - 598)
40-50	592-619	-45	608 (555 - 633)
50-60	619-644	-55	631 (593 - 662)
60-70	644-692	-65	680 (639 - 712)
70-80	692-718	-75	703 (680 - 751)
80-90	718-745	-85	732 (698 - 774)
90-100	745-770	-95	757 (720 - 796)
100-110	770-791	-105	780 (745 - 814)
110-120	791-810	-115	801 (765 - 836)
120-130	810-828	-125	820 (791 - 855)
130-140	828-845	-135	837 (806 - 873)
140-150	845-862	-145	853 (822 - 890)
150-175	862-904	-162.5	882 (850 - 916)
175-200	904-957	-187.5	927 (894 - 964)
200-225	957-1031	-212.5	991 (937 - 1038)
225-250	1031-1117	-237.5	1058 (998 - 1163)
<b>5 ka Dune</b>			
0-5	-69 to -1	-2.5	-42 (-66 - 22)
5-10	-1-93	-7.5	39 (-43 - 185)
10-20	93-263	-15	180 (30 - 347)
20-30	263-834	-25	354 (184 - 456)
30-40	834-1308	-35	1203 (1085 - 1282)
40-50	1308-1462	-45	1425 (1282 - 1661)
50-60	1462-1627	-55	1502 (1361 - 1811)
60-70	1627-1911	-65	1765 (1521 - 2060)
70-80	1911-2104	-75	2056 (1732 - 2211)
80-90	2104-2187	-85	2148 (1875 - 2275)
90-100	2187-2253	-95	2221 (2039 - 2323)

100-110	2253-2333	-105	2296 (2178 - 2392)
110-120	2333-2406	-115	2370 (2263 - 2461)
120-130	2406-2484	-125	2445 (2358 - 2533)
130-140	2484-2553	-135	2523 (2410 - 2605)
140-150	2553-2613	-145	2582 (2459 - 2673)
150-175	2613-2746	-162.5	2696 (2555 - 2752)
175-200	2746-2828	-187.5	2783 (2741 - 2854)
200-225	2828-2932	-212.5	2868 (2811 - 2990)
225-250	2932-3106	-237.5	3009 (2889 - 3180)
250-275	3106-3336	-262.5	3218 (3031 - 3446)
<b>10 ka Dune</b>			
0-5	-69-15	-2.5	-36 (-66 - 52)
5-10	15-131	-7.5	60 (-36 - 265)
10-20	131-327	-15	239 (56 - 406)
20-30	327-861	-25	421 (308 - 493)
30-40	861-1752	-35	1364 (789 - 1722)
40-50	1752-1856	-45	1806 (1685 - 1880)
50-60	1856-2037	-55	1905 (1834 - 1998)
60-70	2037-2235	-65	2174 (2105 - 2271)
70-80	2235-2513	-75	2284 (2225 - 2524)
80-90	2513-2911	-85	2823 (2445 - 3699)
90-100	2911-3392	-95	3008 (2849 - 3960)
100-110	3392-4472	-105	3929 (3269 - 4666)
110-120	4472-5123	-115	4982 (4285 - 5358)
120-130	5123-5381	-125	5273 (4775 - 5500)
130-140	5381-5547	-135	5480 (5158 - 5655)
140-150	5547-5677	-145	5615 (5341 - 5805)
150-175	5677-5997	-162.5	5839 (5641 - 6010)
175-200	5997-6220	-187.5	6123 (6011 - 6235)
200-225	6220-6415	-212.5	6312 (6230 - 6425)
225-250	6415-6689	-237.5	6553 (6442 - 6688)

<sup>a</sup> Age calibration was performed using the Southern Hemisphere calibration curve (SHCal20; Hogg et al., 2020) extended to recent time using the post-bomb atmospheric calibration curve for Southern Hemisphere zone 1–2 (Bomb22SH1-2; Hua et al., 2022), and modelled ages were produced using rbacon (Blaauw and Christen, 2011) in R (R Core Team, 2022).

<sup>b</sup> Median ages for the minimum and maximum sampled depth interval, respectively.

## A.6 Chapters 2-4's original publications

### A.6.1 Chapters 2 – Journal of Maps

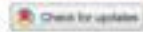
JOURNAL OF MAPS  
2019, VOL. 15, NO. 2, 578–589  
<https://doi.org/10.1080/17445647.2019.1642246>



Taylor & Francis  
Taylor & Francis Group

Science

OPEN ACCESS



## High-resolution remapping of the coastal dune fields of south east Queensland, Australia: a morphometric approach

Nicholas R. Patton , Daniel Ellerton and James Shulmeister

School of Earth and Environmental Sciences, University of Queensland, St Lucia, Australia

### ABSTRACT

The sand islands and shore-attached dune fields of south east Queensland form the world's oldest and largest coastal sand dune system. Here we present updated morphological maps for the dune fields based on topographic expression and geomorphic relationships. Individual dunes were delineated using high-resolution elevation data and were grouped into morphosequences based on the elevation, drainage characteristics and slope characteristics of the individual dunes. The slope characteristics focussed on high resolution derived slope-curvature and slope-elevation parameters. Morphosequences were recognised from cross-cutting relationships and relative position in the dune field. Our method was developed for the Cooloola Sand Mass and then applied to Fraser Island, Moreton Island and North Stradbroke Island, the other major sand islands in south east Queensland. In total, five Holocene and four Pleistocene units have been identified. The new mapping underpins current work on the geomorphic evolution of the dune fields.

### ARTICLE HISTORY

Received 18 January 2019  
Revised 6 June 2019  
Accepted 8 July 2019

### KEYWORDS

Parabolic dunes;  
morphosequence; aeolian  
geomorphology; quaternary;  
geomorphic mapping;  
remote sensing

### 1. Introduction

The dunefields of south east Queensland comprise of one of the largest coastal sand dune systems in the world, incorporating North Stradbroke (Minjerribah), Moreton (Moorgumpin), Bribie and Fraser (K'gari) Islands and the shore-attached Cooloola Sand Mass (Miot da Silva & Shulmeister, 2016; Ward, 2006). They include the world's largest sand island (Fraser Island – 1820 km<sup>2</sup>) and are associated with the longest downdrift sand accumulation system in the world (Figure 1). The net northward longshore sand transport is approximately 500,000 m<sup>3</sup>/year, with the sand sourced from the rivers of central New South Wales more than 1000 km south of Fraser Island (Boyd, Ruming, Goodwin, Sandstrom, & Schröder-Adams, 2008; Roy & Thom, 1981). The dune fields, especially the Cooloola Sand Mass, have been the target of much research, primarily on the soils and biota. The giant podzols of Cooloola are regarded as some of the thickest and most developed soils in the world (Thompson, 1981, 1983). The dune fields have been previously mapped by Ward (2006) who produced a map of all the major dune sequences. His maps were based on aerial photographs and extensive field-mapping. More recently, the dune fields have become the focus of renewed geochronological (e.g. Brooke, Pietsch, Olley, Sloss, & Cox, 2015; Walker, Lees, Olley, & Thompson, 2018) and paleoenvironmental

investigations (e.g. Barr et al., 2013; Cadd et al., 2018; Chang et al., 2015; Levin, 2011; Levin, Jablon, Phinn, & Collins, 2017; Moss, Tibby, Petherick, McGowan, & Barr, 2013; Petherick, McGowan, & Moss, 2008). Previous investigations of the south east Queensland dune fields have defined dune building phases by the soil landscapes (Chen et al., 2015; Thompson, 1981), the periods of active deposition (Tejan-Kella et al., 1990) and morpho-stratigraphic relationships (Ward, 2006). Here, we use geomorphic properties along with these previously used characteristics to describe, identify and map the dune morphosequences of coastal south east Queensland. This study has taken advantage of the improved remotely sensed imagery that is now available for the entire dune fields, most notably complete LiDAR coverage which has permitted a significant refinement of the previous mapping.

Remote sensing has long been an invaluable tool for studying dune fields and has provided researchers with the means to map the global distribution of dune fields (McKee, 1979), study the interaction between sediment supply and wind direction (Roskin, Katra, & Blumberg, 2013; Wasson & Hyde, 1983) and quantify dune morphodynamics (e.g. Ewing & Kocurek, 2010; Hugenholtz & Barchyn, 2010). More recently, LiDAR enables data resolutions down to sub-metre scales and permits the recognition of smaller scale geomorphic features. In the case of sand dunes, it facilitates the recognition of ripples and other small-scale

**CONTACT** Nicholas R. Patton [n.patt@uq.edu.au](mailto:n.patt@uq.edu.au) School of Earth and Environmental Sciences, University of Queensland, St Lucia, 4072 QLD, Australia

© 2019 The Author(s). Published by Informa UK Limited, trading as Taylor & Francis Group on behalf of Journal of Maps

This is an Open Access article distributed under the terms of the Creative Commons Attribution License (<http://creativecommons.org/licenses/by/4.0/>), which permits unrestricted use, distribution, and reproduction in any medium, provided the original work is properly cited.



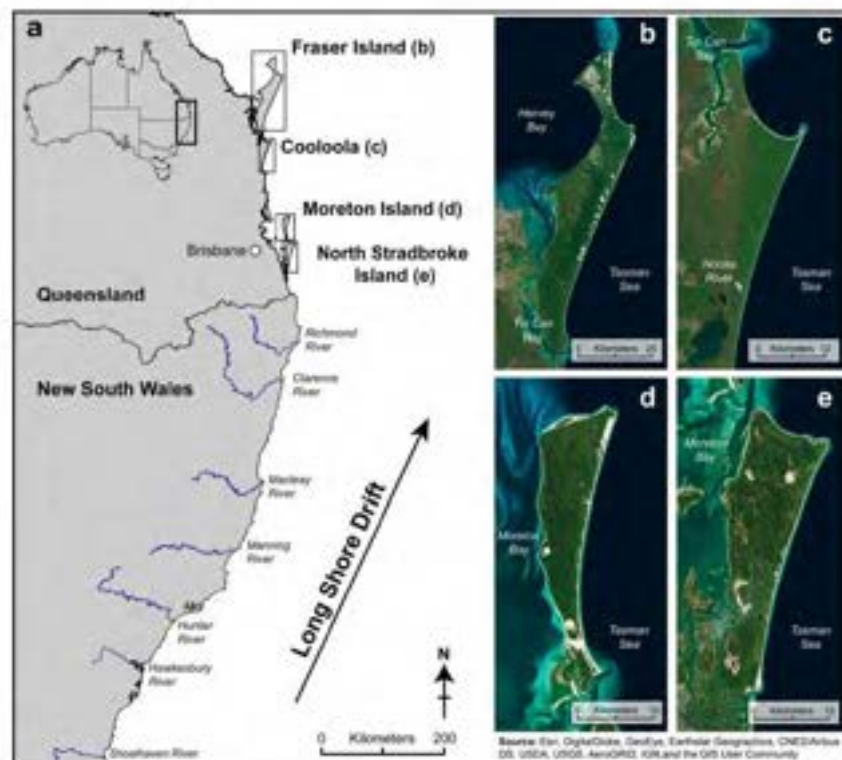


**Figure 1.** Panel a is the location map of the south east Queensland dune fields with the eastern Australian longshore drift system and major rivers along the coast. Satellite images of Fraser Island, Cooloolool Sand Mass, Moreton Island, and Stradbroke Island are presented in panels b through e.

structures on dune surfaces and can be used to track their gradual disappearance with increasing age. We took advantage of such features to examine surface roughness patterns to aid in the individual dune mapping at a much finer scale than was previously possible. This enabled us to distinguish areas of similar geomorphic characteristics within the dune field at a finer scale, thereby enabling us to distinguish late-Holocene units that appear identical on gross morphology. The technique presented in this study provides the foundation for future work to map and quantify phases of dune activity within stable dune fields as well as investigate how dune landscapes evolve through time.

## 2. Study site

The sand islands of south east Queensland form an extensive series of coastal sand dune fields that include Moreton Island (Moorgumpin) and North Stradbroke Island (Minjerribah) to the south and the Great Sandy Region to the north which comprises of the Cooloolool Sand Mass (presently attached to the mainland) and Fraser Island (K'gari) (Figure 1). North Stradbroke Island, situated offshore of Brisbane at  $\sim 27.4^{\circ}\text{S}$  forms the southern extent of these dune

systems while Fraser Island forms the northern extent at  $\sim 25.5^{\circ}\text{S}$ . The dune fields are large, with the Cooloolool Sand Mass, Moreton Island and Stradbroke Island reaching lengths of approximately 40 km and widths of approximately 12 km. Fraser Island is significantly larger with a length of approximately 120 km and an average width of 24 km. The total land area of the dune fields is  $\sim 2350 \text{ km}^2$  and elevation ranges up to 285 m above sea level.

The entire region has a humid subtropical climate (Köppen classification Cfa) with warm, wet summers and mild and dry winters (Peel, Finlayson, & McMahon, 2007). Mean annual precipitation varies from  $\sim 1200$  to  $\sim 1700$  mm. February and March are the wettest months. South easterly winds persist year round with a more southerly component during the winter months and north-easterly winds occur during the spring (BOM, 2017).

The dune fields are notable for containing the world's largest area of rainforest on tall sand dunes (Fraser Island) (Gontz et al., 2015; Wardell-Johnson et al., 2015). Vegetation along the coastal eastern margin of the dune fields comprises of coastal shrubland and grasses that can tolerate strong winds and salty conditions. Moving inland, low open woodland gives way to tall open and closed forest with notophyllous

vine forest in the swale areas. Along the western flanks of the dune fields, vegetation is dominated by open shrubland and heath communities (Donders, Wagner, & Visscher, 2006; Gontz et al., 2015; Longmore, 1997; Longmore & Heijnis, 1999).

The dune fields are composed predominantly of stable parabolic dunes with localised blowouts and several small active transgressive dune sheets. The sediments of the dune fields are homogenous, well sorted and rounded siliceous sands derived from granites and Mesozoic metasediments from the tablelands of eastern New South Wales (Pye, 1983; Roy & Thom, 1981; Thompson, 1981). Bedrock exposures are limited to small rocky outcrops that mostly make up headlands at the northern ends of the dune fields. All of the dune field deposits have formed over successive phases of dune emplacement that have occurred since at least the middle Pleistocene (Pye, 1983; Thompson, 1981; Ward, 2006). The dune emplacements have formed a series of onlapping dune units that increase in age moving away from the present coastline. Ward (2006) recognised nine periods of dune building based on soil development and morphological characteristics. More recently, Walker et al. (2018) identified 10 units at the Cooloola Sand Mass and used single grain optically stimulated luminescence (OSL) dating to identify periods of activity. They found that the oldest units at Cooloola date to about 725 ka, confirming earlier work by Tejan-Kella et al. (1990) and they also observed that dune emplacement has continued episodically.

Soil development across the dune fields ranges from weakly developed podzols to well-developed giant humus podzols that are primarily composed of siliceous sands with <2% heavy minerals, including zircon, rutile and ilmenite (Thompson, 1983). This composition reflects the sand delivered to the coast by the longshore drift system along the east Australian Coast. Marine-derived sands extend to tens of metres below modern sea level (Ball, 1924). Mean grain size ranges between 180 and 210  $\mu\text{m}$  and have high porosity at >600  $\text{mm h}^{-1}$  (Reeve, Thompson, & Fergus, 1985; Thompson & Moore, 1984). Marked increases in soil development occur across the dune sequences with thick A2 and B horizons developed in older dunes located further inland (Thompson, 1981). Thompson (1981) suggested that there is little indication of large climatic, biotic, or lithological shifts within the dune field as indicated by the consistent shape of the dunes and the lack of deviation from podzol soil-forming trends.

### 3. Materials and methods

#### 3.1. Mapping assumptions and workflow

Here we assume that all the south east Queensland coastal dune fields are part of the same depositional system and experience a similar formation and

evolutionary history (Thompson, 1983; Ward, 2006). All changes in the character of the morphosequences are time dependent such that younger dunes will experience similar perturbations as older dunes, with the length of time since emplacement controlling the overall degree of erosion. This results in a unique erosional and depositional history for each dune morphosequence. In addition, we propose that each dune is systematically moving towards a steady state after its emplacement; that is, topography becomes increasingly uniform or 'smoother' with time (Bonetti & Porporato, 2017; Montgomery, 2001). Based on these assumptions we use changes in dune morphological characteristics supported by dune ancillary characteristics to map the dune fields (Figure 2). The Cooloola Sand Mass was the optimal location to establish this method because it contains the most complete dune sequence (Lees, 2006), the most ancillary (e.g. soil, chronology) information and has experienced little human disturbance.

#### 3.2. Individual dune delineation

We utilise high-resolution elevation data, satellite imagery, and historical aerial photographs to identify individual dunes. Principally, we used a 5 m digital elevation model (DEM) derived from Light Detection and Ranging (LiDAR) and 1:5000 digital orthophoto imagery data. Elevation datasets for all areas of interest were obtained from the Digital Elevation Model (DEM) 5 m Grid of Australia created by merging 236 datasets collected between 2001 and 2015. Accuracy of elevation data met the Australian ICSM LiDAR Acquisition Specifications with the vertical and horizontal data having an accuracy of no worse than  $\pm 0.30$  m and  $\pm 0.80$  m (95% confidence), respectively.

Orthophoto imagery was acquired through Queensland Globe (QGlobe), with a pixel resolution of 0.25 m and an accuracy of  $\pm 1.0$  m. In addition, historical aerial photographs were obtained through Queensland Imagery (QImagery) to determine any recent anthropogenic disturbances that may have altered the original topography, such as mining or logging, and provide locations and characteristics of previously visible dunes.

Where little to no anthropogenic disturbances occurred in the landscape, we identified individual dunes through large dune morphological features (> 10  $\text{m}^2$ ) such as crests, trailing arms, and the slip face of the depositional lobes. An example of this process is provided in Figure 3. In ArcGIS 10.6 (ESRI, Redlands, CA) we delineated each dune at the base of their ridges and crests utilising elevation and slope rasters. For all points, slope was calculated using change in elevation in downhill direction which is presented here as degree slope. Curvature was obtained by the rate of change in slope, at a fixed position in all directions and multiplied by -100 to remove the negative curvature convention (i.e. Patton, Lohse, Godsey, Crosby, & Seyfried, 2018).



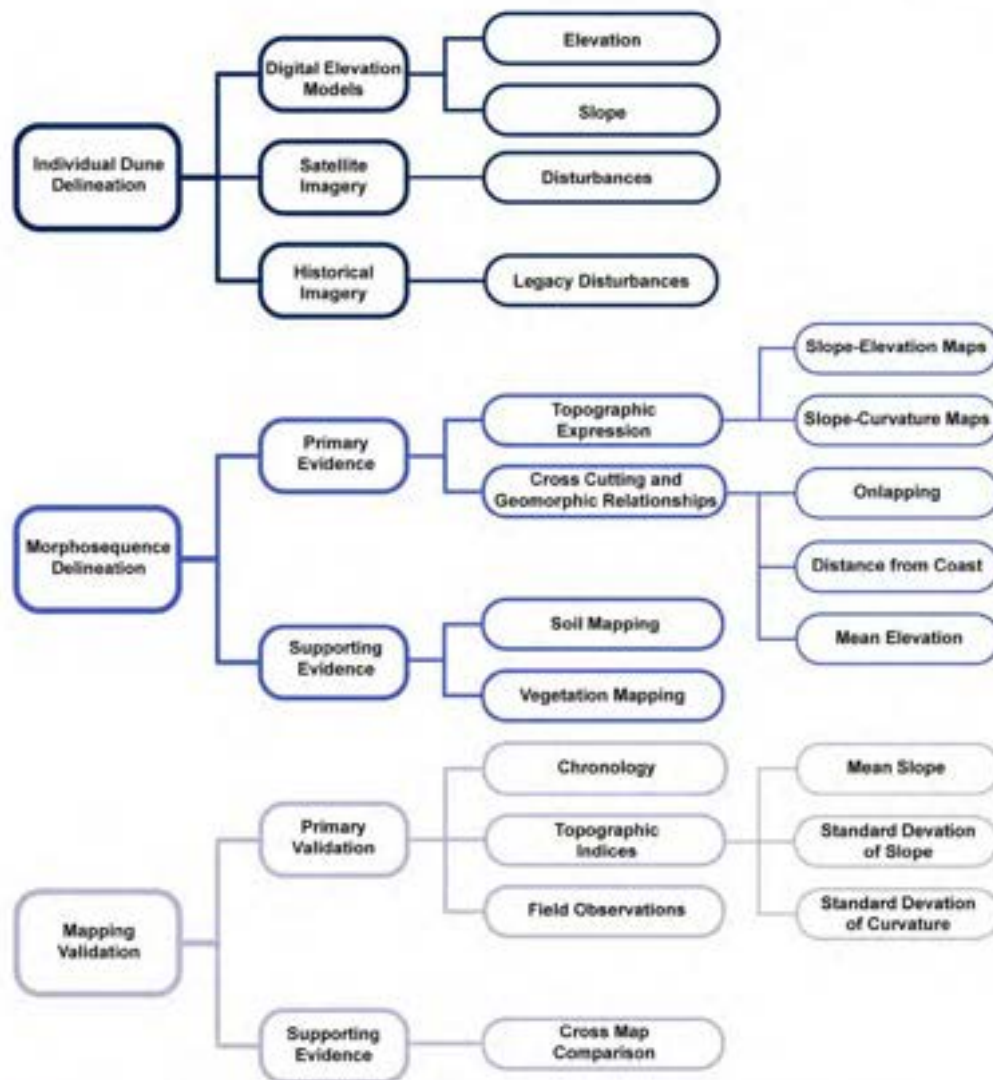


Figure 2. Schematic flow chart of the mapping and validation procedures for dune morphosequence delineation.

### 3.3. Dune morphosequence delineation and supporting evidence

Following individual dune delineation, we categorised dunes into separate morphosequences utilising cross-cutting and geomorphic relationships. The Cooloola Sand Mass forms a classic onlapping dune sequence where dune units become increasingly older from the coast (east) moving inland (west) (Lees, 2006; Walker et al., 2018). In coastal dune fields, onlapping relationships allow us to determine the relative age sequence of the dune emplacements as younger dunes are superimposed on older units. To exemplify this, we measured the shortest mean distance from the furthest inland dune crest to the coast and the mean elevations for each morphosequence.

Where cross-cutting geomorphic relationships are not easily determined due to landscape complexity,

we utilise small (<10 m) internal dune features to help delineate each morphosequence by using the topographic expression to 'fingerprint' each dune emplacement phase. The surface characteristics of the landscape can be defined by the relative surface texture, drainage patterns and landform elements present. The topographic fingerprint is best observed by combining and manipulating elevation, slope and curvature rasters. This was achieved by overlaying a 70% transparent slope raster with a white to black (low to high) gradient on an elevation raster with a continuous brightness colour ramp (Figure 4). Similar to elevation, we combined a transparent slope raster on a curvature raster with a diverging colour ramp. Due to the normal distribution of curvature around planar surfaces ( $0\text{ m}^{-1}$ ) a diverging colour ramp utilising quantile bins, is best suited to emphasise changes from convergent (hollows and valleys) to divergent (ridges and



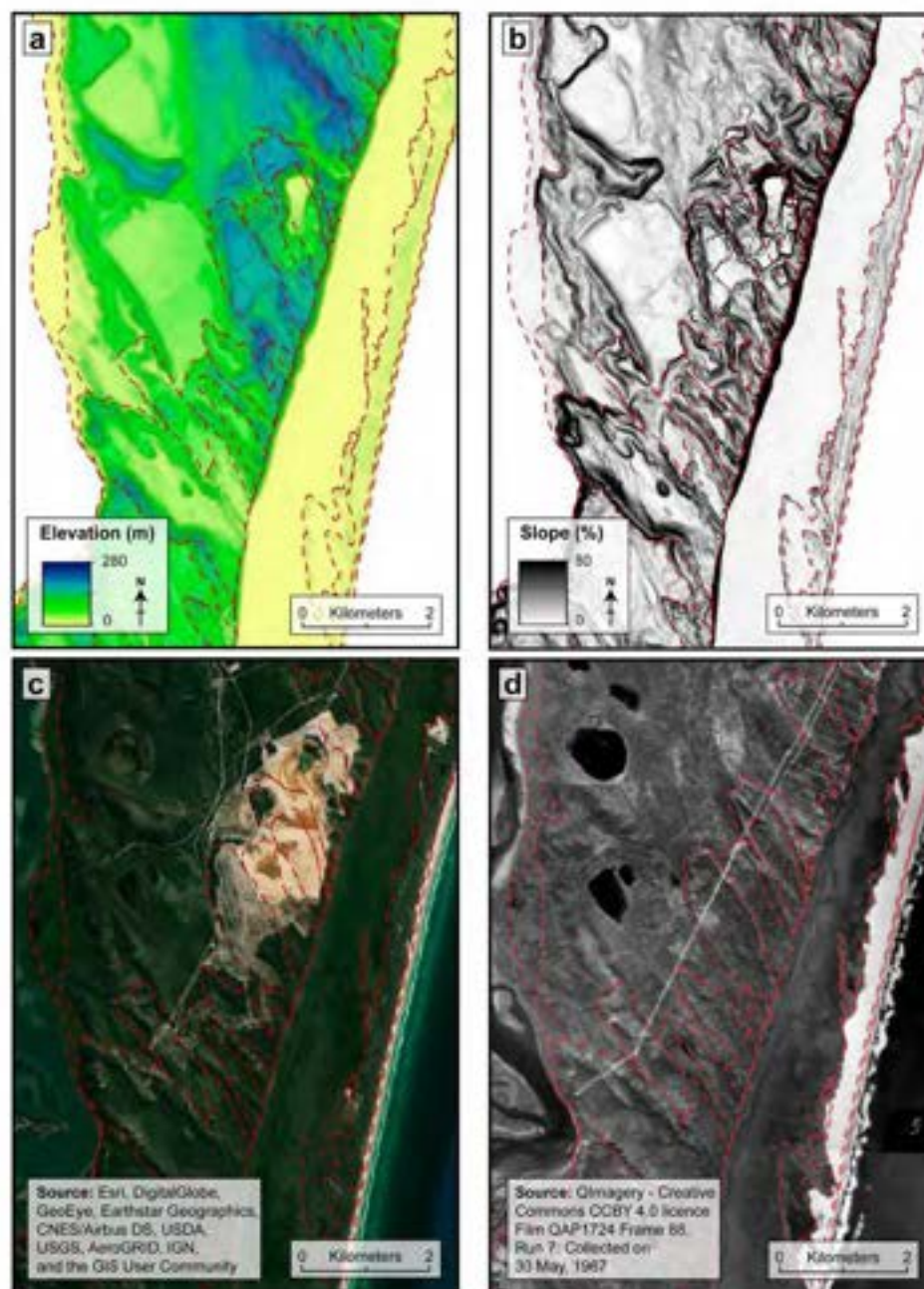


**Figure 3.** Visual sequence of dune delineation using part of North Stradbroke Island as an example. Panel a shows elevation from the DEM. Panel b shows the derived slope map from the DEM. Panel c is an air photo of the same area with dune outlines overlaid. It highlights the areas of human disturbance (mining). Panel d is an example of historical air photo that allows us to map areas currently disturbed and modern dunes.

noses) topography (Figure 4). In combination, both rasters act as visual aids to identify the unique fingerprint of each depositional phase.

This approach allows a simple visual comparison between each individual dune, permitting them to be delineated into separate morphosequence units; however, some discrepancies may still occur. Where internal dune features are limited or difficult to interpret due to

depositional complexity, changes in base level or proximity to higher energy environments (such as Tin Can Bay, Noosa River or the Tasman Sea) (see Figure 1) we used the available soil (Thompson, 1983), vegetation (Queensland Herbarium) and drainage direction data to complement and support our interpretations. Soil information helps provide a relative age sequence of the dunes based on the increasing degree of pedogenesis

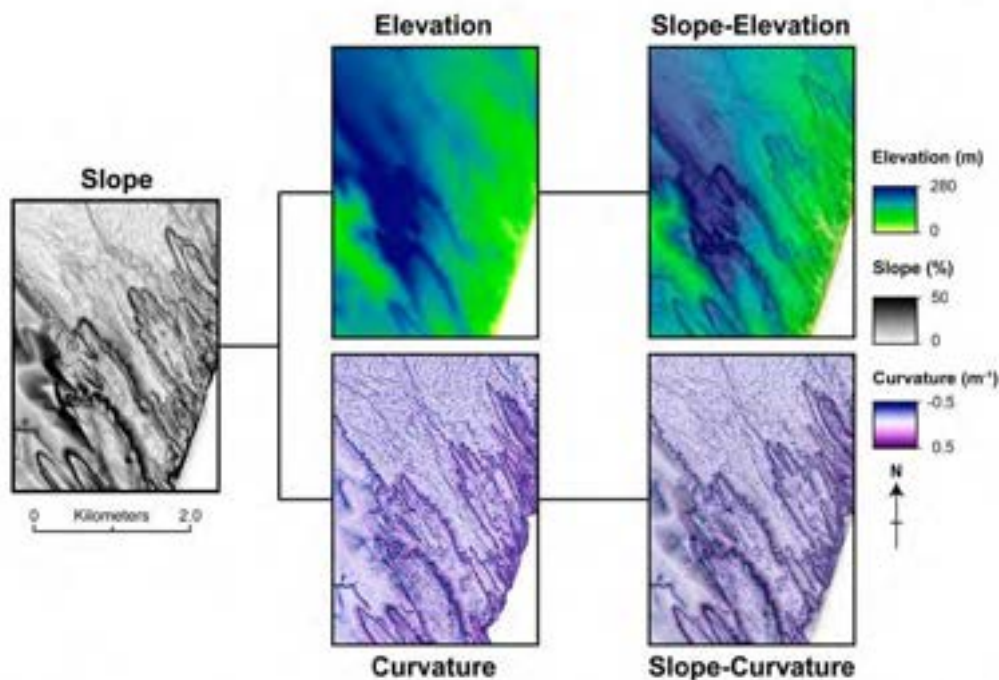


**Figure 4.** This figure demonstrates the methodology used to generate the topographic expressions as seen in the slope-elevation and slope-curvature layers. In each case a slope raster was superimposed at a 70% transparency on the elevation and curvature layers to generate the topographic expression. These topographic expressions were then applied to discriminate between morphosequences.

with time (Chen et al., 2015). Field data was also used to confirm the onlapping relationships of each dune morphosequence (Our unpublished data).

We have opted to use the naming convention of Ward (2006) for the dune morphosequences. We use this convention rather than the numerical convention employed by Thompson (1981) and Walker et al. (2018), as using a number based system can lead to issues if a new unit is identified or an existing unit is eliminated, as happened in our new mapping.

### 3.4. Mapping validation and supporting evidence

To validate our approach for delineating dune field morphosequences, we focus on the Cooloola Sand Mass. Validation was achieved by cross referencing each dune morphosequence with available unpublished chronological data and Walker et al. (2018). This was done to confirm the age relationships of each morphosequence using the weighted mean of the OSL ages. Each morphosequence was plotted as the explanatory variable against mean distance from coast, mean elevation and extracted topographic indices. The topographic indices for each dune morphosequence were determined from ArcGIS zonal statistics as the mean and standard deviation of slope and the standard deviation of curvature. To eliminate any discrepancies that may have altered

the original topographic expression, portions of the landscape such as anthropogenic disturbances (e.g. roads), rock outcrops, and free-standing water were identified and removed from the analyses, along with an additional 10 m buffer.

A complementary assessment of our mapping efforts involved a comparison to the traditional, independently derived geomorphological map by Ward (2006). His study primarily used aerial imagery, soil data and field observations to map the Cooloola Sand Mass and extrapolated his findings across the remaining south east Queensland dune fields. We evaluated and compared each matching morphosequence between the studies. We acknowledge that this is by no means a true validation, however, comparisons of each map provide novel insight into the two techniques. To achieve this, Ward's map was digitised in the ArcGIS georeferencing tool and we report the percent similarity of matching dune morphosequences.

### 3.5. Mapping extrapolation

We extrapolated our approach to the adjacent dune fields. In all dune fields, we delineated individual dunes and then grouped into the appropriate morphosequences based on the same topographic expression and geomorphic relationships seen at the Cooloola Sand Mass.



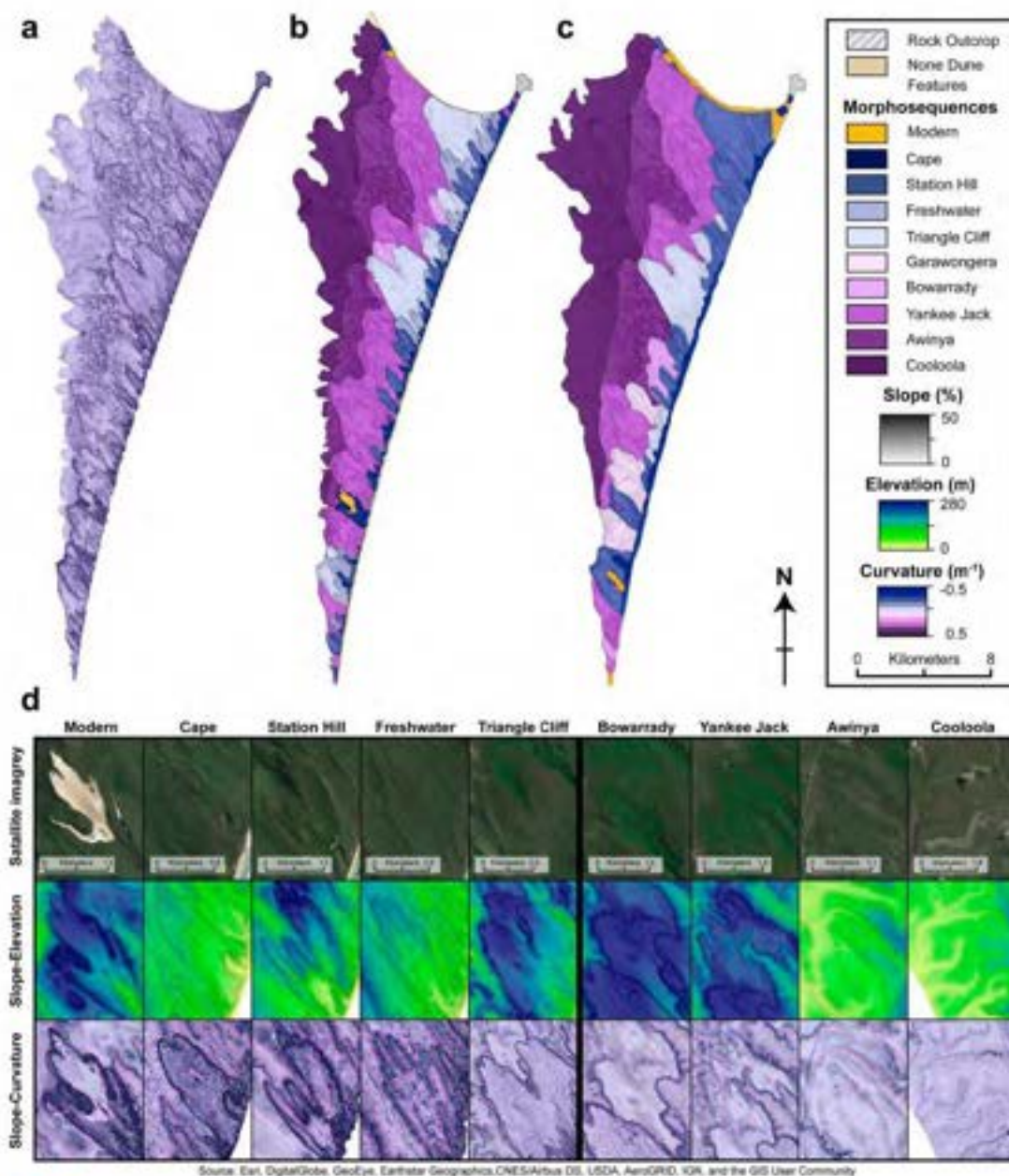


**Figure 5.** Cooloolo Sand Mass morphosequences and their validation. Panel a is the derived slope-curvature raster. Panel b is the final morphosequence map of the Cooloolo Sand Mass. Panel c is the digitised version of Ward's (2006) map. Note the strong similarity between panels b and c. In our final map we have added an extra Holocene unit (Freshwater) but eliminated a Pleistocene unit of Ward (2006) (Garawongera). Panel d displays slope-curvature, slope elevation and satellite images for each of the morphosequences. The heavy black line separating Triangle Cliff from Bowarrady marks the boundary between the Holocene and Pleistocene morphosequences. Note that the dune units become more diffuse and less well defined with increasing age. The units from the Cooloolo Sand Mass were then applied to the sand islands.

#### 4. Results

##### 4.1. Cooloolo morphosequence delineation and validation

We recognise nine dune morphosequences at the Cooloolo Sand Mass composed of five Holocene (Modern, Cape, Station Hill, Freshwater and Triangle Cliff) and four Pleistocene units (Bowarrady, Yankee Jack,

Awinya and Cooloola) see main map (Figures 5 and 6). This study recognises an additional Holocene unit that was not mapped by Ward (2006), which we have named Freshwater. We have also removed one of Ward's Pleistocene units, Garawongera, which was not found in this study. Holocene morphosequences are characterised by decreases in crest sharpness and surface roughness, increases in podzolisation,

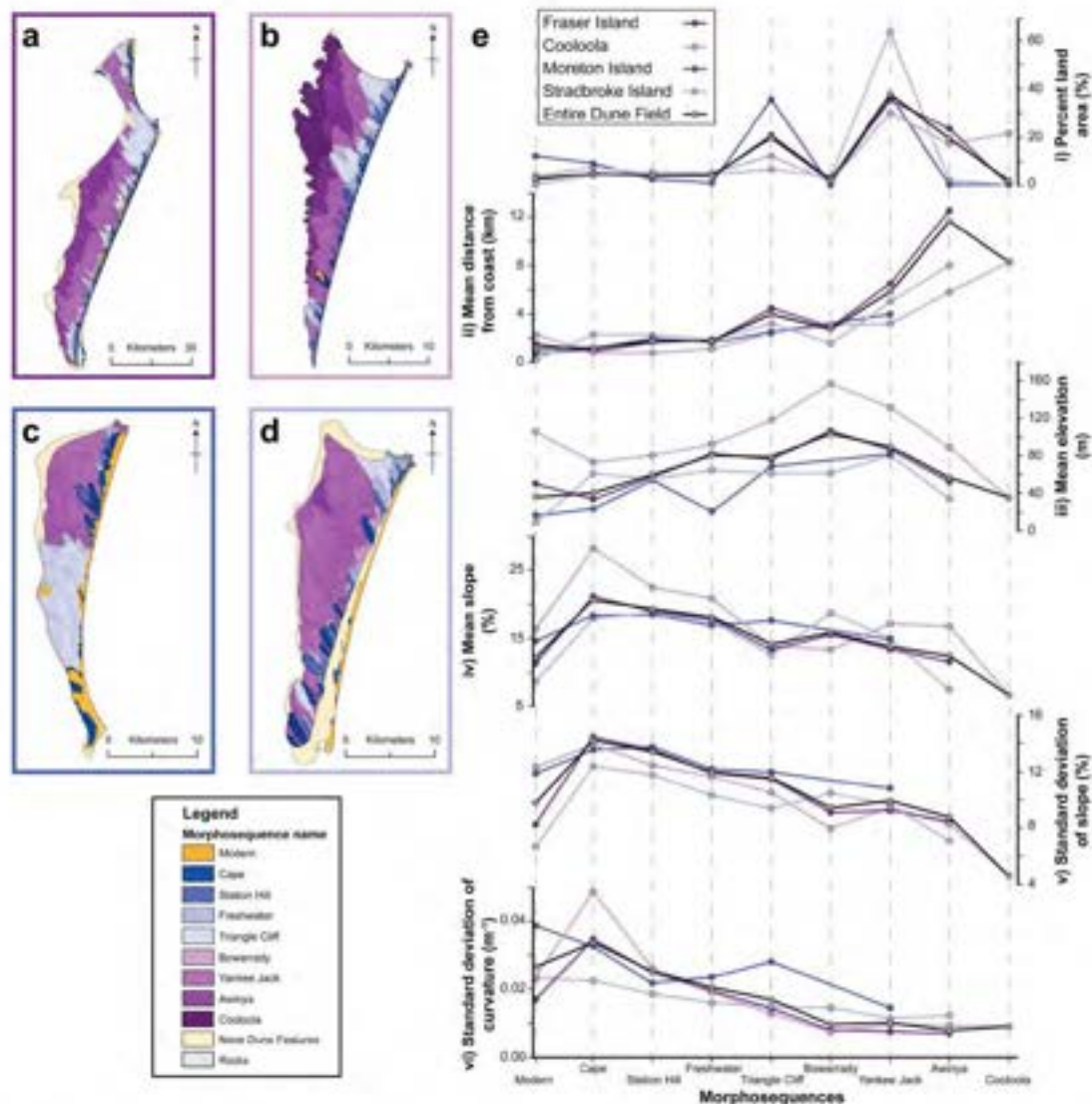


**Figure 6.** On the left-hand side panels a–d display the final maps for each of the dune fields. Panel a: Fraser Island. Panel b: The Cooloola Sand Mass. Panel c: Moreton Island. Panel d: North Stradbroke Island. Dune fields are not to scale. Panel e contains six graphs showing (i) percent land area for each unit; (ii) mean distance from coast, (iii) mean elevation, (iv) mean slope; (v) standard deviation of slope; (vi) standard deviation of curvature. The black line represents the mean values for all dune fields. Note that in all dune fields the parameters follow the same trends. Also note that for geomorphic characteristics there is a general progression from youngest to oldest morphosequences.

elevation, and distance to coast with increasing age. They display little to no stream incision. Pleistocene units exhibit similar trends but all show evidence of increasing fluvial incision and decreasing crest elevation with age (Table 1).

Our results are consistent with the independent chronology of the Cooloola dune field based on OSL ages from both Walker et al., (2018) and our unpublished dataset. The weighted mean and standard error age for Cape, Station Hill, Freshwater, Triangle Cliff, Yankee Jack and Awinya units are  $0.4 \pm 0.04$  ka,  $0.8 \pm 0.1$  ka,  $4.1 \pm 0.24$  ka,  $7.8 \pm 0.26$  ka,  $132 \pm 3.9$  ka,  $648 \pm 32$  ka, respectively. It should be noted here that OSL

dates the last time sand grains were exposed to sunlight and these ages likely reflect the final phase of dune development rather than the time the dune was first initiated. It is likely that the time of initiation predates these ages. The Modern dunes are dunes that are currently active or were visibly active in historical imagery as shown by bare earth (lacking vegetation). The lack of original dune morphology suggests that the Cooloola unit has been extensively reworked, but is older than the Awinya unit ( $> \sim 650$  ka). The Bowrady unit is recognised in our mapping but no age control is available for this dune morphosequence. Based on its morphostratigraphic position, emplacement



**Table 1.** Summary of Cooloola morphosequence units including mean age, surface characteristics, percent land cover, mean elevation, mean slope, standard deviation of slope and standard deviation of curvature.

Morphosequence unit	Mean age (ka)	Surface characteristics	Soil characteristics	Land area (%)	Mean distance from coast (km)	Mean elevation above sea level (m)	Topographic indices		
							Mean slope (%)	St. dev. slope (%)	St. dev. curvature (m <sup>-1</sup> )
Modern	<0.4	Bare, presently active sand	No podsolisation	0.46	2.30	107	16.4	12.3	0.0232
Cape	0.4 ± 0.04	Sharp crested, parabolics that have been recently stabilised	No podsolisation	4.30	0.78	73.6	28.3	14.0	0.0460
Station Hill	0.8 ± 0.1	Elongate, sharp crested parabolics	Incipient podzol	5.77	0.78	80.9	22.6	12.4	0.0262
Freshwater	4.1 ± 0.24	Elongate, sharp crested parabolics	Podzol	5.22	1.12	93.1	20.9	11.7	0.0191
Triangle	7.8 ± 0.26	Elongate, U-shaped parabolics. Large sand ripples within dune interior	Podzol	12.73	2.48	119	14.1	10.5	0.0128
Bowarrady	7.8–132	Prominent dune relief with incised channels. Dune apex and ridges have been truncated. Found blocking major Yankee Jack channels.	Giant Podzol	1.66	3.10	158	13.3	7.89	0.0074
Yankee Jack	132 ± 3.9	Prominent dune relief with large incised channels. Dune apex and ridges have been truncated	Giant Podzol	30.42	3.23	132	17.2	9.51	0.0068
Awinya	648 ± 30	Subdued dune relief with significant incision and complex drainage patterns. Very little original dune morphology	Giant Podzol	17.64	5.81	89.2	16.7	8.32	0.0064
Cooloola	>648	Very subdued dune relief with no original dune morphology	Giant Podzol	21.79	8.33	6.61	6.61	4.62	0.0091

Note: Data were extracted using ArcGIS 10.6 (ESRI, Redlands, CA) zonal statistics tools. For more information on mean age and soil characteristics refer to Ellerton et al. (2018), our unpublished data, Thompson (1981) and Walker et al. (2018).

occurred between the Yankee Jack and Triangle Cliff units and based on its morphology, the unit is clearly Pleistocene, as suggested by Ward (2006).

We observe that 90.3% and 97.8% similarity of our Holocene and Pleistocene mapped units, respectively, when compared to the Holocene and Pleistocene boundaries of the original mapping by Ward (2006). Direct comparisons of each morphosequence are complicated by the change in the number of units but we observe 5.3% Modern, 57.6% Cape, 21.4% Station Hill, 66.0% Triangle Cliff, 0% Bowarrady, 71.2% Yankee Jack, 70.7% Awinya, and 98.2% Cooloola congruence between our study and Ward's (2006). The new mapping of the Cooloola dune field agrees well with the chronology of the dune systems and is largely consistent with past mapping efforts, but provides increased resolution, especially in the Holocene dune units.

#### 4.2. Mapping extrapolation

Like Ward (2006), we extrapolated our morphosequence units across the south east Queensland coastal dune fields. When plotting the topographic indices and geomorphic characteristics against each morphosequence unit, we observe similar landscape relationships between all study sites (Figure 6). The Cooloola Sand Mass contains all of the morphosequences recognised at other dune fields while none of the other dune fields contain the whole sequence. This confirms that the Cooloola Sand Mass is the most complete dune field sequence in south east Queensland and reinforces the need for conservation of this dune field.

### 5. Discussion

#### 5.1. Geomorphic evolution-foundation of this approach

Our mapping is based on the fundamental concept that all landforms are evolving towards a topographic steady-state, where the balance between processes which create topography and the processes that destroy it are equal and landforms are converging towards the local base level (Willett, Slingerland, & Hovius, 2001). This assumption can be problematic in dune fields as dunes can be easily reworked following a perturbation (Hugenholtz & Wolfe, 2005; Tsoar, 2005), especially in coastal environments (Hesp, 2002). The coastal dunes of south east Queensland show evidence of long term stability despite the deep podsolisation, extensive incision and great antiquity of the Pleistocene units (Lees, 2006; Tejan-Kella et al., 1990; Walker et al., 2018). Following the earliest dune building events, subsequent phases of activation have not fully overrun and reworked previous deposits due to the high elevation and steep slopes of the antecedent topography. It is very likely that there have been periods of reworking

(Walker et al., 2018), however, we argue that this has been more local and has not lead to the complete destruction of previous units. The patterns that we observed from our morphometric analyses at the Cooloola Sand Mass, indicates that these assumptions are reasonable and that, especially in the Holocene dune sequences, the approach allows us a better discrimination of dune units than was previously possible (Figure 5). Consistent with the Cooloola Sand Mass, we observe the same topographic patterns across the south east Queensland dune fields, indicating that our assumptions are reasonable and that all the dune fields are part of the same depositional system (Figure 6).

The previous mapping effort by Ward (2006) successfully delineated dune units based on cross-cutting relationships and large-scale features. This can be seen in the similarity of the Holocene and Pleistocene boundaries in both studies (Figure 5; panels b and c). Where dune units are separated by a significant gap in time (e.g. Awinya and Yankee Jack) he was also able to accurately distinguish between the units. However, limitations with his map occurred in areas with complex terrain, dense vegetation cover and/or where dune units were very similar in age. Where these conditions occurred his maps became less reliable. Our approach helps to improve and update the geomorphic mapping. For example, along the north eastern boundary of the Cooloola Sand Mass where significant dune onlapping and dense vegetation occurs, Ward mapped the entire area as Cape and Station Hill, whereas we were able to individually delineate all Holocene morphosequences in this area.

With respect to limitations of this work, the main constraints are around the manual nature of dune delineation which makes the procedure quite time-consuming. There are specific challenges in areas of complex topography because the mapping requires the operator to identify individual dunes. In areas of heavy drainage dissection or complex dune interactions, this may not always be accurate and depends on the familiarity of the operator with the dune forms. Only a few small areas of the dune field are affected by this phenomenon.

In order to apply this method to other systems, high-resolution elevation data are needed along with an understanding of the processes dominating the landscape. How changes to base level, climate and antecedent topography have influenced the depositional and erosional history is important to understand the patterns observed. An example of this is the role of pre-existing topography on dune unit extent. In areas where high dunes are preserved (e.g. The Cooloola Sand Mass) younger dune units are compressed, as they need energy to migrate up and over the older systems. In contrast, in north-central Fraser Island, early Holocene dunes propagated onto a lower topography and succeeded in migrating many kilometres to the west.

## 6. Conclusion

Here we have presented a novel method to interpret and delineate dune morphosequences across the coastal dune fields of south east Queensland, Australia based on work from the Cooloola Sand Mass. This study combined traditional approaches with the assumption that landscapes are systematically smoothing through time. We used two primary parameters to undertake this work, topographic expression and geomorphic relationships to define the morphosequences. The mapped units were validated using chronology, topographic indices and field observations. Using these parameters we have been able to successfully sub-divide the dunes into five Holocene and four Pleistocene units.

The mapping approach presented in this study has advantages over visual mapping of the dune morphosequences in that it is (a) semi-objective and (b) could be automated. Based on our analyses, it is likely to be more robust than traditional mapping. Future coastal dune field studies can use the techniques we provide here as a first-order approach to delineate landforms based on relative age. In addition, we were able to extrapolate with confidence across the entire south east Queensland dune fields into areas with little to no previous chronological information. The mapping will help underpin ongoing paleoclimate and geomorphological research in the south east Queensland dune fields.

## Software

ESRI ArcGIS 10.6 was used to georeference imagery, digitise, extract data using zonal statistics and generate the morphometric map. Queensland Globe (QGlobe) and Queensland Imagery (QImagery) was utilised for viewing orthophoto imagery and historic photographs.

## Acknowledgements

The field mapping at Cooloola was undertaken using permit WITK15791415. We also acknowledge the assistance provided to us by the National Parks and Wildlife Service, Natural Resources and Mines, Queensland Government, Queensland Globe, licensed under Creative Commons Attribution 4.0 sourced on 20th December 2018. We acknowledge the traditional owners of Fraser Island (K'gari), Cooloola, Moreton Island (Moorgumpin) and North Stradbroke Island (Minjerribah) and elders past, present and emerging.

## Disclosure statement

No potential conflict of interest was reported by the authors.

## Funding


Funding for this study was provided by the Australian Research Council (ARC) grant number DP150101513.



## ORCID

Nicholas R. Patton  <http://orcid.org/0000-0002-4137-0636>

Daniel Ellerton  <http://orcid.org/0000-0003-1998-1817>

James Shulmeister  <http://orcid.org/0000-0001-5863-9462>

## References

- Ball, L. E., (1924). Report on oil prospecting, near Tewantin. *Queensland Government Mining Journal*, 25, 354–360.
- Barr, C., Tibby, J., Marshall, J. C., McGregor, G. B., Moss, P. T., Halverson, G. P., & Fluin, J. (2013). Combining monitoring, models and palaeolimnology to assess ecosystem response to environmental change at monthly to millennial timescales: The stability of Blue Lake, North Stradbroke Island, Australia. *Freshwater Biology*, 58(8), 1614–1630.
- BOM. (2017). Climate data online [online] (Vol. 2017), Australian Government, Bureau of Meteorology.
- Bonetti, S., & Porporato, A. (2017). On the dynamic smoothing of mountains. *Geophysical Research Letters*, 44, 5531–5539.
- Boyd, R., Ruming, K., Goodwin, I., Sandstrom, M., & Schröder-Adams, C. (2008). Highstand transport of coastal sand to the deep ocean: A case study from Fraser Island, southeast Australia. *Geology*, 36(1), 15–18.
- Brooke, B. P., Pietsch, T. J., Olley, J. M., Sloss, C. R., & Cox, M. E. (2015). A preliminary OSL chronology for coastal dunes on Moreton Island, Queensland, Australia – marginal deposits of a large-scale quaternary shelf sediment system. *Continental Shelf Research*, 105, 79–94.
- Cadd, H. R., Tibby, J., Barr, C., Tyler, J., Unger, L., Leng, M. J., ... Baldock, J. (2018). Development of a southern hemisphere subtropical wetland (Welsby Lagoon, south-east Queensland, Australia) through the last glacial cycle. *Quaternary Science Reviews*, 202, 53–65.
- Chang, J. C., Shulmeister, J., Woodward, C., Steinberger, L., Tibby, J., & Barr, C. J. Q. S. R. (2015). A chironomid-inferred summer temperature reconstruction from subtropical Australia during the last glacial maximum (LGM) and the last deglaciation. *Quaternary Science Reviews*, 122, 282–292.
- Chen, C. R., Hou, E. Q., Condron, L. M., Bacon, G., Esfandbod, M., Olley, J., & Turner, B. L. (2015). Soil phosphorus fractionation and nutrient dynamics along the Cooloola coastal dune chronosequence, southern Queensland, Australia. *Geoderma*, 257–258, 4–13.
- Donders, T. H., Wagner, F., & Visscher, H. (2006). Late Pleistocene and Holocene subtropical vegetation dynamics recorded in perched lake deposits on Fraser Island, Queensland, Australia. *Palaeogeography, Palaeoclimatology, Palaeoecology*, 241(3–4), 417–439.
- Ellerton, D., Rittenour, T., Miot da Silva, G., Gontz, A., Shulmeister, J., Hesp, P., ... Welsh, K. J. (2018). Late-Holocene cliff-top blowout activation and evolution in the Cooloola Sand Mass, south-east Queensland, Australia. *The Holocene*, 28(11), 1697–1711.
- Ewing, R., & Kocurek, G. (2010). Aeolian dune interactions and dune-field pattern formation: White Sands Dune Field, New Mexico. *Sedimentology*, 57(5), 1199–1219.
- Gontz, A. M., Moss, P. T., Sloss, C. R., Petherick, L. M., McCallum, A., & Shapland, F. (2015). Understanding past climate variation and environmental change for the future of an iconic landscape – K'gari Fraser Island, Queensland, Australia. *Australasian Journal of Environmental Management*, 22(2), 105–123.
- Hesp, P. (2002). Foredunes and blowouts: Initiation, geomorphology and dynamics. *Geomorphology*, 48, 245–268.
- Hugenholtz, C., & Barchyn, T. (2010). Spatial analysis of sand dunes with a new global topographic dataset: New approaches and opportunities. *Earth Surface Processes and Landforms*, 35(8), 986–992.
- Hugenholtz, C. H., & Wolfe, S. A. (2005). Biogeomorphic model of dunefield activation and stabilization on the northern great Plains. *Geomorphology*, 70, 53–70.
- Lees, B. G. (2006). Timing and formation of coastal dunes in northern and eastern Australia. *Journal of Coastal Research*, 22(1), 78–89.
- Levin, N. (2011). Climate-driven changes in tropical cyclone intensity shape dune activity on earth's largest sand island. *Geomorphology*, 125(1), 239–252.
- Levin, N., Jablon, P. E., Phinn, S., & Collins, K. (2017). Coastal dune activity and foredune formation on Moreton Island, Australia, 1944–2015. *Aeolian Research*, 25, 107–121.
- Longmore, M. E. (1997). Quaternary palynological records from Perched Lake sediments, Fraser Island, Queensland, Australia: Rainforest, forest history and climatic control. *Australian Journal of Botany*, 45(3), 507–526.
- Longmore, M. E., & Heijnis, H. (1999). Aridity in Australia: Pleistocene records of palaeohydrological and palaeoecological change from the perched lake sediments of Fraser Island, Queensland, Australia. *Quaternary International*, 57–58, 35–47.
- McKee, D., (1979). Sedimentary structures in dunes: A Study of Global Sand Seas. U.S. Geological Survey, 1052, 83–134.
- Miot da Silva, G., & Shulmeister, J. (2016). A review of coastal dunefield evolution in Southeastern Queensland. *Journal of Coastal Research*, 75, 308–312.
- Montgomery, D. (2001). Slope distributions, threshold hillslopes, and steady-state topography. *American Journal of Science*, 301, 432–454.
- Moss, P. T., Tibby, J., Petherick, L., McGowan, H., & Barr, C. (2013). Late quaternary vegetation history of North Stradbroke Island, Queensland, eastern Australia. *Quaternary Science Reviews*, 74(0), 257–272.
- Patton, N., Lohse, K., Godsey, S., Crosby, B., & Seyfried, M. (2018). Predicting soil thickness on soil mantled hillslopes. *Nature Communications*, 9(1), 3329.
- Peel, M. C., Finlayson, B. L., & McMahon, T. A. (2007). Updated world map of the Köppen–Geiger climate classification. *Hydrology and Earth System Sciences*, 11(5), 1633–1644.
- Petherick, L., McGowan, H., & Moss, P. (2008). Climate variability during the last glacial maximum in eastern Australia: Evidence of two stadials? *Journal of Quaternary Science*, 23(8), 787–802.
- Pye, K. (1983). Formation and history of Queensland coastal dunes. *Zeitschrift fuer Geomorphologie*, 45, 175–204.
- Reeve, R., Thompson, C. H., & Fergus, I. F. (1985). *Studies in landscape dynamics in the Cooloola-Noosa River area, Queensland* (4. Hydrology and water chemistry).
- Roskin, J., Katra, L., & Blumberg, D. G. (2013). Late Holocene dune mobilizations in the northwestern Negev dunefield, Israel: A response to combined anthropogenic activity and short-term intensified windiness. *Quaternary International*, 303, 10–23.
- Roy, P. S., & Thom, B. G. (1981). Late quaternary marine deposition in New South Wales and southern Queensland — An evolutionary model. *Journal of the Geological Society of Australia*, 28(3–4), 471–489.

- Tejan-Kella, M. S., Chittleborough, D. J., Fitzpatrick, R. W., Thompson, C. H., Prescott, J. R., & Hutton, J. T. (1990). Thermoluminescence dating of coastal Sand dunes at Cooloola and North Stradbroke Island, Australia. *Soil Genesis, Morphology and Classification*, v. 28, 465–481.
- Thompson, C. H. (1981). Podzol chronosequences on coastal dunes of eastern Australia. *Nature*, 291(7), 59–61.
- Thompson, C. H. (1983). Development and weathering of large parabolic dune systems along the subtropical coast of eastern Australia. *Zeitschrift fuer Geomorphologie*, 45, 205–225.
- Thompson, C. H., & Moore, A. W. (1984). *Studies in landscape dynamics in the Cooloola-Noosa River area, Queensland*. Divisional Report – CSIRO, Australia, Division of Soils Article, v. 73.
- Tsoar, H. (2005). Sand dunes mobility and stability in relation to climate. *Physica A: Statistical Mechanics and its Applications*, 357, 50–56.
- Wasson, R. J., & Hyde, R. (1983). Factors determining desert dune type. *Nature*, 304(5924), 337–339.
- Walker, J., Lees, B., Olley, J., & Thompson, C. (2018). Dating the Cooloola coastal dunes of south-eastern Queensland, Australia. *Marine Geology*, 398, 73–85.
- Ward, W. T. (2006). Coastal dunes and strandplains in southeast Queensland: Sequence and chronology. *Australian Journal of Earth Sciences*, 53(2), 363–373.
- Wardell-Johnson, G., Schoeman, D., Schlacher, T., Wardell-Johnson, A., Weston, M. A., Shimizu, Y., & Conroy, G. (2015). Re-framing values for a world heritage future: What type of icon will K'gari-Fraser Island become? *Australasian Journal of Environmental Management*, 22 (2), 124–148.
- Willett, S. D., Slingerland, R., & Hovius, N. (2001). Uplift, shortening, and steady state topography in active mountain belts. *American Journal of Science*, 301, 455–485.



## A.6.2 Chapters 3 – Earth and Planetary Science Letters



### Measuring landscape evolution from inception to maturity: Insights from a coastal dune system

Nicholas R. Patton<sup>a,b,\*</sup>, James Shulmeister<sup>a,b</sup>, Daniel Ellerton<sup>b,c</sup>, Gilles Seropian<sup>a</sup>

<sup>a</sup> School of Earth and Environment, University of Canterbury, New Zealand

<sup>b</sup> School of Earth and Environmental Sciences, The University of Queensland, Australia

<sup>c</sup> Department of Geological Sciences, Stockholm University, Sweden

#### ARTICLE INFO

##### Article history:

Received 31 August 2021

Received in revised form 18 January 2022

Accepted 18 February 2022

Available online xxx

Editor: J.-P. Avouac

Dataset link: <https://elevation.fdl.org.au/>

Dataset link: <https://qldglobe.information.qld.gov.au/>

##### Keywords:

surface roughness  
curvature  
soil diffusion  
soil transport  
parabolic dunes  
holocene

#### ABSTRACT

The concept of the geomorphic cycle is a foundational principle in geology and geomorphology, but the topographic evolution of a single landscape from inception to maturity has been difficult to demonstrate in nature. The onlapping dunes of the Cooloola Sand Mass (CSM) in eastern Australia provide an ideal chronosequence to evaluate landscape evolution. Here commonly assumed properties on which landscape models are based (i.e., conservation of mass and major factors contributing to landscape change) can be physically measured and accounted for. Our field based measurements and forward numerical models demonstrate that dunes, like other landscapes, relax in an exponential manner. The emplaced dunes evolve through an initial phase of rapid topographic adjustment associated with the dominance of landsliding. This phase continues for ~1 kyr until hillslope gradients are lowered below their angle of repose ( $0.65 \text{ m m}^{-1}$  or  $33^\circ$ ). Once sufficiently lowered, the dunes evolve through slow, soil creep processes. These findings of dual transport regimes are validated by stratigraphic records at all excavated dune foot-slopes and we propose that this evolution can be measured by the distribution of curvature ( $C$ ) of a landform, specifically its standard deviation ( $\sigma_C$ ), as a measure of surface roughness. Surface roughness smooths with time through diffusional sediment transport that lowers local relief. The value and its rate of smoothing can define the stage in evolutionary development and help infer processes, which makes it an important morphometric tool for understanding landscapes. These observations highlight that under stable evolutionary conditions, the development of the landscape is governed by the physical properties of the dune's parent material. In addition, our findings support landscape evolution inferences from numerical and physical models and the coupling of granular material physics with landscape change.

© 2022 Elsevier B.V. All rights reserved.

#### 1. Introduction

The idea of the geomorphic cycle is embedded in our understanding of landscape evolution (Davis, 1892; Gilbert, 1909). The underpinning concept is that gravitationally driven transport processes and consequential erosion and deposition, relax landscapes towards their base-levels while reducing mean local relief (Carson and Kirkby, 1972; Montgomery, 2001). However, it is difficult to measure and describe the complete process in a natural setting. This is due to the fact that landscape evolution typically occurs over geological time scales (Fernandes and Dietrich, 1997) and few systems have adequate dating control over the full duration of ero-

sion to investigate the entire process; nor are many intermediate stages usually preserved. Nevertheless, studies utilize space-for-time substitutions for their experimental design (e.g., Rosenbloom and Anderson, 1994; Stolar et al., 2007; Hilley and Arrowsmith, 2008; Fryirs et al., 2012; Micallef et al., 2014). However, tectonic, lithologic, biologic and climatic forcings that contribute to landscape change are rarely uniform in time and space and cannot be accurately constrained nor can critical assumptions be verified (McKean et al., 1993; Whipple, 2001).

As highlighted by reviews across the geosciences (e.g., Tucker and Hancock, 2010; Minasny et al., 2015; Pawlik and Šamonil, 2018; Jerolmack and Daniels, 2019; Richter et al., 2020), identifying landscapes that can facilitate the use of interdisciplinary methods is vital for understanding earth systems' processes. In this study, we first highlight that the Cooloola Sand Mass (CSM) dune field in Australia provides a true time-for-space substitution to evaluate landscape evolution, see Fig. 1. Here we note that this

\* Corresponding author at: School of Earth and Environment, University of Canterbury, New Zealand.

E-mail address: [Nicholas.Patton@pg.canterbury.ac.nz](mailto:Nicholas.Patton@pg.canterbury.ac.nz) (N.R. Patton).

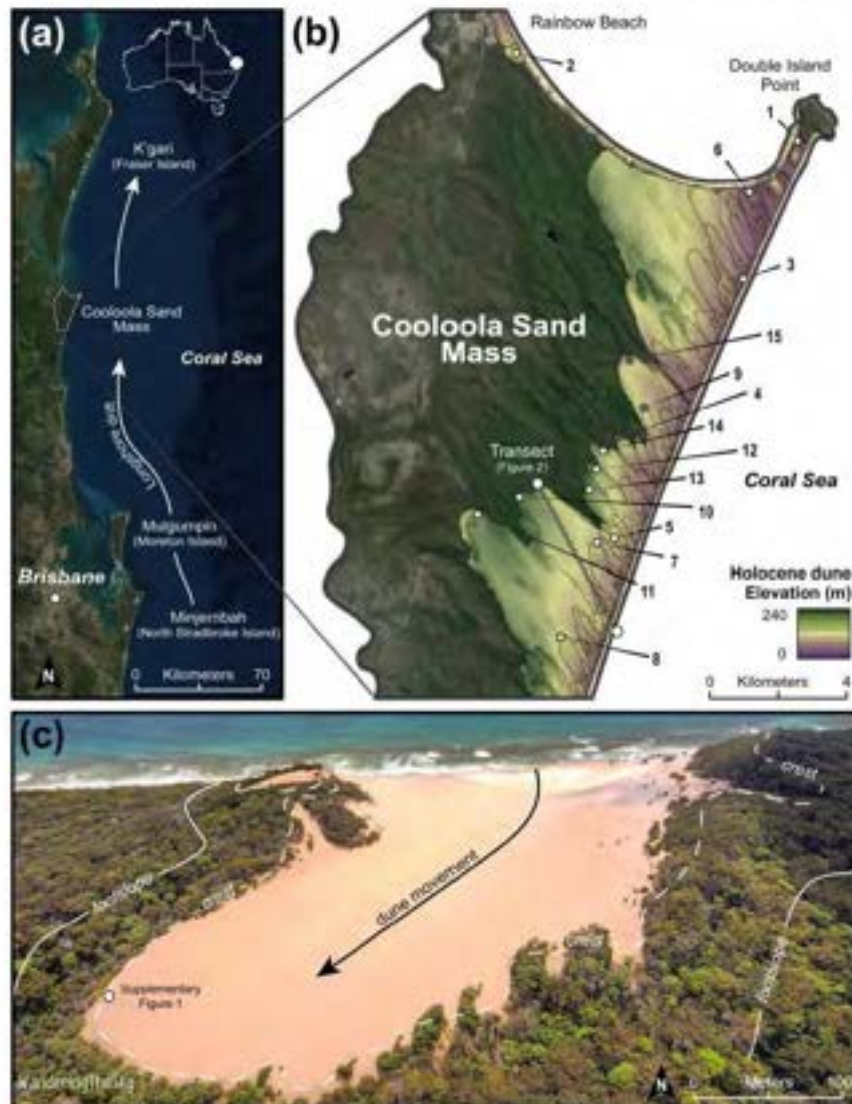


**Fig. 1.** Regional and site location. (a) Satellite imagery of the South East Queensland dune fields in Australia, emphasizing the location of the Cooloola Sand Mass (CSM). (b) Delineated Holocene dunes and their associated elevation at a 5 m resolution (black lines) and location of the 15 dated dunes and 4 soil pits used in this study (white circles and black dots, respectively) (obtained from Walker et al. (2018) and Ellerton et al. (2020), see Table S1, S2, and S3). Note, one soil pit was collected on a dune of a preliminary age of ~2 ka was not utilized in our topographic analyses (white triangle with black dot). A topographic transect aligned parallel to the dominant wind direction, (southeast to northwest), from juvenile to mature dunes is highlighted, see Fig. 2. (c) Aerial view of an incipient parabolic dune forming along the margins of the Carlo Sand Blow near the township of Rainbow Beach (drone photography: "WanderingtheSky"). Note, this active dune (inception) is blown off the coast and extends inland through vegetation and over previously emplaced dunes creating over-steepened lee faces, see Figure S1. (For interpretation of the colors in the figure(s), the reader is referred to the web version of this article.)

dune field offers the closest real world approximation to sandbox models and the application of purely diffusional transport theory is appropriate (a commonly used laboratory based analogue to illustrate erosion and deposition). We then demonstrate this evolution is well characterized by surface roughness, as defined by the standard deviation ( $\sigma_C$ ) of curvature ( $C$ ), due to curvature's mechanistic and empirical relationship with landscape drivers. Lastly, we validate our inferences with sedimentological records and by simulating dune evolution using a two-dimensional numerical evolutionary model.

## 1.1. Study area: the world's premier chronosequence

The Cooloola Sand Mass (CSM) in southeast Queensland, Australia contains coastal dunes that extend back nearly 800 ka (Ellerton et al., 2020) (Fig. 1). The Holocene dunes comprise ~30% of the total area containing >190 parabolic dunes (Patton et al., 2019a), which were created and evolved under similar conditions. The dunes are composed of sands derived from one of the world's longest longshore drift systems (~1500 km) which has generated a nearly limitless supply of homogenous parent material that is



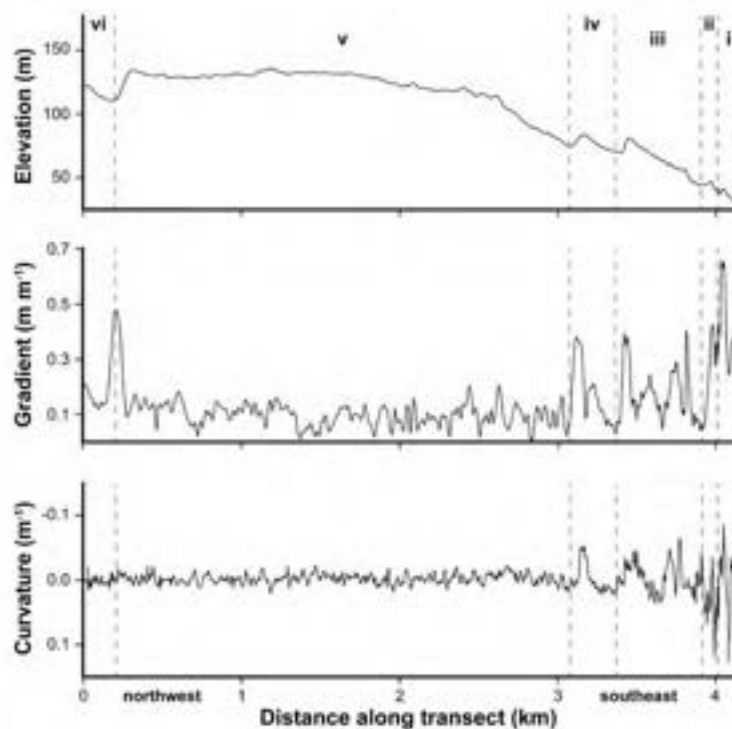


Fig. 2. Changes in topographic variability at the Cooloola Sand Mass (CSM) at a 5 m resolution. A transect aligned parallel to the dominant wind direction (northwest to southeast), seen in Fig. 1b, indicates the transition from juvenile dunes (i) to more mature dunes (ii to vi) moving from the coast inland (right to left). When dunes are stabilized, they have highly variable surface topography. As time continues, their slope relaxes such that morphology is time independent and this evolution can best be described by the dune's curvature, specifically a dune's standard deviation of curvature ( $\sigma_c$ ) as a measure of surface roughness,  $(\sigma_c)/(\sigma_e \rightarrow 0)$ .

>98% medium-fine quartz sand (Boyd et al., 2008). The CSM has been tectonically inactive during this period and experienced only minor eustatic/hydro-isostatic changes in local elevation (sea-level) since the Holocene sea-level highstand (Lewis et al., 2008). In addition, the regional climate has been stable and pollen/palynological proxy records indicate no major changes in vegetation types (e.g., Barr et al., 2017; Schreuder et al., 2019).

Consistent dune activation and emplacement mechanisms promote remarkably uniform morphology. Initiating near the Coral Sea coastline, dunes advance inland by the prevailing wind (dune inception) (Thompson, 1981). The dunes migrate through stands of tall (20–30 m in height) open and closed Eucalyptus forest (canopy cover of 50–80% and >80%, respectively). Their path inland gradually steepens, limiting their progress and permitting rapid colonization of vegetation on the bare hillslopes, thereby emplacing dunes and preserving older dunes. The buttressing of hillslopes and rapid growth of vegetation enable dunes to have over-steepened lee faces built near or above the sand's unmodified angle of repose (gradient of  $0.65 \text{ m m}^{-1}$  or an angle of  $33^\circ$ ) (see Figure S1). As a result, the overlapping dune sequences create a landscape that increases in age while decreasing in topographic variability moving inland from the coast (Fig. 2).

Dune emplacement marks the onset of topographic relaxation (juvenile through old-age stages). The CSM dunes evolve by the reduction of local relief with time under a limited set of sediment (soil) transport processes. The smooth, undissected topography reflects the absence of fluvial transport, which is suppressed by high soil infiltration rates ( $>600 \text{ mm hr}^{-1}$ ) (Reeve et al., 1985). There is consequently a dominance of diffuse grain-by-grain processes. Since the dune sands and the soils they generate are virtually iden-

tical with regard to transportability (i.e., similar bulk density, grain size, and structure), the landscape is not defined and/or limited by development of soil horizons (pedogenesis) – a truly transport limited system. The lack of hillslope-scale water-driven transport and the presence of dune onlapping, limits sediment removal from internal basins, effectively making the Holocene dunes a closed system. As a result, mass is conserved within the boundaries of the CSM, such that all sediment eroded (loss of elevation) is transported only through gravitational hillslope processes and can be accounted for in depositional locations adjacent to the dune ridges as gain of elevation (Fig. 3). Thus, the CSM presents a true space-for-time substitution and illuminates the evolution of an initial topographic form by purely hillslope processes. The dunes retain the depositional legacy of those processes in inland basins, allowing process style and tempo to be inferred. Because of these conditions, we can apply conservation of mass equations to this landscape.

## 1.2. Capturing landscape evolution with surface roughness

On shallow hillslopes, soil transport is commonly described by a linear slope-dependent transport law where soil flux is solely gradient dependent. In this circumstance, sediment flux ( $q_s$ ) per unit width is proportional to hillslope gradient (i.e.,  $\nabla z$ ) (Davis, 1892; Gilbert, 1909):

$$q_s = -K \nabla z, \quad (1)$$

where  $K$  is the soil transport coefficient. Here erosion rates ( $E$ ), can be determined by the divergence of  $q_s$ :

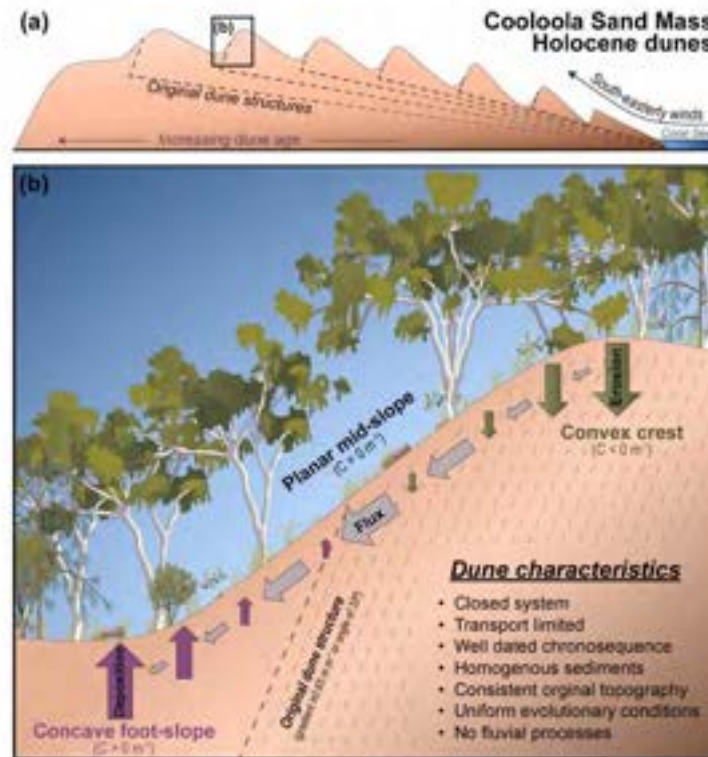


**Fig. 3.** Idealized topography, chronosequence, and hillslope processes of Cooloolo Sand Mass (CSM), Australia. (a) The CSM dunes move inland from the coast across antecedent topography (dashed lines) until wind speeds decrease and dunes emplace (stabilize). With every subsequent dune emplacement, antecedent topography gradients increase therefore decreasing the distance dunes travel inland. (b) Conceptual diagram of hillslope positions and the contribution of erosion, deposition and flux (size of arrow). Once dunes' hillslopes are lowered below their angle of repose (gradient of  $0.85 \text{ m m}^{-1}$  or angle of  $33^\circ$ ), we posit that nonlinear sediment transport effects become negligible. Here only diffusive hillslope processes are active and all sediment removed from crest and ridges can be accounted for in the hollows and valleys (a closed system). As time progresses ridges lower and hollows fill, reducing hillslope gradients and the maximum and minimum curvature values. Combined we hypothesize a systematic decrease in erosion, deposition and flux rates with time.

$$E = \nabla \cdot \mathbf{q}_s = -K \nabla^2 z = -KC, \quad (2)$$

such that curvature ( $C$ ) ( $\nabla^2 z$ , where  $z$  is elevation) is proportional to erosion rate ( $E$ ) (Hurst et al., 2013). As a result, where only diffusive hillslope processes act, the smoothing of the landscape will depend on surface roughness, expressed in terms of standard deviation of  $C$  ( $\sigma_C$ ):

$$\sigma_E = -K\sigma \left( \nabla^2 z \right) = -K\sigma_C, \quad (3)$$

where  $\sigma_C$  captures the spatial variability of erosion rates ( $\sigma_E$ ) such that  $\sigma_E \propto \sigma_C$ . However, when gradients are steep,  $\mathbf{q}_s$  responds nonlinearly to gradient (nonlinear slope-dependent transport) (Roering et al., 1999):

$$\mathbf{q}_s = -K \nabla z \left[ 1 - \left( \frac{|\nabla z|}{S_c} \right)^2 \right]^{-1}, \quad (4)$$

such that  $\mathbf{q}_s$  becomes infinite as a hillslope's gradient approaches a critical gradient or threshold slope ( $S_c$ ), which is associated with the angle of repose (Roering et al., 1999). In this circumstance,  $E$  is no longer linearly related to  $C$ , showing instead greater sensitivity at higher gradients.

Despite this apparent theoretical limitation on steeper slopes, recent studies have highlighted surface roughness as a promising metric to empirically measure and characterize landscape form. It shows consistent relationships to erosion rates and processes

in landscapes where diffusional processes act. While evaluating catchment-wide soil thicknesses, Patton et al. (2018) found that across diverse sites, catchments with broad  $C$  distributions (high surface roughness), relate to a general increase in catchment  $E$ , soil thickness variability and sediment transport styles (i.e., soil creep to landslides), even when landscapes are steep and suggest nonlinear transport (Eq. (1) or Eq. (4)). Moreover, it has been observed on landslide deposits, that changes in surface roughness can be used to define landform ages and this evolution is best described through nonlinear sediment transport (Booth et al., 2017; LaHusen et al., 2020). Combined, the results of these studies and others (e.g., Korzeniewska et al., 2018; Berti et al., 2013), suggest that surface roughness is an essential morphometric tool to measure and define a landscape's stage of geomorphic evolution. We hypothesize surface roughness ( $\sigma_C$ ) to have enhanced utility in the CSM where transport is purely diffusional (juvenile through old age stages) because of the linear relationship between  $E$  and  $C$ , except where slopes approach the angle of repose, which only comprises <2% of the CSM's total land area, see Fig. 4.

## 2. Methods

### 2.1. Dune selection and OSL dating overview

We focus on the Holocene sections of the Cooloolo Sand Mass (CSM), as mapped by Ward (2006) and Patton et al. (2019a). We acquired all previously published small aliquot (Ellerton et al.,



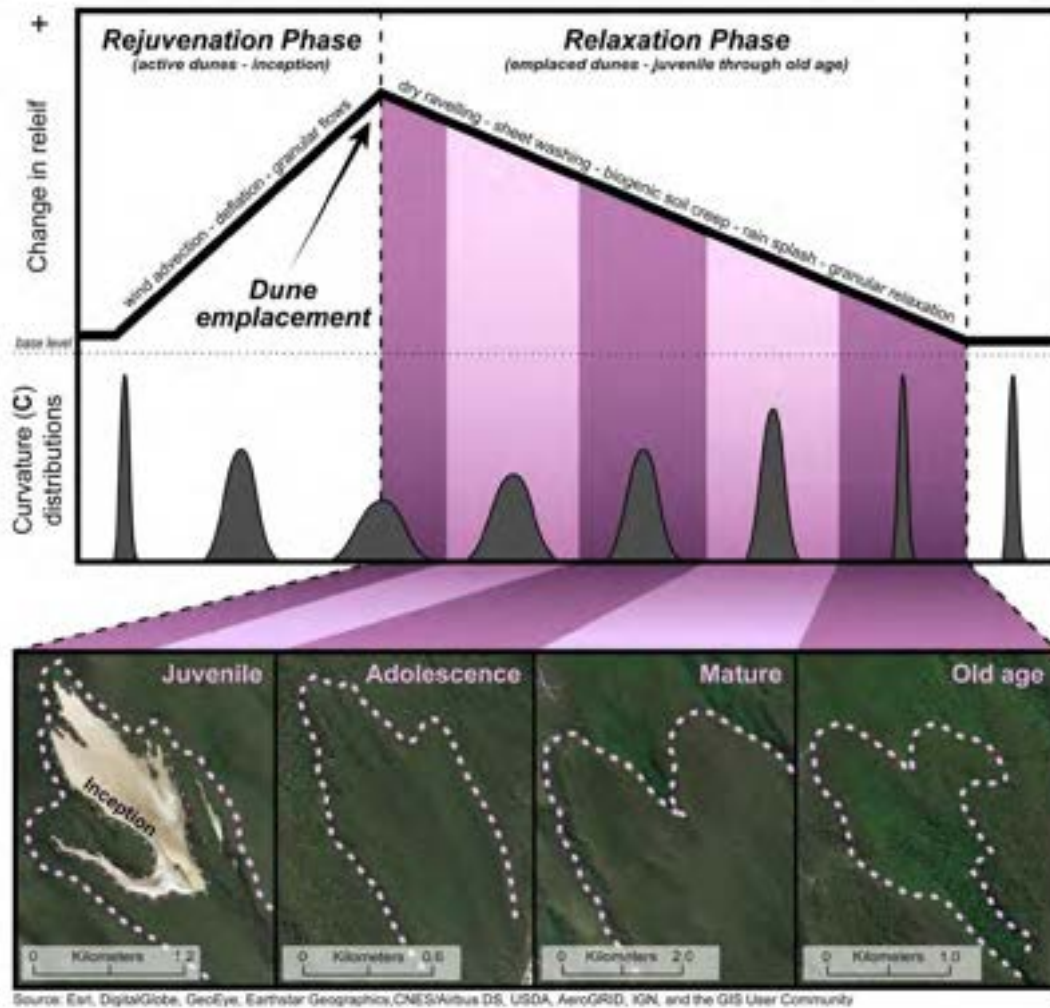


Fig. 4. Conceptual diagram (summarizes hypotheses and main findings) inspired by Montgomery (2001). The relationship between change in elevation from base level, dominant transport styles, and curvature ( $C$ ) distributions ( $\sigma_C$ ) for a dune landscape with time is shown. The dunes found at Cooloola Sand Mass (CSM) are initially smooth (low  $\sigma_C$  and narrow  $C$  distributions) when they are actively migrating across the landscape (dune inception). As the dunes begin to stabilize, the competition between wind advection and vegetation stabilization, results in an increase in topographic variability, broadening the  $C$  distribution (greater  $\sigma_C$ ) and thus increasing erosion rates. This positive change in  $\sigma_C$  represents a phase of landscape rejuvenation. Surface roughness reaches their highest values once dunes are fully stabilized (dune emplacement) and sediment transport is limited to hillslope processes, thus marking the relaxation phase (juvenile through old age stages). The lowering of crest and filling of hollows narrows  $C$  distribution (lower  $\sigma_C$ ) thus decreasing the dune's erosion rates. Given ample time in a relaxation phase, the landscape will evolve towards senescence ( $(\partial\sigma_C)/\partial t \rightarrow 0$ ) where no local relief remains. We hypothesize that dune  $\sigma_C$  can only smooth (decrease) in the relaxation phase. Aerial images of the delineated dunes and the stage of their evolutionary development highlight these changes. Further description of dune stages can be found in Table S1 and S2.

2020) and single grain (Walker et al., 2018). Optically Stimulated Luminescence (OSL) ages from emplaced Holocene dunes within the CSM (juvenile through mature dunes). Dates represent the time of dune emplacement and consequently the initiation of dune relaxation. We choose to select ages either from dune apices or along the crest of the trailing ridges to ensure primary aeolian deposition. If dunes have multiple ages, we preferentially select dates obtained at dune crests and from stratigraphically lower positions. In total, 15 dunes met our criteria and were utilized to produce the age-roughness relationship, see Table S1.

## 2.2. Dune delineation

We use high resolution elevation data, satellite imagery and a series of field campaigns to identify and validate our mapping ef-

forts. Principally, we used publicly available 1 m resolution digital elevation model (DEM) derived from Light Detection and Ranging (LiDAR) (2011 Queensland LiDAR data) and Orthophoto imagery (1:5000) acquired through Queensland Globe. Dated dunes are individually defined as polygons in ArcMAP and delineated at the base of crests and trailing arms. Each dune was allocated into a geomorphic stage according to definitions given in Table S2. A more detailed explanation of our mapping procedures can be found in Patton et al. (2019a).

## 2.3. Foot-slope excavation and depositional characterization

We utilize depositional foot-slope positions from parabolic dunes ranging in age and surface roughness ( $\sigma_C$ ) to evaluate and characterize records of sediment transport and erosion. Sites are

selected with similar aspects and hillslope lengths (parallel to contemporary sediment transport direction). At each site, we identify and record depositional and erosional features (scarps, lobes, burrows, pits and mounds) to help infer active sediment transport styles (landsliding, sheet-washing, biogenic soil creep, etc.). Soil profiles (1 m by 2 m) are excavated to a depth >1.75 m and described using standard field protocols (i.e., grain size, sorting, roundness, bedding structures, Munsell color and texture).

#### 2.4. Selection of topographic indices

In this study, we have evaluated the application of common morphometric variables such as elevation, slope, and curvature for all delineated dunes. Ultimately curvature ( $C$ ), and more specifically the standard deviation of curvature ( $\sigma_C$ ), as a measurement of surface roughness was chosen for our study for four main reasons:

1) Curvature governs the convergence and divergence of sediment transport hence influences water flow paths (Bogaart and Troch, 2006), nutrient redistribution (Ritchie et al., 2007; Patton et al., 2019b), and soil characteristics (Minasny and McBratney, 2016). These consequently affect landscape evolution. In particular,  $C$  has been used as a surrogate for mobile soil (regolith) thickness (Dietrich et al., 1995; Catani et al., 2010; Patton et al., 2018) and in the derivation of soil production functions and erosion rates (Heimsath et al., 1997; Hurst et al., 2012; Gabet et al., 2021; Struble and Roering, 2021). This makes  $C$  a logical candidate to describe landscape evolution.

2)  $C$  and  $\sigma_C$  normalize for antecedent topography on which dunes were emplaced and allow us to compare dunes of varying ages across the whole dune field. Curvature is the spatial rate of change of gradient from a fixed position in all directions and hence is insensitive to gradient biases introduced by broad-scale topography. Despite initial similarity in most respects, antecedent topography plays a role in controlling initial slope conditions. Dunes that have advanced over a flat plain have internal basins with different (lower) slopes than those that have advanced through previously emplaced dune sequences (Fig. 2 and 3). A desirable feature of  $C$  is that all landforms' curvature distributions are centered at zero (Patton et al., 2018), which makes it possible to make straightforward comparisons between dunes'  $\sigma_C$  values.

3)  $\sigma_C$  follows Hani et al.'s (2011) recommendations for ideal morphometric variables. In short,  $\sigma_C$  provides unique values that are independent of rotations or translations, discriminates between varying surfaces (i.e., amplitudes, frequencies, and correlations), describes innate properties of the landscape surfaces, represents local (not global) measurements, is physically meaningful, and easy to derive.

4) More complex methods have been used to describe topographic variability (e.g., root mean squared-based models, two dimensional variograms, and wavelet lifting schemes); however, the difference between each method's outcome is likely insignificant and largely site specific, see Berti et al. (2013) for a discussion on this.

#### 2.5. Calculation of curvature and surface roughness

Curvature ( $C$ ) was calculated using the equation derived from Zevenbergen and Thorne (1987) and Moore et al. (1991) in ArcGIS (version 10.8.1) spatial analysis tools. This calculation utilizes a 3 by 3 matrix around a central node ( $z_5$ ) (Figure S2) and fits a surface ( $z$ ) to the surrounding nine nodes using a moving window:

$$z = Ax^2y^2 + Bx^2y + Cxy^2 + Dx^2 + Ey^2 + Fxy + Gx + Hy + I, \quad (5)$$

where the nine coefficients (A through I) are:

$$A = [(z_1 + z_3 + z_7 + z_9) \div 4 - (z_2 + z_4 + z_6 + z_8) \div 2 + z_5] \div L^4 \quad (5a)$$

$$B = [(z_1 + z_3 - z_7 - z_9) \div 4 - (z_2 - z_8) \div 2] \div L^3 \quad (5b)$$

$$C = [(-z_1 + z_3 - z_7 + z_9) \div 4 + (z_4 - z_6) \div 2] \div L^3 \quad (5c)$$

$$D = [(z_4 + z_6) \div 2 - z_5] \div L^2 \quad (5d)$$

$$E = [(z_2 + z_8) \div 2 - z_5] \div L^2 \quad (5e)$$

$$F = (-z_1 + z_3 + z_7 - z_9) \div 4L^2 \quad (5f)$$

$$G = (-z_4 + z_6) \div 2L \quad (5g)$$

$$H = (z_2 - z_8) \div 2L \quad (5h)$$

$$I = z_5 \quad (5i)$$

Curvature is calculated from the above equations:

$$\nabla^2 z = C = 2(D + E). \quad (6)$$

The original equation by Zevenbergen and Thorne (1987) and Moore et al. (1991) differentiates the slope in percent rather than the actual gradient, and reverses the sign, so to compute curvature values in units  $1 \text{ m}^{-1}$ ; we removed -100 from their equation. This makes positive values represent concavity (hollows) and negative values represent convexity (ridges/crest).

We elected to resample the original DEM using bilinear interpolation to a 5 m resolution to dampen topographic noise, remove DEM artefacts, decrease roughness associated with dense vegetation (Berti et al., 2013; Patton et al., 2019a), and to help place our curvature values in the context of previous work (Patton et al., 2018). Surface roughness ( $\sigma_C$ ) was determined by calculating the standard deviation of  $C$  for the defined polygon of each dune. All areas presently undergoing active local reactivation, recently disturbed (e.g., streets, mines, and buildings), and/or currently water affected (e.g., lakes and swamps) were removed and not included within our statistical analysis. Note,  $C$  and  $\sigma_C$  are extremely sensitive to the quality of the original elevation model or changes to boundary conditions (i.e., extent of the DEM and/or shape and size which statistics are calculated), methodology, and/or processes. Minor variability in absolute values may occur; however, overall trends remain consistent.

#### 2.6. Two-dimensional dune evolution models

We utilized two-dimensional (2-D) sediment transport models to provide a general explanation of landscape evolution for the dune field and to examine the ability of surface roughness ( $\sigma_C$ ) to change with time. We applied the 5 m DEM from the CSM and ran linear and nonlinear landscape evolution with  $K$  values (spanning from  $0.001 \text{ m}^2 \text{ yr}^{-1}$  to  $0.100 \text{ m}^2 \text{ yr}^{-1}$  covering a range of previously reported values (Hurst et al., 2013)) for a model time of 10 ka.

The linear simulated land surface evolved by solving Eq. (2), using a forward finite difference scheme with yearly time steps. At each time step,  $C$  and  $E$  were calculated and  $E$  was then multiplied by the time step to compute land surface lowering (erosion) or rise (deposition). For nonlinear evolution, we utilized a 2-D model from Booth et al. (2017) which uses Eq. (4). Similar to the linear model, we make multiple simulations with different parameterizations of the physical properties of the dune sands. We used a selected  $S_c$  value of  $0.65 \text{ m m}^{-1}$  to represent the angle of repose of the original dune material. We performed simulations and calculated  $\sigma_C$  and the standard deviation of  $E$  ( $\sigma_E$ ) for each dune every 1 ka. We selected  $K$  values and chose one (based on observed goodness of fit with all of our measured dune  $\sigma_C$ ). Note, simulated



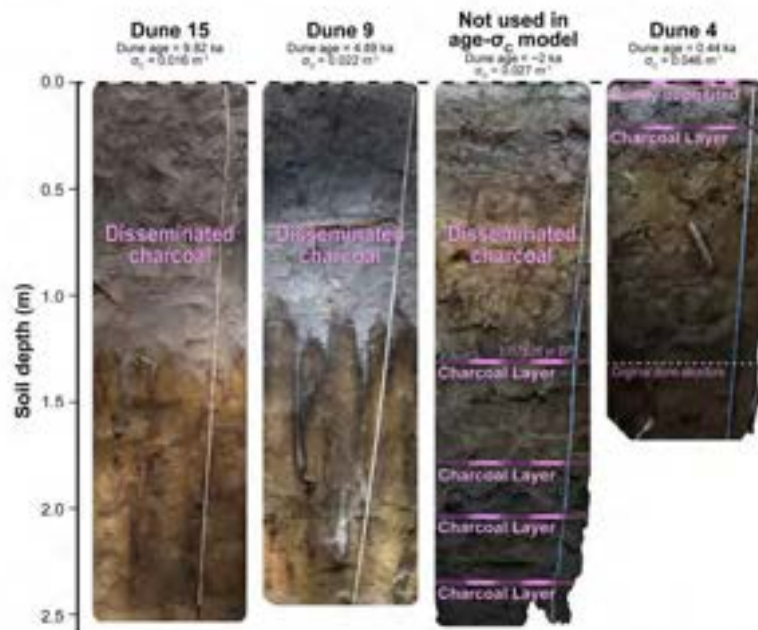


Fig. 5. Excavated depositional foot-slope soil profiles used to characterize erosion and sediment transport styles. Oldest profiles display disseminated charcoal through the full profile whereas the two youngest deposits have charcoal layers. Note the ~2 ka dune record (preliminary age) with disseminated charcoal near the surface that switches to stratified charcoal layers near the base. This transition at ~1.1 m corresponds with a depositional age of ~1 kyr (determined by a radiocarbon age of  $1017 \pm 26$  yr BP (Wk50298) at 1.2–1.3 m, Table S4). We infer the presence of these layers is associated with fire induced mass-movement (dry raveling and sheet-washing) when dunes are young and have steep slopes. As time progresses, hillslope gradients lower and charcoal layers become more diffuse and eventually become disseminated throughout the profile. These records highlight the transition between episodic to continuous sediment transport on dune evolution.

dune evolution is utilized to produce general age-roughness relationships, such that  $(\partial\sigma_c)/\partial t$  or  $\sigma_c$  and modelled  $\sigma_c \propto \sigma_c$  can be evaluated.

### 3. Results

Four ( $n=4$ ) depositional soil profiles at the base of ~70 m hillslopes were excavated from dunes ranging in  $\sigma_c$  (from 0.046 to 0.016  $m^{-1}$ ) and ages (from 0.44 to 9.82 ka) to ~1.75 m in depth, Fig. 5 and Table S3. All sites contain evidence of soil creep processes (burrows, pit and mounds, and root growth and decay); whereas, only the youngest dune displayed evidence of mass-movement with a 10 cm sheet-wash deposit from a recent fire event. All soil profiles have abundant charcoal records with the highest concentrations near the surface. The oldest two sites (4.89 ka and 9.82 ka) have charcoal evenly disseminated through the full excavated profile. In contrast, the ~2 ka site has disseminated charcoal within the top 1.1 m; however, below this depth (marking the first thousand years of sediment deposition, Tables S3 and S4) charcoal is present in distinct layers. The youngest site (0.44 ka) only contains one charcoal layer near the surface.

In total, 15 OSL dated dunes were used in this study, Table S1. All CSM dunes exhibit normal distributions of C of mean ~0  $m^{-1}$  and their surface roughness ( $\sigma_c$ ) declines by a factor of about 5 (from 0.083 to 0.015  $m^{-1}$ ) as dunes increase in age and decrease in local relief and hillslope gradients (Fig. 6a). The time series of  $\sigma_c$  depicts a “horizontal hockey stick” with two distinct phases: 1) an initial rapid decay within the first thousand years after dune emplacement; 2) transitioning to a phase of gradual decline between a  $\sigma_c$  of 0.035–0.045  $m^{-1}$  (Fig. 6b). We define this measured  $\sigma_c$  interval as the “transitional zone” where the presence of episodic mass movement is no longer observed as dunes increase in age (values between Dunes 4 and 5).

The evolution of surface roughness ( $\sigma_c$ ) for the entire CSM is best explained by nonlinear sediment transport with a fixed K value of 0.002  $m^2 yr^{-1}$  and a  $S_c$  of 0.65  $m m^{-1}$ . In reality, simulated topography appears to be more closely represented by an initial K value of 0.06  $m^2 yr^{-1}$  then switching to 0.002  $m^2 yr^{-1}$  at the “transitional zone” near ~1 ka (Figure S3 and S4). Our selected K values are comparable to other values derived from transport-limited systems and sand pile experiments (e.g., Hurst et al., 2013 and Roering et al., 2001). All simulated dune topography continues to have normally distributed C with means centered on ~0  $m^{-1}$ , and distributions that gradually narrow with time. Regardless of the transport mode (linear or nonlinear), dune  $\sigma_c$  has a positive monotonic relationship with its modelled variability of erosion rate ( $\sigma_c$ ), and this relationship continues as dunes relax (Figure S3b).

### 4. Discussion

#### 4.1. Parent material controls on dune evolution

Our results indicate that the measured break in topographic decay at the transitional zone reflects a shift in dominant transport styles associated with soil transport efficiency (K). Booth et al. (2017) observed a similar rapid decay in surface roughness within the first thousand years on landslide deposits. They suggested this phase change was likely due to higher K values during the initial emplacement linked to shifts in climate and vegetation. In the CSM, climate and vegetation are stable throughout this period, so we propose this break reflects an internal transition to a reduction of slope below the critical gradient ( $S_c$ ). In fact, this topographic adjustment has been demonstrated in sandbox experiments and modelled as the transition between episodic to continuous sediment transport processes (Roering et al., 2001). The transitional

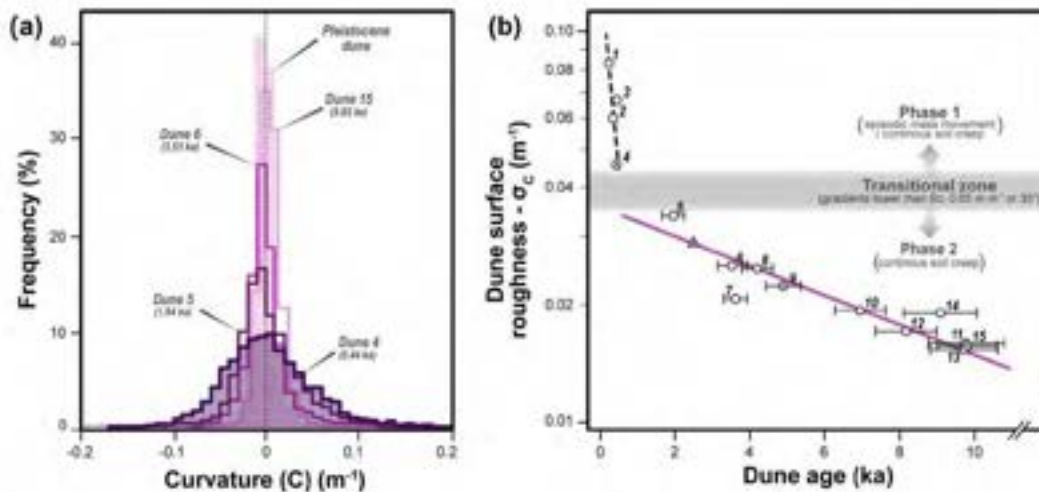


Fig. 6. Measuring landscapes evolution through time at the Cooloola Sand Mass (CSM). (a) Observed curvature ( $C$ ) distributions for four Holocene and one Pleistocene dune at the CSM. Note the normal distribution of  $C$  centered on planar topography ( $0 \text{ m}^{-1}$ ) and the gradual narrowing of distributions with time (dark to light frequency). (b) Measured dune age (with error bars,  $\pm 1 \text{ ka}$ ) with surface roughness ( $\sigma_c$ ) (white circles) and observed dominant transport styles. All dunes with excavated soil profiles are indicated with black dots. Additionally, the  $\sim 2 \text{ ka}$  dune with the excavated soil profile (not utilized in our topographic analyses) is represented by the white triangle. Initially, dunes are emplaced with over-steepened hillslopes at or above the critical gradient ( $S_c$ ). During this phase, there is a dominance of episodic mass movement (dry ravel and sheet-wash ( $n=4$ )), purple dashed line. After dunes'  $\sigma_c$  are lowered below a "transitional zone" (at  $\sim 1 \text{ kyr}$ ), only slow and continuous soil transport occurs (soil creep ( $n=11$ )), pink line. This behavior continues and remains true for the Pleistocene dunes (grey diamonds, not included in this analysis).

zone value is set by the physical properties of the dune sands (i.e., surface roughness values associated with the presence or absence of gradients greater than its angle of repose) and as a result, the measured transition zone is specific to the CSM.

The early phase of evolution of the youngest dunes, which retain steep slopes, corresponds with the period when episodic mass movement on steeper slopes is significant (purple dashed line Fig. 6b). When hillslope gradients are below the  $S_c$ , slow continuous soil creep prevails and a simple first order relationship of the form  $(\partial \sigma_c) / \partial t \propto \sigma_c$  is apparent (pink line Fig. 6b). In this phase, all dune erosion rates become increasingly uniform and their evolution behaves in a linear slope dependent way (Figure S3b). These results follow our field observations that younger dunes experience a wider variety of sediment transport styles that are both discontinuous in frequency and magnitude compared to older dunes. We infer that disturbances, such as burning or storms, switch the dunes from essentially slow continuous soil transport to episodic mass movement, but mass movement is only manifested on the younger, steeper dunes with higher surface roughness (increased  $\sigma_c$  values).

#### 4.2. Field observations and stratigraphic records

Field observations support the presence of two phases of dune evolution (Fig. 5 and 7). On active dunes built above their  $S_c$ , episodic mass movement (i.e., dry raveling and sheet-washing) is observed. After emplacement, episodic mass movement continues to operate as a result of disturbance events, mostly fires. Fires temporarily generate hydrophobic surface soils and increase local soil transport efficiency ( $K$ ) (Bridge and Ross, 1983), thereby promoting rapid lowering of relief. Although fires occur with constant frequency and across dunes of all ages (Moss et al., 2013), higher erosion and flux rates caused by episodic mass movement are limited to the first thousand years of dune development (Fig. 6b). After the dunes' gradients are reduced below the  $S_c$ , gradual transport regimes controlled by soil creep dominate (i.e., granular relaxation, bioturbation, and rain splash) and podsolization is well expressed.

As a result, these degraded dunes are resistant to episodic mass movement.

A major fire event in 2019 only shows evidence of mass movement on younger dunes, initiating on over-steepened, lee faces near dune crests. Though short-lived, the landscape was efficiently smoothed by lowering local highs and filling local lows (Jyotsna and Haff, 1997) (Fig. 7b) and within just three months, the disturbed portions of the landscape were stabilized by new vegetation growth.

These types of disturbance events are recorded in depositional foot-slopes (Fig. 5) (Roering and Gerber, 2005). Within the early stages of dune evolution, sedimentary infills are characterized by stratified layers of charcoal, associated with episodic mass movement. As time progresses, these layers become more diffuse and eventually charcoal is disseminated through the profile due to the influence of slow continuous transport and mixing. These records of dual transport regimes are found at all excavated foot-slope positions and demonstrate the consistency of the landscape to transition from landsliding to soil creep processes.

#### 5. Conclusions

The Holocene dunes in the Cooloola Sand Mass (CSM) provide a highly resolved space-for-time substitution where most major factors contributing to landscape evolution are known. The fidelity of the landscape to preserve dunes from inception to topographic maturity makes it possible to demonstrate how transport processes, erosion, and deposition act on topography to relax landscapes. The dominance of diffusional processes and the assumption of sediment mass balance from erosional into depositional positions is valid, whereas this is not demonstrable in most landscapes. As a result, the dunes' topographic and stratigraphic records validate the presence of dual soil transport regimes. The early phase of dune development evolves through episodic mass movement which is facilitated by wildfires on over steepened gradients. Once lowered below their  $S_c$ , the later phase of continuous soil creep processes persists. This transition is preserved as infill at all foot-



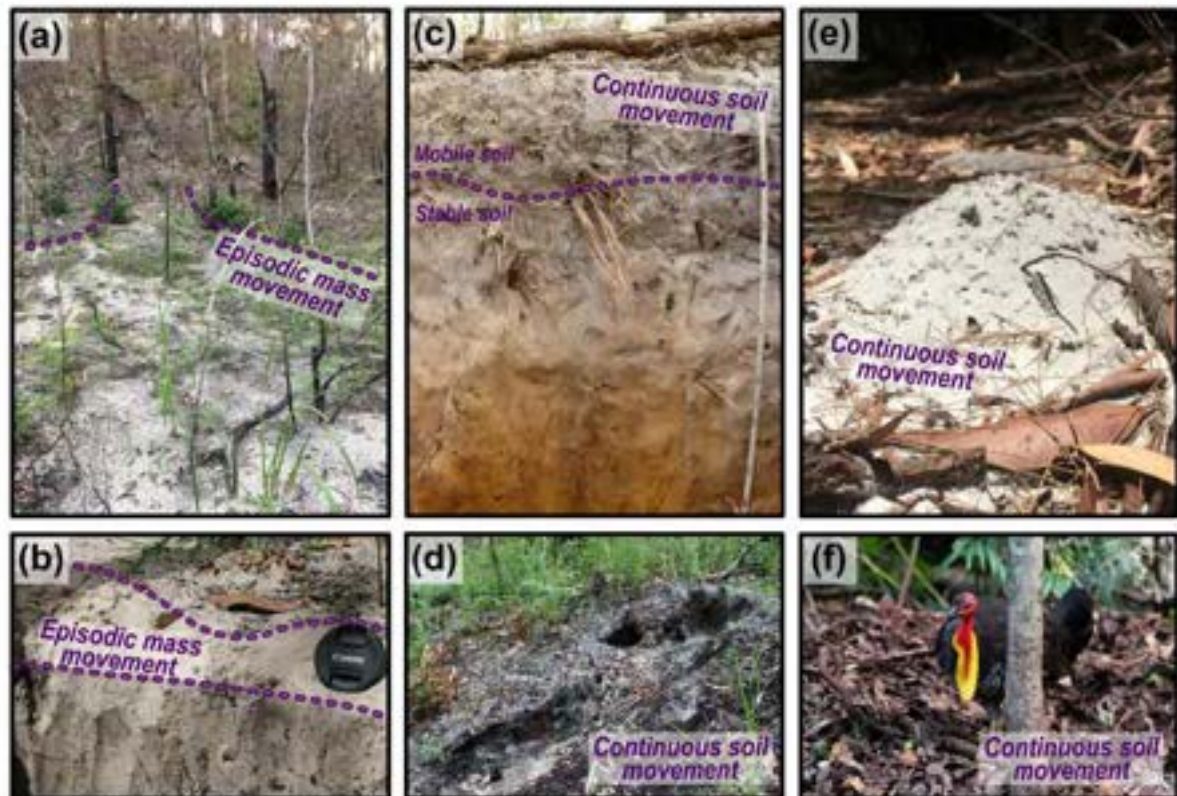


Fig. 7. Field images of typical soil transport styles. Commonly observed episodic (panels (a) and (b)) and continuous (panels (c), (d), (e), and (f)) soil transport mechanisms at the Cooloola Sand Mass. (a) Fire induced sand ravel and sheet-wash movement on the steep lee facing hillside of a 0.44 ka dune shortly after fire event and its associated (b) deposition. (c) Common mid-slope soil profile on a Holocene age dune highlighting the abundance of biogenic disturbed soil near the surface in the A-horizon, where it becomes increasingly stable moving down profile as shown by the intact E- and B-horizons. Typical perturbation includes root growth and decay, (d) tree throw, (e) burrowing invertebrates, and (f) bird nest construction (photo credit: (c) Patrick Adams and (f) Kesham Hovsepian).

slope positions and confirms that variations in sediment delivery to depositional areas are due to changes in hillslope steepness and not a shift in climate.

Adopting  $C$  as a surrogate for landscape change, we evaluate dunes'  $C$  distribution ( $\sigma_C$ ) as a measure of surface roughness and capture the CSM's full morphological evolution. When  $C$  distributions are broad (larger  $\sigma_C$  values) erosion and deposition rates reach more extreme values with a wider variety of transport styles compared to narrow distributions (smaller  $\sigma_C$  values). Once gradients are lowered below their  $S_C$  and soil creep dominates, the landscape can be numerically explained through process-based conservation of mass equations (Eq. (1)–(3)). The marked shift of  $\sigma_C$  coinciding with the transition between landsliding to soil creep provides evidence that evaluating  $\sigma_C$  with time can highlight changes in geomorphic processes and/or their rates (Paton et al., 2018). Our findings reveal the complete evolution of a dune sequence and identify these systems as an ideal natural laboratory to understand landscape change. We demonstrate that forward numerical models generate outcomes that closely parallel the evolution of the CSM. The physical properties of the original dune material are the primary control on how the dune evolves and the  $\sigma_C$  value associated with the transitional zone. Consequently, our observations validate landscape evolution inferences from sandbox modelling (e.g., Roering et al., 2001) and support the coupling between granular material physics and landscape change (e.g., Deshpande et al., 2021).

## Funding

Funding for this study was provided by the Australian Research Council (ARC) grant number DP150101513.

## CRediT authorship contribution statement

N.R.P. formulated the idea of the manuscript. N.R.P., D.E. and J.S. carried out fieldwork and the analyses. N.R.P. and J.S. drafted the manuscript with inputs from G.S., and D.E. G.S. and N.R.P. modelled landscape evolution. All authors assisted with writing and editing the manuscript.

## Declaration of competing interest

The authors declare that they have no known competing financial interests or personal relationships that could have appeared to influence the work reported in this paper.

## Data and materials availability

All data necessary to generate results for this study are available in the supplementary information. All LiDAR datasets were downloaded from <https://elevation.ssf.org.au/> and all aerial photographs were downloaded from <https://qldglobe.information.qld.gov.au/>.



## Acknowledgements

We acknowledge the traditional owners of the Cooloola Sand Mass (the Butchulla and Kabi Kabi peoples) and their elders past, present and emerging. The field work and mapping was undertaken using permit WTK15791415. Funding for this study was provided by the Australian Research Council (ARC) grant number DP150101513. We thank the assistance provided to us by the National Parks and Wildlife Service. We would also like to thank Peter Almond, Tim Stahl, Jiawei Zheng, and the two anonymous reviewers for their valuable modelling advice and comments on this manuscript.

## Appendix A. Supplementary material

Supplementary material related to this article can be found online at <https://doi.org/10.1016/j.epsl.2022.117448>.

## References

- Barr, C., Tibby, J., Moss, R.T., Halverson, G.P., Marshall, J.C., McGregor, G.B., Stirling, E., 2017. A 25,000-year record of environmental change from Weibey Lagoon, North Stradbroke Island, in the Australian subtropics. *Quat. Int.* 449, 106–118. <https://doi.org/10.1016/j.quaint.2017.04.011>.
- Berti, M., Corsini, A., Darbush, A., 2013. Comparative analysis of surface roughness algorithms for the identification of active landslides. *Geomorphology* 182, 1–18.
- Bogaart, P.W., Troch, P.A., 2006. Curvature distribution within hillslopes and catchments and its effect on the hydrological response. *Hydrol. Earth Syst. Sci. Discuss.*, European Geosciences Union 3 (3), 1071–1104. <https://doi.org/10.5194/hess-10-825-2006>.
- Booth, A.M., LaHusen, S.R., Davall, A.R., Montgomery, D.R., 2017. Holocene history of deep-seated landsliding in the North Fork Stillaguamish River valley from surface roughness analysis, radiocarbon dating, and numerical landscape evolution modeling. *J. Geophys. Res., Earth Surf.* 122 (2), 456–472. <https://doi.org/10.1002/2016JF003934>.
- Boyd, R., Rinning, K., Goodwin, I., Sandstrom, M., Schröder-Adams, C., 2008. High-stand transport of coastal sand to the deep ocean: a case study from Fraser Island, southeast Australia. *Geology* 36 (1), 15–18. <https://doi.org/10.1130/G24215A.1>.
- Bridge, S.J., Ross, P.J., 1983. Water erosion in vegetated sand dunes at Cooloola, South-East Queensland. *Z. Geomorphol., Suppl.* 45, 227–244.
- Carson, M.A., Kirkby, M.J., 1972. *Hillslope Form and Process*. Cambridge University Press, New York.
- Catani, F., Segoni, S., Falconi, G., 2010. An empirical geomorphology-based approach to the spatial prediction of soil thickness at catchment scale. *Water Resour. Res.* 46 (5). <https://doi.org/10.1029/2009WR007450>.
- Davis, W.M., 1902. The convex profile of hilly land. *Science* 20, 245.
- Dietrich, W.E., Reis, R., Hou, M.L., Montgomery, D.R., 1995. A process-based model for colluvial soil depth and shallow landsliding using digital elevation data. *Hydrol. Process.* 9, 383–400. <https://doi.org/10.1002/hyp.3360090311>.
- Deshaies, N.S., Furbish, D.J., Asanisi, P.E., Jerolmack, D.J., 2021. The perpetual fragility of creeping hillslopes. *Nat. Commun.* 12 (1), 1–7. <https://doi.org/10.1038/s41467-021-23979-z>.
- Ellerton, D., Rittenour, T., Shulmeister, J., Gontz, A., Welsh, K.J., Paton, N.R., 2020. An 800 kyr record of dune emplacement in relationship to high sea level forcing, Cooloola Sand Mass, Queensland, Australia. *Geomorphology* 354, 106999. <https://doi.org/10.1016/j.geomorph.2019.106999>.
- Fernandes, N.F., Dietrich, W.E., 1997. Hillslope evolution by diffusive processes: the timescale for equilibrium adjustments. *Water Resour. Res.* 33, 1307–1318. <https://doi.org/10.1029/97WR00534>.
- Fryin, K., Brierley, G.J., Erskine, W.D., 2012. Use of ergodic reasoning to reconstruct the historical range of variability and evolutionary trajectory of rivers. *Earth Surf. Process. Landf.* 37 (7), 763–773. <https://doi.org/10.1002/esp.3210>.
- Gabet, E.J., Mudd, S.M., Wood, R.W., Grieve, S.W.D., Binnie, S.A., Dunai, T.J., 2021. Hillslope curvature increases with the square root of erosion rate. *J. Geophys. Res., Earth Surf.* 126 (5). <https://doi.org/10.1029/2020JF005858>.
- Gilbert, G.K., 1908. The convexity of hillslopes. *J. Geol.* 17 (4), 344–350.
- Hani, A.P., Sathiyamoorthy, D., Asirvadam, V.S., 2011. A method for computation of surface roughness of digital elevation model terrain via multiscale analysis. *Comput. Geosci.* 37, 177–192. <https://doi.org/10.1016/j.cageo.2010.05.021>.
- Heinsath, A., Dietrich, W., Nishizumi, K., et al., 1997. The soil production function and landscape equilibrium. *Nature* 388, 358–361. <https://doi.org/10.1038/41056>.
- Hilley, G.E., Arrowsmith, J.R., 2008. Geomorphic response to uplift along the Dragon's Back pressure ridge, Carrizo Plain, California. *Geology* 36 (5), 367–370. <https://doi.org/10.1130/G24517A.1>.
- Hurst, M.D., Mudd, S.M., Walcott, R., Attal, M., Yoo, K., 2012. Using hilltop curvature to derive the spatial distribution of erosion rates. *J. Geophys. Res., Earth Surf.* 117 (F2). <https://doi.org/10.1029/2011JF002057>.
- Hurst, M.D., Mudd, S.M., Yoo, K., Attal, M., Walcott, R., 2013. Influence of lithology on hillslope morphology and response to tectonic forcing in the northern Sierra Nevada of California. *J. Geophys. Res., Earth Surf.* 118 (2), 832–851. <https://doi.org/10.1002/jgrf.20045>.
- Jerolmack, D.J., Daniels, K.E., 2019. Viewing Earth's surface as a soft-matter landscape. *Nat. Rev. Phys.*, 1–15. <https://doi.org/10.1038/s42254-019-0111-z>.
- Joynt, R., Huff, P.K., 1997. Microtopography as an indicator of modern hillslope diffusivity in arid terrain. *Geology* 25, 695–698. [https://doi.org/10.1130/0091-7613\(1997\)025<0695:MAAOM>2.3.CO;2](https://doi.org/10.1130/0091-7613(1997)025<0695:MAAOM>2.3.CO;2).
- Korzeniowska, K., Pfeifer, N., Landtwing, S., 2018. Mapping gullies, dunes, lava fields, and landslides via surface roughness. *Geomorphology* 301, 53–67. <https://doi.org/10.1016/j.geomorph.2017.10.011>.
- LaHusen, S.R., Davall, A.R., Booth, A.M., Grant, A., Mohkin, B.A., Montgomery, D.R., Struble, W., Roering, J.J., Wartman, J., 2020. Rainfall triggers more deep-seated landslides than Cascadia earthquakes in the Oregon Coast Range, USA. *Sci. Adv.* 6 (38), eab6790. <https://doi.org/10.1126/sciadv.abd790>.
- Lewis, S.E., Wüst, R.A., Webster, J.M., Shields, G.A., 2008. Mid-late Holocene sea-level variability in eastern Australia. *Terra Nova* 20 (1), 74–81. <https://doi.org/10.1111/j.1365-3113.2007.00780.x>.
- McKean, J.A., Dietrich, W.E., Finkel, R.C., Southon, J.R., Caffee, M.W., 1993. Quantification of soil production and downslope creep rates from cosmogenic <sup>10</sup>Be accumulations on a hillslope profile. *Geology* 21 (4), 343–346.
- McKee, A., Ribó, M., Canals, M., Puig, P., Lastras, G., Tubau, X., 2014. Space-for-time substitution and the evolution of a submarine canyon-channel system in a passive progradational margin. *Geomorphology* 221, 34–50. <https://doi.org/10.1016/j.geomorph.2014.06.008>.
- Ministry, B., Finke, P., Stockmann, U., Vanwallendael, T., McBratney, A.B., 2015. Resolving the integral connection between pedogenesis and landscape evolution. *Earth-Sci. Rev.* 150, 102–120. <https://doi.org/10.1016/j.earscirev.2015.07.004>.
- Ministry, B., McBratney, A.B., 2016. Digital soil mapping: a brief history and some lessons. *Geoderma* 264, 301–311. <https://doi.org/10.1016/j.geoderma.2015.07.017>.
- Moore, I.D., Grayson, R.B., Landson, A.R., 1991. Digital terrain modeling: a review of hydrological, geomorphological, and biological applications. *Hydrol. Process.* 5, 3–30. <https://doi.org/10.1002/hyp.3360050103>.
- Montgomery, D.R., 2001. Slope distributions, threshold hillslopes, and steady-state topography. *Am. J. Sci.* 301, 432–454. <https://doi.org/10.2475/aj.s.301.4-5.432>.
- Moss, P., Dodgson, A., Shupland, F., Withers, L., Brownhill, C., Terrano, D., Sims, C., 2013. Investigation into the vegetation and fire history of the EPBC Ramsar and WHA wetlands of the Great Sandy Straits, South East Queensland. Unpublished report to the Burnett Mary Regional Group, Bundaberg, Queensland.
- Paton, N.R., Lohse, K.A., Godsey, S.E., Crosby, B.T., Seyfried, M.S., 2018. Predicting soil thickness on soil mantled hillslopes. *Nat. Commun.* 9 (1), 1–10. <https://doi.org/10.1038/s41467-018-05743-y>.
- Paton, N.R., Ellerton, D., Shulmeister, J., 2019a. High-resolution remapping of the coastal dune fields of South East Queensland, Australia: a morphometric approach. *J. Maps* 15 (2), 578–589. <https://doi.org/10.1080/17445647.2019.1642446>.
- Paton, N.R., Lohse, K.A., Seyfried, M.S., Godsey, S.E., Parsons, S.B., 2019b. Topographic controls of soil organic carbon on soil-mantled landscapes. *Sci. Rep.* 9 (1), 1–15. <https://doi.org/10.1038/s41598-019-42556-5>.
- Pawlik, L., Samoni, P., 2018. Soil creep: the driving factors, evidence and significance for biogeomorphic and pedogenic domains and systems—a critical literature review. *Earth-Sci. Rev.* 178, 257–278. <https://doi.org/10.1016/j.earscirev.2018.01.008>.
- Rever, R., Ferguson, I.F., Thompson, C.J., 1985. Studies in landscape dynamics in the Cooloola-Nocera River area, Queensland. 4. Hydrology and water chemistry. In: CSIRO Aust. Div. Soils Divisional Report No. 73, p. 42.
- Richter, D.D., Eppes, M.C., Austin, J.C., Bacon, A.R., Billings, S.A., Brecheisen, Z., Ferguson, T.A., Markewitz, D., Pachon, J., Schroeder, P.A., Wade, A.M., 2020. Soil production and the soil geomorphology legacy of Grove Karl Gilbert. *Soil Sci. Soc. Am. J.* 84 (1), 1–20. <https://doi.org/10.1002/ssa2.20030>.
- Richie, J.C., McCarty, G.W., Venters, E.R., Kaspar, T.C., 2007. Soil and soil organic carbon redistribution on the landscape. *Geomorphology* 89 (1–2), 163–171. <https://doi.org/10.1016/j.geomorph.2006.07.021>.
- Roering, J.J., Gerber, M., 2005. Fire and the evolution of steep, soil-mantled landscapes. *Geology* 33 (5), 349–352. <https://doi.org/10.1130/G21260.1>.
- Roering, J.J., Kirchner, J.W., Dietrich, W.E., 1999. Evidence for nonlinear, diffusive sediment transport on hillslopes and implications for landscape morphology. *Water Resour. Res.* 35 (3), 853–870. <https://doi.org/10.1029/1998WR000080>.
- Roering, J.J., Kirchner, J.W., Sklar, L.S., Dietrich, W.E., 2001. Hillslope evolution by nonlinear creep and landsliding: an experimental study. *Geology* 29 (2), 143–146. [https://doi.org/10.1130/0091-7613\(2001\)029<0143:HBNCA>2.0.CO;2](https://doi.org/10.1130/0091-7613(2001)029<0143:HBNCA>2.0.CO;2).
- Rosenbloom, N.A., Anderson, R.S., 1994. Hillslope and channel evolution in a marine terraced landscape, Santa Cruz, California. *J. Geophys. Res., Solid Earth* 99 (B7), 14013–14029. <https://doi.org/10.1029/94JB00048>.
- Schneider, L.T., Donders, T.H., Metz, A., Hopmann, E.C., Damsté, J.S.S., Schouten, S., 2019. Comparison of organic and palynological proxies for biomass burning and

- vegetation in a lacustrine sediment record (Lake Allom, Fraser Island, Australia). *Org. Geochem.* 133, 10–19. <https://doi.org/10.1016/j.orggeochem.2019.03.002>.
- Stolar, D.B., Willett, S.D., Montgomery, D.R., 2007. Characterization of topographic steady state in Taiwan. *Earth Planet. Sci. Lett.* 261 (3–4), 421–431. <https://doi.org/10.1016/j.epsl.2007.07.045>.
- Struble, W.T., Roering, J.J., 2021. Hilltop curvature as a proxy for erosion rate: wavelets enable rapid computation and reveal systematic underestimation. *Earth Surf. Dyn.* 9, 1279–1300. <https://doi.org/10.5194/esurf-9-1279-2021>.
- Thompson, C.H., 1981. Podzol chronosequences on coastal dunes of eastern Australia. *Nature* 291 (5819), 59–61. <https://doi.org/10.1038/291059a0>.
- Tucker, G.E., Hancock, G.R., 2010. Modelling landscape evolution. *Earth Surf. Process. Landf.* 35 (1), 28–50. <https://doi.org/10.1002/esp.1952>.
- Walker, J., Lees, B., Olley, J., Thompson, C., 2018. Dating the Cooloola coastal dunes of South-Eastern Queensland, Australia. *Mar. Geol.* 398, 73–85. <https://doi.org/10.1016/j.margeo.2017.12.010>.
- Ward, W.T., 2006. Coastal dunes and strandplains in southeast Queensland: sequence and chronology. *Aust. J. Earth Sci.* 53 (2), 363–373.
- Whipple, K.X., 2001. Fluvial landscape response time: how plausible is steady-state denudation? *Am. J. Sci.* 201 (4–5), 313–325.
- Zevenbergen, L.W., Thorne, C.R., 1987. Quantitative analysis of land surface topography. *Earth Surf. Process. Landf.* 12, 47–56. <https://doi.org/10.1002/esp.3290120107>.



## A.6.3 Chapters 4 – Earth Surface Processes and Landforms

Received: 21 February 2022 | Revised: 10 April 2022 | Accepted: 15 April 2022  
DOI: 10.1002/esp.5387

## RESEARCH ARTICLE

ESPL WILEY

# Using calibrated surface roughness dating to estimate coastal dune ages at K'gari (Fraser Island) and the Cooloola Sand Mass, Australia

Nicholas R. Patton<sup>1,2</sup> | James Shulmeister<sup>1,2</sup> | Tammy M. Rittenour<sup>3</sup> | Peter Almond<sup>4</sup> | Daniel Ellerton<sup>2,5</sup> | Talitha Santini<sup>6</sup>

<sup>1</sup>School of Earth and Environment, University of Canterbury, Christchurch, New Zealand

<sup>2</sup>School of Earth and Environmental Sciences, The University of Queensland, Brisbane, Australia

<sup>3</sup>Department of Geology, Utah State Luminescence Laboratory, Utah State University, Logan, UT, USA

<sup>4</sup>Department of Soil and Physical Sciences, Lincoln University, Christchurch, New Zealand

<sup>5</sup>Department of Geological Sciences, Stockholm University, Stockholm, Sweden

<sup>6</sup>School of Agriculture and Environment, The University of Western Australia, Perth, Australia

## Correspondence

Nicholas R. Patton, School of Earth and Environment, University of Canterbury, Christchurch 8140, New Zealand.  
Email: nicholas.patton@pg.canterbury.ac.nz

## Abstract

Here we present a novel application of landscape smoothing with time to generate a detailed chronology of a large and complex dune field. K'gari (Fraser Island) and the Cooloola Sand Mass (CSM) dune fields host thousands of emplaced (relict) and active overlapping parabolic dunes that span 800 000 years in age. While the dune fields have a dating framework, their sheer size (~1930 km<sup>2</sup>) makes high-resolution dating of the entire system infeasible. Leveraging newly acquired ( $n = 8$ ) and previously published ( $n = 20$ ) optically stimulated luminescence (OSL) ages from K'gari and the CSM, we estimate the age of Holocene dunes by building a surface roughness ( $\sigma_c$ )-age relationship model. In this study, we define  $\sigma_c$  as the standard deviation of topographic curvature for a dune area and we demonstrate an exponential relationship ( $r^2 = 0.942$ , RMSE = 0.892 ka) between  $\sigma_c$  and timing of dune emplacement on the CSM. This relationship is validated using ages from K'gari. We calculate  $\sigma_c$  utilizing a 5 m digital elevation model and apply our model to predict the ages of 726 individually delineated Holocene dunes. The timing of dune emplacement events is assessed by plotting cumulative probability density functions derived from both measured and predicted dune ages. We demonstrate that both dune fields had four major phases of dune emplacement, peaking at <0.5, ~1.5, ~4, and ~8.5 ka. We observe that our predicted dune ages did not create or remove major events when compared to the OSL-dated sequence, but instead reinforced these patterns. Our study highlights that  $\sigma_c$ -age modelling can be an easily applied relative or absolute dating tool for dune fields globally. This systematic approach can fill in chronological gaps using only high-resolution elevation data (3–20 m resolution) and a limited set of dune ages.

## KEYWORDS

dune chronology, dune emplacement, dune stabilization, Holocene, OSL dating, parabolic dune, quaternary, sea-level change

## 1 | INTRODUCTION

Coastal dunes are important environmental systems that are found globally around both seas and lakes (Lancaster et al., 2016; Martínez & Psuty, 2004; Yan & Baas, 2015) and provide a rich record of climatic, geologic, and geomorphic information (e.g.

Lindhorst & Betzler, 2016; Patton et al., 2022; Pye, 1983; Swezey, 2001; Wells & Goff, 2007). However, uncovering and deciphering the information from these systems is challenging because they lie at the interface of terrestrial, aquatic, and atmospheric processes, which vary on decadal to millennial timescales (Pye, 1983).

This is an open access article under the terms of the [Creative Commons Attribution License](https://creativecommons.org/licenses/by/4.0/), which permits use, distribution and reproduction in any medium, provided the original work is properly cited.  
© 2022 The Authors. Earth Surface Processes and Landforms published by John Wiley & Sons Ltd.

The timing and mechanisms of dune-field activation and consequent stabilization (dune emplacement hereafter) are ascribed to changes in climate and sediment supply, which affect vegetation, storminess, fire frequency, sea-surface temperatures, and sea level (e.g. Han et al., 2021; Shumack & Hesse, 2018; Vimperi et al., 2021; Yan & Baas, 2017). These interpretations have largely been demonstrated on active and/or recently emplaced sections of dune fields, where physical measurements or repeat aerial/satellite imagery are available (e.g. Levin et al., 2017; Marin et al., 2005; Tsoar, 2005). These mechanisms have been extended to emplaced dune systems; however, the direct landscape–process relationship is unknown and it is difficult to infer these processes unless a strong chronological framework is established.

Coastal dune fields' temporal relationships appear chaotic, and it is difficult to determine whether emplaced dunes were once active simultaneously or asynchronously across the dune field. Stochastic (random) dune activity can be indicative of local perturbations but not related to regional changes in environmental conditions, because dunes can simultaneously be active and emplace under the same conditions (Yizhaq et al., 2007). In contrast, mass activation or emplacement of entire dune fields may provide clues about regional environmental forcings (e.g. Lees, 2006). While the direct dating of dunes can be achieved using optically stimulated luminescence (OSL) and/or radiocarbon dating, these techniques are costly and finding suitable dating targets for radiocarbon is often challenging. To offset these limitations, it is common to either establish geobotanical chronosequences (morphological, biological, or pedological units) (e.g. Shulmeister & Lees, 1992; Thompson, 1981), or date organic-rich sediments in adjacent deposits as a means to help place the dunes into a chronosequence (e.g. Wilson, 2002). In both scenarios, these estimates often have large spatial and temporal uncertainty, even in locations where there are clear sequences of overlapping dunes (e.g. Lees, 2006; Swezey, 2001). Consequently, dune sequences that are composed of tens or even thousands of individual dunes are typically secured by only a handful of ages, with wide age constraints that can lead to misinterpretation (e.g. Ward, 2006).

In order to validate age inferences, and hence improve our understanding of former dune activation and stabilization, a means of extending dune ages to all (or most) dunes within a dune field would be a useful tool. In this paper, we explore the implications of recently observed relationships between dune surface roughness ( $\kappa_c$ ) and dune age to explain landscape smoothing with time. We test whether this provides a basis for dating dunes where high-resolution elevation data and a rough geochronological framework are in place.

## 2 | BACKGROUND

### 2.1 | Surface roughness as a proxy for landform age

In most aeolian research, surface roughness characterizes the near-surface meteorological boundary layer over dunes as a means to understand airflow and sediment transport (e.g. Gillette & Stockton, 1989; Jerolmack et al., 2012; Lancaster & Baas, 1998; Levin et al., 2008; Pelletier, 2013; Raupach et al., 1993; Wiggs et al., 1996). For this study, surface roughness is used to measure and define a

dune's topographic development (colluvial not aeolian processes). Surface roughness has been defined as a metric of topographic variability (local relief) within a defined spatial area or window (e.g. Korzeniewska et al., 2018). Its application has been utilized across earth science disciplines as a metric to identify and map spatial patterns and as a surrogate to build empirical relationships (Smith, 2014). An important application of  $\kappa_c$  is its utility as a proxy for relative age. This relationship has been predominantly applied to constrain the timing of landslide deposition (e.g. Bell et al., 2012; Booth et al., 2009, 2017; Glenn et al., 2006; Goetz et al., 2014; LaHusen et al., 2020; McKean & Roering, 2004), but has also been used on alluvial fans (Frankel & Dolan, 2007), earth flows (Schanz & Cole, *in review*), and planetary surfaces (Pommerol et al., 2012).

Surface roughness gradually smooths due to diffusive processes of sediment transport (Booth et al., 2017; Patton et al., 2022). The basic principle is that local relief reduces with time due to weathering and erosion, such that features smooth (ridges erode and valleys fill) on surfaces that are not affected by advective processes (e.g. sediment transport by water-driven processes). LaHusen et al. (2020) utilized this principle to build a  $\kappa_c$ –age relationship from a minimal set of dated landslide deposits and predicted ~10 000 ages in the Pacific Northwest, USA. The utility of this model was not only that ages could be predicted, but more particularly that previously undated landforms could be placed into the context of regional records of climate and landscape change. Consequently, they determined that rainfall, not earthquake activity, was the major driver of landslide activation inland of the Cascadia Subduction Zone.

### 2.2 | Surface roughness in dune systems

Surface roughness has been used to map dune landforms (e.g. Korzeniewska et al., 2018); however, the application of  $\kappa_c$  as an indicator of landform age ( $\kappa_c$ –age relationship) has not yet been applied and tested in a dune system. A recent study by Patton et al. (2022) highlighted the utility of  $\kappa_c$  within the Cooloola Sand Mass (CSM) dune field as an important metric, and to characterize and define the stage of geomorphologic development of dune forms. They demonstrated that dune  $\kappa_c$ , as measured by standard deviation of curvature for a given dune area, could be related to sediment transport theory. They found that dunes are initially emplaced with remarkably uniform surface roughness, which smooths with time, and this evolution can be simulated using a combination of non-linear and linear sediment transport models (Figure 1).

In their study, they determined that dunes evolve in two distinct phases (Figure 1c). The first phase occurs within ~1 kyr after dune emplacement and is explained through non-linear sediment transport. This is a period when dune gradients and  $\kappa_c$  are large, erosion and deposition rates are more rapid, and there is a wider variety of transport styles. During this initial period, dune-surface gradients are lowered as a result of disturbance-driven perturbations such as fires and storms. These disturbances may remove vegetation, increase hydrophobicity, and consequently increase the soil's efficiency to move downslope, promoting dry ravel and sheetwash processes (similar to avalanching and grain flows observed on active dune slip faces). This phase continues until dune relief is lowered and  $\kappa_c$  values reach the 'transitional zone', as seen in Figure 1c. This zone was defined by



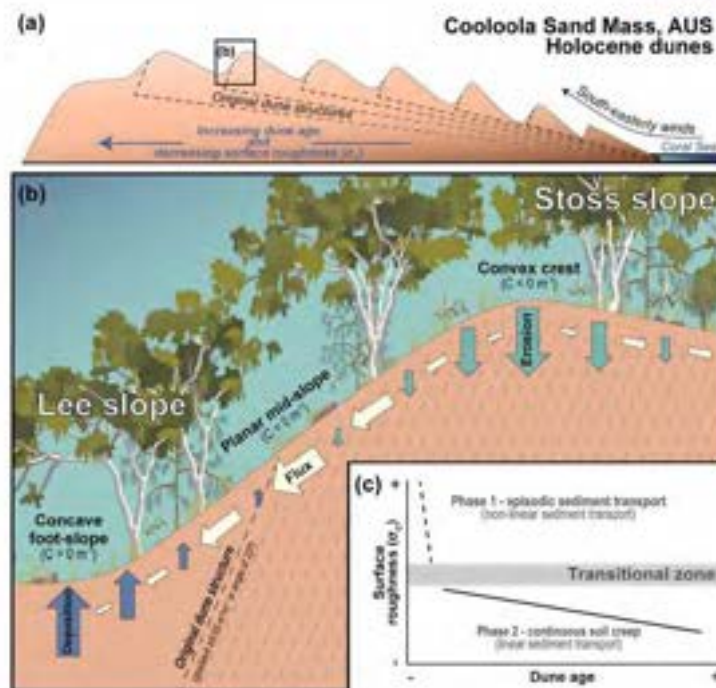


**FIGURE 1** Conceptual diagram and result summary from Patton et al. (2022) between surface roughness ( $n_c$ ) and dune age within the Cooloolool Sand Mass (CSM) dune field, Australia. (a) An idealized elevation profile of the CSM dune field. The dunes move inland from the coast through sclerophyll forest and over antecedent topography (dashed lines) via the dominant south-easterly wind. Dunes are emplaced when wind speeds decrease and vegetation stabilizes the dune surface. With every successive dune emplacement, antecedent topography gradients generally increase, thereby decreasing the distance dunes travel inland whilst preserving older dunes. Consequently, most dunes increase in age while decreasing in  $n_c$  moving away from the coast. (b) Conceptual diagram of hillslope positions as defined by curvature ( $C$ ) and the contribution of erosion, deposition, and flux (size of arrow). All sediment removed from crest can be accounted for in the foot-slopes (a closed system). As time progresses, ridges lower and hollows fill, reducing hillslope gradients and the maximum and minimum curvature values, thus decreasing dune  $n_c$ . (c) The general relationship between dune age, surface roughness, and sediment transport phases. Dunes with high  $n_c$  (phase 1) are best explained through non-linear sediment transport where episodic processes such as dry raveling and sheet washing (comparable to grain flows and/or avalanching) occur. Once dune gradients are lowered below their angle of repose (gradient of  $0.65 \text{ m m}^{-1}$  or angle of  $33^\circ$ ) associated with the defined 'transitional zone', sediment transport is limited to slow and continuous processes (phase 2) where their evolution can be explained with linear sediment transport

an observed shift in dominant transport style and the absence of gradients greater than the sand's angle of repose ( $33^\circ$ , or gradients of  $0.65 \text{ m m}^{-1}$ ). Once gradients are lowered beyond this zone, the second phase of dune evolution begins; wherein sediment transport is proportional to hillslope gradient (linear sediment transport). During this period, dune  $n_c$  is small and sediment transport is limited to slow and continuous processes (e.g. biogenic soil creep, rain-splash, and granular relaxation), where erosion occurs at the dune crests and sediment is deposited within the adjacent foot-slopes (Figure 1b). This mechanism is inferred to continue until all relief is either removed or increased due to dune activation or sea-level fall.

Patton et al. (2022) alluded to an apparent exponential relationship between dune  $n_c$  and age; however, they chose not to prescribe a single function to explain the dune field's evolution. Instead, they elected to retain the two distinct erosional phases to ensure sediment transport processes were not conflated. Despite this decision, they argued that because the dune fields have limited hillslopes that exceed the angle of repose and a dominance of linear sediment

transport, dune  $n_c$  will smooth with time and ascribing a single exponential fit is appropriate.

The goal of this study is to test and, if appropriate, apply  $n_c$ -age modelling to a pair of adjacent coastal dune fields, the CSM and K'gari (Fraser Island) in southeast Queensland. These large and once connected systems are dominated by active and emplaced parabolic dunes. At the CSM, many of these dunes have been dated and the younger parabolic sequences span the Mid- to Late Holocene. Once emplaced, the evolution of the dunes (erosion and deposition) is controlled by a limited set of known diffusional processes that are morphologically trackable through time. We first establish a  $n_c$ -age relationship on the CSM and test its validity on K'gari. If the model proves to be successful for the dated dunes, we will utilize it to estimate the ages of the remaining Holocene-age dunes in both dune fields. Although our study focuses specifically on two locations, the research provides insights on the evolution of overlapping coastal dune systems and a means to produce a more complete chronological framework for multi-phase dune fields globally.



**FIGURE 2** (a) Satellite imagery of K'gari (Fraser Island) and the Cooloola Sand Mass (CSM), which make up the northern section of the southeast Queensland (SEQ) dune field in Australia. The dune sediments are derived from the longshore drift system (dashed line and arrow) that is delivered to the coast by the dominant south-easterly winds (small arrows). (b) Close-up imagery of the coastline and dunes on K'gari. Photo credit: Jürgen Wallstabe

### 2.3 | Site description: K'gari and Cooloola Sand Mass

The southeast Queensland (SEQ) dune fields in Australia (Figure 2) are composed of K'gari (Fraser Island) and the mainland-attached CSM immediately to the south. The dune fields have been developing for over 800 kyr (Ellerton et al., 2020; Walker et al., 2018). These dune systems are currently separated by the entrance to the Great Sandy Strait and the Inskip Peninsula, but recent work (Köhler et al., 2021) has demonstrated that this separation dates back only to the early Mid-Holocene. Stretching for more than 200 km of coastline (26.17–24.41°S), these two systems cover a combined land area of ~1930 km<sup>2</sup>, with most of the dune fields on K'gari. They contain one of the longest and most complete coastal dune field sequences in the world (Thompson, 1981) and include over 700 Holocene dunes (Patton et al., 2019; Ward, 2006) covering roughly 640 km<sup>2</sup>, which are the focus of this study.

Both dune fields have nearly limitless sediment supply, with an estimated 500 000 m<sup>3</sup> of sediment transported yearly along the regional longshore drift system (Boyd et al., 2008; Patterson & Patterson, 1983). The parent material is a uniform 98% medium to fine quartz sand (180–250 µm) that is well sorted and sub-rounded to rounded (Thompson, 1992). The majority of onlapping dunes are parabolic with local transgressive dune waves, which travel inland under the influence of the dominant south-easterly winds (Coaldrake, 1962; Ellerton et al., 2018). The region has been tectonically inactive (Roy & Thom, 1981), with only minor variability in local base level, between +2 and –0.5 m since the Holocene sea-level highstand (Lewis et al., 2008). The vegetation communities have been relatively stable (e.g. Atahan et al., 2015; Moss et al., 2013) with tall open/close sclerophyll forest making up the majority of the inland vegetation and coastal scrubland dominating the eastern side of the dune fields (Harrold et al., 1987). Additionally, the climate has remained sub-tropical (Cfa) during this period (Donders et al., 2006).

## 3 | METHODS

### 3.1 | Dune mapping and remote sensing

In this study, we individually remap the Holocene and modern dunes for both the K'gari and the CSM. Dunes were identified using a 1 m-resolution digital elevation model (DEM) derived from LiDAR (publicly available from Geoscience Australia; Fraser Coastal Project). 1:5000 orthophoto imagery retrieved from Queensland Globe, and field observations. Each dune was delineated by hand in ArcGIS (version 10.6) at the base of slip faces and trailing arms, and defined as polygons.

### 3.2 | Calculating surface roughness

Surface roughness is calculated by determining the standard deviation of curvature ( $C$ ) for each mapped dune area, defined by a map polygon. This calculation of  $\sigma_C$  is utilized because  $C$  distributions are centred at 0 (Patton et al., 2018), making it possible to compare dunes without biases introduced by broad-scale topography (e.g. variations in initial morphology caused from the antecedent topography) (Patton et al., 2022). Curvature was generated in ArcMap, which utilizes equations from Moore et al. (1991) and Zevenbergen and Thorne (1987) that calculate curvature from the slope as a percentage and reverse the sign (negative curvature convention). Therefore, we divide ArcMap's curvature output by –100 such that positive values represent concavity (hollows/foot-slopes) and negative values represent convexity (ridges/crest); see the online Supplementary Information and Figure S1. It is important to highlight that  $\sigma_C$  values are sensitive to methodology and boundary conditions and/or processes. Minor variabilities in  $\sigma_C$  values may occur, but overall trends remain consistent.



Prior to the  $\alpha_C$  calculation, we chose to resample the original DEM using bilinear interpolation to 5 m resolution. The reduction in resolution dampened noise and lowered elevation uncertainty by removing DEM processing artefacts and vegetation effects (Berti et al., 2013) while preserving dune morphology (Patton et al., 2022). Our assumption in calibrating a  $\alpha_C$ -age relationship was that dune  $\alpha_C$  values decline monotonically with dune age. Hence, we limited our areas of calibration and application to where diffusive processes and not advective processes (e.g. wind and fluvial transport, which can increase relief and roughness) prevailed. Additionally, all water (water bodies, bogs, coastal cliffs, etc.) and/or anthropogenic modifications (roads, built-up areas, mining, etc.) were also excluded. Once removed, the 'zonal statistics' tool in ArcMap was used to determine  $\alpha_C$ .

### 3.3 | Optically stimulated luminescence dating

OSL dating provides an age estimate of the time since quartz grains were last exposed to sunlight (burial) (Huntley et al., 1985); therefore, OSL dates represent timing of dune emplacement (Lancaster, 2008). For each dune, OSL samples were collected at dune crests utilizing a sand auger with a 15 cm bucket. Dune stratigraphy was described using standard field protocols (i.e. grain size, sorting, roundness, bedding structures, Munsell colour, and texture). An OSL sampling head was attached with an aluminium insert and once the sample was recovered, the tube was capped, sealed, and stored for later analysis. Dose rate and moisture content samples were collected from the auger samples above and below the OSL sample depth. Eight samples were collected, dating six dunes. On two dunes, we collected multiple OSL samples to increase confidence in measured ages and field interpretations. One dune had samples from the same auger hole and is believed to be equivalent in age. The other dune had samples collected on separate parallel ridges on a transgressive wave, and these ages may vary slightly. These ages are used to supplement those previously collected and reported by Ellerton et al. (2020), Köhler et al. (2021), and Walker et al. (2018).

All OSL samples were processed and analysed at the Utah State University Luminescence Laboratory. Ages were determined utilizing single-aliquot regenerative dose (SAR) analysis of small aliquots of quartz sand (Murray & Wintle, 2000; Murray et al., 2021). Samples were analysed using small aliquot (~10 grains) analysis to reduce scatter caused by grain-to-grain variability in dose rate (micro-dosimetry) (e.g. Ellerton et al., 2020; Guérin et al., 2015). Sample preparation followed standard luminescence protocols (i.e. Wintle, 1997).

All dose rates were determined using representative sub-samples that were analysed using ICP-MS and ICP-AES techniques to determine the concentrations of K, Rb, Th, and U in the sediment. Moisture content (in situ) was calculated for all samples. If the measured value was below 5%, we assumed a value of  $5 \pm 2\%$ , which represents the average moisture history (Ellerton et al., 2020). Dose rates are determined from sediment chemistry, cosmic ray contribution, and water content (Aitken, 1998; Aitken & Xie, 1990) using conversion factors from Guérin et al. (2011). The contribution of cosmic radiation to the dose rate was calculated using sample depth, elevation, and latitude/longitude following the calculations of Prescott and Hutton (1994).

Optical measurements were performed on small aliquot (1 mm diameter, ~10 grains per disk) samples using Rise TL/OSL Model DA-20 readers with blue-green light-emitting diodes (LEDs) ( $470 \pm 30$  nm) as stimulation source. The luminescence signal was measured through 7.5 mm ultraviolet filters (U-340) over 40–60 s (250 channels) at 125°C with LED diodes at 70–90% power (~45 mW/cm<sup>2</sup>) and calculated by subtracting the average of the last 5 s (background signal) from the first 0.7 s (four channels) of the signal decay curve. The luminescence signals show rapid decay dominated by the fast component of the signal (Murray & Wintle, 2003). For those samples with <1 Gy equivalent dose ( $D_E$ ), dose-response curves were fitted linearly between the zero dose and repeated regenerative doses. Results of a preheat-plateau dose-recovery (PP-DR) test (Wintle & Murray, 2006) suggest that a 200°C preheat for 10 s produces the best results for samples in this study.  $D_E$  values were calculated using the Central Age Model (CAM) of Galbraith and Roberts (2012) using at least 14 accepted aliquots of quartz sand. Aliquots were rejected if they had evidence of feldspar contamination, a recycling ratio beyond 20% of unity (<0.8 or >1.2), recuperation >1 Gy, or natural  $D_E$  greater than the highest regenerative dose given. Errors in  $D_E$  and age estimates are reported at 1 $\sigma$  standard error and include errors related to instrument calibration and dose rate/equivalent dose calculations. Errors were calculated in quadrature using the methods of Aitken and Aldred (1972) and Guérin et al. (2011).

### 3.4 | Criteria for utilizing previously OSL-dated dunes

We utilize the following sampling criteria for dune ages from previously published studies. (1) Dates must reflect the age of the dune surface morphology (i.e. the uppermost dune unit that forms the surface morphology was dated). (2) Dunes must be emplaced (i.e. stabilized, not active). Lastly, (3) ages must be collected from dune apices or the crest of the trailing ridges and in physically little altered (B/C, C, soil parent material) soil horizons. These criteria were set to ensure that ages represented primary aeolian deposition.

### 3.5 | Surface roughness-age analysis and age extrapolation

A signal empirical relationship was generated using all OSL-dated dunes within the CSM. We hypothesize that both the CSM and K'garri dune fields are governed by identical mechanisms controlling dune activation and evolution, because they were once part of a connected dune field (Köhler et al., 2021) and have been mapped as part of the same dune system (Patton et al., 2019; Ward, 2006). As a result, we assume that we can apply the same  $\alpha_C$ -age relationship at both sites.

For use in the  $\alpha_C$ -age model and validation subset, where dunes have multiple dates, we preferentially selected ages that were collected nearest to the dune crest and/or from sand with minimal pedogenic alterations (C-horizon). Any ages that met our sampling criteria but were not used in the model are recorded. All OSL-dated dunes from the CSM were utilized to build our  $\alpha_C$ -age model (model set). The remaining OSL-dated dunes from the Inskip Peninsula and K'garri are used as validation subset. We fit our  $\alpha_C$ -age data with an



exponential curve, given that relief lowers through diffusional processes with time (Booth et al., 2017; LaHusen et al., 2020; Patton et al., 2022). We demonstrate our model output by predicting dune ages from our validation subset, and using reduced major-axis regression we compare the slope of the predicted versus measured dune ages to 1.

A map of estimated dune ages is produced using our  $\kappa_c$ -age model to convert dune  $\kappa_c$  to time since dune emplacement. Mapped dune polygons are reclassified to their estimated ages. Given that the  $\kappa_c$ -age relationship is constructed from dunes that are emplaced, we do not predict ages for active sections of the dune field, but rather assign them absolute ages of 0 ka. Active sections are identified by aerial imagery as landforms constructed with little to no vegetation and steep lee faces with gradients  $> 0.65 \text{ m m}^{-1}$  (slopes  $> 33^\circ$ , which is at or above the angle of repose). All areas previously removed during the calculation of  $\kappa_c$  (e.g. sections of dunes with water bodies or anthropogenic disturbances) are incorporated back into the total area to show the full extent of the dune fields and produce the final predictive age map, but their surface roughness is not incorporated in the results.

### 3.6 | Determination of dune emplacement through time

To evaluate the frequency of dune emplacement through time, we determine cumulative probability density functions (PDFs) for the K'gari, CSM, and combined Holocene dune fields (not including active sections). We calculate separate PDFs for OSL-dated and modelled dune ages with 0.05 kyr bin intervals for 12 kyr (240 total bins) and assume that the age estimates represent the median value with normally distributed errors. As a conservative estimate of error, we utilize a constant 10% relative standard error (RSE) for predictive age, which is frequently applied for OSL dating (Murray et al., 2021). We normalize each PDF by total number of dunes used to generate the curve. Additionally, PDFs produced from predictive ages are also normalized by dune area (dune area divided by total Holocene dune area—not including active dune area). This is to remove bias towards younger dunes caused by the preservation of numerous small, younger dunes. We visually compare PDFs and assess dune emplacement through time.

### 3.7 | Sensitivity analysis

We calculate  $\kappa_c$  for all map dune polygons at a range of DEM resolutions (1–50 m). For each resolution, a  $\kappa_c$ -age relationship is produced and its  $r^2$  and RMSE are recorded. We predict all dune ages and generate cumulative PDFs utilizing these relationships and their respective DEM resolutions. We compare all PDFs to the OSL-derived PDF. Although the latter does not provide a quantitative assessment of our analysis, it does offer a sense of uncertainty and a foundation to examine how enhanced resolution and bin intervals may influence our interpretations.

## 4 | RESULTS

### 4.1 | OSL results and previously reported OSL ages

The eight newly acquired OSL ages from six individual dunes are shown in Table 1 and Figure 3. For each sample, supporting information such as soil descriptions, geochemistry, water content, and over-dispersion are found within the online Supplementary Information (Figure S2; Tables S1 and S2). From previously published work, 20 OSL ages met our sample criteria, dating 16 dunes (specifically Ellerton et al., 2020; Köhler et al., 2021; Walker et al., 2018) (Table 2, Figure 3). All dunes with multiple ages were consistent with our expectations. Samples collected from the same auger hole indicate equivalent ages (e.g. Dune 11), whereas samples from different locations from the same dune yielded ages that increased consistently, moving towards the dune's inland limit (e.g. Dunes 16 and 17). In total (newly acquired and previously published), 28 OSL ages met our criteria, dating 22 dunes. All ages that met our sampling criteria but were not preferred are denoted by italicized text in Table 2.

### 4.2 | Surface roughness–age relationship

The dune calibration ages ( $n = 16$ ) span from  $0.23 \pm 0.05 \text{ ka}$  to  $9.82 \pm 0.98 \text{ ka}$  with surface roughness declining from  $0.068$  to  $0.016 \text{ m}^{-1}$  with age (see Table 2). An exponential regression fits our data well, dune age =  $32.1 \cdot \exp(-108.9 \cdot \kappa_c)$ , with  $r^2 = 0.942$ .

TABLE 1 OSL results and map location

Dune number	Map ID	Location	Depth (m)	Lab number	Number of aliquots <sup>a</sup>	Dose rate (Gy/kyr) <sup>b</sup>	Equivalent dose ( $D_e \pm 2\sigma$ ) (Gy) <sup>c</sup>	OSL age $\pm 1\sigma$ (ka)
4	4	K'gari	1–1.13	USU-2742	20 (34)	$0.59 \pm 0.04$	$0.27 \pm 0.07$	$0.45 \pm 0.07$
5	5	K'gari	1–1.16	USU-2743	14 (35)	$0.34 \pm 0.03$	$0.16 \pm 0.06$	$0.47 \pm 0.10$
6	6	K'gari	1.97–2.24	USU-2730	16 (22)	$0.40 \pm 0.03$	$0.51 \pm 0.07$	$1.27 \pm 0.16$
11	11a	CSM	1.90–2.05	USU-3020	19 (31)	$0.56 \pm 0.04$	$1.41 \pm 0.23$	$2.51 \pm 0.32$
11	11a'	CSM	3.88–4.07	USU-3021	20 (32)	$0.62 \pm 0.04$	$1.33 \pm 0.23$	$2.14 \pm 0.27$
12	12	K'gari	4.40–4.50	USU-2397	17 (31)	$0.25 \pm 0.03$	$1.00 \pm 0.14$	$4.05 \pm 0.63$
17	17a	K'gari	3.15–3.20	USU-2390	18 (22)	$0.30 \pm 0.03$	$1.79 \pm 0.21$	$5.96 \pm 0.82$
17	17b	K'gari	3.05–3.15	USU-2389	20 (27)	$0.35 \pm 0.03$	$2.5 \pm 0.27$	$7.24 \pm 0.92$

<sup>a</sup>OSL age analysis using the single-aliquot regenerative dose procedure of Murray and Wintle (2000) on 1 mm small aliquots of quartz sand. Number of aliquots used in age calculation and number of aliquots analysed in parentheses.

<sup>b</sup>See online Supplementary Information for radioisotope concentrations of surrounding sediment and cosmic contribution to dose rate.

<sup>c</sup>Equivalent dose ( $D_e$ ) calculated using the Central Age Model (Galbraith & Roberts, 2012).

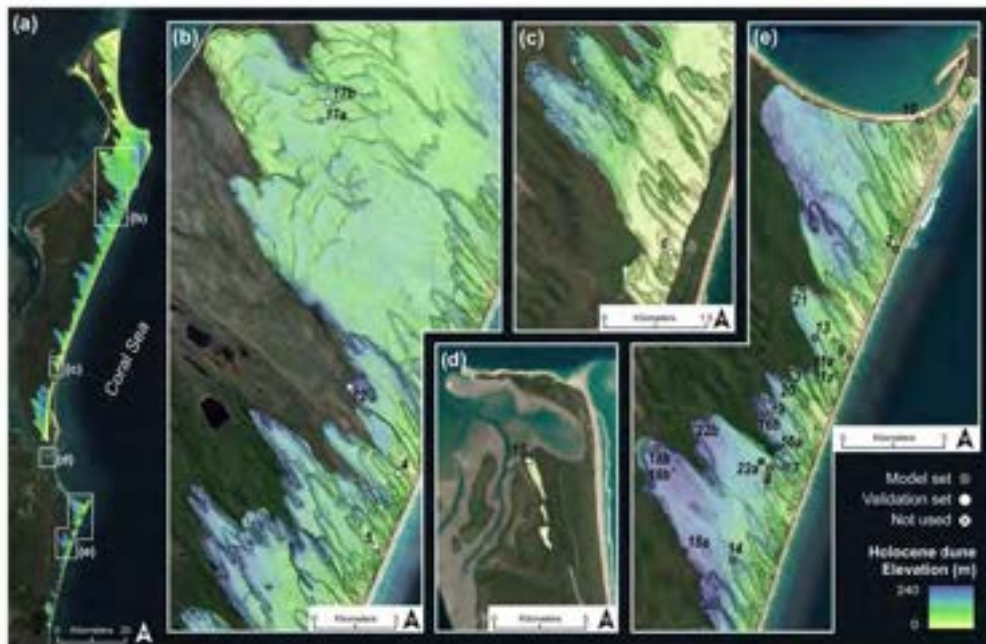


FIGURE 3 Locations of OSL-dated dunes used in this study. Dunes utilized in our  $\sigma_C$ -age relationship are represented by grey dots, whereas dunes used in the validation subset are white. For dunes with multiple dates, we preferentially selected ages from crest and/or stratigraphically lower positions. Samples that met our selection criteria but were not used in our model are marked with an 'X'

RMSE = 0.892 ka, and  $p$ -value < 0.0001 (Figure 4a). Our validation subset from dunes on K'gari and Inskip Peninsula ( $n = 6$ ) falls within the predictions of our model set and demonstrates the predictive power of this model, with a slope of 0.805 (Figure 4b). Similar to past studies, high  $\sigma_C$  associated with younger dunes rapidly decreases within the first 1000 years, and after this period  $\sigma_C$  values decrease more gradually, which is best described by a negative exponential function (Booth et al., 2017; Lakkus et al., 2020; Patton et al., 2022).

### 4.3 | Predicted dune ages and their spatial relationships and characteristics

In this study, we remotely mapped 92 and 11 active dunes (total 103), and 535 and 191 emplaced Holocene dunes (total 726) on K'gari and the CSM, respectively, covering a total area of 640 km<sup>2</sup>—33% of both dune fields' total land area. Utilizing the  $\sigma_C$ -age function above, we estimate the emplacement ages for the Holocene dunes. Generally, the oldest dunes (lowest surface roughness) were located further inland, despite having large sections overlapped by subsequent dune emplacement (Figure S3). Dunes become progressively younger moving towards the east coast (west to east) (Figures 5 and S3). The oldest dunes tend to be larger and less numerous across the landscape, whereas younger dunes are smaller in size but greater in number (Figure S3). Overlapping relationships revealed by the roughness analysis obey the principle of superposition, consistently showing younger dunes superimposed on older dunes.

### 4.4 | Temporal frequency of dune emplacement

Overall, there is good visual correspondence between PDF peaks from the OSL age control and predicted dune ages (Figure 6 vertical teal areas). Utilizing dated dunes and their measurement error ( $n = 22$ ), PDFs depict four major peaks that occur at 0.5, ~2.2, ~4, and ~9.5 ka. When separating the OSL ages into two unique PDFs for both locations, we observe similar trends between K'gari ( $n = 6$ ) and the CSM ( $n = 16$ ), suggesting our sampling efforts captured consistent emplacement events despite having limited OSL dates (white PDFs in Figures S4b and c, respectively).

Using predicted ages derived from the  $\sigma_C$ -age model (not including active dunes) ( $n = 726$ ), we produce PDFs for dune emplacement. PDFs derived from non-normalized estimated dune ages depict one major significant peak at ~1 ka that rapidly decreases with increasing dune age (Figure 6b). This is observed for both the combined and separated PDFs and is a reflection of the abundant number of mapped dunes (~60%) emplaced during the last 1 kyr (Figure S3a). When accounting for dune area, the combined normalized PDF has four peaks centred at <0.5, ~1.5, ~4, and ~8.5 ka (Figure 6c). The same peaks are common to the PDFs generated for the two areas when treated separately (Figures S4b and c).

### 4.5 | Sensitivity analysis

Surface roughness-age relationships for a range of DEM resolutions (1–50 m) and their associated  $r^2$  and RMSE are reported in Table S3.



TABLE 2 All dunes with their locations (Figure 3) and ages utilized in this study. Note: all italicized rows indicate the OSL ages that are not used in the  $\sigma_c$ -age model and validation sets and are indicated with an 'X' in Figure 3

Dune number	Map ID	Location	Latitude, longitude (°S, °E)	Surface roughness ( $m^{-1}$ )	Model or validation set	Lab number	Mean depth (m)	OSL age $\pm 1\sigma$ (ka)	Study
1	1	CSM	25.93, 153.18	0.0684	Model	USU-2011	7.40	$0.23 \pm 0.05$	Elerton et al. (2020)
2	2	CSM	25.98, 153.16	0.0506	Model	USU-2010	1.50	$0.43 \pm 0.06$	Elerton et al. (2020)
3	3	CSM	26.01, 153.13	0.0368	Model	USU-2283	2.19	$0.44 \pm 0.10$	Elerton et al. (2020)
4	4	K'gari	25.16, 153.27	0.0465	Validation	USU-2742	1.07	$0.45 \pm 0.12$	This study
5	5	K'gari	25.19, 153.26	0.0593	Validation	USU-2743	1.08	$0.47 \pm 0.18$	This study
6	6	K'gari	25.60, 153.08	0.0406	Validation	USU-2730	2.20	$1.27 \pm 0.22$	This study
7	7	CSM	26.04, 153.12	0.0275	Model	USU-2267	3.45	$1.94 \pm 0.28$	Elerton et al. (2020)
8	8	CSM	26.04, 153.12	0.0154	Model	Map 2 Sample 2	0.80	$3.6 \pm 0.30$	Walker et al. (2018)
9	9	CSM	26.01, 153.14	0.0236	Model	USU-2265	2.15	$2.37 \pm 0.23$	Elerton et al. (2020)
10	10	CSM	25.95, 153.16	0.0191	Model	USU-2012	3.25	$3.53 \pm 0.38$	Elerton et al. (2020)
11	11a	CSM	26.01, 153.13	—	—	USU-3020	1.98	$2.51 \pm 0.32$	This study
11	11a'	CSM	26.01, 153.13	0.0268	Model	USU-3021	4.00	$2.14 \pm 0.27$	This study
12	12	K'gari	25.13, 153.25	0.0189	Validation	USU-2397	4.45	$4.05 \pm 0.80$	This study
13	13	CSM	25.13, 153.25	0.0178	Model	USU-2284	3.62	$4.89 \pm 0.45$	Elerton et al. (2020)
14	14	CSM	26.06, 153.11	0.0200	Model	Map 3 Sample 3	0.85	$4.2 \pm 0.40$	Walker et al. (2018)
15	15	Inskip	25.82, 153.05	0.0190	Validation	USU-2744	2.55	$4.84 \pm 0.46$	Köhler et al. (2021)
16	16a	CSM	26.02, 153.12	—	—	USU-2268	8.90	$5.91 \pm 0.61$	Elerton et al. (2020)
16	16b	CSM	26.03, 153.12	0.0138	Model	USU-2269	1.48	$6.96 \pm 0.71$	Elerton et al. (2020)
17	17a	K'gari	25.04, 153.24	—	—	USU-2390	3.15	$5.96 \pm 1.03$	This study
17	17b	K'gari	25.04, 153.25	0.0120	Validation	USU-2389	3.10	$7.24 \pm 1.13$	This study
18	18a	CSM	26.06, 153.09	—	—	Map 6 Sample 7	0.75	$6.7 \pm 0.60$	Walker et al. (2018)
18	18b	CSM	26.03, 153.08	—	—	Map 4 Sample 4	0.80	$6.2 \pm 0.80$	Walker et al. (2018)
18	18b'	CSM	26.03, 153.08	0.0113	Model	Map 4 Sample 5	1.05	$9.8 \pm 0.80$	Walker et al. (2018)
19	19	CSM	26.02, 153.12	0.0120	Model	USU-2282	6.85	$8.17 \pm 0.82$	Elerton et al. (2020)
20	20	CSM	26.02, 153.12	0.0138	Model	USU-2270	1.48	$9.1 \pm 0.96$	Elerton et al. (2020)
21	21	CSM	25.99, 153.13	0.0108	Model	USU-2285	2.62	$9.82 \pm 0.98$	Elerton et al. (2020)
22	22a	CSM	26.03, 153.10	—	—	Map 5 Sample 6	0.80	$8.3 \pm 0.70$	Walker et al. (2018)
22	22b	CSM	26.04, 153.12	0.0109	Model	USU-2748	6.40	$9.74 \pm 0.90$	Elerton et al. (2020)

We find that a wide range of resolutions provide a good fit (3–20 m), with  $r^2 > 0.90$  and RMSE  $< 1.1$  ka, with the best resolutions being 5 and 6 m. We observe the poorest relationship (low  $r^2$  and high RMSE) for the highest and lowest resolutions (1 and 50 m). Generally,

we observe that PDFs determined from DEM resolution between 3 and 20 m show similar frequency, magnitude, and timing of dune emplacement compared to PDFs derived from measured OSL-dated dunes (Table S3, Figure S5).

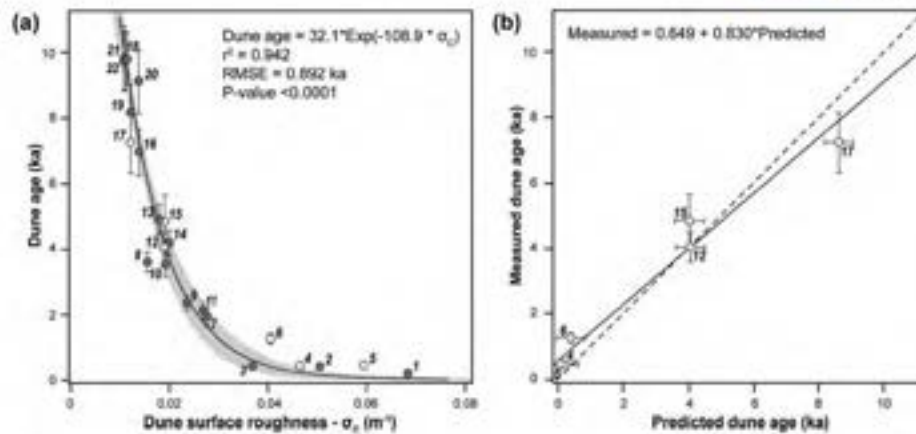


FIGURE 4 Calculated  $\sigma_c$ -age relationship from measured OSL-dated dunes. (a) Dune  $\sigma_c$  depicts a strong exponential relationship with age ( $\pm 1\sigma$ ) (black line) bounded by 95% confidence intervals (shaded area) within the CSM and K'gari dune fields. Our calibration ages (grey dots) come from the CSM ( $n = 18$ ), whereas the remaining dates used as a validation subset (white dots) come from Inskip and K'gari ( $n = 6$ ). (b) Model validation using predicted versus measured dune ages and their associated best-fit line (black line) using reduced major-axis regression to account for uncertainty in both variables compared to a 1:1 line (solid black dashed line)

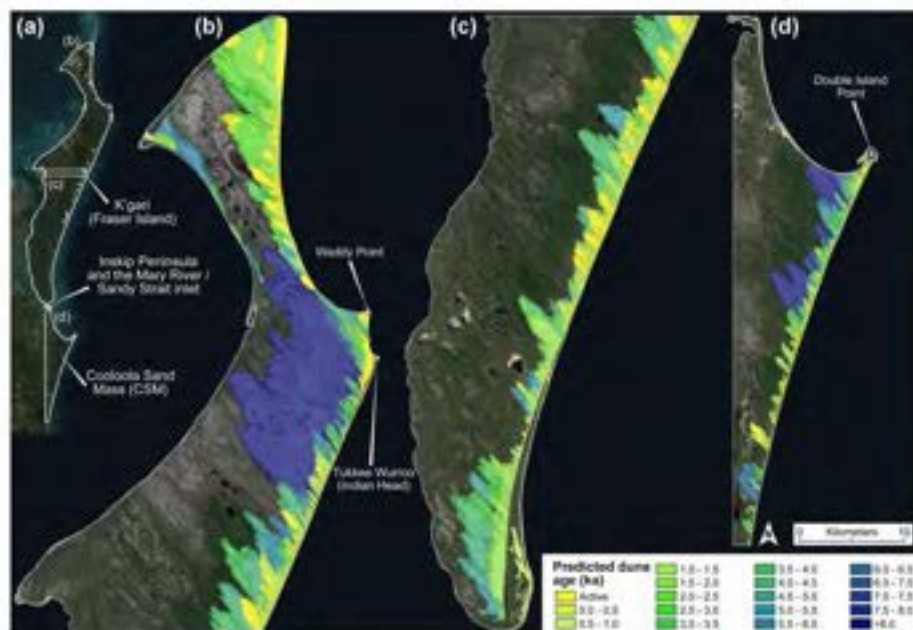


FIGURE 5 Predicted Holocene dune ages using  $\sigma_c$ -age model. (a) Aerial imagery of K'gari to the north and the CSM to the south with locations of panels (b) northern K'gari, (c) southern K'gari, and (d) CSM

## 5 | DISCUSSION

### 5.1 | Dune surface roughness and evolutionary processes

While dunes are active, they are dominated by wind advection and deflation that controls their movement near the lee-slope slip face (Hesp, 2002; Pye, 1982). The migrating dunes' surfaces are barren of vegetation, with shallow stoss gradients and over-steepened lee faces

that are smooth (low  $\sigma_c$ ). The dune continues to move while vegetation begins to stabilize dune segments along the trailing arms and furthest from the active sections (Levin, 2011; Yan & Baas, 2017). Topographic variability begins to emerge as sand is entrained within and/or forced around vegetation patches. This increases local relief, roughening the dune surface and resulting in an increase in  $\sigma_c$ . This progresses until the vegetation has fully covered and stabilized the dune's surface, marking the onset of dune emplacement and the highest recorded  $\sigma_c$  values (Figure S6). Our observations match those seen in other dune systems

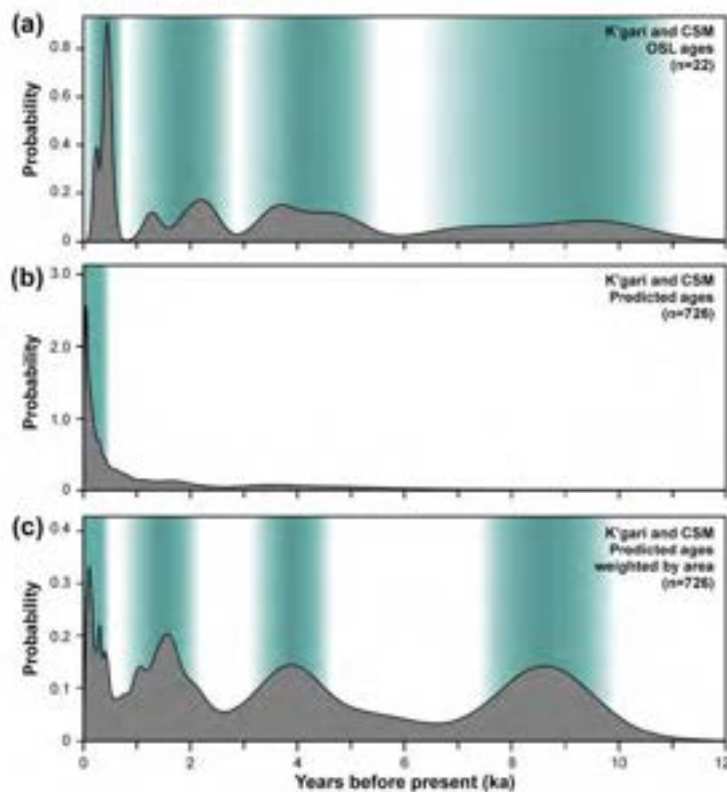


**FIGURE 6** Normalized probability density functions (PDFs) of the combined K'gari and CSM dune fields derived from (a) OSL-dated dunes and (b) predicted ages. (c) Predicted ages normalized by total dune area. Vertical teal areas highlight phases of dune emplacement. By far the largest number of dunes are small coastal blowouts, but cumulatively these dunes represent very little land area and are of only local significance. Area occupied by the dunes is critical as during major activation phases, blowouts coalesce into much larger parabolic and transverse dune fields

(e.g. Hesp, 2002; Pelletier et al., 2009; Stallins & Parker, 2003), indicating that dune emplacement through to the stage of vegetation stabilization is a mechanism that roughens topography.

Once dunes are emplaced, their topographic evolution can be described by diffusive sediment transport theory, which includes two phases of smoothing (decreasing  $\sigma_C$  with time) (Patton et al., 2022). The first phase of rapid smoothing is induced by frequent episodic transport from dry ravel and sheetwash processes. This persists until all slopes are lowered below their angle of repose. This is followed by the second phase, which is dominated by slow and continuous transport processes such as bioturbation and granular relaxation. We hypothesize that this will continue as erosion rates lower and the styles of transport become increasingly uniform until no relief remains,  $\sigma_C \rightarrow 0 \text{ m}^{-1}$  (Figure S6). This general evolution is supported by our field observations that steep slopes persist on young dunes (<1 ka); geomorphic processes are consistent on K'gari, and the validation subset fits well.

## 5.2 | Timing of dune emplacement and regional story

The  $\sigma_C$ -age relationship calibrated from the CSM accurately predicts the ages of the OSL-dated dunes on K'gari. The findings support the idea that both dune fields are part of the same system, undergoing similar evolutionary development with distinct emplacement phases in the Holocene (e.g. Ellerton et al., 2020; Patton et al., 2019; Ward, 2006). Critically, we are able to predict the age of every emplaced Holocene dune in the dune field, which significantly

amplifies our ability to extract chronological signals from dune fields that have, to this point, been limited.

Our approach allows us to observe patterns within the dune fields that would otherwise be obscure. For example, the oldest of the Holocene emplacement phases at the CSM and K'gari is the so-called 'Triangle Cliff' unit (Patton et al., 2019; Ward, 2006). This is comprised of large parabolic dunes, and more locally, large transverse dune waves. This unit was mapped uniformly across the dune fields (Patton et al., 2019; Ward, 2006), suggesting that the entire coastline was simultaneously active during the early Holocene. This is consistent with the expectation that the dune fields would generally be active during the main post-glacial transgression (e.g. Cook, 1986; Lees, 2006; Pye, 1983; Pye & Bowman, 1984; Shulmeister & Lees, 1992; Thom, 1978; Thompson, 1981). However, the age estimates indicate a slightly different pattern; we observe the main preservation of these older Holocene dunes immediately (within ~20 km) south of rocky headlands (i.e. Double Island Point on the CSM; Tukkee Wurroo [aka Indian Head] and Waddy Point on K'gari) (Figure 5). We hypothesize that these headlands act as pinning points for the beaches and long-term rotation of the coastline into swash alignment south of the headlands, which has resulted in enhanced erosion and the consequential loss of older Holocene dunes in the southern parts of both dune fields (Stephens et al., 1981). In addition, eroded sediment tends to accumulate south of the headlands, as can be observed inland from Tukkee Wurroo. The one exception is near the southern limit of K'gari, where the northward migration of the Mary River/Sandy Strait inlet during the Mid- to Late Holocene (Köhler et al., 2021) has increased local sediment supply, promoting



coastal accretion (Figure 5). This has consequently preserved some Mid-Holocene parabolic dunes behind beach-ridge complexes.

Paleoenvironmental interpretations from dune fields are constrained by dune chronologies and are often based on a handful of ages (e.g. Shulmeister & Lees, 1992). In fact, many of the current interpretations for the coastal dune fields are from sparse datasets which are limited to inferred key events, for example, the onset/intensification of the El Niño Southern Oscillation (ENSO) or even the post-glacial transgression. Our method provides a systematic and inexpensive means to substantially expand these chronologies, and a way to increase the robustness of interpretations by providing realistic ages for all the dunes in the dune field. The enhanced chronology is important because patterns of dune activation and emplacement are complex and may encompass significant, region-dependent, time lags and local signals (Lancaster et al., 2016).

### 5.3 | Dune emplacement ages and sea-level variability

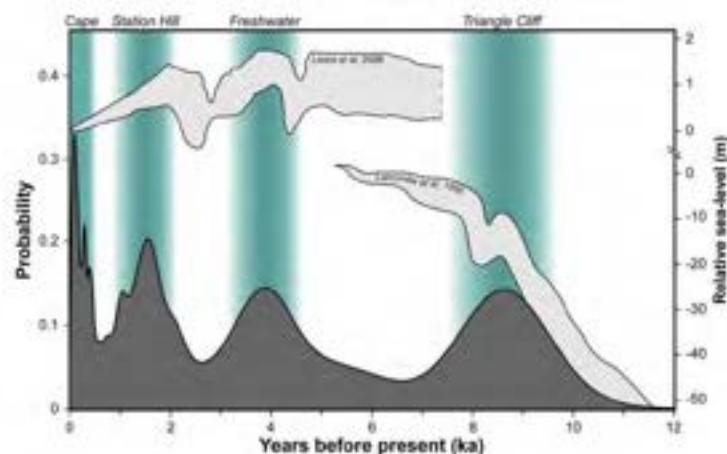
Overall, the predicted ages support previous inferences about the dune fields. Whether the SEQ dune fields, including the CSM and K'gari, have been activated by sea-level or climate change has been strongly debated (e.g. Elerton et al., 2020; Thompson, 1981; Walker et al., 2018; Ward, 1978; Young et al., 1993), but the idea that the main dune-forming events were associated with the glacial maximum has become embedded in the popular literature (e.g. the listing for the Fraser Island/K'gari World Heritage Area). The most comprehensive chronology comes from Elerton et al. (2020), who constrained the ages of the mapped Pleistocene and Holocene dune units and related these emplacement phases to sea level. In their study, they noted that sea-level rise is likely the main driver inducing dune activity owing to the erosion of sand from the coast and nearshore, and consequent reworking of sediment into the dune fields (Cooper-Thorn model) (Cooper, 1958; Thorn, 1978).

We re-examine this hypothesis by comparing our PDF results from the  $\kappa_c$ -age model with local sea-level curves from Larcombe et al. (1995) and Lewis et al. (2008). Similar to Elerton et al. (2020), our findings support the Cooper-Thorn model. We observe four major peaks in the Holocene at  $\sim 0.5$ ,  $\sim 1.5$ ,  $\sim 4$ , and  $\sim 8.5$  ka that are primarily tied to sea-level variability (Figure 7).

The clear advantage of our method compared with OSL-generated PDFs is that the peaks are much better defined. This is particularly true for the two older events, which are larger and more pronounced, while this is not the case for the OSL-derived PDF (Figure 6). To maintain consistency with previous papers, we use names of dune units to represent phases of dune emplacement (Elerton et al., 2020; Patton et al., 2019; Ward, 2006). The oldest emplacement phase (Triangle Cliff) changes from a poorly defined period between  $\sim 6.5$  and 11 ka (Elerton et al., 2020), to a tighter-defined event at  $8.5 \pm 1.0$  ka. This coincides well with the termination of the rapid component of post-glacial transgression (e.g. Larcombe et al., 1995). For the two younger events there is a shift in their peaks, in both cases making the peak slightly younger than the OSL-based peaks. For the Freshwater ( $\sim 4 \pm 0.5$  ka) and Station Hill ( $\sim 1.5 \pm 0.5$  ka) emplacement phases, the revised ages are clearly younger than the sea-level rise they are interpreted to be associated with. This is sensible as the dune ages reflect the timing of sand burial, hence dune emplacement. New dune activation ceases when sea-level rise stops, but the dunes that are active can remain active for decades to centuries after the initiation process has stopped (e.g. Houser et al., 2015; Levin, 2011; Levin et al., 2017).

The most recent dune emplacement event (Cape) occurred within the last 0.5 kyr, which does not correspond with increased sea level. This phase has been ascribed to increased human activity (Aboriginal fires and European clearance and fires) (Cook, 1986), but it has also been proposed that sea-surface temperatures (SST), specifically the intensification of ENSO and the Interdecadal Pacific Oscillation (IPO), may account for this activation (Levin, 2011). While very little is known about the long-term history of the IPO, its direct effect on beach processes in this area has recently been confirmed (Kelly et al., 2019) and it is associated with a change in incident wave direction and effective wave height (McSweeney & Shulmeister, 2018). More positive IPO conditions in the last few centuries may account for this increased coastal dune formation. There is one caveat, Coastal blowouts are formed continuously and are a function of local storms, fires, and other disturbances, as well as regional events (Hesp, 2002; Levin, 2011). The large number of very young dunes may well simply be a reflection of stochastic process, where these dunes have little long-term preservation potential.

**FIGURE 7** The combined K'gari and CSM dune field PDFs from predicted (dark grey) dune ages compared to local sea-level curves from Larcombe et al. (1995) and Lewis et al. (2008). Note that there is a break in the relative sea-level axis so that both curves could be displayed on the same graph. We observe four emplacement phases (vertical teal areas) that are closely associated with the termination of the rising limb of sea-level events. The addition of our estimated ages permits us to better constrain the timing of dune emplacement (Elerton et al., 2020), which has been associated with mapped dune units (Patton et al., 2019; Ward, 2006): Cape  $< 0.5$  ka; Station Hill  $\sim 1.5 \pm 0.5$  ka; Freshwater  $\sim 4 \pm 0.5$  ka; Triangle Cliff  $8.5 \pm 1.0$  ka



It is important to note that we observe little evidence to support the hypothesis that climate is the major control on widespread dune activity, as proposed by Young et al. (1993) (Figure 8). It has been inferred from paleoclimate records that there was an intensification of ENSO during the mid-Holocene, which may have led to increased storminess and climate variability (Barr et al., 2019; Conroy et al., 2008; Donders et al., 2006; Moy et al., 2002; Shulmeister & Lees, 1995), resulting in widespread dune activity. However, this is unlikely in these dune fields. Pollen studies have shown that vegetation type in the dune field was not modified by climate change in the Holocene. In fact, dune vegetation was remarkably consistent. Instead, any impact of ENSO will be through interactions with the IPO on wave climate and on enhanced SST, triggering more frequent or stronger storms.

#### 5.4 | Surface roughness-age model application

In this study we have demonstrated that the  $\alpha_C$ -age model is a potentially powerful tool to apply in dune settings. The advantage of this approach is that it produces systematic dune ages and only requires high-resolution elevation data and a limited number of constraining dune ages. It also has the ability to detect previously non-identified map units. Dunes can be placed in clusters of similar  $\alpha_C$  to help infer the number of emplacement events and their relative sequence, even when dune units are not contiguous and/or age control is absent. Furthermore, reasonable age estimates can be obtained for these undated events. These analyses can be used to target and direct future sampling strategies to ensure all events are confirmed and sampled for dating, while avoiding areas of reactivation so that a robust chronology can be constructed.

In contrast to dune ages, high-resolution elevation data is becoming increasingly available as unmanned aerial vehicles and other remote sensing techniques are being employed extensively to capture

topographic information. Indeed, our sensitivity analysis highlights that a wide range of DEM resolutions can produce robust age predictions, the PDFs of which correspond well with previously described emplacement events. We determine that  $\alpha_C$  calculated with DEM resolutions of between 3 and 20 m produces similar results. Beyond this range (i.e. finer or coarser resolution), the relationships deteriorate (Table S3, Figure S5). Additionally, it is important to recognize that not all elevation models are equal, and researchers must use their own discretion to determine if their data adequately describe the dune surface at the necessary resolution. For example, for areas with dense vegetation and/or canopy cover, UDAR should be considered because of its vegetation-penetrating abilities (i.e. bare-earth DEM) rather than a photogrammetry derived DEM which may not capture the 'true topography'.

We expect that our  $\alpha_C$ -age model will be applicable in many other dune settings. The model has three major assumptions: initial landforms are formed with significant surface roughness, landscape evolution is time dependent, and only diffusive hillslope processes are active. These suggest that all dunes within the same system will have identical evolutionary trajectories ( $\alpha_C$ -age regression) and their topography will only smooth with time (decreasing  $\alpha_C$ ). Within K'gari and the CSM, these assumptions are known to be valid and are clearly demonstrated by the strength of our model in both locations. Similar to K'gari and the CSM, many coastal dune systems have relatively stable base levels in the Mid- to Late Holocene, well-defined and stable wind fields, and have uniform, well-sorted, and unconsolidated material. These boundary conditions apply on the Oregon coast (Peterson et al., 2007) and Great Lakes of the United States (Hansen et al., 2020), Northern Ireland and Scotland (Sommerville et al., 2007; Wilson et al., 2004), the southeast Brazil coast (Giannini et al., 2007), and Israel (Levin et al., 2008), amongst many others.

Despite superficial similarities, each of these dune systems vary dramatically in climate and biota, which may lead to changes in the rate at which  $\alpha_C$  decays with time between sites. As discussed by

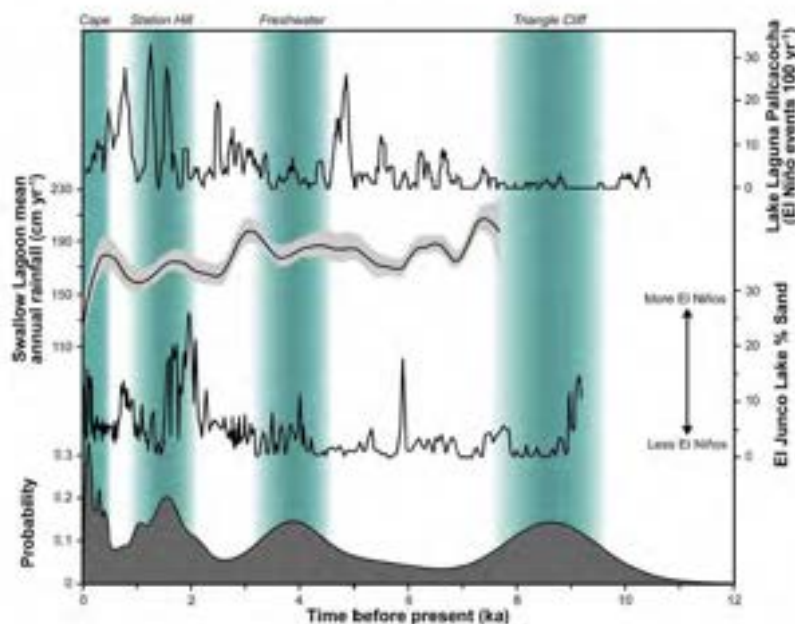


FIGURE 8 Paleoclimate records through the Holocene from Laguna Palicacocha in southern Ecuador (Moy et al., 2002), Swallow Lagoon in eastern Australia (Barr et al., 2019), and El Junco Lake in the Galápagos Islands (Conroy et al., 2008) compared to timing of major dune emplacement phases at K'gari and the CSM. Climate appears to have little direct link to dune emplacement



Booth et al. (2017) and Patton et al. (2022), the rate of decline for the regression is controlled by soil diffusivity (which is the combined effect of all environmental factors influencing the efficiency of sediment to move downslope). As a result, there is no one dune field  $\sigma_c$ -age regression that is applicable at all sites. A new model calibration and validation is critical in each case. Nevertheless, the decline in  $\sigma_c$  with time and its value can help infer transport processes, characterize dune evolution, and place tighter constraints on dune-field development with respect to regional climate/sea-level models.

The key limitation of the method is when non-diffusive (advective) processes such as knickpoint erosion also affect dune evolution. For this reason, applications of the method should initially be limited to Holocene dunes and avoid sites with significant fluvial reworking and/or rapid base-level change. Our intention is to adapt the model to Pleistocene sections of the CSM and K'gari dune fields in due course, a process that will involve developing a model that incorporates the effect of base-level changes into the evolving  $\sigma_c$ .

## CONCLUSIONS

Determining age control for landforms is important within the earth sciences for several reasons, notably providing the rates of processes driving landscape evolution. However, acquiring the volume of ages necessary to develop the complete record of dune emplacement events for a field area is challenging and, in most cases, not feasible. This is mainly due to sample availability, time, cost, and methodological constraints, but may also arise from environmental degradation caused by sampling and travel in sensitive areas. The K'gari and CSM dune fields are ideal locations to validate this approach as within the Holocene, most major factors contributing to landscape evolution can be measured and constrained. We apply an exponential fit to our dune  $\sigma_c$ -age measurements, and this relationship can be numerically explained through conservation of mass equations. K'gari and the CSM provide a field site where >700 dunes spanning the last 10 kyr are preserved, and which can readily be compared with paleo-records of climate, sea level, and vegetation. Despite numerous dating campaigns, only slightly over 20 luminescence-dated Holocene dunes are reported (Ellerton et al., 2020; Köhler et al., 2021; Tejan-Kella et al., 1990; Walker et al., 2018). This only accounts for <3% of dunes preserved and <1% of the total land area (Patton et al., 2019). To fully understand the spatial and temporal relationship of dune emplacement, many additional ages are required. Utilizing a roughness-age empirical model provides the first high-resolution coastal dune chronology. Its application gives a more robust insight on coastal system evolution than can be derived from limited chronological constraints.

This model provides realistic estimates for every Holocene dune, which is not only useful in understanding where dunes of certain ages are located, but also adds significance to the timing of major dune emplacement events. For example, when only OSL-dated dunes are utilized, the timing of these events is broad and poorly defined. With the addition of the predicted ages, the time constraints on the events narrow, and peaks are more pronounced [e.g. the Triangle Cliff dune unit is reclassified from ~6.5–11 ka by Ellerton et al. (2020) to an  $8.5 \pm 1.0$  ka event]. At K'gari and the CSM, our results confirm that major phases of dune activity are governed by sea-level fluctuations. In addition, the age pattern allows us to demonstrate that their spatial

distributions are controlled by changes in swash/drift alignment of the coast. The oldest Holocene dunes are concentrated near headlands that act as pinning points for coastal rotation and are less erosion prone. These observations highlight the power of the method to yield new insights on landform evolution in a coastal dune field.

## ACKNOWLEDGEMENTS

Field work and mapping was undertaken using permit WITK15791415. Funding for this study was provided by the Australian Research Council (ARC) Grant No. DP150101513. We thank the National Parks and Wildlife Service for their assistance. The authors would like to acknowledge the traditional owners of the Cooloolo Sand Mass (the Kabi' Kabi' people) and K'gari (the Butchulla people), and thank the Butchulla Aboriginal Corporation (BAC) for their permission and support of work on K'gari (Fraser Island).

## AUTHOR CONTRIBUTIONS

NRP conceptualized the idea of the manuscript. JS received funding for this project NRP, DE, JS, TMR, and TS completed all field work. TMR and NRP carried out dating analyses. NRP created applied modelling. NRP and JS drafted the manuscript. JS, TMR, and PCA are the primary supervisors of NRP. All authors assisted with writing and editing the manuscript.

## DATA AVAILABILITY STATEMENT

All data necessary to generate the results for this study are available in the online Supplementary Information. All LiDAR datasets were downloaded from <https://elevation.fidf.org.au/> and all aerial photographs were downloaded from <https://qldglobe.information.qld.gov.au/>.

## ORCID

Nicholas R. Patton  <https://orcid.org/0000-0002-4137-0636>  
James Shulmeister  <https://orcid.org/0000-0001-5863-9462>  
Tammy M. Rittenour  <https://orcid.org/0000-0003-1925-0395>  
Peter Almond  <https://orcid.org/0000-0003-4203-1529>  
Daniel Ellerton  <https://orcid.org/0000-0003-1998-1817>  
Taliha Santini  <https://orcid.org/0000-0002-6396-3731>

## REFERENCES

- Aitken, M.J. (1998) *Introduction to Optical Dating: The Dating of Quaternary Sediments by the Use of Photon-Stimulated Luminescence*. Oxford: Clarendon Press.
- Aitken, M.J. & Aldred, J.C. (1972) The assessment of error limits in thermoluminescent dating. *Archaeometry*, 14(2), 257–267. Available from: <https://doi.org/10.1111/j.1475-4754.1972.tb00068.x>
- Aitken, M.J. & Xie, J. (1990) Moisture correction for annual gamma dose. *Ancient TL*, 8(2), 6–9.
- Atahan, P., Hejnis, H., Dodson, J., Grice, K., Le Metayer, P., Taffs, K., Hembrow, S., Woltering, M. & Zawadzki, A. (2015) Pollen, biomarker and stable isotope evidence of late Quaternary environmental change at Lake McKenzie, southeast Queensland. *Journal of Paleolimnology*, 53(1), 139–156. Available from: <https://doi.org/10.1007/s10933-014-9813-3>
- Barr, C., Tibby, J., Leng, M.J., Tyler, J.J., Henderson, A.C.G., Overpeck, J.T., Simpson, G.L., Cole, J.E., Phipps, S.J., Marshall, J.C., McGregor, G.B., Hua, Q. & McRobie, F.H. (2019) Holocene El Niño–Southern Oscillation variability reflected in subtropical Australian precipitation. *Scientific Reports*, 9(1), 1–9. Available from: <https://doi.org/10.1038/s41598-019-38626-3>



1. Bell, R., Petschko, H., Röhrs, M. & Dix, A. (2012) Assessment of landslide age, landslide persistence and human impact using airborne laser scanning digital terrain models. *Geografiska Annaler, Series A: Physical Geography*, 94(1), 135–156. Available from: <https://doi.org/10.1111/j.1468-0459.2012.00454.x>
2. Bert, M., Corsini, A. & Daehne, A. (2013) Comparative analysis of surface roughness algorithms for the identification of active landslides. *Geomorphology*, 182, 1–18. Available from: <https://doi.org/10.1016/j.geomorph.2012.10.022>
3. Booth, A.M., LaHusen, S.R., Duvall, A.R. & Montgomery, D.R. (2017) Holocene history of deep-seated landsliding in the North Fork Stillaguamish River valley from surface roughness analysis, radiocarbon dating, and numerical landscape evolution modeling. *Journal of Geophysical Research – Earth Surface*, 122(2), 456–472. Available from: <https://doi.org/10.1002/2016JF003934>
4. Booth, A.M., Roering, J.J. & Perron, J.T. (2009) Automated landslide mapping using spectral analysis and high-resolution topographic data: Puget Sound lowlands, Washington, and Portland Hills, Oregon. *Geomorphology*, 109(3–4), 132–147. Available from: <https://doi.org/10.1016/j.geomorph.2009.02.027>
5. Boyd, R., Roering, K., Goodwin, I., Sandstrom, M. & Schröder-Adams, C. (2008) Highstand transport of coastal sand to the deep ocean: A case study from Fraser Island, southeast Australia. *Geology*, 36(1), 15–18. Available from: <https://doi.org/10.1130/G24211A.1>
6. Coaldrake, J.E. (1962) The coastal sand dunes of southern Queensland. *Proceedings of the Royal Society of Queensland*, 72, 101–116.
7. Conroy, J.L., Overpeck, J.T., Cole, J.E., Shanahan, T.M. & Steinitz-Karnan, M. (2008) Holocene changes in eastern tropical Pacific climate inferred from a Galapagos lake sediment record. *Quaternary Science Reviews*, 27(11–12), 1166–1180. Available from: <https://doi.org/10.1016/j.quascirev.2008.02.015>
8. Cook, P.G. (1986) A review of coastal dune building in Eastern Australia. *Australian Geographer*, 17(2), 133–143. Available from: <https://doi.org/10.1080/00049188608702912>
9. Cooper, W.S. (1958) Coastal sand dunes of Oregon and Washington. *Geological Society of America: Boulder, CO*. <https://doi.org/10.1130/MEM72-p1>
10. Donders, T.H., Wagner, F. & Visscher, H. (2006) Late Pleistocene and Holocene subtropical vegetation dynamics recorded in perched lake deposits on Fraser Island, Queensland, Australia. *Palaeogeography, Palaeoclimatology, Palaeoecology*, 241(3–4), 417–439. Available from: <https://doi.org/10.1016/j.palaeo.2006.04.008>
11. Ellerton, D., Rittenour, T., Miot da Silva, G., Gontz, A., Shulmeister, J., Hesp, P., Santini, T. & Welsh, K.J. (2018) Late-Holocene cliff-top blowout activation and evolution in the Cooloola Sand Mass, southeast Queensland, Australia. *The Holocene*, 28(11), 1697–1711. <https://doi.org/10.1177/0959683618788679>
12. Ellerton, D., Rittenour, T., Shulmeister, J., Gontz, A., Welsh, K.J. & Patton, N.R. (2020) An 800 kyr record of dune emplacement in relationship to high sea level forcing, Cooloola Sand Mass, Queensland, Australia. *Geomorphology*, 354, 106999. Available from: <https://doi.org/10.1016/j.geomorph.2019.106999>
13. Frankel, K.L. & Dolan, J.F. (2007) Characterizing arid region alluvial fan surface roughness with airborne laser swath mapping digital topographic data. *Journal of Geophysical Research – Earth Surface*, 112, F02025. <https://doi.org/10.1029/2006JF000644>
14. Galbraith, R.F. & Roberts, R.G. (2012) Statistical aspects of equivalent dose and error calculation and display in OSL dating: An overview and some recommendations. *Quaternary Geochronology*, 11, 1–27. Available from: <https://doi.org/10.1016/j.quageo.2012.04.020>
15. Giannini, P.C., Sawakuchi, A.O., Martinho, C.T. & Tatum, S.H. (2007) Eolian depositional episodes controlled by Late Quaternary relative sea level changes on the Imbituba-Laguna coast (southern Brazil). *Marine Geology*, 237(3–4), 143–168. Available from: <https://doi.org/10.1016/j.margeo.2006.10.027>
16. Gillette, D.A. & Stockton, P.H. (1989) The effect of nonerodible particles on wind erosion of erodible surfaces. *Journal of Geophysical Research – Atmospheres*, 94(D10), 12885–12893. Available from: <https://doi.org/10.1029/JD094D10p12885>
17. Glenn, N.F., Streutker, D.R., Chadwick, D.J., Thackray, G.D. & Dorich, S.J. (2006) Analysis of LIDAR-derived topographic information for characterizing and differentiating landslide morphology and activity. *Geomorphology*, 73(1–2), 131–148. Available from: <https://doi.org/10.1016/j.geomorph.2005.07.006>
18. Goetz, J.N., Bell, R. & Brenning, A. (2014) Could surface roughness be a poor proxy for landslide age? Results from the Swabian Alb, Germany. *Earth Surface Processes and Landforms*, 39(12), 1697–1704. Available from: <https://doi.org/10.1002/esp.3630>
19. Guérin, G., Jain, M., Thomsen, K.J., Murray, A.S. & Mercier, N. (2015) Modelling dose rate to single grains of quartz in well-sorted sand samples: The dispersion arising from the presence of potassium feldspars and implications for single grain OSL dating. *Quaternary Geochronology*, 27, 52–65. Available from: <https://doi.org/10.1016/j.quageo.2014.12.006>
20. Guérin, G., Mercier, N. & Adamiec, G. (2011) Dose-rate conversion factors: Update. *Ancient TL*, 29(1), 5–8.
21. Han, M., Kim, J.C., Yang, D.Y., Lin, J. & Yi, S. (2021) The main periods and environmental controls of coastal dune development along the west coast of the Korean Peninsula during the mid to late Holocene. *Palaeogeography, Palaeoclimatology, Palaeoecology*, 569, 110345. Available from: <https://doi.org/10.1016/j.palaeo.2021.110345>
22. Hansen, E., DeVries-Zimmerman, S., Davidson-Arnett, R., Dijk, D.V., Bodenbender, B., Kilbardo, Z., Thompson, T. & Yurk, B. (2020) Dunes of the Laurentian Great Lakes. In: Lancaster, N. & Hesp, P. (Eds.), *Inland Dunes of North America*. Cham: Springer, pp. 65–120. [https://doi.org/10.1007/978-3-030-40498-7\\_3](https://doi.org/10.1007/978-3-030-40498-7_3)
23. Harrold, A.G., McDonald, W.J., Hopkins, M.S., Walker, J., Sandercoe, C.S., Thompson, C.H. 1987. Studies in landscape dynamics in the Cooloola-Noosa River area, Queensland. CSIRO: Canberra.
24. Hesp, P. (2002) Foredunes and blowouts: Initiation, geomorphology and dynamics. *Geomorphology*, 48(1–3), 245–268. Available from: [https://doi.org/10.1016/S0169-5550\(02\)00184-8](https://doi.org/10.1016/S0169-5550(02)00184-8)
25. Houser, C., Wemette, P., Rentschler, E., Jones, H., Hammond, B. & Trimble, S. (2015) Post-storm beach and dune recovery: Implications for barrier island resilience. *Geomorphology*, 234, 54–63. Available from: <https://doi.org/10.1016/j.geomorph.2014.12.044>
26. Huntley, D.J., Godfrey-Smith, D.I. & Thewalt, M.L. (1985) Optical dating of sediments. *Nature*, 313(5998), 105–107. Available from: <https://doi.org/10.1038/313105a0>
27. Jerolmack, D.J., Ewing, R.C., Falcini, F., Martin, R.L., Masteller, C., Phillips, C., Reitz, M.D. & Buynevich, I. (2012) Internal boundary layer model for the evolution of desert dune fields. *Nature Geoscience*, 5(3), 206–209. Available from: <https://doi.org/10.1038/ngeo1381>
28. Kelly, J.T., McSweeney, S., Shulmeister, J. & Gontz, A.M. (2019) Bimodal climate control of shoreline change influenced by Interdecadal Pacific Oscillation variability along the Cooloola Sand Mass, Queensland, Australia. *Marine Geology*, 415, 105971. Available from: <https://doi.org/10.1016/j.margeo.2019.105971>
29. Köhler, M., Shulmeister, J., Patton, N.R., Rittenour, T.M., McSweeney, S., Ellerton, D.T., Stout, J.C. & Hüneke, H. (2021) Holocene evolution of a barrier-spit complex and the interaction of tidal and wave processes, Inskip Peninsula, SE Queensland, Australia. *The Holocene*, 31(9), 1476–1488. Available from: <https://doi.org/10.1177/09596836211019092>
30. Korzenkowska, K., Pfeifer, N. & Landtwing, S. (2018) Mapping gullies, dunes, lava fields, and landslides via surface roughness. *Geomorphology*, 301, 53–67. Available from: <https://doi.org/10.1016/j.geomorph.2017.10.011>
31. LaHusen, S.R., Duvall, A.R., Booth, A.M., Grant, A., Mishkin, B.A., Montgomery, D.R., Struble, W., Roering, J.J. & Wartman, J. (2020) Rainfall triggers more deep-seated landslides than Cascadia earthquakes in the Oregon Coast Range, USA. *Science Advances*, 6(38), eaba6790. Available from: <https://doi.org/10.1126/sciadv.aba6790>
32. Lancaster, N. (2008) Desert dune dynamics and development: Insights from luminescence dating. *Bones*, 37(4), 559–573. Available from: <https://doi.org/10.1111/j.1502-3885.2008.00055.x>
33. Lancaster, N. & Baas, A. (1998) Influence of vegetation cover on sand transport by wind: Field studies at Owens Lake, California. *Earth Surface Processes and Landforms*, 23(1), 69–82. Available from: <https://doi.org/10.1016/j.espl.1998.08.001>



- doi.org/10.1002/(SICI)1096-9837(199801)23:1<69::AID-ESP823>3.0.CO;2-G
- Lancaster, N., Wolfe, S., Thomas, D., Bristow, C., Bubenzer, O., Burrough, S., Duller, G., Halfen, A., Hesse, P., Roskin, J., Singhvi, A., Tsao, H., Tripaldi, A., Yang, X. & Zitate, M. (2016) The INQUA Dunes Atlas chronologic database. *Quaternary International*, 410, 3–10. Available from: <https://doi.org/10.1016/j.quaint.2015.10.044>
- Larcombe, P., Carter, R.M., Dye, J., Gagan, M.K. & Johnson, D.P. (1995) New evidence for episodic post-glacial sea-level rise, central Great Barrier Reef, Australia. *Marine Geology*, 127(1–4), 1–44. Available from: [https://doi.org/10.1016/0025-3227\(95\)00059-8](https://doi.org/10.1016/0025-3227(95)00059-8)
- Lees, B. (2006) Timing and formation of coastal dunes in northern and eastern Australia. *Journal of Coastal Research*, 22(1), 78–89. Available from: <https://doi.org/10.2112/JCOA-0007.1>
- Levin, N. (2011) Climate-driven changes in tropical cyclone intensity shape dune activity on Earth's largest sand island. *Geomorphology*, 125(1), 239–252. Available from: <https://doi.org/10.1016/j.geomorph.2010.09.021>
- Levin, N., Ben-Dor, E., Kifron, G.J. & Yaakov, Y. (2008) Estimation of surface roughness ( $z_0$ ) over a stabilizing coastal dune field based on vegetation and topography. *Earth Surface Processes and Landforms*, 33(10), 1520–1541. Available from: <https://doi.org/10.1002/esp.1621>
- Levin, N., Jablon, P.E., Phinn, S. & Collins, K. (2017) Coastal dune activity and foredune formation on Moreton Island, Australia, 1944–2015. *Aeolian Research*, 25, 107–121. Available from: <https://doi.org/10.1016/j.aeolia.2017.03.005>
- Lewis, S.E., Wüst, R.A., Webster, J.M. & Shields, G.A. (2008) Mid-late Holocene sea-level variability in eastern Australia. *Terra Nova*, 20(1), 74–81. Available from: <https://doi.org/10.1111/j.1365-3121.2007.00789.x>
- Lindhorst, S. & Bettler, C. (2016) The climate-archive dune: Sedimentary record of annual wind intensity. *Geology*, 44(9), 711–714. Available from: <https://doi.org/10.1130/G38093.1>
- Marin, L., Forman, S.L., Valdez, A. & Burch, F. (2005) Twentieth century dune migration at the Great Sand Dunes National Park and Preserve, Colorado, relation to drought variability. *Geomorphology*, 70(1–2), 163–183. Available from: <https://doi.org/10.1016/j.geomorph.2005.04.014>
- Martinez, M.L. & Puzy, N.P. (2004) *Coastal Dunes*. Berlin: Springer Verlag 10.1007/978-3-540-74002-5.
- McKean, J. & Roering, J. (2004) Objective landslide detection and surface morphology mapping using high-resolution airborne laser altimetry. *Geomorphology*, 57(3–4), 331–351. Available from: [https://doi.org/10.1016/S0169-555X\(03\)00164-8](https://doi.org/10.1016/S0169-555X(03)00164-8)
- McSweeney, S. & Shulmeister, J. (2018) Variations in wave climate as a driver of decadal scale shoreline change at the Inskip Peninsula, southeast Queensland, Australia. *Estuarine, Coastal and Shelf Science*, 209, 56–69. Available from: <https://doi.org/10.1016/j.ecss.2018.04.034>
- Moore, I.D., Grayson, R.B. & Landson, A.R. (1991) Digital terrain modeling: A review of hydrological, geomorphological, and biological applications. *Hydrological Processes*, 5(1), 3–30. Available from: <https://doi.org/10.1002/hyp.3360050103>
- Moss, P., Dudgeon, A., Shupland, F., Withers, L., Brownhill, C., Terzano, D., Petherick, L. & Sloss, C. (2013) Investigation into the Vegetation and Fire History of the EPBC, Ramsar and WHA Wetlands of the Great Sandy Straits, South East Queensland. Unpublished report to the Burnett Mary Regional Group, Bundaberg, Queensland.
- Moy, C.M., Seltzer, G.O., Rodbell, D.T. & Anderson, D.M. (2002) Variability of El Niño/Southern Oscillation activity at millennial timescales during the Holocene epoch. *Nature*, 420(6912), 162–165. Available from: <https://doi.org/10.1038/nature01194>
- Murray, A., Arnold, L.J., Buylaert, J.P., Guérin, G., Qin, J., Singhvi, A.K., Smedley, R. & Thomsen, K.J. (2021) Optically stimulated luminescence dating using quartz. *Nature Reviews Methods Primers*, 1(1), 1–31. Available from: <https://doi.org/10.1038/s43586-021-00068-5>
- Murray, A.S. & Wintle, A.G. (2000) Luminescence dating of quartz using an improved single-aliquot regenerative-dose protocol. *Radiation Measurements*, 32(1), 57–73. Available from: [https://doi.org/10.1016/S1350-4487\(99\)00253-X](https://doi.org/10.1016/S1350-4487(99)00253-X)
- Murray, A.S. & Wintle, A.G. (2003) The single aliquot regenerative dose protocol: Potential for improvements in reliability. *Radiation Measurements*, 37(4–5), 377–381. Available from: [https://doi.org/10.1016/S1350-4487\(03\)00053-2](https://doi.org/10.1016/S1350-4487(03)00053-2)
- Patterson, C.C. & Patterson, D.C. (1983) Gold Coast longshore transport. In: *Proceedings of the 6th Australian Coastal and Ocean Engineering Conference*. Gold Coast: The Institute of Engineers, pp. 251–256.
- Patton, N.R., Ellerton, D. & Shulmeister, J. (2019) High-resolution remapping of the coastal dune fields of south east Queensland, Australia: A morphometric approach. *Journal of Maps*, 15(2), 578–589. Available from: <https://doi.org/10.1080/17445647.2019.1642246>
- Patton, N.R., Lohse, K.A., Godsey, S.E., Crosby, B.T. & Seyfried, M.S. (2018) Predicting soil thickness on soil mantled hillslopes. *Nature Communications*, 9(1), 1–10. Available from: <https://doi.org/10.1038/s41467-018-05743-y>
- Patton, N.R., Shulmeister, J., Ellerton, D. & Seropian, G. (2022) Measuring landscape evolution from inception to maturity: Insights from a coastal dune system. *Earth and Planetary Science Letters*, 584, 117448. Available from: <https://doi.org/10.1016/j.epsl.2022.117448>
- Pelletier, J.D. (2013) Deviations from self-similarity in barchan form and flux: The case of the Salton Sea dunes, California. *Journal of Geophysical Research – Earth Surface*, 118(4), 2406–2420.
- Pelletier, J.D., Mitasova, H., Harmon, R.S. & Overton, M. (2009) The effects of interdune vegetation changes on eolian dune field evolution: A numerical-modeling case study at Jockey's Ridge, North Carolina, USA. *Earth Surface Processes and Landforms*, 34(9), 1245–1254. Available from: <https://doi.org/10.1002/esp.1809>
- Peterson, C.D., Stock, E., Price, D.M., Hart, R., Reckendorf, F., Erlanson, J. M. & Hostetler, S.W. (2007) Ages, distributions, and origins of upland coastal dune sheets in Oregon, USA. *Geomorphology*, 91(102), 80–102. Available from: <https://doi.org/10.1016/j.geomorph.2007.02.005>
- Pommerol, A., Chakraborty, S. & Thomas, N. (2012) Comparative study of the surface roughness of the Moon, Mars and Mercury. *Planetary and Space Science*, 73(1), 287–293. Available from: <https://doi.org/10.1016/j.jss.2012.08.020>
- Prescott, J.R. & Hutton, J.T. (1994) Cosmic ray contributions to dose rates for luminescence and ESR dating: Large depths and long-term time variations. *Radiation Measurements*, 23(2–3), 497–500. Available from: [https://doi.org/10.1016/1350-4487\(94\)90086-8](https://doi.org/10.1016/1350-4487(94)90086-8)
- Pye, K. (1982) Morphological development of coastal dunes in a humid tropical environment, Cape Bedford and Cape Flattery, North Queensland. *Geografiska Annaler, Series A: Physical Geography*, 64(3–4), 213–227. Available from: <https://doi.org/10.1080/04353676.1982.11880067>
- Pye, K. (1983) Coastal dunes. *Progress in Physical Geography*, 7(4), 531–557. Available from: <https://doi.org/10.1177/03091333830700403>
- Pye, K. & Bowman, G.M. (1984) The Holocene marine transgression as a forcing function in episodic dune activity on the eastern Australian coast. In: Thom, B.G. (ed.), *Coastal Geomorphology in Australia*. Academic Press: New York; 179–196.
- Raupach, M.R., Gillette, D.A. & Leys, J.F. (1993) The effect of roughness elements on wind erosion threshold. *Journal of Geophysical Research – Atmospheres*, 98(D2), 3023–3029. Available from: <https://doi.org/10.1029/92JD01922>
- Roy, P.S. & Thom, B.G. (1981) Late Quaternary marine deposition in New South Wales and southern Queensland—an evolutionary model. *Journal of the Geological Society of Australia*, 28(3–4), 471–489. Available from: <https://doi.org/10.1080/00167618108729182>
- Schanz, S.A. & Colee, A.P. (in review, 2021) Development of a surface roughness curve to estimate timing of earthflows and habitat development in the Tearaway River, central Washington State, USA. *Earth Surface Dynamics Discussions*. [Preprint]. Available from: <https://doi.org/10.5194/esurf-2021-61>



- Shulmeister, J. & Lees, B.G. (1992) Morphology and chronostratigraphy of a coastal dune field, Grootte Eylandt, northern Australia. *Geomorphology*, 5(6), 521–534. Available from: [https://doi.org/10.1016/0169-555X\(92\)90023-H](https://doi.org/10.1016/0169-555X(92)90023-H)
- Shulmeister, J. & Lees, B.G. (1995) Pollen evidence from tropical Australia for the onset of an ENSO-dominated climate at c. 4000 BP. *The Holocene*, 5(1), 10–18. Available from: <https://doi.org/10.1177/095968369500500102>
- Shumack, S. & Hesse, P. (2018) Assessing the geomorphic disturbance from fires on coastal dunes near Esperance, Western Australia: Implications for dune de-stabilisation. *Aeolian Research*, 31, 29–49. Available from: <https://doi.org/10.1016/j.aeolia.2017.08.005>
- Smith, M.W. (2014) Roughness in the earth sciences. *Earth-Science Reviews*, 136, 202–225. Available from: <https://doi.org/10.1016/j.earscirev.2014.05.016>
- Sommerville, A.A., Hanson, J.D., Housley, R.A. & Sanderson, D.C.W. (2007) Optically stimulated luminescence (OSL) dating of coastal aeolian sand accumulation in Sanday, Orkney Islands, Scotland. *The Holocene*, 17(5), 627–637. Available from: <https://doi.org/10.1177/0959683607078987>
- Stallins, J.A. & Parker, A.J. (2003) The influence of complex systems interactions on barrier island dune vegetation pattern and process. *Annals of the Association of American Geographers*, 93(1), 13–29. Available from: <https://doi.org/10.1111/1467-8306.93102>
- Stephens, A., Roy, P. & Jones, M. (1981) Geological model of erosion on a littoral drift coast. In *Proceedings of the 5th Australian Conference on Coastal and Ocean Engineering: Offshore Structures*. Institute of Engineers: Barton, ACT, 174–179. <https://search.informit.org/doi/10.3316/informit.925679732664746>
- Swezey, C. (2001) Eolian sediment responses to late Quaternary climate changes: Temporal and spatial patterns in the Sahara. *Palaeogeography, Palaeoclimatology, Palaeoecology*, 167(1–2), 119–155. Available from: [https://doi.org/10.1016/S0031-0182\(00\)00235-2](https://doi.org/10.1016/S0031-0182(00)00235-2)
- Tejan-Kella, M.S., Chittleborough, D.J., Fitzpatrick, R.W., Thompson, C.H., Prescott, J.R. & Hutton, J.T. (1990) Thermoluminescence dating of coastal sand dunes at Cooloola and North Stradbroke Island, Australia. *Soil Research*, 28(4), 465–481. Available from: <https://doi.org/10.1071/SR9900465>
- Thom, B.G. (1978) Coastal sand deposition in southeast Australia during the Holocene. In: Davies, J.L. & Williams, M.A.J. (Eds.), *Landform Evolution in Australasia*. Canberra: ANU Press, pp. 197–214.
- Thompson, C.H. (1981) Podzol chronosequences on coastal dunes of eastern Australia. *Nature*, 291(5810), 59–61. Available from: <https://doi.org/10.1038/291059a0>
- Thompson, C.H. (1992) Genesis of podzols on coastal dunes in southern Queensland. I. Field relationships and profile morphology. *Soil Research*, 30(5), 593–613. Available from: <https://doi.org/10.1071/SR920593>
- Tsoar, H. (2005) Sand dunes mobility and stability in relation to climate. *Physica A: Statistical Mechanics and its Applications*, 357(1), 50–56. Available from: <https://doi.org/10.1016/j.physa.2005.05.067>
- Vimpere, L., Watkins, S.E. & Castelltort, S. (2021) Continental interior parabolic dunes as a potential proxy for past climates. *Global and Planetary Change*, 206, 106622. Available from: <https://doi.org/10.1016/j.gloplacha.2021.106622>
- Walker, J., Lees, B., Olley, J. & Thompson, C. (2018) Dating the Cooloola coastal dunes of south-eastern Queensland, Australia. *Marine Geology*, 398, 73–85. Available from: <https://doi.org/10.1016/j.margeo.2017.12.010>
- Ward, R. (1978) Australian legend re-visited. *Australian Historical Studies*, 18(71), 171–190. Available from: <https://doi.org/10.1080/10314617808595586>
- Ward, W.T. (2006) Coastal dunes and strandplains in southeast Queensland: Sequence and chronology. *Australian Journal of Earth Sciences*, 53(2), 363–373. Available from: <https://doi.org/10.1080/08120090500507354>
- Wells, A. & Goff, J. (2007) Coastal dunes in Westland, New Zealand, provide a record of paleoseismic activity on the Alpine fault. *Geology*, 35(8), 731–734. Available from: <https://doi.org/10.1130/G23554A.1>
- Wiggs, G.F., Livingstone, I., Thomas, D.S. & Bullard, J.E. (1996) Airflow and roughness characteristics over partially vegetated linear dunes in the southwest Kalahari Desert. *Earth Surface Processes and Landforms*, 21(1), 19–34. Available from: [https://doi.org/10.1002/\(SICI\)1096-9837\(199601\)21:1<19::AID-ESP508>3.0.CO;2-P](https://doi.org/10.1002/(SICI)1096-9837(199601)21:1<19::AID-ESP508>3.0.CO;2-P)
- Wilson, P. (2002) Holocene coastal dune development on the South Emerald peninsula, Western Ross, Scotland. *Scottish Journal of Geology*, 38(1), 5–13. Available from: <https://doi.org/10.1144/sjg38010005>
- Wilson, P., McGourty, J. & Bateman, M.D. (2004) Mid- to late-Holocene coastal dune event stratigraphy for the north coast of Northern Ireland. *The Holocene*, 14(3), 406–416. Available from: <https://doi.org/10.1191/0959683604NH716p>
- Wintle, A.G. (1997) Luminescence dating: Laboratory procedures and protocols. *Radiation Measurements*, 27(5–6), 769–817. Available from: [https://doi.org/10.1016/S1350-4487\(97\)00220-5](https://doi.org/10.1016/S1350-4487(97)00220-5)
- Wintle, A.G. & Murray, A.S. (2006) A review of quartz optically stimulated luminescence characteristics and their relevance in single-aliquot regeneration dating protocols. *Radiation Measurements*, 41(4), 369–391. Available from: <https://doi.org/10.1016/j.radmeas.2005.11.001>
- Yan, N. & Baas, A.C. (2015) Parabolic dunes and their transformations under environmental and climatic changes: Towards a conceptual framework for understanding and prediction. *Global and Planetary Change*, 124, 123–148. Available from: <https://doi.org/10.1016/j.gloplacha.2014.11.010>
- Yan, N. & Baas, A.C. (2017) Environmental controls, morphodynamic processes, and ecogeomorphic interactions of barchan to parabolic dune transformations. *Geomorphology*, 278, 209–237. Available from: <https://doi.org/10.1016/j.geomorph.2016.10.033>
- Yizhuo, H., Ashkenazy, Y. & Tsoar, H. (2007) Why do active and stabilized dunes coexist under the same climatic conditions? *Physical Review Letters*, 98(18), 188001. Available from: <https://doi.org/10.1103/PhysRevLett.98.188001>
- Young, R.W., Bryant, E.A., Price, D.M., Wirth, L.M. & Pease, M. (1993) Theoretical constraints and chronological evidence of Holocene coastal development in central and southern New South Wales, Australia. *Geomorphology*, 7(4), 317–329. Available from: [https://doi.org/10.1016/0169-555X\(93\)90061-6](https://doi.org/10.1016/0169-555X(93)90061-6)
- Zevenbergen, L.W. & Thorne, C.R. (1987) Quantitative analysis of land surface topography. *Earth Surface Process Landforms*, 12(1), 47–56. Available from: <https://doi.org/10.1002/esp.3290120107>

# SUPPORTING INFORMATION

Additional supporting information may be found in the online version of the article at the publisher's website.

How to cite this article: Patton, N.R., Shulmeister, J., Rittenour, T.M., Almond, P., Ellerton, D. & Santini, T. (2022) Using calibrated surface roughness dating to estimate coastal dune ages at K'gari (Fraser Island) and the Cooloola Sand Mass, Australia. *Earth Surface Processes and Landforms*, 1–16. Available from: <https://doi.org/10.1002/esp.5387>



## A.6.4 Chapters 5 – Quaternary Research

*Quaternary Research* (2023), 1–23  
doi:10.1017/qua.2023.14

## Research Article

## Reconstructing Holocene fire records using dune footslope deposits at the Cooloola Sand Mass, Australia

Nicholas R. Patton<sup>a,b,c</sup>, James Shulmeister<sup>a,b</sup>, Quan Hua<sup>d</sup>, Peter Almond<sup>e</sup>, Tammy M. Rittenour<sup>f</sup>, Johanna M. Hanson<sup>a</sup>, Aloysius Grealy<sup>b</sup>, Jack Gilroy<sup>b</sup> and Daniel Ellerton<sup>b,g</sup>

<sup>a</sup>School of Earth and Environment, University of Canterbury, Christchurch 8041, New Zealand; <sup>b</sup>School of Earth and Environmental Sciences, University of Queensland, Brisbane 4072, Australia; <sup>c</sup>Desert Research Institute, 2215 Raggio Parkway, Reno, Nevada 89512, USA; <sup>d</sup>Australian Nuclear Science and Technology Organisation, Kirrawee DC, New South Wales, 2232, Australia; <sup>e</sup>Department of Soil and Physical Sciences, Lincoln University, Christchurch 7647, New Zealand; <sup>f</sup>Department of Geosciences, Utah State University, Logan, Utah 84322, USA and <sup>g</sup>Department of Geological Sciences, Stockholm University, SE 10961 Stockholm, Sweden

## Abstract

In this study, we assess charcoal records from eolian deposits within the Cooloola Sand Mass, a subtropical coastal dune system in eastern Australia, to determine whether they can be used as a proxy for Holocene fire history. We excavate four profiles in depositional wedges at the base of dune slipfaces (footslope deposits) and calculate charcoal concentrations for three size classes (180–250 µm, 250–355 µm, and 355 µm–2 mm) at predetermined depth intervals. Age–depth models are constructed for each profile using radiocarbon measurements ( $n = 46$ ) and basal optically stimulated luminescence ages ( $n = 4$ ). All records appear intact with little evidence of postdepositional mixing as demonstrated by minimal age reversals and consistent trends in charcoal concentration and accumulation rates (CHAR) among size classes. Combining all four records, we generate a ca. 7 cal ka BP terrestrial fire history that depicts distinct peaks representing periods of increased local fire activity at <0.3, 1.1–0.4, 2.2–1.6, 3.4–2.6, and 6.7–5.3 cal ka BP. Our findings parallel regional records and highlight the utility of dune footslopes as ecological and sedimentary archives. As dune fields are much more common than wetlands and lakes in semiarid and arid areas, these deposits have the potential to increase the spatial resolution of fire records globally.

**Keywords:** Paleofire; Fire history; Charcoal; CHAR; Hillslopes; Eolian sediments; Sediment transport; Erosion; Colluvial; Landscape evolution

(Received 5 October 2022; accepted 9 March 2023)

## INTRODUCTION

Wildfires are prevalent across much of the world; however, fire records are primarily limited to regions with abundant aquatic archives (e.g., Power et al., 2008; Harrison et al., 2022). As a result, identifying a potential sediment deposit commonly found within these areas, such as drylands, would provide a valuable target for paleodimate studies and a means to evenly distribute fire records globally. The goal of this study is to assess the utility of dune footslope deposits to reconstruct fire histories. As a case study, we focus on stabilized Holocene dunes at the Cooloola Sand Mass (CSM) within the southeast (SE) Queensland dune fields (Fig. 1). The dunes are well dated (Walker et al., 2018; Ellerton et al., 2020; Patton et al., 2022b), their evolution is well understood (Levin, 2011; Patton et al., 2022a), and there are several aquatic records that can be used for comparison and validation (Donders et al., 2006; Mariani et al., 2019; Hanson et al., 2023). Specifically, the main objectives were to (1) assess whether sites

contain stratigraphically intact units with preserved depositional charcoal for developing a fire record; (2) evaluate the sensitivity of the records to charcoal size classes; (3) place the spatially aggregated charcoal records into the context of other records found in the SE Queensland dune fields; and (4) consider improvements to the data gathering and/or interpretation techniques. The outcomes will aid in the development of charcoal records from areas where fire is a rare event (wetlands/lakes) into regions where fire may be the dominant geomorphic and ecological process.

## Fire in the Australian landscape

Fire is one of the most dominant landscape disturbances on Earth (Hennessy et al., 2005; Bowman et al., 2009; McLauchlan et al., 2020). This was clearly demonstrated in the 2019–2020 Black Summers bushfires in Australia, which burned ~240,000 km<sup>2</sup>, destroyed more than 3000 houses, killed an estimated 1 billion animals, and displaced thousands of people (DAWE, 2020; Filkov et al., 2020; Richards et al., 2020; Canadell et al., 2021; Gallagher et al., 2021; Fig. 1). Fire activity (both frequency and severity) has been projected to increase due to changes in land use and climate (McKenzie et al., 2004; IPCC, 2021). It is therefore imperative to understand the role, frequency, and intensity

Corresponding author: N.R. Patton; Email: [nicholaspatton@pg.canterbury.ac.nz](mailto:nicholaspatton@pg.canterbury.ac.nz)  
Cite this article: Patton NR, Shulmeister J, Hua Q, Almond P, Rittenour TM, Hanson JM, Grealy A, Gilroy J, Ellerton D (2023) Reconstructing Holocene fire records using dune footslope deposits at the Cooloola Sand Mass, Australia. *Quaternary Research* 1–23. <https://doi.org/10.1017/qua.2023.14>



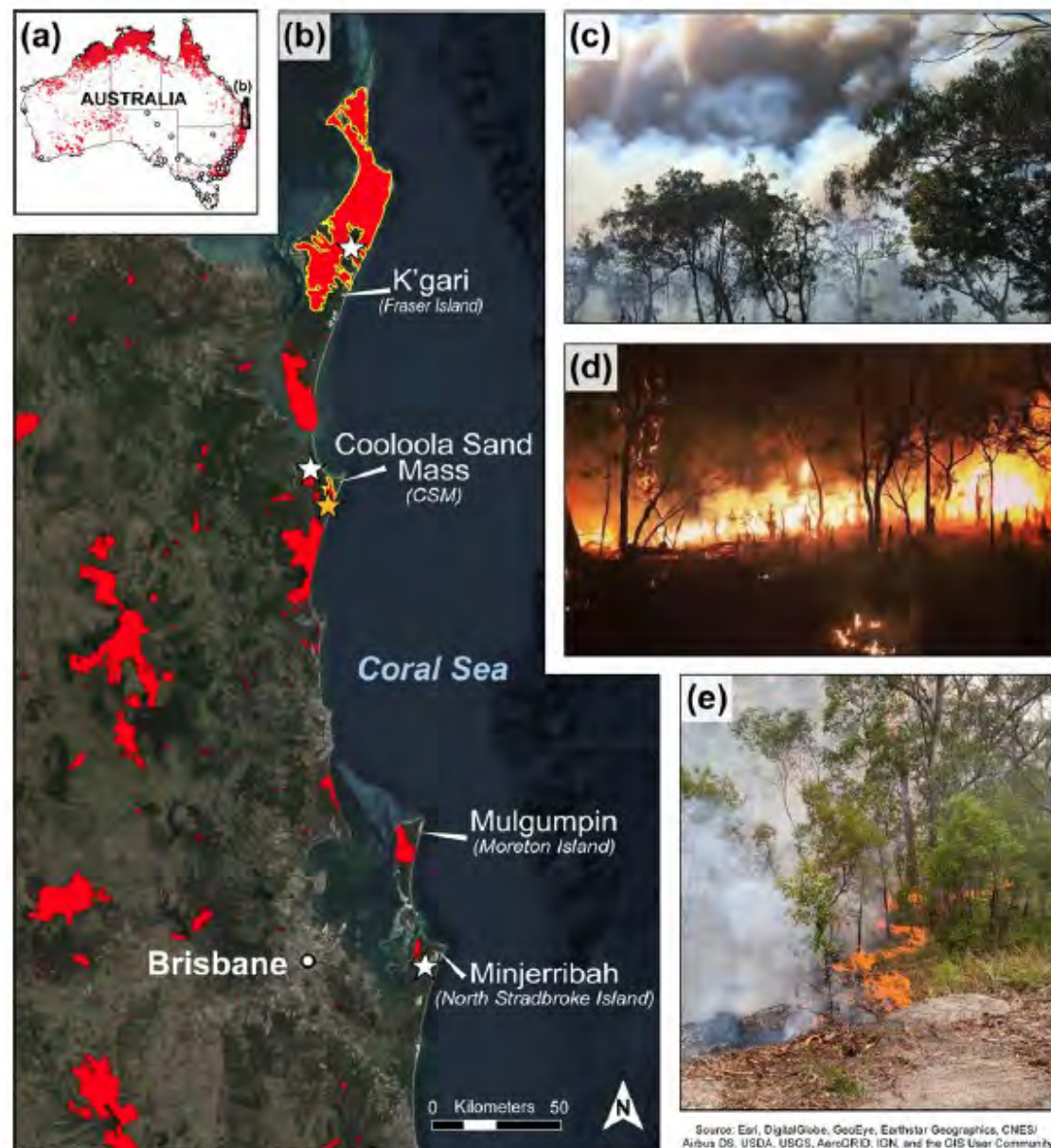


**Figure 1.** (a) Total area burned in Australia during the 2019–2020 Black Summers bushfires (red area) (DAWE, 2020) and the locations of sediment cores (white dots) used to generate Late Quaternary fire records in Mooney et al. (2011). (b) Satellite imagery of the SE Queensland dune fields and location of fires during the 2019–2020 fire season with the yellow outlines representing the Fraser Fire and Freshwater Road Fire on K'gari and the Cooloolool Sand Mass (CSM), respectively. The orange star marks the field site for this study, whereas the white stars indicate the locations of fire records used for comparative purposes in this research. Images of (c) the Kings Bore Wildfire, (d) the Thannaie Fire, and (e) the Freshwater Road Fire are provided as examples of wildfires that occurred within the SE Queensland dune fields during the Black Summers. Photo credits: (c) Michael Ford; (d and e) Erin Atkinson.

of fire in Australia, as it is one of the world's most fire-prone landscapes (Bradstock et al., 2002; Russell-Smith et al., 2007; Bradstock, 2010; van der Werf et al., 2017) and one that has a long legacy of both natural and anthropogenic fire occurrence.

Before the arrival of humans ca. 70–65 ka, evidence of fire in sedimentological records is intermittent and sparse and is

presumed to be of minor importance in Australia (Singh et al., 1981; Moss and Kershaw, 2000; Clarkson et al., 2017). After this period, the subsequent substantial increase in fire activity is commonly ascribed to Indigenous arrival (Kershaw, 1986; Turney et al., 2001) due to their frequent use of small, low-intensity fire across the landscape, aka "fire-stick farming"



(Russell-Smith et al., 1997; Bowman, 1998). However, more recent studies have suggested little evidence of variations in fire regimes after human arrival, instead ascribing increased fire activity to changes in climate (e.g., Mooney et al., 2011).

The relationship between humans and fire is difficult to address in sedimentological records, because the timing of initial human arrival is not precisely known and there are autocorrelations between climate, vegetation, and fire (Bowman, 1998; Archibald et al., 2013). Not until European arrival and a shift to fire suppression and cessation in the last 200 yr, do we see a clear anthropogenic signal (Moss et al., 2011, 2015; Hanson et al., 2022). Indeed, the transition from traditional fire management to fire suppression is inferred to be responsible for not only increased fire severity, but also a shift in vegetation structure, boundaries, and community composition (Thompson and Moore, 1984; Pyne, 1998; Fletcher et al., 2021; Mariani et al., 2022; Stone et al., 2022).

Regardless of its origin, the role of fire in controlling Australian ecosystems and landscapes is widely accepted as significant (Bowman, 1998). There are large and growing paleofire data sets (e.g., Marlon et al., 2015; Gross et al., 2018; Hawthorne et al., 2018; Harrison et al., 2022), but the records in these databases are strongly biased toward wetland areas, and consequently, for Australia, there is a strong emphasis on the SE region (Fig. 1a). To broaden the coverage of fire histories, there is a need to extend records beyond peat bogs, swamps, and lakes; however, much of the Australian landscape is not suitable to sustaining long-term organic records (Bridgman and Timms, 2012; Chang et al., 2014, 2017), and finding suitable sites for the preservation of sedimentary charcoal is therefore challenging (e.g., Leys et al., 2018). As a result, there are spatial discrepancies in data coverage across the continent, particularly in the interior and in the tropics and subtropics. A means to extend fire histories to the continental interior, where fires may be the dominant ecological process, is needed. In this study, we examine dune deposits as potential archives of fire history within the SE Queensland dune fields, because these landforms are abundant within the interior and along the coastlines of Australia (Lees, 2006; Hesse, 2016) and many parts of the world (Lancaster et al., 2016).

### SE Queensland dune field vegetation

The SE Queensland dune fields (aka the Great Sandy Coast) in Australia (24.4°S–27.5°S) include the three largest sand islands in the world—K'gari (Fraser Island), Minjerribah (North Stradbroke Island), and Mulgumpin (Moreton Island)—and the CSM on the mainland (Fig. 1b). These dune fields have existed since ca. 800 ka (Ellerton et al., 2020, 2023). They are composed of large parabolic dunes that contain the world's largest rainforest and unconfined aquifer on a sand island and are home to rare flora and fauna (UNESCO, 2021). Their vegetation structure follows a climax succession moving inland from the coast (Walker et al., 1981, 2010). Biozones change from coastal pioneer communities, through dry sclerophyll forest (e.g., *Eucalyptus*, *Casuarina*, and *Banksia*), to wet sclerophyll forest (e.g., satinay [*Syncairpia hillii*], *Amucaria*, and ferns), and rainforest landward, with heathlands and coastal wetlands on the western (inland) side of the dune sequences (Queensland Herbarium, 2021).

While this shift in vegetation structure and composition is inferred to be reliant on nutrient and water availability (Walker et al., 1981, 1987; Thompson, 1992; Thomas, 2003), fire plays an important role in shaping this landscape (Thompson and

Moore, 1984; Walker et al., 1987; Spencer and Baxter, 2006). For example, heathlands and dry sclerophyll forest often require frequent, low-intensity fires at a minimum spacing of 8 yr to reduce ground cover and canopy shading and incorporate nutrients into the soils (Keeley, 1995; Bowman et al., 2014; Queensland Herbarium, 2021).

Wet sclerophyll forest (composed of tall sclerophyll trees with relatively dense understory vegetation such as ferns) is characterized by less frequent fires occurring in SE Queensland at a minimum of 20 yr intervals (Queensland Herbarium, 2021). In these areas, fires are generally suppressed by the forest moisture content. Even wetter are the rainforests, or more accurately, notophyllous vine thickets, that typically avoid burning in all but the driest and most extreme conditions. Local patches of rainforest within the dune fields are associated with the low-lying dune swales that are perennially wet, and when fires penetrate, they are usually low intensity; however, these systems are extremely sensitive to fire (Collins, 2019; Queensland Herbarium, 2021).

### SE Queensland dune field fire history and geomorphic response

The oldest fire record from the dune island of Minjerribah, ca. 160 km south of the CSM, has preserved fire activity for at least the last ca. 210 ka. There are documented Indigenous traditions of frequent, low-intensity burning on these dune fields (Fensham, 1997; Mulholland, 2021). The oldest archaeological site on Minjerribah is at Wallen Wallen Creek and is dated to 21 ka (Neal and Stock, 1986). Dated archaeological sites on K'gari and the CSM are much younger, with the oldest published age at ca. 5.5 ka (McNiven, 1991), but it is likely that these areas have been inhabited at least as long as Minjerribah.

More recently, Indigenous land management has been absent from the dune fields and replaced by a fire-suppression regime that dates to the expansion of the timber industry ca. AD 1870 (Hawkins, 1975; Spencer and Baxter, 2006). The consequent shift to less frequent fires is easily identified in paleoecological studies (e.g., Moss et al., 2015) and has led to the transition of wet sclerophyll forests to rainforest through local fire exclusion (Krishnan et al., 2018). It is also linked to rare, higher-intensity fire events. For example, in late AD 2020, the Fraser Island Fire burned over 50% (~870 km<sup>2</sup>) of K'gari (Fig. 1b) and is believed to have had a devastating effect on the biota of the dune fields and may be responsible for an acceleration of dune migration (Mulholland, 2021).

Indeed, fire plays a critical role in transforming the landscape (Fig. 1c–e). It is well documented that fire may lead to the formation, accretion, and/or erosion of dunes (Levin et al., 2012; Shumack and Hesse, 2018; Ellerton et al., 2018; Patton et al., 2022a). Ellerton et al. (2018) discovered that the most recent activation of the Carlo Blowout in the CSM was initiated by fire and posited that this was unlikely to be a onetime occurrence. As was discussed in Patton et al. (2022a), fire is one of the primary factors creating the necessary conditions to destabilize steep dune hillslopes. We found that the burned sections of the 2019 Freshwater Road Fire (Fig. 1e) induced dry-ravel and sheetwash (similar to sand avalanching), but these processes were limited to the youngest dunes (Fig. 1b, Supplementary Fig. 1). We hypothesized that this was due to changes in sediment transport styles associated with hillslope gradients after fire. This study aims to help elucidate the effects of fire on dune erosional and depositional processes over multimillennial periods, and how these changes may influence our interpretations of charcoal records.



Landscapes such as the SE Queensland dune fields, with high fuel loads and proximity to consistent winds, are prone to wildfires (Filion, 1984; Thompson and Moore, 1984; Srivastava et al., 2012; Shumack et al., 2017; Ellerton et al., 2018); however, dune environments are rarely targeted for paleofire reconstruction. This is most likely because they are regarded as too ephemeral or present difficulties for extracting reliable multimillennial environmental records. There are few bogs in the CSM, so there are no fire records documented within the immediate dunes, despite the inferred importance of fire in maintaining the local environment. This is in contrast to the other SE Queensland dune fields (i.e., K'gari and Minjerribah), which have multiple charcoal records (e.g., Donders et al., 2006; Barr et al., 2013, 2017; Moss et al., 2013; Atahan et al., 2015; Mariani et al., 2019; Schreuder et al., 2019; Kemp et al., 2021; Maxson et al., 2021) from bog, lake, and fen settings. The closest records from the CSM dune field are from the Rainbow Beach patterned fen complexes approximately 10 km northwest of the dune field (Moss, 2014; Hanson et al., 2023; Fig. 2), which provide local records to compare with records from the CSM.

## METHODS

### Site selection and sampling design

The CSM in SE Queensland, Australia, is positioned approximately 150 km north of Brisbane and immediately south of the sand island K'gari. The dune field has an area of 240 km<sup>2</sup> and is composed of large parabolic dunes with crests up to 240 m above sea level. They are composed of >98% well-sorted siliceous sands (180–250 µm) (Thompson, 1983, 1992; Tejan-Kella et al., 1990). The freely drained soils and the humid subtropical climate with its warm, wet summers and mild, dry winters (mean annual precipitation = 1500 mm) (Peel et al., 2007; BOM, 2019) promote podzolization. Sediments are retained within interdune and foot-slope positions due to the lack of fluvial and eolian erosion following stabilization by vegetation (Patton et al., 2022a). The land-surface stability coupled with high porosity and permeability lead to the unabated development of giant podzols (Thompson, 1981). Changes in dune-form age correspond with systematic changes in soil and vegetation development. The dune field has been extensively dated (Tejan-Kella et al., 1990; Walker et al., 2018; Ellerton et al., 2020, 2023; Patton et al., 2022b) and mapped (Ward, 2006; Patton et al., 2019).

Most dunes initiate near the coastline from disturbances such as sea-level rise, storms, and/or fires (Levin, 2011; Patton et al., 2022b). Their path inland is maintained by the nearly limitless sediment supply from the longshore-drift system (Boyd et al., 2008) and consistent SE winds (Coaldrake, 1962) until they are ultimately stabilized by vegetation (Levin, 2011). The timing of dune stabilization is penecontemporaneous with the initiation of dune sediment erosion and deposition (i.e., the transition from eolian to colluvial processes) (Patton et al., 2022b). These processes have been occurring for at least 800 ka, resulting in one of the oldest and most complex coastal dune sequences in the world (Ellerton et al., 2020, 2023).

In this study, we sampled depositional wedges at the base of four closely adjacent Holocene parabolic dunes with emplacement (stabilization) ages of  $0.44 \pm 0.10$  ka,  $2.14 \pm 0.27$  ka,  $4.89 \pm 0.45$  ka, and  $9.82 \pm 0.98$  ka, hereafter referred to as the 0.5 ka, 2 ka, 5 ka, and 10 ka dunes, respectively (Fig. 2b). The age of each dune was

determined by optically stimulated luminescence (OSL) dating from dune crest positions, representing each of the four major Holocene dune activation/stabilization phases (Patton et al., 2019, 2022b; Ellerton et al., 2020; Supplementary Fig. 2). Sample sites were chosen from depositional settings at the base of the lee-side slipface of each dune (Fig. 2b). All sampled soil pits have a similar upslope source area (a planar hillslope length of <70 m to the dune crest) on a north-facing dune slipface (Fig. 2c and d) and are located in "dry" sclerophyll forest with similar vegetation types and canopy cover. The dominant taxa include pink bloodwood (*Corymbia intermedia*), scribbly gum (*Eucalyptus signata*), forest-oak (*Casuarina torulosa*), black she-oak (*Casuarina littoralis*), banksia (*Banksia serrata*), and blackbutt (*Eucalyptus pilularis*) with a canopy cover between ~60% and 80%.

Each site was hand excavated to a minimum depth of 1.75 m (Fig. 2d). Additionally, we augered at the base of each pit to determine the depth of the underlying dune surface (i.e., deposit thickness), which was identified by the presence of buried horizons (Fig. 2c). This depth is inferred to represent the initiation of sediment deposition and the timing of dune stabilization (i.e., the transition from eolian to colluvial sediment transport); therefore, we utilized the OSL ages collected from dune crest to reflect the maximum basal age of dune footslope deposits (white dot in Fig. 2c). The profile face was cleaned and described using standard soil description protocols (i.e., Schoenberger et al., 2002). Descriptions included characterizing soil horizons, grain size, boundaries of horizons, rooting depths, and soil structure. All charcoal layers and bioturbation features (e.g., ant burrows, nest construction, root growth and decay, and/or evidence of tree throws) were recorded. Charcoal fragments visible on the exposure face were sampled, labeled, and saved for radiocarbon (<sup>14</sup>C) analysis.

For each soil profile, sediment samples and bulk density cores were extracted (~2000 cm<sup>3</sup> and ~260 cm<sup>3</sup>, respectively) at predetermined depths, with the highest sampling density near the surface. Samples were extracted contiguously across the profile face at 0.05 m intervals from 0 to 0.1 m and then at 0.1 m intervals to 1.5 m, after which intervals of 0.25 m were used. In this study, we assign the midpoint for each sample depth interval when placing them in the context of depth and time (e.g., a depth range of 0.1–0.2 m would be reported as being at 0.15 m). Bulk density was measured using the short core extraction method (Blake and Hartge, 1986), which involves driving a core into the pit face and carefully removing it with a flat-edged soil knife. All samples were collected from the bottom of the profile upward to avoid contamination. The sampling was not initially designed with a fire record in mind, and limitations created by the sampling design are discussed later.

### Sediment sample preparation

All samples were dried for 48 h at 50°C. Dried samples were passed through a 2 mm stainless steel sieve to remove the coarse fraction (CF). Very little CF was present (average  $0.34 \pm 0.73\%$  by mass) and only consisted of root and charcoal fragments. This is not surprising in an eolian sand deposit. Coarse charcoal particles in the CF were handpicked and saved for radiocarbon dating. The remaining fine fraction (FF) (<2 mm) soil samples were saved and labeled to be subsampled later for charcoal counting.



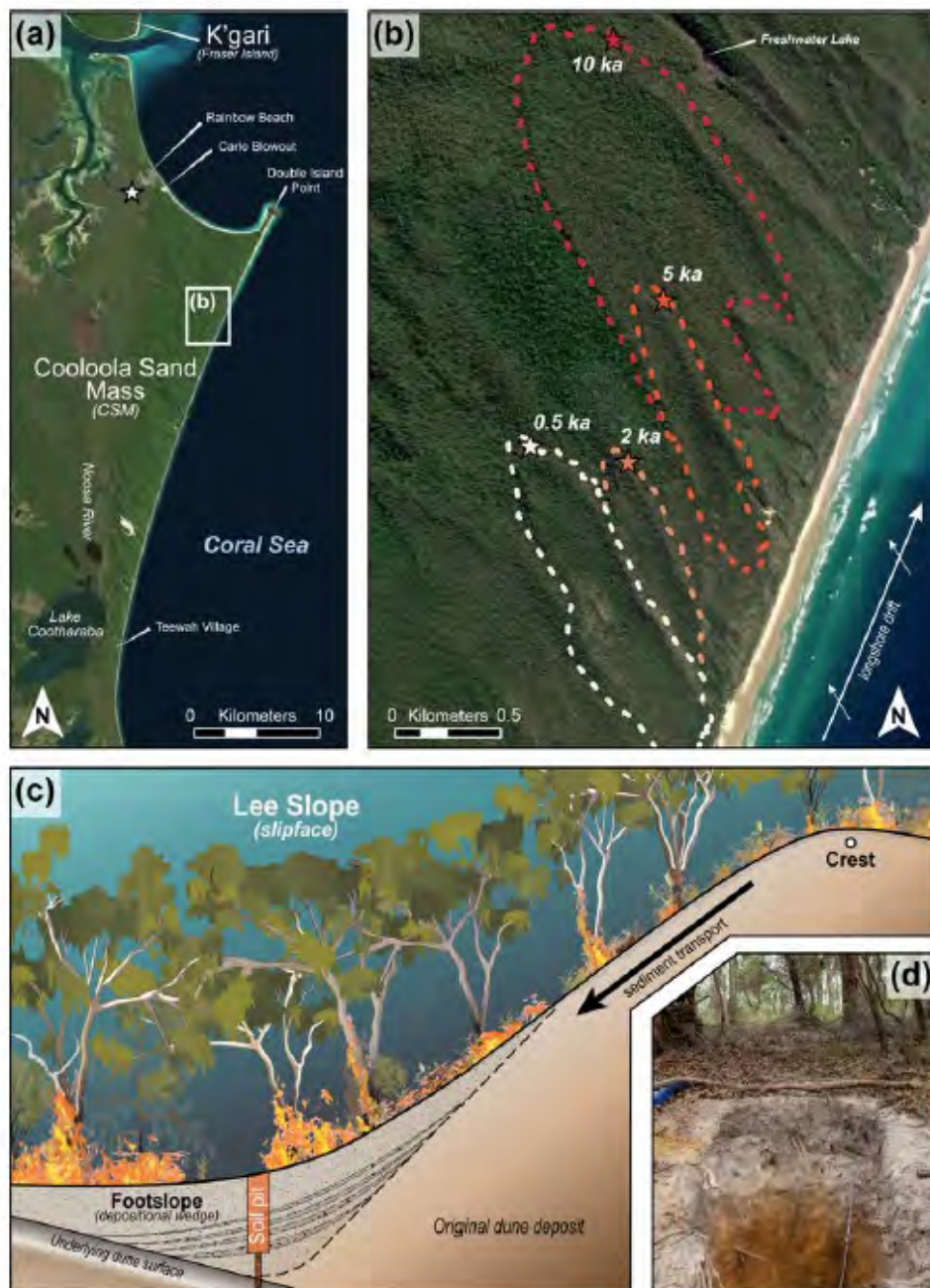


**Figure 2.** Site location. (a) Satellite imagery of the Cooloolo Sand Mass (CSM) with areas of interest, and the Rainbow Beach patterned fen complex (white star). (b) Closeup of the four dunes used in this study (dashed lines) and locations of the depositional footslope sites (stars) found on each dune's north-facing slipface. The dunes selected in the research represent each of the four major Holocene dune activation/stabilization phases (Patton et al., 2019, 2022b; Ellerton et al., 2020; see Supplementary Fig. 2). (c) Conceptual diagram of sediment transport and deposition on a dune's slipface. Charcoal particles are produced on the dune's surface during fires (small black dots), transported down gradient, and deposited in the footslope as disseminated charcoal or charcoal layers. We hypothesize that charcoal analyzed in this study remains in stratigraphic order and is produced locally, because sediment is retained within the CSM's dune basins (Patton et al., 2022a) and charcoal particles are large (between 180  $\mu$ m and 2 mm). The orange box indicates the location where soil pits were excavated to obtain a fire record for this study. A sand auger was used at the base of each pit to determine the depth of the underlying dune surface (i.e., deposit thickness). This surface is inferred to represent when sediment deposition initiated and reflects the emplacement (stabilization) ages collected from optically stimulated luminescence (OSL) samples on the dune crest (white dot). (d) Soil profile looking up to the crest on the 10 ka dune.



### Bulk density

Bulk density cores retrieved from the field were oven dried for 48 h at 105°C to remove all moisture and then weighed. A 2 mm sieve was used to partition soils into CF and FF, and each fraction was weighed ( $m_{CF}$  and  $m_{FF}$ , respectively). The volume of the CF ( $V_{CF}$ ) was determined for each core by dividing the  $m_{CF}$  by the density of the CF, which is assigned a constant 0.5 g/cm<sup>3</sup> (Eq. 1a). This density value was selected because charcoal and fine roots range between 0.4 g/cm<sup>3</sup> and 0.6 g/cm<sup>3</sup> as determined through water displacement. The  $V_{CF}$  was subtracted from the bulk density core volume ( $V_T$ ), ~260 cm<sup>3</sup>, to obtain the FF volume ( $V_{FF}$ ) (Eq. 1b). Finally, FF bulk density ( $BD_{FF}$ ) was calculated by dividing the mass by the volume (Eq. 1c) of the FF.

$$m_{CF}/0.5 = V_{CF} \quad (\text{Eq. 1a})$$

$$V_T - V_{CF} = V_{FF} \quad (\text{Eq. 1b})$$

$$m_{FF}/V_{FF} = BD_{FF} \quad (\text{Eq. 1c})$$

### Charcoal counting

Charcoal retained in sedimentological records has been used as a proxy for fire activity and regimes (e.g., Whitlock and Larsen, 2001; Marlon et al., 2016; Hennebelle et al., 2020). Most traditional aquatic archives, such as lakes and bogs, utilize microcharcoal particles (e.g., <125 µm) that are associated with distal sources through either airborne fallout (generally ca. 1–2 km) and/or by inlet streams from the surrounding catchment area (Whitlock and Millspaugh, 1996; Whitlock and Larsen, 2001; Higuera et al. 2007). As a result, these records typically represent broad, regional fire signals that may include an amalgamation of vegetation types and biozones (Marlon et al., 2006; Vachula et al., 2018). In this study, we focus our analyses on larger macrocharcoal, which represents local (in situ) fire production originating within ca. 100 m of the dune soil profiles (e.g., Clark et al., 1998; Gavin et al., 2003; Higuera et al., 2005; Sanborn et al., 2006; Iglesias et al., 2015; Itter, et al., 2017; Leys et al., 2017; Morris et al., 2017). We analyzed charcoal >180 µm, because smaller fragments are more susceptible to eluviation processes (the vertical transport of particles through the soil profile), due to the homogenous (180–250 µm) and well-drained (600 mm/h) dune sands (Reeve et al., 1985).

FF soil samples for all depth intervals were homogenized, subsampled using a riffle splitter (~5 g), and if necessary, treated with 15 mL of 10% HCl for 24 h to remove any sesquioxide coatings on sand grains (i.e., samples collected from well-developed B horizons). Each sample was sequentially wet sieved at 355 µm, 250 µm, and 180 µm. Care was taken to not damage the charcoal fragments. Under a dissecting microscope (2×–20× magnification) all charcoal was counted (no.) in the following size classes (180–250 µm, 250–355 µm, and 355 µm–2 mm). Charcoal counts are converted to charcoal concentration by dividing the charcoal count by the subsample volume ( $V$ ). The volume is calculated by using the initial subsample mass ( $m_i$ ) divided by the  $BD_{FF}$  from the appropriate depth interval (see Eq. 2). This was completed for all samples for each profile, and results are plotted against depth. Additionally, we compare charcoal concentrations between

each size class.

$$\text{Charcoal concentration} = \left( \frac{\text{no.}}{[m_i/BD_{FF}]} \right) = \left( \frac{\text{no.}}{[V]} \right) \quad (\text{Eq. 2})$$

### Charcoal selection and preparation for radiocarbon (<sup>14</sup>C) dating

Even in regions with homogenous geomorphology and ecology, it is necessary to acquire a large number of dates to adequately resolve fire history. To build a chronological framework for each depositional profile, we selected charcoal samples to be radiocarbon (<sup>14</sup>C) dated by accelerator mass spectrometry (AMS). Our primary targets were >2-mm-diameter charcoal fragments picked directly from the profile face of known absolute depths ( $n = 24$ ). We supplemented these samples with charcoal within the CF ( $n = 22$ ), and although these charcoal samples have inherently higher uncertainty with regard to depth (i.e., they come from intervals of 0.05 m to 0.25 m), they provide a means to evenly distribute radiocarbon dating across all profiles.

Radiocarbon samples were dated at two laboratories, with 46 samples dated in total. Twelve samples were dated at the Waikato Radiocarbon Dating Laboratory in 2019 and 2021. A further 34 samples were dated at the Australian Nuclear Science and Technology Organisation (ANSTO) radiocarbon laboratory in 2021 and 2022 (Fink et al., 2004). At both laboratories, the charcoal samples were pretreated using the standard acid-base-acid (ABA) protocol before being combusted and graphitized (Hua et al., 2001). Sample graphite was then loaded into aluminum cathodes and measurements were determined by AMS. The results were reported in conventional radiocarbon age or percent modern carbon (pMC) (see Table 1).

### Age-depth model and combining charcoal records

For all profiles, age-depth models were created using the rbacon package (Blaauw and Christen, 2011) in R (R Core Team, 2020), with the calibration data being the Southern Hemisphere calibration curve (SHCal20; Hogg et al., 2020) extended to recent time using the post-bomb atmospheric calibration curve for Southern Hemisphere zone 1–2 (Bomb22SH1-2; Hua et al., 2022). All the modeled ages were reported in calibrated years before 1950 (cal yr BP) at 95% confidence interval. Additionally, we set the surface age to 2019 (i.e., –69 cal yr BP; date of sample collection) and the basal ages to the OSL-dated dune ages collected from dune crest (Fig. 2c). We attributed the age for each sample to the midpoint of each sample depth range. Charcoal records were evaluated by plotting sample depth to charcoal concentration (particles/cm<sup>3</sup>). We normalize for changes in sedimentation rates within and between sites by calculating charcoal accumulation rates (CHAR) expressed in units of particles/cm<sup>2</sup>/yr (Long et al., 1998). Charcoal production can vary among sites due to local conditions (i.e., moisture content, fire intensity, and biomass); therefore, we rescaled each record to range from 0 to 1 by dividing by the maximum CHAR value (Power et al., 2008). Once normalized, records were combined and plotted against time to establish a composite master charcoal record for the Holocene dune field. For all charcoal records, CHAR peaks were identified visually.



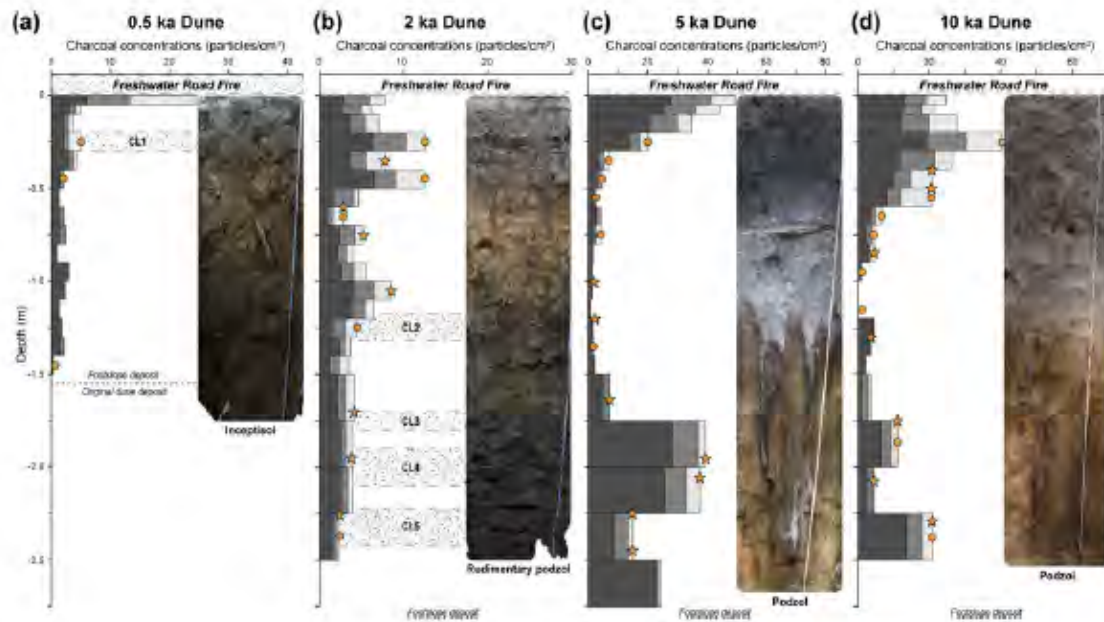


**Figure 3.** Charcoal concentrations for the (a) 0.5 ka, (b) 2 ka, (c) 5 ka, and (d) 10 ka dune depositional sites. For each depth interval (width of bar) charcoal was counted for size classes 180–250  $\mu\text{m}$  (dark gray), 250–355  $\mu\text{m}$  (gray), and 355  $\mu\text{m}$ –2 mm (light gray). Charcoal layers identified in the profile face are indicated by a band of black dots and labeled (CL1–CL5). Samples collected for radiocarbon analysis are indicated with an orange star or an orange circle depending on whether they were collected at a discrete depth or from a sample depth interval, respectively. Charcoal layers only occur on the two youngest dunes and were incorporated in multiple sample intervals due to predetermined sampled depths. Note, the Freshwater Road Fire severely burned and deposited fresh charcoal at the surface of all sites (dashed lines labeled “Freshwater Road Fire”) after pit excavation and sample collection, but only produced a 0.1 m charcoal-rich dry-ravel deposit at the 0.5 ka site. As a result, no charcoal concentrations were recorded for this interval. For more information on each soil profile see Supplementary Figs. 4–8.

Our results were compared with published charcoal records from a nearby patterned fen complex (Hanson et al., 2023) and two lake records with similar forest types and, presumably, similar fire histories (Donders et al., 2006; Mariani et al., 2019) (white stars in Fig. 1b, Supplementary Fig. 3). Additionally, we compared the results with Mooney et al.’s (2011) and Williams et al.’s (2015) subtropical high-pressure belt (25°S–45°S) record of biomass burning. The purpose of this cross-site comparison was to assess whether our master charcoal record depicted reasonable local trends and/or evidence of broad regional fire-regime changes as compared with those derived from more traditional (aquatic) archives.

## RESULTS

### Field observations and soil characterization

Soil profiles were excavated to a maximum depth of 2.75 m and were classified from youngest to oldest as an inceptisol, rudimentary podzol, podzol, and podzol (Fig. 3). As expected, all soils have uniform grain-size distributions concentrated between 180  $\mu\text{m}$  and 250  $\mu\text{m}$ . The younger profiles from the 0.5 ka and 2 ka dunes have minimal pedogenic development, and charcoal is dispersed throughout the profile; however, distinct charcoal layers (CL) are observed. The 0.5 ka profile had one layer (CL1: 0.2–0.3 m), and no charcoal was observed >1.5 m. All sediment below 1.6 m was classified as primary dune sediment due to its lack of soil development and absence of organic material. The 2 ka profile had four charcoal layers near the base (CL2:

1.20–1.30 m; CL3: 1.70–1.80 m; CL4: 1.90–2.10 m; and CL5: 2.20–2.40 m). In contrast, the oldest profiles from the 5 ka and 10 ka dunes have distinct transitions between the pedogenic horizons, with the exception of the boundary between the A and E horizons, which is diffuse. Charcoal was disseminated throughout the profile, with elevated concentrations at the base and near the surface. Additionally, several months after pit excavations the Freshwater Road Fire (Fig. 1b and e) burned all site locations. The fire removed vegetation and deposited charcoal at the surface, but only induced a ~0.1 m sand ravel deposit on the 0.5 ka dune footslope (Fig. 3a, Supplementary Fig. 1). This deposit was not included in our charcoal analyses and is only utilized as a point of discussion.

For all sites, root growth and decay are the most prevalent forms of postdepositional mixing. This activity is greatest at the surface and rapidly decreases with depth, such that most roots are confined within the A horizon (<0.5 m depth). Unexpectedly, we observed little evidence of other common forms of bioturbation (i.e., ant mounds, rodent burrows, tree throws, and/or nest construction). This is in stark contrast to the upslope, eroding positions at the CSM, where all these processes are commonly observed and where we visually estimated up to 3 ant colonies/m<sup>2</sup> along the hill-slope surface.

### Charcoal concentrations

Charcoal at all sites was well preserved (black, angular, and opaque). Concentrations were consistent across all the sites, and all size classes depicted similar trends with depth (Fig. 3,

**Table 1.** All ages used to produce age–depth models in this study are from woody macrocharcoal ( $^{14}\text{C}$ ) and primary dune sands (optically stimulated luminescence [OSL]) are reported in years relative to 1950 (Fig. 4).<sup>a</sup>

Sample no.	Lab ID <sup>b</sup>	Depth (m)	OSL ages (ka $\pm$ 1 $\sigma$ )	Conventional $^{14}\text{C}$ ages (yr BP $\pm$ 1 $\sigma$ )	Calibrated ages (95% confidence interval) (cal yr BP)	Modeled calibrated ages (95% confidence interval) (cal yr BP)
0.5 ka Dune						
—	Surface	0	—	—	–69 <sup>c</sup>	–69 (–66 to –72)
1	OZAF02	0.20–0.30	—	102.61 $\pm$ 0.32 <sup>d</sup>	–5 (0 to –9)	11 (49 to –4)
2	OZAF03	0.40–0.50	—	170 $\pm$ 25	116 (278 to –3)	59 (102–17)
3	OZAF04	1.40–1.50	—	220 $\pm$ 25	192 (298 to –4)	266 (300–178)
—	USU-2283 <sup>e</sup>	1.60 <sup>f</sup>	0.44 $\pm$ 0.10	—	—	292 (344–205)
2 ka Dune						
—	Surface	0	—	—	–69 <sup>c</sup>	–69 (–66 to –72)
4	OZAE96	0.20–0.30	—	335 $\pm$ 25	389 (448–300)	398 (463–299)
5	Wk-52211	0.35	—	718 $\pm$ 18	628 (666–565)	575 (598–512)
6	OZAE97	0.40–0.50	—	625 $\pm$ 25	604 (635–535)	608 (633–555)
7	Wk-52212	0.60	—	640 $\pm$ 19	608 (636–545)	644 (673–613)
8	OZAE98	0.60–0.70	—	980 $\pm$ 30	852 (924–771)	680 (712–639)
9	Wk-52213	0.75	—	882 $\pm$ 21	745 (793–683)	703 (751–680)
10	Wk-52214	1.05	—	960 $\pm$ 19	852 (907–768)	780 (814–745)
11	Wk-50298 <sup>g</sup>	1.20–1.30	—	1017 $\pm$ 26	857 (930–798)	820 (855–791)
12	OZAE99	1.70	—	955 $\pm$ 30	834 (917–740)	895 (928–864)
13	Wk-50299	1.95	—	1023 $\pm$ 24	859 (955–800)	945 (981–908)
14	OZAF01	2.25	—	1080 $\pm$ 25	944 (1047–908)	1031 (1082–957)
15	Wk-50300	2.35–2.41	—	1166 $\pm$ 24	1013 (1062–960)	1060 (1169–1002)
—	USU-3021 <sup>h</sup>	5.10 <sup>f</sup>	2.14 $\pm$ 0.27	—	—	2373 (2679–2109)
5 ka Dune						
—	Surface	0	—	—	–69 <sup>c</sup>	–69 (–66 to –72)
16	OZAE83	0.2–0.3	—	270 $\pm$ 25	285 (322 to –4)	354 (456–184)
17	OZAE84	0.3–0.4	—	1350 $\pm$ 25	1225 (1285–1177)	1203 (1282–1085)
18	OZAE85	0.4–0.5	—	1815 $\pm$ 25	1662 (1747–1590)	1425 (1661–1282)
19	OZAE86	0.5–0.6	—	1535 $\pm$ 20	1367 (1411–1314)	1502 (1811–1361)
20	Wk-50296	0.7–0.8	—	2397 $\pm$ 26	2381 (2671–2179)	2056 (2211–1732)
21	OZAE87	1.0	—	2290 $\pm$ 25	2225 (2341–2143)	2253 (2343–2148)
22	OZAE88	1.20	—	2410 $\pm$ 25	2401 (2684–2332)	2406 (2489–2336)
23	OZAE89	1.30–1.40	—	2585 $\pm$ 25	2626 (2753–2493)	2523 (2605–2410)
24	OZAE90	1.65	—	2665 $\pm$ 25	2752 (2845–2718)	2717 (2767–2570)
25	OZAE92	1.75–2.00	—	2695 $\pm$ 25	2769 (2849–2737)	2783 (2854–2741)
26	OZAE91	1.90	—	2795 $\pm$ 25	2848 (2946–2772)	2796 (2868–2760)
27	OZAE93	2.10	—	2630 $\pm$ 30	2734 (2777–2516)	2858 (2979–2805)
28	Wk-50297	2.25	—	2624 $\pm$ 25	2733 (2767–2518)	2932 (3076–2840)
29	OZAE94	2.45	—	2760 $\pm$ 30	2818 (2920–2754)	3059 (3246–2922)
—	USU-2284 <sup>e</sup>	5.30 <sup>f</sup>	4.89 $\pm$ 0.45	—	—	5716 (6328–5197)

(Continued)



Table 1. (Continued.)

Sample no.	Lab ID <sup>b</sup>	Depth (m)	OSL ages (ka ± 1σ)	Conventional <sup>14</sup> C ages (yr BP ± 1σ)	Calibrated ages (95% confidence interval) (cal yr BP)	Modeled calibrated ages (95% confidence interval) (cal yr BP)
10 ka Dune						
—	Surface	0	—	—	–69 <sup>c</sup>	–69 (–66 to –72)
30	OZZ591	0.20–0.30	—	560 ± 25	—	—
31	OZZ592	0.20–0.30	—	365 ± 35	392 (487–309)	421 (493–308)
32	OZAE76	0.40	—	1905 ± 25	1792 (1875–1725)	1752 (1824–1611)
33	OZAE77	0.50	—	1955 ± 25	1858 (1928–1749)	1856 (1924–1761)
34	OZZ594	0.50–0.60	—	1950 ± 35	1852 (1985–1746)	1905 (1998–1834)
35	OZAE78	0.60–0.70	—	2275 ± 25	2231 (2337–2140)	2174 (2271–2105)
36	OZZ596	0.70–0.80	—	2160 ± 35	2087 (2298–2003)	2284 (2524–2225)
37	Wk-50293	0.85	—	3534 ± 24	3768 (3871–3652)	2823 (3699–2445)
38	OZAE79	0.90–1.00	—	2860 ± 25	2926 (3060–2848)	3008 (3960–2849)
39	OZZ597	1.10–1.20	—	5040 ± 70	5743 (5900–5600)	4982 (5358–4285)
40	OZAE80	1.30	—	4815 ± 25	5522 (5590–5334)	5381 (5570–5074)
41	Wk-50294	1.75	—	5305 ± 26	6062 (6183–5934)	5997 (6152–5922)
42	OZAE81	1.75–2.00	—	5485 ± 30	6240 (6308–6125)	6123 (6235–6011)
43	OZAE82	2.07	—	5495 ± 30	6246 (6385–6128)	6277 (6385–6197)
44	Wk-50295	2.30	—	5648 ± 26	6375 (6483–6305)	6455 (6602–6359)
45	OZZ598	2.25–2.50	—	5880 ± 35	6659 (6778–6502)	6553 (6688–6442)
46	OZZ599	2.90	—	5995 ± 35	6788 (6895–6670)	7124 (7393–6834)
—	USU-2285 <sup>d</sup>	4.50 <sup>e</sup>	9.82 ± 0.98	—	—	10,215 (11,196–9414)

<sup>a</sup>Age calibration was performed using the Southern Hemisphere calibration curve (SHCal20; Hogg et al., 2020) extended to recent time using the post-bomb atmospheric calibration curve for Southern Hemisphere zone 1–2 (Bom52SH1.2; Hua et al., 2022), and modeled ages were produced using rbacon (Blasuw and Christen, 2011) in R (R Core Team, 2020).

<sup>b</sup>Lab numbers beginning with Wk, OZ, and USU were analyzed at the Waikato Radiocarbon Dating Laboratory, Australian Nuclear Science and Technology Organisation (ANSTO), and Utah State University Luminescence Laboratory, respectively.

<sup>c</sup>Surface date in cal yr BP.

<sup>d</sup>A modern sample, whose measured <sup>14</sup>C content was reported in percent modern carbon (pMC) instead of conventional <sup>14</sup>C age.

<sup>e</sup>Originally published in Ellerton et al. (2020) in years relative to AD 2018.

<sup>f</sup>Depth indicates the maximum depth of each footslope deposit (depositional wedge). These depths are assigned a basal age that represents timing of dune stabilization and are obtained from OSL ages collected from dune crests.

<sup>g</sup>Originally published in Patton et al. (2022a) in years relative to AD 1950.

<sup>h</sup>Originally published in Patton et al. (2022b) in years relative to AD 2020.

Supplementary Fig. 4). The 180–250 µm size class contributes approximately half of the cumulative charcoal concentrations for each depth interval, whereas the larger size classes (250–355 µm and 355 µm–2 mm) each contributed about a quarter of the cumulative charcoal concentrations. For this reason, we simplify our results by only reporting aggregate charcoal concentrations hereafter. Combined charcoal concentrations from all size classes (i.e., combined charcoal counts from 180 µm to 2 mm) are measured from 0 to 49.4 particles/cm<sup>3</sup>, with the highest values found near the surface. Out of the 78 sampled depth intervals, only three samples lacked charcoal (not including samples at depths >160 cm from the 0.5 ka dune, which constitutes the original dune deposit). The average charcoal concentrations for each profile generally increased with dune age from 3.9 ± 5.7, through 5.8 ± 2.8, and 14.5 ± 16.6, to 13.9 ± 11.6 particles/cm<sup>3</sup>.

#### Radiocarbon (<sup>14</sup>C) analysis and age–depth modeling

Radiocarbon results from 46 charcoal particles produced ages ranging from 0.01 to 7,125 cal ka BP (Table 1). We analyzed

12, 14, and 17 radiocarbon samples from the 2 ka, 5 ka, and 10 ka dunes, respectively. The 0.5 ka dune had few radiocarbon targets and only yielded three ages. Due to our sampling strategy, 52% of the total dates are younger than 2 cal ka BP. We observe consistent trends with depth, with only four age reversals (> ±2σ) (Fig. 4). The ages of the sampled intervals represent a range of ages owing to the contiguous sampling design (see Supplementary Table 1); however, we find samples from the same depth interval within sites yield similar ages (e.g., samples 33 and 34; samples 44 and 45 in the 10 ka dune). Sedimentation rates are the highest where charcoal layers are present (i.e., the entire 0.5 ka dune and below 1.20 m on the 2 ka dune). In general, rates decrease moving up the excavated profiles toward the surface.

#### CHAR records

Charcoal concentrations are converted into CHAR using accumulation rates derived from the age–depth models. We find that all CHAR values ranged from 0 to 11.6 particles/cm<sup>2</sup>/yr, and each



record shows distinct peaks in CHAR that are detected among sites and size classes (Fig. 5, Supplementary Fig. 4). The 0.5 ka dune has one peak at the surface, whereas the 2 ka dune has a peak between ca. 1.1 and 0.4 cal ka BP. The 5 ka dune record has two peaks. The most recent occurred within the last 0.3 ka and the earlier peak at ca. 3.4–2.6 cal ka BP. The 10 ka dune has four peaks at ca. 6.7–5.3 cal ka BP, peaks between ca. 3.0–2.6 and 2.2–1.6 cal ka BP, and the most recent started ca. 0.5 cal ka BP. When the individual records are combined into a composite master record, we observe five peaks occurring between ca. <0.3, 1.1–0.4, 2.2–1.6, 3.4–2.6, and 6.7–5.3 cal ka BP (vertical orange bars in Fig. 5e) regardless of inclusion or exclusion of CHAR values associated with episodic sediment transport (white line or black area in Fig. 5e, respectively). In general, CHAR peaks increase in frequency after ca. 3.4 cal ka BP, with the highest values in the last century.

Not all CHAR peaks register as visible charcoal layers in the soil profiles. Charcoal layers (CL1–CL5) are only observed within the two youngest sites (Fig. 3a and b). These differences are due to the relatively coarse and contiguous sampling intervals and not all charcoal used for radiocarbon dating being from discrete depths. This caused charcoal layers to be incorporated in multiple samples (Fig. 3), including those with low charcoal concentrations, resulting in a smoothed CHAR record.

## DISCUSSION

### Charcoal preservation within dune footslope deposits

Previous studies have successfully used charcoal records from paleosols in blowouts, deflation basins, and swales to understand dune activity with respect to changes in climate and fire regimes (e.g., Filion, 1984; Seppälä, 1995; Käyhkö et al., 1999; Mann et al., 2002; Arbogast and Packman, 2004; Carcaillet et al., 2006; Matthews and Seppälä, 2014). This study represents the first attempt to systematically target dune footslopes (depositional wedges in front of dune slipfaces) to reconstruct a fire record. We propose that dune footslopes are appropriate targets for paleofire reconstruction. Footslopes at the CSM are depositional systems that produce sequences of locally derived sediments. Most or all inorganic sediments produced on the adjacent hillslope (dune front avalanche face) are inferred to be deposited and preserved with little disruption or mixing. Short-term hiatuses are likely present, but field observations demonstrate only minor physical postdepositional mixing of particles >180 µm. These are limited to the near surface through root growth and decay. The lack of physical mixing is supported by intact and distinct soil horizons, consistent charcoal concentrations among size classes, and consistent increases in age with depth. Only four age reversals are observed in our records, and they likely record minor reworking in upbuilding soil A horizons (Almond and Tonkin, 1999; Fig. 4).

Fires are common in the dune field (e.g., Mulholland, 2021), and charcoal is present throughout the profile of the colluvial footslope deposits. As the sites are located within a ca. 2 km radius from each other, the similarity of the records is expected, and indeed necessary, if these types of sites are to be used to produce reliable fire histories. As depicted in the 0.5 ka dune (Fig. 3a), there is no evidence of macrocharcoal (>180 µm) found within the original dune deposit (>1.6 m depth), which suggests charcoal in these depositional profiles must be incorporated after dune emplacement (stabilization). In fact, our previous studies indicated no evidence of charcoal in the primary eolian

deposits from our sampled Holocene dunes (Ellerton et al., 2020; Köhler et al., 2021; Patton et al., 2022b). The absence of charcoal from primary dune sands within the CSM likely reflects the limited area for fire to initiate in the upwind direction (i.e., the Coral Sea) and the challenge for fire to penetrate into active dunes due to their limited woody fuel loads (Fig. 2b).

Our local records indicate wildfires that occurred within the CSM's dry sclerophyll forest impacted most dune slopes. Perhaps the best evidence for the preservation of paleofire records is that CHAR peaks are traceable between the different profiles (Fig. 5), and the trends are consistent regardless of charcoal size classes (Supplementary Fig. 4). For instance, the 0.5 ka, 5 ka, and 10 ka deposits identified the same ca. <0.3 ka CHAR peak, the 5 ka and 10 ka footslope share the CHAR peak at ca. 3 cal ka BP, and all sites had fresh charcoal deposited on their surfaces from the Freshwater Road Fire (Fig. 3).

An important observation is that we observe minor variability between our records. Fires can be extremely localized and confined to specific sections of the dune field due to the direction of fire propagation or naturally occurring firebreaks (i.e., low-lying swales with high humidity and/or barren sand patches). Indeed, this may explain the differences between our depositional records, especially when episodic sediment transport dominates (within the first ca. 1.5 ka of sediment deposition). However, it could be the result of our sampling design, which lacks the necessary resolution to capture all changes in charcoal production and/or events (Fig. 5). For instance, the 2 ka dune depicts one CHAR peak that incorporates four charcoal layers (CL2–CL5) from ca. 1.1 to 0.4 cal ka BP but did not register at the older sites despite being positioned windward of those sites. This is inferred to be the result of the coarse sample size, which incorporated both periods of low and high biomass burning within the same sample, thereby obscuring potential CHAR peaks (see sample locations: dots in Fig. 5c and d).

Alternatively, the discrepancies could reflect variations in charcoal production or preservation between sites. Cohen-Ofri et al. (2006) demonstrated that oxidizing conditions like those found within the CSM (<5 pH) may degrade charcoal structure, thereby lowering charcoal preservation potential. The charcoal found within our depositional footslopes are large, woody, and structurally strong (slightly hard to hard consistency). Moreover, we find that average charcoal concentrations between the oldest and youngest sites are nearly four times greater despite having been exposed to acidic conditions longer. Although our coarse sampling design prohibited us from addressing this concern, we believe that chemical degradation of charcoal into fragments smaller than our analyses (180 µm–2 mm) is minor and thus does not affect our interpretations. Nevertheless, future studies should consider the preservation potential of charcoal in acidic soil conditions when constructing a fire history.

### Sedimentation inferences from the age–depth models

In our previous work, we characterized the first phase of dune hillslope development as occurring through episodic sediment transport (dry-ravel and sheetwash) induced by disturbances such as fire on the steep initial dune gradients (Patton et al., 2022a). These perturbations resulted in rapid topographic adjustments (increased footslope sedimentation rates). We discovered that once dune gradients are lowered below their angle of repose (0.65 m/m or 33°), which occurs ca. 1 ka after dune stabilization, a second phase of gradual hillslope evolution with steady and



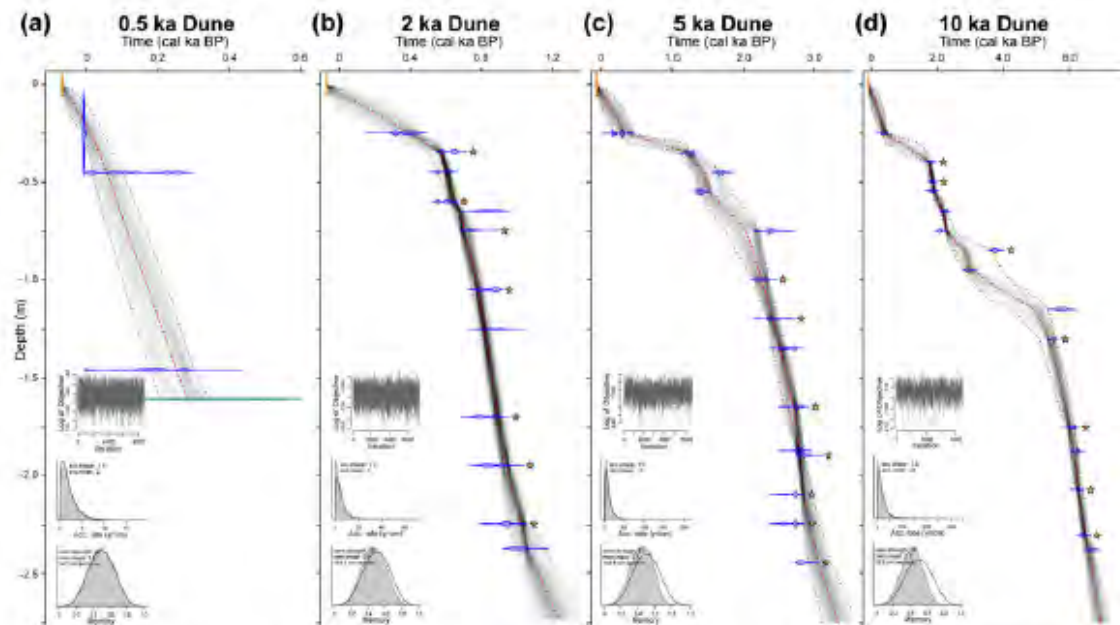


**Figure 4.** Bayesian age-depth models generated for the (a) 0.5 ka, (b) 2 ka, (c) 5 ka, and (d) 10 ka dune depositional sites. For each site, we set the age of the surface (0 m) to the date of pit excavation (vertical orange marker), and the basal age to the optically stimulated luminescence (OSL) dated dune age collected from dune crest. All cal. ages are obtained through radiocarbon ( $^{14}\text{C}$ ) dating of charcoal fragments using the Southern Hemisphere calibration curve (SHCal20; Hogg et al., 2020) extended to the recent time using the Post-bomb Atmospheric calibration curve for Southern Hemisphere zone 1-2 (Bomb22SH1-2; Hua et al., 2022). Graphs were produced using 'rbacon' (Blaauw and Christen, 2011) in R (R Core Team 2020). The calibrated year probability distributions estimates are shown as blue and orange markers for  $^{14}\text{C}$  and OSL ages, respectively. The red dashed line bounded by the gray dotted lines represents the age-depth model best fit and the 95% confidence intervals, respectively. Note, the y-axis only extends to 2.75 m, which covers all sample intervals, and does not include the complete age-depth model that extends to the base of each deposit (original dune deposits or overlapped topography). Additionally, samples collected from discrete depths are labeled with an orange star.

continuous sediment transport (soil creep processes) begins. Indeed, the geochronological and sedimentological data in this study support these assertions.

The age-depth models from the four deposits yield similar trends of increasing age with depth (Fig. 4) and indicate no substantial break in sedimentation or evidence of erosion (truncated horizons), supporting the idea that these dune positions are consistently depositional (Patton et al., 2022a). Additionally, we find that sedimentation rates decrease with dune age, which is to be expected due to the "Sadler effect" (Sadler, 1981), which may lead to biases in sedimentological records if not accounted for (Vachula et al., 2022). We attempt to account for this effect by averaging the median sediment rate in 100 yr intervals for each footslope deposit and find that sedimentation rates decrease with age from  $0.34 \pm 0.17$ , through  $0.16 \pm 0.13$  and  $0.05 \pm 0.05$ , to  $0.03 \pm 0.02$  cm/yr.

When plotting our sedimentation rates for each sample interval as a function of time since dune stabilization, we find a distinct transition at ca. 1.5 ka (Fig. 6a). Interestingly, the abrupt shift in sedimentation rates coincides with the presence or absence of charcoal layers found within the excavated sections of the footslope deposits. For example, the ca. 1.5 ka transition occurs at 0.35 m depth on the 2 ka dune, which is above the boundary between charcoal preserved in distinct layers and charcoal dispersed throughout (Fig. 3b).

We find a substantial difference in the average sedimentation rate between sampled intervals before and after the 1.5 ka transition (i.e., sections associated with either charcoal layers or

disseminated charcoal) with mean values of  $0.57 \pm 0.13$  and  $0.10 \pm 0.07$  cm/yr, respectively (Fig. 6b). Our results support that differences in sedimentation rates are associated with the transition from the dominance of episodic to continuous sediment transport on the dune hillslopes (Patton et al., 2022a; Fig. 6). Moreover, these findings highlight the idea that the change from presence to absence of charcoal layers reflects a geomorphic process (the transition from dominance of episodic to continuous sediment transport).

In fact, the observed 0.1 m deposit during the Freshwater Road Fire of 2019 (Fig. 3a, Supplementary Fig. 1) onto the footslope of the 0.5 ka dune is consistent with the sedimentation rates during the first phase of sedimentation when charcoal layers are present. For sclerophyll forests, such as those found on the CSM, fires are estimated to occur at ca. 20 yr intervals (Keith, 2004). Assuming the Freshwater Road Fire is representative of past fires and that the multimillennial fire frequency-magnitude relationship is appropriate, we would expect a fire to deposit  $\sim 10$  cm of sediment on average within each 20 yr interval (equivalent to a fire-induced sedimentation rate of 0.5 cm/yr). This estimate is consistent with the sedimentation rates observed in the 0.5 ka and 2 ka deposits, and reflects the contribution associated with episodic sediment transport. Sediment will also actively move downslope even without the perturbation of fire through continuous soil transport processes (e.g., granular relaxation, rain splash, and biogenic soil creep), which we estimated to be an order of magnitude lower (Patton et al., 2022a).

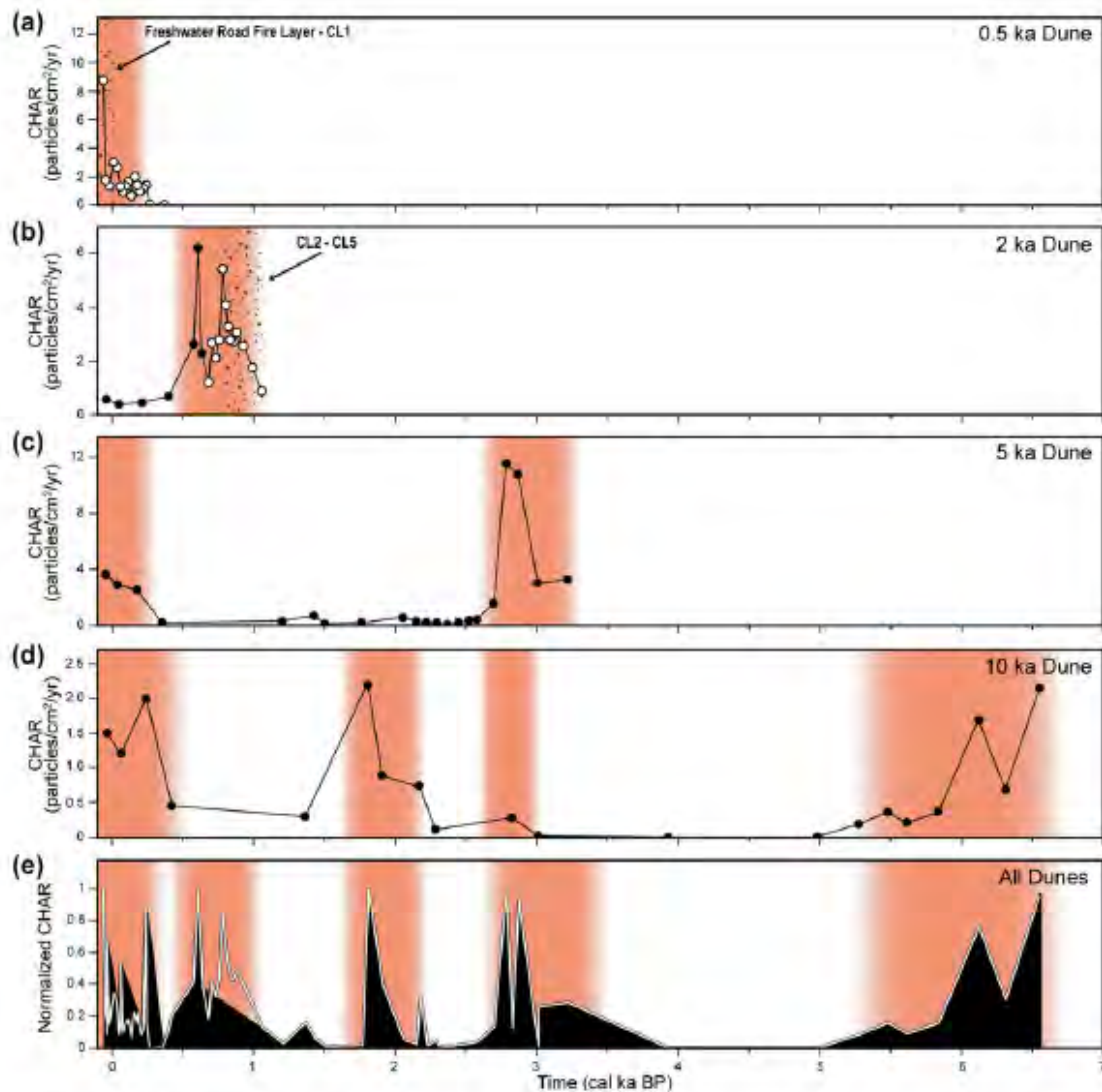


**Figure 5.** Charcoal accumulation rates (CHAR) and the inferred timing of increased fire activity (peaks are vertical orange areas) for the (a) 0.5 ka, (b) 2 ka, (c) 5 ka, and (d) 10 ka dune depositional sites. Locations for all samples are marked with dots, such that white dots indicate episodic sediment transport (sheetwash or dry-ravel) associated with the first 1.5 ka of sediment deposition, while black dots indicate slow and continuous sediment transport (soil creep). Charcoal layers (CL) found in profile faces (Fig. 3) are indicated by a band of black dots and labeled (CL1–CL5). For more information on CHAR for each size class and the locations for all charcoal layers, see Supplementary Fig. 4. (e) A composite master charcoal record was derived from all four sites by dividing each record by its maximum CHAR value and then plotting the normalized CHAR with time. The white line represents a record composed of all CHAR values ( $n = 77$ ), whereas the black area represents samples that only experienced continuous sediment transport ( $n = 48$ ).

#### Implications of charcoal layers in dune deposits

Rates of sedimentation and the presence or absence of charcoal layers (CL) are intimately coupled with geomorphic and ecological processes and must be considered when generating fire records. In the section, we discuss whether CHAR peaks and/or charcoal layers in pit faces represent fire-based events (Figs. 5 and 3, respectively) and provide plausible mechanisms for their presence within our dune deposits.

It is not straightforward to determine whether CHAR peaks or charcoal layers represent individual wildfires. For CHAR peaks, sampling intervals could span more than one fire event, and even where sampling intervals are narrow, these intervals may reflect several centuries of accumulation. This is particularly true for fire records that lack a strong chronological framework (limited age constraints) and/or have charcoal samples with large inbuilt ages, both of which can make interpretations difficult. Although we are confident in our age–depth modeling due



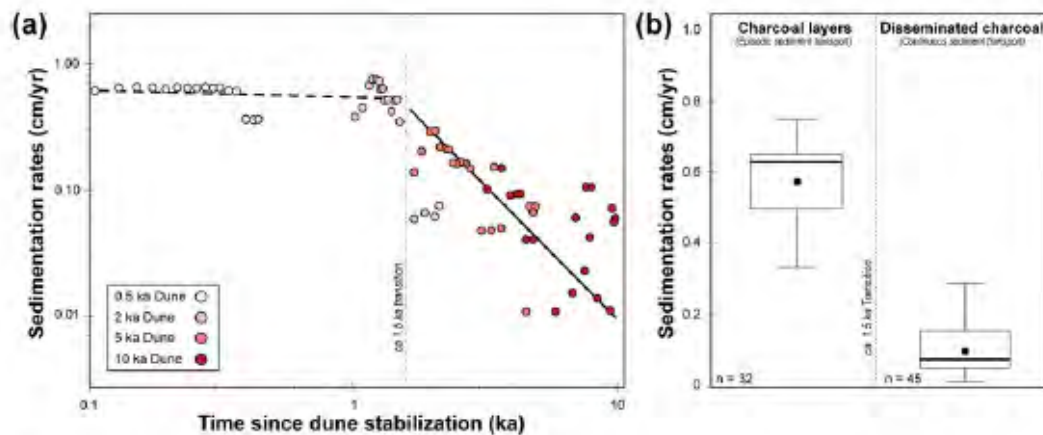


**Figure 6.** (a) A log-log plot of the median sedimentation rate for all sampled intervals (dots) from each footslope deposit as a function of time since dune stabilization. Sedimentation rates are initially high (dashed line) then abruptly decrease after ca. 1.5 ka (solid line). (b) Box and whisker plots for sedimentation rates before and after this transition. Boxes are the interquartile range, with the whiskers representing maximum and minimum values. The black dot is the mean, and the horizontal black line represents the median. We hypothesize that the shift in sedimentation rates reflects the transition from episodic (dry-ravel and sheetwash) to continuous sediment transport styles (soil creep) and is associated with the presence or absence of charcoal in layers, respectively. Note that the separation between these two sedimentation rates occurs ca. 1.5 ka after dune emplacement, which is comparable to the findings in Patton et al. (2022a), where we estimated ca. 1 ka for this transition to occur.

to our large quantity of radiocarbon and OSL dates ( $n = 50$ ) and small inbuilt ages (ca. 10 yr; sample 2 in Table 1), there are always uncertainties in these analyses (e.g., Whitlock and Larsen, 2001). Therefore, it is inappropriate to claim elevated CHAR values represent single fire events, such as those found in sections where sedimentation rates are low (e.g., peak at ca. 2.2–1.6 cal ka BP in Fig. 5d). We propose that individual fire events cannot be identified from CHAR peaks alone, but rather should be used to indicate phases of increased biomass burning (Long et al., 1998; Remy et al., 2018).

Charcoal layers, however, are likely an event-based deposit (Mathews and Seppälä, 2014) (i.e., CL1–CL5 in Fig. 5a and b and Supplementary Figs. 5 and 6). As discussed earlier, layers are only formed before ca. 1.5 ka after dune stabilization, when dune hillslope gradients are above their angle of repose and perturbations such as fires can induce episodic sediment transport near the dune crest. The short (<70 m) and steep (0.65 m/m or 33°) hillslopes promote the rapid delivery of sediments to their subjacent footslopes (e.g., as we observed following the Freshwater Road Fire; Supplementary Fig. 1). These observations indicate that long-term storage of charcoal on hillslopes during this phase is unlikely; therefore, we propose that charcoal layers in pit faces are associated with individual fire events.

An important caveat is that not all fires on oversteepened slopes induce episodic sediment transport, and those that do, do not induce sediment transport evenly across the landscape. To initiate dry-ravel and sheetwash (similar to a sand avalanche), soil cohesion needs to be decreased (Reid and Dunne, 1996; Roering and Gerber, 2005). This can occur through the removal of organic matter, reduction of water content and roots, or production of hydrophobic surface soils (Bridge and Ross, 1983; Doerr et al., 2000; Shakesby and Doerr, 2006). These disturbances to the hillslope are dependent on the severity of the fire and are unlikely to be consistent between events (DeBano, 1981). This was demonstrated during the Freshwater Road Fire, where

episodic sediment transport styles were not observed evenly across all slipfaces near or at the angle of repose. It is reasonable to assume that only the largest and hottest fires are likely to be represented as woody charcoal layers across multiple sampling locations, whereas layers that occur at only one sample site are likely to reflect local fire conditions.

From our dune footslope sites, we find that there is a clear geomorphic and ecological record preserved within the stratigraphy. We observe three stratigraphic deposits within our sites: (1) sand lacking charcoal; (2) sand with charcoal in layers; and (3) sand with dispersed charcoal. We hypothesize that these records directly relate to the vegetation structure and composition and the dominant active sediment transport style (Fig. 7). While dunes are active or stabilizing, woody charcoal-producing fire is rare. In this phase, sand is exposed with only minor patches of vegetation that are composed of grasses and small shrubs (Levin, 2011). The ability of fire to spread is limited, and the lack of woody biomass hinders the production of charcoal, specifically in the larger size classes utilized in this study. Consequently, the sediment delivered from the dune crest to the footslopes through slipface avalanching and granular flows is barren of macrocharcoal (Fig. 7a).

Once the dunes are stabilized, dry sclerophyll forest begins to develop through vegetation succession (Walker et al., 1981); hence fire becomes more prevalent and woody charcoal production increases. We estimate this succession in the CSM to occur ca. 0.3 ka after dune stabilization due to the presence of ~1-m-diameter *Corymbia intermedia* found on the 0.5 ka dune upslope positions that are estimated to be ca. 175–350 yr old (Ngugi et al., 2020; Supplementary Fig. 1a). Charcoal produced on the slopes is rapidly transported down gradient through dry-ravel and sheetwash, forming charcoal layers (Fig. 7b). However, episodic sediment transport only occurs while the gradients are above the angle of repose of the dry unconsolidated dune sands. Once gradients are lowered below this threshold, only continuous sediment processes such as granular relaxation or soil creep



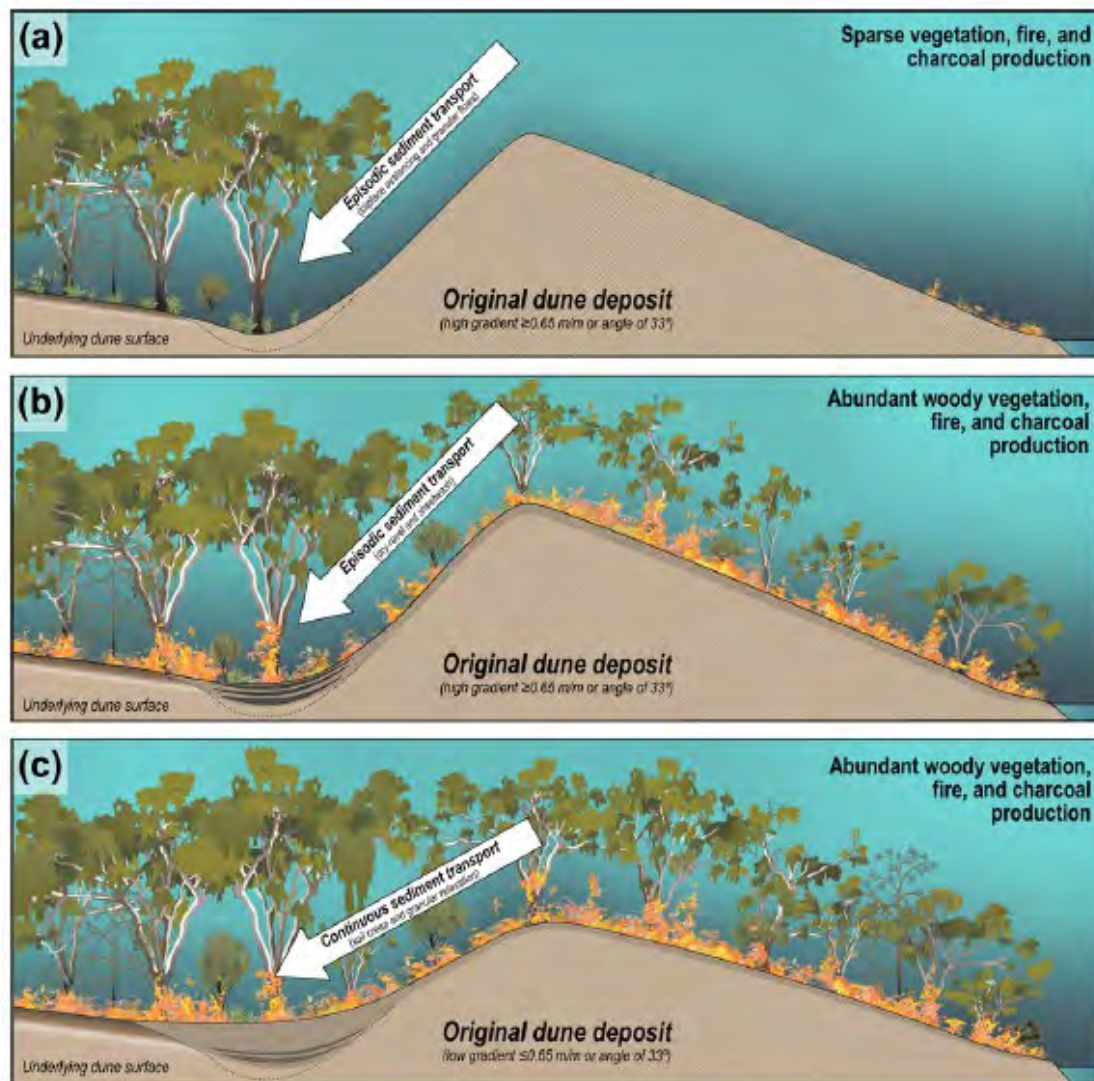


**Figure 7.** Conceptual diagram of progressive vegetation succession, fire activity, charcoal production, and stratigraphic deposit for an (a) active dune with steep gradients, (b) recently emplaced (stabilized) dune with steep gradients, and (c) emplaced dune with shallow gradients. When dunes are active, vegetation is sparse and fires are assumed to be infrequent and unproductive (a). As woody vegetation such as *Eucalyptus* spp. or *Corymbia* spp. becomes established, charcoal production increases (black dots). Charcoal can either be deposited in the footslope positions as layers (black lines in b) or disseminated throughout the profile (gray areas in b and c). The presence or absence of charcoal layers is the result of episodic sediment transport processes (e.g., dry-ravel and sheetwash) and elevated charcoal production on dune gradients that are above the sand's angle of repose (b). The absence of layers but the presence of disseminated charcoal implies slow and continuous sediment transport (i.e., granular relaxation and biogenic soil creep) (c).

prevail (Roering et al., 1999; BenDror and Goren, 2018; Patton et al., 2022a). This transition is estimated to occur ca. 1.5 ka after dune stabilization, as indicated by the significant decrease in the sedimentation rates beginning at 0.35 m in the 2 ka dune (Figs. 4b and 6). Despite the potential for fire and charcoal production to remain high during this phase, the absence of episodic sediment transport results in only the preservation of disseminated charcoal, with higher and lower CHAR rates representing increasing or decreasing biomass burning, respectively (Fig. 7c).

#### Comparison of CSM's dune paleofire records with records from the wider region

CHAR values from charcoal layers provide useful insights on sediment transport styles and local fire events; however, these layers should be used cautiously when developing fire records due to their spatial variability within a small area. Therefore, to compare our findings with other local and regional records, we utilize the composite master charcoal record from CHAR values linked to consistent sedimentation styles and rates (disseminated charcoal) (black area in Figs. 5e and 8a), as these deposits should reflect



general trends of biomass burning without conflating geomorphic and ecological processes.

Our composite master charcoal record indicates three major periods of fire activity in the past ca. 7 cal ka BP that reflect those records derived from lake and swamp deposits in the SE Queensland dune fields and in the wider subtropical high-pressure belt of eastern Australia (24°S–45°S) (Fig. 8). We observe that the earliest peak at ca. 6.7–5.3 cal ka BP corresponds with charcoal records from Minjerribah (Fig. 8d) and a compilation of sites across the nontropical east coast of Australia (Fig. 8e). The Lake Allom record on K'gari (Fig. 8c) registers elevated CHAR values at ca. 7 cal ka BP before a hiatus from ca. 6.5 to 5.4 cal ka BP (Donders et al., 2006). In the wider region, a downward trend in CHAR is observed during this period (Mooney et al., 2011). The only exception is the ca. 4.5 ka charcoal event at the Rainbow Beach patterned fen complex (Moss, 2014; Hanson et al., 2023), where a local fire close to the patterned fen is the likely source of the elevated CHAR (Fig. 8b). This period of reduced burning was followed by an upswing in fire activity with a large CHAR peak from ca. 3.4 to 2.6 cal ka BP, with a smaller peak in CHAR at ca. 2.2–1.6 cal ka BP that is observed in all local and regional records. These late Holocene events are only observed in SE Queensland. At ca. 1.1–0.4 cal ka BP, there is a gradual increase in burning and CHAR peaks at the CSM, at the Rainbow Beach patterned fen complex, and Lake Allom. Although this peak is absent from the macrocharcoal record from Swallow Lagoon on Minjerribah (Fig. 8b), it is present within its microcharcoal record (Mariani et al., 2019). All records show a marked increase in CHAR over the last few centuries between ca. 5 and 0.2 cal ka BP. In summary, the CSM's dune footslope fire records are compatible with those from traditional fire records found within SE Queensland.

#### Causes of the high CHAR periods

As noted in Figure 8, the charcoal records in the SE Queensland dune fields can be divided into three major periods. Period 1, before ca. 5.3 cal ka BP, shows elevated charcoal indicating increased local burning, while Period 2 has little evidence of fires between ca. 5.3 and 3.4 cal ka BP. This matches records obtained from K'gari and Minjerribah (Donders et al., 2006; Atahan et al., 2015; Schreuder et al., 2019; Mariani et al., 2019) and across the subtropical high-pressure belt (Mooney et al., 2011; Williams et al., 2015). The disruption in biomass burning coincides with increases in total rainfall with lower relative variability associated with less frequent El Niño events during period 2 (Barr et al., 2019; Fig. 9b–d). An alternative explanation for the transition may be the result of the termination of the postglacial transgression (Lewis et al., 2008). Before ca. 5.5 cal ka BP, the coastline would have extended significantly seaward from its modern position, which would result in more dune field (land) being seaward of all footslope deposits and increasing the likelihood of fire reaching the sample sites. These hypotheses are not mutually exclusive and indeed likely are the result of both scenarios.

Period 3 shows that fire frequency has gradually increased over the last ca. 3.4 cal ka BP (Fig. 8). This increase in CHAR is observed within many SE Queensland records. K'gari records indicate that after ca. 4 cal ka BP, fire activity progressively increased (e.g., Donders et al., 2006; Atahan et al., 2015; Schreuder et al., 2019). The elevated fire activity was ascribed to increased occupation and amplified Indigenous burning practices

(Schreuder et al., 2019); however, this is difficult to evaluate due to the limited archaeological data available. Alternatively, the increased fire activity is hypothesized to relate to changes in the hydrological cycle primarily through the intensification of the El Niño–Southern Oscillation (ENSO) (Shulmeister and Lees, 1995; Moy et al., 2002; Donders et al., 2006; Conroy et al., 2008; Barr et al., 2019) with minor shifts in vegetation type (Donders et al., 2007; Mariani et al., 2019). Again, it is likely that both intensification of human usage and ENSO affected the fire records but may also reflect an artifact of increased sampling frequency in these sediment sections.

At the end of period 3, there is an increase in biomass burning that is widely observed in records across Australia and the world (e.g., Kershaw et al., 2002; Power et al., 2008; Mooney et al., 2011; Williams et al., 2015). This elevated biomass burning in Australia is inferred to be a direct result of climate change (Power et al., 2008; Mooney et al., 2011) exacerbated by European fire suppression (Hanson et al., 2022; Mariani et al., 2022).

Climate variability drives vegetation communities and thereby available fuel load and fire frequency in the dry sclerophyll forest of subtropical Australia (Mariani et al., 2019). In years with higher water availability, fuel loads increase but fires are suppressed by the moisture content. Dry years enable fires to occur, but the reduced fuel loads make them less intense and frequent. In both scenarios, stable wet or dry climates result in relatively reduced fire risk. In contrast, when interannual climate varies strongly, a condition the SE Queensland dune fields have experienced in the Late Holocene (Barr et al., 2019), fuel loads are able to build up in wet years and cure in the subsequent dry ones, resulting in increased fire activity and intensity (Bradstock, 2010).

#### Geomorphic and ecological controls on dune paleofire records

Biomass burning can be primarily ascribed to climate-mediated vegetation changes; however, it is important to consider how geomorphic processes may influence vegetation, fire activity, and charcoal deposition (Fig. 7). Across the SE Queensland dune field, CHAR records closely reflect progressive vegetation succession associated with phases of dune activation and emplacement (stabilization) (Fig. 9, Supplementary Fig. 9). We observe that CHAR peaks are inversely related to the timing of major phases of dune emplacement and likely reflect the inability of fire to penetrate through active dune fields. The presence of charcoal in the dune footslope deposits is partially controlled by the local composition of vegetation in the windward direction (SE) on the dune hillslopes (Fig. 7). The first evidence of charcoal occurs directly after the first phases of dune activation at  $8.5 \pm 1.0$  ka during the postglacial transgression (Ellerton et al., 2020; Patton et al., 2022b) (Fig. 9, Supplementary Fig. 9). As sea level rose, dunes were active off the coast and migrated inland (vegetation-free landscape) for years to centuries before stabilizing (e.g., Levin, 2011; Houser et al., 2015; Levin et al., 2017). While the dunes are active, they act as a natural fire break that hinders the encroachment of fire spreading from the windward direction (Fig. 7a). Not until the emergence of woody vegetation such as *Eucalyptus* spp. or *Corymbia* spp. do woody charcoal-bearing fires occur (Fig. 7b and c). These findings matched those found in the Nebraska Sand Hills in the United States, where fire frequency and pollen abundance were inversely related to eolian activity (Schmieder et al., 2013).



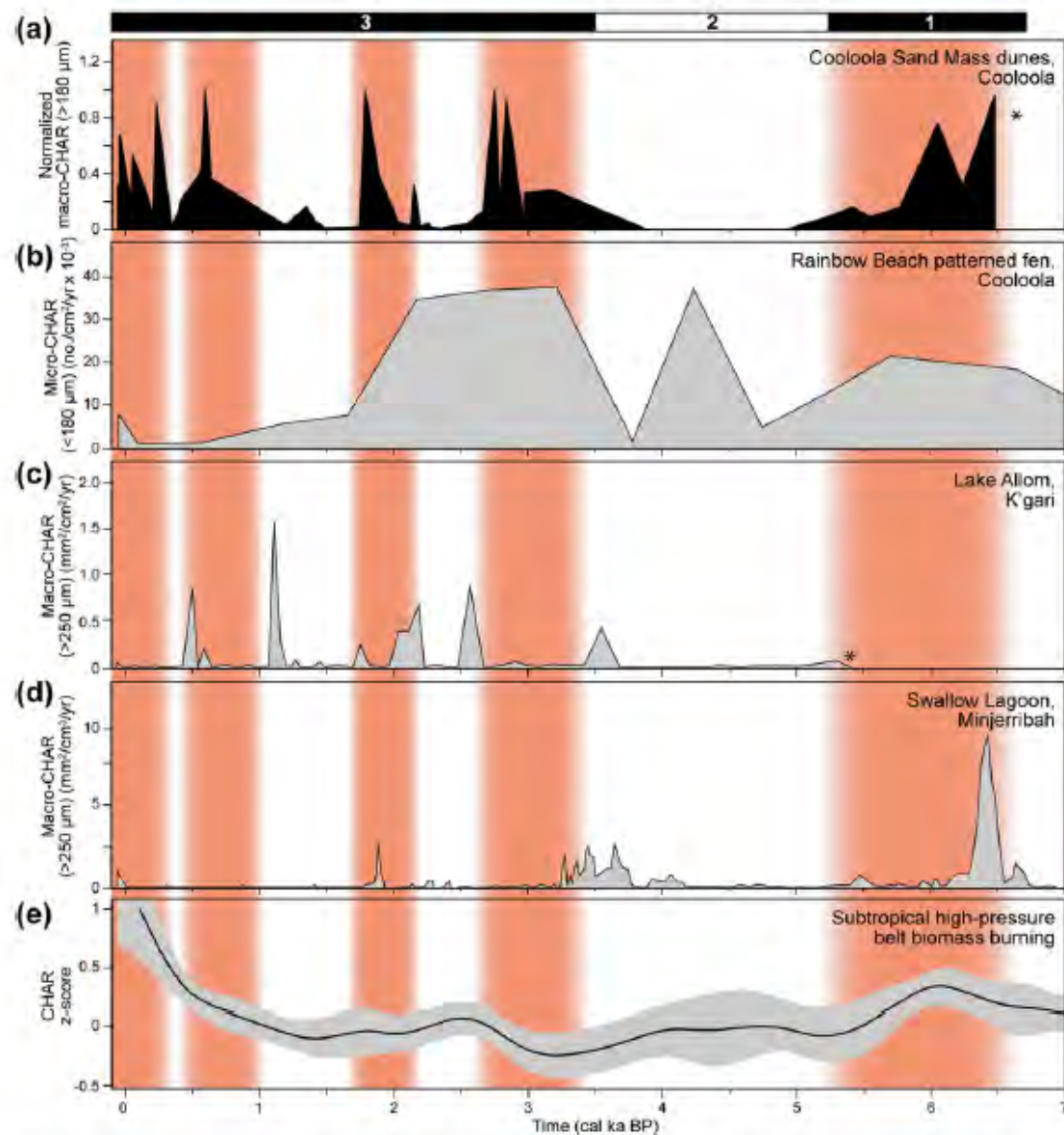


**Figure 8.** (a) Master charcoal record derived from only slow and continuous sediment transport for all sites in this study with increases in biomass burning (vertical orange bars) over three proposed periods of fire activity (black and white bar). Our data are compared with other (b) local (Hanson *et al.*, 2023) and (c and d) regional sites (Dondos *et al.*, 2006; Mañani *et al.*, 2019), as well as (e) a compilation of records from the subtropical high-pressure belt in eastern Australia (125 sites) (Mooney *et al.*, 2011). Locations of local and regional records are indicated in Fig. 1 as white stars. The fire records from the Cooloola Sand Mass (CSM) sites are compatible with those from traditional fire records within SE Queensland (i.e., peats, bogs, and lakes). An asterisk (\*) indicates the lack of data.

An important caution is that dune activation does not influence fire records equally. Although, dune activation will result in some form of disruption to the vegetation, only the largest dunes will significantly impact the charcoal records. For example, only large active dunes that extend several kilometers inland would pose a substantial barrier for fires. Once vegetated with grasses and shrubs, these dunes become highly flammable

ignition sources. These same processes will occur on small dunes but to a lesser extent and under localized conditions.

#### Recommendations and future applications

Wildfires are prevalent across the world, but fire histories are limited to where wetland sediment records are relatively abundant

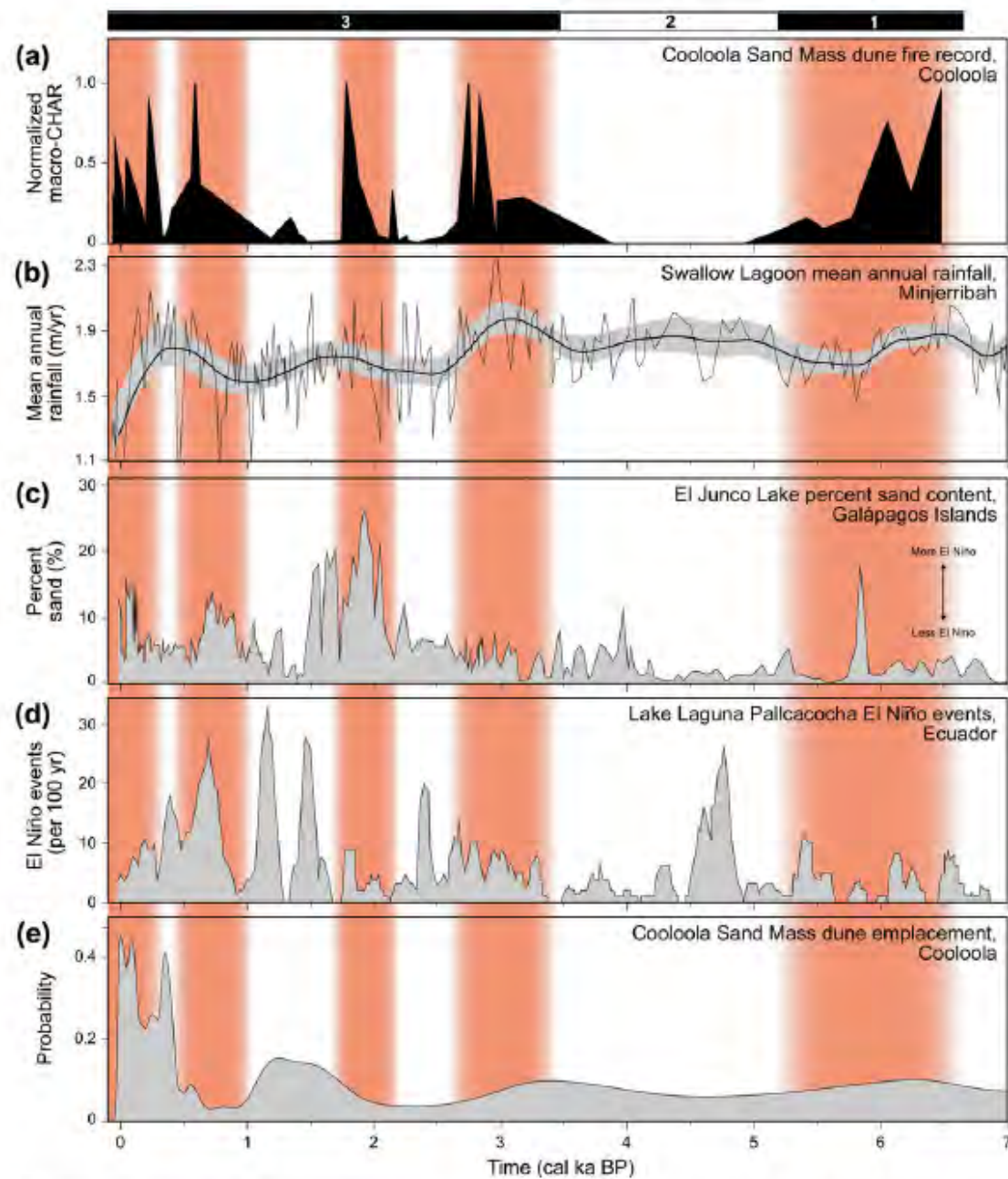


**Figure 9.** (a) Master charcoal record derived from only slow and continuous sediment transport for all sites in this study (black area). We compare our results with (b) the Swallow Lagoon precipitation record (Barr et al., 2019) and (c) the El Junco Lake in the Galápagos Islands and (d) the Lake Laguna Pallcacocha in southern Ecuador records of past El Niño event frequency (Moy et al., 2002; Conroy et al., 2008). Finally, we compare the (e) probability density function for the timing of dune emplacement at the Cooloola Sand Mass (CSM) (Patton et al., 2022b).

(Fig. 10). Our study identifies dune footslope deposits as a previously unrecognized record that can help explain past fire regimes and/or provide evidence for how ecosystems, such as those found in Australia, are adapted or not adapted to fire (Fig. 10). Although, this study is based on large, coastal dunes in SE

Queensland, we believe these outcomes are not unique to this area. Other similar high-quality records should be present in smaller and older dunes across the world, and we encourage further exploration and methodological development in these archives. A clear path of future research would be to target



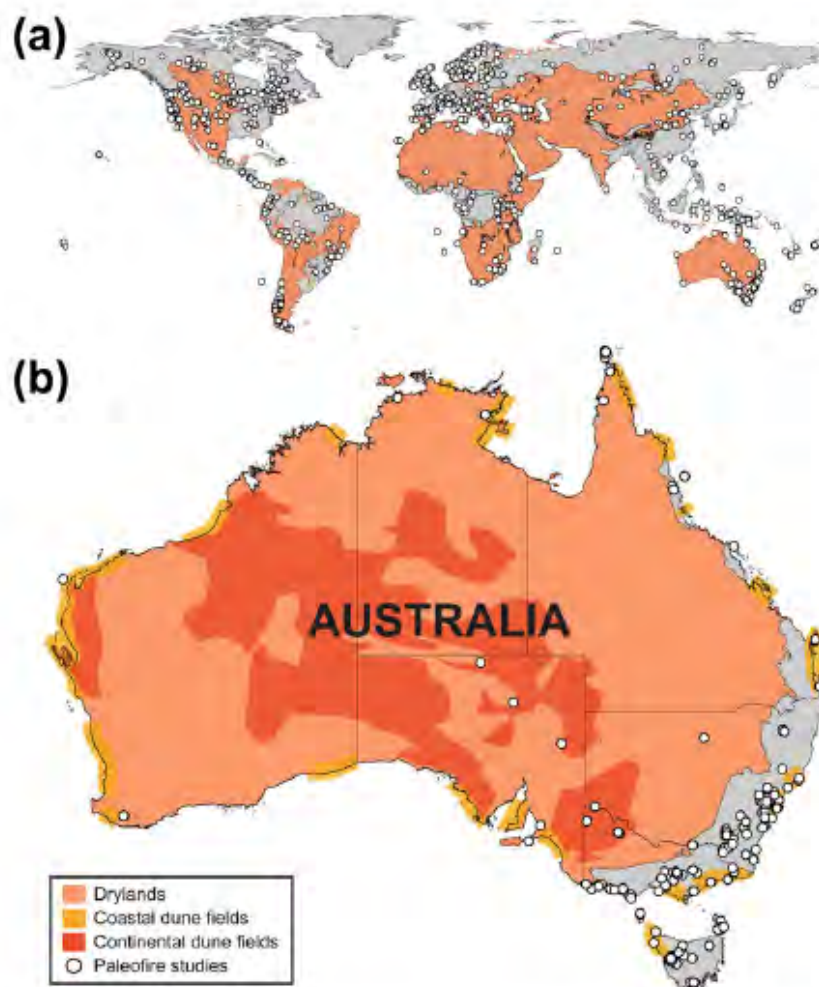


**Figure 10.** (a) World dryland distribution (orange areas) (Sorensen, 2007) and published paleofire records (white dots) from the Global Paleofire Database (Harrison *et al.*, 2022). (b) Closeup view of Australia and the general locations of coastal (yellow) and continental (orange) dunes (Lees, 2006; Hesse, 2016). Note the abundant land area in Australia and the world that is both covered in drylands and lacking fire histories. Dune depositional deposits present an opportunity to expand fire records from wetland areas into dryland regions, which to this point have been underrepresented in paleofire studies.

underrepresented regions such as drylands, where fire records are sparse. We highlight Mediterranean regions, California, and the southwestern United States, northern and southern Africa, and central China as likely high-value targets for this work (Fig. 10a). We provide suggestions on selecting sites and sampling strategies in future studies.

As developed in this study, a network of depositional sites to construct a fire record is encouraged but not necessary. A singular site of significant antiquity coupled with a higher-resolution sampling design can provide useful and continuous local fire records. However, we suggest targeting multiple older, Pleistocene-aged dunes that cover similar time periods. This will increase record length, improve comparison between sites, and reduce biases created by oversampling younger depth intervals. Moreover, it is critical to avoid dunes that have experienced recent reactivations, as their foot-slopes are prone to hiatuses and large shifts in sediment rates. These

data sets are necessary if we are attempting to understand broadscale shifts in fire regimes over glacial-interglacial cycles.

The largest improvement to this study is to undertake a higher-resolution, consistent sampling regime, like those used on lake sediment cores (e.g., 1 cm samples collected every 2 or 5 cm). This would ensure that CHAR peaks are not obscured,  $^{14}\text{C}$  dates are collected at discrete depths, and age-depth models are representative of each site. Furthermore, it is important to select samples for fire reconstruction from intervals with consistent sedimentation rates and styles to decrease the risk of conflating geomorphic and ecological processes. As our work highlights, the first ca. 1.5 ka of sediment deposition is dynamic, and fire records may reflect extremely localized and stochastic signals (i.e., CL2–CL5 in Fig. 5b). After this point, sedimentation rates are reduced, and the dominant signal is inferred to represent more regional trends in biomass burning. Determining the timing



of this transition is critical, as this shift from episodic to continuous sediment transport is unique to each site and relates to the physical properties of the dune sands (Patton et al., 2022b). However, the transition can be easily recognized from the change-over from charcoal layers to dispersed charcoal. While charcoal layers (CL) do not record regional trends in fire activity, they should not be discounted or ignored. Their presence in deposits elucidates processes and relative rates and indicates local fire events. Moreover, this simple identification of charcoal layers in deposits can rapidly aid in site selection, without the immediate need for  $^{14}\text{C}$  dating and age-depth modeling.

## CONCLUSIONS

The largest spatial gaps in fire records come from semiarid and arid regions, which lack the aquatic records favorable for preserving charcoal (Leys et al., 2018; Harrison et al., 2022). However, dunes are abundant in these regions (Thomas and Wiggs, 2008) and may provide a useful target for paleofire reconstruction. In this study, we demonstrate the potential of dune footslope deposits as an archive of multimillennial fire records. We establish that the sclerophyll forest on the stabilized dunes in the CSM in Australia have burned repeatedly and produced abundant charcoal over a ca. 7 ka period.

The large charcoal size classes (180–250  $\mu\text{m}$ , 250–355  $\mu\text{m}$ , and 355  $\mu\text{m}$ –2 mm) selected to represent the presence of local fires show consistent concentrations and accumulation rates (CHAR) with depth from all our sites. These findings support the hypothesis that footslope deposits have experienced limited postdepositional mixing and that sites contain intact and reliable stratigraphic records of fire activity. We find that the dune depositional stratigraphy reflects one of three distinct phases with respect to charcoal production and preservation:

1. **Absent to sparse charcoal:** As dunes are active or becoming stabilized, there is insufficient vegetation to allow fires to fully develop and penetrate.
2. **Charcoal layers:** Once the dunes are stabilized by the colonization of vegetation, charcoal production increases and episodic sediment transport dominates. This results in the creation of charcoal layers associated with individual major fire events.
3. **Dispersed charcoal:** After dune slopes drop below their angle of repose and transition to slow and continuous sediment transport (at ca. 1.5 ka), charcoal continues to be deposited but is dispersed throughout the profile. During these times, individual fires cannot be identified but relative biomass burning can be inferred.

We observe five CHAR peaks found within the three major periods that are traceable between dune footslope records. In general, fire becomes more abundant after ca. 3.4 cal ka BP, which is seen in other records from lakes and swamps in the SE Queensland dune fields (i.e., K'gari's Lake Allom, CSM's patterned fen complex, and Minjerribah's Swallow Lagoon). Our findings correlate with earlier inferences that the shift in fire activity is partially due to changes in the hydrological cycle through the ENSO intensification and its impact on fuel loads. This increase may also reflect intensification of fire usage by the Indigenous people. However, we also propose an alternative hypothesis: the mechanism causing fire variability is

through vegetation changes in the dune field driven by dune activity itself.

The consistent trends of increasing age with depth and relatively minor uncertainty make these depositional footslope positions ideal targets for paleofire reconstruction. We propose that other dune deposits will yield comparable findings and that these records can expand fire histories from areas where fire is a rare event (wetlands/lakes) into the parts of the landscape where fire may be an important or the dominant ecological process. Furthermore, this method opens many new regions for paleofire studies and can give new insights on fire frequency and intensity in regions globally (Fig. 10).

**Acknowledgments.** The fieldwork and sample collection were undertaken using permit WITK15791415. Funding for this study was provided by the Australian Research Council (ARC) grant no. DP150101513, ANSTO Portal Grants (AP12211, AP12614, and AP12591), and the Mason Trust Fund. We thank the helpful comments from Nicholas Lancaster and Kevin Norton and the assistance by the National Parks and Wildlife Service. We would also like to thank Yuzhu Zhang, Dongliang Ning, and Patrick Adams for their assistance in the field. The authors acknowledge the traditional owners of the Cooloola Sand Mass, the Kabi' Kabi' people.

**Data availability statement.** All data necessary to generate results for this study are available in the article and Supplementary Information. The Black Summers fire extent (DAWE, 2020), world dryland distribution information (Sorensen, 2007), and the global paleofire data (Harrison et al., 2022) used in this study were downloaded from [www.environment.gov.au/fed/catalog/search/resource/details.page?uuid=%7B9ACDCB09-0364-4FE8-9459-2A56C792C743%7D%20](http://www.environment.gov.au/fed/catalog/search/resource/details.page?uuid=%7B9ACDCB09-0364-4FE8-9459-2A56C792C743%7D%20), and <http://datadownload.unep-wcmc.org/datasets>, and [www.paleofire.org/index.php](http://www.paleofire.org/index.php), respectively.

**Supplementary material.** The supplementary material for this article can be found at <https://doi.org/10.1017/qua.2023.14>

## REFERENCES

- Almond, P.C., Tonkin, P.J., 1999. Pedogenesis by upbuilding in an extreme leaching and weathering environment, and slow loess accretion, south Westland, New Zealand. *Geoderma* 92(1–2), 1–36.
- Arbogast, A.F., Packman, S.C., 2004. Middle-Holocene mobilization of aeolian sand in western upper Michigan and the potential relationship with climate and fire. *The Holocene* 14, 464–471.
- Archibald, S., Lehmann, C.E., Gómez-Dans, J.L., Bradstock, R.A., 2013. Defining pyromes and global syndromes of fire regimes. *Proceedings of the National Academy of Sciences USA* 110, 6442–6447.
- Atahan, P., Heijnis, H., Dodson, J., Grice, K., Le Métayer, P., Taffs, R., Hembrow, S., Woltering, M., Zawadzki, A., 2015. Pollen, biomarker and stable isotope evidence of late Quaternary environmental change at Lake McKenzie, southeast Queensland. *Journal of Paleolimnology* 53, 139–156.
- Barr, C., Tibby, J., Marshall, J.C., McGregor, G.B., Moss, P.T., Halverson, G.P., Fluin, J., 2013. Combining monitoring, models and paleolimnology to assess ecosystem response to environmental change at monthly to millennial timescales: the stability of Blue Lake, North Stradbroke Island, Australia. *Freshwater Biology* 58, 1614–1630.
- Barr, C., Tibby, J., Moss, P.T., Halverson, G.P., Marshall, J.C., McGregor, G.B., Stirling, E., 2017. A 25,000-year record of environmental change from Welsby Lagoon, North Stradbroke Island, in the Australian subtropics. *Quaternary International* 449, 106–118.
- Barr, C., Tibby, J., Leng, M.J., Tyler, J.J., Henderson, A.C.G., Overpeck, J.T., Simpson, G.L., et al., 2019. Holocene El Niño–Southern Oscillation variability reflected in subtropical Australian precipitation. *Scientific Reports* 11, 7634.
- BenDror, E., Goren, L., 2018. Controls over sediment flux along soil-mantled hillslopes: insights from granular dynamics simulations. *Journal of Geophysical Research: Earth Surface* 123, 924–944.



- Blauw, M., Christen, J.A., 2011. Flexible paleoclimate age-depth models using an autoregressive gamma process. *Bayesian Analysis* 6, 457–474.
- Blake, G.R., Hartge, K.H., 1986. Bulk density. In: Klute, A. (Ed.), *Methods of Soil Analysis. Part 1, Physical and Mineralogical Methods* 5.1. 2nd ed. American Society of Agronomy–Soil Science Society of America, Madison, WI, pp. 363–375.
- [BOM] Bureau of Meteorology, 2019. Climate Data Online. Australian Government, Bureau of Meteorology (accessed April 8, 2019). [www.bom.gov.au/climate/data/index.shtml](http://www.bom.gov.au/climate/data/index.shtml).
- Bowman, D.M., 1998. The impact of Aboriginal landscape burning on the Australian biota. *New Phytologist* 140, 385–410.
- Bowman, D.M., Murphy, B.P., Neyland, D.L., Williamson, G.J., Prior, L.D., 2014. Abrupt fire regime change may cause landscape-wide loss of mature obligate seeder forests. *Global Change Biology* 20, 1008–1015.
- Bowman, D.M.J.S., Balch, J.K., Artaxo, P., Bond, W.J., Carlson, J.M., Cochran, M.A., D'Antonio, C.M., *et al.*, 2009. Fire in the Earth system. *Science* 324, 481–484.
- Boyd, R., Ruming, K., Goodwin, I., Sandstrom, M., Schröder-Adams, C., 2008. Highstand transport of coastal sand to the deep ocean: a case study from Fraser Island, southeast Australia. *Geology* 36, 15–18.
- Bradstock, R.A., 2010. A biogeographic model of fire regimes in Australia: current and future implications. *Global Ecology and Biogeography* 19, 145–158.
- Bradstock, R.A., Williams, J.E., Gill, A.M. (Eds.), 2002. *Flammable Australia: The Fire Regimes and Biodiversity of a Continent*. Cambridge University Press, Cambridge.
- Bridge, B.J., Ross, P.J., 1983. Water erosion in vegetated sand dunes at Cooloola, south-east Queensland. *Zeitschrift für Geomorphologie, Supplementband* 45, 227–244.
- Bridgman, H., Timms, B.V., 2012. Australia, climate and lakes. In: Bengtsson, L., Hensch, R.W., Fairbridge, R.W. (Eds.), *Encyclopedia of Lakes and Reservoirs*. Springer, Dordrecht, Netherlands, pp. 73–80.
- Canadell, J.G., Meyer, C.P., Cook, G.D., Dowdy, A., Briggs, P.R., Knauer, J., Pepler, A., Haverd, V., 2021. Multi-decadal increase of forest burned area in Australia is linked to climate change. *Nature Communications* 12, 1–11.
- Carcaillet, C., Richard, P.J., Asnong, H., Capece, L., Bergeron, Y., 2006. Fire and soil erosion history in East Canadian boreal and temperate forests. *Quaternary Science Reviews* 25, 1489–1500.
- Chang, J.C., Woodward, C., Shulmeister, J., 2014. A snapshot of the limnology of eastern Australian water bodies spanning the tropics to Tasmania: the land-use, climate, limnology nexus. *Marine and Freshwater Research* 65, 872–883.
- Chang, J.C., Woodward, C., Shulmeister, J., 2017. Reconstructing terrestrial temperatures in the Australian sub-tropics and tropics: a chironomid based transfer function approach. *Quaternary International* 449, 136–148.
- Clark, J.S., Lynch, J., Stocks, B.J., Goldammer, J.G., 1998. Relationships between charcoal particles in air and sediments in west-central Siberia. *The Holocene* 8, 19–29.
- Clarkson, C., Jacobs, Z., Marwick, B., Fullagar, R., Wallis, L., Smith, M., Roberts, R.G., *et al.*, 2017. Human occupation of northern Australia by 65,000 years ago. *Nature* 547, 306–310.
- Coldrake, J.E., 1962. The coastal sand dunes of southern Queensland. *Proceedings of the Royal Society of Queensland* 72, 101–116.
- Cohen-Orli, L., Weiner, L., Boaretto, E., Mintz, G., Weiner, S., 2006. Modern and fossil charcoal: aspects of structure and diagenesis. *Journal of Archaeological Science* 33, 428–439.
- Collins, L., 2019. Eucalypt forests dominated by epicormic resprouters are resilient to repeated canopy fires. *Journal of Ecology* 108, 310–324.
- Conroy, J.L., Overpeck, J.T., Cole, J.E., Shanahan, T.M., Steinitz-Kannan, M., 2008. Holocene changes in eastern tropical Pacific climate inferred from a Galápagos lake sediment record. *Quaternary Science Reviews* 27, 1166–1180.
- [DAWE] Department of Agriculture, Water and the Environment, 2020. *Preliminary Analysis for Environmental Analysis—2019/20 Fires*. Department of Agriculture, Water and the Environment, Canberra (accessed May 15, 2022). [www.environment.gov.au/led/catalog/search/resource/details.page?uuid=%7B9ACDCB09-0364-4FEB-9459-2A56C792C743%7D](http://www.environment.gov.au/led/catalog/search/resource/details.page?uuid=%7B9ACDCB09-0364-4FEB-9459-2A56C792C743%7D).
- DeBano, L.F., 1981. *Water Repellent Soils: A State-of-the-Art*. Vol. 46. U.S. Department of Agriculture, Forest Service, Pacific Southwest Forest and Range Experiment Station, Berkeley.
- Doerr, S.H., Shakesby, R.A., Walsh, R., 2000. Soil water repellency: its causes, characteristics and hydro-geomorphological significance. *Earth-Science Reviews* 51(1–4), 33–65.
- Donders, T.H., Wagner, F., Visscher, H., 2006. Late Pleistocene and Holocene subtropical vegetation dynamics recorded in perched lake deposits on Fraser Island, Queensland, Australia. *Palaeogeography, Palaeoclimatology, Palaeoecology* 241, 417–439.
- Donders, T.H., Haberle, S.G., Hope, G., Wagner, F., Visscher, H., 2007. Pollen evidence for the transition of the Eastern Australian climate system from the post-glacial to the present-day ENSO mode. *Quaternary Science Reviews* 26, 1621–1637.
- Ellerton, D., Rittenour, T., Miot da Silva, G., Gontz, A., Shulmeister, J., Hesp, P., Santini, T., Welsh, K.J., 2018. Late-Holocene cliff-top blowout activation and evolution in the Cooloola Sand Mass, south-east Queensland, Australia. *The Holocene* 28, 1697–1711.
- Ellerton, D., Rittenour, T., Shulmeister, J., Gontz, A., Welsh, K.J., Patton N.R., 2020. An 800 kyr record of dune emplacement in relationship to high sea level forcing, Cooloola Sand Mass, Queensland, Australia. *Geomorphology* 354, 106999.
- Ellerton, D., Rittenour, T., Shulmeister, J., Roberts, A.P., Miot da Silva, G., Gontz, A., Hesp, P., *et al.*, 2023. Fraser Island (K'gari) and initiation of the Great Barrier Reef linked by Middle Pleistocene sea-level change. *Nature Geoscience* 15, 1017–1026.
- Fensham, R.J., 1997. Aboriginal fire regimes in Queensland, Australia: analysis of the explorers' record. *Journal of Biogeography* 24, 11–22.
- Filion, L., 1984. A relationship between dunes, fire and climate recorded in the Holocene deposits of Quebec. *Nature* 309, 543–546.
- Fillard, A.L., Ngo, T., Matthews, S., Telfer, S., Penman, T.D., 2020. Impact of Australia's catastrophic 2019/20 bushfire season on communities and environment. Retrospective analysis and current trends. *Journal of Safety Science and Resilience* 1, 44–56.
- Fink, D., Hotchkiss, M., Hua, Q., Jacobsen, G., Smith, A.M., Zoppi, U., Child, D., *et al.*, 2004. The ANTARES AMS Facility at ANSTO. *Nuclear Instruments and Methods in Physics Research B* 223–224, 109–115.
- Fletcher, M.S., Hall, T., Alexandra, A.N., 2021. The loss of an Indigenous constructed landscape following British invasion of Australia: an insight into the deep human imprint on the Australian landscape. *Ambio* 50, 138–149.
- Gallagher, R.V., Allen, S., Mackenzie, B.D., Yates, C.J., Gosper, C.R., Keith, D.A., Merow, C., *et al.*, 2021. High fire frequency and the impact of the 2019–2020 megafires on Australian plant diversity. *Diversity and Distributions* 27, 1166–1179.
- Gavin, D.G., Brubaker, L.B., Lertzman, K.P., 2003. An 1800-year record of the spatial and temporal distribution of fire from the west coast of Vancouver Island, Canada. *Canadian Journal of Forest Research* 33, 573–586.
- Gross, W., Morrill, C., Wahl, E., 2018. New advances at NOAA's World data service for paleoclimatology—Promoting the FAIR principles. *Past Global Changes Magazine* 26(2), 58–58.
- Hanson, J.M., Vandergragt, M.L., Welsh, K.J., Moss, P.T., 2022. Variations in wetland conditions within the Fitzroy Basin, north-eastern Australia: a palaeoecological approach. *Marine and Freshwater Research* 73, 35–47.
- Hanson, J.M., Welsh, K.J., Moss, P.T., Gadd, P., 2023. Implications of sea level variability on the formation and evolution of subtropical Rainbow Beach patterned fen complexes, Queensland, Australia. *The Holocene* 33, 49–60.
- Harrison, S.P., Villegas-Diaz, R., Cruz-Silva, E., Gallagher, D., Kesner, D., Lincoln, P., Shen, Y., *et al.*, 2022. The Reading Palaeofire Database v1.0: an expanded global resource to document changes in fire regimes from sedimentary charcoal records. *Earth System Science Data* 14, 1109–1124.
- Hawkins, P.J., 1975. Forest management of Cooloola State Forest. In: Kikkawa, J., Nix, H.A. (Eds.), *Managing Terrestrial Ecosystems. Proceedings of the Ecological Society of Australia* 9, 328–333.
- Hawthorne, D., Mustaphi, C.J.C., Aleman, J.C., Blarquez, O., Colombaroli, D., Danian, A.L., Marlon, J.R., *et al.*, 2018. Global Modern Charcoal



- Dataset (GIMCD): a tool for exploring proxy-fire linkages and spatial patterns of biomass burning. *Quaternary International* 488, 3–17.
- Hennebelle, A., Aleman, J.C., Ali, A.A., Bergeron, Y., Carcaillet, C., Grondin, P., Landry, J., Blarquez, O., 2020. The reconstruction of burned area and fire severity using charcoal from boreal lake sediments. *The Holocene* 30, 1400–1409.
- Hennessey, K., Lucas, C., Nicholls, N., Bathols, J., Suppiah, R., Ricketts, J., 2005. *Climate Change Impacts on Fire Weather in South-East Australia*. Climate Impacts Group, CSIRO Atmospheric Research and the Australian Government Bureau of Meteorology, Aspendale.
- Hesse, P.P., 2016. How do longitudinal dunes respond to climate forcing? Insights from 25 years of luminescence dating of the Australian desert dunefields. *Quaternary International* 410, 11–29.
- Higuera, P.E., Sprugel, D.G., Brubaker, L.B., 2005. Reconstructing fire regimes with charcoal from small hollow sediments: a calibration with tree-ring records of fire. *The Holocene* 15, 238–251.
- Higuera, P.E., Peters, M.E., Brubaker, L.B., Gavin, D.G., 2007. Understanding the origin and analysis of sediment-charcoal records with a simulation model. *Quaternary Science Reviews* 26, 1790–1809.
- Hogg, A.G., Heaton, T.J., Hua, Q., Palmer, J.G., Turney, C.S., Southon, J., Bayliss, A., et al., 2020. SHCal20 Southern Hemisphere calibration, 0–55,000 years cal. BP. *Radiocarbon* 62, 759–778.
- Houser, C., Wernette, P., Rentschler, E., Jones, H., Hammond, B., Trimble, S., 2015. Post-storm beach and dune recovery: implications for barrier island resilience. *Geomorphology* 234, 54–63.
- Hua, Q., Jacobson, G.E., Zoppi, U., Lawson, E.M., Williams, A.A., Smith, A.M., McGann, M.J., 2001. Progress in radiocarbon target preparation at the ANTARES AMS Centre. *Radiocarbon* 43(2A), 275–282.
- Hua, Q., Turnbull, J.C., Santos, G.M., Rakowski, A.Z., Anicichien, S., De Pol-Holz, R., Hammer, S., et al., 2022. Atmospheric radiocarbon for the period 1950–2019. *Radiocarbon* 64, 723–745.
- Iglesias, V., Yoojin, G.L., Whitlock, C., 2015. Reconstruction of fire regimes through integrated paleoecological proxy data and ecological modeling. *Frontiers in Plant Science* 5, 785.
- [IPCC] Intergovernmental Panel on Climate Change, 2021. *Climate Change 2021: The Physical Science Basis*. Contribution of Working Group I to the Sixth Assessment Report of the Intergovernmental Panel on Climate Change. Cambridge University Press, Cambridge.
- Itter, M.S., Finley, A.O., Hooten, M.B., Higuera, P.E., Marlon, J.R., Kelly, R., McLauchlan, J.S., 2017. A model-based approach to woodland fire reconstruction using sediment charcoal records. *Environmetrics* 28, e2450.
- Kjallik, J.A., Worsley, P., Pys, K., Clark, M.L., 1999. A revised chronology for aeolian activity in subarctic Fennoscandia during the Holocene. *The Holocene* 9, 195–205.
- Keeley, J.E., 1995. Seed germination patterns in fire-prone Mediterranean-climate regions. In: Arroyo, M.T.K., Zedler, P.H., Fox, M.D. (Eds.), *Ecology and Biogeography of Mediterranean Ecosystems in Chile, California, and Australia*. Springer, New York, pp. 239–273.
- Keith, D., 2004. *Ocean Shores to Desert Dunes: The Native Vegetation of New South Wales and the ACT*. Department of Environment and Conservation, Hurstville, NSW, Australia.
- Kemp, C., Tibby, J., Barr, C., Arnold, L., 2021. Climate, fire and vegetation history from subtropical North Stradbroke Island (Manjeribah), eastern Australia, during the last three interglacials. *Journal of Quaternary Science* 36, 1201–1213.
- Kershaw, A.P., 1996. Climatic change and Aboriginal burning in north-east Australia during the last two glacial/interglacial cycles. *Nature* 322, 47–49.
- Kershaw, A.P., Clark, J.S., Gill, A.M., D'Costa, D.M., 2002. A history of fire in Australia. In: Bradstock, R.A., Williams, J.E., Gill, A.M. (Eds.), *Hammable Australia: The Fire Regimes and Biodiversity of a Continent*. Cambridge University Press, Cambridge, pp. 3–25.
- Köhler, M., Schmalzer, J., Patton, N.R., Rittenour, T.M., McSwiney, S., Ellerton, D.T., Hünke, H., 2021. Holocene evolution of a barrier-spit complex and the interaction of tidal and wave processes, Indip Peninsula, SE Queensland, Australia. *The Holocene* 31, 1476–1488.
- Krishnan, V., Robinson, N., Finn, J., Applegate, G., Herbohn, J., Schmidt, S., 2018. Without management interventions, endemic wet-sclerophyll forest is transitioning to rainforest in World Heritage listed K'gari (Fraser Island), Australia. *Ecology and Evolution* 9, 1378–1393.
- Lancaster, N., Wolfe, S., Thomas, D., Britow, C., Bohner, O., Burroughs, S., Dußer, G., et al., 2016. The INQUA Dunes Atlas chronologic database. *Quaternary International* 410, 3–10.
- Lees, B., 2006. Timing and formation of coastal dunes in northern and eastern Australia. *Journal of Coastal Research* 22, 76–89.
- Levin, N., 2011. Climate-driven changes in tropical cyclone intensity shape dune activity on Earth's largest sand island. *Geomorphology* 125, 239–252.
- Levin, N., Levental, S., Moring, H., 2012. The effect of wildfires on vegetation cover and dune activity in Australia's desert dunes: a multisensor analysis. *International Journal of Wildland Fire* 21, 459–475.
- Levin, N., Jablon, P.E., Phinn, S., Collins, K., 2017. Coastal dune activity and foreshore formation on Morton Island, Australia, 1944–2015. *Australian Research* 25, 107–121.
- Lewis, S.E., Wint, R.A., Webster, J.M., Shields, G.A., 2008. Mid-late Holocene sea-level variability in eastern Australia. *Terra Nova* 20, 74–81.
- Ley, B.A., Connerford, J.L., McLauchlan, K.K., 2017. Reconstructing grassland fire history using sedimentary charcoal: considering count, size and shape. *PLoS ONE* 12, e0176445.
- Ley, B.A., Marlon, J.R., Umbanhowar, C., Vannière, B., 2018. Global fire history of grassland biomes. *Ecology and Evolution* 8, 8831–8852.
- Long, C.J., Whitlock, C., Bartlein, P.J., Millspaugh, S.H., 1993. A 9000-year fire history from the Oregon Coast Range, based on a high-resolution charcoal study. *Canadian Journal of Forest Research* 23, 774–787.
- Mann, D.H., Helser, P.A., Finney, B.P., 2002. Holocene history of the Great Kobuk sand dunes, northwestern Alaska. *Quaternary Science Reviews* 21, 709–731.
- Mariani, M., Tibby, J., Barr, C., Mow, P., Marshall, J.C., McGregor, G.B., 2019. Reduced rainfall drives biomass limitation of long-term fire activity in Australia's subtropical sclerophyll forests. *Journal of Biogeography* 46, 1974–1987.
- Mariani, M., Connor, S.E., Theuerkauf, M., Herbert, A., Kunz, P., Bowman, D., Fletcher, M.S., et al., 2022. Disruption of cultural burning promotes shrub encroachment and unprecedented wildfires. *Frontiers in Ecology and the Environment* 20, 292–300.
- Marlon, J., Bartlein, P.J., Whitlock, C., 2006. Fire-fuel-climate linkages in the northwestern USA during the Holocene. *The Holocene* 16, 1059–1071.
- Marlon, J.R., Kelly, R., Danian, A.L., Vannière, B., Power, M.J., Bartlein, P., Higuera, P., et al., 2015. Reconstructions of biomass burning from sediment-charcoal records to improve data-model comparisons. *Ringsedenas* 13, 3225–3244.
- Matthews, J.A., Suppiah, M., 2014. Holocene environmental change in subarctic aeolian dune fields: the chronology of sand dune re-activation events in relation to forest fires, palaeosol development and climatic variations in Finnish Lapland. *The Holocene* 24, 149–164.
- Maxon, C., Tibby, J., Marshall, J., Kent, M., Tyler, J., Barr, C., McGregor, G., Cadd, H., Schulz, C., Lomas, B.H., 2021. Fourier transform infrared spectroscopy as a tracer of organic matter sources in lake sediments. *Paleogeography, Paleoclimatology, Paleontology* 581, 110622.
- McKenzie, D., Godalof, Z., Peterson, D., Mote, P., 2004. Climatic change, wildfire and conservation. *Conservation Biology* 18, 890–902.
- McLauchlan, K.K., Higuera, P.E., Miesch, J., Rogers, B.M., Schweitzer, J., Shuman, J.K., Tepley, A.J., et al., 2020. Fire as a fundamental ecological process: research advances and frontiers. *Journal of Ecology* 108, 2047–2068.
- McNiven, I.J., 1991. Teewah Beach: new evidence for Holocene coastal occupation in southeast Queensland. *Australian Archaeology* 33, 14–27.
- Mooney, S.D., Harrison, S.P., Bartlein, P.J., Danian, A.L., Stevenson, J., Brownlie, K.C., Buckman, S., et al., 2011. Late Quaternary fire regimes of Australia. *Quaternary Science Reviews* 30, 28–46.
- Morris, J.L., Higuera, P.E., Haberle, S., Whitlock, C., 2017. Modern pollen from small hollows reflects *Athanasia depressoides* density across a wildfire gradient in subalpine forests of the Central Plateau, Tasmania, Australia. *The Holocene* 27, 1781–1788.
- Moss, P., Mackenzie, L., Ulm, S., Sloss, C., Rosendahl, D., Petherick, L., Steinberger, L., Wallis, L., Heijink, H., Petchey, F., Jacobsen, G., 2015. *Environmental context for late Holocene human occupation of the South*



- Wellesley Archipelago, Gulf of Carpentaria, northern Australia. *Quaternary International* 385, 136–144.
- Moss, P.T., 2014. *Investigation of the Vegetation and Fire History of the EPBC, RAMSAR and WHA Wetlands of the Great Sandy Strait* (Unpublished report). University of Queensland, Brisbane, Australia.
- Moss, P.T., Kershaw, P.A., 2000. The last glacial cycle from the humid tropics of northeastern Australia: comparison of a terrestrial and a marine record. *Palaeogeography, Palaeoclimatology, Palaeoecology* 155, 155–176, 162–176.
- Moss, P.T., Petherick, L., Neil, D., 2011. Environmental change at Myora Springs, North Stradbroke Island over the last millennium. *Proceedings of the Royal Society of Queensland* 117, 133–140.
- Moss, P.T., Tibby, J., Petherick, L., McGowan, H., Barr, C., 2013. Late Quaternary vegetation history of North Stradbroke Island, Queensland, eastern Australia. *Quaternary Science Reviews* 74, 257–272.
- Moy, C.M., Seltzer, G.O., Rodbell, D.T., Anderson, D.M., 2002. Variability of El Niño/Southern Oscillation activity at millennial timescales during the Holocene epoch. *Nature* 420, 162–165.
- Mulholland, C., 2021. Fighting to save an international icon—K'gari (Fraser Island). *Australian Journal of Emergency Management* 36, 40–43.
- Neal, R., Stock, E., 1986. Pleistocene occupation in the south-east Queensland coastal region. *Nature* 323, 618–621.
- Ngugi, M.R., Knight, J., Hua, Q., Dowling, R., Kington, D., Burns, D., 2020. Ageing culturally significant relic trees in southeast Queensland to support bushfire management strategies. *Ecological Management Restoration* 21, 147–150.
- Patton, N.R., Ellerton, D., Shulmeister, J., 2019. High-resolution remapping of the coastal dune fields of south east Queensland, Australia: a morphometric approach. *Journal of Maps* 15, 578–589.
- Patton, N.R., Shulmeister, J., Ellerton, D., Seropian, G., 2022a. Measuring landscape evolution from inception to maturity: insights from a coastal dune system. *Earth and Planetary Science Letters* 584, 117448.
- Patton, N.R., Shulmeister, J., Rittenour, M.T., Almond, P., Ellerton, D.T., Santini, T., 2022b. Using calibrated surface roughness dating to estimate coastal dune ages at K'gari (Fraser Island) and the Cooloola Sand Mass, Australia. *Earth Surface Processes and Landforms* 47, 2455–2470.
- Peel, M.C., Finlayson, B.L., McMahon, T.A., 2007. Updated world map of the Köppen-Geiger climate classification. *Hydrology and Earth System Sciences* 11, 1633–1644.
- Power, M.J., Marlon, J., Ortiz, N., Bartlein, P.J., Harrison, S.P., Mayle, F.E., Ballouche, A., et al., 2008. Changes in fire regimes since the Last Glacial Maximum: an assessment based on a global synthesis and analysis of charcoal data. *Climate Dynamics* 30, 887–907.
- Pyne, S.J., 1998. *Burning Bush: A Fire History of Australia*. Henry Holt, New York.
- Queensland Herbarium, 2021. Regional Ecosystem Description Database (REDD). Version 12.1. Queensland Department of Environment and Science, Brisbane (accessed April 1, 2022). [www.qld.gov.au/environment/plants-animals/plants/ecosystems](http://www.qld.gov.au/environment/plants-animals/plants/ecosystems).
- R Core Team, 2020. *R: A Language and Environment for Statistical Computing*. R Foundation for Statistical Computing, Vienna, Austria. [www.R-project.org](http://www.R-project.org).
- Reeve, R., Fergus, L.F., Thompson, C.H., 1985. Studies in landscape dynamics in the Cooloola-Noosa River area, Queensland. 4. Hydrology and water chemistry. In: *CSIRO Australia, Division of Soils Divisional Report No. 77*. CSIRO, St. Lucia, QLD, pp. 1–42. <https://doi.org/10.25919/5c8fcd51bd55>.
- Reid, L.M., Dunne, T., 1996. *Rapid Evaluation of Sediment Budgets*. Vol. 29. Catena, Reiskirchen, Germany.
- Remy, C.C., Fouquemberg, C., Aswelin, H., Andrieux, B., Magnan, G., Brossier, B., Grondin, P., et al., 2018. Guidelines for the use and interpretation of palaeofire reconstructions based on various archives and proxies. *Quaternary Science Reviews* 193, 312–322.
- Richards, L., Brew, N., Smith, L., 2020. 2019–2020 Australian Bushfires—Frequently Asked Questions: A Quick Guide. Parliament of Australia, Research Paper Series 2019–2020 (accessed June 2, 2020). [www.aph.gov.au/About\\_Parliament/Parliamentary\\_Departments/Parliamentary\\_Library/pubs/rp/rp1920/Quick\\_Guides/AustralianBushfires](http://www.aph.gov.au/About_Parliament/Parliamentary_Departments/Parliamentary_Library/pubs/rp/rp1920/Quick_Guides/AustralianBushfires).
- Roering, J.J., Gerber, M., 2005. Fire and the evolution of steep, soil-mantled landscapes. *Geology* 33, 349–352.
- Roering, J.J., Kirchner, J.W., Dietrich, W.E., 1999. Evidence for nonlinear, diffusive sediment transport on hillslopes and implications for landscape morphology. *Water Resources Research* 35, 853–870.
- Russell-Smith, J., Lucas, D., Gapindi, M., Gunbunuka, B., Kapirigi, N., Namingum, G., Lucas, K., Giuliani, P., Chaloupka, G., 1997. Aboriginal resource utilization and fire management practice in western Arnhem Land, monsoonal northern Australia: notes for prehistory, lessons for the future. *Human Ecology* 25, 159–195.
- Russell-Smith, J., Yates, C.P., Whitehead, P.J., Smith, R., Craig, R., Allan, G.E., Thackway, R., et al., 2007. Bushfires “down under”: patterns and implications of contemporary Australian landscape burning. *International Journal of Wildland Fire* 16, 361–377.
- Sadler, P.M., 1981. Sediment accumulation rates and the completeness of stratigraphic sections. *Journal of Geology* 89, 569–584.
- Sanborn, P., Geertsema, M., Jull, A.J.T., Hawkes, B., 2006. Soil and sedimentary charcoal evidence for Holocene forest fires in an inland temperate rainforest, east-central British Columbia, Canada. *The Holocene* 16, 415–427.
- Schmieder, J., Fritz, S.C., Grimm, E.C., Jacobs, K.C., Brown, K.J., Swinehart, J.B., Porter, S.C., 2013. Holocene variability in hydrology, vegetation, fire, and eolian activity in the Nebraska Sand Hills, USA. *The Holocene* 23, 515–527.
- Schoenberger, P.J., Wysodki, D.A., Benham, E.C., Broderick, W.D., 2002. *Field Book for Describing and Sampling Soils*. Version 2.0. Natural Resources Conservation Service, National Soil Survey Center, Lincoln, NE.
- Schreuder, L.T., Donders, T.H., Mets, A., Hopmans, E.C., Damsté, J.S.S., Schouten, S., 2019. Comparison of organic and palynological proxies for biomass burning and vegetation in a lacustrine sediment record (Lake Allon, Fraser Island, Australia). *Organic Geochemistry* 133, 10–19.
- Seppälä, M., 1995. Deflation and redeposition of sand dunes in Finnish Lapland. *Quaternary Science Reviews* 14, 799–809.
- Shakesby, R.A., Doerr, S.H., 2006. Wildfire as a hydrological and geomorphological agent. *Earth-Science Reviews* 74, 269–307.
- Shulmeister, J., Lees, B.G., 1995. Pollen evidence from tropical Australia for the onset of an ENSO-dominated climate at c. 4000 BP. *The Holocene* 5, 10–18.
- Shumack, S., Hesse, P., 2018. Assessing the geomorphic disturbance from fires on coastal dunes near Esperance, Western Australia: implications for dune de-stabilisation. *Avian Research* 31, 29–49.
- Shumack, S., Hesse, P., Turner, L., 2017. The impact of fire on sand dune stability: surface coverage and biomass recovery after fires on Western Australian coastal dune systems from 1988 to 2016. *Geomorphology* 299, 39–53.
- Singh, G., Kershaw, A.P., Clark, R., 1981. Quaternary vegetation and fire history in Australia. In: Gill, A.M., Groves, R.H., Noble, L.R. (Eds.), *Fire and the Australian Biota*. Australian Academy of Science, Canberra, pp. 23–54.
- Sorensen, L., 2007. A Spatial Analysis Approach to Global Delineation of Dryland Area of Relevance to CBD Programme of Work on Dry and Subhumid Lands. UNEP-WCMC, Cambridge, UK (accessed May 22, 2022). <http://data.download.unep-wcmc.org/datasets>.
- Spencer, R.J., Baxter, G.S., 2006. Effects of fire on the structure and composition of open eucalypt forests. *Austral Ecology* 31, 638–646.
- Srivastava, S.K., King, L., Mitchell, C., Wiegand, A., Carter, R.W., Shapcott, A., Russell-Smith, J., 2012. Ecological implications of standard fire-mapping approaches for fire management of the World Heritage Area, Fraser Island, Australia. *International Journal of Wildland Fire* 22, 381–393.
- Stone, Z.L., Maron, M., Tasker, E., 2022. Reduced fire frequency over three decades hastens loss of the grassy forest habitat of an endangered songbird. *Biological Conservation* 270, 109570.
- Tejan-Kella, M.S., Chittleborough, D.J., Fitzpatrick, R.W., Thompson, C.H., Prescott, J.R., Hutton, J.T., 1990. Thermoluminescence dating of coastal sand dunes at Cooloola and North Stradbroke Island, Australia. *Soil Research* 28, 465–481.
- Thomas, A., 2003. *Fraser Island World Heritage Area Fire Management Systems: Fire Strategy*. Queensland Government, Queensland Parks and Wildlife Service, Brisbane.
- Thomas, D.S., Wiggs, G.F., 2008. Aeolian system responses to global change: challenges of scale, process and temporal integration. *Earth Surface Processes and Landforms* 33, 1396–1418.
- Thompson, C.H., 1981. Podzol chronosequences on coastal dunes of eastern Australia. *Nature* 291, 59–61.



- Thompson, C.H., 1983. Development and weathering of large parabolic dune systems along the subtropical coast of Eastern Australia. *Zeitschrift fuer Geomorphologie*, Suppl. 45, 205–225.
- Thompson, C.H., 1992. Genesis of podzols on coastal dunes in southern Queensland. Field relationships and profile morphology. *Soil Research* 30, 593–613.
- Thompson, C.H., Moore, A.W., 1984. Studies in landscape dynamics in the Cooloola-Noosa River area, Queensland. 1. Introduction, general description and research approach. CSIRO Australia, Division of Soils Divisional Report No. 73. CSIRO, St. Lucia, QLD, pp. 1–93. <https://doi.org/10.25919/5c8fdcef11537>.
- Turney, C.S., Kershaw, A.P., Moss, P., Bird, M.I., Fifield, L.K., Cresswell, R.G., et al., 2001. Redating the onset of burning at Lynch's Crater (North Queensland): implications for human settlement in Australia. *Journal of Quaternary Science* 16, 767–771.
- [UNESCO] United Nations Educational, Scientific and Cultural Organization World Heritage Convention, 2021. K'gari (Fraser Island) listing (accessed January 1, 2022). <https://whc.unesco.org/en/list/630/>
- Vachula, R.S., Russell, J.M., Huang, Y., Richter, N., 2018. Assessing the spatial fidelity of sedimentary charcoal size fractions as fire history proxies with a high-resolution sediment record and historical data. *Palaeogeography, Palaeoclimatology, Palaeoecology* 508, 166–175.
- Vachula, R.S., Sheppard, R.Y., Cheung, A.H., 2022. Preservation biases are pervasive in Holocene paleofire records. *Palaeogeography, Palaeoclimatology, Palaeoecology* 602, 111165.
- van der Werf, G.R., Randerson, J.T., Giglio, L., van Leeuwen, T.T., Chen, Y., Rogers, B.M., Mu, M., et al., 2017. Global fire emissions estimates during 1997–2016. *Earth System Science Data* 9, 697–720.
- Walker, J., Thompson, C.H., Fergus, I.F., Tunstall, B.R., 1981. Plant succession and soil development in coastal sand dunes of subtropical eastern Australia. In: West, D.C., Shugart, H.H., Botkin, D.B. (Eds.), *Forest Succession*. Springer, New York, pp. 107–131.
- Walker, J., Thompson, C.H., Lacey, C.J., 1987. Morphological differences in lignotubers of *Eucalyptus intermedia* RT Bak and *E. signata* F. Muell. associated with different stages of podzol development on coastal dunes, Cooloola, Queensland. *Australian Journal of Botany* 35, 301–311.
- Walker, J., Lees, B., Olley, J., Thompson, C., 2018. Dating the Cooloola coastal dunes of south-eastern Queensland, Australia. *Marine Geology* 398, 73–85.
- Walker, L.R., Wardle, D.A., Bardgett, R.D., Clarkson, B.D., 2010. The use of chronosequences in studies of ecological succession and soil development. *Journal of Ecology* 98, 725–736.
- Ward, W.T., 2006. Coastal dunes and strandplains in southeast Queensland: sequence and chronology. *Australian Journal of Earth Sciences* 53, 363–373.
- Whitlock, C., Milsapugh, S.H., 1996. Testing assumptions of fire history studies: an examination of modern charcoal accumulation in Yellowstone National Park. *The Holocene* 6, 7–15.
- Whitlock, C., Larsen, C., 2001. Charcoal as a fire proxy. In: Smol, J.P., Birks, H.J.B., Last, W.M., Bradley, R.S., Alverson, K. (Eds.), *Tracking Environmental Change Using Lake Sediments: Developments in Paleoenvironmental Research* 3. Springer, Dordrecht, Netherlands, pp. 75–97.
- Williams, A.N., Mooney, S.D., Sisson, S.A., Marlon, J., 2015. Exploring the relationship between Aboriginal population indices and fire in Australia over the last 20,000 years. *Palaeogeography, Palaeoclimatology, Palaeoecology* 432, 49–57.